

Lecture Notes in Civil Engineering

Dhruvesh Patel  
Byungmin Kim  
Dawei Han *Editors*

# Innovation in Smart and Sustainable Infrastructure

Select Proceeding of ISSI 2022

 Springer

# Lecture Notes in Civil Engineering

Volume 364

## Series Editors

Marco di Prisco, Politecnico di Milano, Milano, Italy

Sheng-Hong Chen, School of Water Resources and Hydropower Engineering,  
Wuhan University, Wuhan, China

Ioannis Vayas, Institute of Steel Structures, National Technical University of  
Athens, Athens, Greece

Sanjay Kumar Shukla, School of Engineering, Edith Cowan University, Joondalup,  
WA, Australia

Anuj Sharma, Iowa State University, Ames, IA, USA

Nagesh Kumar, Department of Civil Engineering, Indian Institute of Science  
Bangalore, Bengaluru, Karnataka, India

Chien Ming Wang, School of Civil Engineering, The University of Queensland,  
Brisbane, QLD, Australia

**Lecture Notes in Civil Engineering (LNCE)** publishes the latest developments in Civil Engineering—quickly, informally and in top quality. Though original research reported in proceedings and post-proceedings represents the core of LNCE, edited volumes of exceptionally high quality and interest may also be considered for publication. Volumes published in LNCE embrace all aspects and subfields of, as well as new challenges in, Civil Engineering. Topics in the series include:

- Construction and Structural Mechanics
- Building Materials
- Concrete, Steel and Timber Structures
- Geotechnical Engineering
- Earthquake Engineering
- Coastal Engineering
- Ocean and Offshore Engineering; Ships and Floating Structures
- Hydraulics, Hydrology and Water Resources Engineering
- Environmental Engineering and Sustainability
- Structural Health and Monitoring
- Surveying and Geographical Information Systems
- Indoor Environments
- Transportation and Traffic
- Risk Analysis
- Safety and Security

To submit a proposal or request further information, please contact the appropriate Springer Editor:

- Pierpaolo Riva at [pierpaolo.riva@springer.com](mailto:pierpaolo.riva@springer.com) (Europe and Americas);
- Swati Meherishi at [swati.meherishi@springer.com](mailto:swati.meherishi@springer.com) (Asia—except China, Australia, and New Zealand);
- Wayne Hu at [wayne.hu@springer.com](mailto:wayne.hu@springer.com) (China).

**All books in the series now indexed by Scopus and EI Compendex database!**

Dhruvesh Patel · Byungmin Kim · Dawei Han  
Editors

# Innovation in Smart and Sustainable Infrastructure

Select Proceeding of ISSI 2022

 Springer



*Editors*

Dhruvesh Patel  
Department of Civil Engineering  
Pandit Deendayal Energy University  
Gandhinagar, Gujarat, India

Dawei Han  
Department of Civil Engineering  
University of Bristol  
Bristol, UK

Byungmin Kim  
Department of Urban and Environmental  
Engineering  
Ulsan National Institute of Science  
and Technology  
Ulsan, Korea (Republic of)

ISSN 2366-2557

ISSN 2366-2565 (electronic)

Lecture Notes in Civil Engineering

ISBN 978-981-99-3556-7

ISBN 978-981-99-3557-4 (eBook)

<https://doi.org/10.1007/978-981-99-3557-4>

© The Editor(s) (if applicable) and The Author(s), under exclusive license to Springer Nature Singapore Pte Ltd. 2024

This work is subject to copyright. All rights are solely and exclusively licensed by the Publisher, whether the whole or part of the material is concerned, specifically the rights of translation, reprinting, reuse of illustrations, recitation, broadcasting, reproduction on microfilms or in any other physical way, and transmission or information storage and retrieval, electronic adaptation, computer software, or by similar or dissimilar methodology now known or hereafter developed.

The use of general descriptive names, registered names, trademarks, service marks, etc. in this publication does not imply, even in the absence of a specific statement, that such names are exempt from the relevant protective laws and regulations and therefore free for general use.

The publisher, the authors, and the editors are safe to assume that the advice and information in this book are believed to be true and accurate at the date of publication. Neither the publisher nor the authors or the editors give a warranty, expressed or implied, with respect to the material contained herein or for any errors or omissions that may have been made. The publisher remains neutral with regard to jurisdictional claims in published maps and institutional affiliations.

This Springer imprint is published by the registered company Springer Nature Singapore Pte Ltd.

The registered company address is: 152 Beach Road, #21-01/04 Gateway East, Singapore 189721, Singapore

Paper in this product is recyclable.

# Contents

<b>Innovations in Remote Sensing and Water Resources Management</b>	
<b>A Dam Break Analysis of Damanganga Dam Using HEC-RAS 2D Hydrodynamic Modelling and Geospatial Techniques</b> .....	3
Kishanlal R. Darji, Uttamkumar Hasubhai Vyas, Dhruvesh Patel, and Benjamin Dewals	
<b>Enhancing the Optimum Water Requirement for the Crop Using the Contemporary Capillary Wick Irrigation Method a Case of an Experimental Demonstration</b> .....	17
Uttamkumar Vyas, Neelkanth Bhatt, Vinay Vakharia, and Dhruvesh Patel	
<b>A Comparative Assessment of Unsupervised and Supervised Methodologies for LANDSAT 8 Satellite Image Classification</b> .....	31
Kratika Sharma, Ritu Tiwari, Shobhit Chaturvedi, and A. K. Wadhvani	
<b>Comparison of Image Processing Techniques to Identify the Land Use/Land Cover Changes in the Indian Semi-arid Region</b> .....	41
Nikhil Anand, Shweta Kumari, and Ankit Deshmukh	
<b>Application of Open-Source Geospatial and Modeling Techniques for Flood Assessment and Management—A Case of Flood 2017, Rel River Catchment</b> .....	51
Dhruvesh Patel, Kishanlal R. Darji, Amit Kumar Dubey, Praveen Gupta, and Raghavendra Pratap Singh	
<b>Evaluation of Movement of Wetting Front Under Wick Irrigation in Black Cotton Soil</b> .....	63
Uttamkumar Vyas, Kishanlal Darji, Neelkanth Bhatt, Vinay Vakharia, and Dhruvesh Patel	

<b>One Dimensional Steady Flow Analysis Using HEC-RAS—A Case of Sabarmati River, Gujarat, India</b> .....	73
Ujas Deven Pandya and Dhruvesh Patel	
<b>Reliability–Resilience–Vulnerability Analysis of Droughts Over Maharashtra</b> .....	87
Gaurav Ganjir, M. Janga Reddy, and S. Karmakar	
<b>Remote Sensing and GIS Application for Soil Erosion and Sediment Yield Estimation of Purna River Sub-Basin</b> .....	99
Milan Dineshbhai Nadiyapara and Falguni P. Parekh	
<b>A Review of Different Approaches for Boundary Shear Stress Assessment in Prismatic Channels</b> .....	117
Vijay Kaushik and Munendra Kumar	
<b>Water Quality Assessment Using Water Quality Index (WQI) Under GIS Framework in Brahmani Basin, Odisha</b> .....	131
Abhijeet Das	
<b>Meta-heuristic Approach for Flood Control in Reservoir Operation</b> ....	151
Priya Chauhan and Sandeep M. Narulkar	
<b>UAV-Based High-Resolution DEM Application for River Cross-Section Derivation and 1D Flood Assessment</b> .....	163
Mrunalini Rana, Dhruvesh Patel, and Vinay Vakharia	
<b>Stream Flow and Sediment Load Variation in Middle Tapi Basin</b> .....	175
Urvashi Malani and Sanjaykumar Yadav	
<b>Sustainable Development in Water Quality Assessment: Data for Khadakwasla Dam, Pune</b> .....	185
Mohnish M. Waikar and Parag Sadgir	
<b>Innovations in Computational Geotechnics and Advance Concrete Technology</b>	
<b>Qualitative Analysis of Physio-Chemical Parameters of Soil to Underline the Effects of Pipeline Laying on Soil Fertility</b> .....	195
Anirbid Sircar, M. A. Shabiimam, Abdul Rasheed, Shaunak Mehta, Jaini Shah, Ankita Patel, Namrata Bist, Kriti Yadav, and Roshni Singh	
<b>Comparative Study for Compressive and Split Tensile Strengths of Low-Sludge Concrete</b> .....	207
J. R. Pitroda, Reshma L. Patel, Rajesh Gujar, Jaykumar Soni, and Vismay Shah	

**Effect of Chemical Stabilisation in Clayey Soil for Strength and Durability Characteristics** ..... 223  
 Shiva Kumar Mahto and Sanjeev Sinha

**Pull-Out and Rupture Behavior of Geogrid Reinforcements in MSE Wall Subjected to Seismic Conditions** ..... 231  
 Anand M. Hulagabali, C. H. Solanki, C. Thrupthi, N. Sushma, Ruokuolenuo Suokhrie, and S. Sudarshan

**Stabilization of Expansive Soil: A Review** ..... 251  
 Dharmendra Singh, Vijay Kumar, and R. P. Tiwari

**Effect of Bottom Ash on the Properties of Subgrade Soil** ..... 265  
 Manan Vaja, Uma Chaduvula, and Tejaskumar Thaker

**Experimental Study on Mechanical Properties of Concrete Incorporated with Basalt and Polypropylene Fibers** ..... 275  
 Sandeep Sathe, Shahbaz Dandin, Shubham Surwase, and Alina Kharwanlang

**Soil Properties Modification Using PET waste—An Experimental Study** ..... 285  
 Alka Shah and Tejas Thaker

**Use of XRD Technique in Characterising Different Types of Concrete** ..... 295  
 Diksha, Nirendra Dev, and Pradeep Kumar Goyal

**Innovations in Sustainable Building Construction Materials**

**Experimental Study on Quarry Dust Cement Mortar with Bacteria** .... 325  
 Reshma L. Patel, J. R. Pitroda, Rajesh Gujar, and Jaykumar Soni

**Reclaimed Sand Dust Waste as Eco-Friendly Green Construction Materials** ..... 339  
 Reshma L. Patel, J. R. Pitroda, Rajesh Gujar, and Jaykumar Soni

**Innovative Sustainable Solution for High-Strength Quaternary Cement Concrete with Lime Powder** ..... 359  
 Niragi Dave

**Effect of Incorporation of Nano-Silica on Mechanical Properties of Mortar and Concrete** ..... 369  
 Patel Karan and Thakkar Sonal

**Ecobricks—A Sustainable Solution to Plastic Waste** ..... 383  
 Vaishali Sahu, Abhishek, Yash Vats, and Niragi Dave

<b>Development of Rubber Mould Paver Blocks Using Textile Effluent Treatment Plant Sludge</b> .....	395
Reshma L. Patel, J. R. Pitroda, Rajesh Gujar, Jaykumar Soni, Bansari N. Dave, and Vismay Shah	
<b>Sustainable Method for Construction and Demolition Waste: A Review</b> .....	411
Mitali Mistry, Hetvi Chaudhari, and M. A. Shabiimam	
<b>Innovations in Climate Change Assessment</b>	
<b>An Enhanced Bottom-Up Approach to Assess the Catchments' Vulnerability to Climate Change</b> .....	427
Vishal Rakhecha and Ankit Deshmukh	
<b>Identification of Best CMIP6 Climate Models for Offshore Wind Energy Assessment</b> .....	443
Deepjyoti Basak, Nagababu Garlapati, and Jaydeep Patel	
<b>Analysis of Rainfall Using Family of Innovative Trend Methods for Climate Change Detection</b> .....	455
Anishka Priya Suresh, Celina Thomas, Aiswarya K. Ajith, A. V. Amalenth, and Adarsh Sankaran	
<b>Review on Statistical Post-processing of Ensemble Forecasts</b> .....	469
Rashmi Yadav and Sanjaykumar M. Yadav	
<b>Statistical Downscaling Model (SDSM) for Long Term Prediction of Rainfall and Maximum Temperature</b> .....	477
Himanshukumar Babuji Thakor and Falguni P. Parekh	
<b>A Non-parametric Test-Based Trend Analysis of the Rainfall and Temperature Pattern in the District of Bharuch, Gujarat</b> .....	487
Khushboo A. Jariwala and Prasit G. Agnihotri	
<b>Role of Changing Atmospheric Temperature and Radiation on Sea Ice Conditions Over Laptev and Greenland Seas for the Recent Decade</b> .....	501
Dency V. Panicker, Bhasha H. Vachharajani, and Rohit Srivastava	
<b>Innovations in Sustainable Infrastructure Development</b>	
<b>Performance Evaluation of Control Variables for the Development of a Blockchain Model for Construction Projects</b> .....	527
Debasis Sarkar and Purvesh Raval	
<b>Examining Different Job-Site Layout Strategies and Their Effects on Construction Productivity</b> .....	551
Vismay Shah, Jaykumar Soni, Devang Shah, Dhruvi Shah, Rajesh Gujar, and J. R. Pitroda	

**Comparative Study of Prospective PPP Models for Highway Projects of India** ..... 563  
 Naimish Bhatt and Debasis Sarkar

**Factors Affecting Improvements in Labour Productivity in Building Construction Projects—India** ..... 573  
 B. Srikanth, Ashwin Raut, Anuja Charpe, and Rahul Reddy

**Systematic Processing Framework for Identifying, Assessing and Overcoming Delays in Construction Projects in India** ..... 585  
 Chaitanya P. Mali and Ajay P. Shelorkar

**Review of Fire Risk Factors for Fire Risk Assessment in Urban Areas: The Case of Ahmedabad, India** ..... 607  
 Priyanka Raval and Ronak Motiani

**Modelling the Impact of Various Strategies for Improving the Outdoor Thermal Comfort at a City Level** ..... 625  
 Yash G. Bhavsar and Anurag Kandya

**Application of a Global Uncertainty and Sensitivity Analysis for Identifying Influential Sustainable Building Design and Operation Parameters** ..... 643  
 Ankit Rajput, Jishan H. Rajpal, Janak Chaudhary, Naimish Bhatt, and Shobhit Chaturvedi

**Problems and Prospects for Conservation of Traditional Bazaars in Walled City of Jaipur** ..... 655  
 Shipra S. K. Goswami, Ashwani Kumar, and Satish Pipralia

**A Framework of Internet of Things–Cloud–Building Information Modeling Based Life Cycle Management of Precast Components in Prefabricated Buildings** ..... 671  
 Arpit Solanki and Debasis Sarkar

# About the Editors

**Dr. Dhruvesh Patel** is currently working as an associate professor of civil engineering department, School of Technology, Pandit Deendayal Energy University (PDEU), India. His major area of research interests include flood risk assessment and management, flood hazard mapping, flood mitigation and planning of water resources management. He has published 21 research papers in international peer-review high impact factor journals and 50 in national/international conferences. He is a reviewer for journals of national and international repute.

**Dr. Byungmin Kim** is currently working as an associate professor of School of Urban and Environmental Engineering at UNIST, South Korea. Dr. Kim obtained his B.S. (2007) from Hanyang University, South Korea and M.S. (2009) and Ph.D. (2012) from the University of Illinois at Urbana-Champaign, USA. His current research interests include various research topics such as seismic hazard analysis, site characterization, ground motion amplification, landslide, liquefaction, seismic risk assessment; etc. He has published over 45 peer-reviewed journal and conference papers.

**Prof. Dawei Han** is professor of hydroinformatics from Department of Civil Engineering, the University of Bristol, UK. He obtained Ph.D. (1991), M.Sc. (1984) and B.Eng. (1982). His research interest includes hydrological modelling, real-time flood forecasting, flood risk assessment and management, climate change impact, remote sensing and geographic information system, natural hazards, etc. He has carried out various projects on weather radar rainfall and numerical weather prediction to aid flood risk assessment, downscaling of global circulation model for climate change, multi-natural hazards, etc. He has published over 300 peer-reviewed journal and conference papers.

# **Innovations in Remote Sensing and Water Resources Management**



# A Dam Break Analysis of Damanganga Dam Using HEC-RAS 2D Hydrodynamic Modelling and Geospatial Techniques



Kishanlal R. Darji, Uttamkumar Hasubhai Vyas, Dhruvesh Patel, and Benjamin Dewals

**Abstract** The dam is the inline structure constructed over the river connecting the storage area to the downstream river catchment area. Large dam constructs serve multipurpose objectives like irrigation, hydropower generation, and water supply for residential, commercial, and industrial use. Though dams have many benefits, the threat of dam break always remains, either due to a large amount of rainfall in the upstream catchment, earthquake, structure failure, etc. To understand the dam breach scenario and find out the inundation extent, water surface elevation, flow velocity, and wave arrival time, a dam breach study is needed. It contributes to reducing loss of life and damage by guiding the preparation of emergency action plans (EAP). This paper describes the analysis of piping failure of the Damanganga dam, Gujarat, India, using the Hydraulic Engineering Centre's River Analysis System (HEC-RAS) 2D hydrodynamic modelling and geospatial techniques. Inflow hydrograph, Digital Elevation Model (DEM), topography, and area capacity curve of Damanganga reservoir have been utilized to build a 2D hydrodynamic model. Froehlich equation was used to estimate dam breach parameters. Water surface elevation, flow depth and velocity, arrival time, and inundation area were calculated. The inundation area is 153 km<sup>2</sup>, and the number of affected villages including cities is 48. This study helps the site's administrative authority, and the dam owner develops EAP and flood mitigation.

**Keywords** Dam breach analysis · HEC-RAS · Piping failure · Remote sensing and GIS

---

K. R. Darji (✉) · U. H. Vyas · D. Patel  
Pandit Deendayal Energy University, Gandhinagar, India  
e-mail: [darjishan1@gmail.com](mailto:darjishan1@gmail.com)

U. H. Vyas  
e-mail: [uttam.vphd21@sot.pdpu.ac.in](mailto:uttam.vphd21@sot.pdpu.ac.in)

D. Patel  
e-mail: [dhruvesh.patel@sot.pdpu.ac.in](mailto:dhruvesh.patel@sot.pdpu.ac.in)

B. Dewals  
Liege University, Liege, Belgium  
e-mail: [b.dewals@uliege.be](mailto:b.dewals@uliege.be)

# 1 Introduction

In India, the concept of water storage by creating water retention structures like a dam comes from the pre-Harappan civilization. Water storage structures have become increasingly important in modern times, as highlighted by the construction of thousands of dams worldwide (Desta 2020). Dams are structures built across rivers to provide socio-economic and environmental services such as irrigation, drinking water, hydropower, recreation, and flood prevention, among other things. Despite these advantages, floods caused by dam failure have resulted in some of the most severe environmental disasters, resulting in massive loss of life and significant property damage because many of these dams are situated near highly populated regions (Berghout and Meddi 2016; Boussekine and Djemili 2016; Derdous et al. 2015; Wang et al. 2016). More than 800,000 dams store water worldwide. According to ICOLD data, the globe has over 57,000 large dams, with India ranked third after the United States and China with approximately 5334 large dams (Dhiman and Patra 2019). As a result, rather than flood reduction, more focus should be placed on better flood management, such as developing EAP and an warning systems to reduce damage induced by dam breach.

According to the Dam Rehabilitation and Improvement Project (DRIP) guideline of the Indian Central Water Commission, the objective of the dam break analysis is to generate a flood map by analysing the impact that may occur in the event of dam failure. The depth and area determine the effects of flood inundations (Patel et al. 2017). Time of arrival determines the flood risk index associated with flood risk management including evacuation management, hazard mapping, and evacuation mapping (Juliastuti 2017; Ingenieure 1892; Sahoo and Sreeja 2017), which helps preparing EAP and public disaster management. Dam breach can be simulated by means of hydrological and hydrodynamic models. Hydrologic Engineering Centre's Hydrologic modelling System (HEC-HMS) and Hydrologic Engineering Centre's-1 (HEC-1) are examples of hydrological models. Hydraulic models include Hydrologic Engineering Centre's hydraulic river analysis system (HEC-RAS) (Li et al. 2022; Jodhani et al. 2021; Pandya and Patel 2021), MIKE 11, MIKE2, TELEMAC 2D, DELFT-FSL, National Weather Service simple dam break (NWS SMPDBK), and Flood wave (FLDWAV) (Desta 2020; Gaagai et al. 2022; Darji et al. 2019, 2021). Predicting the dam breach parameter is the most challenging task in dam breach analysis due to a lack of awareness of reservoir capacity, hydrological parameters, and spillway capacity (Pathan et al. 2021, 2022; Trambadia et al. 2022; Bruwier et al. 2018).

Several studies investigated prediction equations for the dam breach parameters based on historical dam failures (Froehlich 2008, 1995a, 1995b; Wahl 2004; Walder and O'Connor 1997; Pierce et al. 2010; MacDonald and Langridge-Monopolis 1984; Snorrason et al. 1984; Xu and Zhang 2009; Wahl 1998; US Bureau of reclamation 1982). Froehlich (2008) equation was found to provide better results than other equations for Indian dams (Dhiman and Patra 2019). DRIP also recommends this equation to determine dam breach parameters (Central Water Commission 2019).

Previous dam breach analyses were conducted based on one- and two-dimensional models HEC-RAS and NWS-FLDWAV with GIS (Gee and Brunner 2005; Tamm and Tamm 2020; Albu et al. 2020). Numerical modelling of earthen dam for piping failure (Chen et al. 2019) and one-dimensional models to develop food maps, flood mitigation, flood damage, and EAP using GIS and modelling techniques (Gee and Brunner 2005; Tamm and Tamm 2020; Albu et al. 2020; Chen et al. 2019; Purnama and Jayadi 2021).

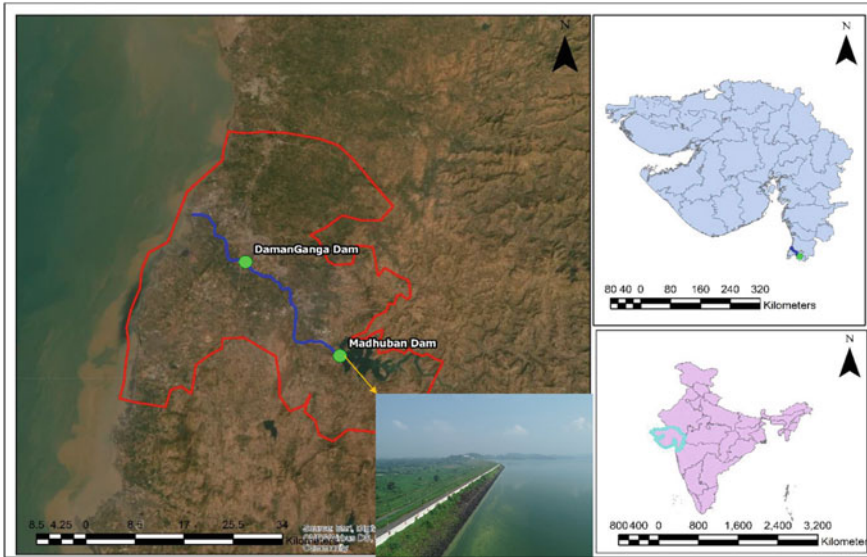
This study aims to analyse dam failure caused by piping and determine the affected villages, towns, and industries of the downstream area. HEC-RAS model was used to simulate in 2D the hydrodynamics. The HEC-RAS model incorporates flow analysis for unsteady flows, GIS tools to aid engineering study, and automated function calculation by the diffusion wave method for developing a map of flood depth, velocity, inundation, water surface elevation, and arrival time, in line with DRIP guidelines. Generated maps help to determine flood risk zones and prepare EAP for dam owners and administrative offices to reduce loss of life and damages.

## 2 Study Area and Data Collection

The Damanganga River originates in the Sahyadri hill near the village of Ambegaon in the Dindori taluka of Maharashtra's Nasik district at an elevation of 950 m above mean sea level. The total length of the Damanganga River is 131 km. It passes through Maharashtra, Gujarat, union territory Daman, and Dadra Nagar Haveli. The total drainage area of Damanganga River is 1813 km<sup>2</sup>, with an average yearly rainfall of 2382 mm.

Damanganga dam was constructed on Damanganga River at Madhuban village in Dharampur taluka of Valsad city, Gujarat (Fig. 1). Damanganga dam is also known as Madhuban Dam, which is an inter-state multifunctional project of the Union territory Daman, Dadra Nagar Haveli, and the Government of Gujarat. Damanganga dam was constructed from 1972 to 1998 for water distribution and irrigation, domestic and industrial use as well as hydropower. It is a composite dam of earth fill, masonry, and saddle dam with a length and height of 2870 m and 58.6 m, respectively. The maximum design flood of this dam is 26,844.37 m<sup>3</sup>/s. The gross storage is 524.86 M m<sup>3</sup>, and live storage is 478 Mm<sup>3</sup>. A total of 10 radial gates of 15.22 \* 14.02 m were designed to discharge 22,030.5 m<sup>3</sup>/s. The 112 villages in the Valsad district, 24 in U.T. Dadra Nagar Haveli, and 26 in the U.T. Daman is irrigated by the Damanganga dam. The Damanganga reservoir provides 58 million gallons each day for domestic and industrial water demands and has a limited power plant capacity of 5.6 MW.

Meteorological data for the study area were obtained from the State Water Data Centre (SWDC), the flood control cell of Damanganga dam (<https://swhydrology.gujarat.gov.in>), the Government of Gujarat, and the Indian Meteorological Department (IMD) (<http://www.imd.gov.in/>). Thematic maps and topography were prepared from the published literature (<https://www.gsi.gov.in/>, <http://cgwb.gov.in/>) of the different



**Fig. 1** Location map of Damanganga Reservoir (Madhuban Dam)

agencies in conjunction with the interpretation of Landsat images, Google Earth images, and SRTM Digital Elevation Model (DEM) using remote sensing and GIS technology. Salient features, inflow-outflow, and capacity area table of Damanganga reservoir were collected from the Damanganga project division no. 1, office.

### 3 Method and Material

The methodology consists of four phases: (1) Data collection (2) Data preparation (3) Model simulation, and (4) Map preparation, as shown in Fig. 2.

#### 3.1 Flow Hydrograph

Inflow hydrograph of an extreme event was collected from flood cell of Damanganga project division-1 office at Madhuban colony, Valsad city, Gujarat (Fig. 3). Over the last 30 years, the highest rainfall fell in the year 2004, leading to an inflow of  $18,075 \text{ m}^3/\text{s}$  into the reservoir. This inflow hydrograph was prescribed as upstream boundary condition for the HEC-RAS model.

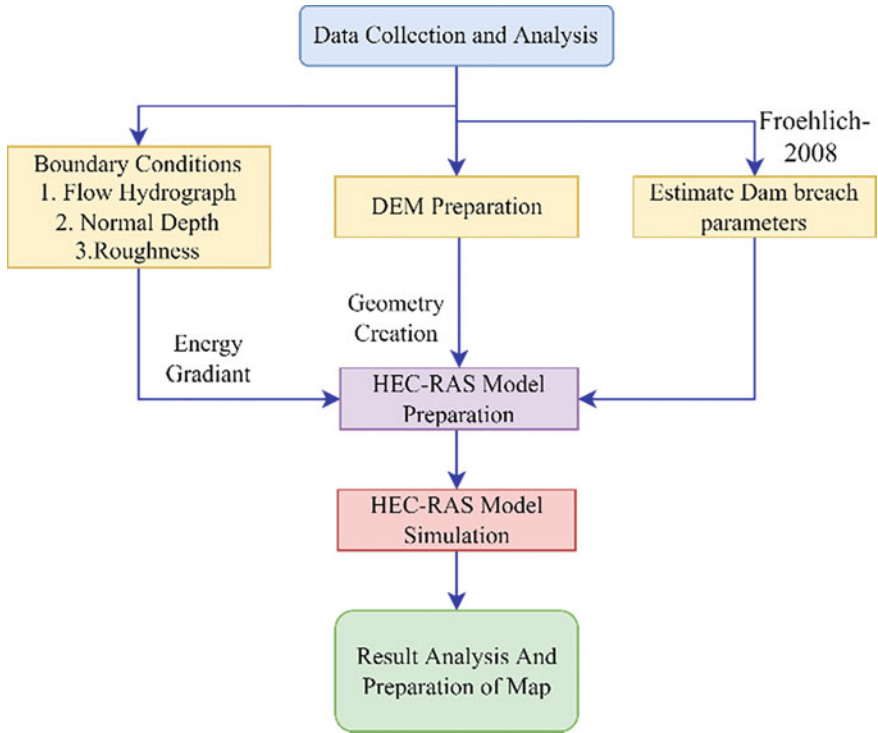


Fig. 2 Methodology chart

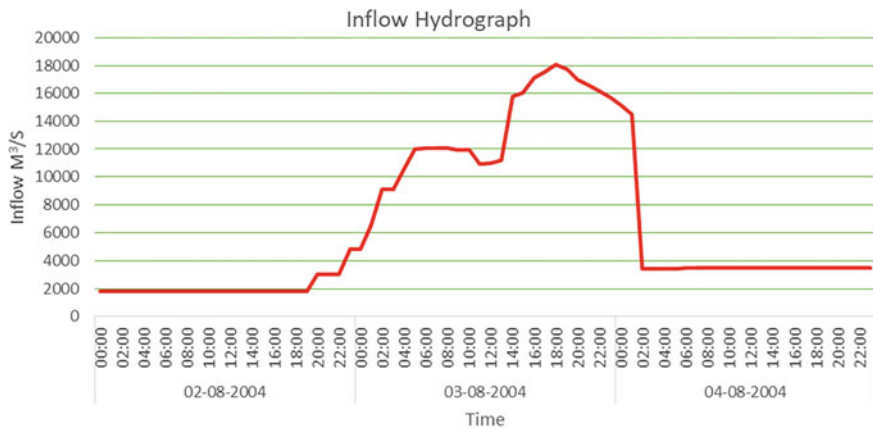
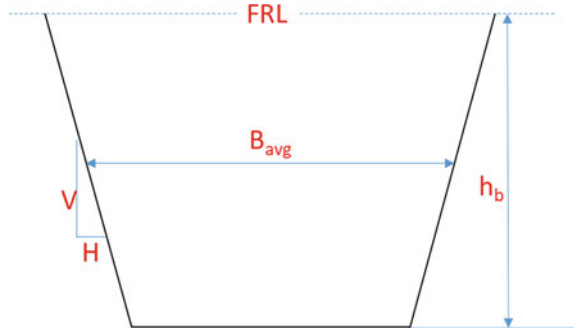


Fig. 3 Inflow hydrograph of Damanganga reservoir

**Fig. 4** Shape of breach section



### 3.2 Dam Breach Parameters

The selection of dam breach parameters, such as breach depth, width, shape, and formation time, is affected by a high level of uncertainty. Several methods are available for estimating dam breach parameters. In this study, we used Froehlich (2008) equation (Pierce et al. 2010), as recommended by the DRIP:

$$B_{avg} = 0.23 * K_m * (V_w)^{1/3} \quad (1)$$

where  $B_{avg}$  = expected value of average width in metres,  $K_m = 1.0$  for internal erosion (Piping) failure, and 1.5 for failure by overtopping,  $V_w$  (in  $m^3$ ) = volume of water stored above breach bottom. The expected breach side-slope ratio is given by  $M = 0.6$  in the case of internal erosion (piping) and 1.0 in the case of overtopping. The breach formation time (in seconds) is given by:

$$T_f = 60 * (V_w / g(H_b)^2)^{1/2}$$

where  $H_b$  = Height of breach in metres (Fig. 4).

### 3.3 Elevation Area Capacity Curve

Elevation area curves are commonly used for reservoir flood routing, determining the surface area of the water and volume corresponding to each elevation, reservoir classification, and sediment distribution in the reservoir. This curve was collected from the Damanganga project division-1 office (Fig. 5). This curve was used to determine the storage capacity at various elevations.

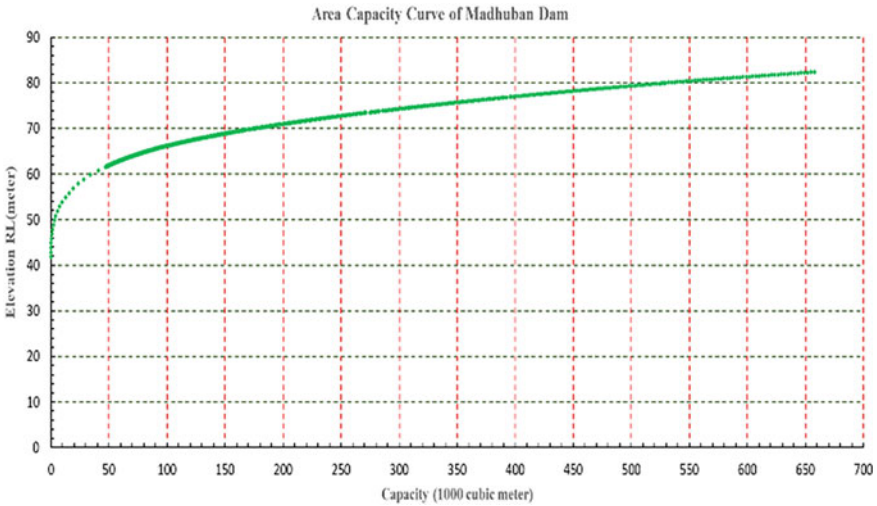


Fig. 5 Elevation capacity curve of dam

### 3.4 Terrain Preparation

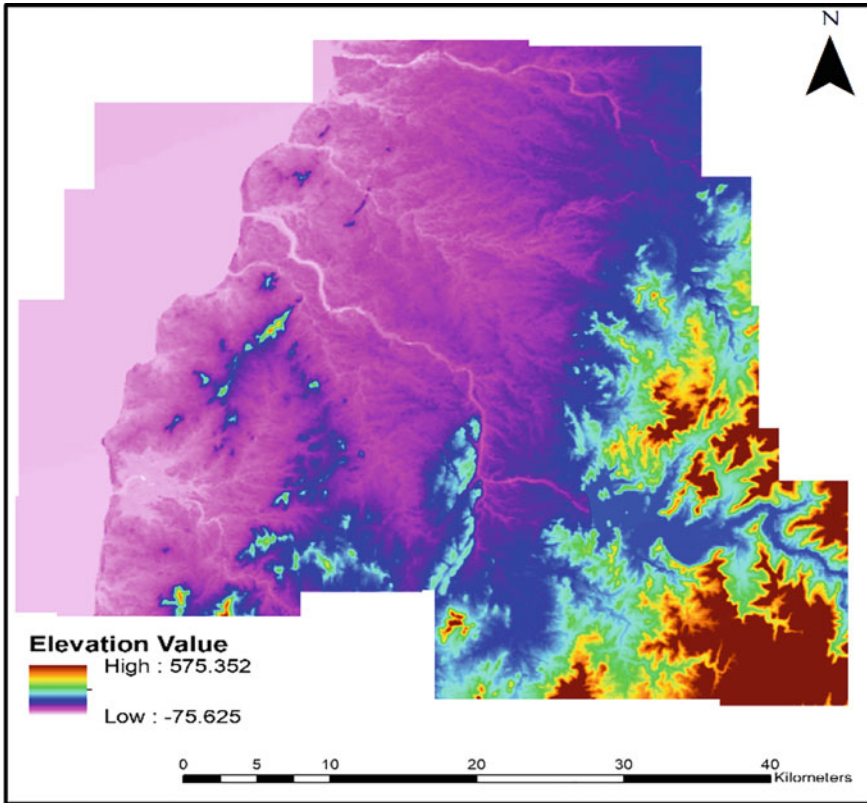
The RAS Mapper was used to prepare the terrain data of the study area (Fig. 6), by inputting the SRTM DEM collected from the United States Geological Survey (USGS) Earth Explore. It has a maximum elevation of 641 m. UTM Zone 43N was used as a projection of the study area.

## 4 Results

According to Froehlich (2008) prediction equation, the bottom breach width is estimated at 164 m, and the breach formation time at 3 h. The discharge inflow series and unsteady flow analysis for the extreme condition of the Damanganga dam were performed using the HEC-RAS model setup. Simulation output maps were created after the results were imported into ArcGIS. Flooding due to piping failure would flood an area of nearly 153 km<sup>2</sup>. This is valuable information for dam owners to prepare EAP and reduce the risk of a life-threatening, catastrophic event. The prepared maps are shown below.

**Flood Depth:** The flood depth map shows the flood depth in metres from the DEM RLs. As per the map, flood depth is more prevalent in the right bank of the river than the left bank. Therefore, the villages located at right bank of the river have more chances to get flooded and need more precaution to prepare a detailed EAP. The usual depth covers the ranges from 3 to 6 m. The area susceptible the depth above 4 m should be considered in emergency conditions and hence needs first priority





**Fig. 6** Terrain of downstream of Damanganga reservoir

for any emergency evacuation. This map is further helpful to decision-makers for preparing a flood defence structure for flood resilience and flood mitigation planning under extreme flooding conditions (Fig. 7).

**Flow velocity:** The river stretch between the Madhuban Dam and the Arabian Sea falls by up to 38 m in 42 km. The slope of the stretch is nearly 0.0009. It shows a steep sloped river in south Gujarat, hence, influences more on river velocity. The results show (Fig. 8) that the flow reaches 7–8 m/s velocity immediately downstream of the dam and further downstream up to 4–5 m/s. The flow velocity has a direct influence on the flood arrival time, hence, high velocity intensifies the flood disaster and flood risk. Furthermore, flood rescue and emergency action need a prompt response in flood susceptible areas and need a more robust mechanism with dam owners to reduce flood fatality.

**Water Surface Elevation:** Maps show the water elevation from the main sea level as shown in Fig. 9, and the WSE is frequently 40–50, 35–40, 20–30, 15–20, 10–15 in the short stretch of river. It shows the need for more prompt action from dam owners during the disaster.



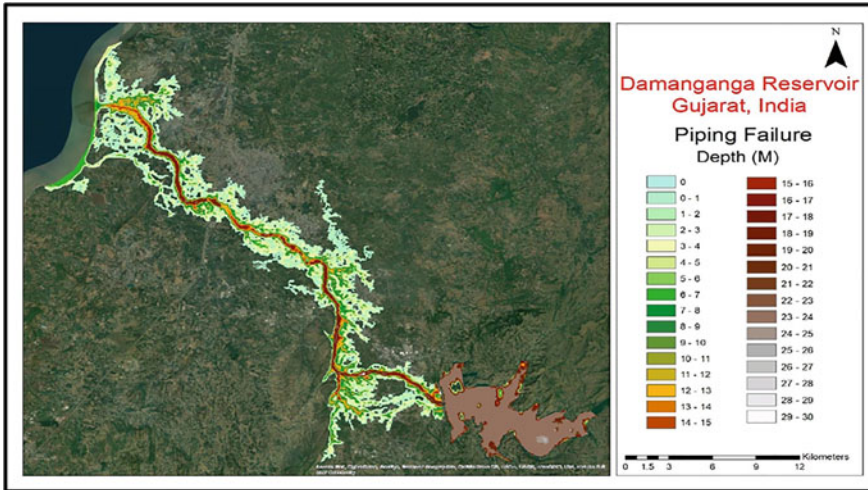


Fig. 7 Flood depth map

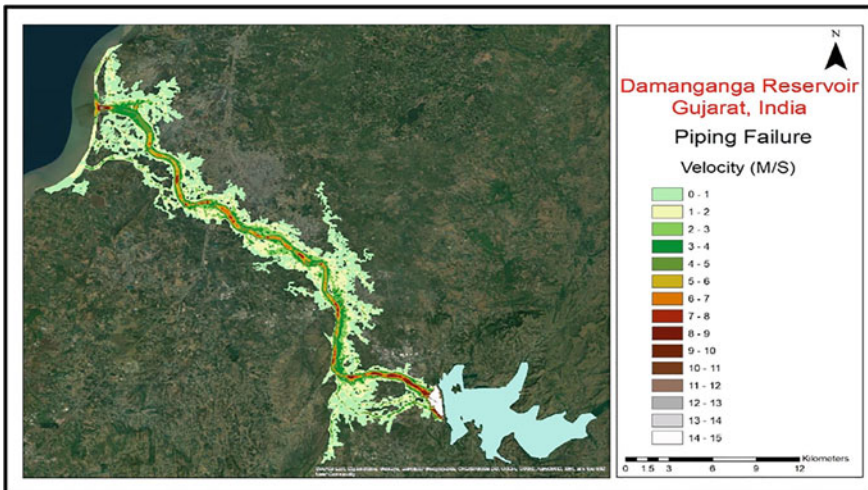


Fig. 8 Flow velocity map

**Flood Arrival Time:** Flood arrival time is one of the major decision-making parameters to reduce flood fatalities. The prepared flood arrival time map shows that water depth reaches inundation depth at the Arabian Sea in 6–9 h. This map would be used to determine where to begin evacuating people, and at what time, to reduce the number of fatalities (Fig. 10).

**Flood Inundation:** Study area is highly vulnerable through the flood, if the dam break case prevails. The inundation maps show that more than 153 km<sup>2</sup> area will be

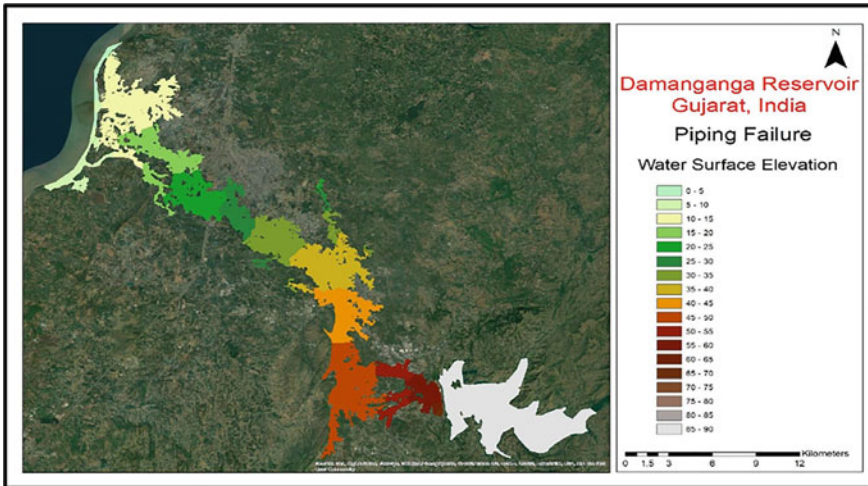


Fig. 9 Water surface elevation map of flood

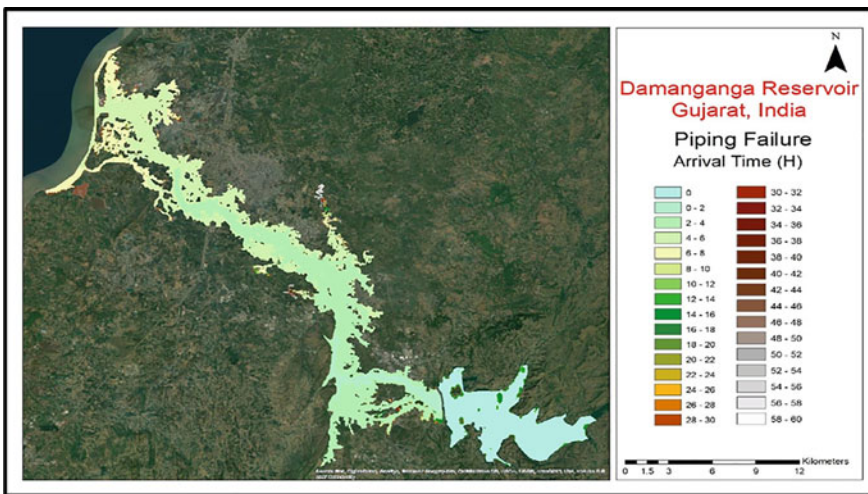


Fig. 10 Flood arrival time map

influenced by flood under piping failure. It would be very useful information for dam owners to prepare and provide flood mitigation plans for flood susceptible areas in the study reach (Fig. 11).

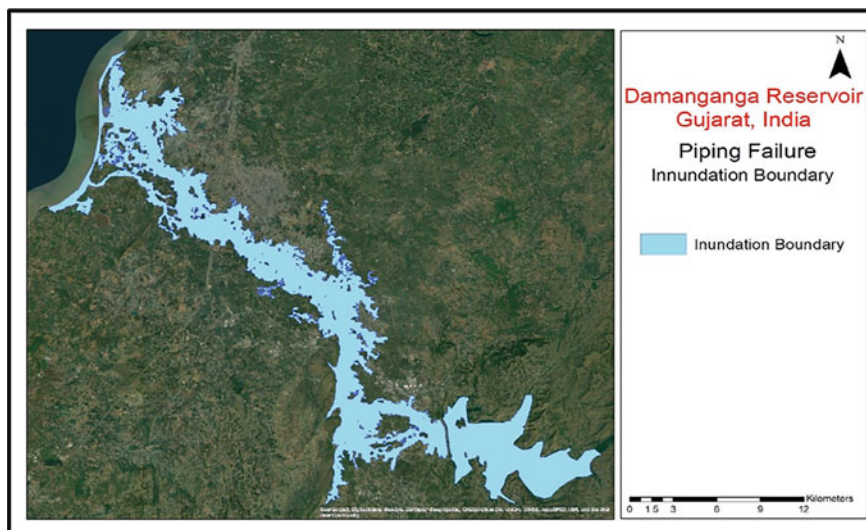


Fig. 11 Inundation boundary map

## 5 Discussion

Prepared dam break case of piping failure condition is an important case study to prepare an EAP for a large dam in the centre part of India. Some important outcomes are abstracted here to improve the performance and flood decision-making system.

- (1) The manning's roughness 'n' has been proposed as per the expert opinion (Patel et al. 2017) and DRIP guideline (Central Water Commission 2019), however, it should be further tested for sensitivity, since model calibration and validation using past flooding events is particularly intricate for extreme scenarios such as dam breaks. In addition, it would be tested using the laboratory test for precise manning's for dam break analysis.
- (2) The model is simulated under SRTM DEM with moderate topographic resolution. The depth, water surface elevation, and arrival time would be further improved using high-resolution DEM. Therefore, in economical cost consideration, it would be recommended to replace the high vulnerable flood extent topography with UAV (Drone) based on precise DEM for robust flood mapping.
- (3) The 2D flood simulation in river starch has been performed considering the base flow projected on DEM, however, surveyed river bathymetry and DEM in replacement of existing DEM will further improve the simulation results and flood decisions making system.

## 6 Conclusion

This study presents a dam break analysis due to piping for the Damanganga dam, using medium resolution terrain data in HEC-RAS. If the Damanganga dam fails due to piping, it is estimated that 46 villages would be affected. People living in Silvassa, the Vapi industrial area, the northern part of Daman, and the low-lying area near the river are highly vulnerable due to dense urbanization. The flood wave arrival time is less than 9 h. Dam breach analysis is instrumental in preparing a dam EAP, and it is recommended that every dam has an EAP to ensure the safety of people living in vulnerable areas. High-quality data and modelling skills are being used to predict a more accurate Damanganga reservoir piping failure flood.

**Acknowledgements** The author (s) would like to thank Damanganga Project Division No-1, Narmada Water Resources Water Supply, and Kalpsar department, GoG, and thank the Survey of India (SOI) for providing the necessary data support to execute the work. The author (s) would also like to thank Dr. R. P. Singh, Scientist-G, Space Applications Centre-ISRO, Ahmedabad, for supporting technical enhancement to improve the research work quality.

## References

- Albu LM, Enea A, Iosub M, Breaban IG (2020) Dam breach size comparison for flood simulations. A HEC-RAS based, GIS Approach for Dracsani Lake, Sitna river, Romania. *Water* (Switzerland) 12. <https://doi.org/10.3390/W12041090>
- Berghout A, Meddi M (2016) Sediment transport modeling in wadi Chemora during flood flow events. *J Water L Dev* 31:23–31. <https://doi.org/10.1515/JWLD-2016-0033>
- Boussekine M, Djemili L (2016) Modelling approach for gravity dam break analysis. *J Water L Dev* 30:29–34. <https://doi.org/10.1515/JWLD-2016-0018>
- Bruwier M, Mustafa A, Aliaga DG, Archambeau P, Ericum S, Nishida G, Zhang X, Piroton M, Teller J, Dewals B (2018) Influence of urban pattern on inundation flow in floodplains of lowland rivers. *Sci Total Environ* 622–623:446–458. <https://doi.org/10.1016/J.SCITOTENV.2017.11.325>
- Central Water Commission (2019) Guidelines-and-manuals | DRIP—Dam Rehabilitation and Improvement Project
- Chen S, Zhong Q, G Shen (2019) Numerical modeling of earthen dam breach due to piping failure. *Water Sci Eng*
- Darji K, Khokhani V, Mehmood K, Prakash I, Pham BT (2019) Rainfall-runoff modelling using HEC-HMS model: an application of regression analysis. *J Emerg Technol Innov Res* 6:226–234
- Darji K, Patel D, Dubey AK, Gupta P, Singh R (2021) An approach of satellite and UAS based Mosaicked DEM for hydrodynamic modelling—a case of flood assessment of Dhanera City, Gujarat, India. *J geomatics* 247–257
- Derdous O, Djemili L, Bouchehed H, Tachi SE (2015) A GIS based approach for the prediction of the dam break flood hazard—a case study of Zardezas reservoir “Skikda, Algeria.” *J Water L Dev* 27:15–20. <https://doi.org/10.1515/JWLD-2015-0020>
- Desta HB, Belayneh MZ (2020) Dam breach analysis: a case of Gidabo dam, Southern Ethiopia. *Int J Environ Sci Technol* 181(18):107–122. <https://doi.org/10.1007/S13762-020-03008-0>
- Dhiman S, Patra KC (2019) Studies of dam disaster in India and equations for breach parameter. *Nat Hazards* 98:783–807. <https://doi.org/10.1007/S11069-019-03731-Z/TABLES/11>



- Froehlich DC (1995a) Peak outflow from breached embankment dam. *J Water Resour Plan Manag* 121:90–97. [https://doi.org/10.1061/\(asce\)0733-9496\(1995\)121:1\(90\)](https://doi.org/10.1061/(asce)0733-9496(1995)121:1(90))
- Froehlich DC (1995b) Embankment dam breach parameters revisited. *ASCE Conf water Resour Eng* 887–891
- Froehlich DC (2008) Embankment dam breach parameters and their uncertainties. *J Hydraul Eng* 134:1708–1721. [https://doi.org/10.1061/\(asce\)0733-9429\(2008\)134:12\(1708\)](https://doi.org/10.1061/(asce)0733-9429(2008)134:12(1708))
- Gaagai A, Aouissi HA, Krauklis AE, Burlakovs J, Athamena A, Zekker I, Boudoukha A, Benaabidate L, Chenchouni H (2022) Modeling and risk analysis of dam-break flooding in a semi-arid montane watershed: a case study of the Yabous Dam, Northeastern Algeria. *Water* 14:767. <https://doi.org/10.3390/W14050767>
- Gee DM, Brunner GW (2005) Dam break flood routing using HEC-RAS and NWS-FLDWAY. *World Water Congr 2005 Impacts Glob Clim Chang Proc 2005 World Water Environ Resour Congr* 401. [https://doi.org/10.1061/40792\(173\)401](https://doi.org/10.1061/40792(173)401)
- Ingenieure AR (1892) Die fortpflanzung der wasserwellen. *Zeitschrift Des Vereines Dtsch Ingenieure* 36:947–954
- Jodhani KH, Patel D, Madhavan N (2021) A review on analysis of flood modelling using different numerical models. *Mater Today Proc*. <https://doi.org/10.1016/J.MATPR.2021.07.405>
- Juliastuti SO (2017) Dam break analysis and flood inundation map of Krisak dam for emergency action plan. *AIP Conf Proc* 1903:100005. <https://doi.org/10.1063/1.5011615>
- Li X, Ercpicum S, Mignot E, Archambeau P, Piroton M, Dewals B (2022) Laboratory modelling of urban flooding. *Sci Data* 91(9):1–10. <https://doi.org/10.1038/s41597-022-01282-w>
- MacDonald TC, Langridge-Monopolis J (1984) Breaching characteristics of dam failures. *J Hydraul Eng* 110:567–586. [https://doi.org/10.1061/\(ASCE\)0733-9429\(1984\)110:5\(567\)](https://doi.org/10.1061/(ASCE)0733-9429(1984)110:5(567))
- Pandya U, Patel DP (2021) Singh SK (2021) A flood assessment of data scarce region using an open-source 2D hydrodynamic modeling and Google Earth Image: a case of Sabarmati flood, India. *Arab J Geosci* 1421(14):1–18. <https://doi.org/10.1007/S12517-021-08504-2>
- Patel DP, Ramirez JA, Srivastava PK, Bray M, Han D (2017) Assessment of flood inundation mapping of Surat city by coupled 1D/2D hydrodynamic modeling: a case application of the new HEC-RAS 5. *Nat Hazards* 89:93–130. <https://doi.org/10.1007/s11069-017-2956-6>
- Pathan AI, Agnihotri PG, Patel D, Prieto C (2021) Identifying the efficacy of tidal waves on flood assessment study—a case of coastal urban flooding. *Arab J Geosci* 1420(14):1–21. <https://doi.org/10.1007/S12517-021-08538-6>
- Pathan AI, Agnihotri PG, Patel D, Prieto C (2022) Mesh grid stability and its impact on flood inundation through (2D) hydrodynamic HEC-RAS model with special use of Big Data platform—a study on Purna River of Navsari city. *Arab J Geosci* 157(15):1–23. <https://doi.org/10.1007/S12517-022-09813-W>
- Pierce MW, Thornton CI, Abt SR (2010) Predicting peak outflow from breached Embankment dams. *J Hydrol Eng* 15:338–349. [https://doi.org/10.1061/\(ASCE\)HE.1943-5584.0000197](https://doi.org/10.1061/(ASCE)HE.1943-5584.0000197)
- Purnama N, Jayadi R (2021) Dam break analysis using 1D geometry at Jatigede Dam, Sumedang. *IOP Conf Ser Earth Environ Sci* 930. <https://doi.org/10.1088/1755-1315/930/1/012088>
- Sahoo SN, Sreeja P (2017) Development of flood inundation maps and quantification of flood risk in an urban catchment of Brahmaputra River. *ASCE-ASME J Risk Uncertain Eng Syst Part A Civ Eng* 3:1–11. <https://doi.org/10.1061/ajrua6.0000822>
- Snorrason Á, Sidek LM, Bt F, Ros C (1984) Sensitivity of outflow peaks and flood stages to the selection of dam breach parameters and simulation models. *J Hydrol*
- Tamm O, Tamm T (2020) Verification of a robust method for sizing and siting the small hydropower run-of-river plant potential by using GIS. *Renew Energy* 155:153–159. <https://doi.org/10.1016/J.RENENE.2020.03.062>
- Trambadia NK, Patel DP, Patel VM, Gundalia MJ (2022) Comparison of two open-source digital elevation models for 1D hydrodynamic flow analysis: a case of Ozat River basin, Gujarat, India. *Model Earth Syst Environ* 2022:1–15. <https://doi.org/10.1007/S40808-022-01426-2>
- US Bureau of reclamation (1982) Guidelines for defining inundated areas downstream from Bureau of Reclamation dams. *Reclam Plan Instr*

- Wahl TL (1998) Prediction of embankment dam breach parameters: a literature review and needs assessment
- Wahl TL (2004) Uncertainty of predictions of Embankment dam Breach parameters. *J Hydraul Eng* 130:389–397. [https://doi.org/10.1061/\(ASCE\)0733-9429\(2004\)130:5\(389\)](https://doi.org/10.1061/(ASCE)0733-9429(2004)130:5(389))
- Walder J, O'Connor JE (1997) Methods for predicting peak discharge of floods caused by failure of natural and constructed earthen dams. *Water Resour Res* 33:2337–2348. <https://doi.org/10.1029/97WR01616>
- Wang B, Chen Y, Wu C, Dong J, Ma X, Song J (2016) A semi-analytical approach for predicting peak discharge of floods caused by embankment dam failures. *Hydrol Process* 30:3682–3691. <https://doi.org/10.1002/HYP.10896>
- Xu Y, Zhang LM (2009) Breaching parameters for earth and Rockfill dams. *J Geotech Geoenviron Eng ASCE* 135:1957. [https://doi.org/10.1061/\(asce\)gt.1943-5606.0000162](https://doi.org/10.1061/(asce)gt.1943-5606.0000162)

# Enhancing the Optimum Water Requirement for the Crop Using the Contemporary Capillary Wick Irrigation Method a Case of an Experimental Demonstration



Uttamkumar Vyas, Neelkanth Bhatt, Vinay Vakharia, and Dhruvesh Patel

**Abstract** Indian farming industry is a major industry globally, comprising a complex group of enterprises that consume a lot of water. India is a predominantly agricultural country. Many sectors are directly or indirectly associated with this agricultural sector, such as employment, food, and industrial raw material. Farming entirely depends on the availability of water. The maximum amount of freshwater is utilized in agriculture, mainly using groundwater. Water scarcity and depletion of groundwater in the recent years due to changes in annual rainfall and climate change in India will be a major challenge in the day to come. Micro-irrigation systems are currently being. Innovative indigenous micro-irrigation techniques like the proposed ‘capillary wick irrigation technique’ would eliminate the limitation of drip irrigation that requires not only electricity but also technical know-how on the part of the irrigator for its effective use. The present experimental study seeks to examine the applicability of the proposed innovative indigenous ‘capillary wick irrigation technique’ through a small underground water reservoir for row crops by comparing the same with the farmers’ traditional method (check basin method) of surface irrigation. The experimentation for row crop of fennel (saunf) (scientific name: *Foeniculum vulgare*), also known as ‘variali’ in vernacular language, was carried out with saline water and on an adverse land. Experimental investigations were conducted by designing and installing capillary wick assembly at an agricultural farm at ‘velavadar,’ district Surendranagar. The effect of wick spacing on the

---

U. Vyas (✉) · D. Patel

Department of Civil Engineering, School of Technology, PDEU, Gandhinagar, India  
e-mail: [uttam.vphd21@sot.pdpu.ac.in](mailto:uttam.vphd21@sot.pdpu.ac.in)

D. Patel

e-mail: [dhruvesh.patel@sot.pdpu.ac.in](mailto:dhruvesh.patel@sot.pdpu.ac.in)

N. Bhatt

Department of Civil Engineering, Lukhdhirji Engineering College, GTU, Morbi, India  
e-mail: [neelkanth78bhatt@gmail.com](mailto:neelkanth78bhatt@gmail.com)

V. Vakharia

Department of Mechanical Engineering, School of Technology, PDEU, Gandhinagar, India  
e-mail: [vinay.vakharia@sot.pdpu.ac.in](mailto:vinay.vakharia@sot.pdpu.ac.in)

© The Author(s), under exclusive license to Springer Nature Singapore Pte Ltd. 2024

D. Patel et al. (eds.), *Innovation in Smart and Sustainable Infrastructure*, Lecture Notes in Civil Engineering 364, [https://doi.org/10.1007/978-981-99-3557-4\\_2](https://doi.org/10.1007/978-981-99-3557-4_2)

crop yield was also studied by employing T1/1, T1/2, T1/3, T2/1, T2/2, T2/3, T3, and T4 types of arrangements. Crop characteristics like height, stem diameter, and yield were studied under various arrangements. Experiments were also conducted to study the wetting front movement under the proposed capillary wick irrigation assembly. Compared to drip irrigation, the additional water saving by the proposed irrigation method was 17.40%. Compared to the regular farmer's irrigation method, the water saving by the proposed irrigation method was around 85%. The results demonstrate the successful applicability of the proposed irrigation method even under adverse agricultural regimes.

**Keywords** Micro-irrigation · *Foeniculum vulgare* · Agriculture · Optimum water requirement

## 1 Introduction

More than 80% of the population in India is generally small landowners with less than 1 hectare of land. These small landholders are vulnerable to poverty and hunger because they neither get enough food production nor do they have domestic food security. There is income to ensure. In an era of greeter irrigation of the global market, if they have advanced technologies and support from the government, they play an important role in increasing food production, generating employment, and additional income (Malik et al. 2020). The agriculture of our country largely depends on the impermanence of nature. More than 60% of farming in India depends on rainfall (Bahinipati and Viswanathan 2019). It becomes very difficult for the agricultural sector to thrive during drought. The promotion is often cited as a strategy to promote poverty reduction, climate adaptation, and food security to save water in irrigation techniques. Therefore, sustainable agricultural development in arid and semi-arid regions, where farmers face farming challenges, holds the key to the future. In general terms of farming, farmers adopt the traditional method of irrigation. It is also known as the surface irrigation method. As per the crop types, first, farmers prepare the land for irrigation and select the irrigation method, i.e., for cotton crops in Gujarat, farmers' crops adapt the furrow irrigation method. The selected method also depends on the availability of water, and the farmer also considers crop water requirements in the traditional irrigation method (Singh 2008). In traditional irrigation methods, the water requirement is very high, and other essential requirements are less like skilled labor is not required, and maintenance and other costs are negligible. In this method, crop yield is not satisfactory compared to the advanced irrigation method like micro-irrigation. Micro-irrigation is planned across the world to achieve water saving in agriculture. Drip irrigation as part of micro-irrigation is expensive to install, and the maintenance cost of assembly is relatively high compared to the other traditional method (Liu et al. 2021; Vyas et al. 2022). Research evidence suggests that presently used micro-irrigation technology due to socio-economic and many other factors, difficult to adopt and maintain assembly setup in study traditional method



and poor quality of water and lower price of the agro product in the market due to certain problems difficult to adopt the drip irrigation in the agriculture sector (Kulecho and Weatherhead 2005). Farmers' voluntary adoption of a sustainable irrigation system requires a need to properly support the resource more broadly through non-voluntary includes such as regulatory incentives (Boland et al. 2005). The use of micro-irrigation systems increases the marginal productivity of water (Malik et al. 2020). The current prevent technology like drip irrigation is more suited for the large area. This system is very sophisticated and expensive and especially impractical for farmers who already make every effort to survive due to very small land and low yield (Malik et al. 2020). As a result, low-cost systems that are technically less complex or simpler should be adopted to suit small and medium farmers and present the largest number of farmers in India (Singh et al. 2008). The drip system helped farmers; instead of improving its access hinders technology. To achieve higher water use efficiency in agriculture, farmers should be encouraged to take affordable indigenous irrigation methods to the drip and sprinkler irrigation system (Semananda et al. 2018). The proposed capillary wick irrigation method in this research study is one such technique.

The soil fertility index for agriculture is low in the Surendranagar district of Gujarat state as per the District Krishi Scheme document. The average annual rainfall in Surendranagar district is only 450 mm. Apart from this, 82.8% of the land in the district is uncultivated. Keeping these facts in research required a local and indigenous capillary wick irrigation system to be developed. It later proposed a capillary wick for growing edema crops on the proposed irrigation system on an agricultural farm in Gujarat's village Velavadar Surendranagar district. Experimental testing has been done for the applicability of irrigation techniques. During the experiment, no fertilizer was used to grow the crop. The proposed irrigation technique was compared with the border strip irrigation method.

## 2 Methodology

The details of the procedure that was followed for the fieldwork are presented here:

The land was prepared by breaking big lumps into small pieces with tractors and spades. The land for the experimental plot was protected by steel wires/railing so that stray dogs and other animals could not enter the experimental plot. The alignment of pipes on the ground was then marked for installation as per the field plan shown in Fig. 1. Representative soil sample from three places was taken for field moisture measurement, soil classification, and nutrients test. Excavation for installation of pipes the earth was excavated with a J.C.B machine (backhoe) and trenches of 45 cm \* 45 cm and 6 m long. 8 numbers of trenches were excavated. Plastic pipe with wicks was installed as per the field plan. Required materials on the experimental plot from the on-farm storage place were then brought to install the same. To keep the wicks straight into the soil. It is with 1 m long pipe head and 10 cm above the ground. The earth was then filled and leveled. Pipes were filled with water.

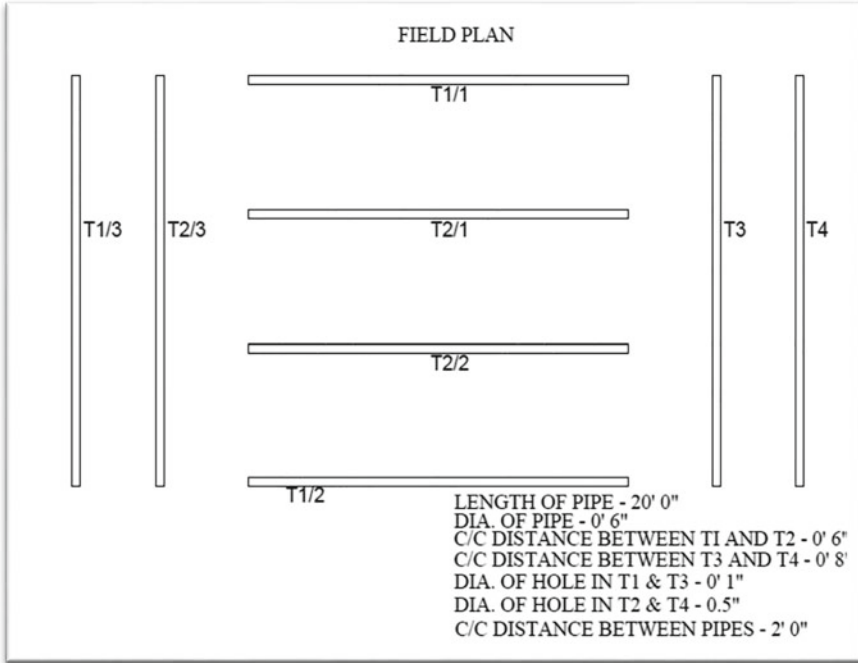


Fig. 1 Field plan of sub surface reservoir with wick

Apply water in pipes and near the wick seeds of the funnel (variyaali) planted. Water sample(s) was collected for the ‘irrigation water quality test.’ The water sample was sent to the laboratory for further testing. The actual field setup on the experimental plot is shown in Fig. 2.

### 3 Experimental Section

#### 3.1 Study Area

Surendranagar district has a geographical area of about 10,489 sq. Km and falls in the survey of I degree sheets 41N and 41 M, between North latitudes 22° 8' and 23° 3' and East longitudes 70° 58' and 72° 12'. The district has 651 villages and 11 towns (populations greater than 100,000) spread over 10 talukas, namely Wadhwan, Limbdi, Dasada, Dhranghadhra, Chotila, Chula, Muli, Sayla, and Lakhtar. This district is one of the largest producers of hybrid cotton globally. The pilot farm was about 23 km by road from Surendranagar in Gujarat shown in Fig. 3.

The soils of Surendranagar district may be classified into three main categories: Medium black soils, red sandy soils, and silty soils in the south, southwest, and

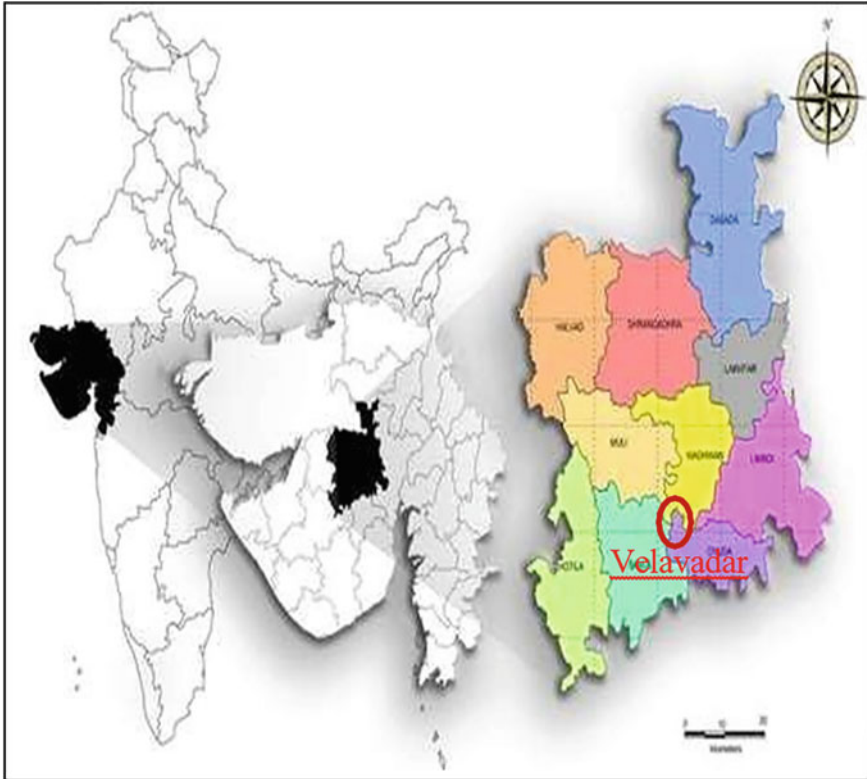


**Fig. 2** Field plan setup in farm

central parts of the area. Medium black soils are found at shallow depths (less than 5 m), where basalts/shale from the major rock block are exposed on the surface. These soils are fertile. However, they aren't suited to extensive irrigation. The red sandy soils can be found in the northeast, east, and southeast. The silty soils can be found in a narrow strip near the tiny Rann of Kachchh in the northeast and shallow alluvial tracts and hard rock sections in the central uplands. The crops are grown in the district mainly cotton 59%, cereals 12%, sesamum 11%, bajra 8%, and wheat 4%.

The district's rivers are mostly ephemeral. Many minor reservoirs and tanks are built to suit the area's irrigation and domestic needs. However, the majority of them dry up in the summer. Ghanshamgad, Satapar, Kankvati, Ramgadh, and Vaodi are the five small irrigation schemes in the district. The total water storage capacity of all minor irrigation schemes is 9.168 MCM. When these projects are combined, the total cultivable command is 2280 acres. The water distribution in these schemes is accomplished using a network of canals. Wadhwan-Bhogava-I, Wadhwan-Bhogava-II, Brahmini, and Limbdi-Bhogava are the four medium irrigation schemes in the area. The combined water storage capacity of all medium irrigation schemes is 139.05 MCM. The total amount of land that can be planted.

The months of March to May saw a progressive rise in temperature, with May being the hottest. In the summer, the highest temperature reaches 46 °C, with an average temperature of 41.9 °C. The beginning of the southwest monsoon, which occurs around June, significantly reduces day temperatures. Day and night temperatures decrease dramatically (up to 5 °C) from the beginning of November to January, which is the coldest month of the year. For the time of observation, the mean daily maximum and minimum temperatures were 28.3 °C and 12.9 °C, respectively. The



**Fig. 3** Experimental farm located in Velavadar village of Surendranagar district

relative humidity in the southwest monsoon is typically over 60%. The rest of the year, especially in the afternoons, the air is quite dry.

The relative humidity ranges between 20 and 30% from November to May. During the southwest monsoon season, the wind direction is westerly to southwesterly.

The wind blows from the north-northeast during the post-monsoon/cold season. During the summer, the wind blows primarily from the northwest to the southwest. The wind speed gradually increases from February to July, when the southwest monsoon is most active, reaching a peak of 20.3 km/h. From August onwards, the speed drops to 6.7 km/h. For this study, the Water Resources Investigation Circle, Department of Irrigation, Gujarat, used rainfall data from Surendranagar, Chotila, Dasada, Dharangadhra, Halvad, and Sayla, Lakhtar, Limbdi, and Muli, Raingage stations. During the monsoon, more than 90% of the rainfall occurs. The amount of rain that falls during the winter and summer months is insignificant. The district's normal annual rainfall is 587.35 mm, although just 298 mm fell in 2012, accounting for less than 49% of the average annual rainfall.

**Table 1** Details of capillary wick assembly setup

Nos. of pipes	Dia. of hole (cm)	C/C distance (cm)	No. of hole
3	1	30	19
3	2	30	19
1	1	38	15
1	2	38	15

### 3.2 Experimental Setup

The setup was prepared from polyester wicks of 10 mm and 20 mm diameter at fixed spacing on a 6 m long P.V.C. pipe. A trench 45 cm wide, 45 cm deep, and 8.2 m long was excavated to install the pipe in the field. The water storage capacity of the pipes was 107.750 L when each pipe used was filled. Initially, capillary growth was studied in a glass box with a wick made of a thread of 1 and 2 cm diameter of cotton, cotton, and polyester. The best capillary growth has been found through the polyester wick, and for this reason, only it was used. T1/1, T1/2 T1/3T2/1T2/2, T2/3 T3, and T4 type arrangements were employed on eight P.V.C. pipes to study the effect of spacing between wicks on crop yield. Under these different systems, plant height, stem diameter, and crop yield were also studied. Experiments were also conducted to study the wetting of farmland under the proposed capillary wick irrigation system. Table 1 assembly arrangement is given and shown Fig. 4 is wick and pipe setup on the field.

Representative soil samples from three locations were also taken for field moisture measurement, soil classification, and nutrient basin testing.

### 3.3 Data Collection and Observation

The surface method of watering the plants to the farmers and the water supplied to the plants from each pipe was recorded. The water requirement of the crops was calculated, and for the present experiment, the required amount of water for both irrigation methods was applied to the crops. In surface irrigation, water was given at 4–5 days, whereas the pipes were filled only at 10 days as the crops had enough moisture in the soil. 1 \* 1 \* 1-m acrylic glass box was installed to observe the moisture moment in black cotton soil under capillary wick irrigation. A 1-m pipe was installed, the actual arrangement of which is the same as the pipe installed on the field. And this pipe was filled with water. The increase of soil moisture over time was monitored, and the soil moisture percentage was recorded using the gravimetric method. In addition, the growth of plants was also monitored regularly. To study the benefit–cost ratio from the respective irrigation method, the cost of both the method and the profit derived from the yield was also recorded in monetary terms.





**Fig. 4** Wick installation in the pipe on field

### ***3.4 Water Application for Crop***

One of the most significant inputs required for crop production is water. Plants require it continuously and in large quantities throughout their lives. It significantly impacts photosynthesis, respiration, absorption, translocation, mineral nutrients, and cell division (Felipe and Bareng 2022). This experiment compares cumulative water applied in the traditional farmer method and capillary wick irrigation method. The actual water requirement for crops is calculated as per the equation below. During the whole crop period, watering has been done twenty times in the traditional farmer method or check basin method on the field. The source of water is used groundwater for irrigation. Crop water requirement increases with the growing stage of the crop.

Water requirement of fennel crop,

$$W_r = E_{pan} * C_f * S * C_w \quad (1)$$

where

$W_r$  Daily irrigation water requirement

Epan Open Pan Evaporation

Cf Crop Factor

S Spacing of plant

Cw Canopy factor

Cf = 0.85 (the initial stage of fennel growth)

= 1.0 (mid-stage of fennel growth)

= 0.9 (final stage of fennel growth)

$$Cw = \frac{\text{wetted area}}{\text{plant area}} = \frac{0.30}{0.60} = 0.5 \tag{2}$$

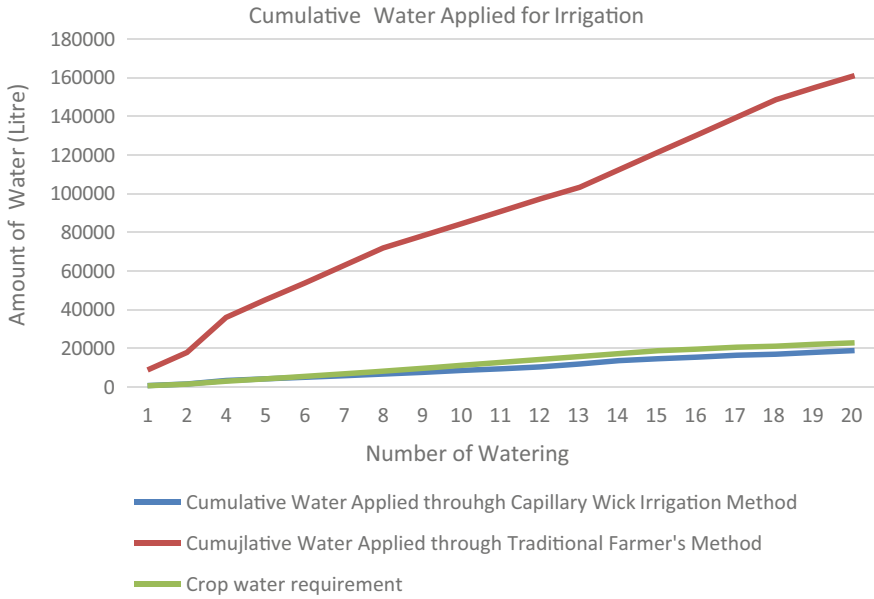
S = 0.3 m<sup>2</sup> (spacing of plant) Epan = 5.34  $\frac{\text{mm}}{\text{day}}$  (Surendra nagar district).

The amount of water supplied to the crop within the traditional farming method is significantly more than the crop needs. In contrast, under micro-irrigation systems like capillary week irrigation, the crop needs to be irrigated as much as required in Fig. 5 amount of cumulative water applied in different irrigation methods is shown. In this experiment, the water supplied in both methods for the whole crop period was calculated cumulatively. It can be seen from the figure that in the traditional method of farming, the expenditure of water is found in abundance. Within the capillary wick irrigation system, there is more to water than just the crop needs in the first two waterings. More water is needed to reach the surface from the water reservoir 1.5 feet below by capillary action. Any crop shows maximum adaptation to fluctuations in water only required for its survival. Crop growth from the conventional and capillary wick irrigation methods is also evaluated over time. The increase in the height of the crop and the increase in the thickness of its stem have also been observed. It can be seen from Table 2 that the increase in the diameter of the stem of the plant is almost the same as in the conventional method and capillary wick irrigation method. Changes in the diameter of the wick used in the capillary wick irrigation method and changes in the diameter growth of the plant stem from a distance between the center and the center for two wicks are also noted.

The increase in plant height is also noted with time. The growth of plants in the traditional method of farmer and capillary wick irrigation methods can be seen from the slightest change. We can see from Table 3.

The growth of plants in T1 and T2 pipes is less than plants in T3 and T4 pipes. But the growth of plants in T3 and T4 pipes is similar to the traditional farming method. The increase in plant growth is observed during the entire crop period, and the growth of the plant depends entirely on the amount of water supplied to the plant or the method followed. At the same time, different factors like temperature, wind velocity, and humidity are considered in the field to be experimented with, which directly changes the growth of plants.

In the traditional method of the farmer, fertilizer and pesticides are used as per the requirement. Still, the crop is groomed in a completely organic manner in the capillary wick irrigation method. The Vernier scale was used to measure the diameter of the stem, and the height of the plant was measured by measuring tape.



**Fig. 5** Comparative graph representing the water applied to the crop by different irrigation methods

**Table 2** Increase of stem diameter with crop growth

Capillary wick irrigation										Regular farmers method
Increase the diameter of stem (mm) avg										
Sr. No	Crop period	T1/1	T1/2	T1/3	T2/1	T2/2	T2/3	T3	T4	Regular farmers method
1	After 12 days	9.35	9.35	9.35	10.05	10.05	10.05	10.05	10.05	7.45
2	After 28 days	26.29	26.29	26.29	29.43	29.43	29.43	29.43	29.43	22.63
3	After 46 days	43.18	43.18	43.18	48.09	48.09	48.09	48.09	48.09	38.18
4	After 59 days	54.09	54.09	54.09	60.53	60.53	60.53	48.09	48.09	51.07
5	After 74 days	65.04	65.04	65.04	69.6	69.6	69.6	72.73	72.73	60.53
6	After 100 days	74.84	74.84	74.84	78.15	78.15	78.15	80.69	80.69	82.08
7	After 125 days	76.15	76.15	76.15	81.05	81.05	81.05	84.94	84.94	94.62
8	Crop Spacing (cm)	30	30	30	30	30	30	37.5	37.5	30
9	Wick Dia. (cm)	1	1	1	2	2	2	1	2	



**Table 3** Increase of height of crop with crop growth

Capillary wick irrigation										Regular farmers method
Height of crop (cm)										
Sr. No	Crop period	T1/1	T1/2	T1/3	T2/1	T2/2	T2/3	T3	T4	Regular farmer method
1	After 12 days	6	6	6	8	8	8	8	8	10
2	After 28 days	20	20	20	25	25	25	25	25	30
3	After 46 days	40	40	40	45	45	45	45	45	50
4	After 59 days	50	50	50	60	60	60	60	60	70
5	After 74 days	60	60	60	80	80	80	85	85	100
6	After 100 days	120	120	120	140	140	140	150	150	165
7	After 125 days	145	145	145	155	155	155	170	170	180

## 4 Results and Discussions

The main goal of the experiment is to use this micro-irrigation method to increase production while conserving water using the capillary wick irrigation system. Capillary wick irrigation method saves water as compared to farmer's traditional method. Capillary wick irrigation technique gave high water use efficiency as compared to conventional irrigation method. This experiment was performed for a row crop with crops having a maximum depth of 1.5 feet in the root zone. The fennel crop was selected in an experiment, in which fennel seeds of the hybrid Mangalam Volleyna brand were used. The crop period is from 120 to 130 days. It is widely cultivated in the Surendranagar district.

Capillary action works on the principle of the passage of a liquid through or along with another substance against an opposing force, such as gravity, which is known as capillary action. Cohesion, or attraction between particles of the same substance, and adhesion, or attraction between particles of different substances, are important in capillary action. In addition to the experiment, the benefit–cost ratio is also calculated. An economic analysis of the system is also done in the traditional farmer and capillary wick irrigation methods 0.75 and 2.78%, respectively. The water supplied to the capillary wick irrigation system plants is self-regulated. More water is just looking for water to reach the surface by the capillary. In the capillary wick irrigation system, the diameter of the wick and the center-to-center distance between



**Fig. 6** Experimental farm after growing crop

two wick also play an important role. It can be seen from the observation that plant growth is good in T3 and T4 pipes, while T1 and T2 pipes are also more suitable for crops with less water requirement like cotton, Castor, etc. Experimental plot with plant shown in Fig. 6.

## 5 Conclusion

Capillary wick irrigation has revealed that the method can be successfully employed to achieve water savings and improve agriculture yields. The method can help small and marginal landholder farmers facing water problems facing water shortages to raise crops for their livelihood. The proposed method can contribute to poverty alleviation among the small farmers and serve as an effective tool for affordable small-scale irrigated agriculture. Capillary wick irrigation technique has no environmental impact, is cost-effective, and most importantly, is either not using electricity for its operation or is subjected to a managerial gaffe by the farmers as in the case of other micro-irrigation techniques. Capillary wick irrigation as an alternative to drip or sprinkler irrigation can be a viable option for water scare areas, particularly for farmers looking to eke a living out of their smallholding land. The water saving is around 85% with the capillary wick irrigation technique compared to the traditional

farmer method. The crop yield in the T4 pipe is higher than in other pipes, so crop spacing and diameter of the Wick play an important role in crop growth. Using the capillary wick irrigation technique requires less manual labor for fitting the pipe and wick at the subsurface level after assembly in the field is completed. In this method, evaporation loss is less, and runoff does not happen, reducing soil erosion because water directly applies to the crop's root zone as per the soil–plant relationship. After all, this technique is autoregulated system. This technology can be used to various types of crops, soils, and environments by leading a new assembly and conducting additional research in the future.

**Acknowledgements** The corresponding authors are sincerely thankful to Mr. Hasubhai Vyas, Mr. Hareshbhai Dodiya, and Mr. Dalsukh Dabhi for supporting the field experiment and executing the research and analysis work.

## References

- Bahinipati CS, Viswanathan PK (2019) Can micro-irrigation technologies resolve India's ground-water crisis? Reflections from dark-regions in Gujarat. *Int J Commons* 13(2):848–858
- Boland AM, Bewsell D, Kaine G (2005) Adoption of sustainable irrigation management practices by stone and pome fruit growers in the Goulburn/Murray Valleys, Australia. *Irrig Sci* 24(2):137–145
- Felipe AJB, Bareng JLR (2022) Growth and yield assessment of lettuce (*Lactuca Sativa* L.): an economic feasibility and performance evaluation of capillary wick irrigation system. *Plant Sci Today* 9(1):62–69
- Kulecho IK, Weatherhead EK (2005) Reasons for smallholder farmers discontinuing with low-cost micro-irrigation: a case study from Kenya. *Irrig Drain Syst* 19(2):179–188
- Liu H, Yuan B, Hu X, Yin C (2021) Drip irrigation enhances water use efficiency without losses in cucumber yield and economic benefits in greenhouses in North China. *Irrig Sci* 40(2):135–149
- Malik RPS, Giordano M, Rathore MS (2020) The negative impact of subsidies on the adoption of drip irrigation in India: evidence from Madhya Pradesh. *Polit Policies Water Resour Manag India* 66–77
- Semananda NPK, Ward JD, Myers BR (2018) A semi-systematic review of capillary irrigation: the benefits, limitations, and opportunities. *Horticulturae* 4(3):23
- Singh AK et al (2008) Small holders' irrigation—problems and options. *Water Resour Manage* 23(2):289–302
- Singh K (2008) Rational pricing of water as an instrument of improving water use efficiency in the agricultural sector: a case study in Gujarat, India. *Int J Water Resour Dev* 23(4):679–690
- Vyas U et al (2022) Matrix irrigation unit

# A Comparative Assessment of Unsupervised and Supervised Methodologies for LANDSAT 8 Satellite Image Classification



Kratika Sharma, Ritu Tiwari, Shobhit Chaturvedi, and A. K. Wadhvani

**Abstract** Developing accurate land cover maps is a fundamental prerequisite for natural resource management, environmental modelling and urban planning studies. Several unsupervised and supervised algorithms are available in the literature for classifying LANDSAT satellite images, and selecting an optimum approach is of critical interest. This paper compares two unsupervised (ISODATA; K Means), and three supervised (Spectral Angle Mapping (SAM), Minimum Distance (MD) and Maximum Likelihood) algorithms for classifying a mid-resolution ( $30 \times 30$ ) m LANDSAT 8 satellite image to develop Land Cover (LC) maps for Nashik city in western India region. Post classification stage, sieve filtering and manual corrections are applied for image enhancements. The Kappa accuracy metric is adopted for comparing the accuracy of LC maps against 100 reference ground points using the Google Earth Engine. The Maximum Likelihood algorithm delivered the highest classification accuracy (73.8%), followed by SAM (70.7%), MD (68.1), K means (41.5%) and ISODATA (31.2%) algorithms. Further, accuracy enhancements are attained by the classification sieve filter (83.2%) and by applying manual corrections (89.7%).

**Keywords** LANDSAT 8 · Unsupervised classification · Supervised classification · Nashik · Producer accuracy

---

K. Sharma (✉)  
IIIT Pune, Pune, India  
e-mail: [kratikasharma@iiitp.ac.in](mailto:kratikasharma@iiitp.ac.in)

R. Tiwari  
PDEU, Gandhinagar, India  
e-mail: [ritu@iiitp.ac.in](mailto:ritu@iiitp.ac.in)

S. Chaturvedi · A. K. Wadhvani  
MITS Gwalior, Gwalior, India  
e-mail: [shobhitchaturvedi101@gmail.com](mailto:shobhitchaturvedi101@gmail.com)

A. K. Wadhvani  
e-mail: [akwadhvani@mitsgwalior.in](mailto:akwadhvani@mitsgwalior.in)

# 1 Introduction

There is an ever-increasing demand for accurate, error-free Land Cover (LC) maps to monitor terrestrial ecosystems (Kavitha et al. 2021). LC maps help assess the impacts of natural and anthropogenic changes on the regional environment, such as global warming, rapid urbanization and urban heat islands (Aburas et al. 2019). However, physically developing LC maps is expensive, time-consuming and error-prone. Instead, high spatial, temporal, radiometric and spectral resolution remote sensing images provide a reliable pathway for rapidly mapping large land masses (Chaturvedi et al. 2023). Most LC maps are developed using the LANDSAT mid-resolution ( $30 \times 30$ ) m data sets. The United States Geological Survey (USGS) and National Aeronautics and Space Administration (NASA) operate LANDSAT, the longest running remote sensing programme for acquiring earth satellite images (Seitzinger et al. 2015). The initial LANDSAT 1 mission was launched on 23 July 1972, whereas the latest LANDSAT 9 satellite was launched on 27 September 2021, continuing the LANDSAT programme's central role in monitoring, understanding and managing the terrestrial resources needed to support human life.

Several image classification techniques are used to develop LC maps from multi-spectral satellite images to extract vital real-world information. Broadly, unsupervised and supervised image classification methods are applied to develop LC maps. Unsupervised classifiers like Iterative Self-Organizing Data Analysis (ISODATA), K means clustering and Fuzzy c means automatically classify satellite imagery into a fixed user-defined number of groups based on similar spectral characteristics (Tarawally et al. 2019). In comparison, supervised classification algorithms like Spectral Angle Mapping, Minimum Distance, Maximum Likelihood, Random Forests, Support Vector Machines and Neural Networks are adopted for extending or extrapolating available LC information from known image segments to classify unknown image segments. Supervised classification begins with users developing a training set containing several segments for each LC class (Macarrigue et al. 2022). Next, spectral signatures are derived for each LC class based on the user-supplied training set. Finally, the entire satellite image is classified by assigning each pixel to the closest matching LC class. Numerous researchers adopted unsupervised and supervised classifications to perform spatiotemporal assessments and predict regional urban growth (Wang et al. 2022).

Generally, unsupervised classifiers are adopted without any ground information, but manual edits are usually needed post-classification stage to eliminate misclassified pixels or merge similar LC classes. In comparison, supervised classification accuracy mainly relies on the quality of the training input supplied. However, generalized conclusions regarding the relative efficiency of various classifiers are still inadequate (Talukdar et al. 2020). In response, this paper presents a comparative assessment of two unsupervised (ISODATA and K means) and three supervised classification algorithms [Spectral Angle Mapping (SAM), Minimum Distance (MD) and Maximum Likelihood (ML)] algorithms for classifying a mid-resolution ( $30 \times 30$ ) m LANDSAT 8 satellite image to develop Land Cover maps for Nashik city in the

western India region. Post classification stage, sieve filters and manual corrections are also applied to estimate the producer accuracy for the developed LC maps.

## 2 Research Methodology

A four-step research methodology has been developed for this study (Fig. 1):

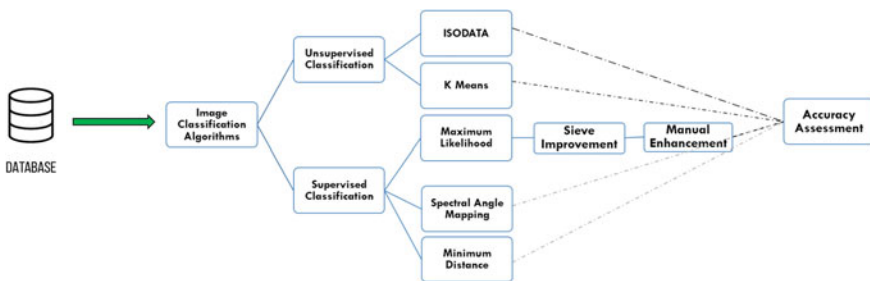
### Step 1 LANDSAT 8 Database Retrieval and Pre-processing

The LANDSAT 8 Operational Land Imager and Thermal Infrared Sensor satellite data for the Nashik, India region for 5 May 2022 is downloaded from the USGS Earth Explorer database. Situated on the banks of river Godavari, Nashik, is the third largest city in Maharashtra, after Mumbai and Pune. This location is chosen for analysis due to its regional importance, as no past study focused on employing RS data sets for developing LC maps for this region. The downloaded image is geo-referenced to the Universal Transverse Mercator (UTM) projection system with World Geodetic System (WGS) 1984 as the datum. Further, the area of interest is clipped using QGIS open-source software, and the Nashik region is shown in Fig. 2.

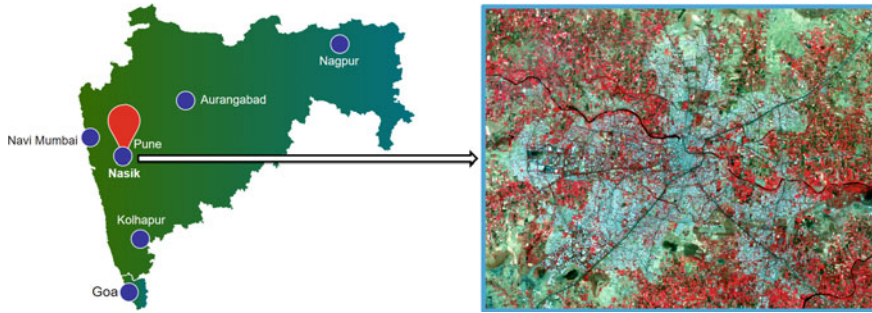
### Step 2 Unsupervised and Supervised Image Classification

In the second step, the Semi-Automatic Classification Plugin (SCP) in QGIS software is adopted for pre-processing, classification and post-processing of Nashik’s LANDSAT images. The theoretical foundations of the different classification algorithms are presented in the Table 1.

The semi-classification plugin within the QGIS software framework is adopted to implement the unsupervised and supervised classification algorithms. The selected Nashik region is categorized under four primary land cover classes: vegetation, water body, built-up area and others. The different terrestrial features under each Land Cover class are given in Table 2. The unsupervised classifiers are executed by affixing four Land cover clusters, whereas supervised classifiers are run by manually providing training sets containing spectral signatures for each Land Cover class.



**Fig. 1** Research methodology adopted to perform unsupervised and supervised LANDSAT 8 image classification



**Fig. 2** Political map and satellite false colour composite images for the Nashik region, India

### Step 3 Application of Image Post-processing Tools

In the third step, post the development of classified LC maps, the Classification Sieve tool is applied to replace isolated pixel values with the largest neighbouring patch value. This tool removes raster polygons smaller than a pre-defined threshold and replaces them with the pixel values of the largest adjacent polygon. Finally, manual edits are applied to the resulting images to produce a final LC map closely resembling the actual satellite image of the region.

### Step 4 Accuracy Assessment

The final stage involves overall and class-wise accuracy assessment of the different LC maps using the Kappa statistic (Arulbalaji 2019). One hundred actual ground points (25 points per LC class) are generated to compare the actual and predicted LC class labels. The accuracy metrics are reported in Table 3. Finally, the most accurate classification approach is identified.

## 3 Results

The LC maps for the Nashik region developed using different unsupervised and supervised classifiers are presented in Figs. 3, 4, 5 and 6. Notably, the waterbody LC class is blue; the built-up LC class is red; the vegetation LC class is green and bare lands are yellow. Further, the classification accuracies for various classifiers are reported in Table 3.

The results of the ISODATA and K means classification algorithms are shown in Fig. 3. The ISODATA algorithm achieves 31.9% overall classification accuracy compared to 41.5% by the K means clustering algorithm. Further, compared with the region's satellite image (refer to Fig. 2), it is seen that the K means algorithm fared better at classifying built-up and vegetated areas than ISODATA, whereas both algorithms significantly over-predict area under waterbodies and bare land LC class.

**Table 1** Theoretical foundations of the different supervised and unsupervised classifiers considered in this study

Unsupervised classification algorithms		References
Name	Theoretical description	
K means	This method is derived from vector quantization which partitions $n$ observations into $k$ clusters, where each observation belongs to the cluster with the nearest cluster mean. This approach doesn't guarantee convergence to the global optimum, and results depend on the initial clusters. Thus, it may be necessary to run this algorithm multiple times with different starting conditions to obtain optimum results	Macarringue et al. (2022), Talukdar et al. (2020), Wang et al. (2022)
ISODATA	Beginning with specified arbitrary cluster centres, this algorithm iteratively converges these centres to the means of the cluster data. This method uses minimum spectral distance to assign the most suitable cluster to each candidate pixel. ISODATA algorithm overcomes K means clustering limitations by merging clusters if their separation distance is smaller than the user-specified value and the rules of splitting a single cluster into two clusters	
<i>Supervised classification algorithms</i>		
Spectral angle mapping	Spectral Angle Mapping (SAM) is a physical spectral classification technique relying on the $n$ -D angle to match pixels to any reference spectra. SAM determines the spectral similarity between two spectra by computing the inter-spectral angle vector in a multi-dimensional space corresponding to the number of multispectral bands	
Minimum distance	The Minimum Distance algorithm classifies image segments into classes that minimize the distance between image data and LC class signatures in a multi-feature space. The computed Minimum Distance is considered analogous to the maximum similarity	
Maximum likelihood	ML classifier assumes that the statistics for each class in each band are normally distributed and estimates the probability of a given pixel belonging to a particular class. Each pixel gets assigned to the class having the highest probability. However, if the highest class association probability is smaller than a threshold, the pixel remains unclassified	

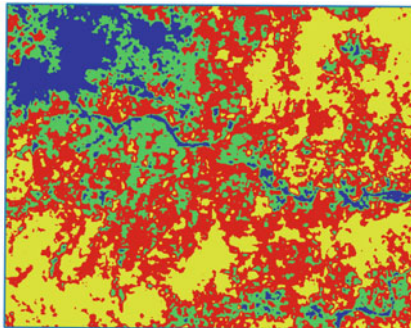


**Table 2** Different terrestrial features considered in different land cover classes

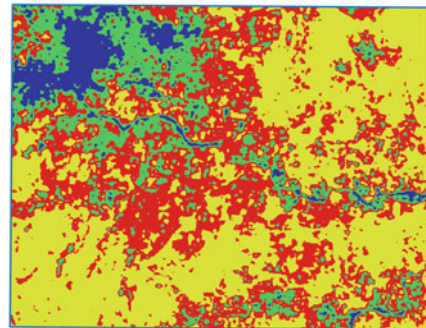
Land cover class	Description
Waterbody	Water bodies, including rivers, lakes, canals and wetlands
Vegetation	Green cover including trees, forests, gardens, cropped agricultural farmlands
Built-up	Physical infrastructure inclusive of roads, bridges, residential, commercial, industrial and institutional buildings
Bare land	Open areas, including uncropped agricultural lands, bare plots, landfill areas and all other remaining land cover types

**Table 3** Classification accuracies (in %) for the different LC classification approaches adopted for developing LC maps for the Nashik region

Methodology	Algorithms	Built-up	Water body	Vegetation	Bare land	Total
Unsupervised classifier	ISO DATA	24.6	61.8	46.9	18.8	31.9
	K means	36.4	69.5	56.8	33.4	41.5
Supervised classifier	Minimum distance	62.2	82.1	60.3	68.3	68.1
	Spectral angle mapping	33.4	97.3	92.5	88.6	70.7
	Maximum likelihood	86.1	100	53.9	77.4	73.8
	ML classification sieve (6 × 8)	86.7	100	88.3	77.1	83.2
	Manually corrected ML-LC image	96	95	95.1	73.1	89.7

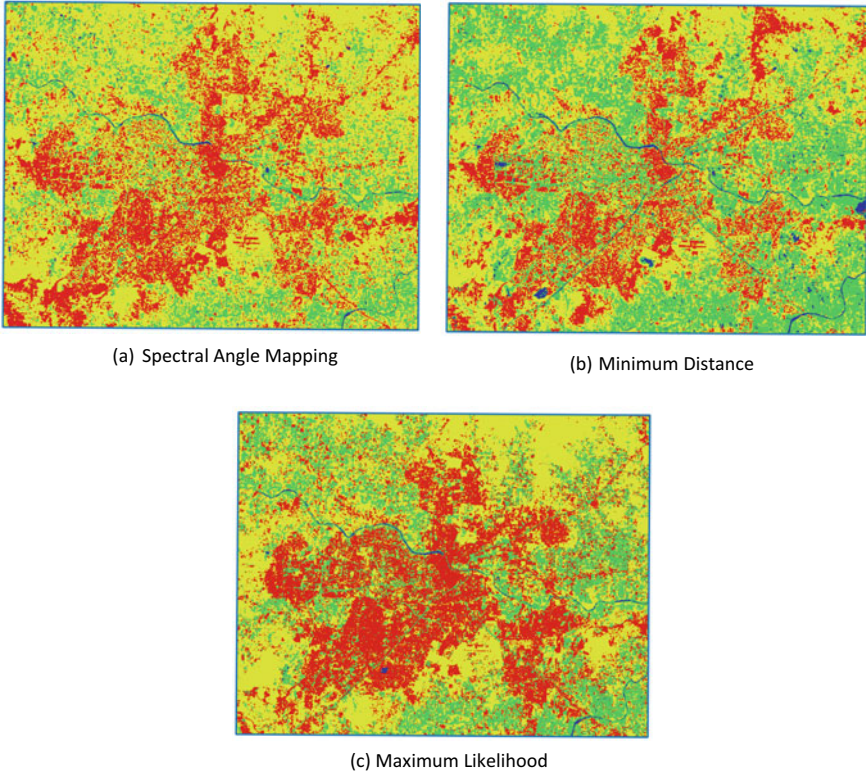


(a) ISODATA Algorithm

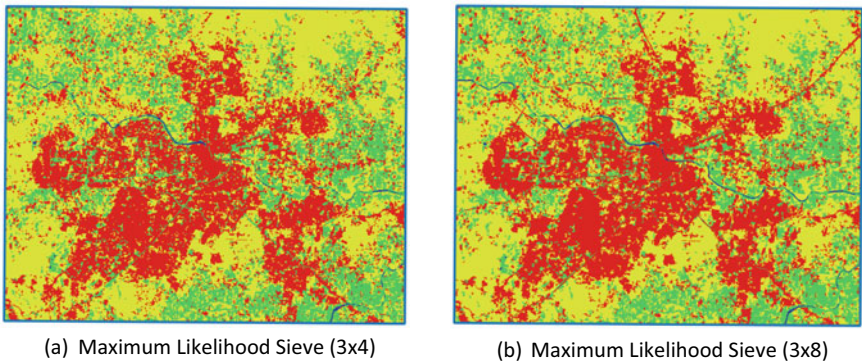


(b) K means Clustering Algorithm

**Fig. 3** Nashik region land cover maps developed using **a** ISODATA, **b** K means clustering unsupervised classifiers



**Fig. 4** Nashik region land cover maps developed using **a** Spectral angle mapping, **b** Minimum distance and **c** Maximum likelihood supervised classifiers



**Fig. 5** Classification sieve filters applied over maximum likelihood land cover maps using **a**  $3 \times 4$  and **b**  $3 \times 8$  pixel threshold and connection values

**Fig. 6** Manual edits applied over the (3 × 8) sieved maximum classified LC map to develop the final LC map for the Nashik region



Inspecting the supervised LC maps in Fig. 4 and Table 3, it is seen that the Maximum Likelihood classifier delivers the highest overall accuracy of 73.8%, followed by 70.7% by Spectral Angle Mapping and 69.24% by the Minimum Distance Algorithm. All three algorithms display similar results for classifying the waterbody LC class, but MD misclassified a road segment as a water body. In comparison, MD produced the maximum vegetation area, whereas ML produced the maximum bare land area. Noteworthy, all three algorithms show a similar expanse of the built-up LC class; however, ML produced built-up area closely resembles the actual built-up extent from Fig. 2. Thus, ML algorithm is identified as a superior supervised classification technique.

However, the ML-classified LC map also suffers from some issues. The ML-LC map contains many isolated raster polygons that do not resemble their large neighbouring LC class, yielding several misleading conclusions like built-up structures in the middle of water bodies, large vegetation and bare lands in dense urban areas. Thus, the ‘Classification Sieve’ image-post-processing tool is applied to remove and replace isolated raster polygons with the pixel values of the largest neighbouring polygon. The result is then saved to generate a new LC map.

Several improvements are visible after applying the classification sieve using different values for its two tuning parameters: pixel threshold and pixel connection. Post-sieving, the overall classification accuracy reached 83.2% and upon visual inspections, each LC class showed a denser texture with fewer mismatched pixels corresponding to other LC classes. Notably, the maximum possible accuracy achievable using image classifiers and post-processing filters hits a ceiling beyond which no further accuracy improvements are possible.

However, the utility of LC maps for various applications is principally governed by their accuracy. Thus, manual edits are performed to improve accuracy and further the resemblance of the final classified image with the actual LANDSAT image for the region.

The final classification accuracy attained after manually classifying the sieved ML-LC map is 89.7%. Notably, a 15.9% accuracy improvement is achieved over the ML-LC map by applying the classification sieve filter and manual edits.

## 4 Conclusion

This study presented a comparative assessment of two unsupervised and three supervised classifiers for developing the LC maps for the Nashik region using the 5 May 2022 LANDSAT 8 satellite data set. All three supervised classifiers outperformed unsupervised techniques, namely ISODATA and K means algorithms which produce 31.9% and 41.5% accuracy. Further, among supervised classifiers, the Maximum Likelihood (ML) algorithm outperformed the Spectral Angle Mapping and Minimum Distance algorithms producing accuracies of 73.8%, 70.7% and 68.1%, respectively. Finally, post-processing and manually correcting the classified ML image improved the classification accuracy by 9.4% and 15.9%, respectively. It is concluded that the ML algorithm outperformed other supervised classifiers, which further outperformed unsupervised algorithms. Thus, ML algorithm should be preferred for the supervised classification of LANDSAT satellite images. Further, classification sieve and manual edits can enhance the accuracy of the LC maps attained from different classification techniques.

## References

- Aburas MM, Ahamad MMS, Omar NQ (2019) Spatio-Temporal Simulation and prediction of land cover change using conventional and machine learning models: a review. *Environ Monit Assess* 191(4)
- Arulbalaji P (2019) Analysis of land cover/land cover changes using geospatial techniques in Salem District, Tamil Nadu, South India. *SN Appl Sci* 1(5). <https://doi.org/10.1007/s42452-019-0485-5>
- Chaturvedi S, Shukla K, Rajasekar E (2023) A spatio-temporal assessment and prediction of Ahmedabad's urban growth between 1990 and 2030 32(9):1791–1812
- Kavitha, AV, Srikrishna A, Satyanarayana C (2021) A review on detection of land cover and land cover from an optical remote sensing image. In: *IOP conference series: materials science and engineering* 1074(1):012002
- Macarringue LS, Bolfe ÉL, Pereira PRM (2022) Developments in land cover and land cover classification techniques in remote sensing: a review. *J Geogr Inf Syst* 14(01):1–28
- Seitzinger SP et al (2015) International geosphere-biosphere programme and earth system science: three decades of co-evolution. *Anthropocene* 12(2015):3–16. <https://doi.org/10.1016/j.ancene.2016.01.001>
- Talukdar, Swapan et al (2020) Land coverland-cover classification by machine learning classifiers for satellite observations-a review. *Remote Sens* 12(7)

- Tarawally M et al (2019) Land cover/land cover change evaluation using land change modeller: a comparative analysis between two main cities in Sierra Leone. *Remote Sens Appl Soc Environ* 16(September):100262. <https://doi.org/10.1016/j.rsase.2019.100262>
- Wang J, Michael Bretz M, Dewan AA, Delavar MA (2022) Machine learning in modelling land cover and land cover-change (LULCC): current status, challenges and prospects. *Sci Total Environ* 822:153559. <https://doi.org/10.1016/j.scitotenv.2022.153559>



# Comparison of Image Processing Techniques to Identify the Land Use/Land Cover Changes in the Indian Semi-arid Region



Nikhil Anand, Shweta Kumari, and Ankit Deshmukh

**Abstract** Several parameters are combined to form a system; if one of the parameters is changed, it also influences the other parameters. Both biophysical components and features made by humans are dynamic and constantly changing. Resources are being used to rapidly meet the growing population demand, causing changes in land use and land cover (LULC). It is believed that LULC change is a significant component of global change that impacts climate change. A significant amount of effort has been into creating methods for remotely sensed data change detection. LULC change detection of Hyderabad using remote sensed images has been performed in this project. Landsat 7 ETM+ imagery for 19 May 2000 and Landsat 8 (OLI/TIRS) imagery for 5 May 2015 has been obtained from the USGS Earth Explorer. ERDAS Imagine 9.1 is used for image rectification, layer stacking, and cloud cover correction. A spectral signature training file is prepared using the pixel values of the image and its properties in the ArcGIS 10.1. Then, the supervised classification was done using the maximum likelihood classifier in 4 different classes (Class 1: Vegetation, Class 2: Barren land, Class 3: Waterbody, and Class 4: Built-up). Post-classification comparison of the two maps is made on a pixel-by-pixel basis using a change detection matrix. Moreover, the changes from the before image (19 May 2000) and after image (5 May 2015) have been done in Arc GIS 10.1 using raster calculator with the image difference method (Before and After images) and ERDAS Imagine 9.1 using the Change Detection tool. ERDAS Imagine 9.1 performed better than ArcGIS 10.1 and shown distinct changes. From the LULC change map, great changes in the stretch of water body have been observed from 2000 to 2015. The different classes of the before map have been merged into other classes or changed as new classes in the

---

N. Anand  
Darbhanga College of Engineering, Darbhanga, India  
e-mail: [nikhil.abhijeet@gmail.com](mailto:nikhil.abhijeet@gmail.com)

S. Kumari (✉)  
Indian Institute of Technology Hyderabad, Hyderabad, India  
e-mail: [contact.shwetakumari.me@gmail.com](mailto:contact.shwetakumari.me@gmail.com)

A. Deshmukh  
Pandit Deendayal Energy University, Gandhinagar, India  
e-mail: [Ankit.Deshmukh@sot.pdpu.ac.in](mailto:Ankit.Deshmukh@sot.pdpu.ac.in)

after map. The area under the water body has been transformed into a built-up area and barren land. LULC change in 15 years also induced two new classes in the study area Class 1 and Class 2. The observed new classes and to distinguish this class from other classes ground survey has been done using Google Earth. In ground survey, the Class 1 has been identified as Nehru zoological park and Class 2 as a planned residential society. LULC change map can be used by the government, decision-makers, and policymakers and can help in proper resource management and policymaking.

**Keywords** Remote sensing · Image processing · Supervised classification · Land use/land cover · GIS

## 1 Introduction

With each passing day, changes can be observed in everything like climate, environment, geography, etc. Several parameters combined together form a system if one of the parameters is changed it influences the other parameters also. Population of the world and urbanisation is increasing at high rate. Due to the growing population the requirements are increasing, to meet the demand, resources are being used at a rapid rate, causing changes in LULC (Wicke et al. 2012; Roy and Roy 2010; Rawat and Kumar 2015; Zope et al. 2016). Land use can be defined as the total of arrangements, activities, and inputs that people undertake in a certain land cover type. Land cover can be defined as physical material at the surface of the earth. Land covers include grass, asphalt, trees, bare ground, water, etc.

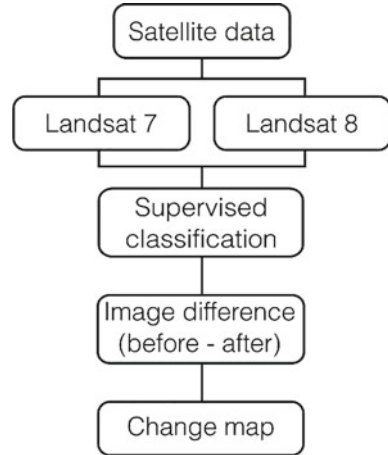
Land use consists the management and alteration of natural environment. One important aspect of global change that might have a bigger influence than climate change is land use and land cover change. Change detection help in management of resources and also helps in determining the solution to the adverse effect. The detailed methodology of change detection and generation of change map is shown as flowchart in Fig. 1.

### 1.1 Materials and Methodology

### 1.2 Site Description

Hyderabad city has been through many changes in a minimal time period. The city population in 1897 was 415,039, and today is 11,723,548 (11.7 million). India's Hyderabad metropolis has a total area of 650 km<sup>2</sup> (250 sq. mi). According to Köppen-Geiger classification, the climate in our study area is hot and semi-arid with low and extremely variable precipitation, high evaporation, and intense solar radiation. BSh (Zope et al. 2016). This region experiences 774 mm of precipitation on average

**Fig. 1** Change map generation methodology flow chart



annually, with lowest and highest temperatures of 27 °C and 41 °C, respectively [IMD report 1901–2015, (Kottek et al. 2006)]. The study area’s minimum and highest temperatures were 27 °C and 41 °C, respectively. The region’s humidity varies from 35% in the summer to 73% during the monsoon season (CGWB 2013). Over the area, the average seasonal wind speed is between 1.5 and 2.7 m/s. The study area is hydro-geologically a part of the Deccan plateau, which is characterised by multiple layers of solidified flood basalt from volcanic eruptions. The groundwater depth in the study area ranges from 12 m pre-monsoon to post-monsoon groundwater depth of 6 m. (CGWB, Central Ground Water Board 2013).

### 1.3 Landsat Imageries and Image Processing

Landsat 7 ETM+ imagery generated via an Enhanced Thematic Mapper Plus (ETM+) sensor produces an 8-bit Image with a 256-greyscale level (Bisht et al. 2018). Landsat 7 imagery consists of a total of 8 spectral bands, including panchromatic and thermal bands. The Landsat 8 (OLI/TIRS) (Barker 2006) imagery consists of a total of 9 bands, including a panchromatic band (Table 1). We use ERDAS Imagine 9.1 for Image processing after stacking all the layers of Landsat 7 in one layer; after that, we apply corrections such as cloud removal. A similar process is used for Landsat 8 imagery. Post-classification change detection techniques using maximum likelihood supervised classification is used to detect the land use/land cover change. This method is used as it has high accuracy across variety of data.



**Table 1** Landsat 7 and Landsat 8 imagery information

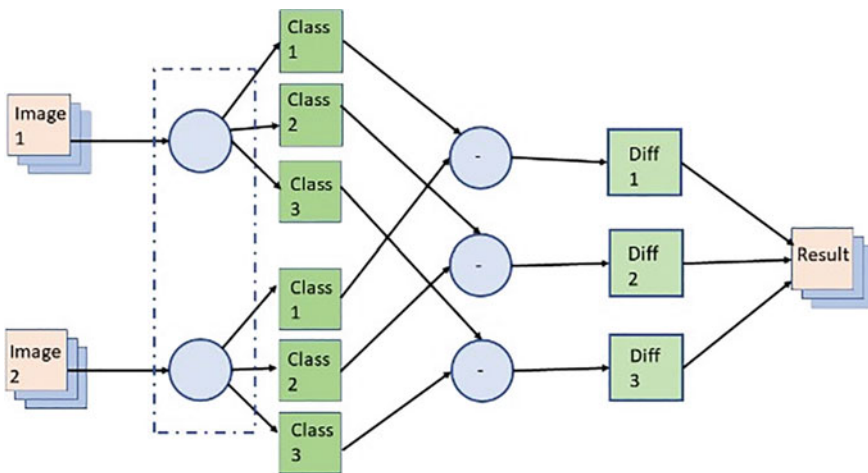
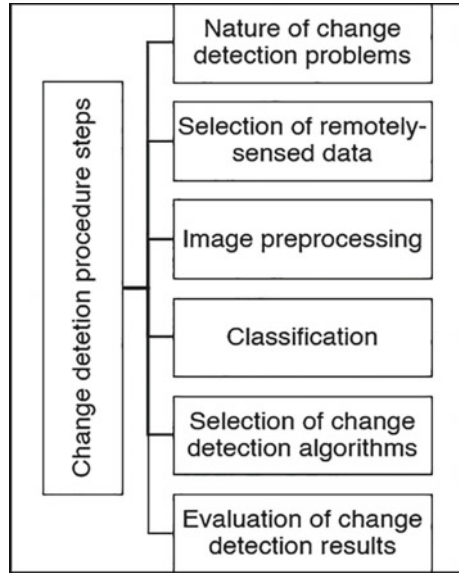
Landsat 7 ETM+ Bands ( $\mu\text{m}$ )			
Band	Resolution (m)	EMR	Range
Band 1	30	Blue	0.441–0.514
Band 2	30	Green	0.519–601
Band 3	30	Red	0.631–0.692
Band 4	30	NIR	0.772–0.898
Band 5	30	SWIR-1	1.547–1.749
Band 6	60	TIR	10.31–12.36
Band 7	30	SWIR-2	2.064–2.345
Band 8	15	Pan	0.515–0.896
Landsat 8 OLI and TIRS band ( $\mu\text{m}$ )			
Band	Resolution (m)	EMR	Range
Band 1	30	Coastal	0.435–0.451
Band 2	30	Blue	0.452–0.512
Band 3	30	Green	0.533–0.590
Band 4	30	Red	0.636–0.673
Band 5	30	NIR	0.851–0.879
Band 6	60	SWIR-1	1.566–1.651
Band 7	30	SWIR-2	2.107–2.294
Band 8	15	Pan	0.503–0.676
Band 9	30	Cirrus	1.363–1.384
Band 10	100	TIR-1	10.60–11.19
Band 11	100	TIR-2	11.50–12.51

## 1.4 Change Detection

The technique of finding differences in an object's or phenomenon's condition by observing it at different times is called as "change detection" (Singh 1989). Change detection is regarded as a crucial procedure in LULC change monitoring because it offers a quantitative examination of the population of interest's spatial distribution. According to Jensen's 2005 statement, there are six primary steps required to detect LULC changes using remotely sensed data (see Fig. 2).

Supervised classification with ERDAS Imagine 9.1 using the class definition of Class 1: Vegetation, Class 2: Barren land, Class 3: Waterbody, Class 4: Built-up area is done. After that, in the change detection, we compare the classified image of both periods (2000 and 2015) and detect the pixel-wise change with ArcGIS 10.1 and ERDAS Imagine 9.1 following the Diallo, Hu and Wen, Bayarsaikhan, Shalaby, Tateishi, Muttitanon, Tripathi Torahi, Rai (Novelli and Tarantino 2015; Irish et al. 2006; Failed 2009; Bayarsaikhan et al. 2009; Shalaby and Tateishi 2007; Muttitanon and Tripathi 2005) (Fig. 3).

**Fig. 2** Major change detection procedures



**Fig. 3** Schematic diagram of post- classification comparison change detection method

This method is based on the rectification of multiple classified images, where each image is classified individually, thematic maps are created, and then the associated labels or themes are examined to identify where change has occurred. This method has a number of benefits, including the reduction of sensor, atmospheric, and environmental differences due to the separate classification of data from two dates, which eliminates the need to normalise for sensor and atmospheric differences between

two dates, and the provision of a complete matrix of land cover change when using multiple images (Torahi and Rai 2011; Fan et al. 2007; Jensen 2005).

## ***1.5 Result and Discussion***

LULC change detection of Hyderabad using remote sensed image has been done in this project. Two satellite imageries have been taken one for year 2000 and other for 2015. Landsat 7 ETM+ imagery for 19 May 2000 and Landsat 8 (OLI/TIRS) imagery for 5 May 2015 has been obtained from the USGS Earth Explorer. As we know, Landsat 7 imagery takes images in 8 bands and Landsat 8 in 11 bands, the image has to be rectified first. For that, we did layer stacking in ERDAS Imagine 9.1. After that, the image is clipped for the Hyderabad region as the image from the satellites covers an extensive area using the shape file. The projection of the images has been changed to WGS\_1984, and the spectral signature training file is prepared using the pixel values of the Image and its properties using the ARC GIS 10.1. Then, the supervised classification was done using the maximum likelihood classifier in 4 different classes. The classes are as follows:

Class 1: Vegetation

Class 2: Barren land

Class 3: Waterbody

Class 4: Built-up

Each remotely sensed image must be rectified and classified for post-classification comparison change detection. We use change detection matrix to compare the two maps pixel-by-pixel for change detection. The post-classification change detection method should use individual classification maps that are as precise as possible. The final change detection map will include each error in the individual date classification map.

The change detection from the before image (19 May 2000) (Fig. 4) and after image (5 May 2015) (Fig. 5) has been done in Arc GIS 10.1 using a raster calculator using the image difference method (before image–after image). The change detection is also performed in ERDAS Imagine 9.1 using the Change Detection tool. Among both software, ERDAS Imagine 9.1 has shown better results.

The LULC change map clearly shows that lots of changes happened over 15 years due to human activities and other factors.

From the LULC change map, great changes in the stretch of the water body has been observed from 2000 to 2015 (Fig. 6). The different classes of the before map have been merged into other classes or changed as new classes has been observed from the after map. The area under the water body has been changed into built-up area and barren land by more than 50%. The area under barren land has tripled in 15 years of time period. LULC change in 15 years also induced two new classes in the study area, Class 1 and Class 2. The new classes have been observed and to distinguish this class from other classes ground survey has been done using Google

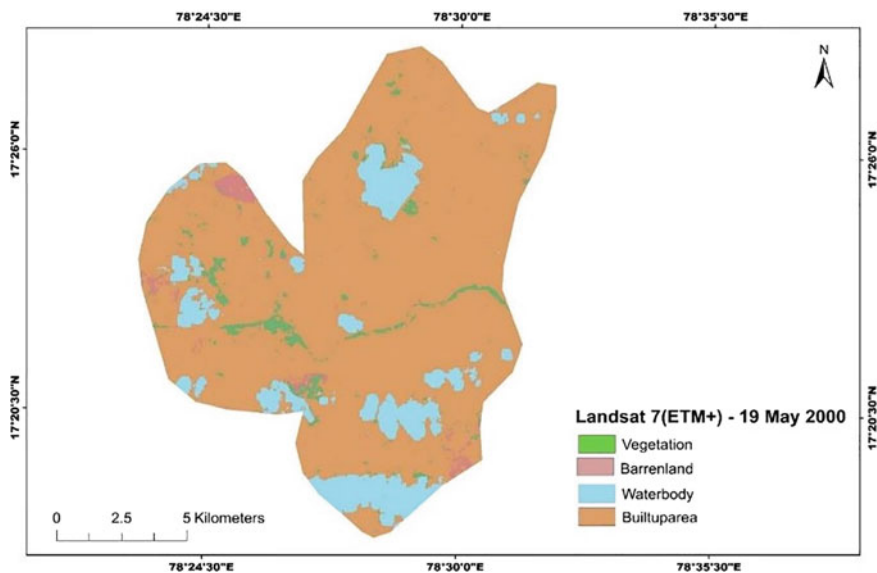


Fig. 4 Map showing the LULC of Hyderabad on 19 May 2000

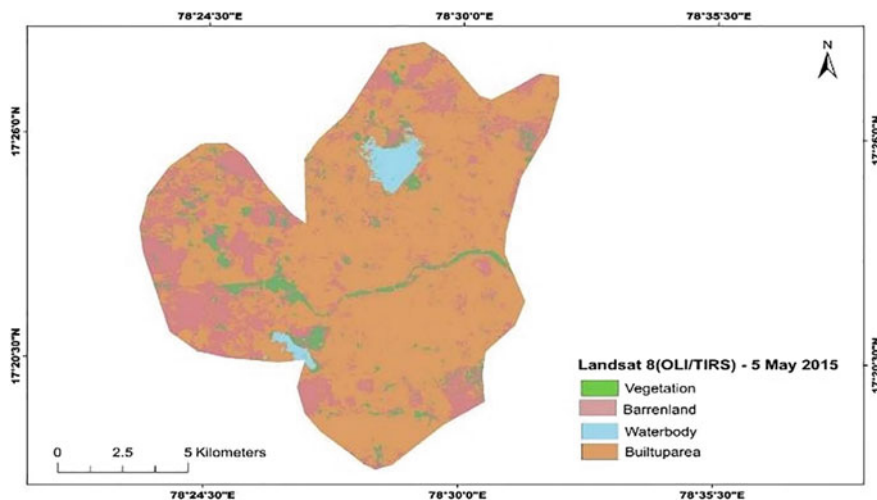


Fig. 5 Map showing the LULC of Hyderabad on 19 May 2000

Earth (Fig. 7). In the ground survey, Class 1 has been identified as Nehru zoological park and Class 2 shows a planned society.

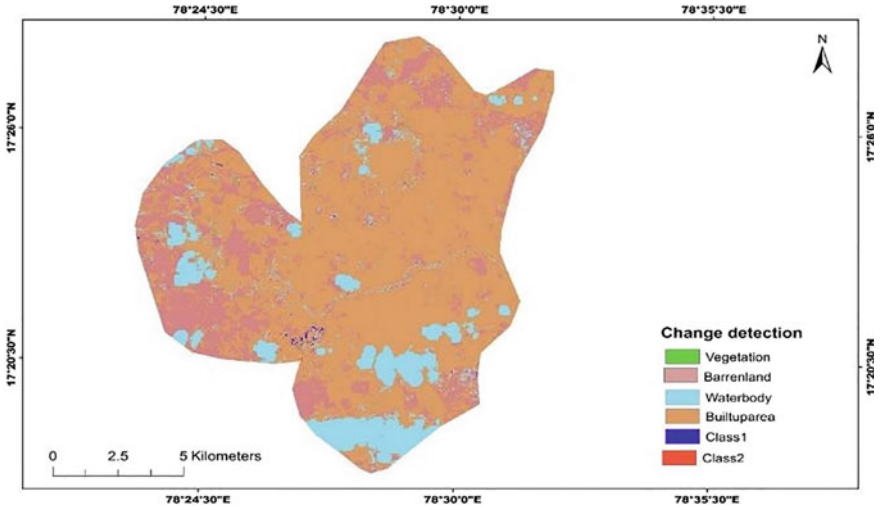


Fig. 6 Map showing the LULC change of Hyderabad from May 2000 to May 2015

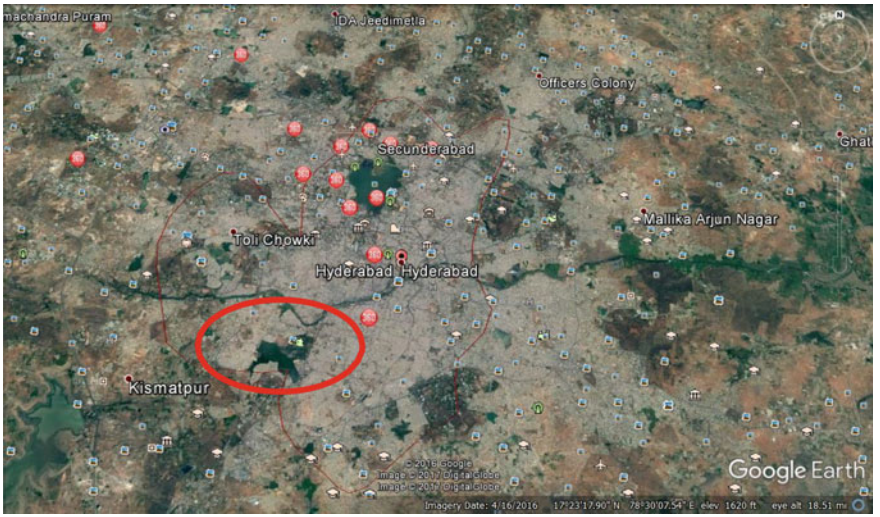


Fig. 7 Ground investigation of the Class1 observed in change map

### 1.6 Conclusions

This study focuses on the changes observed in city of Hyderabad’s land use and land cover in last 15 years using two different satellite imageries. Landsat 7 ETM+ imagery for 19 May 2000 and Landsat 8 (OLI/TIRS) imagery for 5 May 2015 has been obtained from the USGS earth explorer for the same month of the two different

years. Two different popularly used software (ERDAS Imagine and Arc GIS 10.1) are used in the study to understand the land use and land cover changes. ERDAS Imagine 9.1 detected the LULC changes very well with respect to ArcGIS 10.1. Humongous change in the stretch of the water body has been observed from 2000 to 2015 due to human intrusion and climate change. More than half of water body's area has been changed into a built-up area and barren lands. LULC change in 15 years induced two new classes in the study area Class 1 and Class 2. In the ground survey, Class 1 has been identified as Nehru zoological park and Class 2 shows a planned society. LULC change map clearly shows the differences between before and after scenarios of the study area. It can be used by the government, decision-makers, and policymakers and help in proper resource management and policymaking.

## References

- Barker K (2006) Barker review of land use planning: final report, recommendations. The Stationery Office
- Bayarsaikhan U, Boldgiv B, Kim K, Park K, Lee D (2009) Change detection and classification of land cover at Hustai National Park in Mongolia. *Int J Appl Earth Obs Geoinf* 11(4):273–280
- Bisht DS, Chatterjee C, Raghuwanshi NS, Sridhar V (2018) Spatio-temporal trends of rainfall across Indian river basins. *Theoret Appl Climatol* 132(1):419–436
- CGWB, Central Ground Water Board (2013) Dynamic ground water resources of India. Ministry of Water Resources, Government of India. <http://cgwb.gov.in/Documents/Dynamic%20GWRE-2013.pdf>
- Diallo Y, Hu G, Wen X (2009) Applications of remote sensing in land use/land cover change detection in Puer and Simao Counties, Yunnan Province. *J Am Sci*
- Fan F, Weng Q, Wang Y (2007) Land use and land cover change in Guangzhou, China, from 1998 to 2003, based on Landsat TM/ETM imagery. *Sensors* 7(7):1323–1342
- Irish RR, Barker JL, Goward SN, Arvidson T (2006) Characterization of the Landsat-7 ETM+ automated cloud- cover assessment (ACCA) algorithm. *Photogram Eng Remote Sens* 72(10):1179–1188. Fno
- Jensen JR (2005) *Introductory digital image processing: a remote sensing perspective*. Pearson Prentice Hall. Upper Saddle River, NJ, 7458, pp 1–131
- Kottek M, Grieser J, Beck C, Rudolf B, Rubel F (2006) World map of the Köppen-Geiger climate classification updated
- Muttitanon W, Tripathi N (2005) Land use/land cover changes in the coastal zone of Ban Don Bay, Thailand using Landsat 5 TM data. *Int J Remote Sens* 26
- Novelli A, Tarantino E (2015) Combining ad hoc spectral indices based on LANDSAT-8 OLI/TIRS sensor data for the detection of plastic cover
- Rawat JS, Kumar M (2015) Monitoring land use/cover change using remote sensing and GIS techniques: a case study of Hawalbagh block, district Almora, Uttarakhand, India. *Egypt J Remote Sens Space Sci* 18(1):77–84
- Roy PS, Roy A (2010) Land use and land cover change in India: a remote sensing and GIS perspective. *J Indian Inst Sci* 90(4):489–502
- Shalaby A, Tateishi R (2007) Remote sensing and GIS for mapping and monitoring land cover and land-use changes in the Northwestern coastal zone of Egypt. *Appl Geogr*
- Singh A (1989) Digital change detection techniques using remotely-sensed data. *Int J Remote Sens* 10(6):989–1003

- Torahi AA, Rai SC (2011) Land cover classification and forest change analysis, using satellite imagery-a case study in Dehdez area of Zagros Mountain in Iran. *J Geogr Inf Syst* 3(1):1–11. vineyard. *Remote Sens Lett* 6(12):933–941.
- Wicke B, Verweij P, Van Meijl H, Van Vuuren DP, Faaij AP (2012) Indirect land use change: review of existing models and strategies for mitigation. *Biofuels* 3(1):87–100
- Zope PE, Eldho TI, Jothiprakash V (2016) Impacts of land use–land cover change and urbanization on flooding: a case study of Oshiwara River Basin in Mumbai, India. *CATENA* 145:142–154

# Application of Open-Source Geospatial and Modeling Techniques for Flood Assessment and Management—A Case of Flood 2017, Rel River Catchment



Dhruvesh Patel, Kishanlal R. Darji, Amit Kumar Dubey, Praveen Gupta, and Raghavendra Pratap Singh

**Abstract** Floods are disasters; it cannot be prevented; however, their effects can be reduced or minimized using contemporary geospatial and modeling techniques. Floods are unpredictable, though it can be diagnosed and lessen the catastrophic consequences in flood residing areas. India's more than  $40 \times 10^4$  million sq. mt. (12% Geological area) lands are flood-prone, affecting the country's productivity and essential properties. Therefore, flood assessment is a crucial need of the country for societal and economic growth. Remote Sensing (RS) and Geographic Information System (GIS) is an important part of geospatial techniques, help to analyze the flood-prone area; however, due to the coarse resolution of RS techniques, it can't provide the flood inundation information up to sub-metric resolution. To overcome the limitation and apply the contemporary tools, hydrologic and hydrodynamic modeling is a blessing for the hydrologic community to analyze the flood and produce the various flood decision-making maps, i.e., flood arrival, flood velocity, flood inundation, water surface elevation, etc. The hydrologic model is utilized to simulate the runoff from the catchment, and the hydrodynamic model is utilized for flood assessment in 1D and 2D. The present case is the Rel River, which was affected by a flood in 2017. The hydrodynamic model simulates runoff under extreme flooding conditions to identify the flood catastrophe and vulnerability. It helps provide the

---

D. Patel (✉) · K. R. Darji  
Department of Civil Engineering, School of Technology, Pandit Deendayal Energy University (PDEU), Gandhinagar 382426, Gujarat, India  
e-mail: [dhruvesh.patel@sot.pdpu.ac.in](mailto:dhruvesh.patel@sot.pdpu.ac.in)

K. R. Darji  
e-mail: [darjikishan1@gmail.com](mailto:darjikishan1@gmail.com)

A. K. Dubey · P. Gupta · R. P. Singh  
SAC-ISRO, Ahmedabad, India  
e-mail: [a\\_dubey@sac.isro.gov.in](mailto:a_dubey@sac.isro.gov.in)

P. Gupta  
e-mail: [pkgupta@sac.isro.gov.in](mailto:pkgupta@sac.isro.gov.in)

R. P. Singh  
e-mail: [director@iirs.gov.in](mailto:director@iirs.gov.in)



boundary conditions of Rel River and tributaries for flood simulation at Dhanera city. The 2D HEC-RAS-based open-source hydrodynamic modeling is utilized for flood simulation in 2D. Overall, the paper shows the application of geospatial techniques for preparing various files for flood modeling. In contrast, the hydrologic and hydrodynamic model shows the utility of the contemporary method for flood assessment and management.

**Keywords** Disaster management · Flood assessment and management · Geospatial techniques · GIS

## 1 Introduction

Floods constitute a significant threat to the economic growth of developing countries. It causes the loss of life and property (Patel et al. 2017; Darji et al. 2020). Among the flood-affected nations, India is one of the severely flood-affected countries in Asia. One-fifth of global flood deaths and 12% ( $40 \times 10^4$  million sq. mt.) of geographical regions are prone to various floods (Mohanty et al. 2020). The floods in India are accelerated because of the reduced caring capacity of the river, siltation, erotic rainfall, river bank erosion, poor natural drainage, cloudbursts, and much more metrological, topographical, and hydrological factors (Darji et al. 2020). Therefore, flood assessment and risk management are the significant needs of the county to reduce the flood fatality and flood catastrophes in the future (Pathan et al. 2021a).

In India, primary flood risk assessment and preparedness have been performed using satellite techniques and hydrologic and hydrodynamic modeling. Satellite techniques are utilized in India, such as SARAL-Altika Mission (Gairola 2015; Patel et al. 2020), (RISAT-1 SAR Mission (Misra et al. 2013), Cartosat Missions (DEM), Kalpana, Megha Tropiques, and INSAT-3D Missions (Rainfall, Solar Radiation, etc.) (Ranganath and Navalgund 2010), Landsat Program, Sentinel Program, Jason program, SRTM/ASTER topography missions (Swenson et al. 2008) and Tropical Rainfall Measuring Mission (TRMM), etc., however, it has course resolution. It would not provide full coverage for a small flood-prone area. Under these circumstances, an open-source flood assessment model, i.e., HEC-RAS, HEC-HMS, HEC-GeoRAS, would give a modeling platform to simulate the flood events using open-source DEM, rainfall, and boundary condition. Many researchers have successfully applied 1D, 2D, and 1D/2D-coupled HEC-RAS-based hydrodynamic models for flood assessment. It produced flood inundation, flood depth, water surface elevation, and flood arrival maps for the flood decision-making system (Arrighi and Campo 2019; Yalcin 2020; Quiroga et al. 2016). World wised has successfully applied an open-source HEC-RAS hydrodynamic model for generating a flood depth, flood velocity, flood inundation, flood arrival time, and flood hazard maps (Pathan et al. 2021b; Patel 2018; Jodhani et al. 2021; Prieto et al. 2020).

This research paper covers open-source HEC-RAS-based geospatial techniques for flood assessment and management. The Rel River catchment, Gujarat, is considered a case study. The flood of Rel River 2017 has been considered for risk assessment. The open-source 30 m resolution SRTM DEM has been considered for 2D grid modeling; however, the flood hydrograph at the confluence point has been considered for upstream boundary conditions. The normal depth at the D/S boundary condition has been considered for an end-to-end simulation. The entire assembly has been simulated for the flood of 24 and July 25, 2017, and simulated results have been excreted using the open-source geospatial techniques. The flood inundation, flood depth, water surface elevation, and flood arrival maps for the flood decision-making system have been prepared. Overall, the entire approach of modeling and analysis techniques shows the application of recent geospatial and modeling techniques for flood risk assessment and management. It would be utilized for flood risk assessment and preparation of flood mitigation plans for developing countries; hence, it applies to the flood decision-making system.

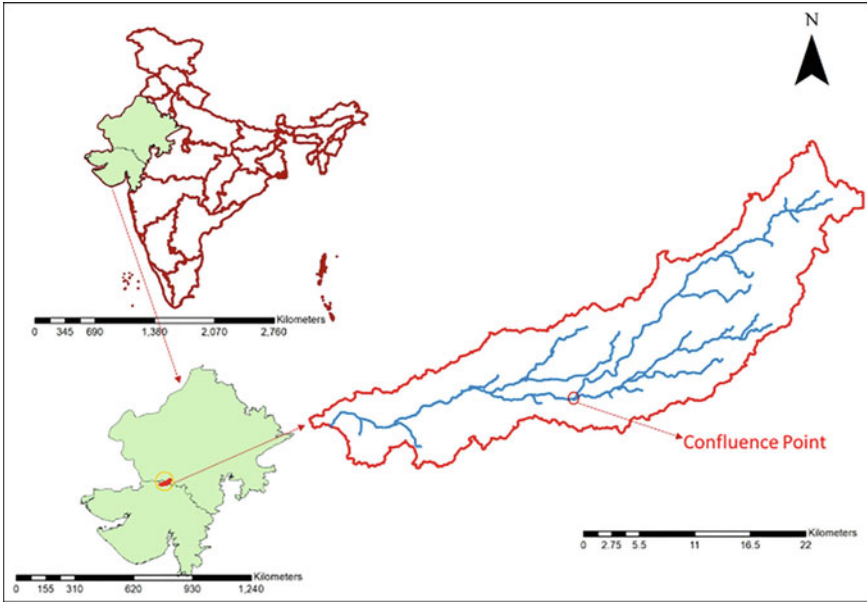
## 2 Study Area and Data Collections

The study area is situated in the northwest part of Gujarat. The Rel River which is non-perennial river originates from the southern part of the Sundhamata mountain and meets the Rann of Kutch in Gujarat. The research is demonstrated in the Rel River basin, situated in Banaskantha district, Gujarat, India (Fig. 1). Its catchment covers an area of 442 km<sup>2</sup> and lies between 24° 50' N to 24° 75' N latitude and 72° 00' E to 72° 45' E longitude. The lowest point is near Dhanera taluka and Dhanera city, near the mouth of the Rel River. The Rel River is an ungauged river with the data-scarce region. The river's width is about 280 m and 180 m at the road bridge and railway bridge, respectively.

The hourly precipitation data was derived from the google earth engine using a NASA-Global precipitation mission (GPM) satellite image as input in hydrological modeling. Thematic maps such as land use, geology, topography, and soil were prepared from the published literature (<https://www.gsi.gov.in/>, <http://cgwb.gov.in/>) of the different agencies in conjunction with the interpretation of the Landsat images, Google Earth images, and DEM using remote sensing and GIS technology.

## 3 Methodology

The current approach shows the state of an arch of flood modeling and flood assessment. The entire approach and modeling work have been performed using open-source software and geospatial techniques. Flowing steps have been adopted and performed for 2D flood simulation:



**Fig. 1** Location map of the study area

### 3.1 HEC-HMS Hydrologic Modeling

HEC-HMS is the open-source hydrological simulation model developed by the United States Army Corps of Engineers (Darji et al. 2019). The soil conservation service Curve number (SCS-CN) method was utilized to create a flow hydrograph at the confluence point of two main tributaries using Initial abstraction ( $I_a$ ), Curve Number (CN), and potential maximum retention ( $S$ ) from the following equations (Subrahmanya 2015):

$$S = \frac{25,400}{CN} - 254 \quad (1)$$

$$I_a = \lambda S \quad (2)$$

where  $\lambda$  is 0.3 for Indian conditions (Ministry of Agriculture 1972).

The direct runoff ( $Q$ ) and net rainfall for the catchment can be determined using Average Precipitation ( $P$ ), Initial Abstraction ( $I_a$ ), and Potential maximum Retention ( $S$ ) values in the following equation:

$$Q = \frac{(P - I_a)^2}{P - I_a + S} \quad (3)$$

The runoff will occur only when rainfall is more than  $I_a$ , that is,  $Q = 0$  when precipitation is lower or equal to initial abstraction ( $P \leq \lambda S$ ). The developed flood hydrograph at the confluence point was utilized as input data to simulate hydrodynamic modeling.

### 3.2 HEC-RAS Hydrodynamic Modeling

The HEC-RAS 5.0.1 is fully solved by using the 2D Saint Venant equation (Quiroga et al. 2016; HEC-RAS 2016; Brunner 2015):

$$\frac{\partial \xi}{\partial t} + \frac{\partial p}{\partial x} + \frac{\partial q}{\partial x} = 0 \quad (4)$$

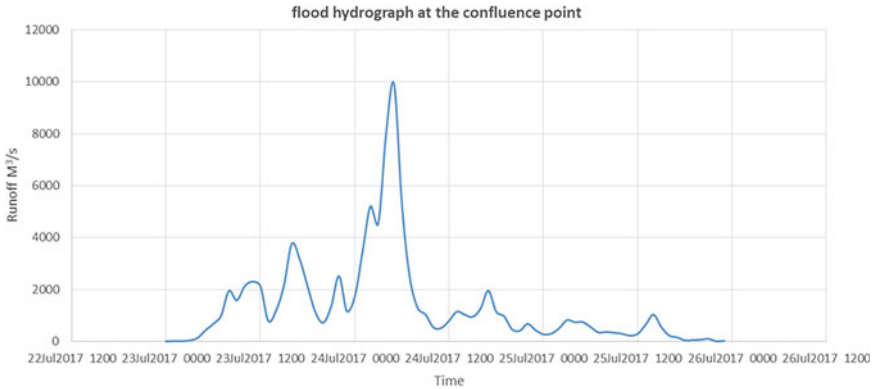
$$\begin{aligned} \frac{\partial p}{\partial t} + \frac{\partial}{\partial x} \left( \frac{p^2}{h} \right) + \frac{\partial}{\partial y} \left( \frac{pq}{h} \right) \\ = - \frac{n^2 pg \sqrt{p^2 + q^2}}{h^2} - gh \frac{\partial \xi}{\partial x} + pf + \frac{\partial}{\rho \partial x} (h\tau_{xx}) + \frac{\partial}{\rho \partial y} (h\tau_{xy}) \end{aligned} \quad (5)$$

$$\begin{aligned} \frac{\partial q}{\partial t} + \frac{\partial}{\partial y} \left( \frac{q^2}{h} \right) + \frac{\partial}{\partial x} \left( \frac{pq}{h} \right) \\ = - \frac{n^2 qg \sqrt{p^2 + q^2}}{h^2} - gh \frac{\partial \xi}{\partial y} + qf + \frac{\partial}{\rho \partial y} (h\tau_{yy}) + \frac{\partial}{\rho \partial x} (h\tau_{xy}) \end{aligned} \quad (6)$$

where  $h$  is the water depth ( $m$ ),  $p$  and  $q$  are the specific flow in the  $x$  and  $y$  direction ( $m^2 s^{-1}$ ),  $\xi$  is the surface elevation ( $m$ ),  $g$  is the acceleration due to gravity ( $ms^{-2}$ ),  $n$  is the Manning resistance,  $\rho$  is the water density ( $kg m^{-3}$ ),  $\tau_{xx}$ ,  $\tau_{yy}$ , and  $\tau_{xy}$  are the components of the effective shear stress and  $f$  is the Coriolis ( $s^{-1}$ ). (Patel et al. 2017; Quiroga et al. 2016) has presented the case of flood assessment of Bolivian Amazonia and Surat city using HEC-RAS-based 2D and 1D/2D-coupled hydrodynamic modeling. DEM is a sensitive parameter for 2D modeling in this study. 2D modeling is performed for 4 DEM using HEC-RAS: (i) Mosaicked DEM based on IDW method (ii) Mosaicked DEM based on NN method (iii) Mosaicked DEM based on HEC-RAS (iv) CARTOSAT DEM. The inundation area and depth results are extracted in QGIS, and maps are produced.

## 4 Results and Discussion

As described in the preceding section, the hydrologic and hydrodynamic model is utilized for flood assessment of the Rel River catchment for Dhanera city. The applied model and the outcomes are discussed for flood risk assessment and management.



**Fig. 2** Flood hydrograph at the confluence point

### 4.1 The Hydrologic Model

The HEC-HMS-based hydrologic model is utilized for rainfall-runoff analysis. The model is set for the Rel River catchments covering 442km<sup>2</sup>; a total of 02 watersheds of tributaries are derived for rainfall-runoff analysis. The CN value as per land use and soil classes has been assigned and identified the 72 over the study reach. The flood hydrograph at confluence points for 2017 at the Rel River catchment is determined using SCS-CN and HEC-HMS models. The simulated flood hydrograph at the confluence point is indicated in (Fig. 2).

### 4.2 The Hydrodynamic Modeling

The HEC-RAS-based 2D hydrodynamic model is simulated for 2D flood analysis. The model was simulated under unsteady hydrodynamic conditions. The outcome from the hydrologic model, irrespective of any changes in flood hydrograph, has been utilized to fix the upstream boundary conditions, and normal depth is set for downstream boundary conditions. The 10-s time simulation has been set for model simulation. The flood depth, water surface elevation, velocity, and flood arrival map are computed and prepared using an open-source geospatial environment. The decision-making maps for flood assessment as an outcome of the HEC-RAS hydrodynamic model are discussed as follows:

**Flood Inundation Map:** 84.5 km<sup>2</sup> area was inundated during the 2017 flood event. Dhanera, Malotra, Rampura, Runi, Sankad, etc., villages were highly affected during the flood, which is beneficial information for administrative and decision-makers to act in emergencies at the flood (Fig. 3).

**Water Depth Map:** The water depth map represents the flooding water depth over the study reach. It shows the difference between the flood water RL to RL of the

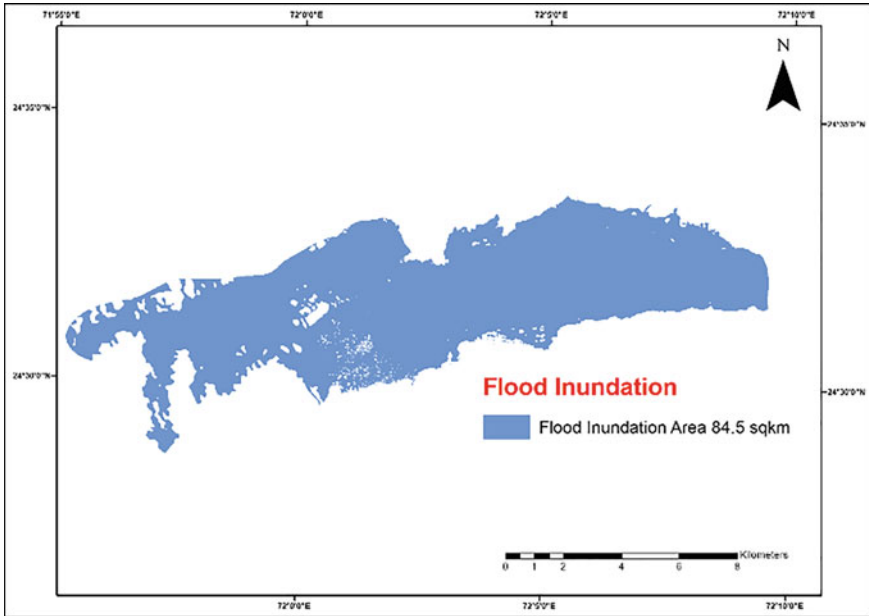


Fig. 3 Flood inundation map

DEM. The maximum water depth from the ground is 8 m, as shown in Fig. 4. This map will be used for decision-makers to get the water depth at a particular location to develop an evacuation plan.

**Water Surface Elevation Map:** WSE for the selected profile represents sea-level water elevation. RL of water level at the flood was used to develop a flood mitigation plan and generate a benchmark point for flood. The maximum water surface elevation is 175 m near the confluence point, and the minimum water surface elevation is 113 m on the downstream side near Dhanera taluka, as shown in Fig. 5.

**Velocity map:** The velocity is directly correlated with arrival time and the relation of water in flood susceptible areas. The high speed shows prompt arrival of flooding water in study reach and affects the sites. The water velocity in the flood plain is 0–5 m/s, as shown in Fig. 6.

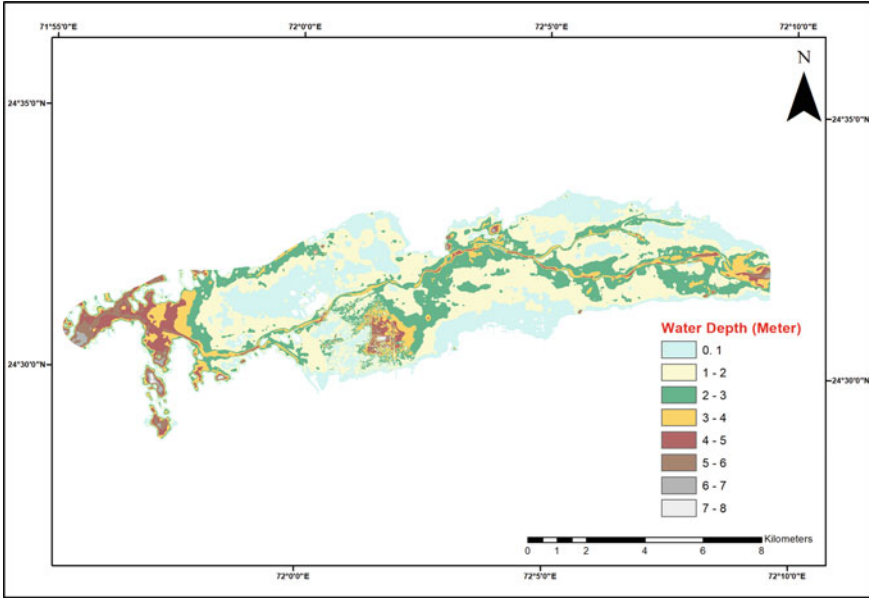


Fig. 4 Water depth map

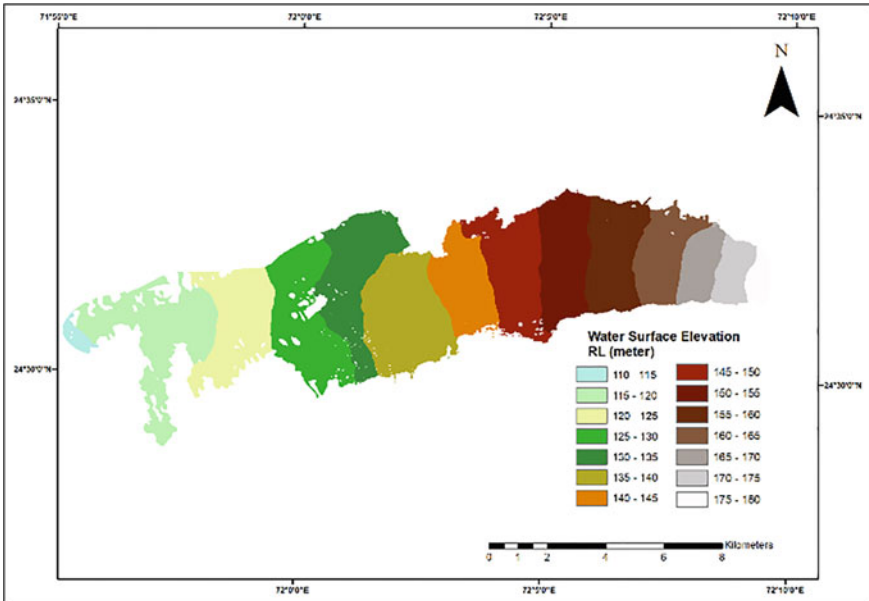
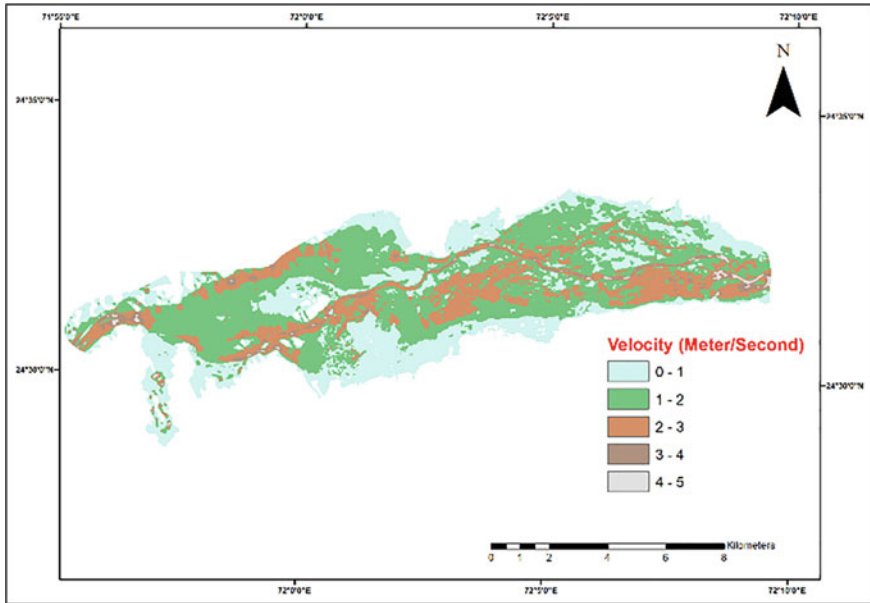


Fig. 5 Water surface elevation map



**Fig. 6** Velocity map

## 5 Conclusion

Flood is the most vulnerable hazard for developing countries, causing damage to properties and productivity to a large extent. However, the appropriate assessment techniques in the urban and riverine areas would decrease the flood catastrophe and reduce the human risk. The present case shows strong evidence of the utility of contemporary flood assessment and modeling techniques. HEC-HMS is an ideal tool utilized for rainfall-runoff modeling at the catchment scale. It will help find the runoff in the ungauged basin and derive a flood hydrograph at the sink point. The simulated hydrography from HEC-HMS is considered one of the essential input parameters for 2D flood hydrodynamic modeling. The paper further presents the utility of the 2D HEC-RAS model for finding the flood inundation, flood depth, water surface elevation, flood velocity, and arrival time maps for flood risk assessment and management. Results reveal that Dhanera, Malotra, Rampura, Runi, and Sankad of villages of Dhanera Taluka were highly affected by flood in 2017. The derived flood maps are an essential tool for decision-makers to take mitigation measures and prepare a robust flood reduction plan to reduce the flood fatality in the future under similar flooding conditions. However, many parameters affect the accuracy of the work. Therefore, the present work will be considered a case of open-source model applications for flood modeling. Although, rigorous analysis is required considering the high-resolution DEM and observed data for model simulations and analysis.



**Acknowledgements** The corresponding author would like to thank SAC-ISRO for providing the financial and technical support to execute the work. The Grant No: SAC/EPSA/GHCAG/LHD/SARITA/01/19. Also thankful to the anonymous reviewer(s) for providing constructive and scientific comments to improve the quality of the manuscript.

## References

- Arrighi C, Campo L (2019) Effects of digital terrain model uncertainties on high-resolution urban flood damage assessment. *J Flood Risk Manag* 12. <https://doi.org/10.1111/JFR3.12530>
- Brunner GW, Piper SS, Jensen MR, Chacon B (2015) Combined 1D and 2D hydraulic modeling within HEC-RAS. *World Environ Water Res Congr* 2015
- Darji K, Khokhani V, Mehmood K, Prakash I, Pham BT (2019) (PDF) Rainfall-runoff modelling using HEC-HMS model: an application of regression analysis. *J Emerg Technol Innov Res* 6:226–234
- Darji K, Prakash I, Pham BT (2020) (PDF) Runoff estimation of Machhu and Watrak Rivers basins of Gujarat India using SCS-CN method and GIS. *Indian J Ecol* 47:726–732
- Darji K, Patel D (PDF) (2020) Creating the high resolution DEM for flood assessment using UAV techniques. In: *Proceedings of the ISRS-ISG national symposium–2020*, p 185
- Gairola RM (2015) SARAL/ALTIKA science and applications: summary of achievement data application-SEAS. In: *National natural resources management system*, pp 1–11
- HEC-RAS (2016) HEC-RAS user's manual
- Jodhani KH, Patel D, Madhavan N (2021) A review on analysis of flood modelling using different numerical models. *Mater Today Proc*. <https://doi.org/10.1016/J.MATPR.2021.07.405>
- Ministry of agriculture (1972) Government of India. *Handbook of hydrology*, New Delhi
- Misra T, Rana S, Desai N, Dave D (2013) Rajeevjyoti synthetic aperture radar payload on-board RISAT-1: configuration, technology and performance. *Curr Sci JSTOR*
- Mohanty M, Mudgil S, Karmakar S (2020) Flood management in India: a focussed review on the current status and future challenges. *Int J Disaster Risk* 49. <https://doi.org/10.1016/j.ijdr.2020.101660>
- Patel DP, Ramirez JA, Srivastava PK, Bray M, Han D (2017) Assessment of flood inundation mapping of Surat City by coupled 1D/2D hydrodynamic modeling: a case application of the new HEC-RAS 5. *Nat Hazards* 89:93–130. <https://doi.org/10.1007/S11069-017-2956-6>
- Patel DP (2018) A comparative study of delineated watersheds through ASTER, SRTM and ALOS for evaluating morphological changes in Hathmati Basin, Gujarat, India, pp 19–20. <https://doi.org/10.13140/RG.2.2.13397.93920>
- Patel DP, Srivastava PK, Singh SK, Prieto C, Han D (2020) One-dimensional hydrodynamic modeling of the River Tapi. *Tech Disaster Risk Manag Mitig* 209–235. <https://doi.org/10.1002/9781119359203.ch16>
- Pathan AI, Agnihotri PG, Patel D, Prieto C (2021b) Identifying the efficacy of tidal waves on flood assessment study—a case of coastal urban flooding. *Arab J Geosci* 14:2132. <https://doi.org/10.1007/s12517-021-08538-6>
- Pathan AI, Agnihotri PG, Patel D, Prieto C (2021a) Identifying the efficacy of tidal waves on flood assessment study—a case of coastal urban flooding. *Arab J Geosci* 14(20):1–21. <https://doi.org/10.1007/S12517-021-08538-6>
- Prieto C, Patel D, Han D (2020) Preface: advances in flood risk assessment and management. *Nat Hazards Earth Syst Sci* 20:1045–1048. <https://doi.org/10.5194/nhess-20-1045-2020>
- Quiroga VM, Kurea S, Udoa K, Manoa A (2016) Application of 2D numerical simulation for the analysis of the February 2014 Bolivian Amazonia flood: application of the new HEC-RAS version 5. *Ribagua* 3:25–33. <https://doi.org/10.1016/J.RIBA.2015.12.001>

- Ranganath R, Navalgund R (2010) The evolution of the earth observation system in India. *J Indian Inst Sci*
- Subrahmanya K (2015) *Engineering hydrology*; Third; Tata McGraw-Hill, New Delhi
- Swenson S, Famiglietti J, Basara J (2008) Estimating profile soil moisture and groundwater variations using GRACE and Oklahoma Mesonet soil moisture data. *Water Resour Res* 44:1413. <https://doi.org/10.1029/2007WR006057>
- Yalcin E (2020) Assessing the impact of topography and land cover data resolutions on two-dimensional HEC-RAS hydrodynamic model simulations for urban flood hazard analysis. *Nat Hazards* 101:995–1017. <https://doi.org/10.1007/S11069-020-03906-Z>

# Evaluation of Movement of Wetting Front Under Wick Irrigation in Black Cotton Soil



Uttamkumar Vyas, Kishanlal Darji, Neelkanth Bhatt, Vinay Vakharia, and Dhruvesh Patel

**Abstract** Irrigation of the crop is a necessity for group growth. Several irrigation techniques have been used for watering the crop and cultivating the crops for maximum production. Applying the different irrigation techniques to crops depends on crop-land suitability; however, finding the optimum water requirements to crop is the primary aim of this case study. The present research aims to identify wetting front movement while using wick irrigation technique. The method has been executed to demonstrate and find the developed wetting front at a small farm in Velavadar, Surendranagar in Gujarat. This study reviews an experiment with capillary wick irrigation for cultivating raw crops. IS 2720 (Part-IV)–1985 and IS 460–1978 were used to analyze a representative soil sample taken from the farm. The electrical conductivity (E.C.) of the irrigation water and the soil was relatively high, according to water quality and soil nutrient tests. The knowledge of wetted width, depth, and maximum wetted width beneath the soil's surface is required to design and manage an efficient wick irrigation system. It can essentially be auto regulated by wick discharge and time of micro-irrigation. Temporal movement of wetting in horizontal and vertical directions under the surface point source was studied in an experimental box size of 1 \* 1 \* 1 m. The wick diameter considerably impacts the yield as per the types of crops. However, a small underground reservoir with 7 L is used for the

---

U. Vyas (✉) · K. Darji · D. Patel

Department of Civil Engineering, School of Technology, PDEU, Gandhinagar 382426, Gujarat, India

e-mail: [uttam.vphd21@sot.pdpu.ac.in](mailto:uttam.vphd21@sot.pdpu.ac.in)

K. Darji

e-mail: [darjishan1@gmail.com](mailto:darjishan1@gmail.com)

D. Patel

e-mail: [dhruvesh.patel@sot.pdpu.ac.in](mailto:dhruvesh.patel@sot.pdpu.ac.in)

N. Bhatt

Department of Civil Engineering, Lukhdhirji Engineering College, GTU, Morbi, India

e-mail: [neelkanth78bhatt@gmail.com](mailto:neelkanth78bhatt@gmail.com)

V. Vakharia

Department of Mechanical Engineering, School of Technology, PDEU, Gandhinagar 382426, Gujarat, India

e-mail: [vinay.vakharia@sot.pdpu.ac.in](mailto:vinay.vakharia@sot.pdpu.ac.in)

© The Author(s), under exclusive license to Springer Nature Singapore Pte Ltd. 2024

D. Patel et al. (eds.), *Innovation in Smart and Sustainable Infrastructure*, Lecture Notes in Civil Engineering 364, [https://doi.org/10.1007/978-981-99-3557-4\\_6](https://doi.org/10.1007/978-981-99-3557-4_6)

best economic returns. The wetting pattern was shaped like a balloon and stretched 30 cm horizontally and 50 cm vertically from the ground level. After 120 h, the wetting front faded and was gone after 12 days. Some shallow-rooted vegetable crops (up to 50 cm depth) such as lettuce, onions, potatoes, radish, and moderately deep-rooted (30–60 cm depth) vegetable crops such as broccoli, beans, cabbages, carrots, cauliflower, cucumbers, muskmelon, peppers, tomatoes, and zucchini can be grown by observing moisture distribution under capillary wick for alkaline soil with saline irrigation water. Tests suggest that this indigenous technology could be used successfully even in adverse land and water conditions.

**Keywords** Micro-irrigation · Wetting front · Black cotton soil · Optimum water requirement

## 1 Introduction

Agriculture is a vital aspect of the economy in a country like India. Agriculture is practiced in the sense of providing a service rather than a business or a trade. With a growing population and dwindling natural resources, it is imperative to increase agricultural production (Kumar and Sharma 2020). Increased agricultural productivity necessitates the use of pure water. Food and fiber need has increased significantly as the world's population has grown tremendously (Talaviya et al. 2020). To meet the rising demand, agricultural yield per unit volume of water application must be optimized. Water is one of the essential resources that is inextricably linked to food production (Manjunatha et al. 2011). Most countries and regions face water scarcity, posing a significant challenge to global food security. India has a population of 1.21 billion people and is expanding at a rate of 17.64% per year (2001–11), compared to the global average of 1.3% per year (Ghosh 2019). The rapid rise of India's population has put pressure on the country's agriculture to produce more and more to feed its 1.21 billion people, but having only 141 million hectares of cultivable land, of which 62 million hectares are exclusively irrigated. Groundwater is still the most significant source of irrigation water. The quality and quantity of groundwater water are deteriorating daily (Kishore et al. 2021). Simultaneously, the need for water is growing by the day. Groundwater levels have dropped dramatically in the recent decades (Manjunatha et al. 2011). Soil fertility is lowered as a result of poor water quality. People gradually rely more on rainfed agriculture, resulting in irrigation water scarcity. Water is the most significant input and is crucial in the plant's critical growth phases. As a result, it must be managed (Sharma et al. 2010). As a result, water management is required, and the most suited option is "micro-irrigation," which provides water to the plant root zone while increasing water efficiency (Rouzaneh et al. 2021; Vyas et al. 2022). Micro-irrigation spread quickly in the 1990s, reaching 0.3 Mha, and its current coverage in India is estimated to be around 3.4 Mha (Saxena et al. 2018).

Each irrigation method has its benefits, drawbacks, and limitations. Irrigation practices depend on location, water availability, cropping practices, water quality, soil types, topography, climate, and the socioeconomic status of the farmers. Farmers must, therefore, carefully select a way most strongly related to their tradition while suiting the local specific environment (Gopal and Lassaad 2009). Micro-irrigation systems can yield more crops with less water in such water-scarce regions (Rouzaneh et al. 2021). The need for water remains high in the traditional irrigation system of agriculture. Drip and sprinkler irrigation systems save half of the water used for irrigation, but technical, economic, and socioeconomic barriers impede their adoption. Drip irrigation adoption is hampered by cultural traditions, low irrigation water quality, and a lack of market for farm products (Abdelraouf et al. 2020). The adoption of micro-irrigation technologies also enhances water's marginal productivity. With the influence of subsidy schemes that indirectly reduce the marginal cost, demand for irrigation water increases, and a rational farmer continues to consume more water. On the other hand, other innovative scientific methods can be utilized to improve agricultural water use efficiency.

The experiment's capillary wick irrigation method is an innovative micro-irrigation technique that provides water according to the crop's needs and is entirely automated (Semananda et al. 2020). Capillary wick irrigation has been utilized to grow crops such as flowering plants and vegetables (Wesonga et al. 2014). Many positive results have been obtained using this method. By developing the procedure and conducting trials, good results can be obtained when utilizing this method to test the viability of additional crops. It is important to understand how the capillary wick irrigation method enhances water flow in the soil. Wetness in the soil was measured in this experiment using the capillary wick irrigation method for black cotton soil. Relative to drip irrigation, these systems are much less expensive, making them accessible to small and medium-scale farmers. On a broad scale, capillary wick irrigation methods required the installation of a cistern and a pipe network to allow for a frequent refill of the setup. Developed using results obtained for temporal changes in parameters of wetting geometry like the horizontal surface wetting width, maximum wetting depth, and maximum horizontal wetting width at a high correlation value. This study conducted laboratory tests, including a capillary rise test and an upward infiltration test, to determine black cotton soil's unsaturated hydraulic conductivity function.

The instantaneous profile technique and wetting have some similarities and differences. The method of front advancing was discussed. The data interpretation, demand specifics, and aspects seen throughout the test process and implementation of the capillary rise and downward infiltration tests were all summarized and examined. The method's flaws and countermeasures were discussed. This technique is better suited for small-scale irrigated agriculture. This technology has no negative environmental effects, is cost-effective, and does not require any electricity to operate. Efficient water management employing this indigenous technology can help alleviate the world's future water issues. The maximum wetted radius at and beneath the soil surface increased. The water and soil samples used in the experiment were tested

in the lab to determine the various parameters. The soil moisture is measured using rapid moisture meters.

## **2 Experimental Section**

### **2.1 Study Area**

The agricultural farm in the Surendranagar area of Gujarat state, the localized approach of “capillary wick irrigation” was tested. By road, the experimental site was around 23.0 km from Surendranagar city. In the district’s south, southwest, and central regions, the soils may be categorized into three primary categories: medium black soils, red sandy soils, and silty soils. Medium black soils are found at shallow depths (less than 5 m) when the primary rock block’s basalts/shale is exposed on the surface. In the central uplands, silty soils may be found in a small strip near the little Rann of Kachchh in the northeast, as well as shallow alluvial tracts and hard rock areas. Cotton accounts for 59% of the district’s agricultural production, followed by cereals (12%), sesamum (11%), bajra (8%), and wheat 4%.

### **2.2 Experimental Setup**

To construct and maintain an effective wick irrigation system, it is necessary to understand the wetted breadth, depth, and maximum wetted width under the soil’s surface. Black cotton soil, a 7-L P.V.C. pipe, and a wick with a diameter of 1 mm have all been included in the experiment box. Wick discharge and the timing of micro-irrigation may essentially auto-regulate it. In this study, an experimental setup consisting of a cubic container with dimensions  $2 \times 2 \times 2$  feet was utilized to investigate the temporal behavior of moisture distribution within soil. The focus was on both horizontal and vertical propagation of moisture from a point source located beneath the soil surface. The investigation centered on the temporal variations of key wetting geometry parameters, specifically, the maximum depth of wetting, the maximum width of horizontal wetting, and the width of wetting on a flat surface. Notably, a strong positive correlation was observed among these parameters. To accurately characterize the unsaturated hydraulic conductivity function of black cotton soil, a crucial aspect in this research, the study employed the wetting front advancement technique. This technique involved a series of laboratory tests, including capillary rise experiments and upward infiltration assessments. A comparative analysis was conducted between the primary profile method and the progressive advancement approach for soaking the front. The data interpretation for capillary rise experiments and downward infiltration tests required meticulous attention, necessitating a comprehensive compilation and examination of procedural aspects and practical applications.



**Fig. 1** Experimental box

Identifying certain limitations inherent to the method, the study outlined potential remedies for the observed drawbacks. Notably, on one side of the experimental container, acrylic material was integrated to mimic water flow dynamics, thereby enabling real-time monitoring of the phenomenon. This research contributes to the broader understanding of soil moisture dynamics and its hydraulic properties, shedding light on the complex interplay between wetting behavior and soil characteristics. On one side of the experiment box, acrylic was used to simulate water flow that could be observed with the self-monitoring (Fig. 1).

### **2.3 Laboratory Tests**

**Soil Quality Test:** According to IS 2720 (Part-IV)–1985 and IS 460–1978, a representative soil sample from the farm was analyzed for soil classification. A test for soil nutrients was also carried out on the soil sample. Testing of soil conducted at Gujarat State Fertilizer and Chemicals Limited (GSFCL), Morbi. As part of the recommendations given by GSFCL, mix well-composted compost while preparing the land in consideration of the laboratory’s report on the soil sample. Necessary biological

**Table 1** Details of quality testing of soil

OC %	0.76
P <sub>2</sub> O <sub>5</sub> (kg/Ac)	27.00
K <sub>2</sub> O (kg/Ac)	175.00
PH (1:2)	7.98
EC (1:2)	1.39
S ppm	16.20
Zn	1.20 (ppm)
Fe	8.56 (ppm)
Mn	27.94 (ppm)
Cu	1.88 (ppm)

**Table 2** Detailed quality of water utilized for irrigation

CO <sub>3</sub>	70 (ppm)
HCO <sub>3</sub>	466 (ppm)
CL	710 (ppm)
SO <sub>4</sub>	602 (ppm)
Ca <sup>++</sup>	72 (ppm)
Mg	48 (ppm)
Na	775 (ppm)
PH	7.33
Electric conductivity	3060

hazards such as azotobacter and phosphate culture should be used to increase agricultural yield, mix nitrogen, phosphorus, potassium (N.P.K.), and Urea, D.A.P., using such fertilizers is necessary. The report of the minerals present in the soil is given in Table 1, according to the soil testing report.

**Water Quality Test:** Water quality test was also conducted in GSFCL. The quality report suggested that the utilizing of this water is not recommended for irrigation. This water is harmful to the land and crop. Using this water for irrigation, thoroughly mix the gypsum into the soil. As often as possible, irrigate using the micro-irrigation method to maintain agricultural productivity with the right balance of soil and water. According to the water test report, the minerals in water can be seen in Table 2.

## 2.4 Wetting Front Movement

Wetting front movement is the horizontal and vertical movement of water in soil. It can be seen from the laboratory test of soil and water that it is possible to make agriculture only by changing the irrigation method and artificial changes in soil





**Fig. 2** Rapid moisture meter to measure water moisture in soil

minerals required for agriculture. Irrigation is done by the capillary wick irrigation method. At the same time, this method is used to study how moisture progresses in the soil, and raw crops are grown using the capillary wick irrigation method. Moisture in soil is tested with the rapid moisture meter. The amount of water in a soil sample is calculated using the gas pressure that results from the interaction of calcium carbide (an absorbent) and free water, where soil samples were collected from various depths, the moisture percentage was exclusively in the soil. Only the amount of moisture left in the soil from capillary action was measured after filling the underground storage tank with water (Fig. 2).

### 3 Results and Discussion

The results of soil nutrient testing and irrigation water quality testing indicated that the electrical conductivity (E.C.) of irrigated water was rather high. Such water is completely improper under regular circumstances. The water's chloride content was unacceptable. Additionally, there was a lot of salt in the water used for irrigation. Wick's exteriors were covered in salt. In addition, there was a reduction in the water diffusion rate via the wick. The strong electrical conductivity of the soil further revealed that the plant's access to water was only marginally constrained. The soil's maximum moisture content, as determined by the moisture measurement instrument, was 12.5%, which is quite close to the amount of moisture that soil of the suitable sand can keep.

Evaporation from the soil may cause reduced moisture content close to the surface. The moisture migration was more vertical than horizontal, as anticipated. Figure 3a–d illustrate the wetting front movement (percent Moisture) at 24, 48, 96, and 360 h, respectively. The moisture was found to be in the soil’s field capacity range after 96 h for a depth of between 30 and 50 cm from ground level (G.L.), but not at that level after 24 h. The moisture had not gotten to the depth of 50 cm from G.L. after 24 h. Additionally, after 24 h, the horizontal spread of water from the wick’s outer wall was far less than it was after 96 h. The wetness pattern resembled a balloon and reached a depth of 50 cm from the G.L. and a horizontal distance of 30 cm.

It is commonly acknowledged that this depth is an efficient zone for plant roots to draw moisture from the soil. After 96 h, the wetness front had begun to diminish, and after 15 days, it had vanished entirely. The wetting front is significantly influenced by how deeply the wick is buried in the dirt. The depth of the water circulation in the box increases with the depth at which the wick was positioned. The wetting front

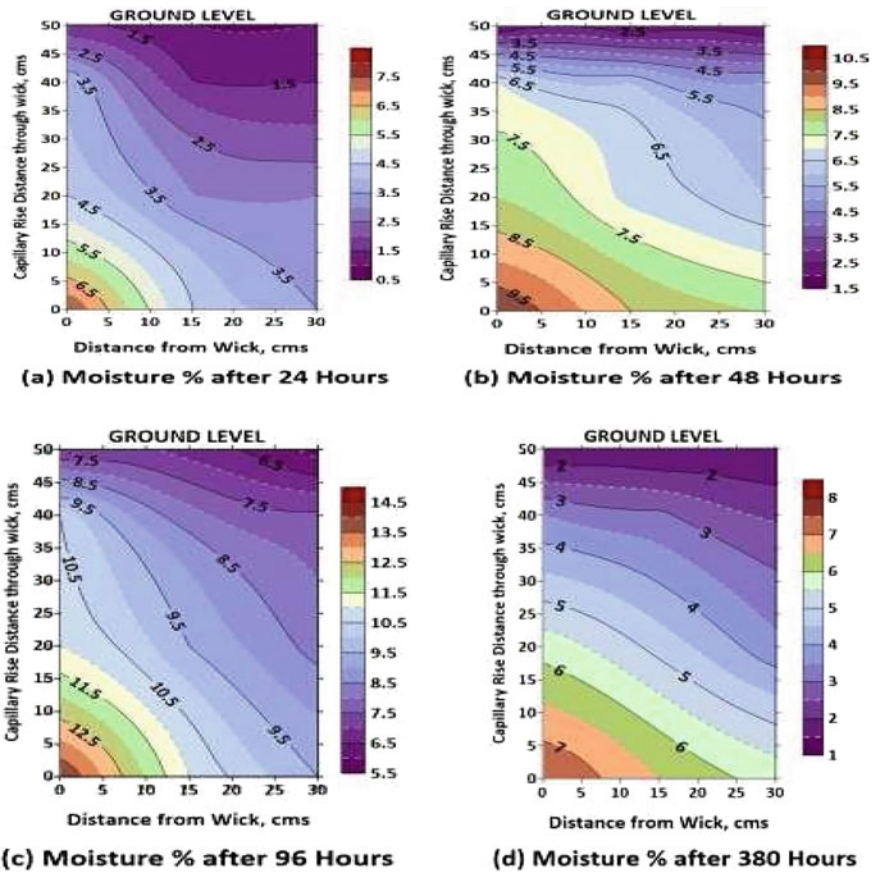


Fig. 3 Moisture level in soil a after 24 h. b after 48 h. c after 96 h. d after 360 h

obtained by the current depth used for the experiments was sufficient for crops with shallow roots, such as peas (root depth of 30–50 cm). It is advised that the farmer conducts a small experiment using a few wicks and the open excavation/pit method. This will allow the farmer to gauge the extent of moisture movement horizontally and vertically.

Broken pots or capsules may interfere with irrigation systems and reduce output in rocky soils, where capillary wick irrigation is difficult. It might be challenging to grow some plants with extensive root systems using this method. The clay pots and capsules could be hard to get or make. Small-scale agriculture is more suited for the usage of capillary wick irrigation. Contrarily, it is important to remember that rainwater harvesting may be used to collect enough water for the entire season in locations with scarcity (Bhatt et al. 2018). The essential aspect of the capillary wick irrigation approach is that it operates without electricity, has no adverse effects on the environment, and is affordable. The technique can be extremely helpful in resolving the water crisis. It can also improve the farmers' economic situation, reducing the number of small and marginal farmer suicides in the nation. Only 0.5% of households in India farm on more than 10 ha of land, and most farmers are typically small-scale or marginal farmers (Dagar et al. 2021).

## 4 Conclusions

As per the experiment, crop root zone depth up to 30–60 cm can be irrigated using the capillary wick irrigation technique, keeping soil moisture solely in effect. Even in places with the adverse condition of soil and water resources, it will be feasible to cultivate using the capillary wick irrigation method. The capillary process speeds up as the depth of the plant's roots grows. The crop will self-regulate as per water requirement of crop. Using this technique, it is essential to recognize row crops where plants thrive. Some shallow-rooted vegetable crops, such as celery, lettuce, onions, potatoes, and radish, as well as some moderately deep-rooted vegetable crops, such as broccoli, beans, cabbages, carrots, cauliflower, cucumbers, muskmelon, peppers, tomatoes, and zucchini, can be grown by using a capillary wick irrigation technique. This is due to the moisture distribution observed under capillary wick irrigation for alkaline soil using saline water for irrigation. In the future, these techniques can be utilized in farm and different types of soil with different types of crops to optimize the water and to save the water during irrigation.

**Acknowledgements** The corresponding authors would like to express their gratitude to Mr. Hasubhai Vyas, Mr. Haresbhai Dodiya, and Mr. Dalsukh Dabhi for their assistance with the field experiment and research and analysis work.

## References

- Abdelraouf RE, El-Shawadfy MA, Ghoname AA (2020) Improving crop production and water productivity using a new field drip irrigation design. *Plant Archives* 20(1):3553–3564
- Bhatt N, Kanzariya B, Motiani A (2018) An experimental investigation on pitcher irrigation technique on alkaline soil with saline irrigation water. *Int J Eng Sci Innov Technol*
- Dagar V, Khan MK, Alvarado R, Usman M (2021) Variations in Technical Efficiency of Farmers with Distinct Land Size across Agro-Climatic Zones: Evidence from India. *J Clean Prod* 315
- Ghosh M (2019) Climate-smart agriculture, productivity and food security in India 4(2):166–87. <https://doi.org/10.1177/2455133319862404>
- Gopal KNC, Lassaad B (2009) Indigenous pest and disease management practices in traditional farming systems in north east India. A review. *J Plant Breed Crop Sci* 1(3):28–038
- Kishore P, Singh DR, Chand P, Prakash P (2021) What determines groundwater depletion in India? A Meso level panel analysis. *J Soil Water Conserv*
- Kumar P, Sharma PK (2020) Soil salinity and food security in India. *Front Sustain Food Syst* 4:174
- Manjunatha AV, Speelman S, Chandrakanth MG, Van Huylenbroeck G (2011) Impact of groundwater markets in India on water use efficiency: a data envelopment analysis approach. *J Environ Manage* 92(11):2924–2929
- Rouzaneh D, Yazdanpanah M, Jahromi AB (2021) Evaluating micro-irrigation system performance through assessment of farmers' satisfaction: implications for adoption, longevity, and water use efficiency. *Agric Water Manag* 246:106655
- Saxena KC, Singh R, Pyasi SK, Mekale AK (2018) Evaluation of movement of wetting front under surface point source of drip irrigation in vertisols. *J Agric Eng* 55(2)
- Semananda NPK, Ward JD, Myers BR (2020) Experimental investigation of wicking bed irrigation using shallow-rooted crops grown under glasshouse conditions. *Irrig Sci* 38(2):117–129. <https://doi.org/10.1007/s00271-019-00651-5>
- Sharma BR et al (2010) Estimating the potential of rainfed agriculture in India: prospects for water productivity improvements. *Agric Water Manag* 97(1):23–30
- Talaviya T et al (2020) Implementation of artificial intelligence in agriculture for optimisation of irrigation and application of pesticides and herbicides. *Artif Intell Agric* 4:58–73
- Vyas U et al (2022) Matrix irrigation unit
- Wesonga JM et al (2014) Wick material and media for capillary wick based irrigation system in Kenya. *Int J Sci Res* 3(4):613–17

# One Dimensional Steady Flow Analysis Using HEC-RAS—A Case of Sabarmati River, Gujarat, India



Ujas Deven Pandya and Dhruvesh Patel

**Abstract** This study aims to examine the probability of over spilling from banks of Sabarmati River in reach between Gandhinagar and Ahmedabad for various return periods. The probable peak discharge for return periods of 20, 25, 30, 50, 60, 75, and 100 years calculated using Gumbel's frequency distribution and further simulated under steady condition in HEC-RAS 5.0.1 software. In present study, integration of Arc Map 10.0.1, HEC GeoRAS 10.0, and HEC-RAS 5.0.1 has been practiced to produce geometric data at every 200 m interval utilizing Cartoset 1 DEM. The flow hydrograph of the respective year at Chiloda Bridge, Gandhinagar, and normal depth at Vasna Barrage, Ahmedabad, have been selected as the upstream and downstream boundary, respectively. The flow is simulated under steady condition by selecting the computational time step of 1 min in HEC-RAS. The simulated maximum water surface levels have been compared for elevations of both the left (east) and right (west) banks of Sabarmati River for all the 190 numbers of cross sections. The cross sections having elevation lesser than relative water surface elevation on corresponding bank have marked as unsafe and have probability of water spill. The analysis concludes that the percentage of cross section prone to spilling of water during high discharge on left bank is 58% and for right bank is 35.33% for 20 year return period, while for 50 year return periods, it has come out as 67.01% on left bank and 44.16% on right bank. For all the return periods, it has been observed that left bank of Sabarmati River which represents east side of old wall city is more prone to water spill from higher water levels in river than the right bank of city locating on west side of river considered as new Ahmedabad city.

**Keywords** Sabarmati river · HEC-RAS · Flood flow modelling · Gumbel's frequency distribution

---

U. D. Pandya (✉)  
Government Engineering College, Gandhinagar, India  
e-mail: [ujaspandya82@gmail.com](mailto:ujaspandya82@gmail.com)

D. Patel  
PDEU, Gandhinagar, India  
e-mail: [dhruvesh.patel@sot.pdpu.ac.in](mailto:dhruvesh.patel@sot.pdpu.ac.in)

# 1 Introduction

Flood is surplus water inundated due to insufficient capacity of rivers to carry a high volume of water from the upstream area within their banks following heavy rainfall (NDMA 2008). India has witnessed total 649 disasters from 1915 to 2015; among which 302 disasters were caused by the flood which accounted approximately 47% of total disasters took place in India in the last 100 years (Tripathi 2015). In India, among all natural hazards, river floods are most recurrent and often destructive causing extensive losses of infrastructures, cultivation, transportation, community health, livestock, and human lives (Alam and Muzzammil 2011).

Hydrological simulation is old since it began discreetly in the 1850s. The development in modeling has occurred at an increasing rate, primarily due to easy access to almost enormous software power (Singh 2018). Researchers like (Kumar et al. 2017) have discussed about application of various 1D and 2D hydrodynamic models like HEC-RAS, HEC-HMS, LISSFLOOD-FP, MIKE-11, MIKE-21 and TELEMAR-2D, DAMBRK, FLDWAV, SMPDBK, and FLO-2D and suggested HEC-RAS as more proficient tool to produce more reliable outcomes in dam break analysis.

In recent years, the HEC-RAS hydraulic model, remote sensing (RS) technology, and geographic information system (GIS) have emerged as the primary tools for flood monitoring (Pallavi and Ravikumar 2022). Together, the GIS's ability to describe topographic characteristics and the hydraulic model's effectiveness in modeling flow for varied return periods produce very good results that can be utilized to create flood risk and hazard maps. (Demir and Kisi 2016). Nowadays researchers are using various hydraulic models in combination with GIS to simulate water flows. Many software packages like DWOPER, MIKE-11, CCHE2D, Infoworks-2D, RiverFLO-2D, etc., have been widely applied for simulating 1D and 2D flow in rivers (Taylor 2012; Bellos 2012). Researchers like Timbadiya et al. (2014) and Pramanik et al. (2010) have developed a stage-discharge relationship using one-dimensional MIKE 11 hydrodynamic model for lower Tapi River, India, and Brahmani River, India, respectively. Among all the available hydrologic models, freely available HEC-RAS (Brunner 2016) model is very handy means for forecasting of likely flood events to occur in future and used worldwide for flood prediction and management (Yamani et al. 2016). HEC-RAS is efficiently used worldwide to develop various and flood risk assessment and management for rivers like Pahang River, Malaysia (Ghani et al. 2019), Mert River, Turkey (ShahiriParsa et al. 2016), Martil River, Northern Morocco (Azouagh et al. 2018), Al Kahlaa and Hilla Rivers of Iraq (Awad 2015; Luay Kadhim and Tawfeek 2013), Senegal River Estuary (Diedhiou et al. 2020), and many more. Also in India HEC-RAS-based hydrodynamic model has been effectively developed for many rivers like Jhelum (Ahmad et al. 2016), Mahanadi (Parhi 2012), Tapi (Timbadiya et al. 2014; Patel et al. 2017), and Yamuna (Kumar et al. 2017).

1D modeling can help to predict the stages of the river while 2D modeling can give best results in terms of inundation and spread of water, which can be utilized to develop the flood warning and forecasting system (HEC-RAS 2016). For both 1D and 2D HEC-RAS models, precise geometry of river is prime requirement. At present,

very few surveyed cross sections are available for development of hydrodynamic model in India.

The case of Sabarmati River has been presented in this paper for flood stages assessment at different locations for flood management in lower Sabarmati catchment. It is also necessary for future flood protection work. Presently, there is no such system is on hand for Sabarmati which calculates water stages for discharge released from upstream. In this study, an attempt has been made to simulate probable peak discharge for various return periods using HEC-RAS hydrodynamic model under the steady flow condition for Sabarmati River, whereas geometric of the river is produced by 10 m grid interval Cartoser-1 DEM using a HEC GeoRAS tool.

## 2 Study Area and Data Collection

### 2.1 Sabarmati River

The Sabarmati basin is located between the longitudes of 70° 58' and 73° 51' East and the latitudes of 22° 15' and 24° 47' north. The River Sabarmati rises from the Aravalli hills at Tepur in Rajasthan's Udaipur district at an elevation of 762 m.

The most significant structure in the Sabarmati River is the 1978-built Dharoi Dam. It is located on the Sabarmati River about 165 km upstream from Ahmedabad, near Dharoi village, Mehsana and 103 km from the river's source. Line diagram shown in Fig. 1 indicates major structures located across Sabarmati River from Dharoi Dam to Vasna Barrage.

There is currently no mechanism in place to forecast how the river will act when a higher flow from the Upstream is released. The specific part of the study area includes the two most significant cities of Ahmedabad and Gandhinagar, the former of which is a major industrial hub and designated as first world heritage city, and the latter of which is state capital. Thus, in terms of flood planning and control, the specific 39 km length of river proves to be very significant.

For the development of a model for the 39 km patch of the Sabarmat, the Chiloda Bridge in Gandhinagar near Palaj village is used as an upstream boundary and

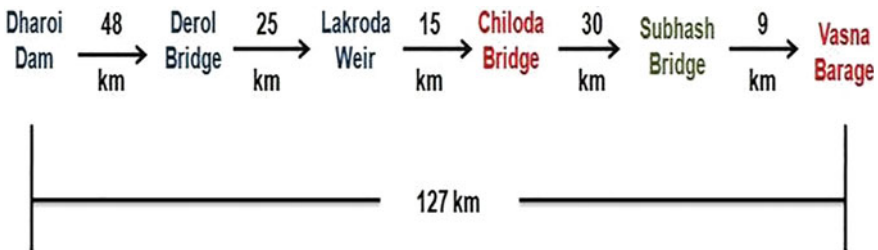


Fig. 1 Line diagram of study area from Chiloda Bridge to Vasna Barrage



the Vasna Barrage as a downstream boundary. Between Chiloda Bridge and Vasna Barrage, there are a total of 12 bridges, including one storage reservoir named Sant Sarovar located around 6 km downstream of Chiloda Bridge.

## ***2.2 Flood History***

The average rainfall of Ahmedabad is about 98.2 cm (36.7 Inches). Infrequent heavy torrential rain causes flood to the River Sabarmati. The city has experienced floods at every two to three years interval. The Sabarmati River basin has a catchments area of about 21,700 km<sup>2</sup>. There are two major dams in upstream River Sabarmati, one at Dharoi and second on a tributary Vatrak River. These dams have been constructed with an objective of conservation of water for agriculture and drinking water purpose. The dams have a gated spillways and outflows aggravating the flood situation in Sabarmati basin. There is also a Vasna Barrage on River Sabarmati within Ahmedabad. During flood situation, the gates on this barrage are opened, and it does not impede flood flows. Ahmedabad reaches a record high flood level at 47.45 m at Subhash Bridge on August 19 and 20, 2006 surpassing the previous record level of 44.09 m in 1993. Initial warning level is 44.09 m, and danger level is 45.35 m. Runoff generated in the lower catchments was increased by release from Dharoi and Vatrak dams. Inflow and outflow were almost same at the time of water release from both the dams. This shows that both the dams have not been constructed with an objective of mitigating floods in downstream area. The city remains flooded for two to three days.

## ***2.3 Data Collection***

The basic data required for the hydrologic model can be mainly divided into two parts, namely hydrologic data and geometric data. Hydrological data like past flood data, discharge of the river, gauge, and water surface elevation for Chiloda Bridge and Subhash Bridge are collected from State Water Data Center (SWDC) and Central Water Commission (CWC) respectively. The Indian Society of Remote Sensing's (ISRS) Cartosat-1 stereo data were used to generate the topology of the Sabarmati River in HEC-RAS. Digital elevation model (DEM) of 10 m grid was generated using Cartosat-1 stereo data with the help of Bhaskaracharya Institute for Space Applications and Geo-Informatics (BISAG) (Table 1).

The very first Indian remote sensing satellite, Cartosat-1, was intended for topographic mapping and is capable of acquiring in-track high-resolution stereo images with a pixel size of 2.5 m. The image quality, tested through radiometric and geometric characteristics of the Cartosat-1 stereo pairs, also gave fine results. Using a suitable method for geometry modeling, the generation of the corresponding DEM produced good results that are appropriate for the operational use in planning and



**Table 1** Details of data required and its application in study

Type data	Details	Source of data	Use in study
Hydrologic data	Hourly discharge and WSE	SWDC, CWC	Simulation of 1 D steady flow model
Annual peak discharge	1981–2015 (35 years)	SWDC	Flood frequency analysis
River geometry data	Every 200 m interval, Major bridge locations	CWC, SWDS, HecGeo RAS, Field Survey	Simulation of 1 D steady flow model
DEM of Ahmedabad city	Cartoset 1 (10 m grid)	ISRO, BISAG	Development of river geometry

development of natural watersheds. According to the findings of Jena et al. (2016), a reasonably accurate DEM developed from a moderate survey in a data-scarce region may be utilized to derive the required river cross sections for hydrodynamic modeling.

### 3 Objective of the Study

The problem is defined in this study as the release of heavy discharge from Dharoj Dam, such as 8800 cumec (approximately 3 Lac cusec), causes water spillover from the banks in low lying areas due to increased depth of water in river, after discussion with officials of the state irrigation department and Ahmedabad Municipal Corporation, followed by a literature review. There is currently no tool or model available that estimates the likely region of water spill on either bank of the river for equivalent upstream discharge. As a result, the primary goal of this research is to create a one-dimensional steady model of the Sabarmati River in order to estimate river stages for peak discharge corresponding to 5-year–100-year return periods at various locations.

### 4 Methodology

The study has started by surveying literature about flood history of Sabarmati River followed by various hydrodynamic models and its application for flood mitigation and management practices in recent decades. A study of flood history and Gumbel's flood frequency analysis has been done for last 35 years before development of hydrodynamic model. It has been observed from literature study that generally all research works done are by taking mostly physically surveyed geometric data or by collecting surveyed data from concern government agencies. During data collection from various state and central government departments like SWDC, CWC, and AMC, it has been faced and observed that the availability of latest and authentic surveyed

data specially required for development of hydrodynamic model is a major problem. Hence, DEM-generated geometric data have been used in this study for simulation of 1D steady HEC-RAS hydrodynamic model.

#### ***4.1 Flood Probability Analysis—Gumbel’s Method***

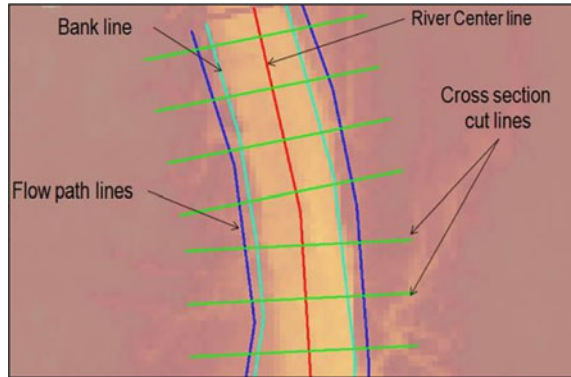
A flood frequency analysis attempts to determine how often a specific area can encounter a flood of a specific size. We can predict floods with the aid of estimated recurrence intervals and discharge incidence probabilities, which may also be applied to flood management planning. Recurrence interval is the length of time (years) between occurrences of a specific flood magnitude. The probability of happening of a particular discharge is the reciprocal of the recurrence interval. Flood frequency information can be determined from past information of peak discharge in any given year.

After studying literature regarding flood history of Sabarmati River and Ahmedabad city, the flood frequency analysis has been carried out using Gumbel’s flood frequency analysis. In this analysis, annual peak discharge of past 35 years from 1981 to 2015 has been considered and following Gumbel’s steps mean, standard deviation has been calculated. Flood flow for different return periods has been calculated using Gumbel’s coefficient K, mean and standard deviation. The graph has been plotted for return period versus flow discharge and best fit function for this graph comes out as fifth-order polynomial having  $R^2$  as 0.995. This function has been used further in study to calculate future discharge for various return periods to run 1D steady flow in HEC-RAS.

#### ***4.2 Geometry Generation in HEC GeoRAS***

For development of any hydrodynamic model, an accurate representation of ground surface elevations is a primary requirement. A high-quality terrain model precisely illustrates the elevations of the river and floodplain by including various physical features like the channel banks and channel bed and other high ground features such as roadways and levees by which the flow is directed. For this study, availability of geometric data at desired interval of 200 m is a major challenge. The only data available with government agencies are at Chiloda Bridge and Subhash Bridge. Also, to produce elevation data at every 200 m interval for the entire patch of 39 km was time consuming and practically not possible. So, desired geometric data of study area have been generated using Cartosat 1 digital elevation model (DEM) of 10 m resolutions. Following are the stepwise procedure, adopted for generating geometric data in HEC GeoRAS tool.

**Fig. 2** River geometry created in HEC GeoRAS



- Add DEM in Arc Map using Add Data tool
- Select terrain type and desired DEM in layer setup for HEC-RAS pre-processing
- Create and digitize various RAS layers like stream center line, banks, flow paths, and cross sections from RAS geometry one by one as shown in Fig. 2. The layers can be modified by using Editor Tool.
- Digitize stream center line in reference with DEM and available base map and assign suitable river code and reach code to stream.
- Assign stream center line attributes like topology, lengths, stations, and elevations.
- Digitize bank lines in reference with selected DEM and base map.
- Digitize flow path center lines in direction of flow in both sides along the river center line.
- Assign line type attributes line right, channel and left to relative flow path lines. For this, left and right banks are considered in direction of flow.
- Generate cross sections directly (of desire width and at desired interval) by using construct XS cut line tools or by manually digitizing. For generating cross sections directly, the maximum width of the channel has to be considered, and accordingly, single value of cross section width needs to be considered so that all the directly generated cross sections can either touch or cross the flow path lines on both the sides. For this study, cross sections are generated directly for spacing of 200 m and width of 1000 m as shown in Fig. 3.
- Assign XS cut line attributes like River and Reach name, stationing, bank stations, downstream reach lengths, and elevations from RAS geometry tool.
- Export GIS to RAS using export RAS data from RAS geometry tool and save to your directory.
- Import geometry data by selecting GIS format in geometric data in HEC-RAS.

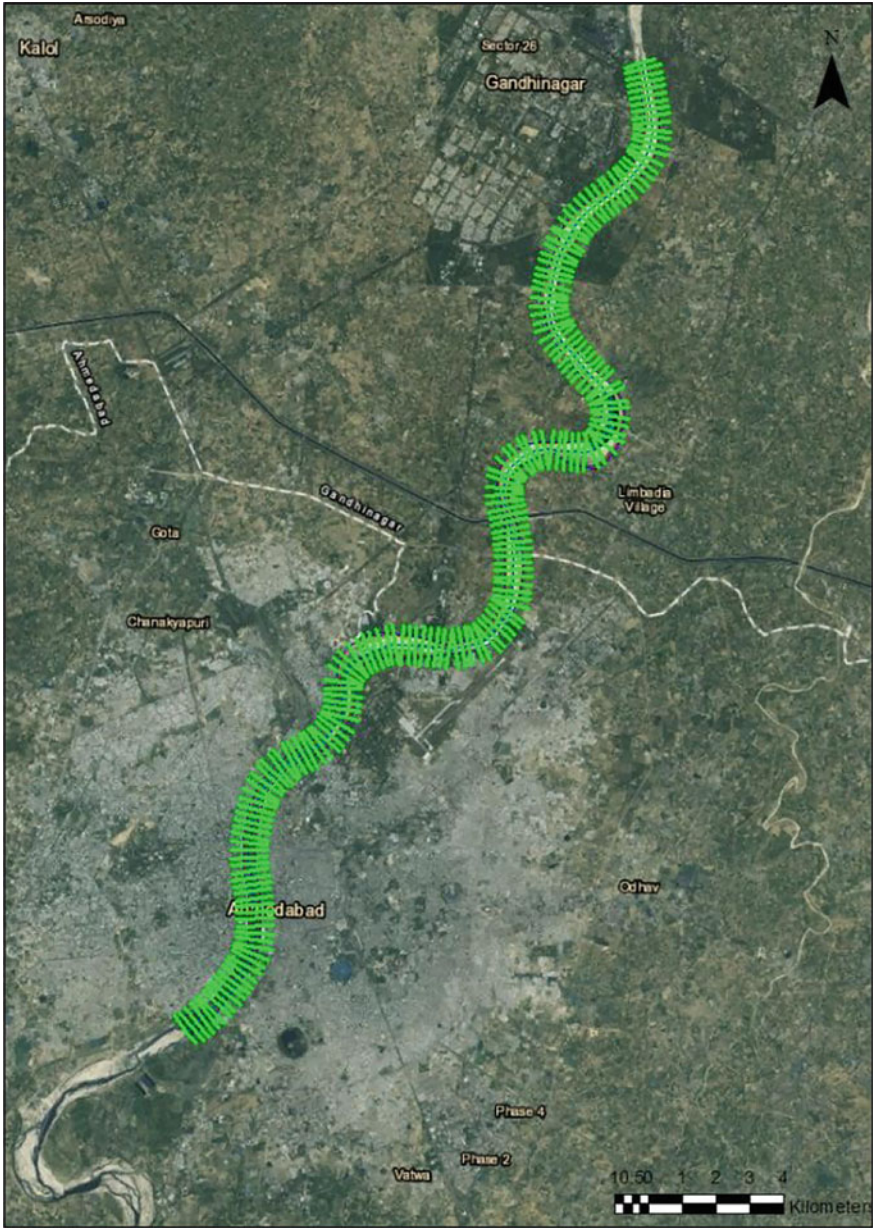


Fig. 3 Cross sections of Sabarmati River extracted from HEC GeoRAS

### 4.3 1D Steady Flow Simulation

To simulate a one-dimensional model in HEC-RAS, prime inputs are geometric data in terms of cross sections and bank levels, hydrologic data in terms of upstream and downstream conditions, and manning’s roughness coefficient. The required geometric data at every 200 m interval along the entire study reach have been generated using the HEC GeoRAS tool in ArcGIS 10.0.1 software. Further, the hydrological data are required to assign upstream and downstream boundaries of the river. The upstream boundary conditions can be given as either stage hydrograph or flow hydrograph of that location and the downstream boundary can be given as any of among stage hydrograph, flow hydrograph, rating curve, and normal depth. As given in Fig. 4, following steps are adopted for development of 1D HEC-RAS steady flow simulation integrating HEC GeoRAS and HEC-RAS.

To determine the upstream and downstream boundary conditions for this study, the flow hydrograph from the year 2006 at Chiloda Bridge and the normal depth at Vasna Barrages are considered. The model is simulated for 1 min of computation time step and 1 h of output storage interval for peak discharge of year 2006 flood event. Manning’s ‘*n*’ of 0.025 has been considered for the whole reach for simulation of the aforesaid model (Chow 1959). The simulated stage hydrographs for various return periods have been studied and compared with R.L. of left and right bank of the Sabarmati for entire length of 38 km considered for study.

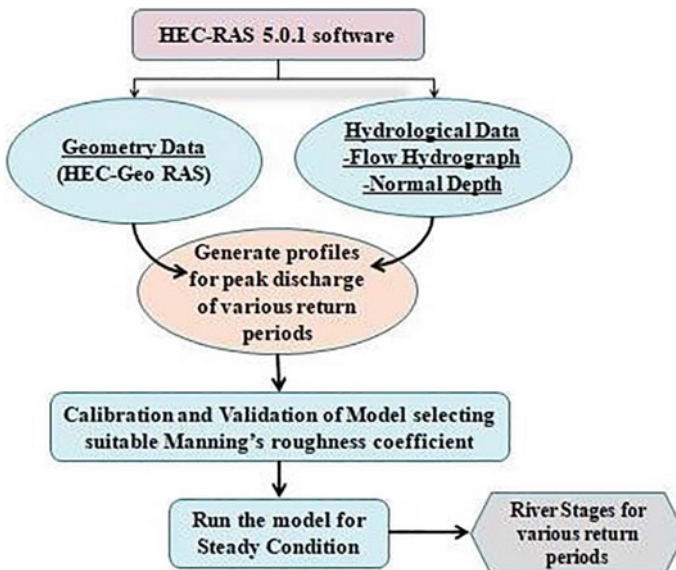


Fig. 4 Methodology chart for 1D steady HEC-RAS model

### 5 Results

The one-dimensional simulation of flow under steady condition has been performed for probable discharge of return period of 20, 25, 30, 50, 60, 75, and 100 years using HEC-RAS. The probable discharge calculated for various return periods using Gumbel's flood frequency analysis has been used to simulate steady HEC-RAS model. The geometric data and hydrological data have been considered the same as of unsteady flow simulation. The maximum water surface elevation for each profile has been simulated and maximum water surface elevation of 20 year and 100 year return period have been plotted against elevations of both side banks as presented in Figs. 5 and 6 respectively to check for overflowing of water from the either banks.

From the above graphical representation of maximum water surface elevation corresponding to elevations of left and right bank gives probability of water to get spill over from the particular banks. It has been observed that the left bank representing the east side of the river is more vulnerable to water spill than the right bank representing the west side of the river. The river is represented as total 190 number of cross sections from Gandhinagar city of Ahmedabad city, and probability of number of cross sections on both the sides of banks has been calculated to check the vulnerable

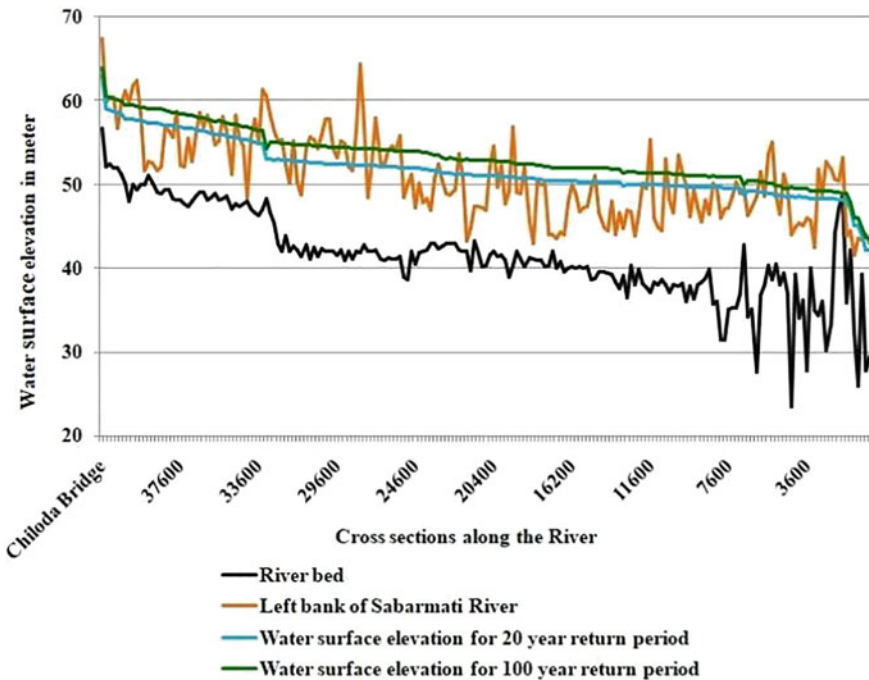
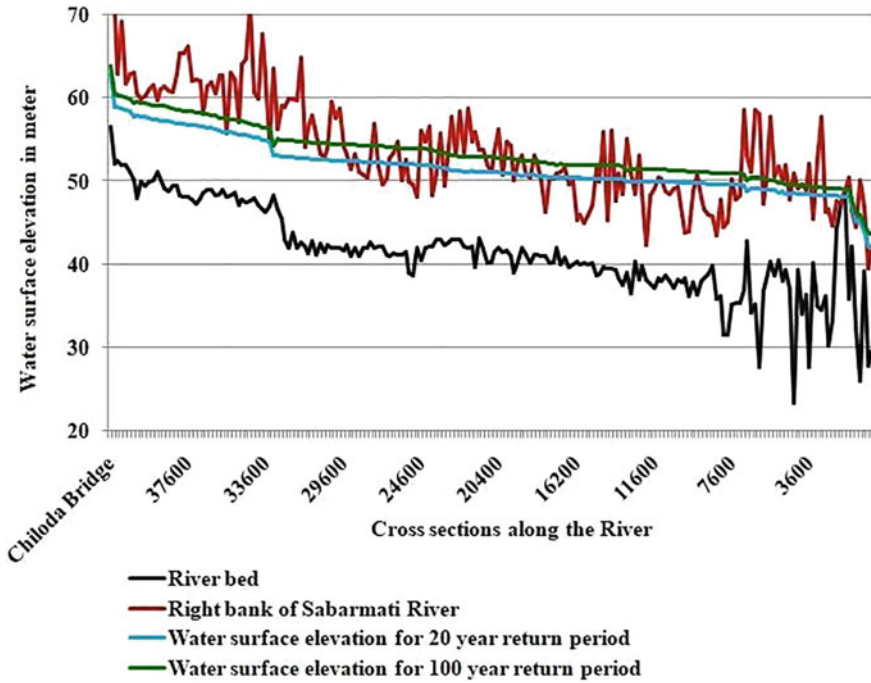


Fig. 5 River stages for peak discharge of 20 years and 100 years return period, Left bank of Sabarmati River





**Fig. 6** River stages for peak discharge of 20 years and 100 years return period, Right bank of Sabarmati River

zone for high water level for different return period of the Sabarmati River as shown in Table 2.

The probable peak discharge for return periods of 20, 25, 30, 50, 60, 75, and 100 years calculated from Gumbel’s frequency distribution has been simulated under

**Table 2** Calculation of probability of inundation of cross sections along left and right bank of Sabarmati for various return periods

Return period in years	Discharge in cumec	Percentage of C/s inundated on left bank (East)	Percentage of C/s inundated on right bank (West)
20	4845.27	58.88	35.53
25	5185.84	60.41	36.55
30	5465.72	61.93	37.06
50	6239.59	67.01	44.16
60	6514.41	69.54	45.18
75	6849.93	71.07	48.73
100	7451.83	74.11	51.27

steady condition, and maximum water surface levels have been compared for elevations of both the left (east) and right (west) banks of Sabarmati River for all the 190 numbers of cross sections. River sections that are identified as dangerous and likely to have a water spill are those where the elevation is lower than the relative water surface elevation on the respective banks. As shown in Table 1, the percentage of cross section prone to spilling of water during high discharge on left bank is 58.88% and for right bank is 35.53% for 20 year return period, while for 50 year return periods, it has come out as 67.01% on left bank and 44.16% on right bank. For all the return periods, it has been observed that left bank of Sabarmati River which represents east side of old wall city is more prone to water spill from higher water levels in river than the right bank of city locating on west side of river considered as new Ahmedabad city. Though, during literature study and discussion with government authorities, it has been learned that the west side of the city faces more inundation problems than east side due to insufficient storm water drainage network and difficulty of rainwater to drain out during torrential rain.

## 6 Conclusion

Through the establishment of a one-dimensional HEC-RAS model, the prime objective of the current effort is to determine the efficacy and usability of DEM generated cross sections in conjunction with the HEC-RAS model for calculating water surface elevation in a river. The manning's value has been calibrated as part of the creation of a 1 D model, and the influence of changes in model output corresponding to DEM resolution and cross section spacing has also been examined and analyzed.

Results generated by comparing various stages in the river with corresponding bank levels indicate the percentage of probable areas to be inundated for equivalent discharge released from upstream. Despite the limitations of the 1D HEC-RAS model and the lack of sufficient gauging stations for results validation, the model has the capacity to compute river stages for relative discharge from upstream for varied return periods. The current approach will simplify 1D modeling and fill in the gaps in essential modeling data sets for the construction of a Dharoi Dam Emergency Action Plan. It also speeds up the modeling process, making it a very important means for engineers to employ in 1D hydrodynamic modeling. Planners and decision-makers can use the hydraulic parameters obtained by the one-dimensional steady HEC-RAS model to construct flood prevention approaches and flood inundation maps considering various return periods. This study acts as a framework for all concerned in developing a decision-making system in places where available record is inadequate.



## 7 Limitation of Study

For this study, surface roughness coefficient is considered same for the whole length of Sabarmati River which can be improved by selecting a different combination of manning's roughness coefficient for different patches of the river as well as the side of banks considering types of surface and vegetation cover to improve results.

## 8 Future Scope

1D simulation gives results in terms of stages only, which can be further replaced by 2D HEC-RAS analysis for a range of return periods to ensure the spread of the inundated water over the nearby area with precise geometric data.

**Acknowledgements** Authors are thankful to the Central Water Commission (CWC), State Water Data Centre (Govt. of Gujarat, India), and Ahmedabad Municipal Corporation (AMC) for providing data to carry out this study. Authors are very thankful to Bhaskaracharya Institute for Space Application and Geo-Informatics (BISAG) for providing all the support in producing DEM.

## References

- Ahmad HF, Alam A, Bhat MS, Ahmad S (2016) One dimensional steady flow analysis using HECRAS—a case of River Jhelum, Jammu and Kashmir. *Eur Sci J ESJ* 12(32):340
- Alam J, Muzzammil M (2011) Flood disaster preparedness in Indian scenario. *Int J Recent Trends Eng Technol* 5:33–38
- Awad AM (2015) Mathematical modeling of unsteady flow for AL-Kahlaa regulator river. *J Eng* 05(02):9–20
- Azough A, El Bardai R, Hilal I, Stitou el Messari J (2018) Integration of GIS and HEC-RAS in Floods Modeling of Martil River (Northern Morocco). *Eur Sci J ESJ* 14(12):130
- Bellos V (2012) Ways for flood hazard mapping in urbanised environments: a short literature review. *Water Util J* 4:25–31
- Brunner GW (2016) HEC RAS\_5.0\_Reference\_Manual.pdf (Feb 2016)
- Chow VT (1959) *Open channel hydraulics*
- Demir V, Kisi O (2016) Flood hazard mapping by using geographic information system and hydraulic model: Mert River, Samsun, Turkey. *Adv Meteorol Hindawi Publ Corp*
- Diedhiou R et al (2020) Calibration of HEC-RAS model for one dimensional steady flow analysis—a case of Senegal River estuary downstream Diama Dam. *Open J Mod Hydrol* 10(03):45–64
- Ghani AA, Kashfy M, Kashfy Zainalfikry M (2019) HEC-RAS one-dimensional hydrodynamic modelling for recent major flood events in Pahang River
- HEC-RAS (2016) *Hydraulic reference manual version 5.0*, p 547
- Jena PP, Panigrahi B, Chatterjee C (2016) Assessment of Cartosat-1 DEM for modeling floods in data scarce regions. *Water Resour Manag* 30(3):1293–1309
- Kumar N, Lal D, Sherring A, Issac RK (2017) Applicability of HEC-RAS and GFMS tool for flood modeling of the river: a case study of River Yamuna at Allahabad (Sangam), India. *Model Earth Syst Environ* 2017(3):1463–1475

- Luay Kadhim H, Tawfeek AS (2013) Estimating of manning's roughness coefficient for Hilla River through calibration using HEC-RAS model
- NDMA (2008) National disaster management guidelines
- Pallavi H, Ravikumar AS (2022) Analysis of unsteady flow using HEC-RAS and GIS techniques. Lecture Notes Civil Eng 234:355–366
- Parhi PK (2012) Calibration of channel roughness for Mahanadi River, (India) using HEC-RAS Model. J Water Resour Prot 04(10):847–850
- Patel DP, Ramirez JA, Srivastava PK, Bray M, Han D (2017) Assessment of flood inundation mapping of Surat city by coupled 1D/2D hydrodynamic modeling: a case application of the new HEC-RAS 5. Nat Hazards 89(1):93–130
- Pramanik N, Panda RK, Sen D (2010) One dimensional hydrodynamic modeling of river flow using DEM extracted river cross-sections. Water Resour Manag 24(5):835–852
- ShahiriParsa A et al (2016) Flood hazard mapping by using geographic information system and hydraulic model: Mert River, Samsun, Turkey. Air, Soil Water Res 7(3):38–45
- Singh VP (2018) Hydrologic modeling: progress and future directions. Geosci. Lett 5(1)
- Taylor P (2012) Flood inundation simulation in Ajoy River using MIKE-FLOOD. J Hydraul Eng 18(2):129–141
- Timbadiya PV, Patel PL, Porey PD (2014) HEC-RAS based hydrodynamic model in prediction of stages of lower Tapi river. ISH J Hydraul Eng 17(2):110–117
- Tripathi P (2015) Flood disaster in India: an analysis of trend and preparedness. Interdiscip J Contemp Res 2(4):91–98
- Yamani K, Hazzab A, Sekkoum M, Slimane T (2016) Mapping of vulnerability of flooded area in arid region. Case study: area of Ghardaïa-Algeria. Model Earth Syst Environ 2(3):147

# Reliability–Resilience–Vulnerability Analysis of Droughts Over Maharashtra



Gaurav Ganjir, M. Janga Reddy, and S. Karmakar

**Abstract** Extreme events are one of the serious challenges society is facing with the changing climate; extreme events like droughts have a significant impact on both human and animal livelihood. In India, one of the most frequent natural calamities is drought, and its assessment is required in order to support policy makers and water managers in the region. This study presented reliability–resilience–vulnerability (R–R–V) analysis of droughts, which uses the duration and severity of drought properties, estimated using the Standardized Precipitation Index (SPI). The study is carried out over Maharashtra (grid-wise) at 0.25° resolution using the precipitation data collected from India Meteorological Department (IMD) for a period of 41 years (1980–2020). The spatial variation of drought parameters, duration and severity at 50, 70, and 90 percentile levels are plotted and analysed to elucidate the regions that have higher drought risks. The most resilient areas are Amaravati, part of the Nashik, and Konkan division. Nagpur and Aurangabad divisions require utmost attention as they have the least reliability. The R-R-V maps of Maharashtra strongly show that the Aurangabad division has the highest drought risk among the other divisions. The results clearly show that Vidarbha and Marathwada are more prone to droughts. The RRV index map showed Latur, Beed, Parbhani, Chandrapur, and Nagpur fall under high to very high category of drought risk. The spatial plots give a clear picture of the areas that require immediate action and thus can be helpful for decision-makers and government bodies.

**Keywords** Reliability · Resilience · Vulnerability · Severity

---

G. Ganjir (✉) · M. Janga Reddy · S. Karmakar  
IIT Bombay, Mumbai, India  
e-mail: [214406001@iitb.ac.in](mailto:214406001@iitb.ac.in)

M. Janga Reddy  
e-mail: [mjreddy@civil.iitb.ac.in](mailto:mjreddy@civil.iitb.ac.in)

S. Karmakar  
e-mail: [skarmakar@iitb.ac.in](mailto:skarmakar@iitb.ac.in)

# 1 Introduction

In the natural climate cycle, drought is a prolonged dry period that can happen anywhere in the world. It is a calamity that develops slowly and is defined by a lack of precipitation that causes a water scarcity. In India, one of the most frequent natural calamities is drought. One third of the country is either prone to drought or covered by desert due to its increased frequency and wider distribution in recent years. Both in terms of agriculture and overall economic growth, these regions fall behind. Drought can have a terrible consequence on agriculture, health, energy, economies, and the environment. Drought is one of the extreme events which not only causes in a short-term impact, but it may also have a severe long-term impact, and it increases with its frequency and duration over the same region. The consequences lead to the migration of people and animals and leave behind barren land; hence it is very important to have a drought assessment for every region. Several studies over the globe and in India have shown an increasing trend of drought with climate change and global warming.

Extreme events are one of the serious challenges society is facing with the changing climate (Ganjir et al. 2022). The underlying processes causing the drought are reduction in precipitation or altered precipitation patterns, as well as increased evaporative demands brought on by higher temperatures. Around 30% of the emerging areas will experience current 100-year droughts (severe droughts that currently only happen once per 100 years) with a 3°C increase in temperature (Naumann et al. 2018). These scenarios show that if appropriate steps are not made to mitigate and adapt to climate change, the risk of drought will increase for many economic sectors and vulnerable areas. Droughts could cause major losses in many areas of the world with large population concentrations and susceptible communities that rely on local agricultural production. Drought management and adaptation will continue to be based on better-targeted impact monitoring and quantification in these areas. One consequence of recent climate change, characterized in particular by rising global temperatures, is a rise in the frequency of weather-related extreme events (IPCC 2014). Drought is not an exception, and in recent years, scientific literature has noted a general trend towards increasingly frequent and severe droughts (Dai 2013).

India is agriculture-based country, and a huge ratio of population is completely dependent on it. The below normal precipitation is great trouble for the farmers as they mostly rely on the monsoon. The drought is like curse for farmers. Mahmoudi et al. (2021) studied the change in spectral patterns of droughts in Iran based on the concepts of reliability, resilience, and vulnerability (RRV). Integration of climatic variables with R-R-V indicators is helpful for generating drought information (Hazbavi and Sadeghi 2017). The Drought Management Index (DMI) was calculated as a five-year time series at each grid point using joint cumulative distribution functions (CDF) of resilience and vulnerability by Chanda et al. (2014).

The reliability–resiliency–vulnerability (R-R-V) framework is used in this study to analyse drought. To evaluate potential changes in the drought features of Maharashtra, an aggregate index of RRV was applied. The region’s drought characteristics can be analysed using this method, and long-term drought planning strategies can be developed for the region. In the following, Sect. 2 contains study area and data details, Sect. 3 gives details of methodology, Sect. 4 discusses the application and results, and finally, the conclusions of the study are given in Sect. 5.

## 2 Study Area

The study area considered for drought analysis is Maharashtra state, in India. Maharashtra occupies 307,713 km<sup>2</sup>, or 9.36% of the nation’s total land area, and is situated in the western peninsular part of the country. The state is bounded on the north by Gujarat and Madhya Pradesh, on the east by Chhattisgarh, on the south by Telangana, Karnataka, and Goa, and on the west by the Arabian Sea. It is situated between 15° 35′ N and 22° 02′ N latitude and 72° 36′ E and 80° 54′ E longitude. Deccan Plateau, Western Ghats, and West Coast are the three physiographic zones of the state. It has a tropical monsoon climate, which includes hot, rainy, and cold seasons as well as dry summers. The yearly temperature varies from 25 to 27 °C, while the annual rainfall ranges from 400 to 6000 mm. Several rivers, including the Bhima, Godavari, Koyna, Krishna, Tapti, and Narmada, drain the state. Thirty-five districts, including 12 tribal and 7 hill districts, make up the state. According to the 2011 census, Maharashtra has a population of 112.37 million, or 9.28% of all the residents in India. While 45.22% of people reside in cities, 54.78% live in rural areas. 9.35% of the state’s population is tribal. The state has a 365 person per square kilometre population density, which is similar to the national average. Semiarid climatic conditions represent about 83% of Maharashtra’s land area. The study area map is shown in Fig. 1.

The rainfall data is taken from IMD daily data at 0.25° × 0.25° resolution for the period of 1980–2020. The daily data is converted into monthly data using the climate data operator (CDO) command.

## 3 Methodology

The meteorological drought is identified by using Standardized Precipitation Index (SPI). For the computation of SPI index, the frequency distribution of precipitation is modelled by a two- parameter gamma probability density function in the original SPI (McKee et al. 1993; Ganguli and Reddy 2012):

$$g(x) = \frac{1}{\beta\Gamma(\alpha)} x^{\alpha-1} e^{-\frac{x}{\beta}} \quad (1)$$



The drought parameters, namely duration and severity, are defined as follows. The number of continuous periods (months) during which the SPI remains below the designated threshold value ( $SPI < 0.8$ ) is considered the length or duration of the drought ( $D$ ). The cumulative SPI readings over the course of the drought duration are drought severity ( $S$ ).

$$S_i = \sum_{t=1}^D SPI_{i,t} \quad (4)$$

The reliability, resilience, and vulnerability are calculated using the following definitions.

### 3.1 Reliability

The probability that a system is in a satisfactory state defines reliability (Hashimoto et al. 1982). Reliability in the context of SPI can be described as the probability that the SPI is higher than a specific threshold. Hence, the reliability is given as (Sung et al. 2018).

$$\text{Reliability} = 1 - \frac{\sum_{j=1}^M d(j)}{T} \quad (5)$$

where  $d(j)$  is the duration of  $j$ th drought event,  $T$  is the total number of time intervals, and  $M$  is the total number of the drought events.

### 3.2 Resilience

Resilience measures how quickly a system can improve once it has dropped below the threshold for satisfactory performance (Sung et al. 2018).

$$\text{Resilience} = \left\{ \frac{1}{M} \sum_{j=1}^M d(j) \right\}^{-1} \quad (6)$$

### 3.3 Vulnerability

Vulnerability is the likely value of deficits  $v(i)$ , if they occur. Vulnerability can be thought of as the average failure because it essentially indicates the intensity of failures. The vulnerability is calculated as the average of the overall deficit, which is calculated by dividing the total number of deficit events by the sum of all the deficits (Sung et al. 2018; Veetil et al. 2018).

$$\text{Vulnerability} = \frac{1}{M} \sum_{j=1}^M v(j) \quad (7)$$

where  $v(j)$  is the value of deficits of  $j$ th drought event. After calculating the reliability, resilience, and vulnerability, using the extreme standardization procedure, they were standardized to range from zero to one (Loucks 1997; Hazbavi and Sadeghi 2017).

$$N = \frac{(X_i - X_{\min})}{(X_{\max} - X_{\min})} \quad (8)$$

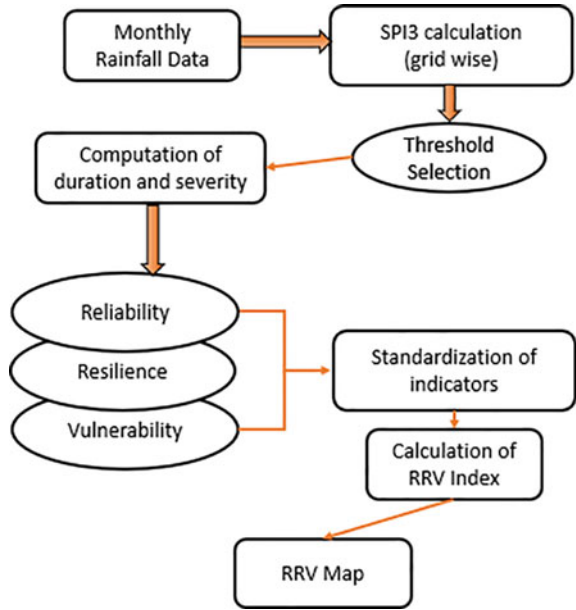
where  $X_i$  is the value being considered,  $X_{\min}$  and  $X_{\max}$  are the minimum and maximum observed values, respectively, and  $N$  is the standardized value of each individual indicator. Since reliability and resilience fall in cost criteria, standardized value is given by  $(1 - N)$  and for vulnerability given by  $N$ . Finally, after standardization of R-R-V indicators, the geometric mean, as indicated in Eq. (9), was used to express the aggregated RRV index. Because it is more sensitive to changes in individual variables than other averages, the geometric mean was chosen for the study (Loucks 1997; Yu et al. 2013).

$$G_{RRV} = [\text{Rel.Rev.Vul}]^{1/3} \quad (9)$$

Where, Rel, Rev and Vul stands for standardized reliability, resilience, and vulnerability respectively. Based on the RRV index, a five-category classification scheme was devised to rate the drought- prone areas from high to low. This was suggested by Ding et al. (2008) and Yu et al. (2013) “Very high (0.81–1.00)”, “high (0.61–0.80)”, “moderate (0.41–0.60)”, “low (0.21–0.40)”, and “very low (0.00–0.20)” are the names of the five classes (I–V). The greater the value, the more susceptible the area is to drought. The flow chart of research methodology is shown in Fig. 2.



**Fig. 2** Flow chart of RRV framework to analyse droughts



## 4 Results and Discussion

### 4.1 Total Number of Drought Events

The spatial variation plot of total number of drought events occurred in the Maharashtra region (grid wise) is shown in Fig. 3. The figures clearly show that the Nagpur division and Aurangabad division and Solapur, Aloka, and Yavatmal districts have the highest number of drought events in years between 1980 and 2020 they have 40–45 drought events and other districts have drought events between 20 and 38. The least number of drought events is seen in the part of Nashik, Buldhana, Thane, and Pune districts.

### 4.2 Spatial Variation of Drought Parameters: Duration and Severity

The duration and severity grid-wise plot is shown in Fig. 4 with quantiles at 50, 70, and 90 percentile levels. The figure depicts duration (in months) and severity values corresponding to the percentile level. It can be clearly seen from the 50-percentile duration and severity plots 4(a) and 4(d) that the Marathwada region has high values of 2–2.5 (both duration and severity), suggesting that the 50% of the value at Marathwada region are high compared to the rest of Maharashtra, except

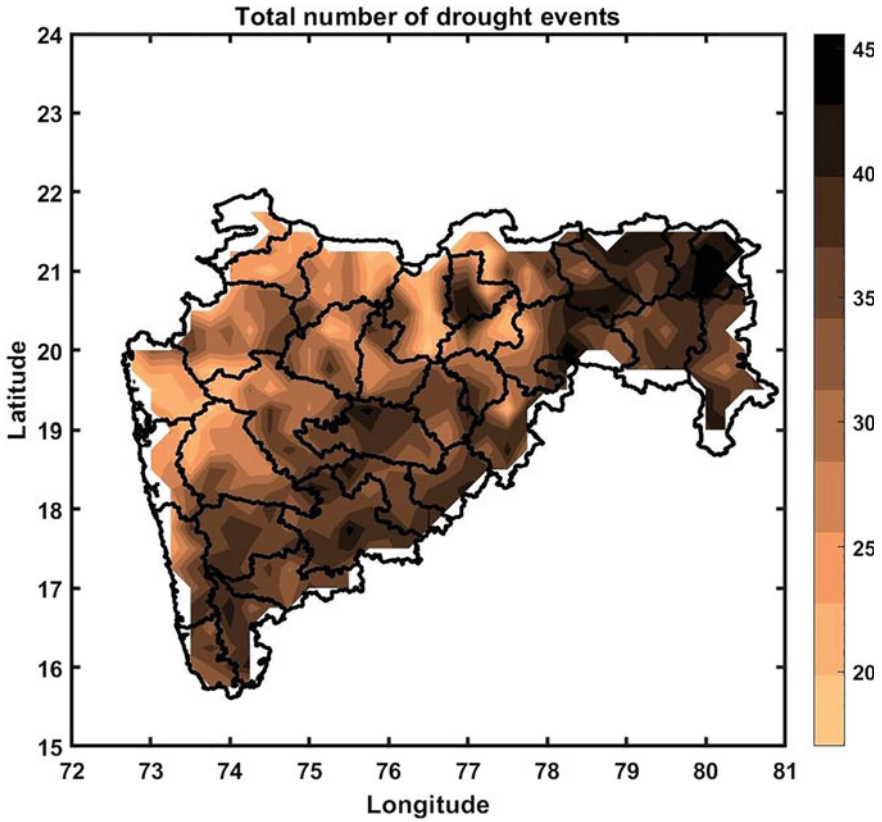
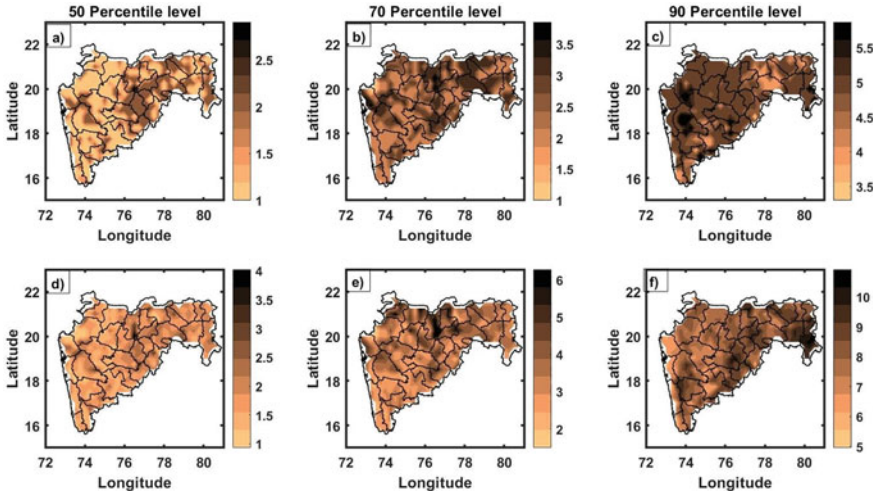


Fig. 3 Spatial variation of total number of drought events over period of 1980–2020

the Marathwada region the rest shows the value of 1–1.5 months of drought duration which means that short duration drought events were more in that region. Buldhana District shows highest value at 50-percentile level with duration of 3 months. The 70- percentile duration and severity plots 4(b) and 4(e) shows that the duration lies between 1 and 4 months and the severity lies between 2 and 6. The spatial variation shows the part of Nagpur, Aurangabad and Amaravati regions have drought duration of 3.5–4 months for 70-percentile values, and the part of Nashik district has shown the highest values corresponding to 70-percentile level. The 70-percentile severity is highest in Buldhana and Washim districts.

The 90-percentile level plot of duration and severity shows that the Pune division (namely Sangli and Pune) and Nashik and Gadchiroli have the highest duration of 5–6 months. The 90-percentile severity plot also shows Pune division and Nagpur division have high severity values of 8–9. From the percentile plot, it can be clearly stated that the Pune division has a contrasting high and low duration and severity variation as 50% of the event have a duration between 1 and 1.5 months, whereas the



**Fig. 4** Spatial variation of drought parameters: Duration (row 1) (a, b, c) and severity (row 2) (d, e, f) at 50, 70, and 90 percentile level, respectively

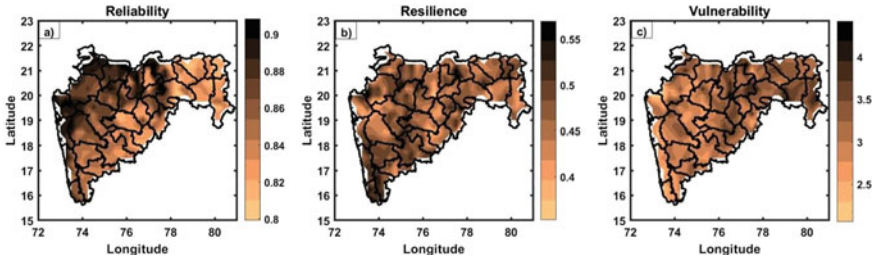
Marathwada region has high values for all the percentile plots except the 90-percentile plot. That is also reflected in the reliability map.

### 4.3 Spatial Variability of Reliability, Resilience, and Vulnerability

The spatial variability of R-R-V is shown in Fig. 5. The Nagpur and Aurangabad division shows the least reliability compared to Nashik, Amravati, and Konkan division as shown in Fig. 5a. The reliability ranges from 0.8 to 0.9 (80–90%). As the probability that a system is in a satisfactory state defines reliability, i.e. the system having the least drought events will have high reliability. Hence, we can compare the total number of drought events in Fig. 3 and see that the area having high drought events have the least reliability. From reliability map (Fig. 5a), we can say that Nagpur and Aurangabad division requires utmost attention.

The spatial plot of drought resilience over Maharashtra at 0.25° grid level is shown in Fig. 5b. How soon a system can achieve a satisfactory condition again is measured by its resilience, and here, higher value of resilience is desirable. From Fig. 5b, we can see that the resilience varies from 0.35–0.55. The most resilient areas are Amravati, part of the Nashik, and Konkan division. The least resilient part is some parts of Chandrapur and the lower part of Nashik. It can be noticed that those having the high mean severity and mean duration have the least resilience.

The spatial variation of vulnerability over Maharashtra is shown in Fig. 5c. The vulnerability ranges from 2.2 to 4.5. The higher vulnerability is the least desirable.



**Fig. 5** Spatial variation of **a** Reliability, **b** Resilience, and **c** Vulnerability

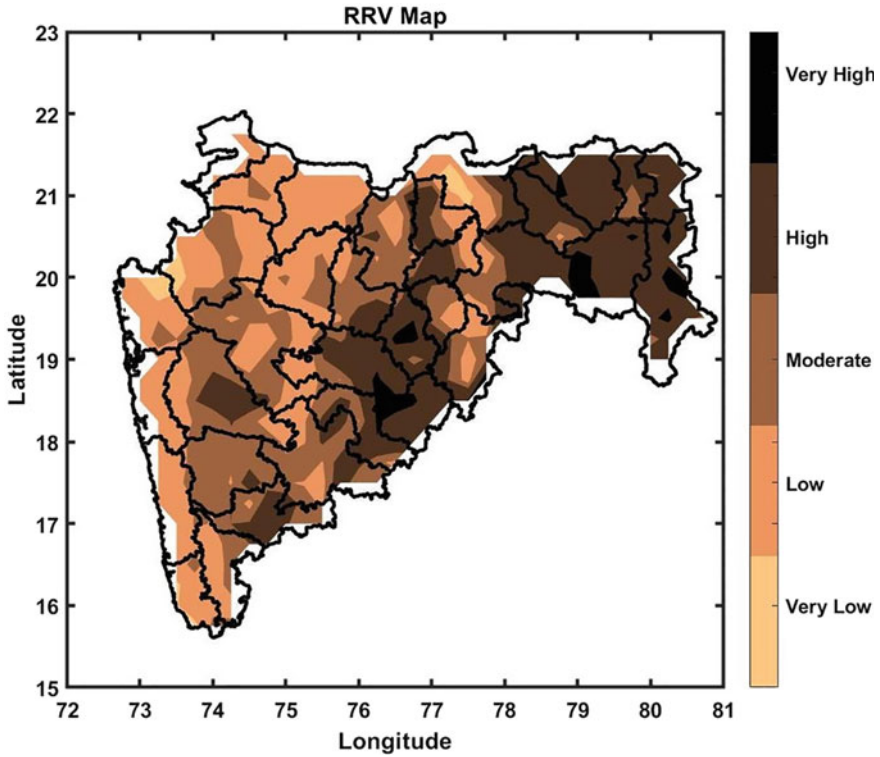
Overall, the vulnerability mostly lies between 2.8 and 3 over most of the grids, but the high vulnerability can be seen at exact same grids, which have high severity as the severity is directly proportional to vulnerability.

#### 4.4 RRV Index Map of Maharashtra

The RRV index map is shown in Fig. 6. The dark colour shows the region which is more prone to drought, and light colour shows region that is comparatively less drought-prone. The regions with very high drought are part of Chandrapur, Gagchiroli, Parbhani, Beed, and Latur. These districts also fall under high drought; other than that districts including Sangli, Satara, and eastern part of Maharashtra come under high drought region. The North-western Maharashtra falls under the low and very low drought scale. Most of the lower part of Maharashtra falls in moderate drought zone. Overall, we can precisely find from Fig. 6, which part of the district falls under which category of drought and accordingly, the action plans can be suggested to bring that region from high to moderate/low drought category.

### 5 Conclusions

This study presented a reliability–resilience–vulnerability (R–R–V) framework for analysing the droughts. The meteorological droughts are characterized using the Standardized Precipitation Index (SPI). The study area of Maharashtra state in India is considered for drought analysis at spatial resolution of  $0.25^\circ \times 0.25^\circ$  utilizing IMD monthly precipitation data over a 41-year period (1980–2020). To understand the spatial variation of drought parameters, duration and severity at 50, 70, and 90 percentile levels are computed and plotted, which clearly show that the Marathwada region has high duration and severity; the 90-percentile plot shows Pune division has high duration and severity, but it has low severity and duration at 50-percentile level. The presented plots depict which areas are more (or less) vulnerable to droughts.



**Fig. 6** RRV combined index map for the periods 1980–2020

Amaravati, part of Nashik, and the Konkan division are the most resilient locations, and they require the least attention. The divisions of Nagpur and Aurangabad deserve special care because they are the least reliable. The R-R-V maps of Maharashtra firmly demonstrate that the Aurangabad and Nagpur division has the highest drought risk among the other divisions. The spatial plots provide a clear picture of locations that demand immediate action, which will be useful to decision-makers and government entities.

**Acknowledgements** The research work is financially supported by the Department of Science and Technology DST—Centre of Excellence in Climate Studies IIT Bombay DST/CCP/CoE/140/2018 (G) Code (RD/0117-DST0000-038).

## References

- Chanda K, Maity R, Sharma A, Mehrotra R (2014) Spatiotemporal variation of long-term drought propensity through reliability-resilience-vulnerability based Drought Management Index. *Water Resour Res* 50(10):7662–7676
- Dai A (2013) Increasing drought under global warming in observations and models. *Nat Clim Change* 3(1):52–58
- Ding Y, Wang W, Cheng X, Zhao S (2008) Ecosystem health assessment in inner Mongolia region based on remote sensing and GIS. *Int Arch Photogramm Remote Sens Spat Inf Sci* 37(B1):1029–1034
- Ganguli P, Reddy MJ (2012) Risk assessment of droughts in Gujarat using bivariate copulas. *Water Resour Manag* 26(11), 3301–3327
- Ganjir G, Pattnaik S, Trivedi D (2022) Characteristics of dynamical and thermo-dynamical variables during heavy rainfall events over the Indian region. *Dyn Atmos Oceans* 99:101315
- Hashimoto T, Stedinger JR, Loucks DP (1982) Reliability, resiliency, and vulnerability criteria for water resource system performance evaluation. *Water Resour Res* 18(1):14–20
- Hazbavi Z, Sadeghi SHR (2017) Watershed health characterization using reliability–resilience–vulnerability conceptual framework based on hydrological responses. *Land Degrad Dev* 28(5):1528–1537
- Hazbavi Z, Baartman JE, Nunes JP, Keesstra SD, Sadeghi SH (2018) Changeability of reliability, resilience and vulnerability indicators with respect to drought patterns. *Ecol Ind* 87:196–208
- IPCC (2014) Climate Change 2014: Impacts, adaptation, and vulnerability. Part A: global and sectoral aspects. Contribution of working group II to the fifth assessment report of the Intergovernmental panel on climate change
- Loucks DP (1997) Quantifying trends in system sustainability. *Hydrol Sci J* 42(4):513–530
- Mahmoudi P, Maity R, Amir Jahanshahi SM, Chanda K (2021) Changing spectral patterns of long-term drought propensity in Iran through reliability–resilience–vulnerability-based drought management index. *Int J Climatol*
- McKee TB, Doesken NJ, Kleist J (1993, January) The relationship of drought frequency and duration to time scales. In *Proceedings of the 8th conference on applied climatology*, vol 17, no 22, pp 179–183
- Naumann G, Alfieri L, Wyser K, Mentaschi L, Betts RA, Carrao H et al (2018) Global changes in drought conditions under different levels of warming. *Geophys Res Lett* 45(7):3285–3296
- Panofsky HA, Brier GW, Best WH (1958) Some application of statistics to meteorology
- Sung JH, Chung ES, Shahid S (2018) Reliability–resiliency–vulnerability approach for drought analysis in South Korea using 28 GCMs. *Sustainability* 10(9):3043
- Veettil AV, Konapala G, Mishra AK, Li HY (2018) Sensitivity of drought resilience-vulnerability-exposure to hydrologic ratios in contiguous United States. *J Hydrol* 564:294–306
- Wiegand AN, Walker C, Duncan PF, Roiko A, Tindale N (2013) A systematic approach for modelling quantitative lake ecosystem data to facilitate proactive urban lake management. *Environ Syst Res* 2(1):1–12
- Yu G, Yu Q, Hu L, Zhang S, Fu T, Zhou X et al (2013) Ecosystem health assessment based on analysis of a land use database. *Appl Geogr* 44:154–164

# Remote Sensing and GIS Application for Soil Erosion and Sediment Yield Estimation of Purna River Sub-Basin



Milan Dineshbhai Nadiyapara and Falguni P. Parekh

**Abstract** Apart from other significant environmental issues, one of the severe threats to the continents is soil erosion. As a result, significant cultivable land has been deteriorated. The Purna River watershed, located at south east of Gujarat, India, was selected as a study area for this research work. The rainfall, DEM, soil map, and satellite imagery were used to compute various factors of soil erosion such as rainfall erosivity, topography, conservation practise factor, soil erodibility, and cover management sequentially. NDVI which reflects the percentage of vegetation was used for the estimation of C-factor. The sediment yield was determined by using the SDR model. After spatial evaluation using RUSLE model within GIS interface, it was seen that  $1131.73 \times 10^3$  t soil was lost annually at average rate, and sediment yield was  $122.68 \times 10^3$  t/year. Resulted soil erosion map showed that in the Purna River basin, the steeper the slope, the more erosion occurs. That leads to conclusion that soil erosion for Purna River watershed was more correlated with the LS-factor than any other factor. Sediment yield was found out using SDR model as a fraction of soil loss. It was seen that SDR model gave closest result to observed sediment load with  $R^2 = 0.99$  for validation of model at Mahuwa station. Net sediment load at the outlet of Purna River into Arabian Sea was found out to be 112,680 t/year with sediment delivery ratio 10.84. All the statistics about soil erosion, SDR model, and sediment yield can be much resourceful for watershed management study of Purna River watershed. On a catchment scale, geospatial technologies proven to be effective tools for evaluation of soil erosion and estimating sediment output at the definite location on the streams.

**Keywords** GIS · RS · RUSLE · Sediment delivery ratio · Soil erosion · Sediment yield

---

M. D. Nadiyapara · F. P. Parekh (✉)  
Water Resources Engineering and Management Institute, Faculty of Technology and Engineering,  
The Maharaja Sayajirao University of Baroda Samiala, Vadodara, Gujarat 391410, India  
e-mail: [fpparekh-wremi@msubaroda.ac.in](mailto:fpparekh-wremi@msubaroda.ac.in)

M. D. Nadiyapara  
e-mail: [nmilan1213@gmail.com](mailto:nmilan1213@gmail.com)

## 1 Introduction

The aim of the study is to determine the soil erosion by RUSLE model into GIS interface and obtain spatial distribution of RUSLE parameter such as R, LS, K, P, and C factors and to compare estimated and observed sediment yield at Mahuwa station. Then evaluate best-suited sediment delivery ratio model for Purna River watershed that finally leads to determination of net sediment yield of Purna River at its outlet in Arabian Sea. Soil erosion leads more and more unproductive lands.

Arekhi et al. (2012) identified the critical area on grid basis working environment, with high erosion rate for watershed conservation planning in western Iran. It was found out that LS parameter of RUSLE ( $r^2 = 0.71$ ) was the major factor affecting soil erosion. Bhattarai and Dutta (2007) carried out study on sub-basin of Mun River using 30 m DEM and 90 m DEM. It was found out that smaller the grid cell of DEM, more accurate will be the result. Jain and Kothiyari (2000) calculated all the required parameter to evaluate the soil erosion like rain distribution, slope, land use, soil data on a little grid pattern as particular formation so jointly establish and equivalent for watershed as whole or for the sub-watershed in addition. Colman et al. (2018) performed an evaluation study between most commonly used SDR models using RUSLE in three sub-basins of Gauriroba Brazil. Lewoye and Rishikesh (2021) studied soil erosion by RUSLE model on Anjeb watershed, Ethiopia concludes that more than 50% severe erosion out of total erosion was occurring from only 7% of total area had steeper topography and major reduction in storage capacity of reservoir designed for a life span of 43 years.

## 2 Materials and Methods

### 2.1 Study Area

Purna is a major river with its drainage area lying in the south east of Gujarat and Maharashtra. (Table 1) Purna has a watershed area of about 2431 km<sup>2</sup> and length of about 185 km. The extent of catchment area of Purna is between 72° 45' E to 74° 00' E and 20° 41' N to 21° 05' N. (Fig. 1) The origin of Purna is Saputara hill, in the Maharashtra state. The vital tributaries of the Purna River are Gira and Jankheri (CWC 2017).

**Table 1** State-wise proportion of study area watershed

S. No	State	Watershed area (k m <sup>2</sup> )	% of total watershed area
1	Gujarat	2373	97.61
2	Maharashtra	58	2.39



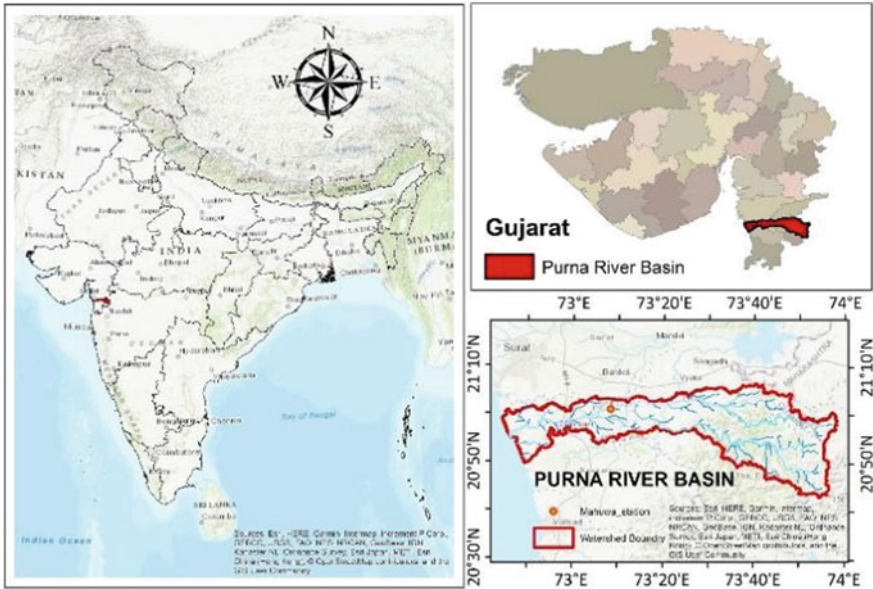


Fig. 1 Study area (Purna River basin)

### 2.2 Data Collection

The various data needed to model revised universal soil loss equation (RUSLE) are rainfall, DEM, soil map, LULC map, and satellite imagery. The data source and description about data are represented in Table 2.

### 2.3 Determination of the Soil Erosion (SE)

Renard et al. (1991) revised all parameters of USLE model which was used for analysis of soil erosion and referred as RUSLE model is extensively used for spatial distribution of soil erosion into GIS interface. During this study, all the parameters of RUSLE model determined in ARCGIS 10.5 tool. The RUSLE expression is presented as (Eq. 1).

$$SE = R.K.LS.C.P \tag{1}$$

where SE is gross soil erosion (t/ha/year), R is rainfall erosivity factor (Mj mm/ha/hr/year), K is soil erodibility factor (t h/Mj/mm), LS is topographic factor, C is land cover and management factor, and P is conservation practice factor. P, C, and LS factors are dimensionless.

**Table 2** Data sources and description of the data used in study

Data	Data source and description
DEM	ASTER DEM used for terrain processing which had spatial resolution of 30 m obtained from USGS database ( <a href="https://earthexplorer.usgs.gov/">https://earthexplorer.usgs.gov/</a> )
Rainfall data	Rainfall data collected from IMD Pune in form of netcdf spatial gridded data set of resolution $0.25^\circ \times 0.25^\circ$ ( <a href="https://cdsp.imdpune.gov.in/home_gridded_data.php">https://cdsp.imdpune.gov.in/home_gridded_data.php</a> )
Soil map	Soil type map for study area extracted from FAO soil database which was in ESRI shape file format and available at FAO soil portal ( <a href="https://www.fao.org/soils-portal/data-hub/soil-maps-and-databases/en/">https://www.fao.org/soils-portal/data-hub/soil-maps-and-databases/en/</a> )
Satellite imagery	RESOURCESAT—1/ RESOURCESAT—2: AWiFS camera of spatial resolution 23.5 m with 4 band. Obtained from NRSC/ISRO Open data and product archive facilitates ( <a href="https://bhuvan-app3.nrsc.gov.in/data/download/index.php">https://bhuvan-app3.nrsc.gov.in/data/download/index.php</a> )
LU/LC map	For land use land cover classification ESRI land cover map was used with spatial resolution of 10 m and had 10 land classification. Available at ESRI land cover portal ( <a href="https://livingatlas.arcgis.com/landcover/">https://livingatlas.arcgis.com/landcover/</a> )
SY data	Sediment yield (SY) data was obtained through sediment year book published by central water commission (CWC), India. Available at Publication section of CWC official portal ( <a href="http://www.cwc.gov.in/hydro_16-17">http://www.cwc.gov.in/hydro_16-17</a> )

### 2.3.1 R-Factor

This factor represents the erosion caused by impact of raindrops which falls with definite momentum, but practically it is very hard to obtain the details of each storm, so the  $R$ -factor is evaluated by (Eq. 2) developed by Arnoldus (1980).

$$R = \sum_{n=1}^{12} 1.735.10^{\left(1.5 \log 10 \frac{P_i^2}{P} - 0.08188\right)} \quad (2)$$

where  $R$  is rainfall erosivity factor (Mj mm/ha/hr/year),  $P_i$  is monthly rainfall (mm), and  $P$  is annual rainfall (mm). The average annual rainfall of Purna river basin is shown in Fig. 2.

### 2.3.2 K-Factor

It is the ability of soil particles to erode per unit of rain erosivity factor ( $R$ ), and for specified soil,  $K$ -factor was calculated by expression (Eq. 3) developed by Williams (1995).

$$K = 0.01317.f_{csand}.f_{cl-si}.f_{orgC}.f_{hisand} \quad (3)$$

$$f_{csand} = 0.2 + 0.3.\exp\left[-0.256.m_s.\left(1 - \frac{m_s}{100}\right)\right]. \quad (4)$$

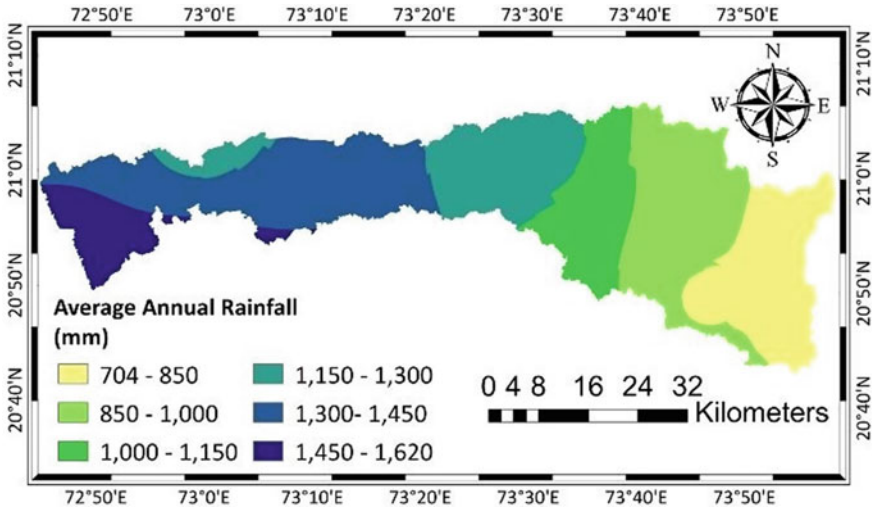


Fig. 2 Average annual rainfall (mm)

$$f_{cl-si} = \left( \frac{m_{silt}}{m_c + m_{silt}} \right)^{0.3} \tag{5}$$

$$f_{orgC} = \left( 1 - \frac{0.256orgC}{orgC + \exp[3.72 - 2.95orgC]} \right) \tag{6}$$

$$f_{orgC} = \left( 1 - \frac{0.7(1 - \frac{m_s}{100})}{(1 - \frac{m_s}{100}) + \exp[-5.51 + 22.9(1 - \frac{m_s}{100})]} \right) \tag{7}$$

where  $K$  is soil erodibility factor (t h/Mj/mm),  $m_s$  is % sand in topsoil,  $m_{silt}$  is % silt in topsoil,  $m_c$  is % clay in top soil, and  $orgC$  is % organic carbon in top soil.

All parameters of (Eq. 3) were identified based on the percentage of silt, sand, clay, and organic carbon content in topsoil. Soil types and texture identified from the soil map given by FAO soil data are presented in Fig. 3 and Table 3.

### 2.3.3 LS-Factor

LS-factor indicates the effect of terrain on the process of soil erosion, more the slope the velocity of overland flow will be more and that phenomenon leads to more soil erosion.

In the ARCGIS 10.5 interface with the use of DEM (Fig. 4), slope map (Fig. 5) and flow map were generated, and then with the use of (Eq. 8) which is stated by Moore and Burch (1986a, b) gives the spatial distribution of LS-factor.

Average elevation of whole study area found out to be 224.22 m from the DEM.

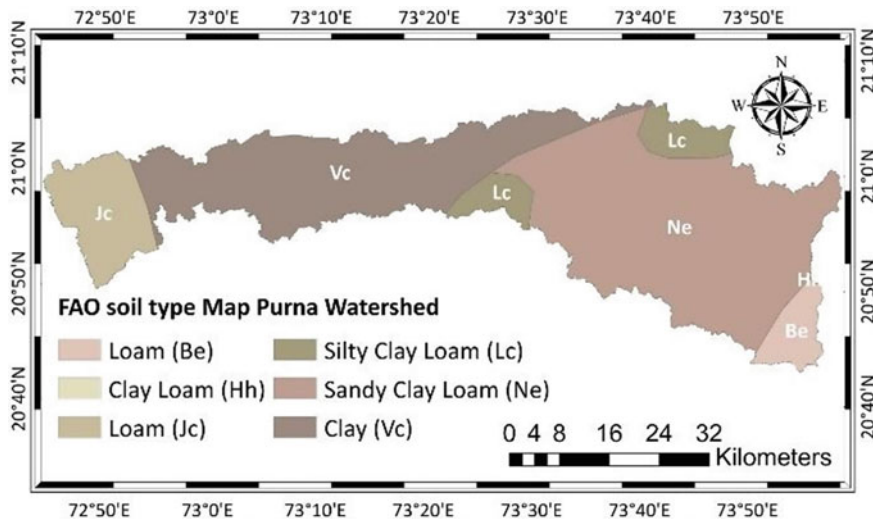


Fig. 3 Soil type map of Purna River catchment obtained from FAO soil data

Table 3 Soil type classification according to FAO soil data and % of soil different soil particles

Soil type by FAO database	Sand %	Silt %	Clay %	OC %	K-Factor
BE	36.4	37.2	26.4	1.07	0.20
HH	37.2	31.2	31.6	1.09	0.18
JC	39.6	39.9	20.6	0.65	0.24
LC	64.3	12.2	23.5	0.63	0.16
NE	68.4	10.5	21.2	0.6	0.15
VC	22.4	24.5	53	0.69	0.16

$$LS = \left( \frac{FA \cdot \text{cell size}}{22.13} \right)^{0.4} \cdot \left( \frac{\sin(\text{slope})}{0.0896} \right)^{1.3} \tag{8}$$

where LS is topographic factor, FA is accumulated upslope contributed area, cell size is size of DEM raster cell (30 m for this study), and sin(slope) is degree of slope value in sin.

### 2.3.4 C-Factor

Vegetation cover reduces the effect of erosion caused by rainfall impact and overland flow. Value of C-factor differs widely from season to season, by place, and by the types of vegetation cover presented on catchment (Fig. 6). Table 4 illustrates the area of different land cover in km<sup>2</sup> of Purna River basin.

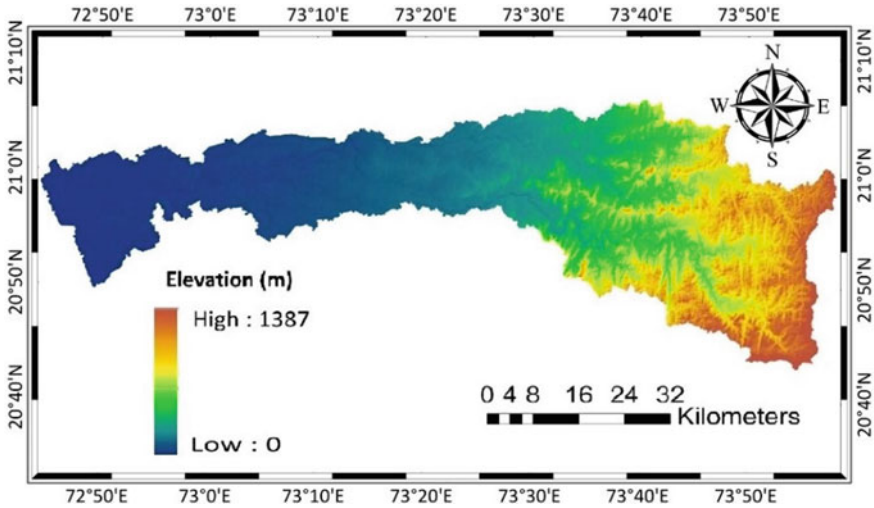


Fig. 4 Elevation map of study area (m)

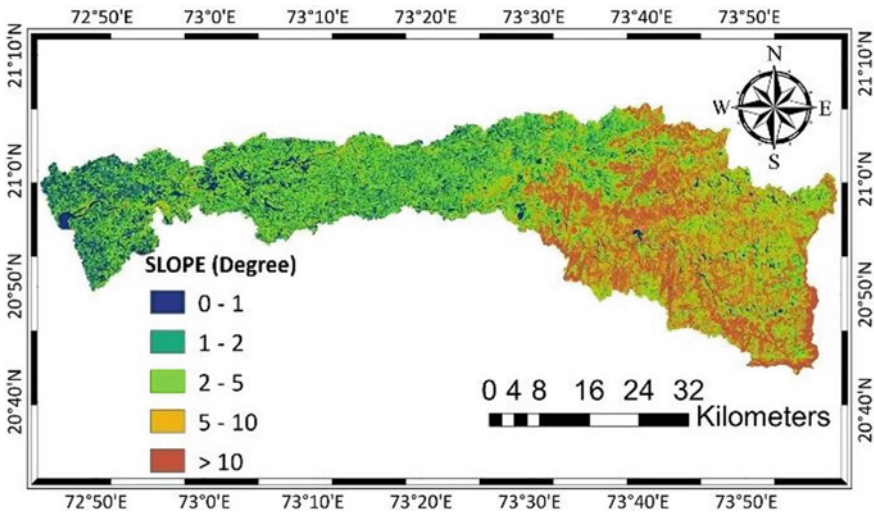


Fig. 5 Spatial representation of slope (degree)

In remote sensing technic most commonly used index of vegetation fraction is NDVI, which is used to calculate *C*-factor. (Eq. 9) depicts relation between NDVI and *C*-factor given by Lin et al. (2002). In this study, multispectral imagery of RESOURCESAT satellite used to make NDVI map of Purna River catchment. (Fig. 7)

$$c = \frac{(1 - NDVI)}{2} \tag{9}$$

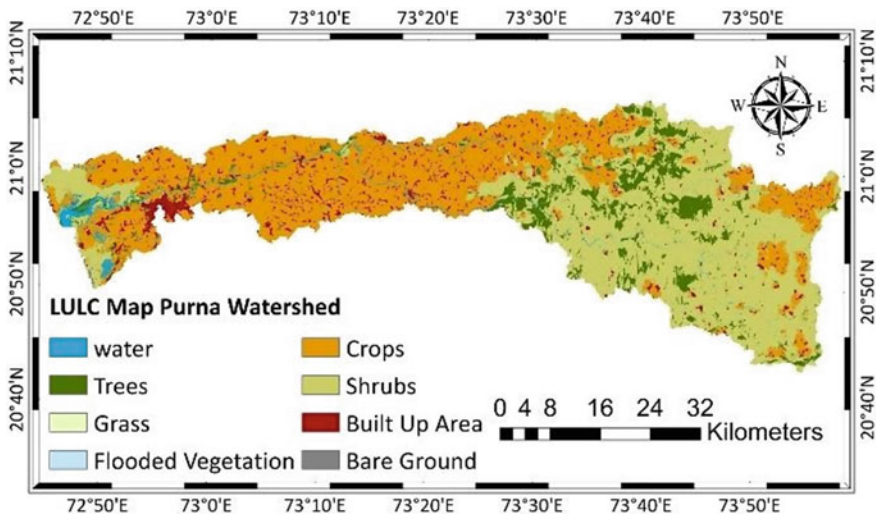


Fig. 6 Spatial representation of LU/LC map

Table 4 Amount of area in km<sup>2</sup> covered by different land class

S. No	LU/LC type	Area (km <sup>2</sup> )
1	Water	43.47
2	Trees	206.44
3	Grass	0.08
4	Flooded vegetation	0.41
5	Crops	990.44
6	Shrubs	991.8
7	Built area	123.03
8	Bare ground	2.73

$$NDVI = \frac{NIR - R}{NIR + R} \tag{10}$$

where *C* is cover management factor, NDVI is normalized difference vegetation index [− 1, + 1], NIR is near infrared band (band 4 of RESOURCESAT imagery), and *R* is red band (band 3 of RESOURCESAT imagery).

### 2.3.5 P-Factor

*P*-factor inversely proportional with an existing conservation practice. *P*-factor is 1 for no conservation practice and vice versa. For this study, *P*-factor is calculated

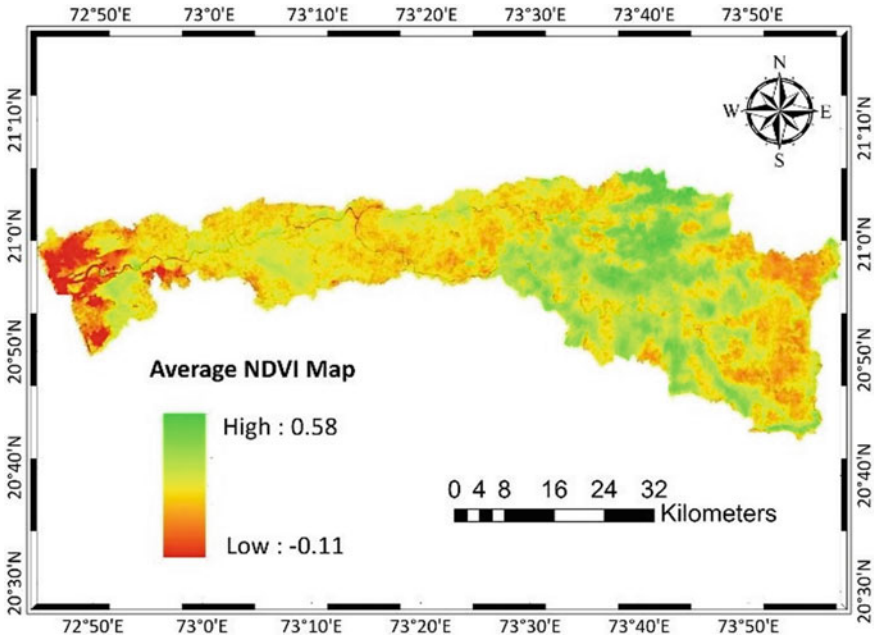


Fig. 7 Spatial representation of average NDVI

directly from the slope map in the ArcGIS environment using the expression (Eq. 11) stated by Wener (1981).

$$P = 0.2 + 0.3S \tag{11}$$

where  $P$  is conservation practice factor, and  $S$  is slope steepness (%).

### 2.4 Sediment Yield (SY)

It is resulted from combined erosion and deposition process of the soil within drainage boundary. SY is estimated as the portion of soil loss from the (Eq. 12)

$$SY = SDR \cdot SE \tag{12}$$

where SY is sediment yield (t/year), SDR is sediment delivery ratio, and SE is soil erosion (t/year).

### 2.4.1 Sediment Delivery Ratio (SDR)

SDR is net sediment received at the outlet of catchment to the gross soil erosion of the upstream contributing area of that catchment. Numbers of study had been conducted to calculate the SDR based on area of watershed, slope of main stream, basin relief, and curve number. Most simple and widely used SDR models are based on power function of watershed area given by Vanoni (1975) (Eq. 13), Boyce (1975) (Eq. 14), and USDA (1972) (Eq. 15).

$$\text{SDR} = 0.4724 A^{-0.125} \quad (13)$$

$$\text{SDR} = 0.3750 A^{-0.2382} \quad (14)$$

$$\text{SDR} = 0.5656 A^{-0.11} \quad (15)$$

On the catchment scale, sediment yield is affected by many other factors like slope, drainage density, soil type, relief of catchment, and types of land cover. So for the current study a better indicator of SDR given by Williams (1977) is used and expressed as (Eq. 16).

$$\text{SDR} = 1.366 A^{-0.1} \cdot (R/L)^{0.363} \cdot \text{CN}^{5.444} \cdot 10^{-11} \quad (16)$$

where SDR is sediment delivery ratio,  $A$  is catchment area ( $\text{km}^2$ ),  $R/L$  is relief to length ratio, and CN is *S.C.S* curve number.

Soil class and land use/land cover distribution determines the CN value. For this study, CN value is calculated as 73 by taking weighted average of CN of different land class. Table 5 given below represents the variation in SDR value calculated using different model.

**Table 5** Values of SDR model estimated by different approach at Mahuwa and outlet of Purna River

SDR model	SDR at Mahuwa	SDR at outlet of Purna River
Vanoni	0.1658	0.1591
Boyce	0.0636	0.0588
USDA	0.2496	0.2407
Williams	0.1437	0.1084



### 3 Results and Discussion

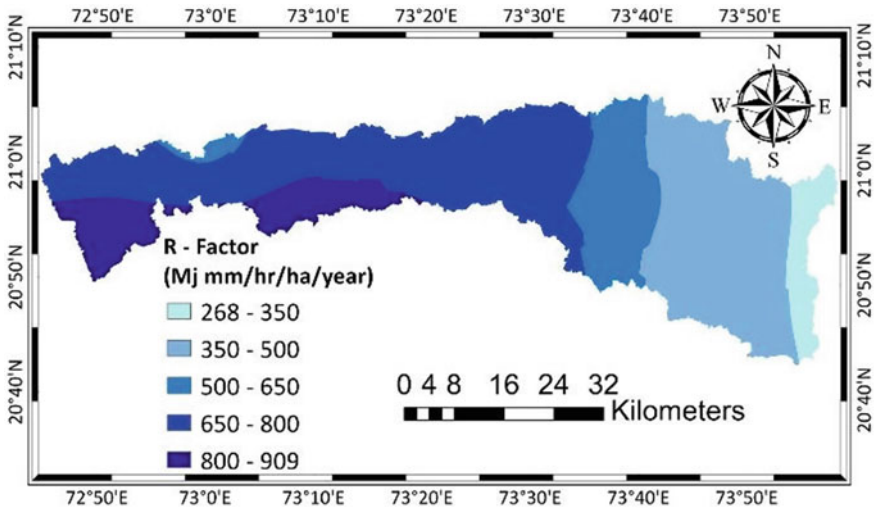
Study was conducted for the five consecutive years from 2012 to 2016. All the parameters of RUSLE model given in (Eq. 1) were found out for all 5 years, and then, average was taken to determine the average annual values of each parameter that were represented in Table 6.

The average annual value of each parameter calculated in ARCGIS 10.5 tool on spatial grid cell for Purna River watershed. The spatially distributed map of *R*-factor (Fig. 8), *K*-factor (Fig. 9), *LS*-factor (Fig. 10), *C*-factor (Fig. 11), and *P*-factor (Fig. 12) of RUSLE is shown below.

The average annual soil loss was found to be 4.7984 t/ha/year with minimum, maximum, and standard deviation of 0 t/ha/year, 1002.5 t/ha/year, and 16.26 t/ha/year, respectively (Fig. 13). From the spatial distribution of soil loss map, it was seen that upper portion of Purna River basin was more erosion prone due to high steepness

**Table 6** Maximum, minimum, average, and standard deviation value of various RUSLE model parameter in their respective units

RUSLE parameter	Max	Min	Mean	SD
<i>R</i> -factor	909.13	267.92	606.15	171.04
<i>K</i> -factor	0.24	0.15	0.16	0.026
<i>LS</i> -factor	22	0	2.14	4.27
<i>C</i> -factor	0.57	0.18	0.32	0.046
<i>P</i> -factor	1	0.02	0.19	0.18



**Fig. 8** Spatial representation of *R*-factor (Mj mm/hr/ha/year)

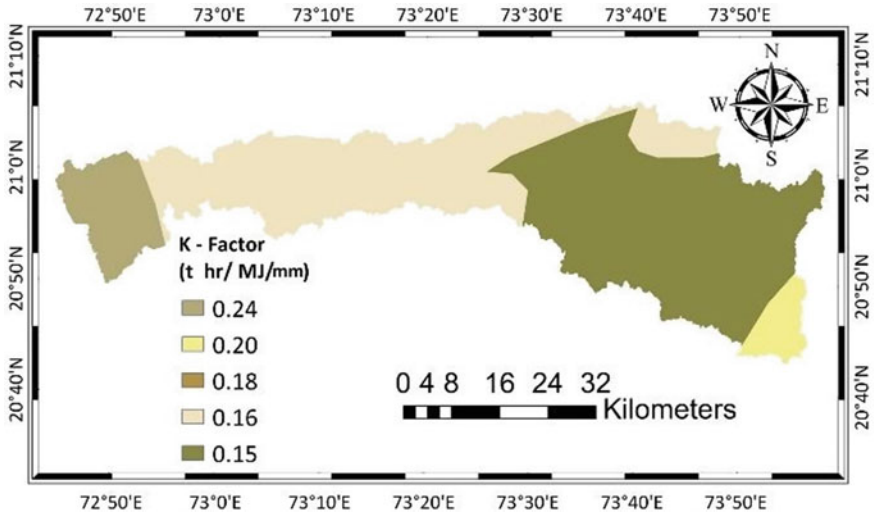


Fig. 9 Spatial representation of K-factor (t hr/Mj/mm)

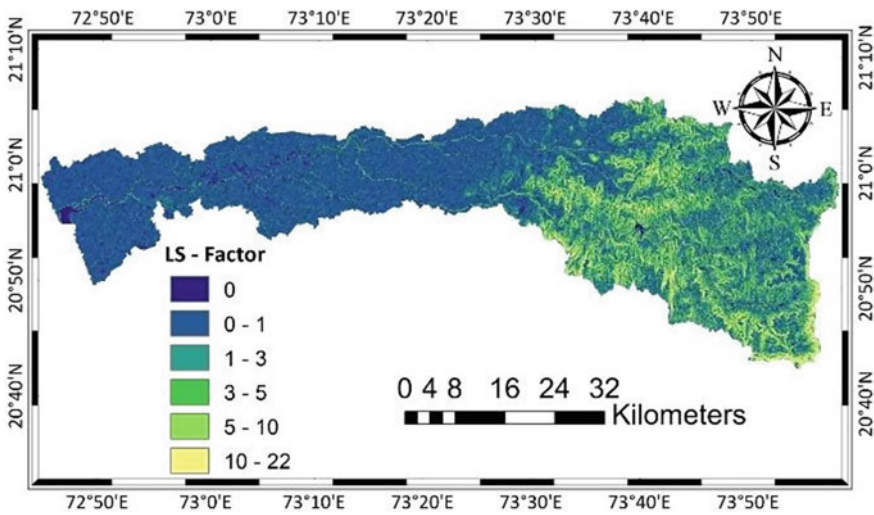


Fig.10 Spatial distribution of LS-factor

of terrain despite having a lowest soil erodibility. For the validation of model at the Mahuwa gauging station, observed and estimated sediment load was compared. For determining sediment load at Mahuwa station upstream contributing area extracted from the whole watershed in ArcGIS 10.5 interface (Fig. 14) and sediment load at outlet was estimated from gross soil erosion by using the various SDR model as discussed in Sect. 2.4.1.

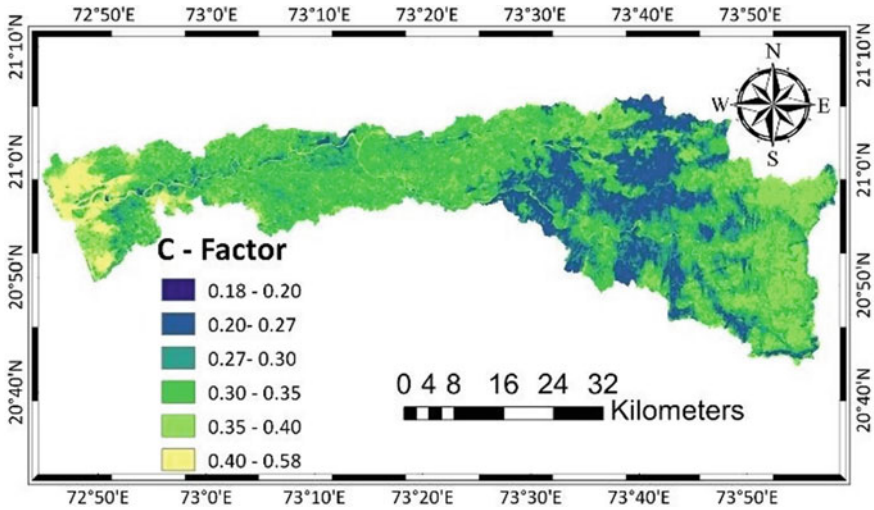


Fig. 11 Spatial distribution of *C*-factor

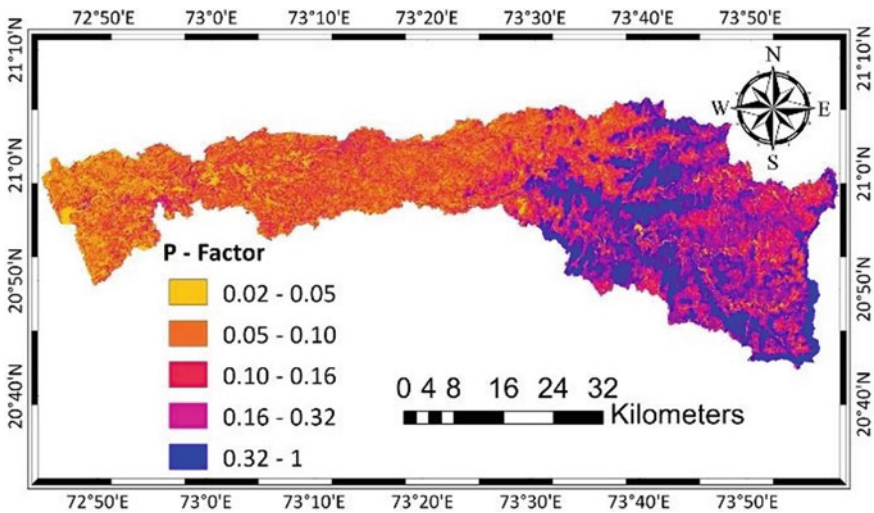


Fig. 12 Spatial distribution of *P*-factor

It was seen that results from the SDR model (Eq. 15) had very close values of sediment load from the observed sediment load. The coefficient of correlation is 0.99 for observed and predicted sediment load which is illustrated in (Fig. 15). Observed and calculated sediment load is shown in Table 7.

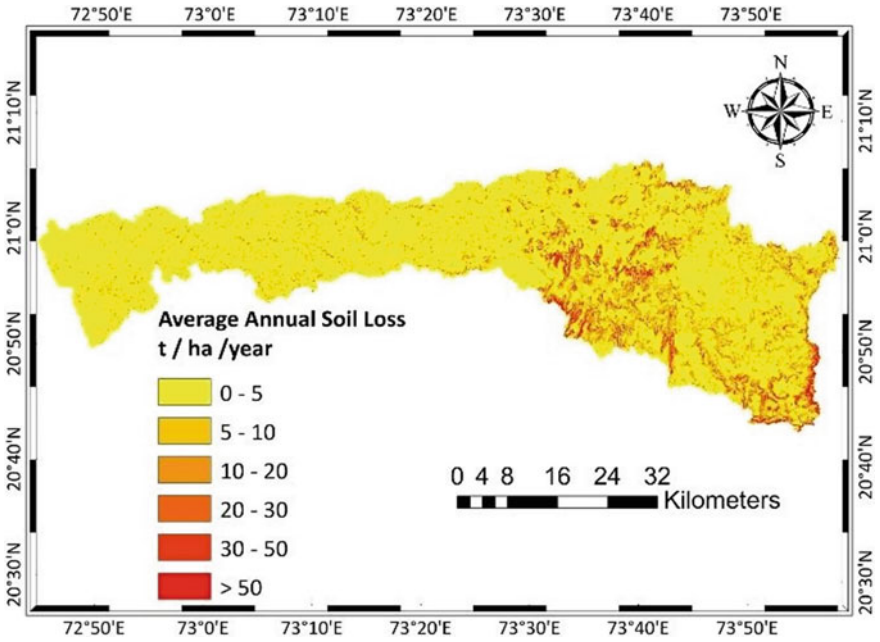


Fig. 13 Spatial distribution of average annual soil erosion

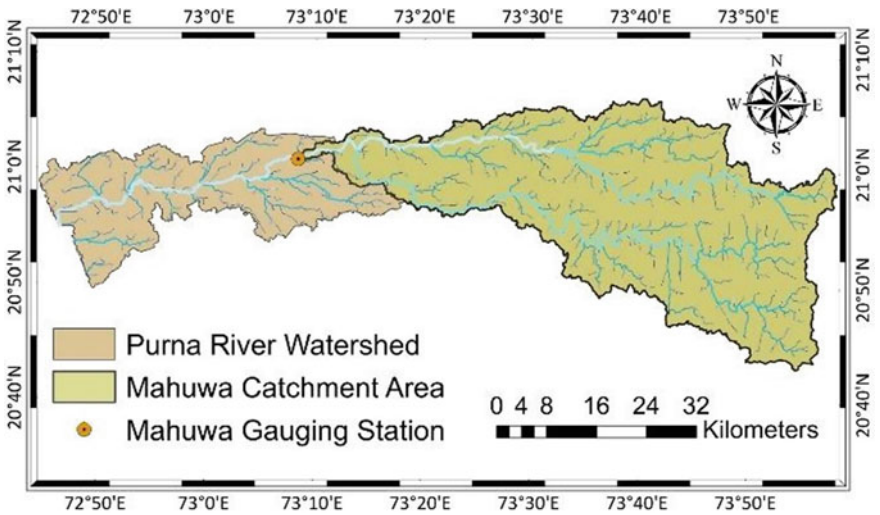
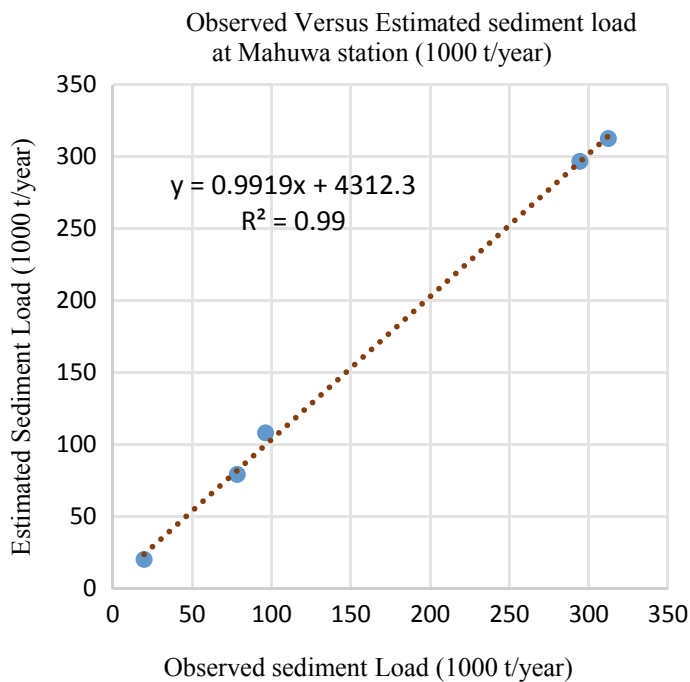


Fig. 14 Location and upstream catchment area of Mahuwa station gauging station on Purna River watershed



**Fig. 15** Observed and calculated sediment yield (1000 t/year) at Mahuwa gauging station

**Table 7** Observed and calculated sediment yield (t/year) at Mahuwa gauging station

Year	Observed sediment load (t/year)	Calculated sediment load (t/year)	Difference (t/year)	% Diff.
2012	78,385	79,107.38	722.38	0.92
2013	294,454	296,615.64	2161.63	0.73
2014	96,262	108,002.26	11,740.26	12.2
2015	19,653	20,100.66	447.66	2.28
2016	312,447	312,479.09	3210	0.01

After validation of model at Mahuwa gauging station, sediment load at outlet of Purna River catchment was estimated using the SDR value calculated from (Eq. 16) by multiplying it to gross erosion obtained from ArcGIS 10.5 as shown in Table 8.

**Table 8** Average annual soil erosion (t/year), SDR, and sediment yield (t/year) for Purna basin and Mahuwa sub-basin

Outlet point	Gross erosion (t/year)	SDR	Sediment yield (t/year)
Last point of Purna River basin	1131,734.34	0.1084	122,680.00
At Mahuwa	1136,300.04	0.1437	163,286.31

## 4 Conclusions

The soil erosion on the Purna River watershed was determined by RUSLE model in the ArcGIS 10.5 GIS interface tool efficiently by considering monthly and annual precipitation, DEM, soil type map, and satellite imagery dataset. All parameter of RUSLE model such as *R*-factor, *K*-factor, *LS*-factor, *C*-factor, and *P*-factor were calculated successfully as spatially distributed map of basin to 30 m resolution in the ArcMAP 10.5 tool. Average annual soil loss found to be 1131,734.34 t/year. The upper portion of watershed covered with medium to dense forest which should have low tendency for erosion had lower *R*-factor value and also the soil type for upper portion of watershed where the forest area situated had the lowest soil erodibility value of 0.15 t h/Mj/mm. Despite these facts, the maximum erosion prone area of Purna watershed was the forest area. The reason behind that the major portion of forest covered with hilly terrain which has very steep slope ranges from 10 to 66°. Due to steep slope value, erosion was dominant in upper portion of catchment.

That leads to conclusion that soil erosion for Purna River watershed was more correlated with the *LS*-factor than any other factor. Any reservoir constructed in vicinity of that terrain will yield more sediment to reservoir due to high sediment transport capacity. Sediment yield was found out using SDR model as a fraction of gross soil loss. It was seen that SDR model gave closest result to observed sediment load with  $R^2 = 0.99$  for validation of model at Mahuwa station. Net sediment load at the outlet of Purna River into Arabian Sea was found out to be 112,680 t/year with sediment delivery ratio 10.84. All the statistics about soil erosion, SDR model, and sediment yield can be much resourceful for watershed management study of Purna River watershed. However, this whole study could not be possible if GIS-based environment tool was not used.

**Acknowledgements** We are very thankful to the State Water Data Center, Gandhinagar for providing data for this research work.

## References

- Arekhi S, Niazi Y, Kalteh AM (2012) Soil erosion and sediment yield modeling using RS and GIS techniques: a case study, Iran. *Arab J Geosci* 5:285–296
- Arnoldus HJM (1980) An approximation of the rainfall factor in the universal soil loss equation. In: De Boodt M, Gabriels D (eds) *Assessment of erosion*. Wiley, Chichester, UK, pp 127–132

- Bhattarai R, Dutta D (2007) Estimation of soil erosion and sediment yield using GISat catchment scale. *Water Resour Manage* 21:1635–1647
- Boyce RC (1975) Sediment routing with sediment delivery ratios. Present and prospective technology for ARS. USDA, Washington, DC
- Colman CB, Garcia KMP, Pereira RB (2018) Different approaches to estimate the sediment yield in a tropical watershed. *Revista Brasileira De Recursos Hídricos* v 23:47
- CWC (2017) Sediment year book 2016–2017, central water commission, Narmada & Tapi Basin organization, Hydrological Observation Circle, Gandhinagar
- Jain MK, Kothyari UC (2000) Estimation of soil erosion and sediment yield using GIS. *Hydrol Sci J* 45(5):771–786
- Lewoye T, Rishikesh B (2021) Soil erosion and sediment yield assessment using RUSLE and GIS-based approach in Anjeb watershed Northwest Ethiopia. *SN Appl Sci* 3:582
- Lin C, Lin W, Chou W (2002) Soil erosion prediction and sediment yield estimation the Taiwan experience. *Soil Tillage Res* 68(2):143–152
- Moore ID, Burch GJ (1986a) Physical basis of the length slope factor in the universal soil loss equation. *Soil Sci Soc Am* 50(5):1294–1298
- Moore ID, Burch GJ (1986b) Modeling erosion and deposition topographic effects. *Trans Am Soc Agric Eng* 29(6):1624–1630
- Renard KG, Foster GR, Weesies GA, Porter JP (1991) RUSLE revised universal soil loss equation. *J Soil Water Conserv* 46(1):30–33
- USDA (1972) Sediment sources, yields and delivery ratios. National Engineering Handbook, section 3, Sedimentation. USDA, Washington, DC
- Vanoni VA (1975) Sedimentation engineering. Manual and report no. 54, American Society of Civil Engineers, New York
- Wener C (1981) Soil conservation in Kenya. Nairobi, Ministry of Agriculture, Soil Conservation Extension Unit
- Williams J (1977) Sediment delivery ratios determined with sediment and runoff models. Erosion and solid matter transport in inland waters. IAHS-AISH Publication 122:168–179
- Williams JR (1995) Chapter 25: The EPIC model In: Singh VP (ed) Computer models of watershed hydrology. Water Resources Publications, pp 909–100

# A Review of Different Approaches for Boundary Shear Stress Assessment in Prismatic Channels



Vijay Kaushik and Munendra Kumar

**Abstract** The stress range of shear at the channel's boundaries has a direct bearing on the flow of fluid inside the channel. Hence, understanding it is critical for defining the fluid field and velocity profile. Many engineering issues, such as design of flood control structures, energy loss calculation, and sedimentation, require shear stress computation. The proportion analysis between width and depth has strong influence over the stress distribution at shear in direct channels. Sinuosity, aspect ratio, and meander length affect shear stress distribution in meandering channels. Henceforth, the necessity of scrutinizing the methods used to determine the stress distribution in the channels. This paper analyzes the pros and cons of several methodologies that helps to estimate the allocating the stress ranges of shear via the prismatic channels. The review states that the vertical depth method, the normal depth method, the Guo and Julien method, the Prasad and Manson method, the Knight et al. method, the merged perpendicular method, and the Preston tube technique are the most popular methods that assist to estimate the distribution of boundary shear passing through the channels. This is due to the fact that these methods are straightforward, reliable, and easy to implement. After examining a number of other approaches, it was determined that the Preston tube technique was by far the most effective way in order to determine the stress range for boundary shear in all different kinds of channel sections.

**Keywords** Open channel flow · Prismatic channels · Boundary shear stress distribution

---

V. Kaushik (✉) · M. Kumar  
Department of Civil Engineering, Delhi Technological University, Delhi 110042, India  
e-mail: [vijaykaushik\\_2k20phdce01@dtu.ac.in](mailto:vijaykaushik_2k20phdce01@dtu.ac.in)

M. Kumar  
e-mail: [munendrakumar@dtu.ac.in](mailto:munendrakumar@dtu.ac.in)



## 1 Introduction

It is well known wherein the allotment of stress ranges around boundary shear does not coordinate with route near the perimeter of wetted via channel cross-partition. It follows a steady flow in cross-partition structures. This phenomenon has been thoroughly researched and documented. This is primarily due to turbulence's anisotropy, resulting in transverse Reynold's stress gradients and secondary circulations. According to Tominaga et al. (1989) and Knight and Demetriou (1983), when secondary currents flow directing the wall, the boundary shear stress increases, and when they flow away from the wall, the shear stress decreases. Shear stress distribution in a straight open channel is controlled using the factors count comprising the geometrical properties of cross-partition, the distribution of roughness along the longitudinal and lateral boundaries, and the concentration of sediment (Khodashenas et al. 2008). The collected information states that the variant solutions available to estimate the stress value of boundary shear via directly or indirectly. The indirect estimation of stress value of boundary shear is done using Preston method. Due to this limitation and deficits, it is difficult to estimate the observed and predicted stress distribution across the wetted area (Patel 1965). Pertaining to it, a variant set of empirical, computational, and the analytical strategies are been introduced to forecast the stress value near the boundary shear.

## 2 State-of-Art

According to Leighly (1932), an estimation of stress distribution in public channel was studied using the conformal mapping process. Due to the mishandling of secondary order constraints, the weight analysis of water flow in upward comprised of boundaries that has to be balanced in orthogonal direction. The investigation of hydraulic radius was studied by Einstein (1942) has been widely used in many parts of academic sectors and also in practice. With the use of Bagnold's three-point suspension technique, the shear distribution in rough and smooth public channels holding the cross-partition of trapezoidal and rectangular was studied by Ghosh and Roy (1970). It was measured and isolated on the part of tested public channels. The outcomes of the distribution of boundary under two-stage channels on the plain and coarse borders are portrayed by Ghosh and Mehta (1974). Finally, the shear distribution is not consistent, and the placements of the various distances in free surface are summarized.

The Rajaratnam and Ahmadi (1979) explored the interaction analysis between direct primary channels with symmetrical plain under a smooth boundary condition was studied. The investigation revealed that the longitudinal momentum of the water was carried via the main river to the floodplain. The bed shear in the floodplain rose dramatically as a result of flow interaction, although it decreased in the primary channel itself. The floodplain is located at the point where the main channel meets

the floodplain. The interaction's influence became less significant since the flow analysis of the depth in floodplain was inclined. As per the knight (1981), the fractional analysis of shear is performed on the walls using breadth and depth proportion analysis. Along with that, the roughness size related to the bed and walls is being studied in Nikuradse. The separation of channels that has been explored in the laboratory research is symmetrical. The analysis of the boundary shear is to calculate the stress value of shear has been done via the primary channels and the floodplain. It is possible to encounter the boundary shear. The identification of channel allocation to compute the discharge value was been studied. By the use of direct channels, the characteristics of boundary shear stress and its distribution are explored in Knight and Demetriou (1983). It was designed on the basis of measuring the shear force under different flows in different sub-partitions.

This was done in relation to two channel features that lacked dimensions: the floodplain and the compound section. Knight and Hamed (1984) concentrated their attention on rocky floodplains, following in the footsteps of Knight and Demetriou (1983). The investigation of the lateral momentum transfer to disclose the discrepancies in roughness is being studied among the primary channels and the floodplain. These floodplains are tightened in different stages to show the discrepancies. A set of equations has been formulated to analyze in vertical, horizontal, diagonal, and bisected interface plains to estimate the force value in shear. A set of equations that are based on four dimensionless channel properties has been supplied. Knight and Patel (1985) have given outcomes in finding out the relation between the stress distribution between the smooth and rectangular cross-partition that achieved the aspect ratios from one to ten. It was discovered that the distributions are controlled by the aspect ratio, as well as the aspect ratio's influence on the amount and type of secondary flow cells.

In order to investigate stress allotment in boundary shear by the use of smooth surface and complete circular parts, Knight and Sterling (2000) employed the Preston tube method as their method of analysis. It has been established that the Froude number and shape have an effect on the distribution of boundary shear stresses. After solving the continuity and momentum equations, Guo and Julien (2005) offered an approach to estimate the mean value for the bed and sidewall shear stress in smooth rectangular public-channel flows. This strategy was developed after the continuity, and momentum equations were solved. According to the findings of the experiment, the shear stresses are a result of three different components: (1) the shear stress at the interface between two different materials; (2) gravity; and (3) secondary flows. The amount of the total boundary shear force that may be attributed to the wall shear force was analyzed as part of a research that was carried out by Lashkar et al. (2010). They analyzed the data using nonlinear regression in order to construct equations that would allow us to calculate the percentages of shear stress near wetted regions that relying on the beds and sidewalls of rectangular cross-partition. In the case of meandering channels, the distribution of shear force was studied by Khatua and Patra (2010) that amends the sinuosity and geometrical properties of adopted channels. Similar to it, the Preston tube was studied by Naik and Khatua (2016) to determine the boundary of non-prismatic channels. Rather than the adoption of theoretical

approaches, the findings of those methodologies were far better than the findings of shear stress with the use of energy related gradient process. Using the Preston tube method, Prasad et al. (2022) were able to make a prediction about the border shear stress in diverging compound channels. According to the data, the strategy achieves favorable outcomes in both the smooth bed and gravel bed circumstances when compared to other approaches. This is the case regardless of the kind of bed. There has been progress made in the understanding of the relationships between boundary shear, geometry, and sinuosity. It is also possible to evaluate the models using data obtained from other researchers who have publicized the results of their study.

### **3 Classes of Variant Methodologies**

#### ***3.1 Geometrical Methods***

With the help of geometrical analysis, the cross-partitions are divided into the set of different sub-partitions. Each shear force may be calculated by first achieving a balance between the forces and fluid weight in each sub-region of the boundary that has been partitioned. Methods such as Leighly's (1932), Einstein's (1942), NDM, NAM, VAM, and NPM are also explored in this study.

#### ***3.2 Empirical Methods***

Curve fitting to experimentally collected data is a common approach in empirical research. Knight's (1981) model may be the first of its sort. Other researchers have incorporated his approach into their work, including Knight and his colleagues (1984). Similar basic models for the boundary shear stress were proposed by Olivero et al. (1999).

#### ***3.3 Analytical Methods***

Continuous, momentum, and energy transport equations are used in analytical approaches. It is possible to solve open-channel shear stress using some of these approaches. Yang and Lim (2005), Guo and Julien (2005), and Bilgil (2005) are a few examples of analytical methods.

### 3.4 Computational Methods

The shear stress value near boundaries, the analysis of turbulence-based closure model, and the motion formulation are employed to yield the accurate outcomes. To forecast the shear stress at boundary in primary flow channels, Cacqueray et al. (2009) have considered the SSG-based Reynolds model in computational fluid dynamics software. Though it permits to resolve the formulation of motion, yet the determination of order in boundary shear is not comparable. Hence, the proper examination of sediments analysis is done to find out the allotment of stress value near the local shear. The accurate estimation of local shear stress is employed on all versions of turbulence model. The other usage of empirical, analytical, and computational techniques has been studied. The main intention of these techniques was to estimate the mean value of wall and bed shear either through prismatic or direct channels. It is applied on the number of assumptions that could lead to the independent shear stress. The adoption of quantitative analysis has led to the estimation of boundary shear stress in coordination with prior models. Each of these approaches was chosen because it makes it possible to calculate the boundary shear stress in a comprehensive manner while at the same time being simple enough to be used in engineering applications.

## 4 Relatable Survey of Prior Methods

### 4.1 Vertical Depth Method (VDM)

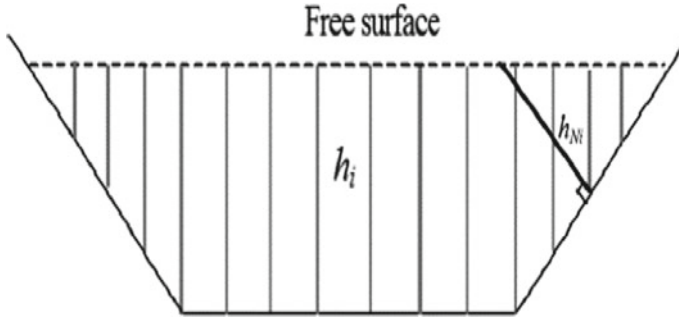
In this way, the local shear stress  $\tau_i$  that is acting on one wetted perimeter point denoted by the symbol  $i$  is relative to the depth estimation of local water, denoted by the symbol  $h_i$ .

$$\tau_i = \rho g h_i J \quad (1)$$

where

- $P$  density representation of water;
- $g$  acceleration representation of gravity;
- $J$  slope value of the observed energy.

The VDM is adaptable to any cross-partition geometry that is considered. On the other hand, it does not encounter the second-order constraints among the channel flow and the relatable floodplains. Added upon, the distribution of roughness under wetted perimeter is consistent across the process.



**Fig. 1** Visualizations of the VDM and NDM in schematic form (Khodashenas et al. 2008)

## 4.2 Normal Depth Method (NDM)

The thought process of vertical depth analysis is not used in the estimation of boundary shear stress of the slope at steep side. Thus, NDM was introduced by Lundgren and Jonsson (1964). This is because the steep side slope has a greater potential for shear deformation. They decided to use the normal depth method (NDM) rather than the vertical depth method (VDM). This method involves replacing  $h_i$  in Eq. (1) with  $h_{Ni}$ , where  $h_{Ni}$  is the depth analysis of the flow which is being circulated along the line of the wetted part. It is expressed as follows (Fig. 1):

$$\tau_i = \rho g h_{Ni} J \quad (2)$$

## 4.3 Merged Perpendicular Method (MPM)

The geometric analysis of the local shear under non-rectangular regions is studied by Khodashenas and Paquier (1999). The merged perpendicular method (MPM) is predicated on the theory of detaching the radius of hydraulic explored by Einstein (1942). This concept is characterized as “a cross-sectional zone bounded by walls splitting into three sub-areas, corresponding to sidewalls and bed, respectively.” With the help of transmission lines, the wetter regions are categorized into several sub-regions. These lines are perpendicular to the perimeter of the wetted region in accordance with the procedure (Fig. 2).

- i. The perimeter  $p$  of the wetted region is partitioned into different tiny segments coordinating with the length  $P_{il}$ .
- ii. The boundary of each segment is used to draw the perpendiculars  $L_{i-1}$  and  $L_i$ . These are scrutinized as first order.

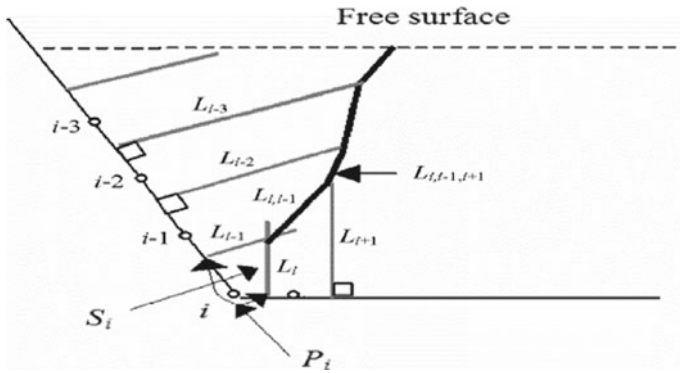


Fig. 2 Illustrations in schematic form of the MPM-determined regions

iii. The common point that meets the perpendicular has the option to elongate for the single line transmission. This is termed as bisector. Henceforth, the angle between the planes and intersection of perpendiculars is represented as

$$\hat{L}_{i,i-1} = 1/2(\hat{L}_i + \hat{L}_{i-1}),$$

wherein the “^” denoting the analysis between the planes and line  $L_i$ .

iv. In the case of joining, the common points of order  $j$  and  $k$  are added up to form order  $j + k$ . The angle formed among the line and the plane is used to estimate the weighted mean of those lines and planes.

Consider an instance, the order of 1 and 2 are 3. Similar to it, Fig. 2 presents the estimation of angles as:

$$\hat{L}_{i,i-1,i+1} = 1/3(\hat{2L}_{i,i-1} + \hat{L}_{i+1})$$

v. Every segment of local hydraulic is used to measure the radius as  $R_{hi} = S_i/P_i$ . This shows the discrepancies with the final lines and the flow area. Therefore, the stress value of the local shear  $\tau_i$  is then

$$\tau_i = \rho g R_{hi} J$$

The numerical integration of the local values is used to get the mean boundary stresses, which are denoted by the symbols  $\bar{\tau}_{(b)}$  and  $\bar{\tau}_{(w)}$  represent, respectively, the bed and the sidewall.

Relied on the stress value of local shear, the corners in convex are higher than the corners in concave due to the lower flow of velocity. This proves that MPM model yields better solution than the other models such as VDM, NAM, and NDM (Khodashenas and Paquier 1999). This is because the MPM takes into account the fact that the local shear stresses obtained at convex corners are larger than in concave

corners. This approach, on the other hand, does not take into account the processing of main channels via momentum to the floodplains and the structural flow of secondary constraints. In addition, when the wetted zone is subdivided into smaller sections, the roughness distribution that exists outside the wetted perimeter is not taken into consideration.

#### 4.4 Guo and Julien Method (GJM)

The mean estimation of bed and sidewall shear under rectangular part is estimated using Guo and Julien method. It assists to resolve the momentum and continuity criteria of the formulated part. With use of mapping the conformal constraints, the average of bed and stress value of sidewalls are calculated. On the other side, it eliminates the second constraints and also added the eddy viscosity which is shown in Eq. 3. By the use of Eq. 4, these two factors are integrated.

The formula for calculating the mean value of stress under bed shear is as follows:

The secondary constraints are

$$\frac{\bar{\tau}_{(b)}}{\rho ghJ} = \frac{4}{\pi^2} \frac{b}{h} \sum_{n=1}^{\infty} (-1)^n \frac{t^{2n-1} - 1}{(2n-1)^2} \text{ with } t = e^{-\frac{\pi h}{b}} \quad (3)$$

With corrections factors

$$\frac{\bar{\tau}_{(b)}}{\rho ghJ} = \frac{4}{\pi} \text{Arctg} \exp\left(\frac{-\pi h}{b}\right) + \frac{\pi}{4} \frac{h}{b} \left(\frac{-h}{b}\right) \quad (4)$$

The average of the shear stress at sidewalls is given as:

$$\frac{\bar{\tau}_{(w)}}{\rho ghJ} = \frac{b}{2h} \left(1 - \frac{\bar{\tau}_{(b)}}{\rho ghJ}\right) \quad (5)$$

#### 4.5 Prasad and Manson Method (PMM)

An analytical equation was presented by Prasad and Manson (2002) for the purpose of determining the proportion of shear force, %SF<sub>w</sub>. It is analyzed on the cross-partition of trapezoidal shape with the prismatic transfer mode. It was not taken into consideration that there were secondary currents. The proportion among the width and depth, b/h, is multiplied by to arrive at the percentage shear force, %SF<sub>w</sub>.

$$\%SF_w = \frac{100\bar{\tau}_{(w)}}{\bar{\tau}_{(w)} + \bar{\tau}_{(b)}\left(\frac{P_{(b)}}{P_{(w)}}\right)} = \left\{ \begin{array}{l} 25\left(4 - \frac{b}{h}\right)\frac{b}{h} \leq 2 \\ \frac{100}{h}\frac{b}{h} \geq 2 \end{array} \right\} \tag{6}$$

Here, the perimeter of bed is represented as  $P_{(b)}$ , and the perimeter of the sidewall is represented as  $P_{(w)}$ . Pertaining to it, the percentage analysis of shear stress value is resolved by exploration of  $\bar{\tau}_{(b)}$  and  $\bar{\tau}_{(w)}$  as:

$$\frac{\bar{\tau}_{(b)}}{\rho gh J} = (1 - 0.01 \%SF_w)\left(1 + \frac{P_{(w)}}{P_{(b)}}\right) \tag{7}$$

$$\frac{\bar{\tau}_{(w)}}{\rho gh J} = (1 - 0.01 \%SF_w)\left(1 + \frac{P_{(b)}}{P_{(w)}}\right) \tag{8}$$

#### 4.6 Knight et al. Method (KAM)

Empirical formulae are provided in order to measure the fraction of the shear force that is being taken up by the sidewall with the cross-partitions of trapezoidal and the roughness estimation of borders by following prismatic transfer mode. A significant number of different experimental data sets were used in order to refine this model. These featured, among other things, subcritical ( $F < 1$ ) flows in straight channels with rectangular and trapezoidal cross-sections, as well as supercritical ( $F > 1$ ) flows in straight channels.

Where  $F = u/(gS/b)^{1/2}$  represents value of Froude constant, flow of the velocity as  $u$ , width of the surface as  $b$ , and the cross-partition area as  $S$ . Experiments that were carried out later on by Knight and Sterling (2000) investigated stress range of boundary shear under smooth circular regions under flatbed. They discovered that for  $P_{(b)}/P_{(w)} > 1$ , denoting the contribution of the force in shear walls by considering a uniform stress values as:

$$\%SF_w = C_{cf} \exp\left[-3.23 \log_{10}\left(\frac{P_{(b)}}{P_{(w)}}C_2 + 1\right) + 4.6052\right] \tag{9}$$

For  $F < 1$ :  $C_2 = 1.50$ ,  $C_{cf} = 1$  for  $P_{(b)}/P_{(w)} < 6.546$ ,  $C_{cf} = 0.5875(P_{(b)}/P_{(w)})^{0.28471}$  for  $P_{(b)}/P_{(w)} \geq 6.546$ , and

For  $F > 1$ :  $C_2 = 1.38$ ,  $C_{cf} = 1$  for  $P_{(b)}/P_{(w)} < 4.374$ ,  $C_{cf} = 0.6603(P_{(b)}/P_{(w)})^{0.28125}$  for  $P_{(b)}/P_{(w)} \geq 4.374$ .



## 4.7 Preston Tube Technique

As a result of how simple it is to use and make the tubes using Preston. It is a kind of technique of measuring stress value of shear that is used rather often. Because of the development of diverse features such as length value of the roughness and the displacement analysis of zero-plane, it is challenging to apply this method to a rough bed, despite the fact that it is straightforward and dependable when used to a bed with a smooth surface. Mohajeri et al. (2017) established a novel Preston tube technique that is applicable for determining the volume of stress value of bed shear in both rough and smooth loose-flow channels. This new device could make formula usage of wall similarity model and the double averaging method. This is in contrast to Preston tube comprising of three tubes of Pitot with a static Prandtl tube. In coordinating to it, other strategies such as laws of logarithmic, stress profile analysis using Reynolds, slope measurement of energy, and the prior use of Preston tube were also tested in order to assure the collection of data quality. In order to do mathematical estimates of the boundary shear stress, Patel (1965) presented the correlations that are as follows:

$$x^* = \log_{10} \left( \frac{\Delta p d^2}{4 \rho \nu^2} \right) \quad (10)$$

$$y^* = 0.5x^* + 0.037 \text{ for } 0 < y^* < 1.5 \text{ and } 0 < x^* < 2.9 \quad (11)$$

$$y^* = 0.8287 - 0.1381x^* + 0.1437x^{*2} - 0.0060x^{*3} \\ \text{for } 1.5 < y^* < 3.5 \text{ and } 2.9 < x^* < 5.6 \quad (12)$$

$$y^* = \log_{10} \left( \frac{\tau d^2}{4 \rho \nu^2} \right) \quad (13)$$

Here, the diameter of outer region of Preston tube is represented as  $d$ ,  $\Delta p$  is the pressure difference between static and total pressure, the density of the liquid is given as  $\rho$ , and  $\nu$  is the viscosity of fluid in kinematic. The equations listed above were tested, and one of the following was selected as the best fit for calculating the stress value of wall shear relying on the count of  $x^*$  values. The aggregate force value of shear to the unit length is carried on the compound parts of walls that combine with the perimeter of entire region. This allowed for the accurate determination of the total shear force. The analyzed component of the weight force exerted by the liquid along the streamwise direction was compared to the total shear that was measured. It portrays the reliability of the considered ranges. In situations when the experiments were not repeated, the error percentages ranged within  $\pm 5\%$ .

## 5 Conclusions

Several unique approaches are introduced to perform a comparative study on the boundary shear stress distribution using prismatic channels. In specific to, a simple cross-sectional shapes like circular, rectangular covering the planar and compound sections under uniform boundary roughness. The experiments were conducted on the strategies such as Preston tube technique, the vertical depth method, the normal depth method, the merged perpendicular method, the Guo and Julien method, the Ramana Prasad and Russell Manson method, the Knight et al. method, and the merged perpendicular method.

Each strategy has shown the incredible support of employing it. Consider an instance, the mean calculation of bed and the sidewall shear stresses with respect to the stress value of local shear stress and perimetric distance are explored and discussed. In line to the experimental analysis, the stress value of local boundary shear and the mean of bed and sidewall shear have strong influence over the cross-sectional shape and the roughness estimation of boundary. However, the VDM strategy cannot express accurately of the local shear stress. The most accurate prediction of mean value of bed and the wall shear is obtained by using GJM method. The adoption of varying the eddy viscosity, factors related to presented and observed effects are employed. This conclusion illustrates the need of taking into consideration the secondary current repercussions. Therefore, the PMM and the KAM strategies has been widely employed to forecast the stress value of the wall and the shear. It is mainly tested on the flatbeds in cross-sections of rectangular and circular. Estimates of the local shear stress may be obtained using MPM for cross-sections that have a trapezoidal, rectangular, or circular shape. The MPM has the advantage of being able to adapt to geometries that have an uneven cross-section as well. For compound cross-sections, the MPM provides a fair estimate of the local shear stress provided that the cross-section is not curved, does not have a sharp edge, and does not intersect the main channel-floodplain interface zone of all compound partition. Because the MPM does not take into account lateral flow exchange among primary channel and the floodplain that could unleash the discrepancies. It affects the exchange of lateral flow in the MPM. In other words, the lack of inclusion of lateral flow exchange in the MPM is the cause of these local discrepancies. The outcomes of Preston tube method have the ability to measure the accuracy ranging from  $\pm 15.0$  to  $\pm 24\%$ , respectively, depending on whether the bed is smooth or rough. Because of these precision ranges, it is certain that this device will be useful in open-channel flow research in the future. The procedures described here are effective engineering tools that are not difficult to implement into numerical models. Even when looking at flows in flumes with trapezoidal or complex cross-sections, it might be difficult to identify the boundary shear stress distribution. This is because of the practical difficulties involved. Any cross-sectional shape that has a roughness distribution that is not uniform may be quickly treated using these procedures. For the overall validation of the approaches that have been provided, there has to be a greater number of boundary shear stress

measurements taken in smooth, intermediate, and rough channels with a variety of cross-sectional forms.

## References

- Bilgil A (2005) Correlation and distribution of shear stress for turbulent flow in a smooth rectangular open channel. *J Hydraul Res IAHR* 43(2):165–173
- Cacueray N, Hargreaves DM, Morvan HP (2009) A computational study of shear stress in smooth rectangular channels. *J Hydraul Res IAHR* 47(1):50–57
- Einstein HA (1942) Formulas for transportation of bed load. *Trans Am Soc Civil Eng ASCE* 68(8, Part 2):561–577
- Ghosh SN, Mehta PJ (1974) Boundary shear distribution in compound channel with varying roughness distribution. *Proc Inst Civ Engg* 57:159–164
- Ghosh SN, Roy N (1970) Boundary shear distribution in open channel flow. *J Hydraul Div ASCE* 96(4):967–994
- Guo J, Julien PY (2005) Shear stress in smooth rectangular open-channel flows. *J Hydraul Engg* 131(1):30–37
- Khatua KK, Patra KC (2010) Evaluation of boundary shear distribution in a meandering channel. In: *Proceedings of ninth international conference on hydro-science and engineering IIT Madras Chennai India ICHE 74*
- Khodashenas SR, ElKadi AK, Paquier A (2008) Boundary shear stress in open channel flow. *J Hydraul Res IAHR* 46(5):598–609
- Khodashenas SR, Paquier A (1999) Geometrical method for computing the distribution of boundary shear stress across irregular straight open channels. *J Hydraul Res IAHR* 37(3):381–388
- Knight DW (1981) Boundary shear in smooth and rough channels. *J Hydraul Div ASCE* 107(7):839–851
- Knight DW, Demetriou JD (1983) Flood plain and main channel flow interaction. *J Hydraul Eng ASCE* 109(8):1073–1092
- Knight DW, Demetriou JD, Hamed ME (1984) Boundary shear in smooth rectangular channels. *J Hydraul Eng ASCE* 110(4):405–422
- Knight DW, Hamed ME (1984) Boundary shear in symmetrical compound channels. *J Hydraul Eng* 110(10):1412–1430
- Knight DW, Patel HS (1985) Boundary shear in smooth rectangular ducts. *J Hydraul Eng ASCE* 111(1):29–47
- Knight DW, Sterling M (2000) Boundary shear in circular pipes running partially full. *J Hydraul Engg* 126(4):263–275
- Lashkar et al (2010) Boundary shear stresses in smooth channels. *J Food Agric Environ* 132–136
- Leighly JB (1932) *Toward a theory of the morphologic significance of turbulence in the flow of water in streams.* University of California Press, vol 6, no 1–9
- Lundgren H, Jonsson IG (1964) Shear and velocity distribution in shallow channels. *J Hydraul Div ASCE* 90(1):1–21
- Mohajeri SH, Akbar S, Salehi N (2017) An innovative Preston tube for determination of shear stress on smooth and rough beds. *Iran J Sci Technol Trans Civil Eng* 41(2):187–195
- Naik B, Khatua K (2016) Boundary shear stress distribution for a converging compound channel. *ISH J Hydraul Eng.* <https://doi.org/10.1080/09715010.2016.1165633>
- Olivero M, Aguirre-Pey J, Moncada A (1999) Shear stress distribution in rectangular channels. In: *Proceeding of XXVIII IAHR Congress Graz Austria* p 6
- Patel VC (1965) Calibration of the Preston tube and limitations on its use in pressure gradients. *J Fluid Mech* 23:185–208

- Prasad BSS, Sharma A, Khatua KK (2022) Distribution and prediction of boundary shear in diverging compound channels. *Water Resour Manage* 36(13):4965–4979. <https://doi.org/10.1007/s11269-022-03286-y>
- Prasad R, Manson JR (2002) Discussion of a geometrical method for computing the distribution of boundary shear stress across irregular straight open channels. *J Hydraul Res* 40(4):537–539
- Rajaratnam N, Ahmadi RM (1979) Interaction between main channel and flood-plain flows. *J Hydraul Div* 105(5):573–588
- Tominaga A, Nezu I, Ezaki K, Nakagawa H (1989) Three dimensional turbulent structure in straight open channel flows. *J Hydraul Res* 27(11):149–173
- Yang SQ, Lim SY (2005) Boundary shear stress distributions in trapezoidal channels. *J Hydraul Res* 43(1):98–102

# Water Quality Assessment Using Water Quality Index (WQI) Under GIS Framework in Brahmani Basin, Odisha



Abhijeet Das 

**Abstract** River water quality has become more important as a result of the numerous human activities that are contaminating it and the need to assure its safe and reliable use. In light of the fact that water quality has been threatened by human activities, apportionments of potential pollution sources are essential for water pollution control. A thorough investigation on the water quality of the Brahmani River has been done while considering these factors in mind. Twelve sampling sites have provided water samples to be examined. Twenty physicochemical parameters were investigated on yearly basis for a period of four year (2017–2021) by using standard procedures. The water quality index (WQI) was generated using the CCME algorithm, and a geostatistical technique called inverse distance weighting (IDW) was employed to create a forecast map for the region. Information from this research also aims to assist policy makers, to take the right decisions for sustainable agriculture in the study area. Between the observed data and the expected values from the predictor maps in both season, regression prediction was conducted on the three predicted stations, namely Biritola, Nandira D/s, and Kabatabandha. The study's quality database is created using the physicochemical analysis results of various water samples collected at various sites. The pH of the river was just mildly alkaline. In the PRM and POM, the overall CCME WQI grades fell into the fair to good and marginal to fair categories, respectively. Regression prediction values of WQI for all parameters in PRM were given the most acceptable values of determination coefficient ( $R^2 = 0.82$ ) than POM. The current investigation reveals that at stations P-3 (Panposh D/s) and P- 4 (Rourkela D/s), the quality of the local surface water has degraded. It was confirmed that both geogenic events and human activities linked to the origin of TC, TDS, TH, TA,  $\text{Ca}^{2+}$ , and  $\text{HCO}_3^-$ . At these places, it is necessary to first reduce the causes of deterioration to which the surface water is exposed, and the water should be treated before consumption. Therefore, future studies should be conducted in the area to precisely state the quality of water used for drinking and domestic purposes. Hence, this research should also emphasize identifying factors

---

A. Das (✉)

Research Scholar, Department of Civil Engineering, C.V. Raman Global University (CGU), Bhubaneswar, Odisha 752054, India  
e-mail: [das.abhijeetlaltu1999@gmail.com](mailto:das.abhijeetlaltu1999@gmail.com); [abhijeetlaltu1994@gmail.com](mailto:abhijeetlaltu1994@gmail.com);  
[2101070005@cgu-odisha.ac.in](mailto:2101070005@cgu-odisha.ac.in)

controlling surface water chemistry in the area. Further, measures should be discussed and implemented in managing downstream areas, sewage treatment facilities, and fertilizer and industrial application.

**Keywords** Brahmani river · Physicochemical parameters · CCME · IDW · Regression

## 1 Introduction

Water is one of important resources for consumption, as well as for additional uses including farming, industry, and recreational opportunities (Anawar and Chowdhury 2020). One of the main sources of freshwater for the world's human populations is the river. They are part of our natural heritage, yet they are constantly being overused, exploited, and polluted to the point where the surface water and aquatic life are being adversely affected (Patil et al. 2013; Das 2022). Furthermore, many riverine systems all over the world are becoming more and more polluted as a result of mounting human demand. Rivers have the ability to detoxify a specific number of contaminants that are dumped into them, but if that amount is exceeded, the water quality suffers (Chen et al. 2017). For instance, factors like precipitation, soil erosion from weathering, and human-induced factors like overusing water resources can all have an impact on the quality of surface water in a given area (Meshram et al. 2021). The river system has been under tremendous pressure over the past few decades due to population increase, urbanization, industrialization, and encroachments (Muhammad et al. 2018). Therefore, in order to create an effective water management system, it is necessary to comprehend the extent of pollution, create and quantify pollution tracking indices, as well as comprehend spatiotemporal changes in pollution in rivers (Fu et al. 2012). Surface water is a rich natural resource that has often been used for agriculture and consumption, especially in dry and semi-arid countries (Ram et al. 2021). It is significant because it has industrial uses and can be directly converted into drinkable water by desalination (Panagopoulos 2021). Also, recent changes in climatic conditions have affected rainfall patterns in the region, causing a significant decrease in crop yield as well as other agricultural productions. They have resulted in an increased demand for water resources exploration in communities within the region, for sustainable agricultural activities. Surface water quality has been impacted by significant pesticide leaching, salinization, topsoil contamination, landfill, and extensive floods (Islam and Mostafa 2021). Numerous studies have been done to evaluate the nation's surface water quality, including Hasan et al. 2019, Sarkar et al. 2019, Nadikatla et al. 2020, and Parvin et al. 2022. Surface water quality has been the subject of numerous investigations, particularly in coastal regions where water sodicity is a major problem (Islam and Majumder 2020). Therefore, it is critical to maintain continual observation to assess the water's suitability for diverse uses and guard against future deterioration of water quality in the research zone (Rahman et al. 2011). Surface water is usually thought to be the purest source of waterbodies, but studies have found that it is not

entirely free of contaminants (Ahmed et al. 2018). The fundamental issue is that once it is corrupted, it can never be made pure again (Sarkar et al. 2019). Water quality is impacted by the direct discharge of industrial waste, which includes detergent, toxic substances, acids, pigments, inorganic salts, and other contaminants (Roy and Shamim 2020a). Almost all of Odisha, India's drinking and irrigation water needs are met by the Brahmani River, the state's primary waterway. Over the past several decades, its river water has been continuously degrading as a result of the emission of untreated effluents and human intrusions (Bhadra et al. 2014). However, there is a lack of pollution source analysis concerning mixing the elements of nutrients, salinity, and heavy metals. This highlights the need for and issue of managing and conserving surface water quality (Said et al. 2004). The water quality index (WQI), that is employed to comprehend the overall water quality role of water supplies, has been employed to determine the water quality including both surface and ground water (Das 2022). Number of studies are carried out related to water quality index (WQI). WQI was initially used as a measure of water contamination by Horton in 1965. Over the past fifty years, literatures on water quality have also addressed the frequent fluctuations of WQIs (Banda and Kumarasamy 2020). It is imperative to create a WQI that is widely accepted and adaptable enough to reflect water that is fit for drinking or other uses for consumers everywhere (Othman et al. 2020). A newer WQI, the Canadian Council of Ministers of Environment Water Quality Index (CCME-WQI), which may be known as the Canadian Water Quality Index (CWQI) in 2001, was introduced in the middle of the 1990s (Lumb et al. 2011). The WQI was evaluated in this model based on the frequency of sample variables, failed variables, and variance from the standard values (Das 2023). This approach has helped to identify the pollution sources in the surface water. In fine, it evaluate contributions of potential pollution sources, have been widely used in the apportionment of water pollution and riverine pollution sources. Later, the United Nations Environmental Program acknowledged this model as a suitable model for evaluating the quality of drinking water around the world (Bharti and Katyal 2011). In the Talcher-Angul Industrial Vicinity, this approach has been used to estimate the grade of water in rivers including the Sabarmati River in Gujarat (Shah and Joshi 2017), the Dokan Lake Ecosystem (Hameed et al. 2010), the Ganges River along various sites in Allahabad (Sharma et al. 2014), and also the Brahmani River (Bhadra et al. 2014) (Mishra et al. 2014). Assessing surface water quality, mapping, vulnerability and appropriateness assessments, and other tasks connected to the management and development of water resources all need the use of geographic information system (GIS). These programmes provide tools for geographical analysis that can handle large amounts of data. An efficient method for interpreting and analysing spatial data has been demonstrated using the Inverse Distance Weighted (IDW) interpolation method with GIS technology (Soujanya et al. 2020). IDW relies on a method of precise local deterministic interpolation (Watson and Philip 1985). IDW was thought to produce the bathymetry of the Panchganga River Basin more precisely than Kriging and Topo to Raster. The WQI and IDW interpolation method has been employed by many researchers, including (Balamurugan et al. 2020; Soujanya et al. 2020), who are interested in evaluating surface water for drinking reasons. Surface water is a

significant supplier of potable water, residential use, and farming in the current field of research (Das 2022). However, just a small amount of study has been done on the Brahmani River's WQI report. There has not been a single study that blends WQI, GIS, and IDW to determine the score of this region. As a result, there is a study gap, and further discussion is required to comprehend the scope and reasons behind its decline. The following study's primary goal is to formulate an improved WQI in attempt to explore how human activities affect the water quality of the Brahmani River throughout the city of Odisha and ascertain whether it is acceptable for human consumption. These latest results could be useful in developing a successful drinking water management framework for the locals who live close to the sampling points. By applying the findings in this study, governments could take more flexible and targeted measures, such as treating eutrophic sewage in villages and controlling vehicle emissions.

## 2 Study Area

The Brahmani River is an important river in the Odisha state in eastern India. It is formed when the South Koel and Sankh rivers confluence at  $22^{\circ} 15' N$  and  $84^{\circ} 47' E$ . It passes through the districts of Sundergarh, Kendujhar, Dhenkanal, Cuttack, and Jaipur. A total of about  $39,628 \text{ km}^2$  of the river basin's drainage area is in the states of Jharkhand ( $15,405 \text{ km}^2$ ), Odisha ( $22,516 \text{ km}^2$ ), and Chhattisgarh ( $1347 \text{ km}^2$ ). The river basin's projected annual renewable water resources total 21,920 million cubic metres. Before it merges with the Bay of Bengal, the river passes through a sizable portion of an agricultural region and a number of industrial facilities. The river basin is in a climate zone with tropical monsoons, and it has three distinct seasons: winter, summer, and rainy season (Das et al. 2023). This region has a semi- arid to arid environment with an annual rainfall average of 1400 mm and a mean temperature of  $25.7^{\circ} C$ . The river basin provides an ideal environment for economic expansion since it has abundant mineral resources and inexpensive manpower. The Sundergarh district's Rourkela integrated steel mill, which also includes nearby mines, ancillary by product, and downstream product facilities, has significantly increased the town's development. In order to collect data for the study, 12 key sample stations were chosen, including Sankh U/s (P-1), Koel U/s (P-2), Panposh D/s (P-3), Rourkela D/s (P-4), Bonaigarh (P-5), Rengali (P-6), Samal (P-7), Talcher U/s (P-8), Dhenkhanal U/s (P-9), Bhuban (P-10), and Dharmsala (P-12). Figure 1 portrays the stream and the sampling spots chosen throughout its length. The water quality indicators taken into account in this study are TC, COD, pH, DO, BOD, TA, B,  $Fe^{2+}$ , TDS, TH, and EC, cations like  $Ca^{2+}$ ,  $Mg^{2+}$ ,  $Na^{+}$ , and  $K^{+}$ , and anions like  $CO_3^{2-}$ ,  $HCO_3^{-}$ ,  $Cl^{-}$ ,  $F^{-}$ , and  $SO_4^{2-}$ . These data were obtained annually for a duration of four years, i.e. (2017–2021).



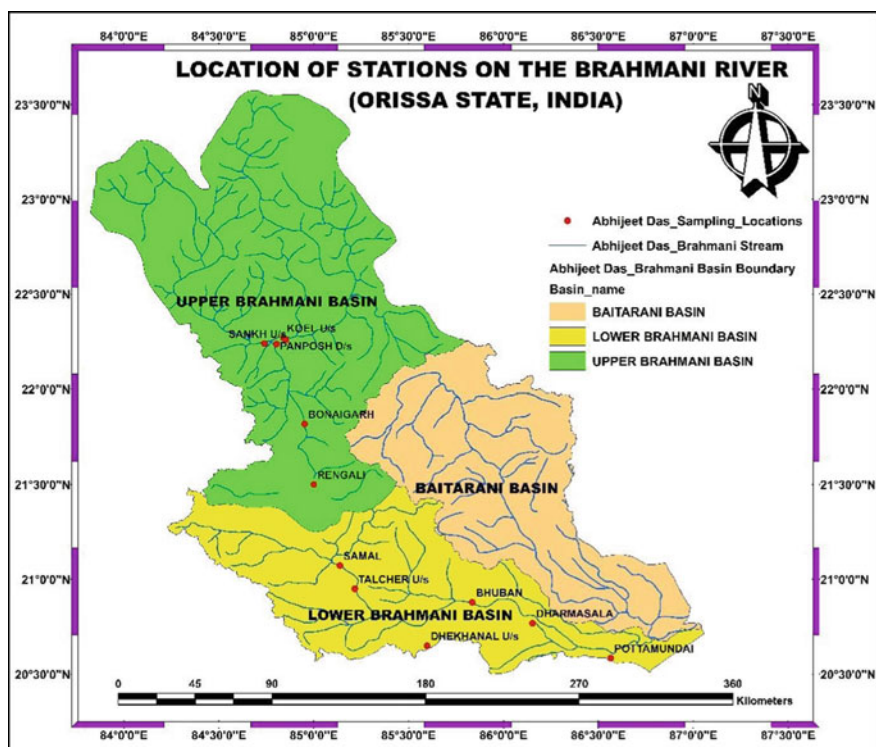


Fig. 1 Map showing study area and sampling locations

### 3 Data Collection and Analysis

Water samples were taken for the current study from 12 (Twelve) previously chosen sampling stations throughout the pre- and post-monsoon periods (PRM and POM), i.e. (2017–2021). The samples were taken between 10:00 am and 12:00 pm following downstream in both seasons. All samples indicate the current water quality at a particular time. Fresh surface water was collected for sampling using dry, clean, and sanitized plastic bottles. Following the steps outlined in APHA (2012), the samples were transferred to the laboratory at a favourable temperature ( $< 4\text{ }^{\circ}\text{C}$ ) after being collected and sealed in airtight bottles. The global positioning system (GPS) was used to gather global references for each place. During the analytical phase, techniques such as procedural blank, duplicates samples, and repetitive tests were carried out as needed for quality assurance. While the other parameters were determined in a laboratory, pH was measured on the spot using a portable metre. The Systronics Water Quality Analyzer 371 instantly measured total dissolved solid (TDS), electrical conductivity, and dissolved oxygen (DO) using a digital DO metre. Sodium ( $\text{Na}^+$ ), potassium ( $\text{K}^+$ ), iron ( $\text{Fe}^{2+}$ ), and calcium ( $\text{Ca}^{2+}$ ) were determined by flame photometer. Fluoride ( $\text{F}^-$ ), chloride ( $\text{Cl}^-$ ), sulphate ( $\text{SO}_4^{2-}$ ), carbonate ( $\text{CO}_3^{2-}$ ), and

bicarbonate ( $\text{HCO}_3^-$ ) were determined by ion chromatography. The majority of the samples were submitted to the Central Water Commission's water quality lab in Bhubaneswar for inspection and analysis. The proportion of TDS/EC is now within acceptable limits, and the charge balance remained typically less than 10%, verifying the accuracy of the data obtained. Below 5% indicated the relative standard deviation values.

## 4 Methodology

### 4.1 CCME WQI

The Canadian Water Quality Index (CWQI), which was first created by the Canadian Council of Ministers of the Environment (CCME WQI), offers a common framework that was created by Canadian jurisdictions to communicate water quality information to managers and the general public (CCME 2001). The following expression can be used to calculate index values, i.e.  $\text{CWQI} = 100 - ([F_1^2 + F_2^2 + F_3^2]^{0.5} / 1.732)$ . There are three components to it, with Scope ( $F_1$ ) equal to the number of elements whose objective limitations are not reached.  $F_1 = (\text{Number of failed variables} / \text{Total number of variables}) * 100$ . Frequency ( $F_2$ ) = The quantity of times the goals were not achieved.  $F_2 = (\text{Number of failed tests} / \text{Total number of variables}) * 100$ . Amplitude ( $F_3$ ) = The extent by which the test results that failed to pass did not attain their objectives. When the test value must not exceed the objective then  $\text{Excursion}_i = (\text{Failed test value}_i / \text{Objective}_j) - 1$ . For the cases in which the test the test value must not fall below the objective then  $\text{Excursion}_i = (\text{Objective}_j / \text{Failed test value}_i) - 1$ . Finally, normalized sum of excursions (NSE) is calculated as  $\text{NSE} = (\sum_{i=1}^N \text{excursion} / \text{Number of tests})$ . However, after scaling the normalizing summation of the excursions towards objectives (NSE) to generate a number ranging from zero and 100, an asymptotic function calculates  $F_3$ . The equation is represented as  $F_3 = (\frac{\text{NSE}}{0.01\text{NSE}+0.01})$ . The rating has been scaled from 0 to 100 using a proportion of 1.732. The five essential criteria are used to rate the quality of water: Excellent (95–100), good (80–94), fair (60–79), marginal (45–59), and poor (0–44).

## 5 Results and Discussions

The surface water quality maps for this research have been created utilizing ArcGIS 10.5, focusing on the parameters that have been chosen and explained previously. The many parameters taken into account for the study are explained in the paragraphs that follow. Table 1 illustrates the characteristics of water chemistry. The World Health Organization's (2011) recommendations for safe drinking water have been employed as a guide in this work. During PRM and POM periods, respectively, surface water

had a pH range of 6.6–8.4 and 7–8.1, which is between the upper acceptable limits of WHO criteria (6.5–8.5). The slight alkalinity may indeed be caused by the outflow of household and industrial wastewater into the river and the action of green organisms, which absorb CO<sub>2</sub> dissolved in water. (Driche et al. 2008). The amount of oxygen freely available in water is measured by dissolved oxygen (DO). The values are in the range of 6.8–8.3 and 6.9–8.3 during PRM and POM period. Increased temperature hampers the chemical interactions and reduces the DO concentration from water (Talling et al. 1957). DO numbers are high everywhere because they depend on a variety of variables, including temperature, microbial population, pressure, and sample period (Patnaik 2005). BOD is the amount of oxygen consumed for microorganisms to digest the organic compounds found in a particular water sample at a particular temperature for a certain period of time. COD describes the amount of DO required for any organic waste dissolved in the air to be oxidized (Das et al. 2023).

The reported BOD values are comparatively low to the WHO threshold of 5 mg/l, during which phase they constitute a risk to aquatic life owing to inadequate oxidative metabolism, and in both seasons varied from 0.75 to 4.5 mg/l. The presence of organic materials and bacterial load may be the cause of the low BOD value (Kumar and Puri 2012). In all seasons, COD ranged from 6.3 to 18.3, which is extremely low when compared to the WHO-recommended minimum limit of 250 mg/l. Reduced COD readings convey the existence of commercial and homemade effluents in the watercourse and give us a sense of the level of toxicity in the river water; the more waste, the lower the oxygen demand (Sharma et al. 2014). Coliform (TC) contamination has a deleterious effect on the river's DO to varying degrees. The waters close to industry, municipal sewage systems, or hospitals have been observed to contain high quantities of coliform bacteria (Niyoyitungiye et al. 2020). In the present study, values are in the range 1310–13,222 in both seasons. P-3 and P-4 levels during PRM and P-6 and P-7 levels during POM are much higher than the WHO-recommended standards (5000 MPN/100 ml). These high readings are an indication of dangerous chemicals and are also caused by bacterial pollutants in river water, household waste, industrial discharge, and food manufacturing runoff. The measuring capacity of alkalinity (TA) of water is to neutralize acids. These values varied as 40–250 and 50–880 during PRM and POM. The WHO's preferred threshold for alkalinity seems to be 120 mg/l. But in our study, maximum locations in both periods were high above the permissible limits and should be the effect of continuous, heavy deposition of domestic sewage, agricultural runoff along with effluents of industry (Sahni et al. 2011). A neutralizing agent can be used to increase the quality of water. The amount of organic matter and inorganic salts inside the water body dictate the TDS of the water; the lesser the TDS, the greater the purity of the water. During the PRM and POM seasons, the TDS of the water was determined to be 150–1200 and 74–622, respectively. Greater TDS observed in P-3 (1200) in PRM when compared with the values given by WHO (1000 mg/l). Extremely high values are a result of industrial discharge, home sewage, and agricultural runoff contaminating river water, and they are a sign of dangerous toxins in mineral form (Ibrahim and Nofal 2020). We can estimate the quantity of calcium and magnesium compounds in water by looking

**Table 1** Statistics of chemical parameters (all in mg/l, TC in MPN/100 ml and EC in  $\mu\text{S/cm}$ )

Parameters	Pre-monsoon (PRM)		Post-monsoon (POM)	
	Min	Max	Min	Max
PH	6.6	8.4	7	8.1
DO	6.8	8.3	6.9	8.3
BOD	0.75	4.5	0.75	4.5
TC	1310	13,222	1310	13,222
COD	6.3	18.3	6.3	18.3
TA	40	250	50	880
TDS	150	1200	74	622
TH	48	244	55	365
EC	55	590	90	240
B	0	0.17	0.03	0.17
F <sup>-</sup>	0.08	0.66	0.2	0.66
Ca <sup>2+</sup>	6.7	57.1	12.6	109.2
Mg <sup>2+</sup>	7.6	31.6	3.2	30.4
Na <sup>+</sup>	8	66	7	123
K <sup>+</sup>	0.2	1.32	0.7	5.3
Fe <sup>2+</sup>	0.01	0.2	0.02	0.09
CO <sub>3</sub> <sup>2-</sup>	0.01	36	0	180
HCO <sub>3</sub> <sup>-</sup>	48.8	292.8	61	1073
Cl <sup>-</sup>	15	179.9	15	129.9
SO <sub>4</sub> <sup>2-</sup>	0.5	45.7	0.7	48.8

at its total hardness (TH). The WHO has established a 600 mg/l hardness standard for drinking water. In the degree of hardness, water is commonly classified as soft (0–75 mg/l), moderately hard (75–150 mg/l), hard (150–300 mg/l), and very hard (> 300 mg/l). As per WHO standard of drinking water, total hardness values are in the range of 300–600. In the present study, the values varied as 48–244 and 55–365 during PRM and POM. P-3 (365 mg/l) in PRM has extremely hard water, and a significant concentration of hardness is visible. Water systems, frequent soap use, artery calcification, urinary concretions, kidney and bladder problems, and stomach disorders can all be impacted by high levels of hardness. Water's EC is typically correlated with the quantity of ions dissolved in the liquid. The river water samples in both seasons met the WHO's recommended maximum permitted limits of EC (750 S/cm), making them fit for human consumption. Higher EC readings can occasionally signify salt enrichment and may result from improperly disposing of nearby home and industrial wastewater. During PRM and POM, the content of boron (B) varied between 0 and 0.17 and 0.03 and 0.17. According to WHO criteria, the ideal level is close to 2 mg/l. A noticeable increase in the boron content of surface water can occasionally be brought on by the entry of wastewater with washing solutions containing borate compounds or leaching from sediment or rock containing borates or borosilicates (Danish et al. 2019). The activity of human cells, hormones, cancer, heart disease, fluid balance within the body, muscle contraction, neurological illness, and testicular descent are all significantly influenced by calcium ( $\text{Ca}^{2+}$ ) (Heaney et al. 1982). Although excessive ingestion of calcium damages the brain and causes hypercalciuria, kidney and vascular illness, urinary tract concretion, and compression of bone restoration, it is beneficial for bones and prevents osteoporosis (Nerband et al. 2003). During PRM and POM, it had levels between 6.7 and 57.1 and 12.6 and 109.2, respectively. According to WHO, the acceptable level for drinking water is 75 mg/l. Except for P-3 and P-10, all of the sampling locations are within the permissible ranges both before and after the monsoon. These sites saw the establishment of some cement and oil refinery companies, which mostly caused the river water's higher  $\text{Ca}^{2+}$  concentration (Potasznik and Szymczyk 2015). Magnesium ( $\text{Mg}^{2+}$ ) supports strong bones, robust nerve and muscle function, and a strong immune system. It also supports the regulation of blood glucose levels and the synthesis of protein and energy. Several different types of rocks, sewage, and industrial wastes are the main sources (Murphy 2007). During PRM and POM,  $\text{Mg}^{2+}$  values vary from 7.6 to 31.6 and 3.2 to 30.4, respectively. The required allowable level of magnesium for drinking is 35 mg/l (WHO). The bulk of the surface water is below the allowable magnesium limit. Additionally, the findings showed that sodium ( $\text{Na}^+$ ) was a dominant cation in both seasons. High  $\text{Na}^+$  concentrations can cause alkaline soils, which can negatively influence the structure and permeability of the soil. 200 mg/l of sodium is the acceptable amount in drinkable water (WHO). During PRM and POM, the values vary between 8 and 66 and 7 and 123, respectively, staying within allowed limits. Due to the physical structure of the soil and rocks, as well as the humidity and temperature of the semi-arid region, low concentrations may be seen in PRM and POM (Nwankwo et al. 2020). When ingested in excess, potassium ( $\text{K}^+$ ) can have laxative consequences such as elevated blood pressure, arteriosclerosis, hyperosmolarity, and

oedema (El-Aziz and Hassanien 2017). According to the WHO, the acceptable potassium limit is 12 mg/L. The limits encompass all sites. The most pertinent issue with rural drinking water is iron (Fe) (Islam and Mostafa 2021). Although a low iron level is necessary for human nutrition and plant metabolism and cannot cause significant harm, it promotes undesirable bacterial growth (iron bacteria) in waterworks and supply systems, which leads to the deposition of a slushy coating on the pipes (Can 1990). The recommended iron limit for drinking water is 1 mg/l (WHO). During PRM and POM, Fe concentrations vary between 0.01 and 0.2 and 0.02 and 0.09, respectively, satisfying the acceptable limits. The hardness and alkalinity of water are influenced by the presence of carbonates ( $\text{CO}_3^{2-}$ ) and bicarbonates ( $\text{HCO}_3^-$ ). Salts made of carbonates and bicarbonates are produced as a result of rock weathering. Low carbonate levels were found within the WHO's (100 mg/l) permissible limits in PRM and POM. Bicarbonate levels in PRM and POM range from 48.8 to 292.8 and 61 to 1073, respectively. According to WHO regulations, 300 mg/l is the permitted maximum. The results showed that carbonate from weathering sources contributed to POM's results, which were marginally greater than those for PRM. From P-6 to P-12, the threshold of bicarbonate greater than 500 mg/l was noticed. The rise in bicarbonate in these locations may be related to agricultural runoff, where the prevalent process in such arid agricultural areas is the dissolution of carbonate minerals being precipitated in the soil by the action of high evaporation rates (Selvam et al. 2013). Chloride ( $\text{Cl}^-$ ) is a sign of sewage-related contamination. According to the WHO, the permissible level of chloride is 250 mg/l (Kumar and Puri 2012). Plants and living things both eat chloride in tiny levels, but at higher doses, it is harmful. The recorded values for PRM and POM, which ranged from 15 to 179.9 and 15 to 129.9, respectively, are well within the permitted limits. Gypsum leaching and anthropogenic activity in a metamorphic environment result in the emission of sulphur gases, which decompose and enter surface water systems, resulting in the formation of sulphate ( $\text{SO}_4^{2-}$ ), which is naturally present in water (Shukla and Saxena 2020a). Throughout PRM and POM, the values ranged from 0.5 to 45.7 and 0.7 to 48.8, respectively. 200 mg/l is the acceptable limit for sulphate in drinking water (WHO 2011). In the current investigation, all  $\text{SO}_4^{2-}$  values are within the permissible range. Numerous studies have found that endemic fluorosis disease affects the rural population, especially children, as a result of excessive fluoride levels in drinking water (Adimalla et al. 2018). The readings were determined to be under the maximum permissible level of 1.5 mg/l of WHO, and they ranged from 0.08 to 0.66 and 0.2 to 0.66 during PRM and POM (2011). Although the human body needs these ions in modest amounts, when they are present in drinking water in large quantities, they can lead to a number of acute and chronic disorders. The current study evaluates the impact of water quality on ecosystem initiatives and makes use of the recently developed CCME WQI (procedure is discussed in the methodology section), which offers an easy way to summarize complicated water quality data that the general public, water distributors, planners, managers, and policymakers can easily understand. To evaluate regional and temporal changes in water quality, the CCME WQI calculator has been used in conjunction with the Canadian Water Quality Guidelines (Magesh and Chandrasekar 2011). This mechanism also, suggesting the

reliability and feasibility of using the variables, that helps in examining the apportionment of water pollution sources. The index was calculated taking into account all water quality factors. Table 2 displays the overall water quality index value for all sampling stations. According to the classifications of water quality assessed by the CCME WQI scores, the majority of the study area is classified as fair to good in the PRM and marginal to fair and fair to good in the POM. In PRM, stations like P3, P4, P2, P5, P9, and P10 indicate fair water quality, and P1, P6, P7, P8, P11, and P12 indicate good water quality. P-3, P-4, and P-9 in POM stand for marginal zone, P-2, P-11, and P-12 for fair, and P-1, P-5, P-6, P-7, P-8, and P-10 for good water quality. To identify the various water quality classifications, such as excellent, good, fair, marginal, and low at each hydro-station for drinking purposes, the spatial distribution map (Fig. 2a and b) was created using ArcGIS 10.5 software. In the case of PRM, the decline in water quality at the aforementioned locations P-3 and P-4 may be felt by domestic and industrial wastewater sources, agricultural runoff including fertilizers, and untreated water discharges. The station (P-1) in the area where the river flows through a mountainous region before approaching the Odisha belt has a good status in both periods owing to the presence of a few smaller towns on both of the river's banks and the unavailability of irrigation projects in the vicinity prior to it and surrounding the place. Owing to the river's capability to self-purify, rising water levels in its channel can also result in lower concentrations of the parameters. Major cities with dense populations grow from Station (P-1) to Station (P-12), indicating that the river's downstream has a significant effect on the water quality. The CWQI categorization indicates an overall good quality, but when it approaches the city, significant WQI alterations were noticed because of contaminating activities, encroachments, and burying activities.

## 5.1 Prediction Maps

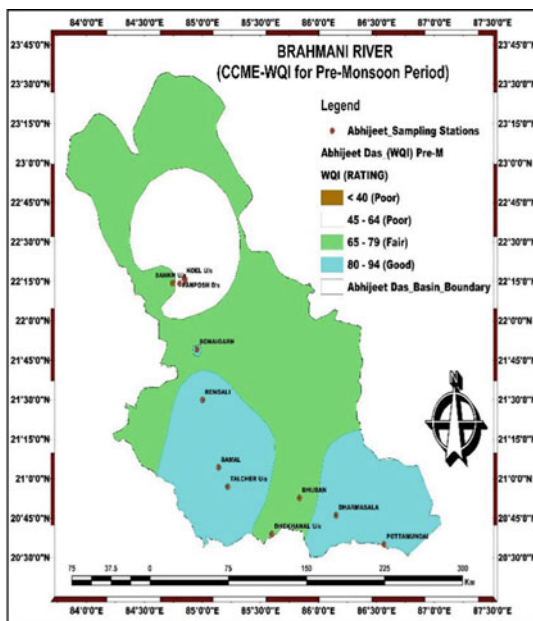
In this study, PRM and POM seasons were used to create prediction maps for 20 physicochemical variables measured from all sites for a period of 4-year timeframe, i.e. (2017–2021) along the Brahmani River. Using IDW and Arc GIS 10.5 tool, predicted maps for three anticipated stations had been created employing 12 observations. The prediction stations are Biritola, Nandira D/s, and Kabatabandha as shown in Fig. 3. The predicted values for the three stations (Fig. 4a and b) for PRM are Biritola (WQI = 69.56) indicates fair, Nandira D/s (WQI = 63.26) indicates fair, and Kabatabandha (WQI = 85.37) indicates good status whereas in POM, Biritola (WQI = 80.16), Nandira D/s (WQI = 55.22), and Kabatabandha (WQI = 78.08). Additionally, the forecast maps include information on the parameter dosages at each place along the river. Regression predictions were conducted across three measured data (observed values) and estimated values (results from predictor maps) for all variables in order to verify the values acquired from either the prediction maps developed by using the IDW and GIS connected to the Brahmani River. Overall, three sites had strong significance level for the coefficient value ( $R^2$ ) among actual and predicted

**Table 2** Water quality index classification

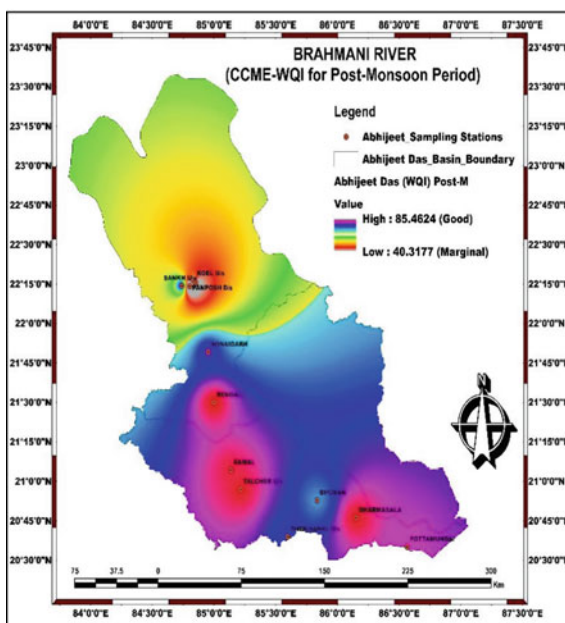
Location no	CWQI (PRM)	CWQI status (PRM)	CWQI (POM)	CWQI status (POM)
P-1	80.48	Good	81.49	Good
P-2	70.98	Fair	74.87	Fair
P-3	39.52	Poor	45.11	Marginal
P-4	43.48	Poor	53.16	Marginal
P-5	79.44	Fair	82.84	Good
P-6	85.47	Good	84.88	Good
P-7	84.6	Good	81.2	Good
P-8	85.19	Good	84.82	Good
P-9	77.66	Fair	52.52	Marginal
P-10	75.18	Fair	83.85	Good
P-11	85.08	Good	73.71	Fair
P-12	82.02	Good	60.46	Fair



Fig. 2 CCME WQI map of the study area



(a)



(b)

values in PRM. The results (Fig. 5) showed the determination coefficient ( $R^2 = 0.82$ ) for values during PRM is quite acceptable whereas in POM,  $R^2 = 0.29$ , shows weak correlation. Evidence shows that a variety of non-point inputs, including fertilizer runoff, urban runoff, toxic pollution, and trash dumping, are contaminating river water. As a corollary, these contributors lower the WQI ratings in the river.

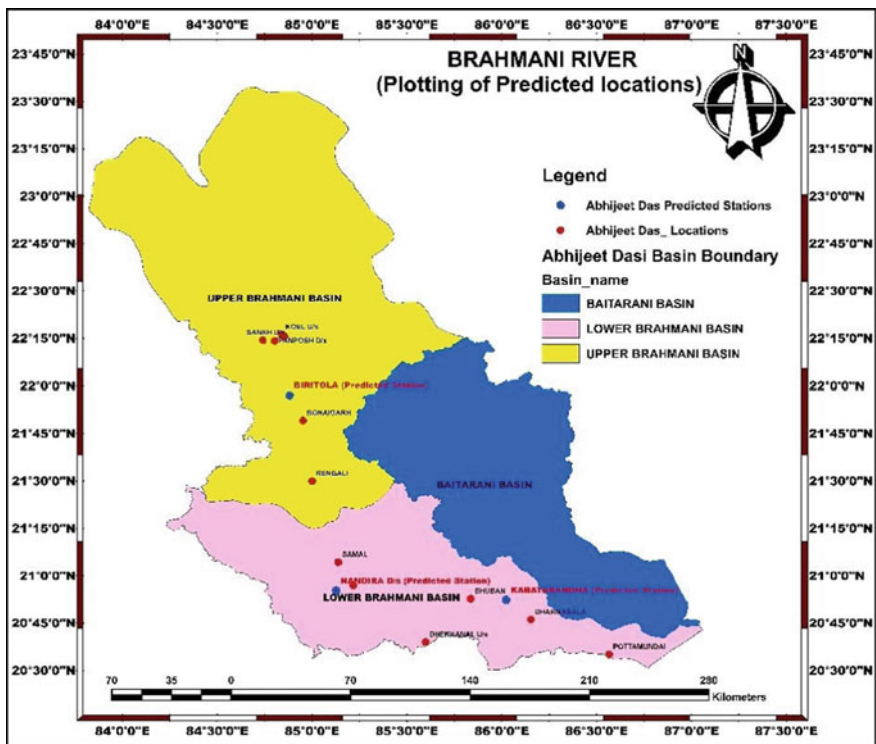
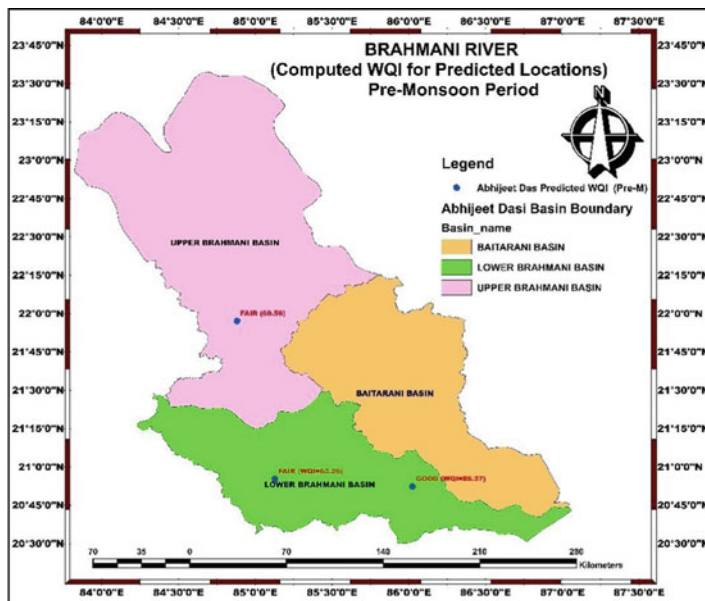
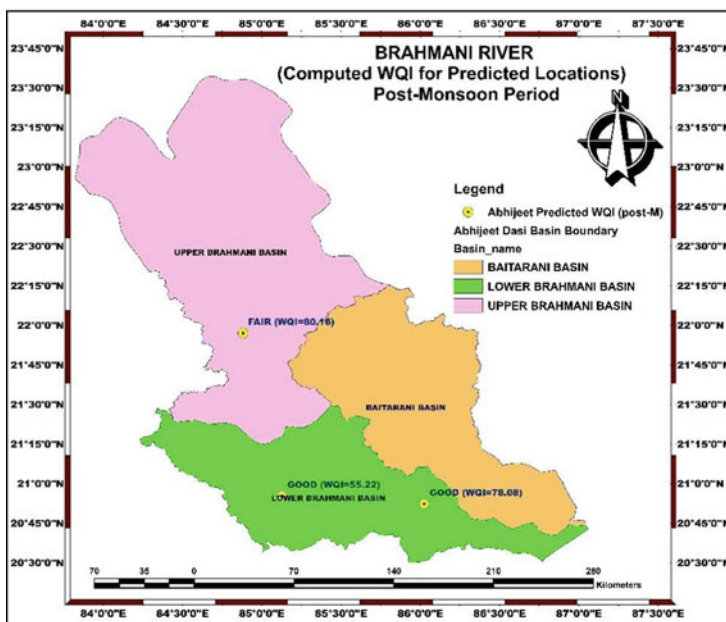


Fig. 3 Location of predicted stations



(a)



(b)

Fig. 4 Prediction map of PRM and POM season

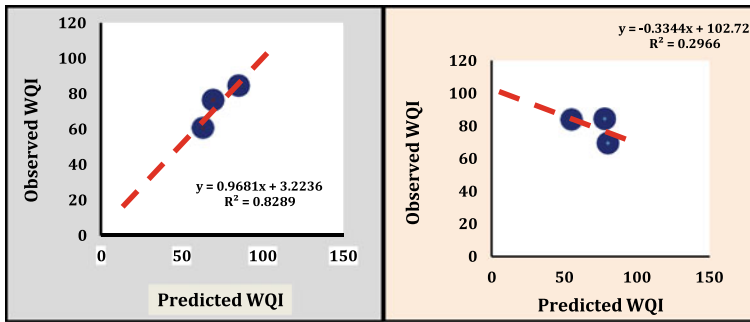


Fig. 5 Results of computed CCME-WQI and observed CCME-WQI

## 6 Conclusion

The latest study is a landmark in examining the water quality of one of the significant rivers in India, the Brahmani, which flows through the region of Odisha. This work, generally addresses a variety of subjects, such as pollution, and its evaluation on water quality. The collected data is combined using GIS to better illustrate the degree of pollution and its influence on public health. Twenty indices were chosen, and 12 study sites were identified. Because of its slightly alkaline composition, the river's water promotes the growth of phytoplankton. Pollutant addition to river water at several locations has raised the DO value. Excellent results were found for the water samples' BOD and COD. A few parameters like TC, TDS, TH, TA,  $\text{Ca}^{2+}$ , and  $\text{HCO}_3^-$  were identified as critical polluting parameters, which may substantially harm the health of the residents in the concerned site. It is evident from the WQI value that areas with a high TC number also have high WQI values. The input of wastewater into the basin, farmers' usage of animal manure, or irrigation of land should be the main causes of this association. On the basis of the CCME WQI scale, it is determined that over 50% of the observations in both periods fit into the good category. Hence, surface water is safe and potable in the study area except for localized pockets such as Panposh D/s and Rourkela D/s. The outcomes of the regression analysis demonstrated that, while the determination coefficients for these three values in the case of PRM were adequate, they are poor in the case of POM. The results of WQI throughout the river for Panposh D/s (P-3) and Rourkela D/s (P-4) could be negatively impacted by anthropogenic sources such as industrial pollution, untreated sewage water, municipal solid waste dumping, and vehicular emissions. With the use of a GIS tool, spatial variability mapping is a viable tactic for surveillance, maintenance, and future modelling. It conveyed potential data regarding the general pattern of water quality in the studied region. Therefore, prior to human intake, the proper treatment and remediation methods are needed. To fill more gaps in our understanding of the water quality aspects in Brahmani River, Odisha, the author may recommend future study efforts in a variety of areas. First of all, an in depth-investigation of how particular pollutants, such as pesticides, heavy metals, and

emerging contaminants, affect the water quality, would provide essential knowledge on potential risks and risk management strategies. Also, more research should be undertaken how climate change impacts water quality parameters including water temperature, DO and nutrient dynamics will also help to understand the long-term effects on the river basin.

**Acknowledgements** The author extend their appreciation to the C.V. Raman Global University (CGU), Bhubaneswar, Odisha, for providing necessary lab facilities, in order to carry out this innovative research work. Also, the author thanks to the anonymous reviewers and editor for the valuable suggestions in revising the manuscript.

**Author Contributions** Abhijeet Das: Investigation, writing and original draft, conceptualization, supervision, funding acquisition, writing, review and editing.

## References

- Adimalla N, Li P, Venkatayogi S (2018) Hydrogeochemical evaluation of groundwater quality for drinking and irrigation purposes and integrated interpretation with water quality index studies. *Environ Process*. <https://doi.org/10.1007/s40710-018-0297-4>
- Ahmed N, Bodrud-Doza M, Didar-UI SM, Choudhry MA, Muhib MI, Zahid A, Hossain S, Moniruzzaman M, Deb N, Bhuiyan MAQ (2018) Hydrogeochemical evaluation and statistical analysis of groundwater of Sylhet, north-eastern Bangladesh. *Acta Geochimica* 38:440–455. <https://doi.org/10.1007/s11631-018-0303-6>
- Anawar HM, Chowdhury R (2020) Remediation of polluted river water by biological, chemical, ecological and engineering processes. *Sustainability* 12:7017
- APHA (2012) Standard methods for the examination of water and wastewater, 22nd edn. American Public Health Association, American Water Works Association, Water Environment Federation, Washington
- Balamurugan P, Kumar PS, Shankar K et al (2020) non-carcinogenic risk assessment of groundwater in southern part of Salem District in Tamilnadu, India. *J Chil Chem Soc* 65:4697–4707
- Banda T, Kumarasamy M (2020) Development of water quality indices (WQIs): a review. *Pol J Environ Stud* 29(3):1–11. <https://doi.org/10.15244/pjoes/110526>
- Bhadra AK, Sahu B, Rout SP (2014) A study of water quality index (WQI) of the river Brahmani, Odisha (India) to assess its potability. *Int J Curr Eng Technol* 4(6):4270–4279
- Bharti N, Katyaj D (2011) Water quality indices used for surface water vulnerability assessment. *Int J Ecol Environ Sci* 2(1):154–173
- Can DNH (1990) Nutrition recommendations. The Report of the Scientific Review Committee, Department of National Health and Welfare (Canada), DSS Cat. no. H49-42/1990E. Ottawa. Available from: <https://catalogue.nla.gov.au/Record/1785247>
- Canadian Council of Ministers of the Environment (CCME) (2001) Canadian water quality guidelines for the protection of aquatic life: CCME Water Quality Index 1.0, Technical report, Canadian Council of Ministers of the environment, Winnipeg. <http://www.ccme.ca/source/tap/wqi.html>
- Chen D, Leon AS, Asce M, et al (2017) Application of cluster analysis for finding operational patterns of multireservoir system during transition period. *J Water Resour Plan Manag* 143(8):1–10
- Danish M, Tripathy GR, Panchang R, Gandhi N, Prakash S (2019) Dissolved boron in a brackish-water lagoon system (Chilika lagoon, India): spatial distribution and coastal behavior. *Mar Chem* 214:103663. <https://doi.org/10.1016/j.marchem.2019.103663>

- Das A (2022) Water criteria evaluation for drinking purposes in mahanadi river basin, Odisha. In: International Conference on Trends and Recent Advances in Civil Engineering, pp 237–260. Singapore: Springer Nature Singapore
- Das A (2022) Multivariate statistical approach for the assessment of water quality of Mahanadi basin, Odisha. *Mater Today Proc* 65:A1–A11
- Das A (2023) Assessment of potability of surface water and its health implication in Mahanadi Basin, Odisha. *Mater Today: Proc*
- Das A, Goyal A, Soni A (2023) Use of water quality indices and its evaluation to verify the impact of Mahanadi river basin, Odisha. In: AIP Conference Proceedings 27 July 2023; 2721 (1): 040003. <https://doi.org/10.1063/5.0153903>
- Das A, Goyal A, Soni A (2023) Deciphering surface water quality for irrigation and domestic purposes: A case study in Baitarani Basin, Odisha. In: AIP Conference Proceedings 2023 Jul 27; 2721(1):040017. <https://doi.org/10.1063/5.0153902>
- Driche M, Abdessemed D, Nezzal G (2008) Treatment of wastewater by natural lagoon for its reuse in irrigation. *Am J Eng Appl Sci* 1(4):408–413. <https://doi.org/10.3844/ajeassp.2008.408.413>
- El-Aziz A, Hassanien S (2017) Evaluation of groundwater quality for drinking and irrigation purposes in the north-western area of Libya (Aligeelat). *Environ Earth Sci* 76(4):1–17
- Fu K, Su B, He D, Lu X, Song J, Huang J (2012) Pollution assessment of heavy metals along the Mekong River and dam effects. *J Geogr Sci* 22:874–884
- Hameed A, Alobaidy MJ, Abid HS, Mauloom BK (2010) Application of water quality index for assessment of dokan lake ecosystem, Kurdistan region. *Iraq J Water Resour Prot* 2:792–798
- Hasan MK, Shahriar A, Jim KU (2019) Water pollution in Bangladesh and its impact on public health. *Heliyon* 5(8):e02145. <https://doi.org/10.1016/j.heliyon.2019.e02145>
- Heaney RP, Gallagher JC, Johnston CC, Neer R, Parfitt AM, Whedon GD (1982) Calcium nutrition and bone health in the elderly. *Am J Clin Nutr* 36:986–1013. <https://doi.org/10.1093/ajcn/36.5.986>
- Horton RK (1965) An index-number system for rating water quality. *J Water Pollut Control Fed* 37:300–306
- Ibrahim LA, Nofal ER (2020) Quality and hydrogeochemistry appraisal for groundwater in Tenth of Ramadan Area. *Egypt Water Sci* 34(1):50–64
- Islam MS, Majumder SMMH (2020) Alkalinity and hardness of natural waters in Chittagong City of Bangladesh. *Int J Sci Business* 4(1):137–150. <https://doi.org/10.5281/zenodo.3606945>
- Islam MS, Mostafa MG (2021) Trends of chemical pesticide consumption and its contamination feature of natural waters in especial reference to Bangladesh: a review. *Am Eurasian J Agric Environ Sci* 21(3):151–167. <https://doi.org/10.5829/idosi.ajeaes.2021.151.167>
- Kumar M, Puri A (2012) A review of permissible limits of drinking water. *Indian J Occup Environ Med* 16:40–44. <https://doi.org/10.4103/0019-5278.99696>
- Lumb A, Sharma TC, Bibeault J-F (2011) A review of genesis and evolution of water quality index (WQI) and some future directions. *Water Qual Expo Health* 3(1):11–24. <https://doi.org/10.1007/s12403-011-0040-0>
- Magesh NS, Chandrasekar N, Vetha Roy D (2011) Spatial analysis of trace element contamination in sediments of Tamiraparani estuary, southeast coast of India. *Estuar Coast Shelf Sci* 92:618–628
- Meshram SG, Singh VP, Kahya E, Sepehri M, Meshram C, Hasan MA, Islam S, Duc PA (2021) Assessing erosion prone areas in a watershed using interval rough-analytical hierarchy process (IR-AHP) and fuzzy logic (FL). *Stochastic Environ Res Risk Assess* 36:297–312
- Mishra TK, Moharana JK, Nanda PM, Gamaik BK (2014) Study of water quality index of brahmani river water in Talcher-angul industrial vicinity, Odisha. *Int J Curr Res* 6(06):704; 9–70
- Muhammad AHR, Malik MM, Sana M (2018) Urbanisation and its effects on water resources: an exploratory Analysis. *Asian J Water Environ Pollut* 15(1):67–74
- Murphy S (2007) General information on dissolved oxygen. City of Boulder/USGS Water Quality Monitoring. Last Page Update–Monday April 23, 2007. Retrieved July 10, 2007, from <http://bcn.boulder.co.us/basin/data/BACT/info/DO.html>

- Nadikatla SK, Mushini VS, Mudumba PSMK (2020) Water quality index method in assessing groundwater quality of Palakonda mandal in Srikakulam district, Andhra Pradesh, India. *Appl Water Sci* 10(1):30
- Nerbrand C, Agréus L, Lenner RA, Nyberg P, Svärdsudd K (2003) The influence of calcium and magnesium in drinking water and diet on cardiovascular risk factors in individuals living in hard and soft water areas with differences in cardiovascular mortality. *BMC Public Health* 18(3):1–21. <https://doi.org/10.1186/1471-2458-3-21>
- Niyoyitungiye L, Giri A, Ndayisenga M (2020) Assessment of coliforms bacteria contamination in Lake Tanganyika as bioindicators of recreational and drinking water quality. *South Asian J Res Microb* 9–16
- Nwankwo CB, Hoque MA, Islam MA, Dewan A (2020) Groundwater constituents and trace elements in the basement aquifers of Africa and sedimentary aquifers of Asia: medical hydrogeology of drinking water minerals and toxicants. *Earth Syst Environ* 4:369–384. <https://doi.org/10.1007/s41748-020-00151-z>
- Othman FME, Seyam AH, Ahmed AN, Teo FY, Fai CM, Afan HA, Sherif M, Sefelnasr A, El-Shafie A (2020) Efficient River water quality index prediction considering minimal number of inputs variables. *Eng Appl Comput Fluid Mech* 14(1):751–763. <https://doi.org/10.1080/19942060.2020.1760942>
- Panagopoulos A (2021) Study and evaluation of the characteristics of saline wastewater (brine) produced by desalination and industrial plants. *Environ Sci Pollut Res* 29:23736–23749. <https://doi.org/10.1007/s11356-021-17694-x>
- Parvin F, Haque MM, Tareq SM (2022) Recent status of water quality in Bangladesh: a systematic review, meta-analysis and health risk assessment. *Environ Chall* 6(100416):1–13. <https://doi.org/10.1016/j.envc.2021.100416>
- Patil S, Ghorade IB (2013) Assessment of physico-chemical characteristics of Godavari River water at Trimbakeshwar and Kopergaon, Maharashtra. *Indian J Appl Res* 3(3):149–152
- Patnaik KN (2005) Studies on environmental pollution of major industries in Paradip Area. Ph.D. Thesis, Utkal University, Bhubneshwar, (Unpublished)
- Potasznik A, Szymczyk S (2015) Magnesium and calcium concentrations in the surface water and bottom deposits of a river-lake system. *J Elementol* 20(3):677–692
- Rahman M, Majumder R, Rahman S, Halim M (2011) Sources of deep groundwater salinity in the southwestern zone of Bangladesh. *Environ Earth Sci* 63:363–373. <https://doi.org/10.1007/s12665-010-0707-z>
- Ram A, Tiwari SK, Pandey HK, Chaurasia AK, Singh S, Singh YV (2021) Groundwater quality assessment using water quality index
- Roy M, Shamim F (2020a) Assessment of anthropogenically induced pollution in the surface water of River Ganga: a study in the Dhakhineswar Ghat, W.B, India. *J Water Pollut Purification Res* 7(1):15–19
- Sahni K, Silotia P, Prabha C (2011) Seasonal variation in physico-chemical parameters of Mansagar lake, Jaipur. *J Env Bio Sci* 25:99–102
- Said A, Stevens DK, Sehlke G (2004) An innovative index for evaluating water quality in streams. *Environ Manage* 34(3):406–414. <https://doi.org/10.1007/s00267-004-0210-y>
- Sarkar AM, Lutfor Rahman AKM, Samad A, Bhowmick AC, Islam JB (2019) Surface and ground water pollution in Bangladesh: a review. *Asian Rev Environ Earth Sci* 6(1):47–69. <https://doi.org/10.20448/journal.506.2019.61.47.69>
- Selvam S, Manimaran G, Sivasubramanian P (2013) Hydrochemical characteristics and GIS-based assessment of groundwater quality in the coastal aquifers of Tuticorin corporation, Tamilnadu, India
- Shah KS, Joshi GS (2017) Evaluation of water quality index for river Sabarmati, Gujarat, India. *Appl Water Sci* 7:1349–1358
- Sharma P, Meher PK, Kumar A, Gautam YP, Mishra KP (2014) Changes in water quality index of Ganges River at different locations in Allahabad. *Sustain Water Qual Ecol* 3:67–76



- Shukla S, Saxena A (2020a) Groundwater quality and associated human health risk assessment in parts of Raebareli district, Uttar Pradesh, India. *Groundwater Sustain Dev* 10:100366
- Soujanya Kamble B, Saxena PR, Kurakalva RM, Shankar K (2020) Evaluation of seasonal and temporal variations of groundwater quality around Jawaharnagar municipal solid waste dumpsite of Hyderabad City, India. *SN Appl Sci* 2:1–22. <https://doi.org/10.1007/s42452-020-2199-0>
- Talling JF (1957) The longitudinal succession of the water characteristics in White Nile. *Hydrobiol* 11:73–89
- Watson DF, Philip GMA (1985) Refinement of inverse distance weighted interpolation. *Geoprocessing* 2:315–327
- WHO (2011) Guidelines for drinking-water quality: third edition incorporating the first and second addenda. World Health Organization, Geneva
- Wu Z, Zhang D, Cai Y, Wang X, Zhang L, Chen Y (2017) Water quality assessment based on the water quality index method in Lake Poyang: the largest freshwater lake in China. *Sci Rep* 7(1):1–10



# Meta-heuristic Approach for Flood Control in Reservoir Operation



Priya Chauhan and Sandeep M. Narulkar

**Abstract** Besides irrigation and power generation, reservoirs in India also play a vital role in protecting the country from floods. During flood, reservoirs store and release the excess water according to its capacity and future requirement. It is imperative that the reservoir has to be operated effectively to conserve water so that competing goals can be accomplished. This requires an extensive investigation and the development of new system analysis approaches using meta-heuristic techniques of soft computing. The Omkareshwar Sagar Project (OSP) Reservoir in India has been designed to satisfy annual demands, protect against flooding, and produce maximum power generation, which is used for analysis in the current study. The present study incorporates one conventional optimization method the nonlinear programming (NLP), a semi-conventional method the genetic algorithm (GA) and a meta-heuristic technique the teaching–learning-based optimization (TLBO) to solve the problem of optimum operation in a flood scenario. A flood-release protocol has to be developed keeping the objective of maximum power output and reach the specified storage target at the end of the operation. Present study has been a successful attempt in getting the desired results, and the adoptability of the TLBO for complex problem is also proven.

**Keywords** Flood control · Meta-heuristics · Nonlinear programming · Genetic algorithm

---

P. Chauhan (✉) · S. M. Narulkar  
Shri G. S. Institute Of Technology And Science, Indore, India  
e-mail: [cpriya14@gmail.com](mailto:cpriya14@gmail.com)

S. M. Narulkar  
e-mail: [snarulkar@gmail.com](mailto:snarulkar@gmail.com)

## 1 Introduction

Irrigation, hydropower, navigation, and flood management are reservoirs' significant economic contributors to the benefit of any country. Besides irrigation and power generation, the reservoirs in India also play a vital role in protecting the country from floods. During the floods, reservoirs store and release the excess water according to its capacity and future requirement. Flood protection and optimizing power generation and storage for future use are important reservoir objectives that are competing with one another. It is imperative that the reservoir has to be operated effectively to conserve water so that competing goals can be accomplished in an optimum manner. Reservoir management has benefited from the development and use of both traditional and more recent meta-heuristic optimization methodologies. Traditional reservoir operation methods include linear programming (LP), nonlinear Programming (NLP), and dynamic programming (DP). Each one had many advantages thus has been applied to many problems in reservoir operation studies. The disadvantages of these strategies outweigh the benefits. LP requires a linear objective function and constraints, whereas DP is bound by dimensionality, and NLP is incapable of addressing the non-convex issue efficiently on its own (Hosseini-Moghari et al. 2015). Many reviews (Yeh 1985; Wurbs 1993; Rani and Moreira 2010) on reservoir planning and operation are available in the literature. To alleviate the difficulties and to overcome the limitations, there has been a constant hunt for new optimization techniques that can produce globally optimal solutions. The advent of soft computing techniques in general and meta-heuristic algorithms [MA] techniques in particular have revolutionized the optimization process. MA are probabilistic approximation techniques that allow efficiently solving optimization problems. (Nesmachnow 2014) A review on MA along with the water resources applications can be seen in Reddy and Kumar (2020) and reservoir optimization problems in particular in Lai et al. (2022). The MA techniques are further classified as evolutionary algorithms (EA), swarm intelligence algorithms (SIA), and other algorithms based on certain natural physical processes or human-induced processes. The basic premise on which EAs work is to generate a population of possible solutions through a selection mechanism, evolution, and reproduction to achieve better solutions. The genetic algorithms (GA) introduced by Holland (1992) is the most commonly applied EA which is applied mostly to the optimization of reservoir operations. The algorithm is straightforward and easy to implement. The limitations of GA are discussed in Lai et al. (2022). GA is considered to be a slower optimization technique, and its chance of sticking to a local optimum is maximum.

The teaching–learning-based optimization (TLBO) algorithm was developed by Rao et al. (2011). When a teacher has a significant impact on student performance, it is referred to as TLBO. Results or grades are used to measure output here. In the field of water resources, the TLBO algorithm has only recently been applied in a few studies, including (Kumar and Yadav 2018) on reservoir operation, (Patel and Balve 2018) on multi-reservoir operation policy, (Patnaik and Swain 2021) on the comparison of PSO and TLBO for Hirakud reservoir operation, (Kumar and Yadav

2021) on water allocation, and (Ajudiya et al. 2022) on optimization of cropping pattern in the command area of multiple reservoir system. To summarize, TLBO is broadly applicable in the field of water resources as a global optimization technique, and these studies show that it is also a reliable technique for producing global optimal solutions.

In this study, target storage generation was optimized to meet annual demands, prevent floods, and maximize power generation at the Omkareshwar Sagar Project (OSP) reservoir in India. The OSP reservoir operations are optimized for a monsoon flood wave situation using a conventional NLP approach and a semi-conventional genetic algorithm method to validate the accuracy of the TLBO results.

The Omkareshwar Sagar Project (OSP) reservoir in India has been designed to satisfy annual demands, protect against flooding, and produce maximum power generation, which is used for analysis in the current study. Present study incorporates one conventional optimization method the nonlinear programming (NLP), a semi-conventional method the genetic algorithm (GA), and a meta-heuristic technique the teaching-learning-based optimization (TLBO) to solve the problem of optimum operation in a flood scenario. A flood-release protocol has to be developed keeping the objective of maximum power output and reach the specified storage target at the end of the operation. Present study has been a successful attempt in getting the desired results, and the adaptability of the TLBO for complex problem is also proven.

## 2 Theoretical Background

### 2.1 Genetic Algorithm

Over other optimization techniques, GA provides a lot of advantages. Both parallelism and the ability to work through challenges of varying complexity are critical. A linear or nonlinear, continuous or random noise objective (fitness) function is just as valid as a non-stationary (changing over time) linear objective (fitness). All of these optimizations can be handled by genetic algorithms. Genetic algorithms, on the other hand, have some downsides. It is vital to take into account the size of the population, mutation and crossover rates, as well as other important aspects, when creating a new population in order to arrive at an accurate fitness function. Choosing the incorrect selection will hinder or eliminate the algorithm's ability to converge. Genetic algorithms, despite these drawbacks, are nevertheless widely used in nonlinear optimization. (Yang 2021) provides a comprehensive description of the algorithm.

## 2.2 Teaching–Learning-Based Optimization

A novel population-based algorithm called TLBO (Rao et al. 2011) simulates classroom teaching and learning. The professor’s approach to getting their students to participate in class and work together more effectively is the basis for the algorithm. You don’t have to worry about making precise modifications with the TLBO. TLBO’s key regulating elements are the number of iterations and the size of the population. It is the major goal of teachers at TLBO to improve the average grade of classes. The two components of the algorithm are: the teacher and the learner.

### 2.2.1 Teacher Phase

The teacher phase is the first step in the TLBO algorithm. Teachers place a high priority on raising the average grade in their classes. A new solution is created using the population’s mean value and the solution’s best fitness value (teacher). This is how each solution ( $x$ ) variable gets changed:

$$x_{\text{new}} = x + r(x_{\text{best}} - t_f x_{\text{mean}}) \quad (1)$$

There are five factors in this equation: the current solution/population value  $x$ , the newly generated solution/population value  $x_{\text{new}}$ , the teacher’s selection of the  $x_{\text{best}}$  solution/population based on the objective function’s minimum and maximum values, the population’s mean value  $x_{\text{mean}}$ , the teaching factor  $T_f$ , which can be either 1 or 2, and a random number between zero and one for each variable.

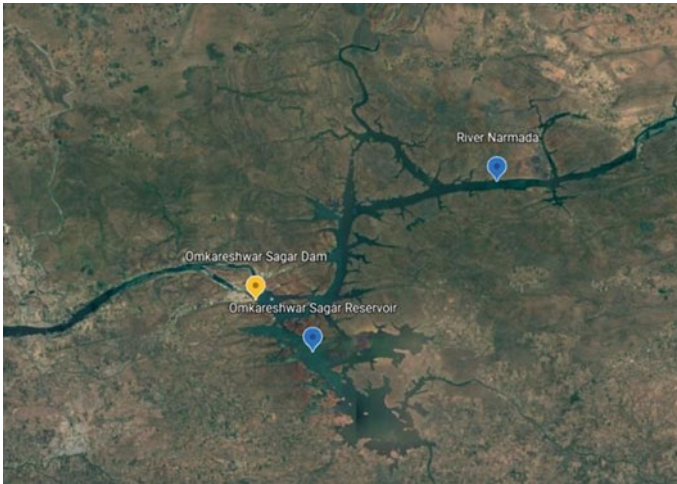
### 2.2.2 Learner Phase

The learner phase requires students to interact with each other. With the help of partner solutions, new ideas might be generated. For the sake of finding the finest potential companion, the population will be culled. As an example, consider the fact that a partner’s answer cannot be the same as a solution that the learner examines. All variables can be changed based on current and partner fitness levels.

$$x_{\text{new}} = x + r(x - x_p) \quad \text{if } f_i < f_p \quad (2)$$

$$x_{\text{new}} = x - r(x - x_p) \quad \text{if } f_i > f_p \quad (3)$$

where the current solution/learner value is  $x$ ,  $x_{\text{new}}$  is the new generated value,  $x_p$  represents the partner solution/learner,  $f_i$  is the current solution/fitness learner’s value,  $f_t$  is the partner solution/fitness learner’s value. The value  $r$  will be randomly chosen between 0 and 1 for each variable.



**Fig. 1** Satellite view of Omkareshwar Sagar project

### 3 Study Area

India's Omkareshwar Sagar Project reservoir in Madhya Pradesh is used to compare nonlinear programming, genetic algorithm, and teaching–learning-based optimization for reservoir operation under a flood scenario. The OSP is made up of eight 65-MW power plants and a gravity dam that stands 53 m tall and 949 m long. The reservoir's total capacity of 987 Mcm is used to irrigate more than 146,800 hectares of crops. India's Sardar Sarovar Project (SSP) and India's Indira Sagar Project (ISP) are two of the country's major reservoir projects. The intercepted flow between ISP and OSP joins with the water already released from ISP, which creates a vast reservoir. OSP's operations have been complicated as a result of the mandatory release of water for SSP. As a result, OSP must be triggered in order to protect the reservoir's downstream side from floodwaters, maximize power output, target storage for future use, and ensure that the reservoir's downstream receives the appropriate release. Figure 1 shows the satellite view of Omkareshwar Sagar Project location.

### 4 Model Formulation

The objective function is defined in light of the following purposes: By adding a continuity constraint to the objective function, the objective function is modified. The release from the hydropower is kept constant at 6.87 Mcm per hour to enhance power generation.

$$\text{Min} \left[ \sum_{t=1}^T V_1(Q_t)^2 + V_2(S_{t+1} - S_t - I_t + Q_t + Q_{pt})^2 + \sum_{t=2}^{T+2} V_3(S_t - T_s)^2 \right] \quad (4)$$

where

$Q_t$  = Outflow through Spillway,  $Q_{pt}$  = Outflow through turbine taken as a constant value equal to 6.87 Mcm per hour,  $S_t$  = Storage at time  $t$ ,  $S_{t+1}$  = Storage at time  $t + 1$ ,  $T_s$  = Target storage in the reservoir,  $Q_t \text{ max}$  = Maximum outflow through the spillway,  $Q_t \text{ min}$  = Minimum Outflow through the spillway,  $Q_{pt} \text{ max}$  = Maximum Outflow through the turbine.

The objective function is confined by variable value boundaries.

$$Q_t \text{ min} \leq Q_t \leq Q_t \text{ max} \quad (5)$$

$$Q_{pt} \text{ min} \leq Q_{pt} \leq Q_{pt} \text{ max} \quad (6)$$

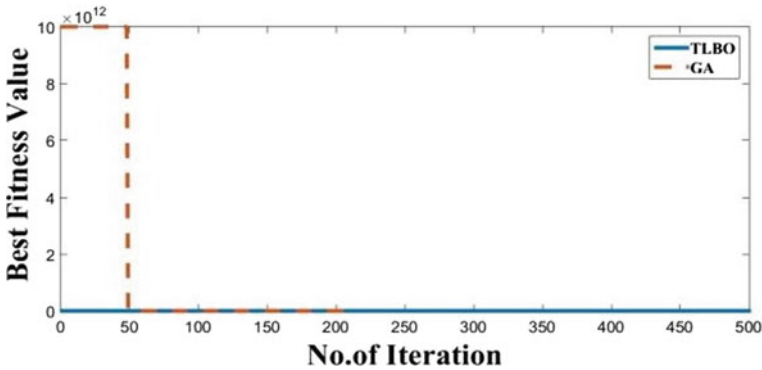
$$S_t \text{ min} \leq S_t \leq S_t \text{ max} \quad (7)$$

$V_1$  is the weight related to the spillage that must be minimized,  $V_2$  is the weight connected to the continuity equation, and  $V_3$  is the weight involved with meeting the reservoir's target storage at the conclusion of operation. The current challenge has 25 release values and 25 storage values. Due to the fact that weights are fixed, multiple objective problems can be treated as a single optimization problem.

## 5 Result and Discussion

Optimizing reservoir operation with aims of maximizing power generation, achievement of storage targets, protecting the downstream side from flooding are the objectives of the present study applied to OSP reservoir during flood. Three techniques, one of them is NLP and other two are meta-heuristic techniques the GA and the TLBO, have been employed to solve the same problem for comparison. MATLAB platform was used for coding of the problem and solving it. The results of the problem are stated in following lines.

All the three algorithms result in to maximization of the hydropower releases and have maintained it to a value of 6.87 Mcm throughout the flood season. The problem is basically a weighed sum of squares and squared. The following are the weights assigned in the objective function: As a result,  $V_1$  is set at 0.1 to reduce spillage,  $V_2$  is set at 100 to achieve maximum power, and  $V_3$  is arbitrarily varied between 0.00001 and 100,000 for the inflow value of a flood wave to emphasize



**Fig. 2** Convergence of TLBO to best fitness value for different flood inflow scenarios

reaching target storage at the end. Using a heuristic method to allocate weights ensures that the study’s many goals are completed in the order they were given in the beginning. The objective function is optimized using genetic algorithms, nonlinear programming, and teaching–learning-based optimization with a population size of 20 and 500 iterations.

The convergence generated by GA and TLBO for a flood inflow scenario of monsoon duration to an optimal solution is shown in Fig. 2. It is clearly seen in the figure that TLBO initiates with lower fitness value, on the other hand GA initiates with very higher value. After 152 iterations, GA stuck in local minima. Details of fitness value at different iteration numbers can be seen in Table 1. By observing Table 1, results of fitness value generated by TLBO ( $3.607e + 5$  in 398 iterations) are much better than GA and NLP on all stages of iteration. Table 1 is restricted to 400 iterations due to the achievement of convergence at 398 iterations of TLBO, while NLP and GA already converge at 319 and 152 iterations, respectively.

Two more distinct algorithms are used to determine the TLBO algorithm’s correctness in achieving the target storage of 299.00 Mcm. The TLBO results were compared to the GA and NLP outcomes. Figure 3 illustrates a comparison of gradually increasing storage plots computed from flood wave inflow values using GA, NLP, and TLBO. As illustrated in Fig. 3, all models take the same path to reach the destination storage with very slight changes.

The final storage values derived by GA, NLP, and TLBO for a flood inflow scenario are shown in Table 2. The model is compressed based on the near target storage value achieved by GA, NLP, and TLBO in terms of Mcm and percentage. From Table 2, it is apparent that the percentages of target storage reached by GA, NLP, and TLBO are 96.1706%, 96.9264%, and 97.1237%, respectively, indicating that TLBO performs well in attaining near target storage.

GA, NLP, and TLBO developed a flood influx scenario inflow and outflow charts are shown in Fig. 4. Outflows formed by each algorithm are clearly shown in Fig. 4; however, TLBO’s path is smoother than those generated by GA and NLP. Outflow plot provided by TLBO is a smoother hydrograph, which reduces the peak flood level

**Table 1** Fitness value at different iteration numbers

	Iteration										Iteration of convergence
	50	100	150	200	250	300	350	400			
NLP	2.9851e + 6	1.0810e + 6	5.6603e + 5	5.5e + 5	5.4905e + 5	5.4891e + 5	5.4885e + 5				319
GA	1.046e + 6	8.148e + 5	7.987e + 5	7.986e + 5							152
TLBO	7.565e + 5	4.04e + 5	4.04e + 5	3.945e + 5	3.922e + 5	3.656e + 5	3.656e + 5	3.607e + 5			398



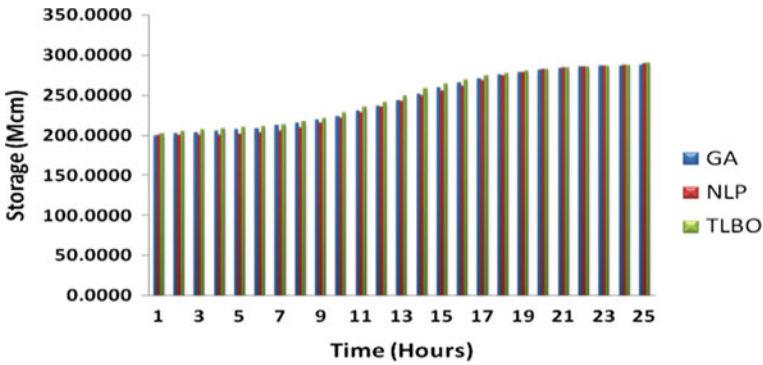


Fig. 3 Comparative gradually increasing storage plot from GA, NLP and TLBO

Table 2 Target storage (299.00 Mcm) achievement by GA, NLP, and TLBO

Optimization	Storage achieved (Mcm)	% Storage achieved
GA	287.55	96.1706
NLP	289.81	96.9264
TLBO	290.40	97.1237

to safeguard downstream areas while also releasing a mandated amount of water to a downstream side water supply system.

Flood peak reduction by GA, NLP, and TLBO can be seen in Table 3. In order to compare the algorithms, GA, NLP, and TLBO result in reducing the flood peak in terms of Mcm and percentage. From Table 3, it is clear that TLBO lowered the flood peak by 18.4764%, which suggests that TLBO’s performance in reducing the flood peak to safeguard the downstream side together with the mandatory release is excellent.

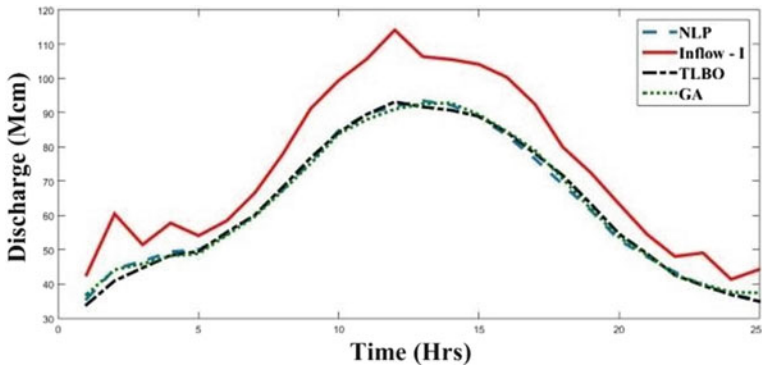


Fig. 4 Comparative inflow versus outflow plot generated from GA, NLP, and TLBO

**Table 3** Flood peak reduced by GA, NLP, and TLBO

Optimization	Flood peak volume 114.2 Mcm	
	Flood peak reduced	% Flood reduced
GA	93.42	18.1961
NLP	93.50	18.1261
TLBO	93.10	18.4764

Results of TLBO model for a flood inflow scenario show that the TLBO is capable of maximizing hydropower output, attaining target storage levels, protecting the downstream sides of reservoirs from flooding, and releasing mandated amounts for the reservoir on the downstream side. TLBO findings were also tested against conventional NLP and semi-conventional GA results, and it was determined that TLBO can be utilized to optimize reservoir operation difficulties during flood situations.

## 6 Conclusion

A nonlinear optimization model is solved with genetic algorithms, teaching–learning-based optimization, and nonlinear programming for the achievement of target storage for future use and maximize hydropower generation and provide flood protection on the downstream side of the reservoir. The model was applied to Omkareshwar Sagar Reservoir to simulate a monsoon flood inflow. For a population of 20, the best fitness outcomes can be achieved by running the TLBO algorithm for 500 iterations. GA achieves and converges at a fitness value of  $7.987e + 5$  in 151 iterations at the same iteration time. TLBO's fitness value is  $4.40e + 5$ , which is much lower than GA. TLBO finally converged at  $3.607e + 5$  in 398 iterations to obtain the global optimal solution, proving its robustness and speed. The highest increased power output has been achieved by maintaining hydropower release at a higher value. GA, NLP, and TLBO achieve 96.1706%, 96.9264%, and 97.1237% of the target storage value, respectively. In addition to helping to safeguard the downstream from flooding, GA, NLP, and TLBO's reduction in flood peak is 18.1961, 18.1261, and 18.4764%, respectively, which offers mandatory release for the downstream side reservoir, and TLBO's results show the highest reduction rate among all algorithms. According to comparative results of GA, NLP, and TLBO results for a convergence plot, target storage achievement, and flood peak reduction flood inflow scenario, TLBO performed better than conventional and semi-conventional approaches. This research shows that teaching–learning-based algorithm approach is capable of optimizing large-scale, sophisticated water resource systems.

## References

- Ajudiya B, Yadav SM, Majumdar PK (2022) Optimization of cropping patterns in the command area of multiple reservoir system using TLBO algorithm. *ISH J Hydraul Eng* 28(3):271–280
- Holland JH (1992) Genetic algorithms. *Sci Am*. <https://doi.org/10.1038/scientificamerican0792-66>
- Hosseini-Moghari SM, Morovati R, Moghadas M, Araghinejad S (2015) Optimum operation of reservoir using two evolutionary algorithms: imperialist competitive algorithm (ICA) and Cuckoo optimization algorithm (COA). *Water Resour Manage* 3749–3769
- Janga Reddy M, Nagesh Kumar D (2020) Evolutionary algorithms, swarm intelligence methods, and their applications in water resources engineering: a state-of-the-art review. *H2Open J* 3(1):135–188. <https://doi.org/10.2166/h2oj.2020.128>
- Kumar V, Yadav SM (2018) Optimization of reservoir operation with a new approach in evolutionary computation using TLBO Algorithm and Jaya Algorithm. *Water Resources. Management* 32:4375–4391. <https://doi.org/10.1007/s11269-018-2067-5>
- Kumar V, Yadav SM (2021) Optimization of water allocation for Ukai reservoir using elitist TLBO. *Water Resour Manage Reserv Oper* 191–204
- Lai V, Huang YF, Koo CH, Ahmed AN, El-Shafie A (2022) A review of reservoir operation optimisations: from traditional models to metaheuristic algorithms archives of computational methods in engineering, vol 29, 3435–3457. <https://doi.org/10.1007/s11831-021-09701-8>
- Nesmachnow S (2014) An overview of metaheuristics: accurate and efficient methods for optimisation. *Int J Metaheuristics* 3(4):320–347
- Patel JN, Balve PN (2018) Optimisation of multi reservoir operation policy using teaching learning based optimisation algorithm. *Pertanika J Sci Technol* 26(3):1155–1168
- Patnaik P, Swain PC (2021) Intelligent operation of hirakund reservoir using metaheuristic techniques (PSO and TLBO). *Water Resour Manage Reserv Oper* 263–276. [https://doi.org/10.1007/978-3-030-79400-2\\_22](https://doi.org/10.1007/978-3-030-79400-2_22)
- Rani D, Moreira MM (2010) Simulation– optimization modeling: a survey and potential application in reservoir systems operation. *Water Resour Manag* 24:1107–1138. <https://doi.org/10.1007/s11269-009-9488-0>
- Rao RV, Savsani VJ, Vakharia DP (2011) Teaching–learning–based optimization: a novel method for constrained mechanical design optimization problems. *Comp Aided Design* 43:303–315
- Wurbs RA (1993) Reservoir-system simulation and optimization models. *J Water Resour Plan Manag ASCE* 119(4):455. [https://doi.org/10.1061/\(ASCE\)0733-9496](https://doi.org/10.1061/(ASCE)0733-9496)
- Yang X (2021) Genetic algorithm. In: Chapter–6, nature-inspired optimization algorithms, 2nd edn., pp 91–100
- Yeh WWG (1985) Reservoir management and operations models: a state-of-the-art review. *Water Resour Res* 21(12):1797–1818. <https://doi.org/10.1029/WR021i012p01797>

# UAV-Based High-Resolution DEM Application for River Cross-Section Derivation and 1D Flood Assessment



Mrunalini Rana, Dhruvesh Patel, and Vinay Vakharia

**Abstract** The precise digital elevation model (DEM) is the need of an hour for flood risk assessment to reduce the loss of lives and properties. The benchmarked free source nationally available DEM is Cartosat and globally available DEM is SRTM, which is widely used for hydrodynamic modeling by developing countries. However, it covers the course resolution. High-resolution DEM is required to execute the hydrodynamic model in 1D and 2D and to improve the flood decision-making system at the sub-metric level for urban flood mapping and assessment. Therefore, to reduce the data deficiency for flood decision-making systems in urban areas in developing countries, high-resolution DEMs are generated. This attempt has been performed over the Sabarmati River with a stretch of 5 km, covering the 8 km<sup>2</sup> of the area and its surrounding. The advanced survey was done using a UAV named 4RTK (Real-Time Kinematic) Phantom for the study area. The data collected were processed with the help of Pix4D. This UAV is then converted into different grids size of 0.5 m × 0.5 m to 10 m × 10 m resolution to perform the simulation for the study area using Global Mapper. These DEMs are used as input parameters for performing any hydrodynamic simulation. The high-resolution DEMs can be utilized for the preparation of river geometry extraction and comparisons of the river bed and river banks. This high-resolution DEM is used in the hydrodynamic model to produce flood inundation, velocity, depth, and water surface elevation maps. The research shows that high-resolution DEM is most applicable to creating a high-resolution map for flood decision-making. Hence, high-resolution DEMs influence the accuracy of flood forecasts, so even the most severe catastrophes can be mitigated.

---

M. Rana (✉) · D. Patel

Department of Civil Engineering, Pandit Deendayal Energy University, Gandhinagar, India

e-mail: [mrunalini.rphd20@sof.pdpu.ac.in](mailto:mrunalini.rphd20@sof.pdpu.ac.in)

D. Patel

e-mail: [Dhruvesh.Patel@sof.pdpu.ac.in](mailto:Dhruvesh.Patel@sof.pdpu.ac.in)

V. Vakharia

Department of Mechanical Engineering, Pandit Deendayal Energy University, Gandhinagar, India

e-mail: [Vinay.Vakharia@sof.pdpu.ac.in](mailto:Vinay.Vakharia@sof.pdpu.ac.in)

**Keywords** Unnamed aerial vehicle (UAV) · Digital elevation model (DEM) · Flood assessment · 1D modeling

## 1 Introduction

Floods are the most damaging, pervasive, and common natural disasters, which account for roughly 30% of all-natural disaster losses (Hashemi-Beni et al. 2018; Govedarcic et al. 2018) causing significant economic damage on a global scale (Darji et al. 2021). The destruction caused by the flood has increased much due to dense urbanization and radical climatic changes, resulting in a massive loss of life and property in recent decades. In the present situation, the frequency and intensity of floods are increasing dynamically every year. A high-tide coastal zone, industrialization, bank erosion, illegal construction, floodplains, valleys, and a thickly urbanized area all play to the mayhem factors toward flood (Trambadia et al. 2022). The International Disasters Database covers the years 1900–2020 and comprises 11,356 both records of hydrological and meteorological disasters that caused 8.6 million fatalities and \$2600 million in economic damage worldwide (2019) (Garrote 2022). In India, the Himalayan Rivers floods 80% of the flood-affected region during the rainy season, which occurs from June to September. During the monsoon season, extreme flooding occurs annually in many Indian states, including Gujarat, Maharashtra, Andhra Pradesh, West Bengal, and Orissa, resulting in massive property and life losses. While it is not possible to control the flood completely, the consequence can be taken care of by identifying the flood-prone areas in advance with the proper implementation of risk management. The associated hazards could be minimized if flood-prone areas are known in advance (Darji et al. 2021). DEMs, such as SRTM or ASTER, are among the most important input data for hydrological modeling; nevertheless, these DEMs are not very precise or have a high spatial resolution, which inevitably reduces the accuracy of the hydraulic model and flood maps (Mazzoleni et al. 2020). According to several case studies, current remote sensing technologies fail to give sufficient detail to determine the effects of micro-topography and the presence of property flood-resistant measures (Darji et al. 2021). Hence, the faults and flaws in global DEMs are carried over into hydraulic modeling, influencing the outcomes. As a result, responsibilities such as flood hazard assessments and flood risk management would be impacted, particularly in data-scarce areas (Garrote 2022). For credible assessments of flooding area mapping and flood hazard analysis, accurate and high spatial resolution topographic data are required as UAV-generated very high-resolution DEM can be used to examine stream features, velocity, and floodplain, improving our scientific understanding of hydrological processes at the very small scale. Several prior research publications have argued that the quality of free global DEMs should be improved in order to generate a more reliable flood hazards map (Garrote 2022). Complex hydrological and hydraulic models have been developed as a result of the socioeconomic relevance of flood research; one-dimensional (1D) and two-dimensional (2D) hydraulic models, for example, have all become critical numerical tools in floodplain planning and hazard identification (Mazzoleni et al. 2020). One-dimensional (1D) simulation models are commonly calibrated and

validated using water level data, whereas 2D simulation models are typically calibrated and validated by comparing extensional flooding areas. Hydraulic models that have been calibrated and validated require a variety of input data to be implemented. One of the most delicate input data is the morphology of the river channel and floodplain, which are frequently described using digital elevation models (Horritt and Bates 2001). In reality, DEM is a critical component in addressing water resource management concerns. These DEMs are produced by UAV surveys, and in recent years, the scientific community has started to look into a number of aspects of UAV survey used in urban and riparian flood modeling (Mazzoleni et al. 2020). UAVs have arisen as a low-cost alternative to traditional photogrammetric systems for image-capturing platforms, allowing for the low-cost generation of high-quality and high-frequency data (Miro Govedaric et al. 2018), and in comparison to traditional data acquisition approaches, it has the ability to quickly deliver high spatial resolution imagery for a temporal event (e.g., the extent of flooding at a particular flood stage) (Trambadia et al. 2022). Numerous nations have shown promising outcomes for a widespread application of UAV survey in hydraulic modeling, showcasing the advantages of drone-based remote sensing with a sharp decrease in risks, costs, and execution time, while delivering products of acceptable quality for the desired use. (Mazzoleni et al. 2020). This paper aims to present the usability of DEM of different grid/resolutions using Global Mapper, created based on UAV images, for flood assessment for Sabarmati River, at Gandhinagar. For quantitative investigations such as flood extension and the building of inundation models, UAV-derived DEMs prove valuable and economical.

## 2 Information About Site

### 2.1 Study Area

The research area is in the district of Gandhinagar, Gujarat. The research region is located in the Sabarmati basin, with flat topography and generally covered by agricultural fields and urbanized areas. During the May 2006 floods, it played an essential role in the flood inundation in the low line area of the Sabarmati River.

### 2.2 Data

The UAV survey is done at the stretch of Sabarmati River between Gandhinagar bypass road, i.e., Dholeswar–Shahpur Bridge with coordinates  $23^{\circ} 11' 12''$  N and  $72^{\circ} 39' 30''$  E and GIFT city PDP Bridge with coordinates  $23^{\circ} 8' 33''$  N and  $72^{\circ} 40' 12''$  E, along with the important landmarks sideways the banks of the river. Pictures taken onsite are used in Fig. 1 to depict the location of the study area of Sabarmati River. A. Displays the Sant Sarovar Dam, which is seen on the upstream side of the Dholeswar–Shahpur Bridge. B. Shows a picture of the Dholeswar–Shahpur

Bridge. The GIFT city PDPU Bridge is shown in picture C. The total area covered is 8.7 km<sup>2</sup>. The stretch of river stream between the two bridges is 4.45 km with a radial coverage of 3.34 km. The UAV used for the project was Phantom 4 RTK (Real-Time Kinematics); refer to Fig. 2.

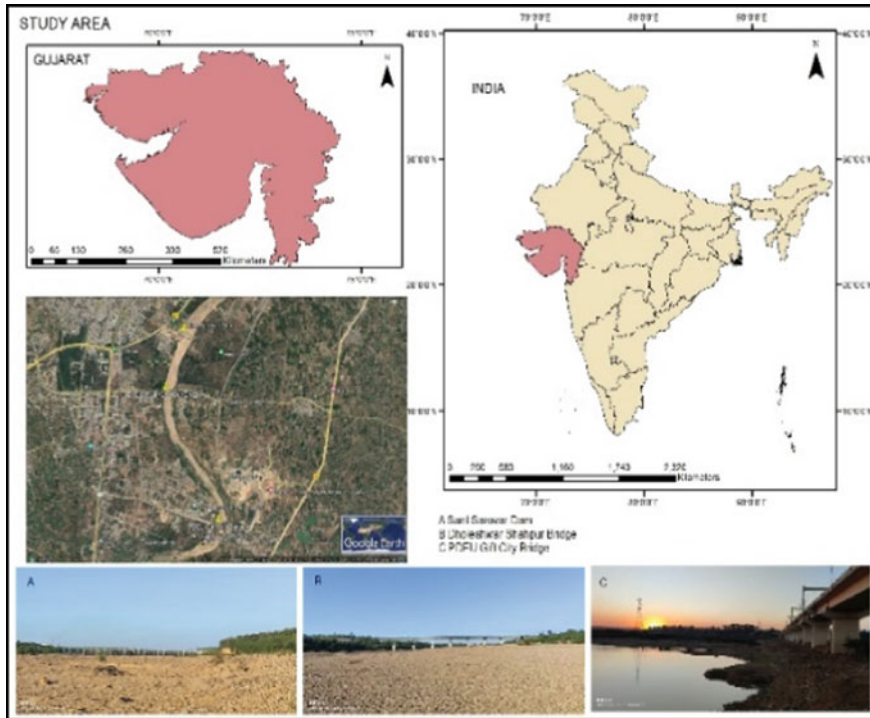


Fig. 1 Study location

Fig. 2 Phantom 4 RTK.  
Reproduced from: <https://www.dji.com/phantom-4-rtk>



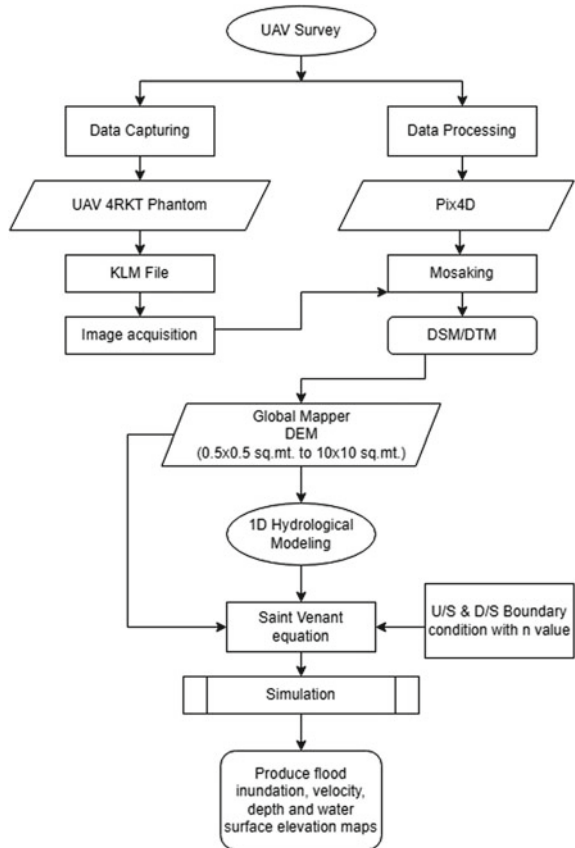
### 3 Methodology

#### 3.1 UAV Survey

The UAV survey for the study area is performed in two courses: 1. Data capturing and 2. Data processing, as shown in the methodology chart in Fig. 3. In data processing, the actual topography is captured by the device. The image capturing is done by a machine named 4RTK Phantom.

To produce an accurate map, Phantom 4 RTK requires some GCP (Ground Control Points). GCP is obtained by continuously georeferencing data using the reference station method. For the convenience of the survey, the study area was divided into three patches. The GCPs were labeled, so each patch has at least one GCP, and auto validation for the camera was made with transverse flight in Phantom 4 RTK for the UAV survey. The UAV then flew over the entire region, capturing aerial photographs along the predefined path. The overlap between the images was adjusted at 75%. Once

Fig. 3 Methodology chart





data are captured in the form of an image, the data processing is done. Therefore, after the image acquisition process, the study was conducted using the Pix4D, which converts photos into digital spatial models. Initial processing, point cloud, and mesh are the three steps of analysis this graphic user performs in final processing. The digital model was generated with near precision of 3-cm spatial resolution.

### 3.2 DEM Generation

Since the DEMs are an integral part of hydrodynamic modeling, various DEMs were generated for the study area with the help of a Global Mapper. Table 1 shows the size of 20 nos. of grid file for  $0.5 \times 0.5 \text{ m}^2$  to  $20 \times 20 \text{ m}^2$ .

**Table 1** Grid size with the storage capacity

Sr. no.	Grid size in ( $\text{m}^2$ )	Storage capacity in (MB)
1	$0.5 \times 0.5$	233.000
2	$1 \times 1$	58.400
3	$1.5 \times 1.5$	26.000
4	$2 \times 2$	14.600
5	$2.5 \times 2.5$	9.370
6	$3 \times 3$	6.500
7	$3.5 \times 3.5$	4.780
8	$4 \times 4$	3.660
9	$4.5 \times 4.5$	2.980
10	$5 \times 5$	2.340
11	$5.5 \times 5.5$	1.940
12	$6 \times 6$	1.630
13	$6.5 \times 6.5$	1.390
14	$7 \times 7$	1.190
15	$7.5 \times 7.5$	1.040
16	$8 \times 8$	0.944
17	$8.5 \times 8.5$	0.833
18	$9 \times 9$	0.744
19	$9.5 \times 9.5$	0.672
20	$10 \times 10$	0.604

### 3.3 1D Hydrodynamic Modeling

For 1D hydrodynamic modeling, Civil GeoHECRAS was used. GeoHECRAS dramatically speeds up the generation and review of HECRAS models, resulting in better and more accurate results. Some of the applications are calculating water surface profiles for steady and unsteady flow models, bridge and culvert roadway crossings, floodplain encroachments, stream restorations, inline reservoir structures, and off-channel storage areas. It is also simple to learn and use, with the ability to work directly on the map and integration with CAD and GIS. Here, the study focuses on developing 1D river hydrodynamic modeling for the case. The main input parameter are as follows: 1. DEM, 2. C/S spacing, 3. boundary condition (U/S and D/S), and 4. Manning’s roughness coefficient  $n$ . The HECRAS unsteady, gradually varied flow simulation function is utilized, which is based on finite-difference solutions to the Saint–Venant equations (Timbadiya et al. 2011).

$$\frac{\partial A}{\partial t} + \frac{\partial Q}{\partial x} = 0 \tag{1}$$

$$\frac{\partial Q}{\partial t} + \frac{\partial \left( \frac{Q^2}{A} \right)}{\partial x} + gA \frac{\partial H}{\partial x} + gA(S_o - S_f) = 0 \tag{2}$$

where

$A$ = cross-sectional area normal to the flow [m <sup>2</sup> ]	$S_o$ = bed slope
$Q$ = discharge [m <sup>3</sup> /s]	$S_f$ = energy slope
$g$ = acceleration due to gravity [m <sup>2</sup> /s]	$t$ = temporal coordinate
$H$ = elevation of the water surface above a specified datum, also called stage [m]	$x$ = longitudinal coordinate

#### 3.3.1 River Geometry and Cross-Section Extraction

Civil GeoHECRAS for 1D simulation boundary conditions, channel geometry, and roughness are necessary for flow simulation. The river’s geometry includes the river centerline, bank lines, flow route lines, and cross-section cut lines, which were digitized using the Civil GeoHECRAS in this work. For the case study, we considered 5 km of the river Sabarmati stretch from Dholeswar Bridge which is 1 km D/S of Sant Sarovar Dam, up to PDEU Bridge. The cross-section width of 600 m and 27 nos. of c/s was plotted with 180 m center to center distance between each of them. Figure 4 illustrates this point.

**Fig. 4** River geometry extraction by Civil GeoHECRAS



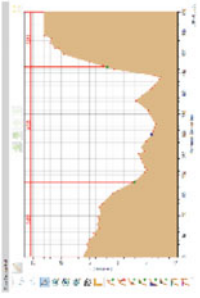
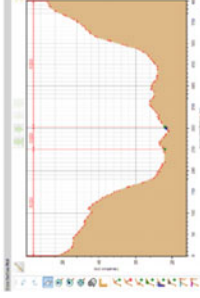

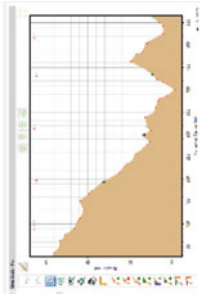
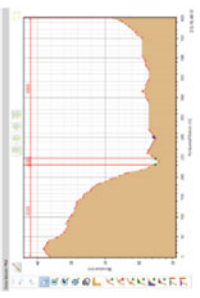
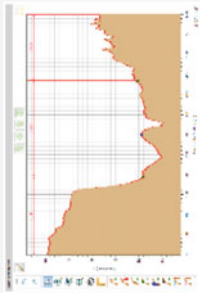
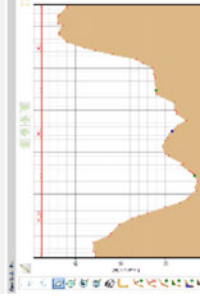
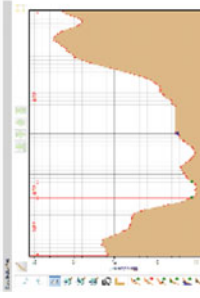
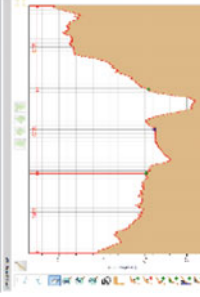
### 3.3.2 Boundary Condition

The constraints of the boundary are dependable on the nature of a river, which necessitates anticipating the flow characteristics as well as the river's range. The boundary conditions represent the input and output aspects of the upstream range under investigation. For the present study of 1D hydrodynamic simulation, the discharge of Dhario Dam is used for the year 2006 (Pandya et al. 2021) to fix the upstream boundary condition. While for the downstream boundary condition, the normal depth of river Sabarmati is used with the unsteady flow condition.

## 4 1D Model Execution in Civil GeoHECRAS

After creating river geometry and cross-section extraction, the model was executed for 1D in Civil GeoHECRAS for SRTM, Cartosat, and DEM  $5 \times 5$  grid. The grid size is considered with a reduction of 50 percent. As shown in Table 2, the cross-sections for all are observed for chainage: 27, 19, 11, and 11. A roughness of 0.033 is analyzed in the cross-sections as shown in Table 2. One of HECRAS's advantages is the ability to study water quality; the research will then be examined for the effects of water quality on water bodies due to the climatic imbalances as done for part of Southern Africa (Kheswa et al. n.d.).

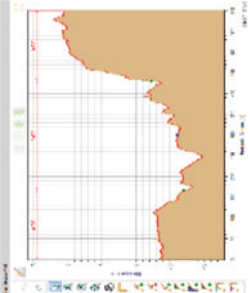
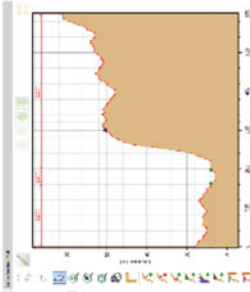
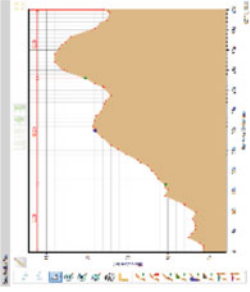
**Table 2** Various cross-section along the study area for SRTM (30 × 30) cell size, Cartosat (10 × 10) cell size, and DEM (5 × 5) grid cell size

<p>SRTM_c/s27</p> 	<p>Cartosat_c/s27</p> 	<p>DEM 5 × 5_c/s27</p> 
<p>SRTM_c/s19</p> 	<p>Cartosat_c/s19</p> 	<p>DEM 5 × 5_c/s19</p> 
<p>SRTM_c/s11</p> 	<p>Cartosat_c/s11</p> 	<p>DEM 5 × 5_c/s11</p> 

(continued)

Table 2 (continued)

SRTM_c/s27	Cartosat_c/s27	DEM 5 × 5_c/s27
SRTM_c/s1	Cartosat_c/s1	DEM 5 × 5_c/s1



## 5 Discussion

The whereabouts of river shorelines, channel geometry, and flora could all be accurately georeferenced using just a UAV. This dataset can also be used to calibrate and validate distributed flood forecasting models. SRTM and Cartosat are available universally, but for a slight stretch, DEM generated from a UAV survey may solve the purpose for the decision-makers. As shown in the tiles Table 2, the various cross-sections of SRTM with grid size ( $30 \times 30$ ) show less clarity than Cartosat with grid size ( $10 \times 10$ ) and  $5 \times 5$  girded DEM. The DEM constructed from the UAV survey is an excellent resource for investigators to evaluate various hydrological processes as it describes the terrain more precisely. Further, this study shall include 2D hydraulic modeling using these UAV-based DEMs. However, the duration of time it needs to process a 2D model is influenced either by pixel density, image information, output precision chosen, or computer used. (Hashemi-Beni et al. 2018). Moreover, there are specific challenges to tackle in UAV surveys to deal onsite, i.e., the battery life, which limits the duration and maximum attitude of flight, payload capacity, reliability, and weather conditions are also factors to consider. The width and length of the river are the most significant challenges in river ecosystems. The flight time required can dramatically rise if the river is too wide to be covered by a single flight line (Govedaric et al. 2018).

## 6 Conclusion

The different size grid DEM generated from UAV will help to analyze 1D hydrodynamic modeling with the output like total discharge, the velocity of the flood, water surface elevation with energy gradient elevation and slope along with flow area, and Froude number in the stream. It will also help in river cross-section generation; the applicability of these results will be helpful in the construction of structures like a bridge across the river. The high-resolution DEM could provide timely and accurate assistance to policymakers in identifying dangerous locations likely to get submerged, defining flood risk reduction strategies, and implementing flood protection policies mainly for the perennial river. It assists policymakers in determining the flood damage mapping hazard. Further, the application of UAV-based DEMs for 2D hydraulic modeling will give good results for the simulation of flood amount, flood submergence, the velocity of flow, and timely arrival of the flood.

**Acknowledgements** This project is funded ORSP, PDEU for the UAV survey.

## References

- Darji K, Patel DP, Kumar Dubey A, Gupta PK, Singh RP (2021) An approach of satellite and UAS based mosaicked DEM for hydrodynamic modelling a case of flood assessment of Dhanera City, Gujarat, India. *J Geomat* 15
- Garrote J (2022) Free global DEMs and flood modelling—a comparison analysis for the January 2015 flooding event in Mocuba City (Mozambique). *Water* (Switzerland) 14(2). Retrieved from <https://doi.org/10.3390/w14020176>
- Govedaric M, Jakovljević G, Álvarez-Taboadac F (2018) Flood risk assessment based on LiDAR and UAV points clouds and DEM
- Hashemi-Beni L, Jones J, Thompson G, Johnson C, Gebrehiwot A (2018) Challenges and opportunities for UAV-based digital elevation model generation for flood-risk management: a case of Princeville, North Carolina. *Sensors* (Switzerland) 18(11). Retrieved from <https://doi.org/10.3390/s18113843>
- Horritt MS, Bates PD (2001) Predicting floodplain inundation: raster-based modelling versus the finite-element approach. *Hydrol Process* 15(5):825–842. Retrieved from <https://doi.org/10.1002/hyp.188>
- Kheswa N, Bloodless Dzwairo R, Kanyerere T, Singh SK (n.d.) Current methodologies and algorithms used to identify and quantify pollutants in sub-basins: a review. *Int J Water Resour Environ Eng* 13(2):154–164. Retrieved from <https://doi.org/10.5897/IJWREE2021.0997>
- Mazzoleni M, Paron P, Reali A, Juizo D, Manane J, Brandimarte L (2020) Testing UAV-derived topography for hydraulic modelling in a tropical environment. *Nat Haz* 103(1):139–163. Retrieved from <https://doi.org/10.1007/s11069-020-03963-4>
- Pandya U, Patel DP, Singh SK (2021) A flood assessment of data scarce region using an open-source 2D hydrodynamic modeling and google earth image: a case of Sabarmati flood, India. *Arab J Geosci* 14(21). Retrieved from <https://doi.org/10.1007/s12517-021-08504-2>
- Timbadiya PV, Patel PL, Porey PD (2011) HEC-RAS based hydrodynamic model in prediction of stages of lower tapi river. *ISH J Hydra Eng* 17(2):110–117. Retrieved from <https://doi.org/10.1080/09715010.2011.10515050>
- Trambadia NK, Patel DP, Patel VM, Gundalia MJ (2022) Comparison of two open-source digital elevation models for 1D hydrodynamic flow analysis: a case of Ozat River basin, Gujarat, India. *Model Earth Syst Environ*. Retrieved from <https://doi.org/10.1007/s40808-022-01426-2>

# Stream Flow and Sediment Load Variation in Middle Tapi Basin



Urvashi Malani and Sanjaykumar Yadav

**Abstract** The discharge and sediment load in natural rivers everywhere are enduring significant changes due to present climate changes and anthropogenic activities. Therefore, to inculcate management of water resources and soil conservation practices, it is crucial to identify variation of discharge and sediment load. In present study, the trend analysis of daily discharge and suspended sediment load is carried out using Mann–Kendall test, Modified Mann–Kendall test, and change point was determined using Pettitt test. Here, Sarangkhedha from Middle Tapi Basin is chosen to understand the variability. Change point is observed at 2008 at Sarangkhedha for both sediment load and discharge. After change point, average annual sediment load has decreased by 50% and average annual water discharge decreased by 20%. The decline in sediment load in Middle Tapi Basin shown major drop of sediment load which has arisen due to sediment entrapment by the dam. Sarangkhedha carries average annual sediment load of  $15.61 \times 10^6$  tons and average annual water discharge of  $7.58 \times 10^9$  m<sup>3</sup>. Incorporating the trend in sediment load and discharge can be helpful for water management. Both climatic and human activities appear to be responsible for variation in flow pattern of the river.

**Keywords** Middle Tapi Basin · Sediment load · Tapi River · Trend

## 1 Introduction

Water is quintessential for human life. Human beings are directly or indirectly dependent on different sources of water for their sheer existence. From all the sources, river water plays a major role in shaping the lives. Rivers are major pathways that link continents and oceans and deliver large quantities of materials along with it. Along with the

---

U. Malani (✉) · S. Yadav  
Department of Civil Engineering, Sardar Vallabhbhai National Institute of Technology,  
Surat 395007, India  
e-mail: [malani.urvashi1232@gmail.com](mailto:malani.urvashi1232@gmail.com)

S. Yadav  
e-mail: [smy@ced.svnit.ac.in](mailto:smy@ced.svnit.ac.in)

© The Author(s), under exclusive license to Springer Nature Singapore Pte Ltd. 2024  
D. Patel et al. (eds.), *Innovation in Smart and Sustainable Infrastructure*, Lecture Notes  
in Civil Engineering 364, [https://doi.org/10.1007/978-981-99-3557-4\\_14](https://doi.org/10.1007/978-981-99-3557-4_14)

175



flowing water, river carries sediment with it. Sediments and water are the most important substance in rivers, and their transportation is important to maintain the dynamic geomorphologic processes in rivers and oceans. Water being a carrier for the sediments, erosion and deposition of sediments thus depends upon the flow properties. But due to change in climatic conditions and alteration in anthropogenic activities, discharge and sediment transport over the world are greatly affected. Researchers all over the world are trying to understand the behaviour of rivers over the years due to change in the flow conditions, rise in population and change in human activities.

Due to changes happening over the course of the years, sediment load carried by the rivers have declined remarkably. Human activities, water and soil conservation practices are proved to be significant for such changes in sediment load. Milliman (1983) found decreasing sediment load in many European rivers in the last 50 years. Panda (2011) analysed river basins of India and found decreasing sediment load for most of the gauging stations, and major reduction is observed in Narmada River due to dam construction. Walling (Walling and Fang 2003) detected sediment load in the major river of the world and found that non-stationary trend is observed more in sediment load as compared to discharge. Bastia and Equeenuddin (2016) have studied sediment load and discharge variation in the Mahanadi River and found sudden decrease in sediment load delivery to the ocean between 1980 and 2010. Wang (2016) determined 90% decrease in the sediment load of Yellow River in China over past 60 years. Due to declining sediment load in the rivers, risk of coastal erosion increases. The need for this study arises due to declining sediment load in major Indian rivers leading to greater risk of coastal erosion.

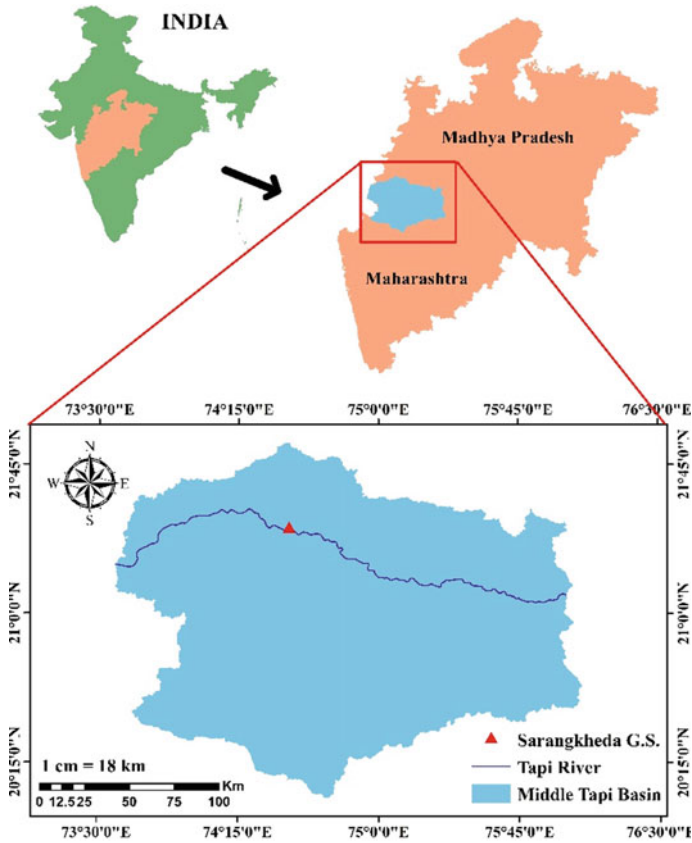
Therefore, the present study aims to focus upon temporal variation of sediment load and discharge of Middle Tapi Basin of India by analysing past data of 35 years. The main objective of this study is to annual mean sediment load, water discharge of the basin. Missing sediment load data are filled by linear regression; then, trend analysis of daily data of sediment load and discharge is carried out using non-parametric Mann–Kendall (MK) test and modified Mann–Kendall (MMK) test along with that change point analysis is done using Pettitt test. The study could provide suggestions regarding management of water resources in Middle Tapi Basin.

## 2 Study Area and Data

### Middle Tapi Basin

Tapi River is one of the largest west flowing rivers of India. The Tapi Basin is situated in the northern part of the Deccan Plateau and extends over an area of 65,145 sqkm which is nearly 2% of the total geographical area of the country. Maharashtra contributes 80% of the Tapi Basin. Middle Tapi Basin extends from Hatnur Dam to Sarangkhedha gauging site (29,970 km<sup>2</sup>) (Fig. 1).

Data



**Fig. 1** Index map of study area

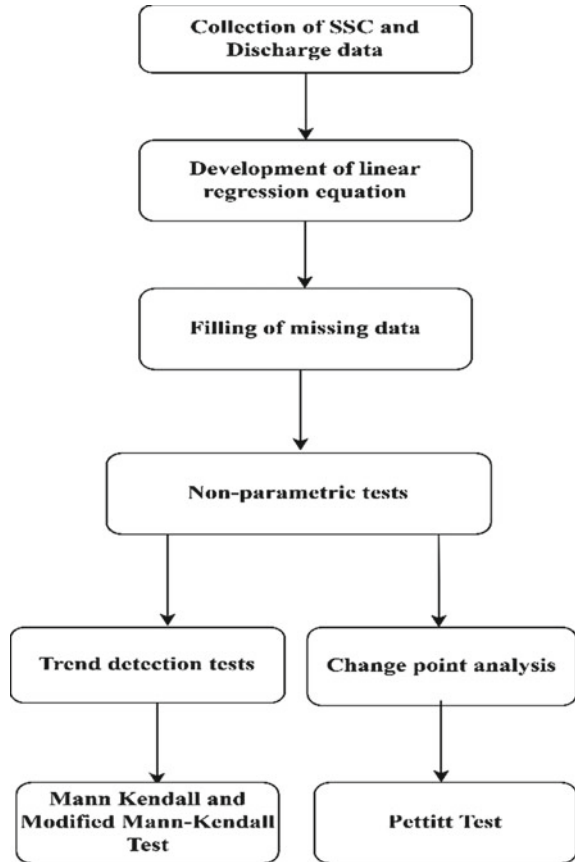
The data of sediment load and discharge at Sarangkheda G. S. for present study is taken from CWC, Surat. Data for 35 years are collected. Sarangkheda is gauging station located in Middle Tapi Basin where discharge and sediment load are measured with catchment area of 58,400 km<sup>2</sup>. Average sediment yield of Sarangkheda G. S. is 267.42 MT/km<sup>2</sup> (Fig. 2).

### 3 Methodology

#### Missing Data

The missing data of sediment load were obtained by linear regression. Logarithmic values of available sediment concentration and discharge were used to develop the relation.

**Fig. 2** Methodology for present study



## Trend Analysis

### Mann–Kendall test

It is a statistical non-parametric test to find out trend in a time series. The following are the definitions of the Mann–Kendall statistics (Mann et al. 1945; Kendall 1970) which are given in Eqs. 1, 2, 3 and 4.

$$S = \sum_{k=1}^{n-1} \sum_{j=k+1}^n \text{sgn}(X_j - X_k) \quad (1)$$

where  $X_j$  and  $X_k$  represent the data values,  $n$  represents the length of the time series, and

$$\text{sgn}(x) = \begin{cases} 1 & \text{if } x > 0 \\ 0 & \text{if } x = 0 \\ -1 & \text{if } x < 0 \end{cases} \quad (2)$$

Mann et al. (1945) and Kendall (1970) stated that when  $n \geq 8$ , where  $S$  tends to follow normal distribution along mean and variance. Thus,

$$E(S) = 0 \quad (3)$$

$$\sigma^2 = \frac{\left\{ n(n-1)(2n+5) - \sum_{j=1}^p t_j(t_j - 10(2t_j + 5)) \right\}}{18} \quad (4)$$

The Mann–Kendall does not determine the magnitude of the trend, so Sen's slope estimator given by (Sen 1968) which is stated below in Eq. 5,

$$d_k = \frac{X_j - X_i}{j - i} \quad (5)$$

Here,  $d$  indicates the slope, i.e. magnitude and  $X_j$  and  $X_i$  are values at times  $i$  and  $j$ , and  $n$  is the number of variables.

#### Modified Mann–Kendall

Hamed and Ramchandra (1998) gave a modified version of MK test in which autocorrelation among the time series is considered which was not taken into consideration in MK test. This method can be used for trend detection as autocorrelation is present between hydrological time series, and this can lead to detect trend which may not be significant.

#### Sen's Slope

Sen's slope measures the trend indicated by MK test. Trend slope is measured by formula given in Eq. 6 given by Sen (1968) and Theil (1950).

$$\beta = \text{median} \left( \frac{x_j - x_i}{j - i} \right) \quad (6)$$

where  $\beta$  indicates the magnitude of trend slope.

#### Pettitt Test

In order to understand the non-homogeneity in time series, Buishand (1982) stated that there are different theories to determine the change point in a time series. Pettitt (1979) gave a method to find change point in a time series by focusing on a null hypothesis that variable of a time series follows same or different distributions with no changes occurring in the location parameter.

## 4 Results and Discussion

### Filing of Missing Data at Sarangkhedha G. S.

Missing data were filled using developing a linear regression equation between sediment concentration and discharge at Sarangkhedha. Equation 7 was developed using logarithmic values of the variables (Fig. 3).

$$\log \text{SSC} = -2.96 + 0.86 \log Q \quad (7)$$

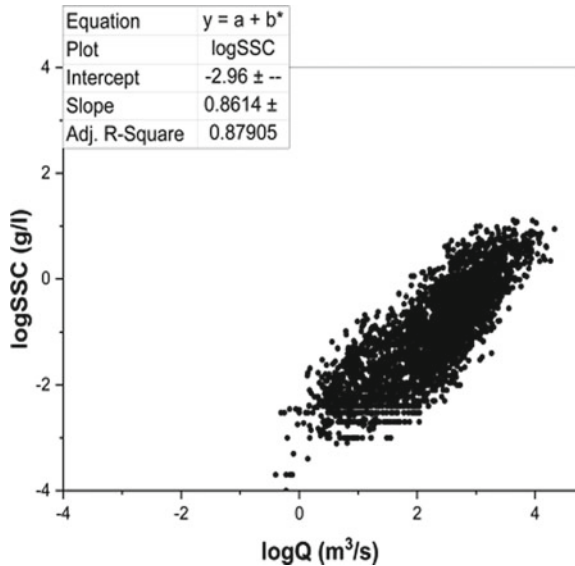
### Decadal Variation of Sediment Load and Discharge

Figure 4 shows the decadal variation of average annual sediment load carried by Sarangkhedha G. S. in four decades. It is seen that sediment load is declining with the time. Major declination is observed in the last decade which is 25% less than the previous decade. Figure 5 shows the decadal variation of average annual water discharge carried by Sarangkhedha G. S. in four decades. It is seen that water discharge is declining with the time.

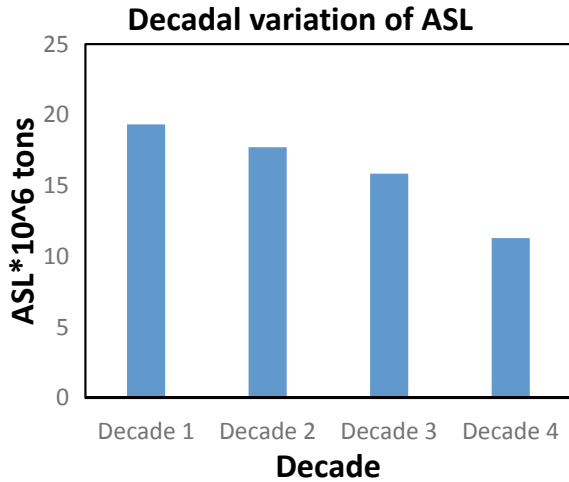
Major declination is observed in the last decade which is 25% less than the previous decade. Major changes are not observed in annual discharge in the four decades. In 2nd decade from 1990 to 2000, in 1994 and 1998, annual water discharge was  $14.6510^9 \text{ m}^3$  and  $14.4210^9 \text{ m}^3$ , respectively, and hence, 2nd decade has shown higher average annual water discharge.

### Trend Analysis of Discharge and Sediment

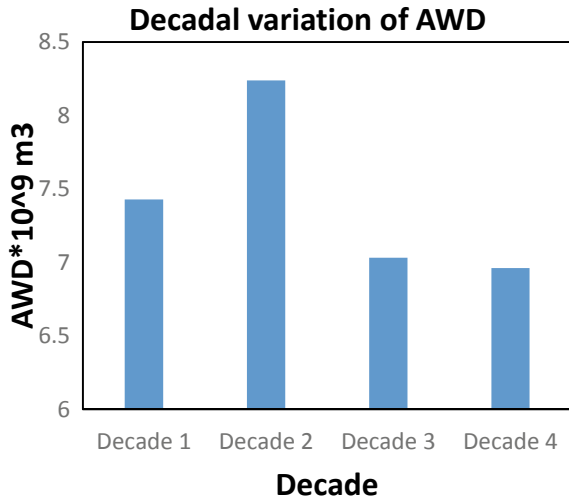
**Fig. 3** Linear regression for missing data



**Fig. 4** Decadal variation of annual sediment load



**Fig. 5** Decadal variation of annual water discharge



Tables 1 and 2 show the results of trend analysis of hydrological parameters. For daily discharge, both the methods are showing decreasing trend as Tau value is less than zero. Considering the autocorrelation of the series, for 5% confidence interval,  $z < -1.96$ ; hence, significant decreasing trend is observed in discharge. Similarly for sediment load, significant decreasing trend is observed. Hence, MK test is unable to detect the correct trend present in the time series.

**Change Point Analysis**

For change point analysis, annual discharge and annual sediment load are considered. Figure shows change point analysis of annual water discharge. Annual water

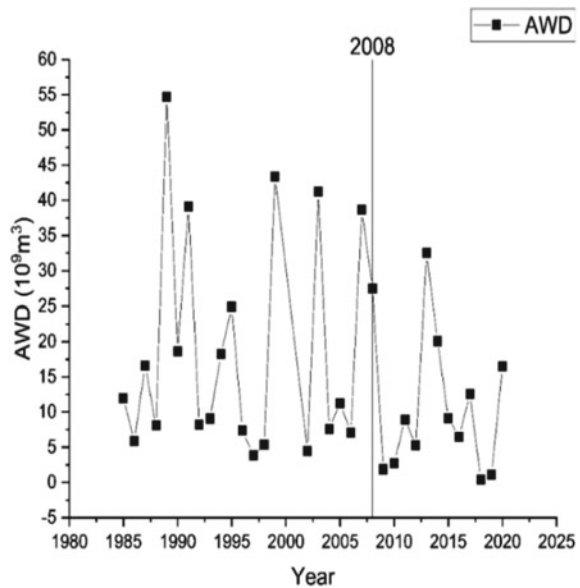
**Table 1** Results of MK test

Parameters	Tau	Z
Discharge	-0.264	-40.68
Sediment load	-0.245	-42.59

**Table 2** Results of MMK test

Parameters	Tau	Z
Discharge	-0.22	-2.04
Sediment load	-0.279	-3.69

**Fig. 6** Pettitt test for discharge

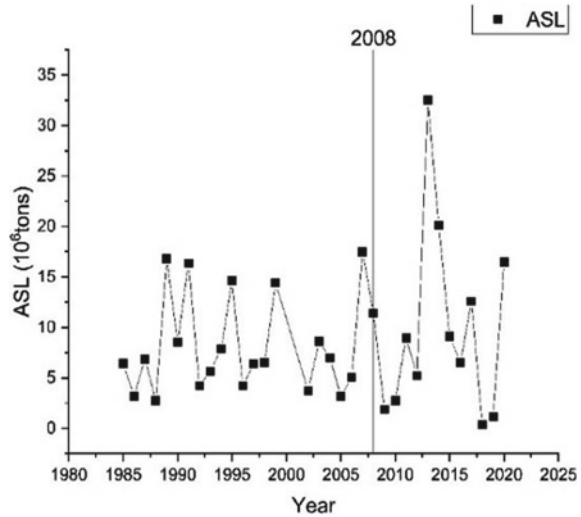


discharge is total amount of water carried by the river throughout the year. Change point is observed at 2008. Figure 6 shows change point analysis of discharge, and Fig. 7 shows change point of sediment load. After change point, 50% decline was observed in sediment load and about 22% decrease in annual water discharge. As compared to discharge, sediment load has decreased significantly.

### 5 Conclusions

The main aim of present study was to study the streamflow and sediment load variation in Middle Tapi Basin. The conclusions of the study are as follows;

**Fig. 7** Pettitt test for sediment load



- Decadal variation of average annual sediment load shows a drop in sediment load in the last decade.
- Trend analysis for discharge and sediment load was carried out at Sarangkhedha G.S. Significant decreasing trend at 5% significance level indicating fall in the value of the parameters was observed for both sediment load and discharge. This change has caused due to climatic variability and human activities.
- Results of different magnitude were observed in MK and MMK tests, and hence, MMK test can be preferred over MK test as its application is certainly advantageous.
- Change point was observed at 2008 for both discharge and sediment load. Sediment load has declined by 50% after change point whilst discharge has decreased by 22% hence, major declination is observed in sediment load.
- This study suggests to implement appropriate actions to reduce the impact of decrease in sediment load and stream flow in order to meet the requirements of increasing population. However, further research is required to determine the influence of different factors that leads to variation in sediment load and streamflow.

## References

- Bastia F, Equeenuddin SM (2016) Spatio-temporal variation of water flow and sediment discharge in the Mahanadi River, India. *Global Planet Change* 144:51–66. <https://doi.org/10.1016/j.gloplacha.2016.07.004>
- Buishand TA (1982) Some methods for testing the homogeneity of rainfall records. *J Hydrol* 23(58):11–27



- Hamed KH, Ramachandra Rao A (1998) A modified Mann-Kendall trend test for autocorrelated data. *J Hydrol* 204(1–4):182–196. [https://doi.org/10.1016/S0022-1694\(97\)00125-X](https://doi.org/10.1016/S0022-1694(97)00125-X)
- Kendall MG (1970) Rank correlation methods. Griffin, London
- Mann HB, Mantua N, SR H, Zhang Y, Wallace J, Francis R (1945) Non-parametric tests against trends. *A Pacoific Decadal* 13:245–259
- Milliman JD, Meade RH (1983) World-Wide delovery of river sediment to the oceans. *J Geol* 91(1):1–21
- Panda DK, Kumar A, Mohanty S (2011) Recent trends in sediment load of the tropical (Peninsular) river basins of India. *Glob Plan Change* 75(3–4):108–118. <https://doi.org/10.1016/j.gloplacha.2010.10.012>
- Pettitt AN (1979) A non-parametric to the approach to the change-point problem. *Appl Stat* 28(2):126–135
- Sen PK (1968) Estimates of the regression coefficient based on Kendall's Tau. *J Am Statist Assoc* 63(324):1379–1389. <https://www.jstor.org/stable/2285891>
- Theil H (1950) A rank-invariant method of lienar and polynomial regression analysis. Part 3. *Proc Koninalijke Nederlandse Akademie Van Weinenschatpen A1* 53:1397–1412
- Walling DE, Fang D (2003) Recent trends in the suspended sediment loads of the world's rivers. *Glob Plan Change* 39(1–2):111–126. [https://doi.org/10.1016/S0921-8181\(03\)00020-1](https://doi.org/10.1016/S0921-8181(03)00020-1)
- Wang S, Fu B, Piao S, Lü Y, Ciais P, Feng X, Wang Y (2016) Reduced sediment transport in the Yellow River due to anthropogenic changes. *Nat Geosci* 9(1):38–41. <https://doi.org/10.1038/ngeo2602>

# Sustainable Development in Water Quality Assessment: Data for Khadakwasla Dam, Pune



Mohnish M. Waikar and Parag Sadgir

**Abstract** The study represents data collection and analysis of the water quality index (WQI) and different parameters considered for calculating water quality index in Khadakwasla dam which is located in Pune district. The dam is major contributor of fresh water in Pune city, and thus, the analysis of the water in Khadakwasla dam is crucial as water for the urban and rural areas as well as for industries is supplied through canals of Khadakwasla dam. The data is acquired and analysed for the study of variation of water quality index, and results were obtained for the year 2011 to 2021. Data is tabulated, and graphs are plotted for better understanding the variation in the data. Precipitation data is also studied for the variation of quality of water and interrelation of precipitation and water quality can be seen from tables and graphs.

**Keywords** Water quality · Water quality index · Sustainable development · Data

## 1 Introduction

Khadakwasla dam is primary source of water in Pune district. Built in 1869 the dam has a capacity of 1.96 TMC (Thousand Million Cubic feet) and is in the downstream of Panshet and Varasgaon Dam. The deterioration of water quality is caused by a growing population, declining usable water resources, increasing rates of usage, global climate change, and a variety of other factors (Bora and Goswami 2017). These sources are, for the most part, made unfit for human eating and other human activity. The minimum needed flow within the river is not maintained at numerous locations due to dry season circumstances and limited releases from dams along the downstream river stretch during dry months. Water shortage is exacerbated by deteriorating water quality and a scarcity of supply, which puts the environment under

---

M. M. Waikar (✉) · P. Sadgir  
College of Engineering, Pune, India  
e-mail: [waikarmm20.civil@coep.ac.in](mailto:waikarmm20.civil@coep.ac.in)

P. Sadgir  
e-mail: [pas.civil@coep.ac.in](mailto:pas.civil@coep.ac.in)

stress (Shah and Joshi 2017). As a result, the efficient and effective management of water resources is becoming increasingly crucial (Arief Dhany Sutadian et al. 2016).

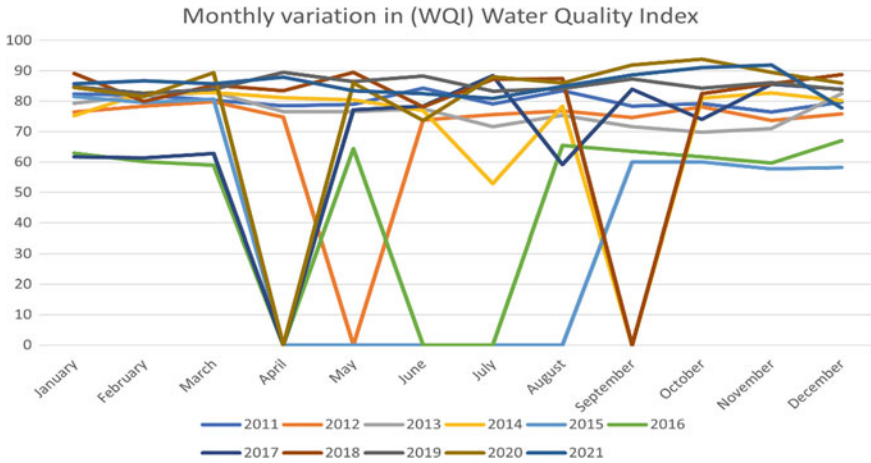
The water quality index is one way for determining the quality of river water (Ichwana et al. 2016). It has been proved to be an effective and practical tool for analysing water quality. This technique provides policymakers with a sense of the overall quality of water. The purpose of this study is to construct a WQI to analyse the quality of water of the Khadakwasla dam and its water quality status (Water Quality Index).

## 2 Water Quality Assessment

Water quality assessment differs with respect to fresh water and wastewater. Our study includes the fresh water that is to be supplied in Pune city and downstream, so the quality assessment of water is done with respect to freshwater study only. The water quality index (WQI) is an important tool to determine the drinking water quality in urban, rural and industrial area (Ichwana et al. 2016). WQI is described as an index that reflects the combined impact of several water quality characteristics that are taken into account and used to calculate the water quality index.

Factors considered in the calculation of water quality index

- i. pH-If the pH of the water is too high or too low, sea creatures living in it will perish. The pH of water affects the stability and hazard of chemicals and heavy metals. Although most marine animals require a pH of 6.5 to 9.0, some may thrive in water with a pH higher than that (Gupta et al. 2017).
- ii. Dissolved Oxygen-Dissolved oxygen is oxygen that has been dissolved in water. The greater the quantity of D.O. of water, the better the quality. The growth potential of aquatic organisms is lowered when dissolved oxygen is depleted (Lkr et al. 2020).
- iii. Bio-Chemical Oxygen Demand-Bio-chemical oxygen demand generally known as BOD is one of the prominent parameters which reflects the quality of water by giving the oxygen demand required to disintegrate the amount of organic contaminants present in the water that is to be tested (Bora and Goswami 2017). This BOD is analogous to water quality and can be treated as same as it consumes oxygen from water, i.e. dissolved oxygen, and hence, if the oxygen level in water depletes, the aquatic life may disrupt.
- iv. Chemical Oxygen Demand-The test is used to evaluate the amount of organic matter that can be oxidised in an acid solution by a powerful chemical oxidising agent (potassium dichromate). For describing water bodies, sewage, industrial pollutants and treatment plant effluents, it is a significant and quickly measurable characteristic (Prabhakar et al. 2018).
- v. Nitrate-Nitrogen mixes with oxygen to generate  $\text{NO}_3$ —when bacteria break down ammonia, urea, or proteins. This reduces the amount of dissolved oxygen



**Fig. 1** Monthly variation in WQI

in the water, which can result in dead zones for any species that rely on oxygen to exist (Lkr et al. 2020).

- vi. Faecal Coliform-Faecal coliform bacteria suggest that a stream has been contaminated with sewage and that other harmful organisms may be present (Fig. 1).

### 3 Methodology







#### 1. Data collection

The data for analysis of WQI is collected from Maharashtra Pollution Control Board (MPCB) website, and the information for the precipitation is collected from Maharashtra Rainfall and recording website, and then, the analysis is carried out.

#### 2. Data processing

Different metrics of the Khadakwasla Dam’s data were observed, processed in excel sheets, and shown as graphs. For each year, monthly data is provided, which is then analysed, and a consolidated graph for the years 2011–2021 is shown.

**Table 1** WQI classification and colour code

WQI	Quality classification	Remarks	Colour code
63-100	Good to Excellent	Non-Polluted	
50-63	Medium to Good	Non-Polluted	
38-50	Bad	Polluted	
38 and less	Bad to very Bad	Heavily Polluted	

The monthly study of precipitation data includes an analysis of how it relates to WQI.

### 3. Variation analysis

It has been noted that after the monsoon, the water quality improves due to the arrival of freshwater, but after winter, the water quality declines because in the summer, water contaminants become concentrated due to evaporation loss, and the oxygen level is found to be lower (Table 1).

Graphical representation of yearly data:

See Figs. 2 and 3.

## 4 Discussion

As we can see from the precipitation chart, due to decrease in rainfall in 2014, there is decrease in water quality, and in 2015, there is enough rainfall but due the rapid industrialisation, the discharged effluents from the factories, etc., have polluted the river making quality to moderate, and in 2016, the rainfall is once again reduced deteriorating the quality which is made up after the monsoon of 2016, and water quality once again increases as water input is consistent thereafter.

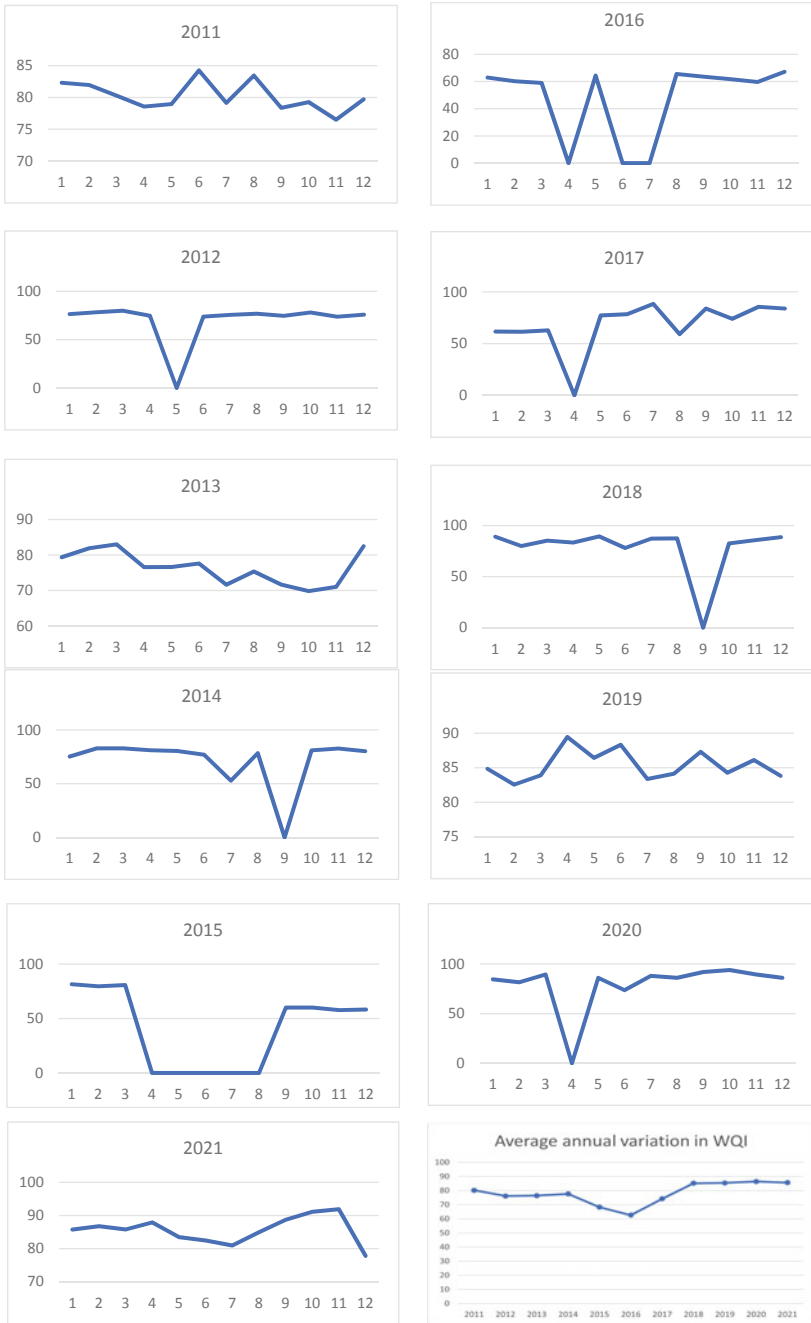
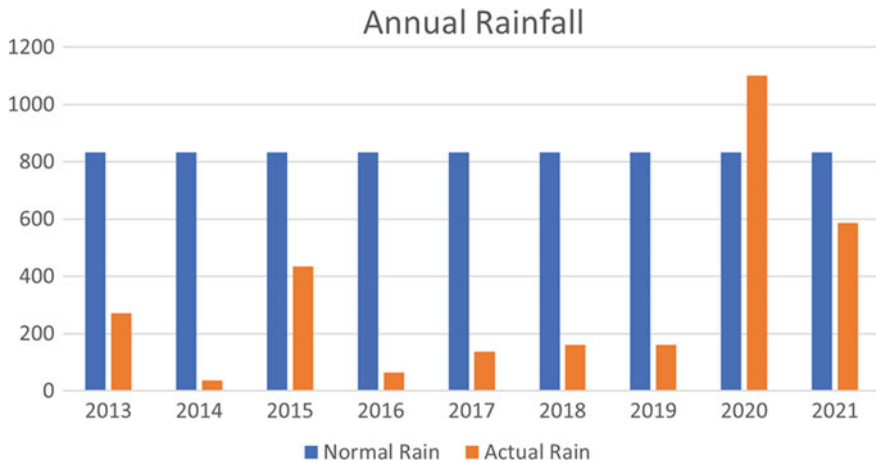


Fig. 2 Average annual variation in WQI



**Fig. 3** Precipitation

## 5 Conclusion

As per the data analysis and plotting, it can be concluded that in the post-monsoon months up to November, the water quality index is apparently going towards the good end, i.e. the river is not polluted and due to addition of freshwater the dissolved oxygen level increases, resulting in reduction of BOD and COD values. Nitrate concentration also decreases due to addition of freshwater so less algal bloom and decrease in growth of aquatic plants is seen. The pH also balances in river water as rainwater is in the range of 5.5–6, but it can vary according to the air quality as sulphates and nitrates oxidise with water and form sulphuric and nitric acid, respectively, causing acid rain which reduces the pH affecting the quality of river water.

## References

- Arief Dhany Sutadian CP, Muttill N, Yilmaz A (2016) Authors' accepted version of the paper  
 Bora M, Goswami DC (2017) Water quality assessment in terms of water quality index (WQI): case study of the Kolong River, Assam, India. *Appl Water Sci* 7(6):3125–3135. <https://doi.org/10.1007/s13201-016-0451-y>
- Gupta N, Pandey P, Hussain J (2017) Effect of physicochemical and biological parameters on the quality of river water of Narmada, Madhya Pradesh, India. *Water Sci* 31(1):11–23. <https://doi.org/10.1016/j.wsj.2017.03.002>
- Ichwana I, Syahrul S, Nelly W (2016) Water quality index by using national sanitation foundation-water quality index (NSF-WQI) method at Krueng Tamiang Aceh, pp 110–117. <https://doi.org/10.21063/ictis.2016.1019>

- Lkr A, Singh MR, Puro N (2020) Assessment of water quality status of Doyang River, Nagaland, India, using water quality index. *Appl Water Sci* 10(1):1–13. <https://doi.org/10.1007/s13201-019-1133-3>
- Prabhakar VM, Patil AR, Swain KK, Mane BB, Nerkar MS, Kharat PC (2018) Assessment of water quality index of Indrayani River, Alandi, Pune, Maharashtra. *Int J Sci Eng Technol Res* 7(6):398–402
- Shah KA, Joshi GS (2017) Evaluation of water quality index for River Sabarmati, Gujarat, India. *Appl Water Sci* 7(3):1349–1358. <https://doi.org/10.1007/s13201-015-0318-7>



# **Innovations in Computational Geotechnics and Advance Concrete Technology**

# Qualitative Analysis of Physio-Chemical Parameters of Soil to Underline the Effects of Pipeline Laying on Soil Fertility



Anirbid Sircar, M. A. Shabiimam, Abdul Rasheed, Shaunak Mehta, Jaini Shah, Ankita Patel, Namrata Bist, Kriti Yadav, and Roshni Singh

**Abstract** Agricultural land constitutes the most important part of a geological component of a country in terms of economy and prosperity. The virtue of an agricultural land solely resides on the type and composition of soil type and quality of that region. The laying of an underground pipeline might affect the soil quality and productivity of the specific area. In addition to this, there is a potential threat of leakage of sediments, pathogens, sewage, waste water or hydrocarbons/chemicals, or other contaminants into the ground. The present study aims to investigate the effects of laying a hydrocarbon pipeline on the soil quality thereby its productivity in two different regions of Gujarat state (Gandhinagar, Bharuch) India. The post-employment effects of pipeline laying on soil quality and productivity were evaluated

---

A. Sircar · M. A. Shabiimam · N. Bist (✉) · K. Yadav · R. Singh  
Pandit Deendayal Energy University, Gandhinagar, India  
e-mail: [namrata.bist@spt.pdpu.ac.in](mailto:namrata.bist@spt.pdpu.ac.in)

A. Sircar  
e-mail: [anirbid.sircar@spt.pdpu.ac.in](mailto:anirbid.sircar@spt.pdpu.ac.in)

M. A. Shabiimam  
e-mail: [shabiimam.ma@sot.pdpu.ac.in](mailto:shabiimam.ma@sot.pdpu.ac.in)

K. Yadav  
e-mail: [kriti.yadav@spt.pdpu.ac.in](mailto:kriti.yadav@spt.pdpu.ac.in)

R. Singh  
e-mail: [roshni.singh@spt.pdpu.ac.in](mailto:roshni.singh@spt.pdpu.ac.in)

A. Rasheed · S. Mehta · J. Shah · A. Patel  
Gujarat Energy Research Management Institute, Gandhinagar, India  
e-mail: [abdul@germi.res.in](mailto:abdul@germi.res.in)

S. Mehta  
e-mail: [shaunak@germi.res.in](mailto:shaunak@germi.res.in)

J. Shah  
e-mail: [jaini@germi.res.in](mailto:jaini@germi.res.in)

A. Patel  
e-mail: [ankita@germi.res.in](mailto:ankita@germi.res.in)

and the results were interpreted. The parameters for quality check of soil contamination due to pipeline laying included pH, electrical conductivity, organic matter content, available nitrogen, and heavy metal content. The results obtained suggested negligible degradation of soil quality by the underlying pipelines and provided positive results for utilization in several purposes including agriculture. The modelling and analysis of various parameters also supported the same.

**Keywords** Underground pipelines · Soil contamination · Soil quality · Soil productivity

## 1 Introduction

Natural gas has made its way into the domestic and commercial sectors as one of the most essential fuel sources for the mankind. Natural Gas Distribution or City Gas Distribution (CGD) is a developing business sector. Its objective is to give constant gas supply to domestic, commercial, and industrial consumers by means of Piped Natural Gas (PNG) and Compressed Natural Gas (CNG) (Kudaisya and Kar 2017). The city gas distribution consists of gas supply mains and service lines which are laid either underground or above ground. Generally, it is designed as a loop system, and pressure is maintained throughout the system to provide a constant gas supply (Sircar et al. 2017). Human interferences like laying of pipelines can have long-term effect on the landscape as well as the soil quality of the surrounding area. Some reports in literature suggested harmful effects of pipeline system on soil that included lower plant growth rate and less vegetation (Khasanova et al. 2017; Ryabukhina et al. 2017; Mayskiy et al. 2017; Zhang et al. 2019). Since, these can lead to reduced stability and productivity as well as soil deterioration and quality degradation. Hence, it is essential to carry out constant monitoring and evaluation of the changes of biotic and abiotic elements of the landscape due to external impacts (Halmová et al. 2017). In Gujarat, India, the genesis of soil is controlled by various macro and microclimates, topography, terrene, geology, and flora. At a given point of time and in a given area, soil characteristics are widely dependent upon natural influences and human activities. The types of soil found in Gujarat are black soil which is the leading soil type (Jangir et al. 2018, 2020; Sharma et al. 2019). Lateritic soil which is good for forests and vegetation (Zinzala et al. 2018). Alluvial soil which are low in nutrient content (Dadhich et al. 2018; Thokchom et al. 2017; Gohel and Singh 2018). Hill soil in the mountain areas with low productivity and desert soil with little or no vegetation (Shinde et al. 2020; Siddiqui and Fatima 2017). The presence of a gas pipelines can cause modifications in the soil content that can affect the flora and fauna of the surrounding (Halmová and Feher 2014). Therefore, there is a need for detailed investigation on the effect on physio-chemical factors of soil like pH, conductivity, organic nutrients, and heavy metals content by the laid underground pipelines.

The present study describes the effect of laid pipelines on soil quality and productivity in samples collected from two different regions of Gujarat, India, namely

Gandhinagar and Bharuch. The detailed analysis of soil quality was carried out using parameters such as pH, electrical conductivity (EC), organic matter content, heavy metals content, and nitrogen content in the affected samples. These results and analysis would suggest the long-term impact of pipeline networking on the vegetation, growth, and ecology of the biosphere as a whole.

## **2 Methodology**

### **2.1 Sampling**

The samples were collected from two regions including Gandhinagar and Bharuch. 5 samples were collected from Kalol region of Gandhinagar and 12 samples were collected from Bharuch region including onsite as well as offsite of the pipeline.

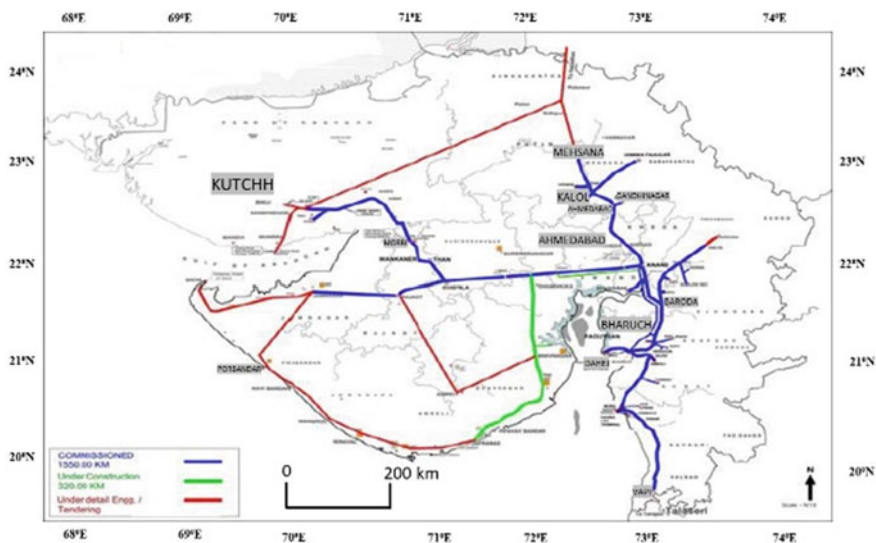
The location of soil samples was identified using Gujarat State Petronet Limited (GSPL) pipeline network map (Fig. 1). The locations were recorded in a Global Positioning System (GPS) unit for tracking, where samples had been collected. At the sample location, crop residue was removed from the soil surface. The soil probe was placed into the soil to the desired depth of around 1 m. The probe was placed vertically into the soil and it was not tilted to the side. The same process was followed at the new location. Between the two consecutive samples, 10 km of distance was kept. To obtain a homogeneous mixture, the soil was mixed thoroughly in the bucket with a trowel and placed in sample bag. After collection, the samples were stored in a refrigerator to reduce the chances of mould forming in the sample bag.

### **2.2 Parameters for Soil Quality Analysis**

There are several parameters that suggest the nature, composition, and quality of soil responsible for their fertility and productivity. The parameters along with their procedures are discussed in detail.

### **2.3 pH**

Electrometric method was applied for pH analysis using digital pH metre. The collected soil samples were dried, crushed, and separated from other impurities. Then, an aqueous suspension of soil was made and stirred for 1 h. After calibration, pH reading was taken and noted down.



**Fig. 1** Map of a gas pipeline network of Gujarat State Petronet Limited (GSPL) (<https://www.gidb.org/gas-pipeline-infrastructure>)

## 2.4 Electrical Conductivity

Argentometric method was performed for finding the chloride content using Standard Potassium Chloride Solution. 20 g of soil and 40 mL of distilled water (1:2) were transferred into a 100 mL beaker at  $25\text{ }^{\circ}\text{C} \pm 1\text{ }^{\circ}\text{C}$ . The beaker was closed and placed in a horizontal position in the shaking machine and shaken for 30 min. The electrical conductivity of each sample was measured.

## 2.5 Organic Matter

After pre-treatment, a measured amount of soil sample was kept in a flask, 10 ml of 1 N potassium dichromate was added and the flask was spun lightly to dissolve the soil in the dichromate solution. Then, 20 ml concentrated  $\text{H}_2\text{SO}_4$  (having 1.25%  $\text{Ag}_2\text{SO}_4$ ) was poured into the flask and spun. After that, 200 ml of distilled water and 10 ml of orthophosphoric acid were added to obtain a precise point of the titration. Then 1 ml of diphenylamine indicator was added, and contents were titrated with ferrous sulphate solution until the colour was changed from blue-violet to green.

## **2.6 Available Nitrogen**

50 g of wet soil was taken into the flask and 250 mL of acidified KCL was added and shaken for 1 h. After filtration, 2–4 g of magnesium oxide was added to the filtrate. 20 mL of 2% boric acid indicator solution was used. After distillation, 40 to 45 ml of distillate was collected in around 30 min. In the end, ammonia was titrated against 0.02 N H<sub>2</sub>SO<sub>4</sub>, and a blank correction was made for the final calculation.

## **2.7 Heavy Metals**

Heavy metals like zinc (Zn), iron (Fe), manganese (Mn), and copper (Cu) were analysed by using Atomic Absorption Spectrophotometer (AAS). All samples were pre-treated using the microwave digestion method.

# **3 Results and Discussion**

## **3.1 Soil Quality Analysis of Samples of Gandhinagar**

### **3.1.1 Effect on Soil pH**

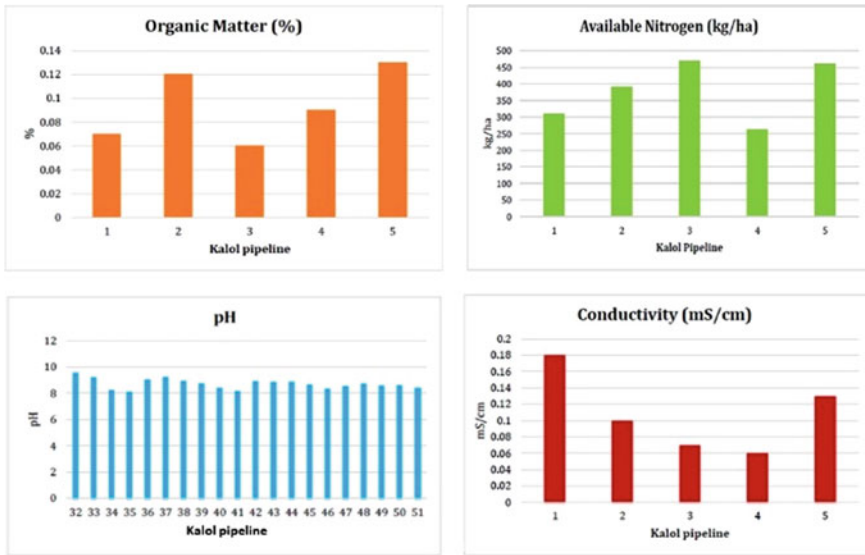
The pH of soil samples collected from the Kalol region of Gandhinagar ranges from 8.5 to 9.5 which indicates that soil is alkaline. The hardness of groundwater needs treatment and remediation for application of water reservoirs of the region is required. The variable pH range in the samples was shown in Fig. 2c.

### **3.2 Effect on Soil Conductivity**

The EC of soil samples varies from 0.06 to 0.18 mS/cm. This range of EC suggests that the soil is not saline in nature (Karlikar and Solanki 2014). The low salinity would be the result of low chloride content in soil samples. The conductivity of different samples is shown in Fig. 2d.

### **3.3 Effect on Soil Organic Content**

Soil organic matter can affect two important characteristics of soil: (i) plant available water capacity and (ii) plant available vital nutrients, particularly nitrogen. Organic



**Fig. 2** a Organic matter of soil sample collected from Kalol region of Gandhinagar; b available nitrogen of soil sample collected from Kalol region of Gandhinagar; c pH of soil sample collected from Kalol region of Gandhinagar d conductivity of soil sample collected from Kalol region of Gandhinagar

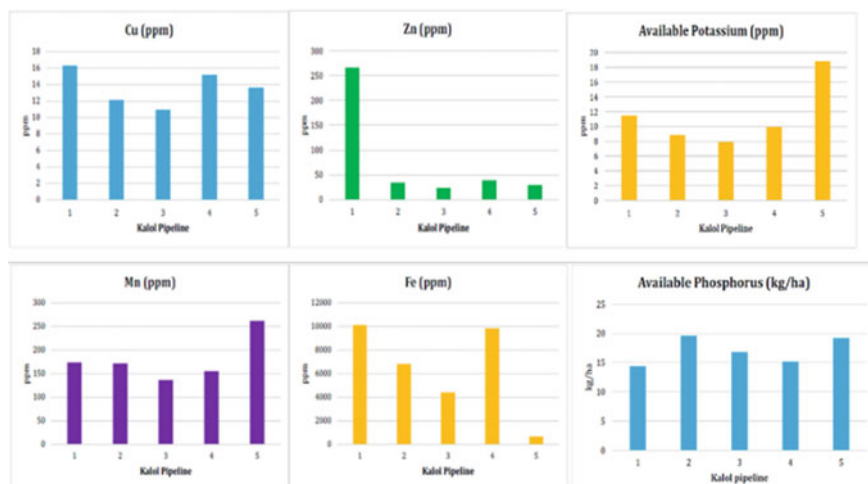
matter content is also very less (0.06–0.13%). The organic content in the samples collected from different regions of Gandhinagar was shown in Fig. 2a.

### 3.4 Effect on Soil Nitrogen

Available Nitrogen in different soil samples of Kalol area ranges from 263 to 470 kg/ha suggesting moderate concentration of nitrogen in the soil. Nitrogen is one of the most essential soil components for plant growth since it forms a part of chlorophyll which in turn is involved in photosynthesis. Therefore, the results of the study reveals that the growth of the plants due to nitrogenous content in these areas remain unaffected by the pipeline looping. The samples nitrogen concentration is shown in Fig. 2b.

### 3.5 Effect on Heavy Metal Content

The soil of the Kalol region contains a low concentration of available phosphorus (14–19 kg/ha) and available potassium (7.89–18.83 ppm). The low concentration



**Fig. 3** Heavy metal content in soil samples of Kalol region of Gandhinagar

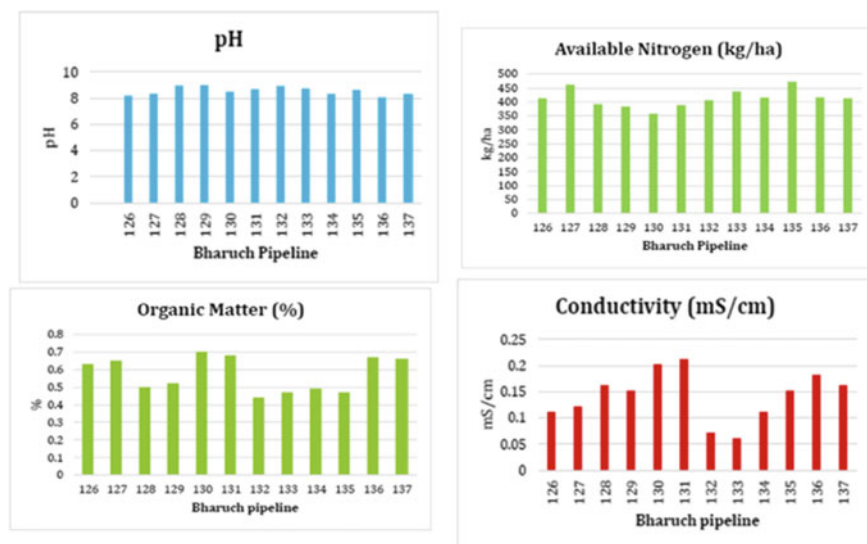
of phosphorus and potassium might be because of the temperature of gas passing through the gas distribution pipeline. For the reproductive development and consumption of proteins, copper (Cu) is significant (Karlikar and Solanki 2014). The copper content in soil samples collected from Kalol region of Gandhinagar is very high (10.91–16.29 ppm). The manganese concentration in the soil varies from 135.6 to 261.7 ppm, and it might be attributed to the corrosion of the pipeline (Miao and Wang 2016). Zinc is important for transportation of carbohydrates and also for the controlled utilization of sugars. Zn concentration in the soil of the Kalol region of Gandhinagar is 23.31–266.5 ppm which is quite high (Karlikar and Solanki 2014). The chemical composition of corrosion products on API steel pipeline liberates 56.06 wt% iron in the soil samples, Fe content is 644.4–10,090 ppm, i.e. 0.064–1.009 wt%. This high value indicates the effect of mild corrosion (Miao and Wang 2016). The heavy metal content of samples in Kalol region is shown in Fig. 3.

### 3.6 Soil Quality Analysis of Samples of Bharuch

#### 3.6.1 Effect on Soil pH

The pH of soil samples collected from Bharuch region ranges from 8.0 to 8.9 which indicates soil alkalinity and hardness (Fig. 4a). The study suggested the scope of fresh water loggings which can be applicable for various purposes after treatment.





**Fig. 4** **a** pH of soil sample collected from Bharuch region; **b** available nitrogen of soil sample collected from Bharuch region; **c** organic matter of soil sample collected from Bharuch-A region; **d** conductivity of soil sample collected from Bharuch region

### 3.7 Effect on Soil Conductivity

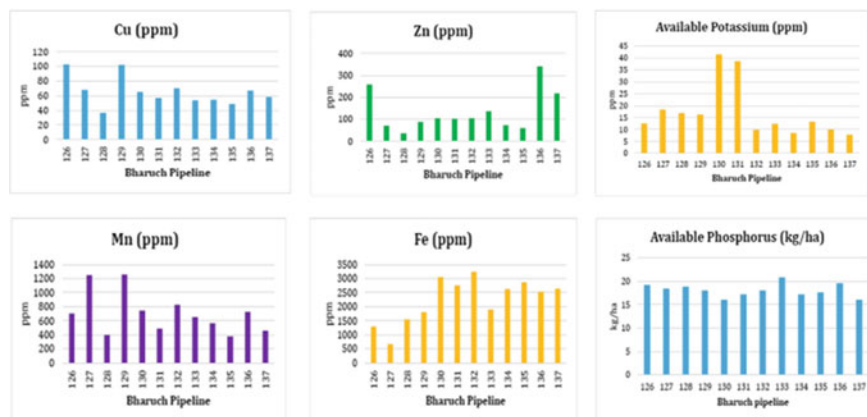
The EC of soil in Bharuch region varies from 0.06 to 0.21 mS/cm which is very less than the permissible limit (4 mS/cm) and hence salinity of soil in these areas is very low (Fig. 4d).

### 3.8 Effect on Soil Organic Content

In the soil samples collected from Bharuch area, organic matter concentration varies from 0.44 to 0.68% (Fig. 4c). This indicates low storage capacity of soil for essential nutrients and less retention potential for toxic elements. Hence, the area under study needs enrichment in organic content for better growth and productivity.

### 3.9 Effect on Heavy Metal Content

The concentration of the toxic heavy metals like Cd, Hg, As, etc., found to be negligible in the soil samples of Bharuch region indicating low toxicity level and proper



**Fig. 5** Heavy metal content in soil samples of Bharuch region

growth. The other heavy metals like phosphorus content is 7.74–41.5 kg/ha, potassium content is 16–20.8 ppm, Cu and Zn contents are 36.32–102.7 ppm, and 36.25–339.8 ppm, respectively. Zinc is the component of the enzyme systems which control plant growth. Cu, K, and P are also important substitutes for growth and development of plants. These ranges suggest suitable plant growth with optimum metallic concentration in the soil samples with negligible effect of pipeline laying.

In case of Mn and Fe, the concentration is 375.2–1257 ppm and 669.7–3237 ppm, respectively. Their higher concentration suggests possible corrosion of underlying gaseous pipelines. The heavy metal content of various samples was shown in Fig. 5.

## 4 Conclusion

The present study summarizes the effect on physio-chemical parameters of soil samples collected from two different regions of Gujarat by the underlying pipeline channels. The higher pH ranges from 8.5 to 9.3 in samples of Gandhinagar region suggest alkaline nature and hardness in the groundwater of that area. The salinity of most of the soil samples is found to be low which could be related to low chloride concentration and hence feasible for vegetation.

Heavy metals like Cu, Zn, Mn, and Fe vary widely for all regions. The concentration of some of the most toxic heavy metals like Hg, As, Cd, etc., was found negligible which is a positive aspect of water resource exploration for that area. In all regions, the concentrations of available nitrogen, phosphorus, and potassium are moderate and sufficient enough as required. The availability of high nutrients increases the uptake quality and productivity of plants. The soil analysis has provided positive results for the utilization in agricultural purposes as soil productivity and nutrients are not

affected after laying of pipelines. The modelling and analysis of various parameters indicates positive results for the vegetation and agricultural use post pipeline laying.

**Acknowledgements** The authors sincerely acknowledge Pandit Deendayal Energy University for providing research facilities. The authors also show their gratitude to Gujarat State Petronet Limited (GSPL) for cooperation in sampling at various locations.

## References

- Dadhich G, Patel PR, Kaluberne MH (2018) Farm level land suitability assessment for wheat and mustard crops using geomatics: a case study of Badipur village in Patan district, Gujarat. *Technol Driv Eng Growth* 93–98
- Gohel SD, Singh SP (2018) Molecular phylogeny and diversity of the salt-tolerant alkaliphilic actinobacteria inhabiting coastal Gujarat, India. *Geomicrobiol J* 35:775–789. <https://doi.org/10.1080/01490451.2018.1471107>
- Halmová D, Poláková Z, Končerková L, Fehér A (2017) Impact of operating temperature of gas transit pipeline on soil quality and production potential of crops. *Agric Pol'nohospodárstvo* 63:120–127. <https://doi.org/10.1515/agri-2017-0012>
- Halmová D, Feher A (2014) Effect of transit gas pipeline temperature on the production potential of agricultural soils. *J Centr Europ Agric* 15. <https://doi.org/10.5513/JCEA01/15.3.1481>  
<https://www.gidb.org/gas-pipeline-infrastructure>
- Jangir A, Tiwari G, Sharma RP, Dash B, Paul R, Vasu D, Malav LC, Tiwari P, Chandran P (2020) Characterization, classification and evaluation of soils of Kamrej taluka in Surat district, Gujarat for sustainable land use planning. *J Soil Water Conserv* 19:347–355. <https://doi.org/10.5958/2455-7145.2020.00046.6>
- Jangir A, Sharma RP, Tiwari G, Dash B, Naitam RK, Malav LC, Narse R, Gautam N, Bhure S, Chandran P, Singh SK (2018) Characterization and classification of soils of Bharuch taluka in Bharuch district of Gujarat
- Karlikar BH, Solanki HA (2014) Estimation of micronutrients and physico-chemical analysis of soils of Gandhinagar district, Gujarat, India. *Life Sci Leaflets* 48:49–54
- Khasanova R, Suyundukov J, Semenova I (2017) Evaluation of the ecological state of soils in the steppe agro-ecosystems indicators of biological activity. *Bull Nizhnevartovsk State Univ* 1:103–108
- Kudaisya SK, Kar SK (2017) A comprehensive review of city gas distribution in India. *Nat Gas Mark India* 113–165. [https://doi.org/10.1007/978-981-10-3118-2\\_7](https://doi.org/10.1007/978-981-10-3118-2_7)
- Mayskiy R, Ryabukhina M, Dodova M (2017) Ecological and economic modeling of the insects elimination effectiveness in the coniferous forests of the Orenburg region. *Vestnik Bashkir State Agrarian Univ* 1:101–103
- Miao J, Wang Q (2016) Corrosion rate of API 5L Gr. X60 multipurpose steel pipeline under combined effect of water and crude oil. *Met Mater Int* 22:797–809. <https://doi.org/10.1007/s12540-016-6175-6>
- Ryabukhina MV, Maiski RA, Salikhova RH (2017) Environmental risks of landscape botanical complexes and minimization of technogenic influence exerted by objects of oil & gas production in steppe zone of the Southern Urals. *IOP Conf Ser Mater Sci Eng* 262:012167. <https://doi.org/10.1088/1757-899X/262/1/012167>
- Sharma RP, Singh RS, Naitam RK, Singh SK (2019) Technique of large scale soil mapping using remote sensing satellite data in basaltic terrain of Peninsular region in the north-west Gujarat, India. *J Indian Soc Soil Sci* 67:151–159. 10.5958/10974-0228.2019.00016.1

- Shinde V, Singh M, Nandgude S, Bharti B (2020) Modeling the effect of conservation measures on potential soil erosion: a USLE and GIS approach. *Curr Sci* 119:00113891
- Siddiqui SA, Fatima N (2017) Indian soils: identification and classification. *Earth Sci India* 10:1–14
- Sircar A, Sahajpal S, Yadav K (2017) Challenges and issues in natural gas distribution industry. *STM J* 7:1–8
- Thokchom S, Rastogi BK, Dogra NN, Pancholi V (2017) Geotechnical investigations in the southern part of Ahmedabad district, Gujarat, India. *J Ind Geophys Union* 21:105–115
- Zhang P, Qin G, Wang Y (2019) Risk assessment system for oil and gas pipelines laid in one ditch based on quantitative risk analysis. *Energies* 12:981. <https://doi.org/10.3390/en12060981>
- Zinzala VJ, Patel AR, Saini LK (2018) Effect of sulphur and boron on growth, yield and economics of summer groundnut in clay loam soil of Dang district. *Trends Biosci* 11:919–922

# Comparative Study for Compressive and Split Tensile Strengths of Low-Sludge Concrete



J. R. Pitroda , Reshma L. Patel , Rajesh Gujar , Jaykumar Soni , and Vismay Shah 

**Abstract** The waste and by-products of today's industries are used as supplemental cementitious materials for cement concrete and serve to strengthen portions made of reinforced concrete. Concrete has advanced to new levels because of its continued development to meet the demanding requirements of the construction industry. The sludge that is produced by the paper industry is referred to as hypo sludge. It has been shown that trash is superior to conventional construction materials. It is possible to make the case that it is an opportunity for growth. To meet the challenge, all domains will need to collaborate and make concentrated efforts to adopt the categorization of waste into co-products. Only then we will be able to rise to the occasion. This research explores how 0, 10, 20, 30, and 40% of hypo sludge is replaced with cement in M25 grade of concrete. The following tests were performed to test the mechanical qualities, such as compressive strength (CS) and split tensile strength 28, 56, and 90. The research discovered that affordable composites containing low-cost hypo sludge in infrastructure applications deliver sufficient strength and lower expected costs. Hypo sludge concrete improves the compressive and split tensile strength of concrete.

**Keywords** Compressive strength (CS) · Concrete · Economic · Hypo sludge · Relationship · Split tensile strength

---

J. R. Pitroda (✉) · R. L. Patel  
BVM Engineering College, Vallabh Vidyanagar, India  
e-mail: [jayesh.pitroda@bvmengineering.ac.in](mailto:jayesh.pitroda@bvmengineering.ac.in)

R. L. Patel  
e-mail: [rlpatel@bvmengineering.ac.in](mailto:rlpatel@bvmengineering.ac.in)

R. Gujar  
School of Technology, Pandit Deendayal Energy University, Gandhinagar, India  
e-mail: [rajesh.gujar@sot.pdpu.ac.in](mailto:rajesh.gujar@sot.pdpu.ac.in)

J. Soni · V. Shah  
LJ Institute of Engineering and Technology, LJ University, Ahmedabad, India  
e-mail: [jay.soni\\_ljiet@ljinstitutes.edu.in](mailto:jay.soni_ljiet@ljinstitutes.edu.in)

V. Shah  
e-mail: [vishmay.shah\\_ljiet@ljinstitutes.edu.in](mailto:vishmay.shah_ljiet@ljinstitutes.edu.in)

## 1 Introduction

Globally, people were concerned with problems related to industrial waste like its disposal, transportation, and utilization in the present era. During the last decades, researchers paid attention to evolving technologies for their fruitful utilization. Greenhouse gas emissions must be mitigated to achieve sustainable development. Various types of cement and hypo sludge (HS) are discussed in this work. Hypo sludge is rich in CaO, and it functions as a suitable alternative construction material in some circumstances. Every day, the carbon footprint grows. Concrete is made by adding sand and gravel to cement, whisking the mixture with water, and pouring it into molds before it dries. Making cement is the most carbon-intensive part, it involves using fossil fuels to heat a mixture of limestone and clay to more than 1400 °C in a kiln.

The paper generating industry generates waste from different paper production machinery, and many recycled paper products are possible. Within the scope of this discussion, there are three general categories of waste produced by paper mills: fibrous sludge, hypo sludge, and lime sludge.

Bio-degradable fibrous sludge is rejected. The natural by-product of causticization is lime sludge, and sludge formed during calcium hypochlorite production is the only alternative. Hypo sludge is pure garbage.

## 2 Literature Review

It is possible to employ hypo sludge as an alternative to cement as a cement substitute (Chenniappan et al. 2020). As an additional cementitious material, Pulp Mill Fly ash (PFA) might be a beneficial resource for the pulp and paper industry (Cherian and Siddiqua 2021). The optimal strength of hypo sludge concrete is achieved when 20% of fine aggregate is replaced with hypo sludge (Devi et al. 2018). Using hypo sludge as a 20% substitute for cement has resulted in better compressive strength than the control specimen. When compared to the price of control specimens, the cost of using 20 percent paper mill waste was less expensive (J et al. 2020). Hypo sludge is a paper industry by-product (Katrolia et al. 2021). Conventional and regular resources are being used less and less, which demands an increase in the utilization of other industrial wastes. It is possible to manage the devastation of the environment to deal with rubbish. Hypo sludge is a chemical waste that requires much disposal space under normal conditions. There is a chance it may replace cement concrete in specific applications. Hypo sludge may be included in cement concrete to alleviate the disposal problem while also cutting the cost of the product. Hypo sludge improves construction functionality and ecological sustainability, which lowers the project's life cycle cost. Because of the multiple weights put on the bed, durability may be a significant concern for construction experts. That is why an experiment is necessary to solve the topic at hand.

Concrete's strength and durability have been enhanced thanks to the addition of hypo sludge to the mix. From 0 to 50% of the cement is replaced with hypo sludge. For 28 days, the maximum compressive strength may be attained with 30% hypo sludge substitution of cement (Kishan et al. 2015). 25–40% of municipal solid waste is generated yearly in the pulp and paper production and recycling sectors. Sludge and the ash produced by its combustion comprise the bulk of the waste stream (Mavroulidou and Shah 2021). Up to 10% of Waste Paper Ash (WPA) may be substituted for standard Portland Cement to improve the compressive strength of the mix (Meko and Ighalo 2021). Adding more hypo sludge to cement improves its workability. It is, however, reducing in strength as the amount of hypo sludge replaced by cement increases (Pandya and Joshi 2017). The early strength growth of M40 grade concrete at 7 days and the requisite strength of 66% at 14 days' age is achieved with replacements of up to 10%. When cement is replaced with a hybrid mixture of fly ash and hypo sludge (10%), the average strength gain is determined to be 5.03% between 28 and 90 days for grade M40 (Pitroda 2015). Using low-sludge concrete may save the paper industry money on waste disposal and produce a more environmentally friendly building material (Pitroda et al. 2012). 10% hypo sludge and 0.5% polypropylene fiber are the best combinations for the highest strength and least brittleness. Hypo sludge incorporation reduces concrete costs by up to 18.35% (Poonia et al. 2020). The hardened concrete's compressive strength dropped as the amount of OPC replaced with hypo sludge increased (Sarma et al. 2016). The compressive and tensile strength rise up to a 20% addition of hypo sludge, however subsequent additions of hypo sludge diminishes the strength (Selvarani 2016). To minimize paper industry waste disposal expenses and generate greener concrete for construction, hypo sludge and brine sludge are better novel supplemental cementitious building materials utilized in concrete (Sharma and Diwan 2020). A 10% increase in hypo sludge replacement enhances the flexural strength of concrete by 8.91% (Solanki and Pitroda 2013a, b, c). Hypo sludge may be used in concrete to save disposal expenses and generate a more environmentally friendly product (Solanki and Pitroda 2013b). Compressive strength (CS) evaluated after 28 days rises as fly ash replacement increases up to 30% and if 20% hypo sludge compressive strength is replaced (Solanki and Pitroda 2013a). When hypo sludge is used instead of cement, concrete percentages rise by up to 20% for cubes and beams and up to 10% for cylinders (Vijayan et al. 2020).

### 3 Experimental Materials

The experimental materials used for preparing a concrete mix are described below.

**Fig. 1** Hypo sludge**Table 1** Properties of OPC

Physical properties of cement	Results	Requirements as per IS: 12269-2013
Specific gravity	3.15	3.10–3.15
Standard consistency (%)	28%	30–35%
Initial setting time (h, min)	91 min	30 min
Final setting time (h, min)	211 min	600 max
CS (7 days) N/mm <sup>2</sup>	38	43
CS (28 days) N/mm <sup>2</sup>	54.9	53

### 3.1 Hypo Sludge

According to the paper industry, they create large amounts of trash. When paper is made from pulp, the damaged and low-quality fibers are separated as sludge and are referred to as HS. Producing in an optimal quantity and pace is possible for paper, too. Concrete is a good substitute for HS since it may last longer. The hypo sludge is sourced from Gujarat, where it is produced in great quantity. Hypo sludge was sun-dried till the moisture exhaust; after that, it was grinded and sieved. It was sieved using a 150-micron sieve. Refer to Fig. 1 for hypo sludge.

### 3.2 Ordinary Portland Cement (OPC)

The OPC of 53, which complies with the criteria of IS: 12269-2013, is used. The cement exhibits several different characteristics, which are listed in Table 1.

Chemical properties of OPC and HS as given in Table 2.

### 3.3 Coarse Aggregate (CA)

The coarse aggregates are made from basalt rock with thicknesses ranging from 20 to 4.75 mm and fulfill the IS: 383. The flakiness index (FI) and elongation



**Table 2** Chemical properties of OPC and HS

Chemical properties	OPC (% by mass)	HS (% by mass)
CaO	57.02	47.84
SiO <sub>2</sub>	21.77	5.28
MgO	2.71	6.41
SO <sub>3</sub>	2.41	0.19
Al <sub>2</sub> O <sub>3</sub>	2.59	0.09
Fe <sub>2</sub> O <sub>3</sub>	0.65	0.73
LOI	2.82	38.26

Source Geo test house, Vadodara, Gujarat

**Table 3** Properties of aggregates

Properties	Fine aggregate	Coarse aggregate	
		20 mm down	10 mm down
Fineness modulus	3.35	7.54	3.19
Specific gravity	2.38	2.76	2.69
Water absorption (%)	1.20	1.83	1.35
Bulk density (gm/cc)	1753	1741	1711

index (EI) were both kept far below the 15 percent threshold. The aggregate has the characteristics listed in Table 3.

### 3.4 Fine Aggregate (FA)

Fine aggregate is defined as natural river sand with fractions ranging from 4.75 mm to 150 microns that complies with the criteria of IS: 383, which is a standard for fine aggregate. Table 3 contains information on the characteristics of FA.

### 3.5 Water

Using portable water that is readily accessible in the workroom and that complies with the requirements of IS 456-2000.

**Table 4** Concrete mix design proportions

CM	W/C ratio	Concrete mix design proportions (by weight in kg)				% Replacement of C by HS
		C	FA	CA (20 mm down)	CA (10 mm down)	
A1	0.50	372.00	558.60	751.14	500.76	0% (0 kg)
C1	0.50	334.80	558.60	751.14	500.76	10% (37.2 kg)
C2	0.50	297.60	558.60	751.14	500.76	20% (74.4 kg)
C3	0.50	260.40	558.60	751.14	500.76	30% (111.6 kg)
C4	0.50	223.20	558.60	751.14	500.76	40% (148.8 kg)

CM concrete mixes, W/C water/cement ratio, C cement, FA fine aggregate, CA coarse aggregate

## 4 Experimental Methodology

### 4.1 Mix Design Proportions

Mix proportions were adopted requirements to IS 10262:2009, and the same was used to prepare the test samples for M25. The mix proportions are given in Table 4.

### 4.2 Compressive Strength (CS) of Cubes

The CS of concrete was measured by performing experiments with and without hypo sludge following IS 516-1959, which was then compared. The specimens were maintained in water for curing for 28, 56, and 90 days. They were examined in a dry environment after being removed from the water. To conduct the test, a compression testing machine (CTM) with a capacity of 2000 kN was used. The cubes were put in the CTM, and the load was applied until the specimen failed. The sample's CS was calculated by taking the mean of three readings. Figure 2 illustrates the results of the compressive strength test.

### 4.3 Splitting Tensile Strength (STS) Test for Cylinders

STS tests were directed as per IS 5816:1999. The dimensions of the cylinder are 300 mm long, and 150 mm dia. was prepared for the various percentages of cement replacements with hypo sludge concrete at 0, 10, 20, 30, and 40%. Figure 3 shows the testing of the split tensile test.

$$STS = 2P/(\pi DL) \quad (1)$$

**Fig. 2** Testing of compressive strength test



**Fig. 3** Testing of split tensile test



where:  $P$  = Load (N),  $D$  = Diameter (mm),  $L$  = Length (mm).

## 5 Discussion of the Findings

The succeeding results and discussion of CS of cubes and STS test for cylinders.

### 5.1 Compressive Strength of Cubes

CS of different concrete mixes was evaluated at 28, 56, and 90 days to study the partial replacement of hypo sludge with cement. Different observations are specified in Table 5.

The use of hypo sludge as a cement substitute increases the CS of concrete at all ages. At 28 days, the control mix's CS was  $38.52 \text{ N/mm}^2$ , whereas the mixes' CS

**Table 5** CS of cubes and % change of CS

CM	CS (N/mm <sup>2</sup> ) at days			% Change in CS at days		
	28	56	28	56	28	56
A1	38.52	40.30	42.52	0	0	0
C1	39.70	40.15	42.67	(+) 3.06	(-) 0.37	(+) 0.35
C2	25.78	27.11	29.19	(-) 33.07	(-) 32.72	(-) 31.34
C3	23.26	24.30	25.19	(-) 39.61	(-) 39.70	(-) 40.75
C4	22.96	23.11	23.85	(-) 40.39	(-) 42.65	(-) 44.14

CM concrete mixes

was 39.70, 25.78, 23.26, and 22.96 N/mm<sup>2</sup>. On the other hand, after 56 days, the control mix's CS was 40.30 N/mm<sup>2</sup>, whereas the mix's CS was 40.15 N/mm<sup>2</sup>. At 90 days, the control mix's CS was 42.52 N/mm<sup>2</sup>, whereas the mixes' CS was 42.67, 29.19, 25.19, and 23.85 N/mm<sup>2</sup>. It implies that the compressive strength of concrete increases with cement replacement level until it reaches a maximum of 10% and then begins to decrease. All concrete mixtures exhibit a similar tendency.

The percent increase and reduction in CS of concrete for C1, C2, C3, and C4 mixes compared to control concrete were 3.06, 33.07, 39.61, and 40.39%, respectively. However, after 56 days, the compressive strength of C1, C2, C3, and C4 concrete mixes decreased by 0.37, 32.72, 39.70, and 42.65%, respectively, compared to control concrete. After 90 days, the CS of C1, C2, C3, and C4 concrete mixes increased or decreased by 0.35, 31.34, 40.75, and 44.14%, respectively, compared to control concrete. Figure 4 compares compressive strengths (N/mm<sup>2</sup>) of several HS mixes in M25 at various ages.

## 5.2 Splitting Tensile Strength (STS) of Cylinders

STS of altered concrete mixes was evaluated at the age of 28, 56, and 90 days to study the effect of partial replacement for hypo sludge with cement, and observations are given in Table 6.

The use of hypo sludge as a cement substitute significantly improves the STS of concrete compared to the control mix. 3.00 N/mm<sup>2</sup>, whereas C1, C2, C3, and C4 concrete mixes had 3.60, 2.59, 2.20, and 1.80 N/mm<sup>2</sup> STS at 28 days. Following a 56-day curing period, STS of the control mix was 3.20 N/mm<sup>2</sup>, whereas STS of the concrete mixes C1, C2, C3, and C4 was 4.30, 2.72, 2.44, and 2.00 N/mm<sup>2</sup> 90-day STS of control mix was 3.40 N/mm<sup>2</sup> but was 4.10, 3.00, 2.62, and 2.20 N/mm<sup>2</sup> for C1, C2, C3, and C4 concrete mixes. The splitting tensile strength of concrete increases with increasing cement replacement level which reaches a maximum at 10% cement replacement level and then decreases. All concrete mixtures exhibit a similar tendency.

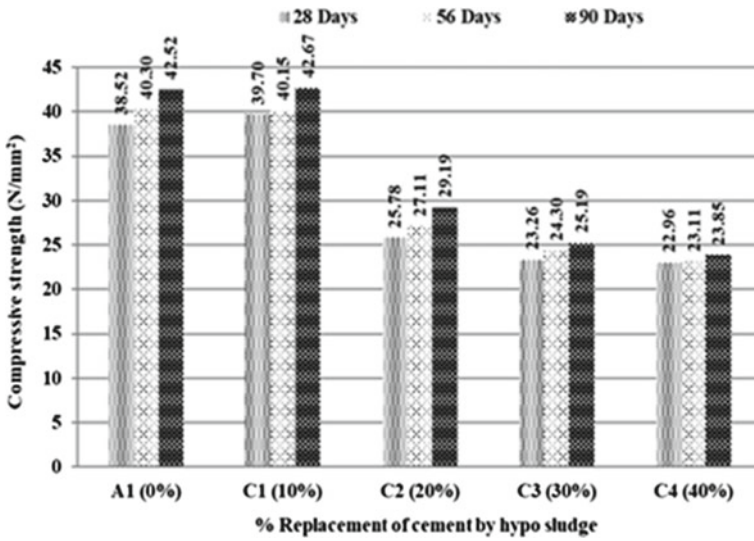


Fig. 4 Comparison of compressive strength (N/mm<sup>2</sup>) of mixes of hypo sludge in M25

Table 6 STS of cylinders and % change of STS

CM	STS (N/mm <sup>2</sup> ) at days			% Change in STS at days		
	28	56	90	28	56	90
A1	3.00	3.20	3.40	0	0	0
C1	3.60	4.00	4.10	(+) 16.66	(+) 25.00	(+) 20.58
C2	2.59	2.72	3.00	(-) 13.66	(-) 15.00	(-) 11.76
C3	2.20	2.44	2.62	(-) 26.66	(-) 23.75	(-) 22.94
C4	1.80	2.00	2.20	(-) 40.00	(-) 37.50	(-) 35.29

CM concrete mixes

Concrete STS increased or decreased by 16.22, 13.66, 26.66, and 40.00% after 28 days compared to control concrete. On the other hand, after 56 days, the rise and reduction in STS of concrete was (+) 25%, (-) 15%, (-) 23.75%, and (-) 37.50% for C1, C2, C3, and C4 mixes, respectively. The increase in STS of concrete for C1, C2, C3, and C4 mixes compared to control concrete was 20.58 percent, 11.76, 22.94, and 35.29%, respectively, at 90 days. Figure 5 compares the splitting tensile strength (N/mm<sup>2</sup>) of several HS mixtures aged M25.

### 5.3 Correlation Concerning STS and CS

Ratios of STS to CS of concrete as percentage are given in Table 7.

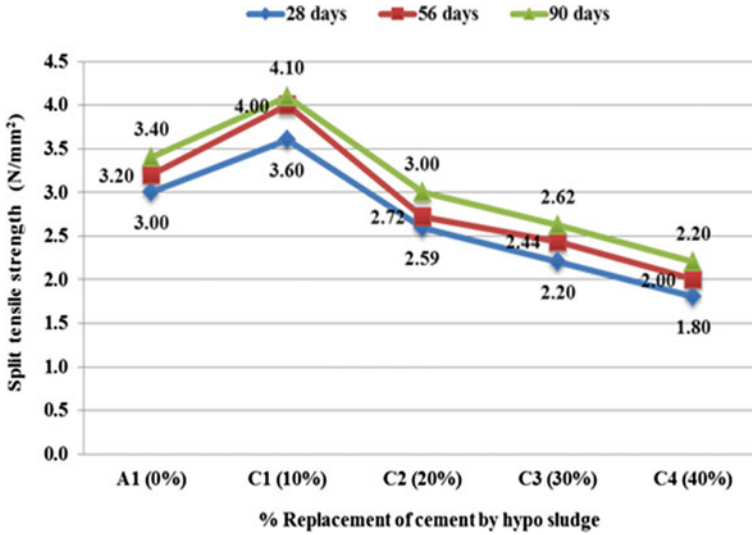


Fig. 5 Comparison of the split tensile strength (cylinders) (N/mm<sup>2</sup>) of different mixes of hypo sludge in M25

Table 7 STS and compressive strength ratios at different days

CM	STS and CS ratio (%) at days		
	28	56	90
A1	7.78	7.94	7.99
C1	9.06	9.96	9.60
C2	10.04	10.03	10.27
C3	9.45	10.04	10.40
C4	7.83	8.65	9.22

CM concrete mixes

A close look at Table 6 reveals that the strength ratios and cement replacement level have no discernible connection. At 28 days, the average STS/CS ratio of concrete is 8.83, 56 days is 9.32, and 90 days is 9.49. As a result, the STS/CS ratio rises with increasing age.

Regression analysis may be utilized to discover the relationship between STS and CS. Using hypo sludge in place of cement, the connection between STS and CS of the resulting concrete may be shown in Fig. 6.

Concrete’s STS and CS are linked together using the equation shown below, along with the coefficient of determination:

$$f_{st} = 0.1393(f_{cu})^{0.8775}, R^2 = 0.8317 \tag{2}$$

where

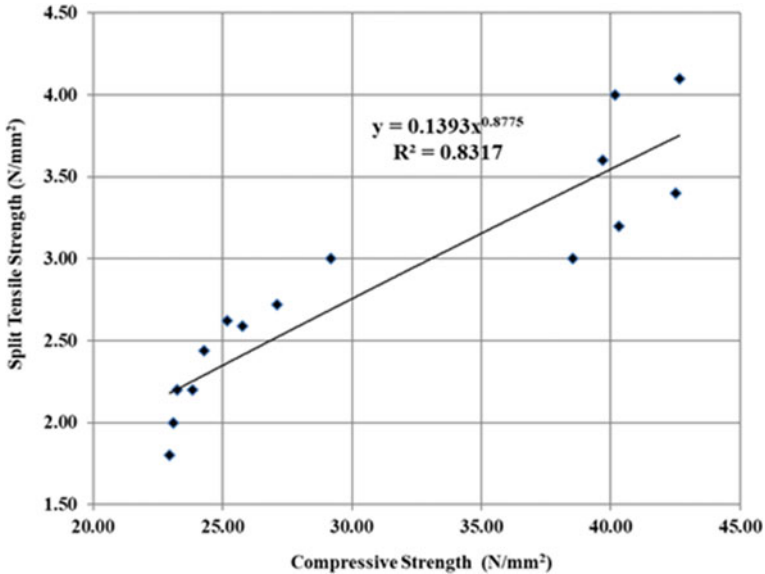


Fig. 6 Relation between STS and CS of hypo sludge concrete

$f_{st}$  STS (N/mm<sup>2</sup>)  
 $f_{cu}$  CS of cube (N/mm<sup>2</sup>).

$R^2$ , the coefficient of determination, indicates that the regression curve and the data points have a strong connection. A comparison is made between the suggested equation and those found in standard literature to see whether it is accurate. ACI 318M-14 and CEB-FIP Model Code, 2010, provide empirical formulae for determining STS from CS in concrete (Eqs. 3 and 4).

$$f_{st} = 0.56(f_{cy})^{0.5} \tag{3}$$

$$f_{st} = 0.3(f_{cy})^{2/3} \tag{4}$$

where

$f_{st}$  = Splitting tensile strength (N/mm<sup>2</sup>).

$f_{cy}$  = Compressive strength of cylinder in (N/mm<sup>2</sup>), which may be taken as 0.8  $f_{cu}$ .

Using the equation presented in this research, we may compare it to those provided by ACI 318-14 and CEB-FIP Model Code, 2010.

It is easy to see from Fig. 7 that the correlation found between CS and STS is quite similar to the equation found in other mainstream publications. Therefore, using the equation presented in this research and the STS values found in ACI 318-14 and

CEB-FIP Model Code, 2010, a regression analysis is performed to get a clearer picture. The results are displayed in Fig. 8.

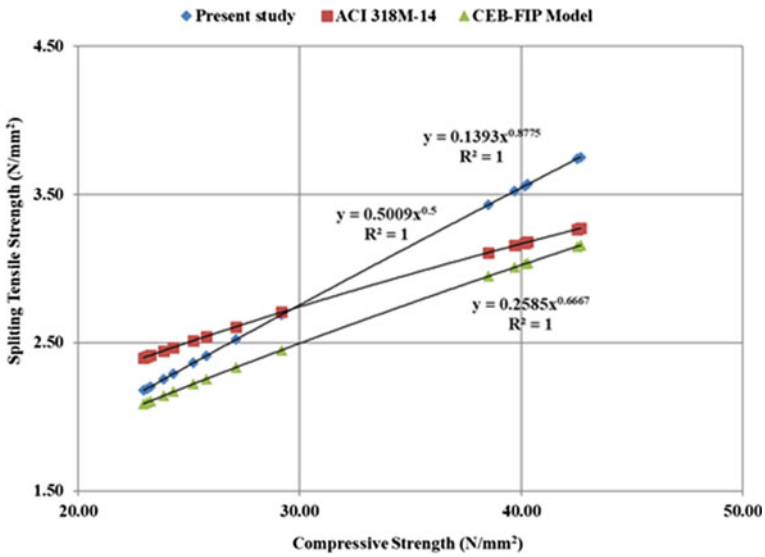


Fig. 7 Comparison between equations proposed by the present study and relations given in other standard literature

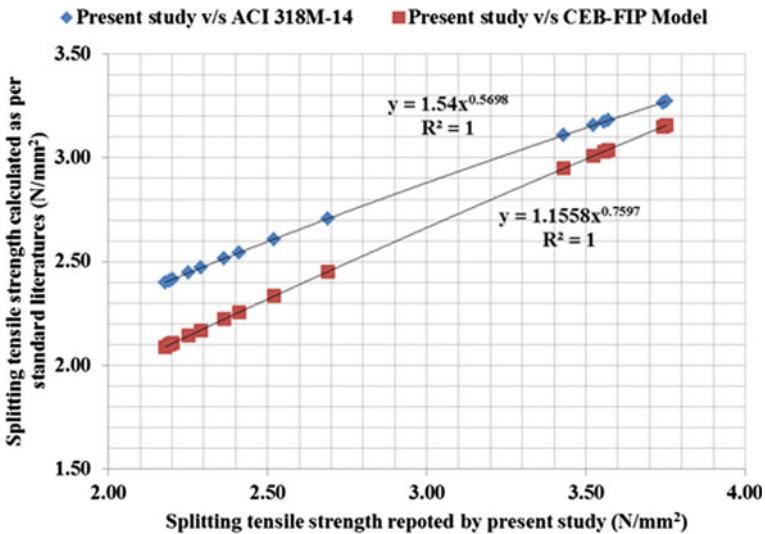


Fig. 8 Relation between splitting tensile strength results as per present study and as per equations given in standard literature



**Table 8** Cost of experimental materials

Materials	Rate (Rs/kg)
C	6.40
HS	0.60
FA	0.60
CA (20 mm down)	0.65
CA (10 mm down)	0.65

**Table 9** Cost of concrete with % change in cost

CM	% Reduction in cement	Total cost [m <sup>3</sup> ]	% Change in cost
	0	3529.70	0
C1	10	3313.94	(-) 6.11
C2	20	3098.18	(-) 12.22
C3	30	2882.42	(-) 18.33
C4	40	2662.66	(-) 24.56

The coefficient of determination ( $R^2$ ) for the splitting tensile strength findings according to the current research and equation provided in ACI 318-14 is 1, as shown in Fig. 8. This research and equation in CEB-FIP Model Code, 2010, show that the coefficient of determination,  $R^2$ , for the splitting tensile strength values is 1. Therefore, we may conclude that since the correlation coefficient is so close to 1, the findings in this research have a lot in common with the previous ones. These also confirm the correctness of the current study's STS and CS findings.

## 6 Economic Feasibility

Table 8 gives the current market prices for various commodities. Table 9 calculates the change in cost due to using hypo sludge instead of cement. Reduced cement use lowers costs. Figure 9 compares the cost per m<sup>3</sup> of different HS mixes in M25 in concrete (m<sup>3</sup>).

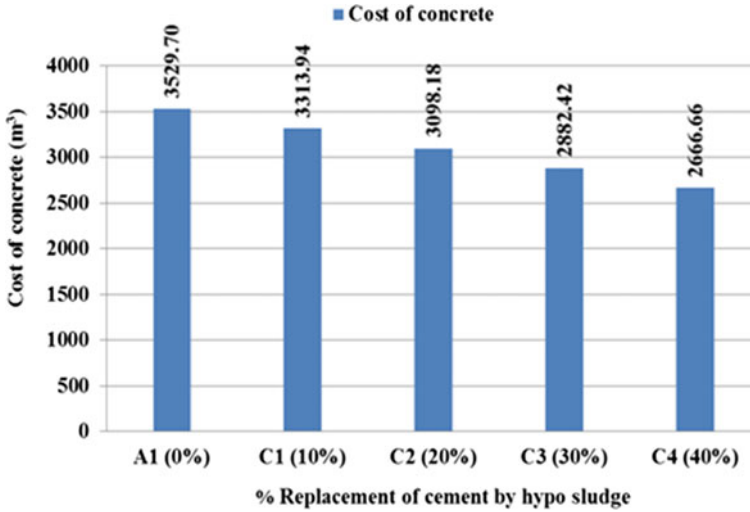


Fig. 9 Cost comparison of concrete ( $\text{m}^3$ ) of various mixes of HS in M25

## 7 Conclusion

Based on experimental work, conclusions are drawn:

1. Comparatively, concrete that contains 10% hypo sludge replacement has higher strength than concrete that does not.
2. It was found that adding HS to concrete improved its compressive strength (CS). As a result, the concrete mix had a maximum CS of 10% cement replacement level on all days.
3. With HS as a partial substitute for cement, the STS of concrete was improved. Concrete with a 10% cement replacement level had the highest STS at all ages.
4. The relationship between CS–STS is given by  $f_{st} = 0.1393 (f_{cu})^{0.8775}$  with coefficient of variation  $R^2 = 0.8317$ .
5. The relationship between CS and STS of hypo sludge concrete follows power's law.
6. Temporary shelter initiatives sponsored by the government would allow this material to be used and make it financially viable.
7. Using this low-cost concrete, these disposal and pollution issues may be prevented, ultimately protecting the environment.
8. Newly formulated building material, e.g., hypo sludge, produces a superior measure.

## References

- Chenniappan A, Shanmugam J, Rajendran V (2020) Analysing mechanical behaviour of concrete with crimped steel fibres and hyposludge as partial replacement of cement. *Int J Adv Sci Technol AIP Conf Proc* 29(3):3158–3163. <https://doi.org/10.1063/5.0011063>
- Cherian C, Siddiqua S (2021) Engineering and environmental evaluation for utilization of recycled pulp mill fly ash as binder in sustainable road construction. *J Clean Prod* 298:126758. <https://doi.org/10.1016/j.jclepro.2021.126758>
- Devi AA, Thenral BG, Bharath P, Sountharya G (2018) Durability study on hypo sludge concrete with replacement of fine aggregate. *Int Res J Eng Technol* 05(03):2127–2132
- J AJ, Peerzada D, Ganesh S, Raina CS (2020) Implementation of paper mill waste as partial replacement material. *Indian J Sci Technol* 13(19):1901–1907. <https://doi.org/10.17485/ijst/v13i19.583>
- Katrolia D, Mudgal BP, Sharma M (2021) Supplementary cementitious materials (SCMs) like fly ash and hypo sludge. *Compl Eng J* 12(8):217–224
- Kishan KH, Lal NV, Konni S (2015) Study of structural performance and durability of concrete by partial replacement of cement with hypo sludge (paper waste). *Int J Eng Res* 4(12):635–639. <https://doi.org/10.17950/ijer/v4s12/1201>
- Mavroulidou M, Shah S (2021) Alkali-activated slag concrete with paper industry waste. *Waste Manage Res* 39(3):466–472. <https://doi.org/10.1177/0734242X20983890>
- Meko B, Ighalo J (2021) Utilization of waste paper ash as supplementary cementitious material in C-25 concrete: evaluation of fresh and hardened properties. *Cogent Eng* 8(1):1–11. <https://doi.org/10.1080/23311916.2021.1938366>
- Pandya A, Joshi T (2017) Gainful utilization of hypo sludge in concrete. *Int J Civ Eng Technol* 8(2):128–134
- Pitroda J (2015) Gainful utilization of fly ash and hypo sludge in concrete. *Int J Construct Res Civ Eng (IJCRCE)* 1(1):1–7
- Pitroda J, Zala LB, Umrigar FS (2012) Hypo sludge management: opportunities for developing low cost concrete with glass fibres. *Glob Res Anal* 1(7):56–58
- Poonia P, Daniyal M, Singh RK (2020) Use of hypo sludge and polypropylene fibers in concrete by partially replacing the cement. *Mukt Shabd J* IX(Vii):1632–1639
- Sarma V, Rambabu PV, Anil NC (2016) Durability studies on concrete with hypo sludge as partial replacement of cement. *J Eng Res Appl* 6(5):81–85. [www.ijera.com](http://www.ijera.com)
- Selvarani S (2016) Structural performance of concrete by partial replacement of cement with hypo sludge. *Int J Adv Res Trends Eng Technol (IJARTET)* 3(2):321–326
- Sharma SK, Diwan PC (2020) A suitability analysis of paper waste sludge in cement concrete. *Int J Innov Eng Res Manage* 7(07):1–6
- Solanki J, Pitroda J (2013a) Flexural strength of beams by partial replacement of cement with fly ash and hypo sludge in concrete. *Int J Eng Sci Innov Technol* 2(1):173–179
- Solanki JV, Pitroda J (2013b) Investigation of low cost concrete using industrial waste as supplementary cementitious materials. *Int J Eng Sci Innov Technol (IJESIT)* 2(1):81–88
- Solanki JV, Pitroda J (2013c) Study of modulus of elasticity of concrete with partial replacement of cement by hypo sludge waste from paper industry. *Global Res Anal* 2(1):40–41
- Vijayan DS, Rose AL, Kumar PD, Gokulnath V, Parthiban D (2020) Sustainable efficiency of hypo sludge in concrete. *Int J Emerg Trends Eng Res* 8(9):5490–5495. <https://doi.org/10.30534/ijer/2020/94892020>

# Effect of Chemical Stabilisation in Clayey Soil for Strength and Durability Characteristics



Shiva Kumar Mahto and Sanjeev Sinha

**Abstract** The use of locally available materials plays an important role in reducing the cost and environmental benefits. It can be such as wastes from industries, plastic fibre, natural fibres, etc. Such materials are found to be effective in the stabilisation process of soils which are having poor geotechnical properties. These materials improve the soil strength by changing the properties and also will be advantageous in reducing the cost of road construction. In the present study, soft clay soil has been considered for its strength and durability assessment. The use of low calcium fly ash (FA) obtained from thermal plants has been used for the stabilisation process. It was mixed with cement in different ratios as per AASHTO guidelines to evaluate the strength and durability parameters. The clayey soil was assessed for the initial consumption of lime (ICL) to reduce the plastic nature. The cylindrical soil samples were prepared and subjected to unconfined compressive strength (UCS) and California bearing ratio (CBR) tests for strength evaluation. The wetting and drying test method was used for durability analysis. The results revealed that the use of fly ash had led to a significant increase in the strength of the soil. The UCS value was so high that it could be a replacement for the GSB layer of rural roads. The CBR test reported a substantial increase in the value by the stabilisation technique. It can be concluded that the thickness of the pavement can be reduced significantly. Also, the results showed a magnificent increase in the durability percentage of the prepared samples.

**Keywords** Fly ash · Clayey soil · Lime · Unconfined compressive strength · CBR

---

S. K. Mahto (✉) · S. Sinha  
Department of Civil Engineering, National Institute of Technology Patna, Bihar 800005, India  
e-mail: [shivam.phd19.ce@nitp.ac.in](mailto:shivam.phd19.ce@nitp.ac.in)

S. Sinha  
e-mail: [sanjeev@nitp.ac.in](mailto:sanjeev@nitp.ac.in)

## 1 Introduction

Due to rapid urbanisation, getting good quality material near the site of road construction is a challenging task. The availability of such material is limited on road sites, especially in rural areas. Also if available, the transportation of good materials may lead to an increase in cost as it is far away from the construction sites. The use of locally available materials plays a great role in reducing the overall cost of construction. The type of soil also has demerits in road construction. One such type is black cotton soil. The black cotton soil is expansive in nature. They are having high clay content which becomes weak when it comes in contact with moisture. It tends to expand, swell or shrink due to the ingress of water and experiences losing engineering properties that lead to a settlement which mainly depends on the stress level and the swell pressure of the soil (Horpibulsuk et al. 2012; Sharma et al. 2012). It becomes problematic and tends to lose its engineering properties such as the decrease in strength, swelling and conversion to highly compressible soils. It contains the two main clay minerals, i.e. montmorillonite and kaolinite which are the reason for low strength and increased swelling index (Latifi et al. 2016). Therefore, a suitable method is required to solve this issue. Soil stabilisation is one of the methods used for several years for the treatment of such soils. It involves the technique which changes the properties of the soil by adding suitable admixtures and thus making it fit for road construction by fulfilling the minimum requirements. Previous studies reported different techniques using waste materials and chemical processes which have been used for treating clayey soils (Horpibulsuk et al. 2012; Koliyas et al. 2005; Roohbakhshan and Kalantari 2013; Sharma et al. 2012; Al-Jabban et al. 2017). Most of them made use of traditional techniques, i.e. cement lime, fly ash, etc. Also, the utilisation of industrial waste such as marble dust and brick dust had influenced the strength of stabilised soil (Patel and Bhavsar 2014). All such techniques showed improved strength and other properties that make them suitable for fulfilling the requirements of road construction. The use of stone dust with lime showed improved strength and bearing properties of clayey soil (Roohbakhshan and Kalantari 2013). In a study, the addition of marble dust has shown significant improvement in engineering properties with clayey soil (Patel and Bhavsar 2014). In another study, the addition of brick kiln dust showed improved strength and CBR value of clayey soil. (Bhavsar and Patel 2014). The use of waste plastic fibre has shown improvement in tensile and compressive strength with increased CBR value (Dhar and Hussain 2019). The properties of clayey soil were significantly changed due to the addition of waste calcium carbide residue which was treated with fly ash (Horpibulsuk et al. 2012). The use of high calcium fly ash showed a magnificent increase in indirect tension and flexure strength test of fine-grained clayey soils (Koliyas et al. 2005).

The literature study reported several methods and materials which led to an enhancement of the strength and durability of clayey soil. However, scanty information was found on the utilisation of low calcium content in fly ash which can be used as stabilisation material. In the present study, the use of fly ash was assessed as locally available materials from nearby thermal plants in the stabilisation process

by varying ratios. The fly ash was obtained from Barh, a thermal power plant in Bihar. It is estimated about 8.92 million tonnes (Central Electricity Authority, New Delhi, India, 2020) of fly ash is generated every year from Bihar thermal plants and disposing of such a large quantity is a serious problem. The cement to fly ash ratio was by determining the initial lime content for high plastic soil, and the samples were subjected to various strength tests such as unconfined compressive strength and California bearing ratio test. Furthermore, the durability test was also conducted for the stabilised soil through a wetting and drying test.

## 2 Materials and Test Methods

In the current study, the soil was taken from the Lakhisarai district in Southern Bihar. The soil was found to be soft and clayey soil. The lime was added initially with different contents to reduce the plasticity. It was varied from 6% by the weight of soil at a 1% increment as per the methodology adopted by Rogers and Glendinning (2000). The content at which the soil becomes plastic free could be taken as the initial consumption of lime (ICL) in such soils. The soil found zero plasticity at 10% lime. Then, the soil was stabilised with cement and fly ash. The ratio of 1:4 was adopted as per the AASHTO R Draft (2008) and national academy of sciences; Recommended Practice for Stabilisation of Subgrade Soils and Base Materials (2009), guidelines for the stabilisation process in clayey soil. The guidelines states that determination of the optimal activator content is best achieved on a trial and error basis realising that the required lime content or Portland cement content to activate the fly ash is typically between one part lime to three parts fly ash (1:3 ratio) to one part lime to four parts fly ash (1:4 ratio). The content of cement varied from 2 to 8% and the corresponding ratio of fly ash was 8–32%. The cylindrical sample of diameter 50 and 100 mm in height was prepared and subjected to an unconfined compressive strength test and California bearing ratio value. The durability test was conducted by the drying and wetting method as per ASTM 559.

## 3 Results and Discussion

*Soil:* The soil was obtained from the Lakhisarai district zone a southern part of Bihar, India. The physical properties of the soil have been assessed and found to be soft clay soil. The result of the various tests is as follows in Table 1.

*Fly ash:* The fly ash was obtained from nearby thermal plants, viz Barh, Bihar in India. It is estimated only 60–70% is been utilised in other sectors such as cement and brick manufacturing industries. The amount of approximately 30–40% is left open to the atmosphere which can be hazardous to the environment. The physical and

**Table 1** Physical properties of soil

Sl no	Properties	Test results	Test codes
1	Liquid limit, %	79	ASTM D4318-10
2	Plastic limit, %	35	ASTM D4318-10
3	Plasticity index, %	44	ASTM D4318-10
4	Type of soil	CH-clay of high plasticity	(ASTM D2487-11)
5	Optimum moisture content, %	24.26%	ASTM D698
6	Maximum dry density, gm/cc	1.54	ASTM D698
7	California bearing ratio, %	3.52%	ASTM D1883
8	Unconfined compressive strength (MPa)	0.31	ASTM D2166

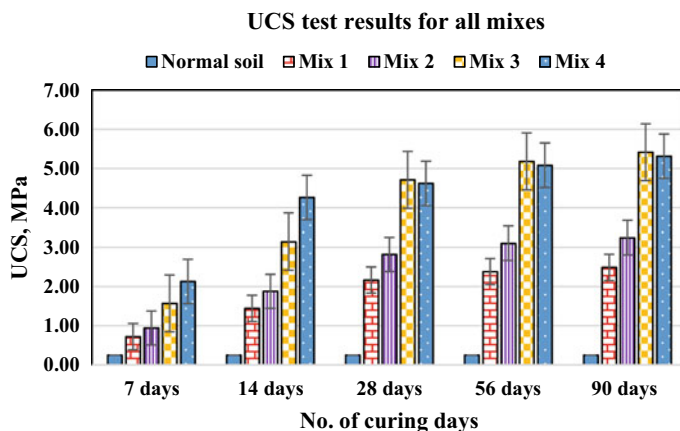
**Table 2** Physical and chemical properties of fly ash

Fly ash composition			
No.	Test conducted	Observed values (%)	Requirement as per IS: 3812 2003
1	Loss of ignition	1.23	5.0 (max)
2	Silica as SiO <sub>2</sub>	57.42	35 (min)
3	SiO <sub>2</sub> + Al <sub>2</sub> O <sub>3</sub> + Fe <sub>2</sub> O <sub>3</sub>	(63.5 + 26.42 + 3.26) = 93.18	70 (min)
4	Available alkalis as Na <sub>2</sub> O	0.4	1.5 (max)
5	Reactive silica	28.12	20 (min)
6	Lime reactivity, N/mm <sup>2</sup>	4.62	4.5 (min)
7	Calcium oxide (CaO)	Practically nil	–
8	Specific surface area (SSA), m <sup>2</sup> /kg	372	–

chemical properties of fly ash are given in Table 2. Based on chemical composition, it was that the fly ash is of the class F category.

### 3.1 Unconfined Compressive Strength (UCS)

The UCS test was conducted on the cylindrical sample conforming to ASTM D2166. This test is adopted because of its simplicity, less cost and reliability way for assessing the strength of the soil. The cylindrical sample of diameter 50 and 100 mm in height was prepared and subjected to the compressive testing machine at a rate of 1.25 mm/min. The results are shown in Fig. 1. Table 3 gives the nomenclature for the ratios adopted.



**Fig. 1** Results of UCS for the mix variants

**Table 3** Content of stabiliser used in stabilised soil sample

Particulars	Mix 1	Mix 2	Mix 3	Mix 4
Cement: fly ash ratio (1:4)	2% cement: 8% FA	4% cement: 16% FA	6% cement: 24% FA	8% cement: 32% FA

Figure 1 demonstrated the UCS values which shows the increase in the value of UCS as compared to that of non-stabilised soil. However, the decrease in UCS is observed with higher content of cement. It might be due to excess cement content; there was insufficient time remained to finish the hydration process. This lead to incomplete formation of CSH gel which maybe the possible reason for decrease in strength at higher cement content.

## 4 Durability

The durability test was calculated for the material reliability and to retain the permanency of the strength for long days exposed to severe climatic conditions. The test was conducted by wetting and drying test conforming to IS 4332 (Part IV) and also followed as per ASTM (D 559). The samples were prepared and subjected to wet-dry cycles. For wetting cycles, the samples were soaked in water for 5 h and kept in an oven for 42 h at 70 °C. For the dry sample, another set was kept in an oven for 48 h, and then, a wire brush was used at the longitudinal axis by giving a firm stroke of 1.4 kgf. The procedure was repeated for 12 cycles. The results are shown in Fig. 2 below. It is observed that the durability value for mix 1 and mix 2 fails to fulfil the minimum requirement of 80% as specified in SP 89 2018 guidelines. The results showed that the mix 3 gained higher durability value with 86.52%.



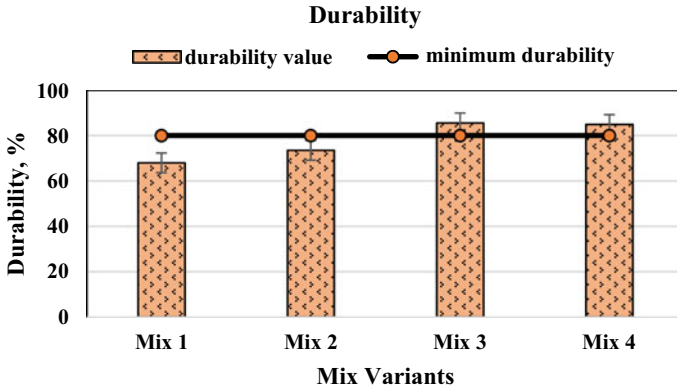
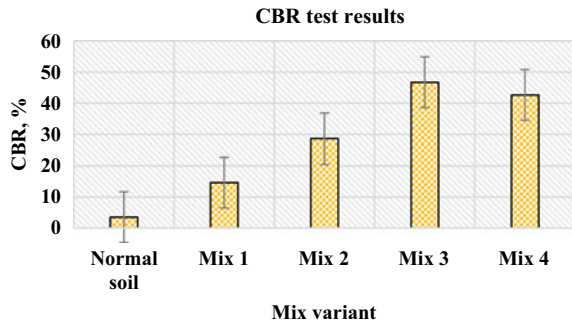


Fig. 2 Durability results for all the mixes

Fig. 3 CBR test plot



### 4.1 California Bearing Ratio

The CBR value was attained for mix 3 which attained the maximum UCS, and durability value was compared with the CBR of normal soil. The procedure was followed conforming to ASTM D1883. The results of CBR are shown in Fig. 3. It is observed that the CBR value for mix 3 was higher as compared to the all mix variant.

## 5 Conclusion

Locally available soil which is soft clay has been utilised in the study. This is due to large cost of transportation and environmental damage occur by the supply of primary aggregates from far distances. The natural soil was stabilised in two stages. Initially, the lime was used for making the soil plastic free. Later, the locally available fly ash has been incorporated with cement as a stabilising agent. The cement and FA ratio were maintained for the determination of optimal dosage in assessing the strength

and durability characteristics of the soft soil. From the result and interpretations made, it can be concluded that the stabilising agent cement and fly ash were found to be effective in gaining higher strength. The clayey soil was found to be plastic free at 10% lime content. It could be taken as the initial consumption of lime in such soils. The 7 days UCS value attained for mix 3 was 1.67 MPa which was higher value than 1.5 MPa for sub-base layer. It is as specified in IRC SP 72, 2015 and SP 89, 2018 guidelines. Also, the maximum durability result was obtained for the mix 3 ratio by 85.62%. The initial mixes, i.e. mix 1 and mix 2 failed to attain the minimum requirement of 80% durability value as per IRC: SP 89, 2018. The CBR value also reported a drastic increase for normal soil and stabilised soil. Therefore, it can be concluded that the cement to fly ash ratio of mix 3 can be adopted for stabilisation by adding lime at 10% initially when working with such soft clay soils. However, further properties such as flexure, tensile strength and linear shrinkage are to be evaluated for better assessment.

## References

- Al-Jabban W, Knutsson S, Laue J, Al-Ansari N (2017) Stabilization of clayey silt soil using small amounts of petrit T. *Engineering* 09(06):540–562. <https://doi.org/10.4236/eng.2017.96034>
- ASTM C618: Standard specification for coal fly ash and raw or calcined natural pozzolan for use in concrete
- Bhavsar SN, Patel AJ (2014) Analysis of swelling and shrinkage properties of expansive soil using brick dust as a stabilizer. *Int J Emerg Technol Adv Eng* 4(12):303–8. <https://www.researchgate.net/publication/269762906>
- Dhar S, Hussain M (2019) The strength behaviour of lime-stabilised plastic fibre-reinforced clayey soil. *Road Mater Pavement Design* 20(8):1757–1778. <https://doi.org/10.1080/14680629.2018.1468803>
- Horpibulsuk S, Phetchuay C, Chinkulkijniwat A (2012) Soil stabilization by calcium carbide residue and fly ash. *J Mater Civ Eng* 24(2):184–193. [https://doi.org/10.1061/\(ASCE\)MT.1943-5533.0000370](https://doi.org/10.1061/(ASCE)MT.1943-5533.0000370)
- IS 1727:1967 (1967) Indian standard methods of test for pozzolanic materials. Bureau of Indian Standards, New Delhi
- Kolias S, Kasselouri-Rigopoulou V, Karahalios A (2005) Stabilisation of clayey soils with high calcium fly ash and cement. *Cement Concr Compos* 27(2):301–313. <https://doi.org/10.1016/j.cemconcomp.2004.02.019>
- Latifi N, Meehan CL, Majid MZA, Horpibulsuk S (2016) Strengthening montmorillonitic and kaolinitic clays using a calcium-based non-traditional additive: a micro-level study. *Appl Clay Sci* 132–133:182–193. <https://doi.org/10.1016/j.clay.2016.06.004>
- National Academies of Sciences, Engineering, and Medicine (2009) Recommended practice for stabilization of subgrade soils and base materials. Washington, DC: The National Academies Press. <https://doi.org/10.17226/22999>
- Patel AJ, Bhavsar SN (2014) Analysis of clayey soil using waste material. *Int J Innov Res Sci Technol* 1(6):125–130
- Rogers CDF, Glendinning S (2000) Lime requirement for stabilization. *Transp Res Rec* 1721:9–18. <https://doi.org/10.3141/1721-02>
- Roohbakhshan A, Kalantari B (2013) Stabilization of clayey soil with lime and waste stone powder. *Int J Sci Res Knowl* 1(12):547–56. <https://doi.org/10.12983/ijrsk-2013-p547-556>

Sharma NK, Swain SK, Sahoo UC (2012) Stabilization of a clayey soil with fly ash and lime: a micro level investigation. *Geotech Geol Eng* 30(5):1197–1205. <https://doi.org/10.1007/s10706-012-9532-3>

# Pull-Out and Rupture Behavior of Geogrid Reinforcements in MSE Wall Subjected to Seismic Conditions



Anand M. Hulagabali, C. H. Solanki, C. Thrupthi, N. Sushma, Ruokuolenuo Suokhrie, and S. Sudarshan

**Abstract** Mechanically Stabilized Earth (MSE) walls are an alternative engineering structure to traditional reinforced concrete retaining walls with significant and adaptable height at a lower cost. The main objective of this study is to perform a detailed numerical analysis of the MSE wall for the effect of parameters such as reinforced soil, the vertical spacing between reinforcements, the tensile strength of reinforcement, surcharge magnitude, and wall height on the internal stability of MSE wall under the static and seismic loading conditions. The analysis has been carried out using the Geo-5 numerical tool to obtain the Factor of Safety (FS) against internal stability checks. Variations of FS against rupture and pull-out for reinforced blocks are compared for various parameters considered in this study. From the detailed parametric analysis for the internal stability of the MSE wall, it has been found that the rupture and pull-out resistance is higher for minimum vertical spacing. FS reduces as surcharge magnitudes increase. The pull-out resistance is substantially larger than the rupture resistance for higher wall heights. In clayey soil, the rupture is larger at the top layer than at the lower layers for a given wall elevation, yet pull-out is greater at the lower levels than at the top layers.

---

A. M. Hulagabali (✉)

Department of Civil Engineering, The National Institute of Engineering, Mysore 570008, India  
e-mail: [anandmh@nie.ac.in](mailto:anandmh@nie.ac.in)

C. H. Solanki

Department of Civil Engineering, SVNIT, Surat, India  
e-mail: [chs@amd.svnit.ac.in](mailto:chs@amd.svnit.ac.in)

C. Thrupthi · N. Sushma · R. Suokhrie · S. Sudarshan

The National Institute of Engineering, Mysore, Karnataka, India  
e-mail: [thrupthiprofessionalmail@gmail.com](mailto:thrupthiprofessionalmail@gmail.com)

N. Sushma

e-mail: [sushmanagaraj16@gmail.com](mailto:sushmanagaraj16@gmail.com)

R. Suokhrie

e-mail: [Rksuokhrie@gmail.com](mailto:Rksuokhrie@gmail.com)

S. Sudarshan

e-mail: [sudarshansachi777@gmail.com](mailto:sudarshansachi777@gmail.com)

**Keywords** MSE wall · Factor of safety · Reinforcement · Rupture · Pull-out

## 1 Introduction

### 1.1 *Mechanically Stabilized Earth Retaining Wall*

The retaining wall takes the eccentric lateral load of soil and live loads and retains the backfill at different slopes and heights. Retaining walls are designed for safety against uplift pressure and overturning due to retained soil mass, utilizing more reinforcement in the stem, toe, and heel construction all through its length.

Mechanically stabilizing the backfill soil by the addition of synthetic polymer reinforcement to hold the soil in place is practiced extensively these days. The friction between geogrids (synthetic polymer reinforcement) and the soil holds the structure in position, reducing the lateral loads on precast panel members, which gives alignment to the structure; supports the geogrid and soil mass. A facing system enables the construction of a steep or even a vertical MSE wall. The structural failure of an MSE wall is attributed to low-quality soil-filled, poor drainage quality of the backfill soil and insufficient reinforcement length and strength, a sudden drawdown of the water table, and a weak foundation soil.

Most of the studies cover external stability checks like overturning and sliding, but there are very few works that consider internal stability checks. Hence, this study describes the importance and the results of internal stability checks, especially those checks for pull-out and rupture which are considered critical in the performance of MSE walls.

### 1.2 *Literature Review*

There are many studies carried out to know the behavior of an MSE wall in different loading conditions. The stability and movement of the existing MSE wall at central Texas major state highway were studied by Konnur et al. (2019) using a finite element (FE) and limit equilibrium (LE) slope stability analysis program, GEO-5 2016 (Konnur et al. 2019). Bathurst et al. (2019) demonstrated the application of the load and resistance factor design (LRFD) for tensile rupture and pull-out internal stability limit states and showed the reduction in required reinforcement strength by using the Simplified Stiffness Method (Bathurst et al. 2019). The advances in reliability-based LRFD calibration of simple linear limit state functions used for tensile rupture and pull-out of the reinforcing elements have been applied to steel-reinforced MSE walls as described by (Allen et al. 2019). The horizontal and vertical movement of the MSE wall decreases as the length of the reinforcement increases which also increased the Factor of Safety for internal stability (Hulagabali et al. 2018).

The effects of soil reinforcement on the excessive movement of the MSE wall were determined by (Kibria et al. 2014). Leshchinsky et al. (2016) studied the behavior of non-uniform reinforcement spacing on the performance of footing surcharged MSE walls using FE analysis (Leshchinsky et al. 2012). While the deformation of walls, facing panels, and ground settlement behind them were observed by Hulagabali et al. (2018a) for different types of reinforcements, backfill, and foundation soil and concluded that the ground settlements were lesser for steel reinforcements behind the wall along with the horizontal profile. Also, the HDPE and steel reinforcements are found to be more reliable as the deformations and settlements are less compared with PET Geogrid (Hulagabali et al. 2018b). Hulagabali et al. (2018) studied the effect of backfill and reinforcement on MSE Wall behavior using the FE numerical tool PLAXIS 2D. Different types of foundations such as rammed aggregate pier (RAP), pile foundations, and drilled shafts were used to analyze the behavior of reinforced earth retaining structures. Wall deformations, settlement of ground, and facing panel deflections were found to be less in drilled shaft compared to RAP and pile foundation (Hulagabali et al. 2018a). Hulagabali et al. (2018b) used design codes to analyze the external and internal stability of MSE walls (AASHTO, 2010; BS8006-1, 2010) (Hulagabali et al. 2018c). Huang et al. (2019) carried out the numerical simulation of the interaction between the drilled shaft and MSE wall using FLAC 3D under a cyclic loading event which resulted in the gradual accumulation of the displacement (Huang et al. 2019). The interaction between back-to-back reinforced walls is strongly dependent on the distance between the walls in synthetic and metallic strips (Lajevardi et al. 2021) (Lajevardi et al. 2021). Back-to-back MSE walls are commonly used for embankments in bridges. In determining internal stability, the strength of the reinforcement and its connection to the facing, as well as its pull-out resistive length are checked. The reinforced mass is designed to have a sufficient long-term margin of safety internally to sustain such as self-weight, surcharge, and seismic loads. (Leshchinsky, Vahedifard, & Leshchinsky, 2012) (Leshchinsky et al. 2012). The design methods used for soil mass structures, such as MSE structures, are based on soil/reinforcement anchorage models which require the knowledge of the soil/reinforcement interface friction capacity. (Abdelouhab et al. 2010) (Abdelouhab et al. 2010).

Many researchers have worked on numerical, analytical, experimental, field, and sustainability studies.

Numerical methods such as FEM and FDM are used using different tools PLAXIS, GEO-5, etc. Numerical analysis results are compared with analytical, experimental, and field wall studies. External and internal stability of the MSE wall has been carried out using AASTHO, FHWA, and BS guidelines. Even after numerous researches, there is still a lot to know about the MSE wall.

This study is carried out to model MSE walls using the Geo-5 program and conduct an internal stability analysis for static and seismic loading conditions. Also, to study the effect of parameters such as reinforcement soil, the vertical spacing between reinforcements, surcharge magnitude, and wall height on the internal stability (pull-out resistance and rupture resistance) of MSE wall modeled, under the static and seismic loading conditions.

## 2 Methodology

### 2.1 Analysis of MSE Wall using Geo-5

In this study, 3D analysis of the MSE wall is carried out using Geo-5 software based on the FE method. Numerical analysis is initialized by creating a model of suitable dimension followed by assigning material properties. Then, the stability of the model is checked. The data thus extracted is used for the study of FS against rupture and pull-out.

### 2.2 Input Parameters

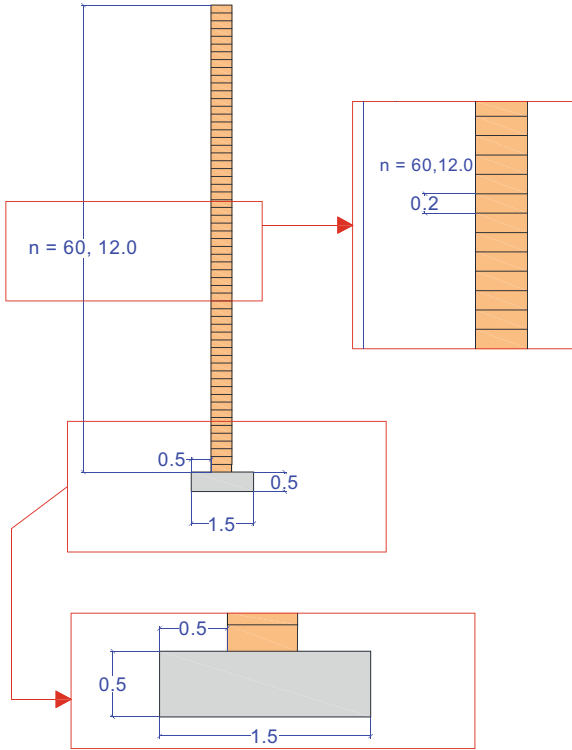
Various parameters are considered as inputs for the analysis done using Geo-5 software (Figs. 1, 2 and 3; Table 1). The parameters varied for the analysis are vertical spacing (varied as 0.4, 0.6, 0.8 m and 1 m), the tensile strength of reinforcement, reinforced soil, surcharge, and wall height. Reinforcement details are summarized in Table 2. In this analysis, reinforcement with different tensile strengths is considered to understand their effect on wall behavior under different loads. To incorporate creep, durability and installation damage reduction factors are considered, which are listed in Table 3.

## 3 Seismic and Static Analysis

Analysis of MSE walls is carried out for both seismic and static conditions as the walls may be constructed in earthquake-prone areas, where earthquake magnitude may be very high. The pseudo-dynamic analysis is considered with varying vertical and horizontal coefficients of earthquake ( $k_v$  and  $k_h$ ) to consolidate the effect of least and high magnitude of seismic effects. The seismic coefficients are dimensionless parameters, which represent the earthquake acceleration as a fraction of acceleration due to gravity. Seismic force is equal to the product of seismic coefficient and block weight, which may be obtained by the area of the block and unit weight of the block.

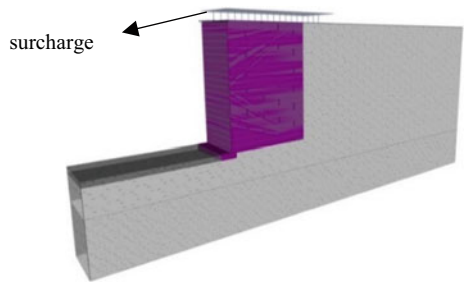
Parameters considered to study internal stability analysis of the structure under seismic and static conditions are vertical spacings, the tensile strength of reinforcement and reinforced soil, surcharge, and wall height.

**Fig. 1** 2D view of MSE wall's wall-facing details, with dimensions in meters, considered for analysis

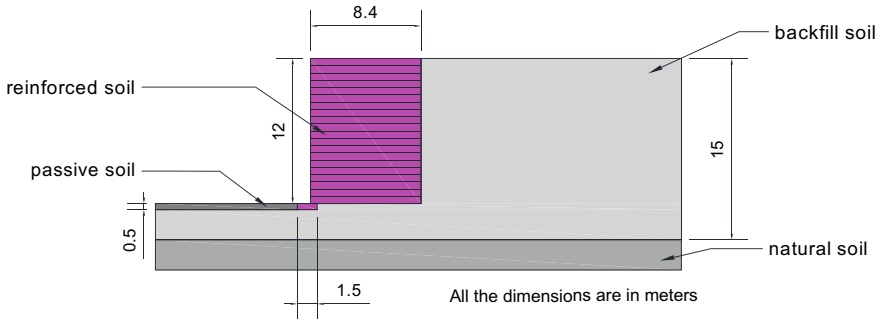


All the dimensions are in meters

**Fig. 2** 3D model of the MSE wall under analysis in Geo-5 software







**Fig. 3** 2D view of MSE wall’s details of soil profiles, with dimensions in meters, considered for analysis

**Table 1** Input parameters for analysis of the MSE wall

Parameter	Quantity	Unit
Total wall height	12	m
No. of facing blocks	60	Number
Block height	0.2	m
Block width	0.5	m
Height of foundation	0.5	m
Width of foundation	1.5	m
Foundation offset	0.5	m

**Table 2** Reinforcement details

Sl. No.	$T_{ult}$ (kN/m)	$RF_{cr}$	$RF_D$	$RF_{ID}$	$FS_{UNC}$	$T_{LTDS}$ (kN/m)
1	138.60	1.60	1.10	1.25	1.5	42

**Table 3** Properties of various soils considered for the analysis

Soil properties	Units	GW	GM	SW	SM	SP	CL
Unit weight ( $\gamma$ )	kN/m <sup>3</sup>	21	19	20	18	18.5	21
The angle of internal friction ( $\Phi$ )	Degree	38.5	32.5	36.5	29	33.5	19
Cohesion (C)	kN/m <sup>2</sup>	0	0	0	5	0	12

## 4 Results

### 4.1 The Factor of Safety (FS) Against Pull-Out and Rupture

#### 4.1.1 Effect of Vertical Spacing of Reinforcement

Figures 4, 5, 6 and 7 show the variation of FS against pull-out and rupture for static and seismic conditions ( $k_v = k_h = 0.5$ ) for vertical spacing ( $S_v$ ) of 0.4, 0.6, 0.8, and 1 m.

The FS against pull-out decreases with an increase in vertical spacing of reinforcement from 0.4 to 1 m by about 4 times. The FS reduces by about ten folds in static conditions with the decrease in wall elevation from 12 to 1 m (Fig. 4). For the earthquake coefficients ( $k_v$ , and  $k_h$ ) 0.5, the structure is not stable for wall elevation less than 8 m for any vertical spacing,  $S_v$  provided. Higher stability against pull-out can be observed for lesser  $S_v$  (a greater number of reinforcements) and more significant wall elevations (Figs. 4 and 5). There is a comparatively lighter load on the topmost layer of reinforcement due to the pavement course, which is appreciably lighter than the dead and live loads acting on the lower layers of reinforcements, at lower wall elevations. This scenario is the reason for the sudden increase in FS at the topmost point of wall elevation, i.e., 12 m.

The FS against rupture decreases with an increase in vertical spacing of reinforcement from 0.4 m to 1 m by about 2 times. The FS increases by about 4 times in static conditions with the decrease in wall elevation from 12 to 1 m (Fig. 6), however, is

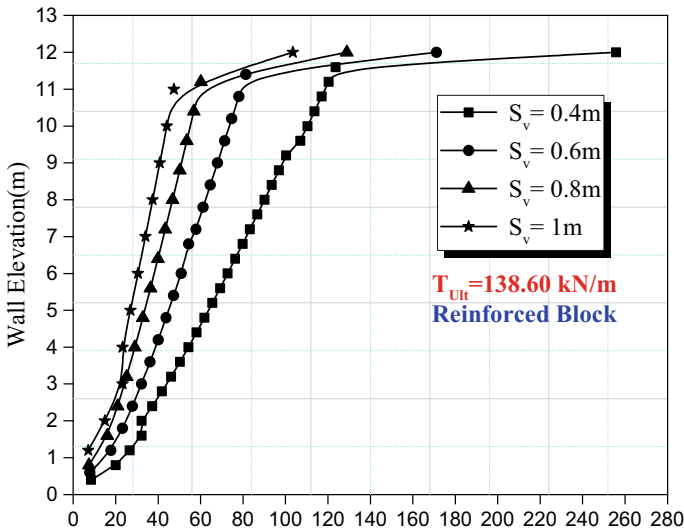


Fig. 4 Variation of FS against pull-out for static conditions ( $S_v$  variation)

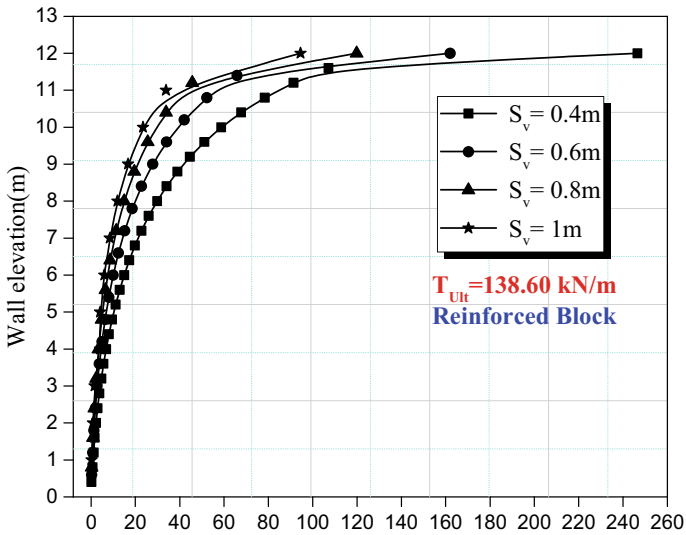


Fig. 5 Variation of FS against pull-out for  $k_v$  and  $k_h$  of 0.5 ( $S_v$  variation)

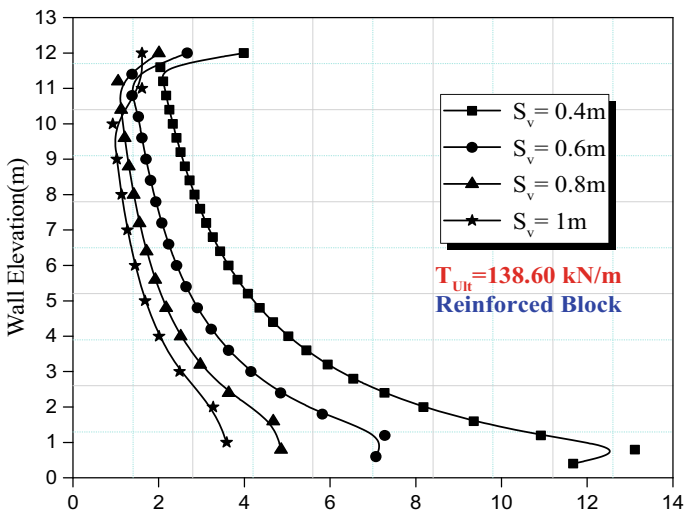


Fig. 6 Variation of FS against rupture for static conditions ( $S_v$  variation)

not suitable for  $S_v$  greater than 0.4 m for wall elevations above 5 m. For the earthquake coefficients ( $k_v$  and  $k_h$ ) 0.5, the structure is not safe for any  $S_v$  provided, due to reduced rupture resistance. Higher stability against rupture can be observed for lesser  $S_v$ , i.e., for the more significant number of reinforcements (Figs. 6 and 7).

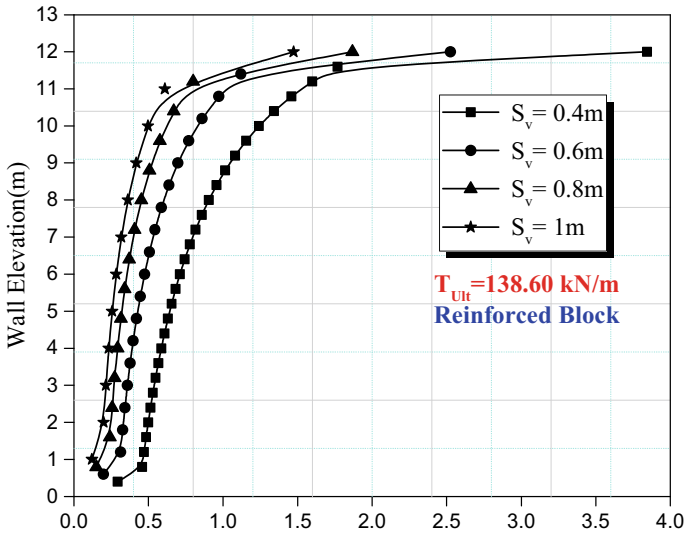


Fig. 7 Variation of FS against rupture for  $k_v$  and  $k_h$  of 0.5 ( $S_v$  variation)

At the bottom of the reinforced block, the FS against rupture is significantly higher because of the anchorage provided to support the reinforced earth along with the wall facing. Whereas, at the top, the increase in rupture resistance is due to the lighter loads acting on the MSE wall at the top. In general, the FS against pull-out and rupture increases with the increase in numbers of reinforcement, i.e., a decrease in  $S_v$  (vertical spacing of reinforcement).

#### 4.1.2 Effect of Reinforced Soil Property

The reinforcement with an ultimate tensile strength of 138.60 kN/m is used for reinforcing the MSE wall modeled. A comparison of static and seismic conditions (with  $k_v = k_h = 0.1$  and 0.5) is done for different reinforced soils (GW, SP, CL) for both pull-out and rupture resistance (Figs. 9, 10, 11 and 12). FS against pull-out for reinforced well-graded gravel (GW) (Fig. 8), for static conditions, increases gradually from 0.5 m wall elevation to 11 m by about 8 times but a sudden increase is seen at wall elevation of 12 m, as the loads to be borne by the reinforced earth is much lesser than other layers below it. For seismic conditions,  $k_v = k_h = 0.5$ , the FS for pull-out shows that the structure is not safe up to the wall elevation of 4 m with FS 1.6 but as the wall elevation increases, the stability also increases with a peak at 12 m which is having an FS of 160.

The seismic conditions,  $k_v = k_h = 0.1$ , is having the intermediate FS against pull-out between the static and seismic conditions with an earthquake coefficient of 0.5(Fig. 8).

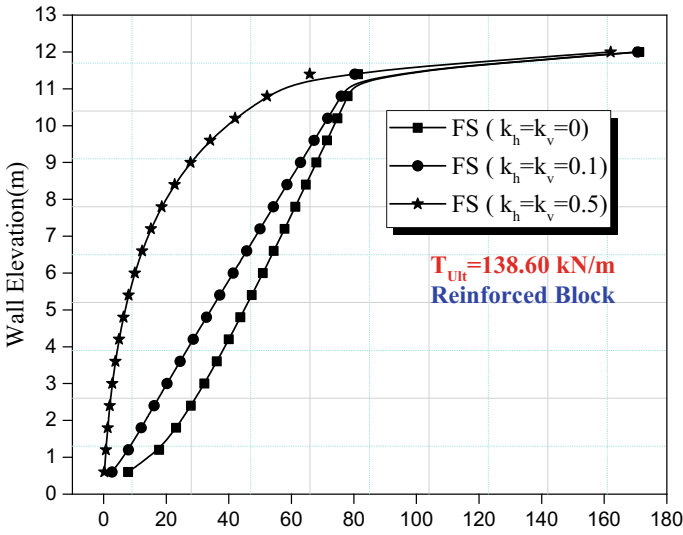


Fig. 8 Variation of FS against pull-out for reinforced well-graded gravel (GW) ( $k_v = k_h = 0, 0.1, 0.5$ )

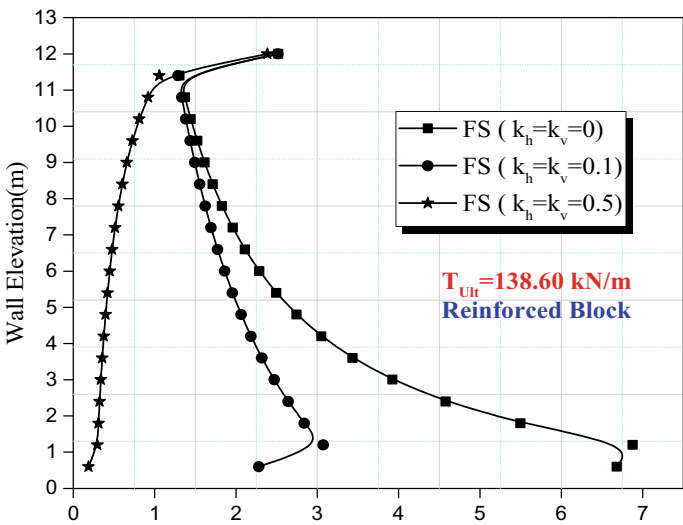


Fig. 9 Variation of FS against rupture for reinforced well-graded gravel (GW) ( $k_v = k_h = 0, 0.1, 0.5$ )

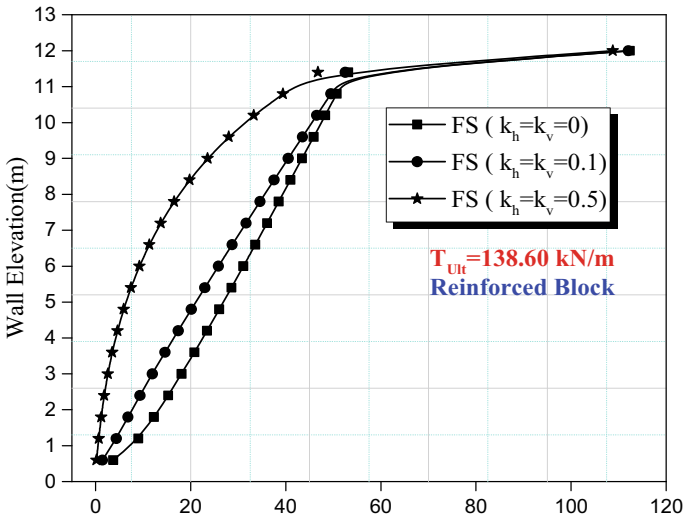


Fig. 10 Variation of FS against pull-out for reinforced poorly graded sand (SP) ( $k_v = k_h = 0, 0.1, 0.5$ )

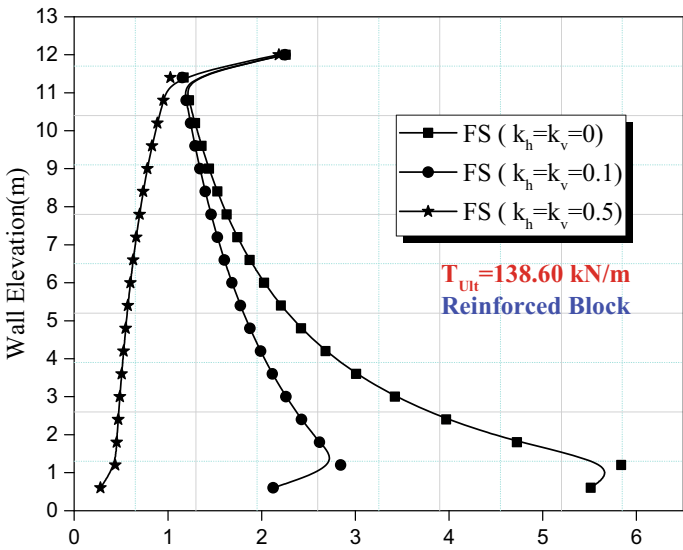
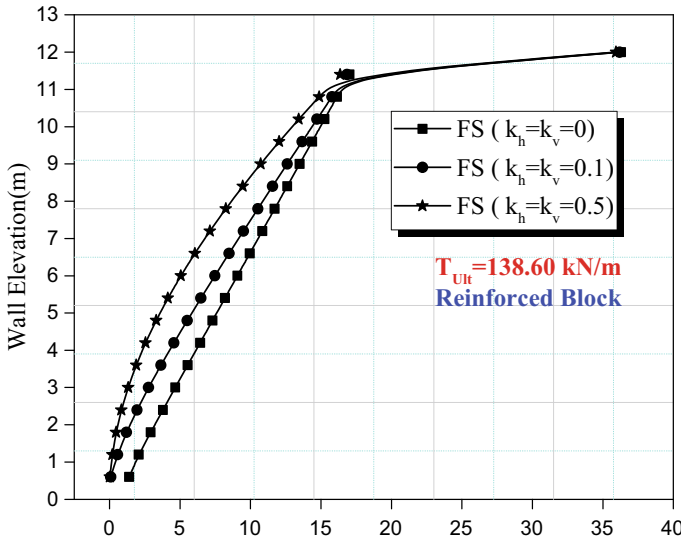


Fig. 11 Variation of FS against rupture for reinforced poorly graded sand (SP) ( $k_v = k_h = 0, 0.1, 0.5$ )



**Fig. 12** Variation of FS against pull-out for reinforced clayey soil (CL) ( $k_v = k_h = 0, 0.1, 0.5$ )

The variation of FS against rupture for reinforced GW has a wide range of FS values for rupture resistance ranging from 0.2, for  $k_v = k_h = 0.5$ , to 2.2, for  $k_v = k_h = 0.1$ , and 6.8 for static conditions at wall elevation of 0.5 m. Figure 9 shows that the structure is stable and resistant to rupture, at lower wall elevations for static and for seismic conditions with an earthquake coefficient of 0.1, but at higher wall elevations, FS against rupture is continuously reduced. Whereas for seismic conditions with  $k_v = k_h = 0.5$ , the FS for rupture resistance is notably within the safe limit only at the wall elevation of 12 m, for all other wall elevations, it is unsafe.

Figures 10 and 11 show the variation of FS against pull-out and rupture, respectively, for reinforced poorly graded sand (SP) for reinforcement with  $T_{Ult} = 138.60 \text{ kN/m}$ , for static and seismic conditions. Though the variations look similar to that of FS for GW soil (Figs. 8 and 9), the FS values are much lesser.

FS against pull-out for reinforced poorly graded sand (Fig. 10), for static conditions, increases gradually from 0.5 m wall elevation to 11 m by about 11 times but a sudden increase is seen at wall elevation of 12 m, as the loads to be borne by the reinforced earth is much lesser than other layers below it. For seismic conditions,  $k_v = k_h = 0.5$ , the FS for pull-out shows that the structure is not safe up to the wall elevation of 2 m with FS 1.56 but as the wall elevation increases, the stability also increases with a peak at 12 m which is having an FS of 110.

The variation of FS against rupture for reinforced SP has FS values for rupture resistance ranging from 0.2, for  $k_v = k_h = 0.5$ , to 2.1, for  $k_v = k_h = 0.1$  and 5.55 for static conditions at wall elevation of 0.5 m. Figure 11 shows that the structure is stable and resistant to rupture, at lower wall elevations for static and for seismic conditions with an earthquake coefficient of 0.1, but at higher wall elevations, FS

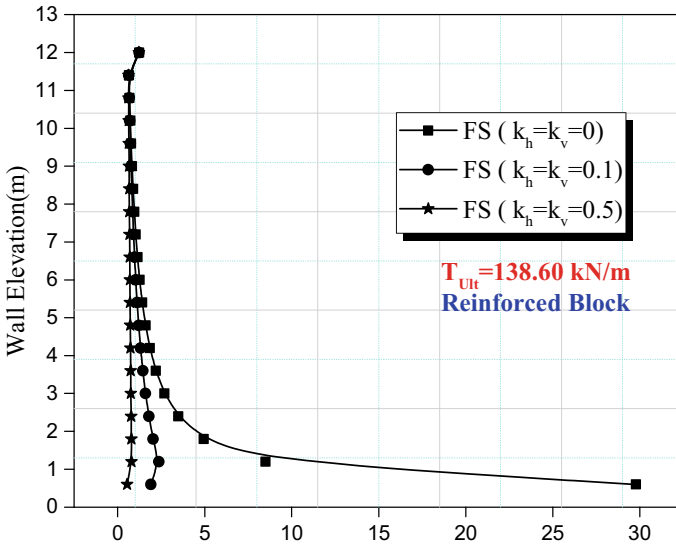


Fig. 13 Variation of FS against rupture for reinforced clayey soil (CL) ( $k_v = k_h = 0, 0.1, 0.5$ )

against rupture is continuously reduced. Whereas for the seismic condition with  $k_v = k_h = 0.5$ , the FS for rupture resistance is notably within the safe limit only at the wall elevation of 12 m, otherwise, it is unsafe.

Figures 12 and 13 show the variation of FS against pull-out and rupture, respectively, for reinforced clayey soil (CL) for reinforcement with  $T_{Ult} = 138.60$  kN/m, for static and seismic conditions. The FS for pull-out resistance increases by about 7.5 times from wall elevation 0.5 to 11 m but has a sudden increase in FS to 37 at wall elevation of 12 m. For seismic conditions at greater wall elevations, the FS against pull-out increases with a significant increase at 12 m wall elevation.

From Fig. 13, it is observed that FS for rupture resistance is about 30 at 0.5 m wall elevation for the reinforced CL, and considerably has FS in safe limits up to the elevation of 5 m as the CL will be highly compressed at lower elevation due to all the combined loading of the above layers of soil. CL at this elevation will be in a highly compacted state, thus having greater stability and resisting rupture than at the higher elevations.

Thus, pull-out resistance in the reinforcement is dependent on the reinforced soil type. Reinforced soil as GW has a better resistance than SP which is better than CL which is the weakest of all the soils considered and highly not suitable. FS against rupture is considerably better for CL at a lower height of the wall otherwise it depends highly on the tensile strength of reinforcement used.



### 4.1.3 Effect of Surcharge

Figures 14–17 show the variation of FS against pull-out and rupture for static and seismic conditions ( $k_v = k_h = 0.5$ ) for surcharge values 15, 25, 35, and 45 kN/m<sup>2</sup>. In Figs. 14 and 15, the FS against pull-out reduces by 50% for static conditions from a surcharge 15–45 kPa. The sudden increase of FS against pull-out in the top layer is due to the anchorage to the top facing panel, and the FS gradually increases with the wall elevation for all surcharges considered. The variations of surcharges are merging for seismic conditions (Fig. 15) indicating that there is little to no effect of surcharge on pull-out resistance. This is because the inertial stresses are the main influence in seismic conditions.

In Figs. 16 and 17, the FS against rupture reduces by 76% for static conditions from a surcharge 15–45 kPa. The sudden increase of FS against rupture in the top layer is due to the anchorage to the top facing panel, and the FS gradually decreases with the wall elevation for all surcharges considered.

The variations of surcharges are merging for seismic conditions (Fig. 17) indicating that there is little to no effect of surcharge on rupture resistance as the inertial stresses are the main influence in seismic conditions.

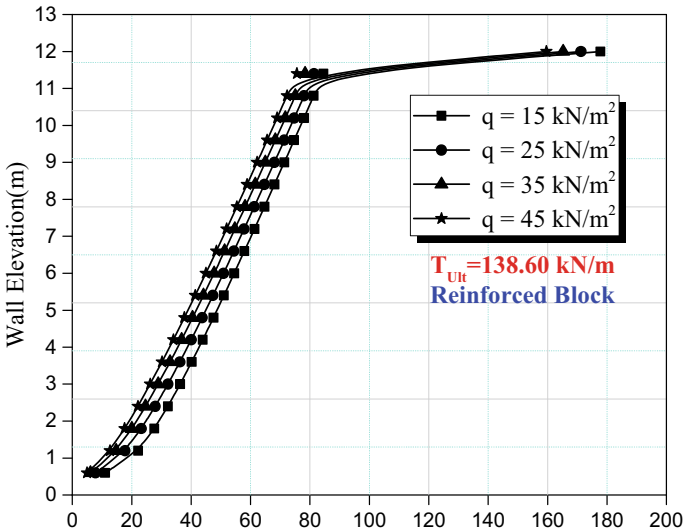


Fig. 14 Variation of FS against pull-out for static conditions (variation of  $q$ )

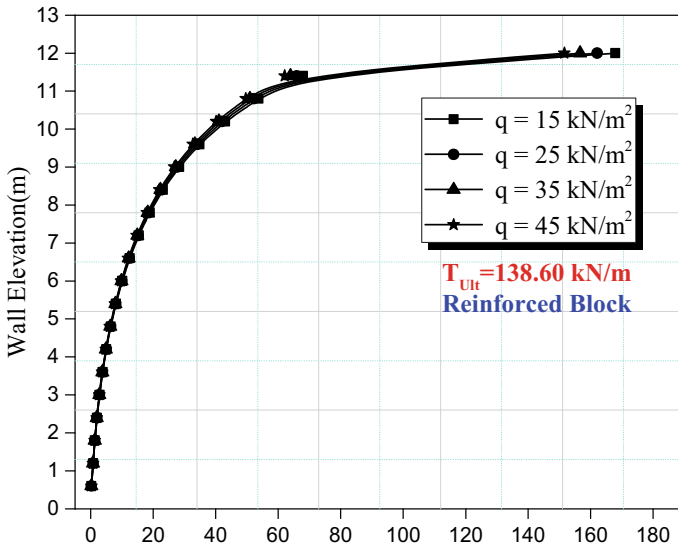


Fig. 15 Variation of FS against pull-out for  $k_v$  and  $k_h$  of 0.5 (variation of  $q$ )

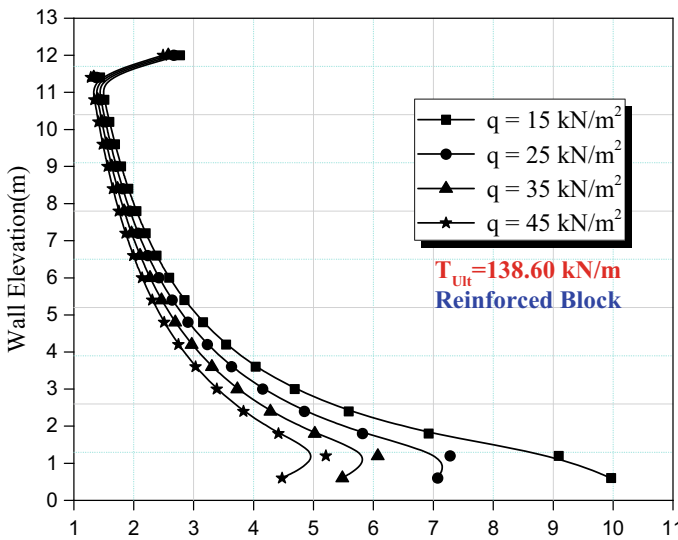


Fig. 16 Variation of FS against rupture for static conditions (variation of  $q$ )

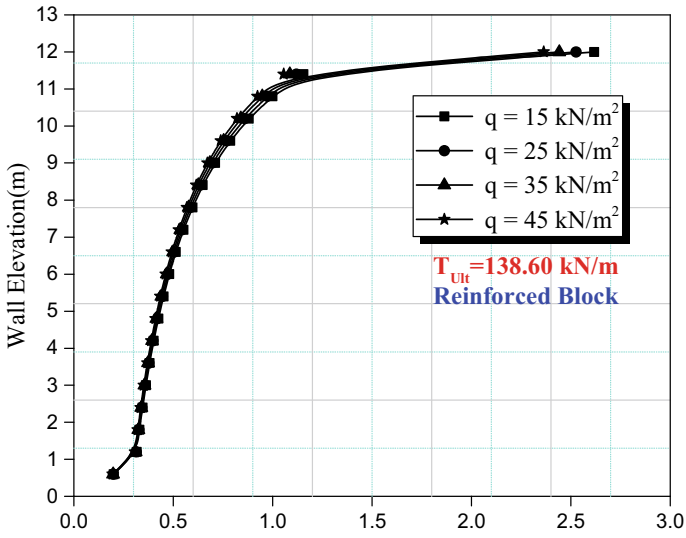


Fig. 17 Variation of FS against rupture for  $k_v$  and  $k_h$  of 0.5 (variation of  $q$ )

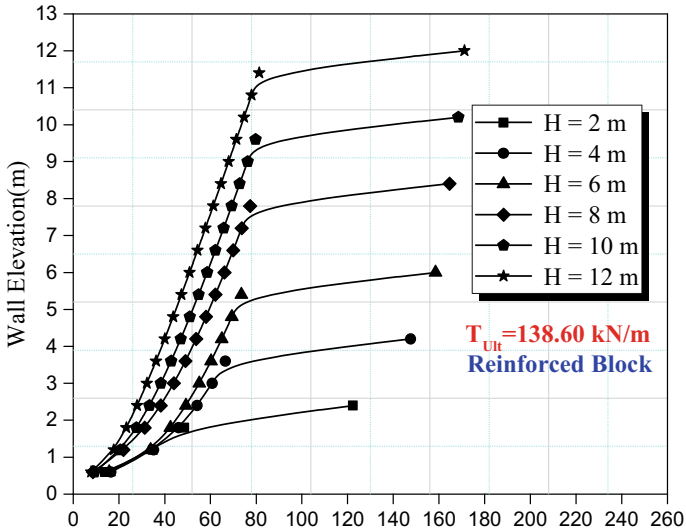


Fig. 18 Variation of FS against pull-out for various wall heights ( $H$ ) for static conditions

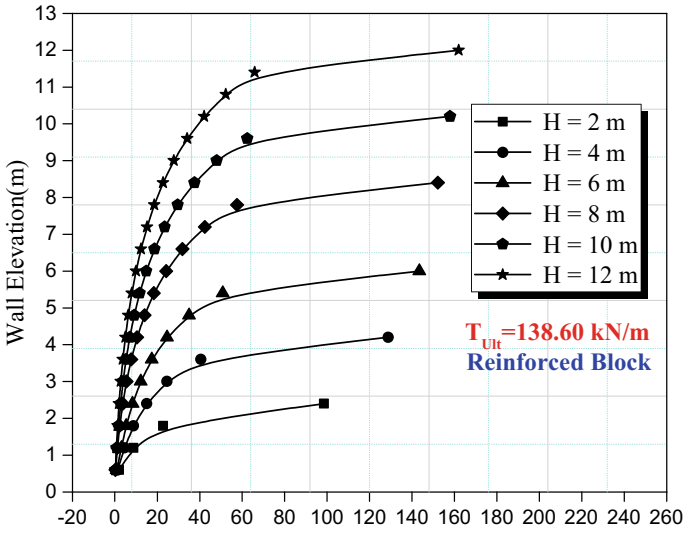


Fig. 19 Variation of FS against pull-out for various wall heights ( $H$ ) for  $k_v$  and  $k_h$  of 0.5

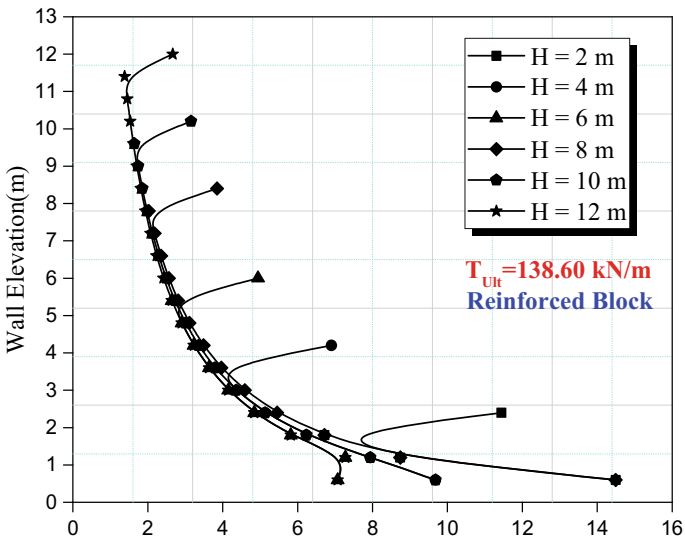


Fig. 20 Variation of FS against rupture for various wall heights ( $H$ ) for static conditions

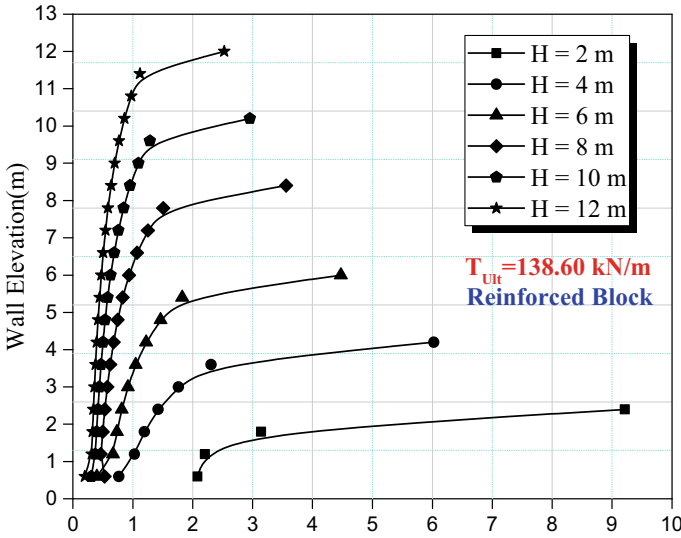


Fig. 21 Variation of FS against rupture for various wall heights ( $H$ ) for  $k_v$  and  $k_h$  of 0.5

### 4.2 Effect of Wall Height

From, Figs. 18 and 19, it has been observed that pull-out resistance in the reinforced block depends on the interaction between reinforcement and backfill soil. Also it is found that tensile strength of the reinforcement and the angle of internal friction of the soil affect the pull-out resistance. Wall height does not affect the pull-out resistance. FS against rupture depends on the vertical stress developed within the reinforced block. This vertical stress, in turn, depends on the depth of the backfill soil, hence it is observed in Figs. 20 and 21, as the depth of the overburdened soil increases, resistance for rupture also increases.

## 5 Conclusions

The conclusions of the study are as follows:

- Factor of Safety values against pull-out and rupture is higher for a greater number of reinforcements.
- Pull-out resistance in the reinforcement is dependent on the reinforced soil type. Reinforced soil as GW has a better resistance than SP which is better than CL which is the weakest of all and highly not suitable.
- FS against rupture is considerably better for CL at a lower height of the wall.

- For lesser magnitudes of surcharge, a Factor of Safety against pull-out and rupture are maximum.
- Factor of Safety values against pull-out increases with an increase in wall height.
- Factor of Safety against rupture increases with a decrease in wall height.

## References

- AASHTO (2010) LRFD bridge design specifications, 5th edn. AASHTO, Washington, D.C.
- Abdelouhab A, Dias D, Freitag N (2010) Physical and analytical modelling of geosynthetic strip pull-out behaviour. *Geotext Geomembr* 28(2010):44–53
- Allen TM, Bathurst RJ, de N (2019) Probabilistic tensile strength analysis of steel strips in MSE walls considering corrosion. *J Geotech Geoenviron Eng* 145(5):1–12. [https://doi.org/10.1061/\(ASCE\)GT.1943-5606.0002043](https://doi.org/10.1061/(ASCE)GT.1943-5606.0002043)
- Bathurst RJ, Allen TM, Lin P, Bozorgzadeh N (2019) LRFD calibration of internal limit states for geogrid MSE walls. *J Geotech Geoenviron Eng* 145(11). [https://doi.org/10.1061/\(ASCE\)GT.1943-5606.0002124](https://doi.org/10.1061/(ASCE)GT.1943-5606.0002124)
- BS8006-1 (2010) Code of practice for strengthened/reinforced soils and other fills. BRIT
- Collin JG, Meyers MS, Berg RR (2007) State-of-the-practice design of segmental retaining walls: NCMA's third edition manual. *Geotech Spec Publ* 7(165). [https://doi.org/10.1061/40909\(228\)7](https://doi.org/10.1061/40909(228)7)
- FHWA-NHI-10-024 (2009) Design and construction of mechanically stabilized earth walls and reinforced soil slopes—Volume I. Fed High Way Admin (FHWA) 1. FHWA-NHI-10-024 and FHWA-NHI-10-025
- Han J, Leshchinsky D (2010) Analysis of back-to-back MSE walls. *Geotext Geomembr* 28:262–267
- Huang J, Rahman S, Bin-Shafique S, Zheng C, Malla S (2019) Effect of lateral cyclic loading on drilled shaft within an MSE wall. In: MATEC web of conferences, vol 271, p 02006. EDP Sciences
- Hulagabali AM, Solanki CH, Dodagoudar GR, Shettar MP (2018b) Effect of reinforcement, backfill and surcharge on the performance of reinforced earth retaining wall. *ARNP J Eng Appl Sci* 13(9):3224–3230
- Hulagabali AM, Solanki CH, Dodagoudar GR, Shettar MP (2018c) Influence of supporting systems on behavior of mse wall. *Int J Civ Eng Technol* 9(4):1000–1007
- Hulagabali AM, Solanki CH, Dodagoudar GR, Konnur SS, Shettar MP (2018a) Analysis of mechanically stabilised earth (MSE) retaining wall using finite element and AASHTO methods. *J Eng Technol Am Soc Eng Educ* 6(Special Issue [Emerg Trends Eng Technol]):139–150
- Kibria G, Sahadat HMD, Khan MS (2014) Influence of soil reinforcement on horizontal displacement of MSE wall. *Int J Geomech* 14(1):130–141. [https://doi.org/10.1061/\(ASCE\)GM.1943-5622.0000297](https://doi.org/10.1061/(ASCE)GM.1943-5622.0000297)
- Konnur SS, Hulagabali AM, Solanki CH, Dodagoudar GR (2019) Numerical analysis of MSE wall using finite element and limit equilibrium methods. *Lect Notes Civ Eng Springer Nature, Singapore* 15(December):199–205. [https://doi.org/10.1007/978-981-13-0562-7\\_22](https://doi.org/10.1007/978-981-13-0562-7_22)
- Lajevardi SH, Malekmohammadi K, Dias D (2021) Numerical study of the behavior of a back-to-back mechanically stabilized earth walls. *Geotechnics* 1:18–37. <https://doi.org/10.3390/geotechnics1010002>
- Leshchinsky D, Vahedifard F, Leshchinsky BA (2012) Revisiting bearing capacity analysis of MSE walls. *Geotext Geomembr* 34:100–107. <https://doi.org/10.1016/j.geotextmem.2012.05.006>

# Stabilization of Expansive Soil: A Review



Dharmendra Singh, Vijay Kumar, and R. P. Tiwari

**Abstract** Black cotton soil (BCS) as an expansive soil (ES) is the most problematic soil which may cause severe risk to the safety of structures that are built over it. These expansive soils may be modified by compacting effort or by introducing some special additives to such soils. For swelling and shrinkage properties of such soils, soil stabilization (SS) method using various materials such as lime, fly ash (FA), stone dust (SD), coir fiber (CF), bagasse ash (BA), and sugarcane straw ash (SSA) may be preferred. Black cotton soil may undergo severe change in its volume when the moisture absorption phenomenon takes place, and this may lead to swelling and subsequently shrinkage after evaporation of moisture from these soils. The expansive soils may possess strength in its dry state, but the strength may wipe out in its wet state. When stabilizing expansive soils with materials suited for such conditions, the strength and bearing capacity of the soils can significantly increase. Unconfined compressive strength (UCS) test as well as California bearing ratio (CBR) test may be performed in order to assess existing bearing capacity and strength of ES prior to SS as well as after the stabilization process too. Stabilization of soil may reduce compressibility as well as permeability of the soil mass. It may also modify shear parameters of the soil, thus increasing the shear strength of ES. The main objective of this paper is to review chemical as well as physical characteristics of expansive soils due to introduction of various materials in these soils. In this paper, also, a number of articles have been reviewed to emphasis on various economical as well as effective expansive additives. This study focuses on the effect of introduction of non-traditional stabilizers in the stabilization of the expansive subgrade with the use of chemical stabilization technique.

---

D. Singh (✉) · V. Kumar · R. P. Tiwari  
Department of Civil Engineering, Motilal Nehru National Institute of Technology Allahabad,  
Prayagraj 211004, India  
e-mail: [dharmendra@mnnit.ac.in](mailto:dharmendra@mnnit.ac.in)

V. Kumar  
e-mail: [vkr@mnnit.ac.in](mailto:vkr@mnnit.ac.in)

R. P. Tiwari  
e-mail: [rpt@mnnit.ac.in](mailto:rpt@mnnit.ac.in)

**Keywords** UCS · Soil stabilization · CBR · Expansive soil · Shrinkage · Swelling

## 1 Introduction

Soil stabilization (SS) is a technique that involves enhancing soil properties through the utilization of various materials, including BA, SD, Lime, CF and FA. The stabilization of expansive soils (ES) using these materials leads to an improvement in geotechnical characteristics such as optimum moisture content (OMC), maximum dry density (MDD), swelling potential, California bearing ratio (CBR), shrinkage behavior and unconfined compressive strength (UCS) test. (Abass 2013; Bhatt et al. 2018; Bhavani et al. 2015; Chakraborty et al. 2016; Dang et al. 2016).

SS is that alteration of any property of a soil to enhance its engineering performance. The aim of SS is to

1. Decrease the tendency for frequent volume fluctuations like swelling and shrinking.
2. Make it more stable in various weather situations or to increase strength.
3. Decrease compressibility.
4. The soil is made more durable and workable by stabilization.
5. The soil's bearing capacity is increased via stabilization.
6. Stabilization increases the soil's strength, which raises the soil's bearing capacity.
7. Reduced permeability.
8. It assists in minimizing the change in soil volume brought on by variations in temperature or moisture content.
9. On slopes and other similar areas, stabilization is also utilized to increase the soil's stability (Chakraborty et al. 2016; Dang et al. 2016; Dalal et al. 2017; Gowda et al. 2019).

### Soil Stabilization Various Techniques

Types of soil stabilization divided into two parts

1. Mechanical stabilization
  - (a) Sand gravel
  - (b) Soil aggregate
  - (c) Stabilization of soil with soft aggregates
  - (d) Soil clay mixture.
2. Chemical stabilization
  - (a) Sodium silicate
  - (b) Bituminous
  - (c) Lime
  - (d) Cement.



**Mechanical Stabilization**—By combining locally available soil with introduced soil/aggregate to get the required particle size distribution and compacting the mixture to desired density, the stability of the soil is enhanced in this method. Soil can be mechanically stabilized by being compacted at an appropriate moisture content [1–4]. **Chemical Stabilization**—In this method, the intended impact of soil stabilization is mostly achieved by chemical interactions between the stabilizer (cementation material) and soil minerals (pozzolanic materials) (Abass 2013; Bhatt et al. 2018; Bhavani et al. 2015; Chakraborty et al. 2016).

## 1.1 Components of Stabilization

In order to increase the geotechnical attributes of poor soils, like permeability, compressibility, durability, and strength, stabilizing agents (binder materials) are used. Soils, soil minerals, and stabilizing agents/binders are among the elements of stabilization technology (Abass 2013; Bhatt et al. 2018; Bhavani et al. 2015; Chakraborty et al. 2016).

1. Soil
2. Stabilizing agent
  - (a) Lime
  - (b) Fly ash
  - (c) Bagasse ash
  - (d) Coir Fiber.

### 1.1.1 Soil

**Expansive Soil**—Where there is a great deal of seasonal change in the weather, expansive soils are produced by the breakdown of basic igneous rocks. These soils are frequently created in India by the weathering of volcanic rock formations. Additionally, these soil deposits are formed from a wide variety of rocks, including extremely old material deposits. Minerals found in clay fractions include the montmorillonite and a combination of illite and montmorillonite (Chakraborty et al. 2016; Dang et al. 2016; Dalal et al. 2017).

The expansive soils of India are known as black cotton or Regur soil, and they span over several states, including Odisha, and encompass around 20% of the country's total geographical area. The soil profile of the eastern region of India (including the states of Odisha) shows that red soil, mixed red and yellow soil, black cotton soil that occurs in sporadic amounts, deltaic and costal saline, and dirt are all present in coastal districts. The expansive soils show swelling after being wet and shrinking after being dried. If erected without sufficient care, this is regarded as perilous for any type of foundation (Rajput et al. 2019).

Expansive soils have been seen around the world, but are most frequently found in Africa, Australia, India, South America, the United States, and some portions of Canada. This in no way implies that expansive soils do not exist elsewhere because they are almost ubiquitous (Surjandari et al. 2017).

### 1.1.2 Stabilizing Agent

**Lime**—The most popular technique for reducing shrink-swell behavior of ES brought on by seasonal fluctuations is lime stabilization. The physio-chemical characteristics of expansive soil are altered by lime's reaction with expansive clay (EC) in presence of water, which also affects treated soil's engineering features. Lime is a cost-effective method of stabilizing soil. Lime is added to the soil to stabilize it. Clayey soil can be stabilized with the use of lime (Dang et al. 2016).

The essential classification of limes is five.

1. CaO (High calcium, quick lime)
2. Ca(OH)<sub>2</sub> (Hydrated, high calcium lime)
3. CaO + MgO (Dolomite lime)
4. Ca(OH)<sub>2</sub> + MgO (Normal, hydrated dolomitic lime)
5. Ca(OH)<sub>2</sub> + Mg(OH)<sub>2</sub> (Pressure, hydrated dolomitic lime).

**Bagasse**—Bagasse is the ash that results from burning bagasse, which is a fibrous substance that may remain after sugarcane has been crushed to obtain its juice. Bagasse fiber has a variety of uses, including as a combustible fuel source for sugar cane factories, a source of pulp for the paper industry, and a component of construction materials such bagasse-cement composites (Dang et al. 2016).

**Fly ash**—FA, a waste by-product of coal, is taken out of the flue gases of a coal-fired furnace that is located in the business. These resemble the volcanic ashes that were once employed as hydraulic cements in a very close way. One of the greatest pozzolanic materials employed up to this point in history worldwide was thought to be these volcanic ashes (Dixit et al. 2016).

**Coir Fiber**—Natural fiber known as coir is taken from the coconut's outer husk. Coconut fiber is another name for coir. The tough, interior shell of a coconut and its outer coating are separated by a fiber substance called coir (Swami et al. 2018).

## 2 Literature Review

The literature review is divided into five parts.

- Literature review of various research paper
- Classification and engineering properties of expansive soil
- Engineering properties of various material
- Chemical composition of various material

- Effect of various material on expansive soil.

## 2.1 Literature Review of Various Research Paper

The use of material to stabilize soil has been the subject of extensive research (like lime, fly ash, coir fiber, and bagasse fiber). The literature review is a component that shows the work that has been done on a particular project. For civil engineering constructions, ES's erratic behavior is a major problem. Many scientists and researchers have worked on and proposed numerous safety measures for ES in order to lessen likelihood of collapse in ES. Along with it, a great deal of materials is used. To stabilize the ES, some researchers have utilized fly ash, lime, coir fiber, and bagasse fiber. The presentation includes some succinct information on treating expansive soil with several types of stabilizers. Rajakumar and Meenambal (2015) in the Indian state of Tamil Nadu, soil samples were taken from Coimbatore Cheran Maanagar, while bagasse ash samples were taken from Sakthi Sugars in Erode. Various amounts of BA, including 2, 4, 6, 8, and 10% were combined with obtained soil sample. Plasticity index of the soil has decreased from 30 to 19% as a result of the rise in bagasse ash content. Its swelling has decreased from 50 to 30% due to the increased amount of bagasse ash in the soil. Dang et al. (2016)—A variation of proportions of randomly dispersed BA in the range of 0.5, 1.0, and 2.0% was added to ES with various bagasse fiber proportions which were also tested in order to assess impact of BA on engineering behavior of ES. Linear shrinkage of ES treated with additives was significantly decreased with varying additive levels and longer curing times. The amounts of hydrated lime-bagasse fiber rose concurrently with the curing period, increasing the UCS values of the treated ES. Hasan et al. (2016)—Bagasse is the ash that results from burning bagasse, which is a fibrous substance that may remain after sugarcane has been crushed to obtain its juice. Given that bagasse ash is a non-plastic substance, stabilizing expansive soil by adding it reduces swelling of ES. With an increase in bagasse ash content, free swell ratio falls. In order to reduce the soil's tendency to swell, using lime in combination with bagasse ash is more feasible than using lime alone. The dry density of expansive soil fell somewhat when the bagasse ash–lime concentration rose from 0 to 25%, while the UCS increased by 80%. Chakraborty et al. (2016)—In the current investigation, soil samples from a depth of 2 m below actual ground level were taken from Gorchuk. By altering the quantity of bagasse ash (5, 10, and 15%) during various curing times, various geotechnical laboratory experiments, such as the CBR, FSI, and UCS, were conducted. The UCS value rises with an extension of the curing time. For a 10% addition of sugarcane straw ash, the UCS value rise is more noticeable. Using 10% ash from sugarcane straw decreases the pavement's thickness by 50%, lowering the overall cost of construction. Surjandari et al. (2017)—This study objective is to assess how BA can improve the engineering qualities of ES. Bagasse is applied to the ES in weight-based treatments of 0, 5, 10, 15, and 20% depending on dry mass. The plasticity index decreases from approx. 53–47% when bagasse ash is mixed to

expansive soils. The sample's MDD rises from 1.13 to 1.24 g/cm<sup>3</sup>. MDD increases as the percentage of bagasse ash mixture increases, whereas the OMC decreases as the percentage of BA mixture increases. Dalal et al. (2017)—Compared to mixed BA and ground-granulated blast furnace slag (GGBS), wood power provides a superior improvement in consistency and a reduction in activity and plasticity. This study used GGBS and wood powder to decrease black cotton soil's swelling percentage and enhance its strength (UCS and CBR). The findings of this study indicate that adding BA and GGBS, as compared to wood powder, can improve compaction and increase the strength of the BCS sample. Sivasubramani et al. (2017)—In this study, ability of egg shell powder and bagasse ash to stabilize soft ES is assessed. Wet sieve analyses, specific gravity measurements, and testing for the liquid and plastic limits have all been used to examine the physical characteristics of ES, bagasse ash, and egg shell powder. Compaction and CBR testing have been carried out. According to this study, when the percentage of bagasse ash is increased while the proportion of egg shell powder remains constant, the OMC decreases and the MDD increases. The CBR values likewise rise when the amount of bagasse ash is increased while the percentage of egg shell powder remains constant. Gowda et al. (2019)—According to IRC guidelines, soil sampling for the current study has been collected from a depth of 1 m below ground level from village—Beekanahalli, district—Chikkamagaluru, Karnataka. The goal of the study is to determine whether adding bagasse ash at various percentages (3, 6, 9, and 12%) will improve the expansive soil's properties. This study found that adding 9% bagasse ash to expansive soil causes the MDD to increase from 1.44 to 1.58 g/cm<sup>3</sup> and the OMC to decrease from 33 to 25%. Additionally, the inclusion of BA increases MDD and decreases the OMC. UCS values rise at 9% of bagasse ash concentration, from 0.32 to 0.46 N/mm<sup>2</sup>. Singh (2013)—This research conducts several tests on soil reinforced with coir fiber. In the CBR mold with and without reinforcement, a soil sample is obtained at its MDD and OMC for CBR value testing. The CBR value of soil increases with the increase in CF content, according to test findings that are both unsoaked and soaked conditions. Additionally, with a fiber level of 1%, it is seen that the CBR value of reinforced soil increases significantly. Devdatt et al. (2015)—It is clear from this study that measurements of soil's physical characteristics such as Atterberg's limit, specific gravity, OMC, and MDD, swelling pressure, permeability, soaked and un-soaked CBR test results, are conducted. Several test investigations using coir fiber at varying percentages of 0.25, 0.50, 0.75, and 1 were carried out on BC soil. The inclusion of coir fiber has also greatly raised the soaking CBR values. The CBR values in BC soil increased from 3.9 to 8.6% with mixed of 1% coir fiber. Coir fiber dose enhances MDD and reduces OMC. Goyal et al. (2015)—The BC soil sample for the evaluation in this study was taken from Gwalior, M. P., India. By excavating trenches that were 1.5 m by 1.5 m, soil samples were taken from levels that were more than 2 m. The shrinkage limit is increased by 7.52–12.62% in the presence of 2% coir fiber, according to test results. OMC also increased by around 20–27% due to the mixing of coir fiber, and UCS increases by 106.89 to 129.45 kN/m<sup>2</sup> due to the mixing of coir fiber. Peter et al. (2016)—Natural fiber known as coir is taken from the coconut's outer husk. Coir is another name for coconut fiber. The tough, interior shell of a coconut and its outer

coating are separated by a fiber substance called coir. The addition of 2% coir pith and 0.6% short coir fiber raise CBR value by approx. 190–340%, respectively, while the total treatment enhanced the CBR value by approx. 4 to 5 times. The higher water absorption capacity of fibers may be the cause of the rise in OMC with high coir fiber content. Prashantha and Mittal (2017)—The BC soil used in this study was obtained from Karnataka, as well as the coir fiber. According to IS: 1498 (1970), the soil is categorized as highly compressible clay (CH). Test results show that adding more coir fiber (up to 1%) enhances OMC and reduces MDD. Swami et al. (2018)—The physical characteristics of soil, including moisture content, Atterberg's limits, grain size distribution, MDD and OMC, specific gravity, swelling pressure, CBR, and permeability test has determined in this study. Coir fibers with a percentage range of 0.25–1.25 are mixed in the soil to stabilize BC soil. According to test results, 1% of mixed coir fiber was found the highest soaking CBR value. With the addition of 1% coir fiber, CBR value rose by approx. 32%. Phanikumar et al. (2009)—Swelling can be decreased by chemically stabilizing expansive clays. In this study, the effect of lime on FSI, swelling potential, consolidation, swelling pressure, compaction, UCS, and CBR is presented. A range of lime doses, from 0 to 6%, was added to the soil sample that has been obtained. With more lime, the plasticity index decreased and the liquid limit reduced and the plastic limit increased. With an increase in lime content, but only up to 4%, swelling pressure and swelling potential are reduced. When the lime was increased from 0 to 4%, the FSI decreased from 250 to 125%. With increasing lime, MDD increased but OMC decreased. Abass (2013) Lime stabilization of expansive soil reduces the clay properties, specific gravity, MDD, and liquid limit. Lime also decreases the FSI and swelling pressure while increasing OMC. With an increase in lime, the plastic limit rises. Bhavani et al. (2015)—The strength of clayey soil is increased by lime. Gypsum and hydrated lime were purchased from Vijayawada, Andhra Pradesh, India. Furthermore, coir fiber was obtained from a supplier in Tadepalligudem, Andhra Pradesh, India. The UCS value can be raised by using lime. The soil's UCS has increased from its initial value of 1.6–4.1 kg/cm<sup>2</sup> with 8% lime.

## 2.2 *Classification and Engineering Properties of Expansive Soil*

Table 1 presents the classification and engineering characteristics of expansive soil as discussed in several kinds of literature, along with a reference list.

**Table 1** Geotechnical properties of soil from various literature review

S. no.	Soil type	Specific gravity	LL (%)	PL (%)	PI (%)	Soil classification	OMC (%)	MDD (g/cc)	References
1	ES	2.52	99.00	30.00	69.00	CH	22.00	1.61	Abass (2013)
2	ES	2.68	82.00	47.22	34.78	CH	24.30	1.55	Bhavani et al. (2015)
3	BCS	2.74	63.79	25.48	38.31	CH	14.40	1.73	Dalal et al. (2017)
4	ES	2.24	51.00	27.40	23.60	CH	20.30	1.54	Rajput et al. (2019)
5	BCS	2.71	47.00	17.00	30.00	CI	15.00	1.66	Rajakumar and Meenambal (2015)
6	ES	2.65	86.00	37.00	49.00	CH	36.50	1.29	Hasan et al. (2016)
7	BCS	2.17	42.05	28.00	14.05	CI	20.00	1.56	Sivasubramani et al. (2017)
8	BCS	2.63	54.20	29.10	25.10	CH	20.10	1.56	Goyal et al. (2015)
9	Clay soil	2.55	52.00	28.00	24.00	CH	31.70	1.68	Peter et al. (2016)
10	BCS	2.35	63.20	28.11	35.09	CH	24.40	1.59	Prashantha and Mittal (2017)
11	ES	2.72	100.00	27.00	73.00	CH	34.00	1.36	Phanikumar et al. (2009)
12	ES	2.68	69.00	34.00	35.00	CH	24.00	1.46	Magdi and Omer (2020)

### 2.3 Engineering Properties of Various Material

Imperative parameters of various material like specific gravity, OMC, and MDD with reference list are presented in Table 2.

### 2.4 Chemical Composition of Various Material

Material content is usually based on the type and composition of parent matter and also on the process of combustion through which material formation may take place. To determine the material's mineralogical composition, X-ray fluorescence spectroscopy was used as indicated in Table 3.

**Table 2** Engineering properties of materials from various literature review

S. no.	Name of materials	Specific gravity	OMC (%)	MDD (g/cc)	References
1	BA	3.38	48.00	1.27	Gowda et al. (2019)
2	SD	2.58	11.50	1.54	Rajput et al. (2019)
3	CF	2.58	27.20	1.51	Goyal et al. (2015)
4	FA	1.90	21.00	1.25	Rajput et al. (2019)
5	CF	1.20	–	–	Prashantha and Mittal (2017)

### 2.5 Effect of Various Material on Expansive Soil

An entire analysis of the behavior of material content on expansive soil has been conducted. The effects, uses, and mixing ratios of various materials are given in Tables 4, 5, and 6, correspondingly.

## 3 Methodology

This review article examines the engineering and index characteristics of expansive soil, as well as how those qualities change when the soil is stabilized with coir fiber, lime, fly ash, and bagasse ash. On expansive soil, the following experiments were performed:

1. Grain size analysis (IS: 2720 (Part IV)-1975).
2. Free swell index test (IS: 2720 (Part XL)-1977).
3. Specific gravity test (IS: 2720 (Part III/Section 1)-1980 for fine-grained soil, I.S: 2720 (Part III/Section 2)-1980 for fine, medium, and coarse grained soil).
4. Liquid and plastic limit test (IS-2720 (Part-V)-1985).
5. Standard proctor compaction test (IS: 2720 (Part VII)-1980).
6. California bearing ratio (CBR) test (IS: 2720 (Part XVI)-1965).
7. Unconfined compression strength (UCS) test (IS 2720 (Part X)-1973).

**Table 3** Chemical composition of various material from literature review

S. no.	Name of ash	SiO <sub>2</sub> (%)	CaO (%)	K <sub>2</sub> O (%)	Al <sub>2</sub> O <sub>3</sub> (%)	Fe <sub>2</sub> O <sub>3</sub> (%)	P <sub>2</sub> O <sub>5</sub> (%)	MgO (%)	TiO <sub>2</sub> (%)	References
1	Sugarcane straw ash	48.65	4.52	4.12	1.22	2.85	–	1.46	–	Chakraborty et al. (2016)
2	BA	65.27	11.16	–	3.11	2.10	–	1.27	–	Gowda et al. (2019)
3	BA	67.33	12.51	4.11	3.45	3.39	3.10	2.04	0.28	Surjandari et al. (2017)
4	BA	66.23	2.81	6.44	1.90	3.09	–	1.54	0.07	Sivasubramani et al. (2017)
5	Lime	5.20	48.0	–	0.70	0.70	–	1.50	–	Magdi and Omer (2020)
6	FA	52.5	6.50	0.20	24.2	3.50	–	1.50	–	Magdi and Omer (2020)
7	FA	47.40	14.80	–	25.50	5.70	–	2.70	–	Nalbantoglu (2004)
8	FA	40.18	1.23	0.18	1.42	6.48	0.19	0.14	0.04	Mahajan and Parbat (2015)



**Table 4** Effect of various material on soil from literature review

S. no.	Type of soil	Mixed material	Soil: material	Result	References
1	ES	Lime	85:15	Reduced FSI and swelling pressure of soil	Abass (2013)
2	ES	Quick lime	92:08	UCS value improved	Bhatt et al. (2018)
3	ES	Lime + gypsum + coir fiber	82:08:08:02	UCS value increased from 157 to 902 kN/m <sup>2</sup>	Bhavani et al. (2015)
4	ES	Sugarcane straw ash	90:10	UCS value improved at 7 days cured sample	Chakraborty et al. (2016)
5	ES	Bagasse ash	91:09	MDD increased with the inclusion of 9% of bagasse ash	Gowda et al. (2019)
6	ES	Bagasse ash	80:20	Reduced the plasticity index	Surjandari et al. (2017)
7	BCS	Coir fiber	99:01	CBR value increased by 31% with 1% of coir	Swami et al. (2018)
8	ES	Bagasse ash	81.25:18.75	UCS and CBR value improved	Hasan et al. (2016)
9	Clay soil	Coir fiber	99:01	CBR value improved	Singh (2013)
10	BCS	Coir fiber	98:02	Increase in shrinkage limit, OMC, and UCS value	Goyal et al. (2015)
11	ES	Lime	96:04	Swelling pressure and FSI value reduced	Phanikumar et al. (2009)
12	BCS	Fly ash	70:30	CBR and UCS value improved	Mahajan and Parbat (2015)

## 4 Conclusions

A major issue in construction that is found all over the world is the expansive soil, which results in structural damage to buildings. This study looked at how admixtures, including lime, fly ash, coir fiber, and bagasse fiber, were used to stabilize expansive soil. Additionally, the engineering characteristics of expansive soil in various materials are discussed. The geotechnical properties of expansive soil (such as index properties, compaction properties (OMC and MDD), UCS, CBR, and swelling properties) are improved by the stabilization of expansive soil employing material. From the aforementioned reviews of the diverse literature, the following conclusions are drawn:

1. By stabilizing fly ash in expansive soil, the properties and strength of excessively expansive soil may be improved.
2. The plasticity index of the soil is effectively increased by the fly ash stabilization with expansive soil.

**Table 5** Use of various materials for soil stabilization from various paper

S. no.	Material name	Maximum proportion (%)	Remarks	Reference
1	BA	12	UCS value improved from 317 to 456 kPa at 9% bagasse ash	Gowda et al. (2019)
2	BA	12	MDD improved from 1.44 to 1.58 g/cc and OMC reduced from 33.33 to 25% at 9% of bagasse ash	Gowda et al. (2019)
3	FA	30	CBR value improved from 3.10 to 3.22% at 25 percent fly ash	Dixit et al. (2016)
4	CF	1.25	CBR value increased by 31% at 1% coir fiber	Swami et al. (2018)
5	Lime	9	FSI decreased from 20 to 0.5%, and swelling pressure reduced from 200 to 23 kPa	Leite et al. (2016)
6	FA	30	Plasticity index decreased from 35 to 17%	Magdi and Omer (2020)

**Table 6** Mixing proportions of material for soil stabilization from literature review

S. no.	Type of soil	Material used	Material quantity mixed with soil (%)	Remarks	Reference
1	ES	Sugarcane straw ash	5, 10, and 15	CBR and UCS value optimum at 10% ash	Chakraborty et al. (2016)
2	ES	Bagasse ash	3, 6, 9, and 12	MDD and UCS value optimum at 9% ash	Gowda et al. (2019)
3	ES	Bagasse ash	5, 10, 15, and 20	Swelling of maximum soil decrease at 15% ash	Surjandari et al. (2017)
4	Clay soil	Fly ash	5, 10, 15, 20, 25, and 30	CBR value maximum at 25% fly ash	Dixit et al. (2016)
5	Clay soil	Coir fiber	0.25, 0.50, 0.75, and 1.00	Optimum CBR value at 1.00% fiber	Singh (2013)
6	ES	Coconut coir fiber	0.25, 0.50, 0.75, and 1.00	Maximum CBR value at 1.00% of coconut fiber	Devdatt et al. (2015)
7	ES	Lime	2, 4, and 6	Soil swelling pressure reduced at 4% lime	Phanikumar et al. (2009)

3. As fly ash dose is increased, maximum dry density (MDD) increases and the optimum moisture content decreases (OMC).
4. Increasing the bagasse ash dose raises the maximum dry density while decreasing the optimum moisture content.
5. Using bagasse ash gives stabilized soil a high compressive strength and raises its hardness.

6. Because bagasse ash is a non-plastic substance, stabilizing expansive soil by adding it reduces the soil's swelling.
7. The use of coir waste and the combination treatment, that is, coir fiber and coir pith, raised the California bearing ratio value by 4 to 6 times, and can stabilize soil's engineering properties.
8. Increasing the coir fiber dose raises the maximum dry density while decreasing the optimum moisture content.
9. Plastic limit increases with the increase of lime percentage.
10. Stabilization of expansive soil by using various percentage of lime improves the geotechnical properties (like index properties, compaction properties, unconfined compressive strength (UCS), California bearing ratio (CBR), and swelling properties) of expansive soil.

## References

- Abass IK (2013) Lime stabilization of expansive soil. *J Eng Develop* 17(1). ISSN 1813–7822
- Bhatt H, Meena M, Bindlish A (2018) Geotechnical properties of an expansive soil stabilized with quick lime. *Int J Eng Develop Res* 6(2). ISSN: 2321-9939
- Bhavani PG, Prasad DSV, Krishnan GR (2015) Strength properties of expansive soil treated with lime, gypsum and coir fibre. *Int J Innov Res Technol. IJIRT* 2(7). ISSN: 2349-6002
- Chakraborty A, Borah A, Sharmah D (2016) Stabilization of expansive soil using sugarcane straw ash (SCSA). *ADBU-J Eng Technol* 4(1). ISSN: 2348-7305
- Dalal SP, Patel R, Dalal PD (2017) Effect on engineering properties of black cotton soil treated with agricultural and industrial waste. In: *Proceedings of the 4th international conference on recent trends in engineering and material sciences (ICEMS-2016)*, pp 9640–9644
- Dang LC, Fatachi B, Khabbaz H (2016) Behavior of expansive soils stabilized with hydrated lime and bagasse fibers. In: *The 3rd international conference on transportation geotechnics (ICTG 2016)*, Vol 143. *Advances in transportation geotechnics* 3, pp 658–665
- Devdatt S, Shikha R, Saxena AK, Jha AK (2015) Soil stabilization using coconut coir fibre. *Int J Res Appl Sci Eng Technol (IJRASET)* 3(IX). ISSN: 2321-9653
- Dixit A, Nigam M, Mishra R (2016) Effect of fly ash on geotechnical properties of soil. *Int J Eng Technol Manage Res* 3(5)
- Gowda AIV, Guruprasada MD, Manoj S, Manu S, Nagaraj K, Goutham DR, (2019) Experimental investigation on expansive soil stabilized using bagasse ash. *Int J Innov Res Sci Eng Technol* 8(6)
- Goyal P, Trivedi AS, Sharma M (2015) Improvement in properties of black cotton soil with an addition of natural fibre (coir) derived from coconut covering. *Int J Eng Res Appl* 5(3):36–37
- Gunjag DA, Kore SB, Lole AA, Kadam SR (2016) Assessment of use of lime in expansive soil subgrade for Sangli—Kolhapur Highway. *Int Res J Eng Technol (IRJET)* vol 03(11)
- Hasan H, Dang L, Khabbaz H, Fatahi B, Terzaghi S (2016) Remediation of expansive soils using agricultural waste bagasse ash. In: *The 3rd international conference on transportation geotechnics (ICTG 2016)*, vol 143, pp 1368–1375. *Advances transport geotechnics* 3
- Leite R, Cardoso R, Cardoso C, Cavalcante E, Freitas OD (2016) Lime stabilization of expansive soil from Sergipe-Brazil. In: *E3S web of conference* 9, 14005, E-UNSAT 2016
- Magdi MEZ, Omer SMH (2020) Improving the characteristics of expansive subgrade soils using lime and fly ash. *Int J Sci Res (IJSR)*. ISSN: 2319-7064

- Mahajan SM, Parbat DK (2015) A study on strength characteristics of BC soil-flyash mixes. *Int J Mod Trends Eng Res* 02(10) [October—2015]. ISSN (Online): 2349-9745; ISSN (Print): 2393-8161
- Nalbantoglu Z (2004) Effectiveness of class C fly ash as an expansive soil stabilizer. *Constr Build Mater* 18(2004):337–381
- Peter L, Jayasree PK, Balan K, Raj SA (2016) Laboratory investigation in the improvement of subgrade characteristics of expansive soil stabilized with coir waste. In: 11th transportation planning and implementation methodologies for developing countries TPMDC 2014, 10–12 December 2014, Mumbai, India
- Phanikumar BR, Amshumalini C, Karthika R (2009) Effect of lime on engineering behaviour of expansive clays. IGC 2009, Guntur India
- Prashantha TR, Mittal A (2017) Change in the properties of black cotton soil due to addition of coir fibres. *Int J Eng Technol Manage Appl Sci* 5(4). ISSN 2349-4476
- Rajakumar C, Meenambal T (2015) Experimental study of bagasse ash utilisation for road application on expansive soil. *Nature Environ Pollut Technol Int Quart Sci J* 14(4):903–908
- Rajput Y, Sakale R, Singh HP (2019) Performance analysis of expansive soil treated with stone dust and fly ash. *Int J Sci Res Eng Develop* 2(1)
- Singh HP (2013) Effects of coir fiber on CBR value of Itanagar soil. *Int J Curr Eng Technol* 3(4). ISSN 2277-4106
- Sivasubramani PA, Arya C, Karunya R, Mohammed N, Jalaludeen (2017) Experimental study on stabilization of black cotton soil subgrade using bagasse ash and egg shell powder for the design of flexible pavement. *Int J ChemTech Res* 10(8):662–669
- Surjandari NS, Djarwanti N, Ukoi NU (2017) Enhancing the engineering properties of expansive soil using bagasse ash. In: International conference on science and applied science
- Swami A, Kushwaha PK, Gangwar M (2018) Studies on effect of different environmental conditions on CBR of black cotton soil reinforced with coir fibre. *Asian J Eng Appl Technol* 7(1):20–28. ISSN 2249-068X
- Thirumalai R, Babu SS, Naveennayak V, Nirmal R, Lokesh G (2017) A review on stabilization of expansive soil using industrial solid wastes. Scientific Research Publishing
- Verma K, Mitra A, Sagar D, Fayaz M, Kumar R (2017) A review study of effect of flyash on engineering properties of soil. *Int Res J Eng Technol (IRJET)* 04(04). e-ISSN: 2395-0056, p-ISSN: 2395-0072

# Effect of Bottom Ash on the Properties of Subgrade Soil



Manan Vaja, Uma Chaduvula, and Tejaskumar Thaker

**Abstract** The utilization of biodegradable substances for the improvement of poor soil has given better outcomes in the field of geotechnical engineering. They diminish the void proportion and thickness of absorbed water in the soil particles and boost the compaction of the subgrade. A decrease in moisture content causes an increase in shrinkage. This will bring about harm to the construction. In the recent years, manufacturers are claiming the increase in soil shear strength, decreasing in liquid limits, and swell index of the soil. Recent studies suggest that adding industry waste products like bottom ash or fly ash into the subgrade soil increases the California bearing ratio (CBR) values of the soil and decreases the swelling potential. In the present study, literature review and laboratory work were carried out on the mechanical stabilization of pavement subgrade mixed with industrial bottom ash (BA). In this study, bottom ash (BA) has been used as a filler material. An attempt has been made to evaluate the properties of soil, such as bearing capacity by replacing it with bottom ash (BA). Environmental scanning electron microscope (ESEM) study conducted to study shape and texture of particles of bottom ash and soil. Different proportions of bottom ash were mixed with locally available (well-graded sand) soil to assess their effect on the engineering properties of soil. Series of tests like California bearing ratio (CBR) of soil were carried out with different dosages of bottom ash with a varying range of 0 to 30% to compare the results. The addition of bottom ash up to a certain limit increased the CBR value by increasing its load bearing capacity and compressive strength of the soil. Using laboratory tests, it is concluded that bottom ash can be used as a filler material in road construction like embankments when they are properly compacted because their dry density is low as their lightweight particles.

**Keywords** Bottom ash (B.A.) · Stabilization · California bearing ratio (CBR)

---

M. Vaja · U. Chaduvula (✉) · T. Thaker  
Pandit Deendayal Energy University, Gandhinagar, Gujarat, India  
e-mail: [uma.chaduvula@sot.pdpu.ac.in](mailto:uma.chaduvula@sot.pdpu.ac.in)

M. Vaja  
e-mail: [manan.vmtct20@sot.pdpu.ac.in](mailto:manan.vmtct20@sot.pdpu.ac.in)

T. Thaker  
e-mail: [Tejas.Thaker@sot.pdpu.ac.in](mailto:Tejas.Thaker@sot.pdpu.ac.in)

## 1 Introduction

Before we begin any construction on soil with poor bearing strength, low shear strength, high water absorption, and high plasticity, we must incorporate an additional mechanism to ensure its stability. A mechanical approach or chemical stabilizers can be used to improve soil stability. The black cotton soil shares a significant proportion of the area concerning the total land. It is spread over 5.46 lakh square kilometers, around 16.6 percent (Shirsath et al. 2017). Montmorillonite is a part of clayey mineral. The black cotton soil is extremely spongy of dampness (Shirsath et al. 2017). It expands fundamentally and becomes sticky and wet in the monsoon season. Under such conditions, it is inordinately difficult to chip away at such soil on account of the mud. In the hot, dry season, the dampness dissipates, and the soil shrinks and forms large and deep fractures, which are usually 10 to 15 cm broad and a meter deep. Medium to high compressibility and plasticity, high shrinkage, and swelling properties forms an inferior foundation material for road construction (Oza and Gundaliya 2013).

Significant research has been done to establish a property process to monitor swelling behavior and increase the strength of expansive soil. Soil stabilization can be accomplished through a variety of methods, including physical, mechanical, and chemical methods. The shearing strength and compressibility of such soils are both poor, and it has a low bearing capacity (Mekonnen et al. 2020). It is extremely difficult to calculate with this soil since it lacks adequate strength to support the masses that are imposed on it during construction and during the structure's service life. The performance characteristics of such soils should be enhanced for structures designed on them to perform better (Reddy et al. 2018). Chemical and mechanical approaches to increasing the strength of expanding soil are potential fundamental techniques. Chemical treatments are excellent for stabilizing expansive soil subgrades, yet this procedure caused the stabilized soil to become brittle. To overcome the chemical stabilization limitation, a new strategy integrating the coupling influence of mechanical and chemical stabilization approaches has been devised (Mekonnen et al. 2020).

The use of industrial wastes for soil stabilization is being studied, which includes coal waste, such as bottom ash (B.A.) and fly ash (F.A.). Mechanical stabilization is compacting the soil with mechanical devices such as rollers, jumps, and vibrators in order to increase its bearing and shearing strength. Chemical stabilizers change the chemical properties of the parent soil and enhance it; examples include lime, cement, bitumen, fly ash, and other admixtures. Coal combustion generates a large amount of solid waste in the form of B.A. and F.A., which must be reused rather than disposed of to avoid polluting the environment (Vasiya and Solanki 2021). It is also harmful to humans, causing respiratory issues (Mekonnen et al. 2020). There are various research publications on the use of F.A. alone, but bottom ash has only been considered in a few circumstances. Several of the researcher's works are presented here. (Sharma and Singh 2020) investigated the beneficial characteristics of coal ashes and used coal ashes from a variety of countries as examples. Low

relative density, low compressibility, a faster rate of consolidation, high resistance strength, high CBR, and pozzolanic reactivity are all beneficial qualities. F.A. and B.A. are often disposed of jointly, with an 80% fly ash to 20% bottom ash ratio. According to the American Coal Ash Association (ACAA), over 123 MT of coal combustion wastes was produced in 2005. About 71 MT of fly ash and 18 MT of B.A. was produced, accounting for 72% of coal combustion waste. Thermal power plants provide for over 80% of India's total electricity generation (Sharma and Singh 2020; Tiwari et al. 2021, Navagire et al. 2022, Randhawa and Chauhan 2022).

## 2 Materials and Methodology

### 2.1 Materials

The materials used in the present investigation are soil and bottom ash (B.A.).

#### Soil

A soil sample was taken from village Raysan on the AFCONS Construction site in Gandhinagar, Gujarat, to appraise the properties. At a depth of 1–2 m, the soil was collected. The collected soil was taken to the Geotech Lab for analysis of the index and engineering properties. The soil was stored in the oven for 72 h at a temperature of 100–110°C to preserve the clay's components. The powdered oven-dried soil was sieved through a 4.75 mm I.S. Sieve. Physical and chemical parameters were determined by laboratory studies. Soil has a specific gravity (S.G.) of 2.41. According to the grain size distribution analysis, the soil is well-graded sand (SW). Table 1 summarizes the physical and chemical characteristics of this soil (Fig. 1).

An environmental scanning electron microscope (ESEM) study was conducted to study the shape and texture of the particles; approximately 1 g of soil sample was obtained and placed over the instrument after passing through a 75-micron sieve. The sample was then placed on top of the equipment, and the electron beam was triggered once the vacuum conditions met the necessary criteria in the ESEM's vacuum chamber. With the use of a focused beam, an environmental SEM scans the sample's surface. By using 1000× and 5000× magnification, it was discovered that soil particles were flake shaped and had a smooth texture, as illustrated in Fig. 2.

#### Bottom Ash (B.A.)

Bottom ash is coarser, the granular component of by-products collected from the coal combustion from the bottom of furnaces in thermal power plants. Large volumes of ash, as well as carbon dioxide and other gases, are produced during coal burning. Rather than floating into the exhaust stacks, it sinks to the bottom of the thermal power plant's boiler. The bottom ash sample is collected from the dumping area near the thermal power plant at Gandhinagar for this investigation as shown in Fig. 3. At the time of sample collection, there is no moisture observed. The experiments

**Table 1** Physical and chemical properties of soil

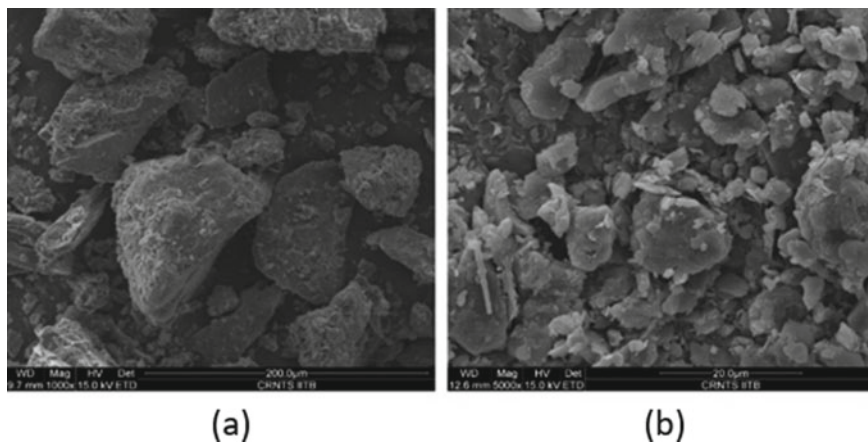
Properties	Result obtained	Specifications
Moisture content (%)	14.50	IS 2720 Part-3
Specific gravity	2.41	IS 2720 Part-3
Liquid limit (%)	31.83	IS 2720 Part-5
Plastic limit (%)	14.26	IS 2720 Part-5
Plasticity index (%)	17.57	IS 2720 Part-5
Shrinkage limit (%)	23.42	IS 2720 Part-6
Free swell index (%)	31.5	IS 2720 Part-40
Grain size distribution	Gravel (%) = 13.65 Sand (%) = 72.63 % Finer (%) = 13.72	IS 2720 Part-4
pH	9.06	IS 2720 Part-26
Maximum dry density (g/cc)	1.92	IS 2720 Part-7
Optimum moisture content (%)	11.16	IS 2720 Part-7

**Fig. 1** Soil sample

were carried out to characterize bottom ash through specific gravity and pH test. The physical and chemical properties of bottom ash are given in Table 2.

Environmental scanning electron microscope (ESEM) study was conducted to study the shape and texture of particles of bottom ash. Around 1 g of bottom ash sample was obtained and deposited over the instrument after passing through a 75  $\mu$ m I.S. sieve. The sample was then placed in the ESEM's vacuum chamber, and the electron beam was triggered once the vacuum conditions met the recommended criteria. As illustrated in Fig. 4 by 10,000  $\times$  magnification, ash particles were spherical in shape and had a smooth texture in ESEM pictures of bottom ash. Physically, B.A. has a diverse morphology with a rough surface roughness and semispherical to spherical particle shapes. Bottom ash typically increases particle interlocking and restricts





**Fig. 2** ESEM images of soil particles 2 **a** 1000 $\times$  magnification 2 **b** 2000 $\times$  magnification

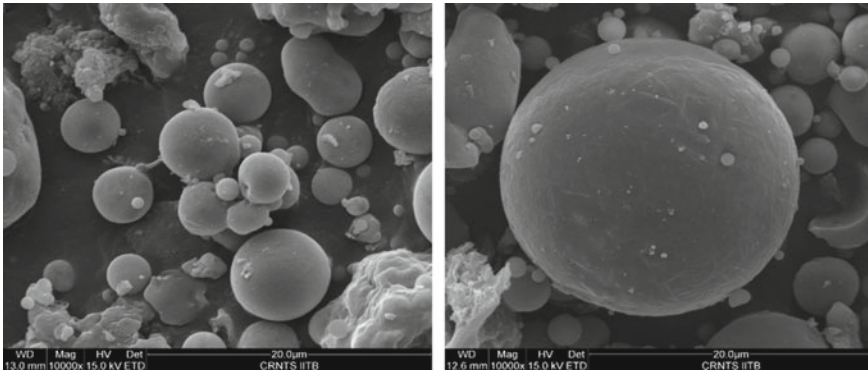
**Fig. 3** Dumping area near thermal power plant, Gandhinagar



**Table 2** Physical and chemical properties of bottom ash

Properties	Result obtained	Specifications
Specific gravity	1.87	IS 2720 Part-3
pH	7.53	IS 2720 Part-26
Color	Gray to black	–

movement from one particle to another due to its rough surface and angular form, which mechanically stabilizes soil.



**Fig. 4** ESEM images of bottom ash particles

## 2.2 Laboratory Experiments

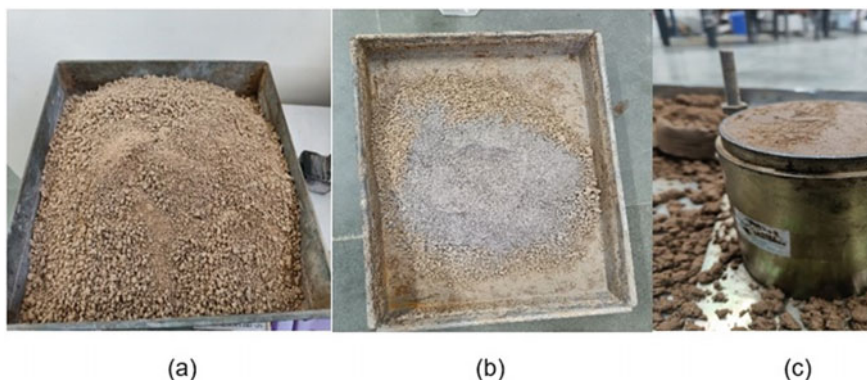
In this research study, the content of bottom ash to be used are 0, 10, 20, 25, and 30%, respectively, as per the literature study. The research plan of California bearing ratio (CBR) test is followed by soil mixed with (0, 10, 20, 25, and 30%) bottom ash content. The number of samples that have been carried out with different dosages of bottom ash is mentioned in Table 3.

### Compaction Test

For the maximum dry density (MDD) and optimum moisture content (OMC), a compaction test was used to measure the density of the soil, and B.A. 4.75 kg of air-dried soil passing through the I.S. sieve was used in the test. For each test, 3 kg of dirt was divided; a total of 20 compaction tests were performed. As indicated in Fig. 5, soil and B.A. samples were sieved and combined to compact this sample in a proctor mold. For maturation, water was mixed into the soil with varying water content and maintained in an airtight container for 24 h. The compaction test was carried out following I.S. 2720 part 8. A compaction test was performed for five different samples SB0, SB10, SB20, SB25, and SB30 to determine MDD and OMC for each one.

**Table 3** Soil and bottom ash mixes

Sr no	Sample name	Bottom ash (%)	Soil (%)	Soaking period (days)
1	SB0	0	100	4
2	SB10	10	90	4
3	SB20	20	80	4
4	SB25	25	75	4
5	SB30	30	70	4



**Fig. 5** a soil b soil + bottom ash c compacted sample

### **California Bearing Ratio (CBR) Test**

The CBR test was carried out to get the optimum dosage of soil and bottom ash mixes that had been obtained. The CBR test was essential because, according to the IRC-37, the pavement thickness is determined by the CBR value of the soil. The CBR test samples were made at their OMC and samples were made, and the samples were soaked for four days in accordance with IS 2720 part 16. The mixes were made with different bottom ash percentages (10 to 30%), the specimens compacted at the OMC, and CBR tests were performed on the mix. CBR test specimen is placed in CBR test apparatus as shown in Fig. 6.

**Fig. 6** CBR test apparatus



### 3 Results and Discussion

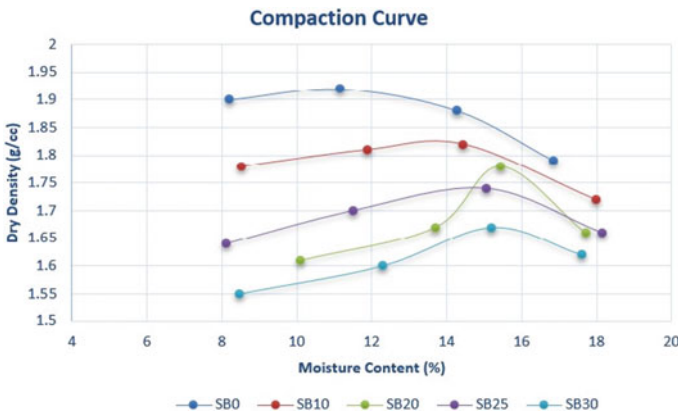
#### 3.1 Compaction Test

A compaction test was conducted to determine MDD and OMC of prepared soil samples followed by 0, 10, 20, 25, and 30% bottom ash (B.A.) content. The IS 2720 part 7 (1980) code was used to execute the compaction test. The values of optimum moisture content (OMC) and maximum dry density (MDD) of bottom ash added to the soil are given in Table 4 and Fig. 7.

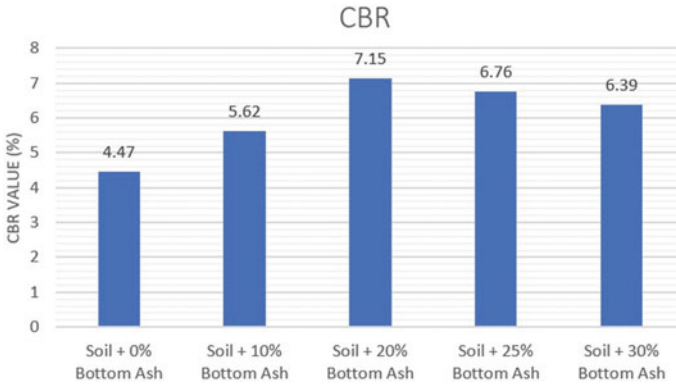
With the addition of bottom ash (B.A.), OMC drops. Untreated soil (0% bottom ash) gives MDD of 1.92 g/cc with 11.16% OMC. The 10% bottom ash (SB10) gives MDD of 1.82 g/cc with 14.44% OMC. The MDD decreases with the addition of bottom ash percentage in the soil mix up to 30% B.A. probably because of bottom ash's light pozzolanic particles having a specific gravity of about 1.87 as mentioned above. The MDD is observed in the soil with 0% bottom ash at about 1.92 g/cc. This could be caused by the replacement of high-density soil particles with low-density lightweight bottom ash particles. As observed from Fig. 7, SB20 sample exhibits

**Table 4** Compaction of soil and bottom ash mixes

Sr no	Sample name	Bottom ash (%)	Soil (%)	MDD (g/cc)	OMC (%)
1	SB0	0	100	1.92	11.16
2	SB10	10	90	1.82	14.44
3	SB20	20	80	1.78	15.44
4	SB25	25	75	1.74	15.05
5	SB30	30	70	1.67	15.20



**Fig. 7** Moisture content and dry density of soil and bottom ash mix



**Fig. 8** CBR values of soil and bottom ash mixes

different compaction characteristics as compared to others, which is due to soil with 20% B.A. shows higher load bearing capacity and 20% bottom ash consumes more water as shown in Fig. 8.

### 3.2 California Bearing Ratio (CBR)

A normal increase in CBR values was seen when the bottom ash % increased. The percentage of bottom ash determines the increase in CBR values. For the mix that was examined, the bottom ash stabilization significantly raised the CBR values. The highest CBR value measured in the soil with 20% bottom ash is 7.15%, which is 60% higher than the reference sample's CBR of 4.47% at 2.5 mm penetration as illustrated in Fig. 8. The CBR value is slightly reduced by adding more bottom ash to the soil. As per IRC-37, a CBR value greater than 5% can be used in subgrade soil. So, the criteria also match the value of the CBR value of the soil. This behavior also matches with the maximum dry density values obtained.

## 4 Conclusion

The purpose of the preceding research was to determine the effect of combining soil and bottom ash mixes for mechanical stabilization to improve the engineering properties of the soil. The CBR value has improved significantly, according to the findings of the soil when mixed with bottom ash dosages.

- The MDD of local soil and B.A. (SB0) was found out 1.92 g/cc and OMC to be 11.16%. Changes are observed for MDD when increasing in percentage of bottom ash. The MDD decreased from 1.92 to 1.83 g/cc by adding 10% bottom ash to the

reference soil sample and OMC increases from 11.16 to 14.44%. Furthermore, the decrease is observed in MDD when an increase in dosage of bottom ash is about 20, 25, and 30%. This is most likely because high-density soil particles have been replaced by low-density, lightweight bottom ash particles.

- ESEM analysis observed lightweight particles of bottom ash. Due to pozzolanic activity between soil and bottom ash, this will further help to reduce air voids and increase bonding between them.
- The highest CBR value measured in the soil with 20% bottom ash is 7.15%, which is 60% higher than the reference sample's CBR of 4.47% at 2.5 mm penetration which helps to increase the bearing capacity of soil up to a certain limit.

Bottom ash's key advantages are its lightweight particles and strong compressive strength. Bottom ash's pozzolanic activity adds strength and reduces settlements, making it a better choice for in-fill embankment material. It facilitates in the disposal of large volumes of solid waste from power plants and its reuse as ash for soil stabilization without producing any environmental problems, as well as being a cost-effective construction material.

## References

- IS 2720-3-1 (1980) Methods of test for soils. Part 3: determination of specific gravity
- IS 2720-5 (1985) Methods of test for soils. Part 5: determination of liquid and plastic limit
- IS 2720-6 (1972) Methods of test for soils. Part 6: determination of shrinkage factors
- IS 2720-7 (1980) Methods of test for soils. Part 7: determination of the water content-dry density relationship by light compaction
- IS 2720-26 (1987) Methods of test for soils. Part 26: determination of pH value
- IS 2720-40 (1977) Methods of test for soils. Part 40: determination of free swell index of soils
- Mekonnen E, Kebede A, Tafesse T, Tafesse M (2020) Application of microbial bioenzymes in soil stabilization. *Int J Microbiol* 2020(1725482):1-8. <https://doi.org/10.1155/2020/1725482>
- Navagire OP, Sharma SK, Rambabu D (2022) Stabilization of black cotton soil with coal bottom ash. *Mater Today Proc* 52(3):979-985
- Oza JB, Gundaliya PJ (2013) Study of black cotton soil characteristics with cement waste dust and lime. *Procedia Eng* 51:110-118
- Randhawa KS, Chauhan R (2022) Stabilizing black cotton soil in subgrade with municipal solid waste incineration ash for lowering greenhouse gas emission : a review. *Mater Today Proc* 50(5):1145-1151. <https://doi.org/10.1016/j.matpr.2021.08.037>
- Reddy CS, Mohanty S, Shaik R (2018) Physical, chemical, and geotechnical characterization of fly ash, bottom ash, and municipal solid waste from Telangana state in India. *Int J Geo-Eng* 9(23):1-23. <https://doi.org/10.1186/s40703-018-0093-z>
- Sharma V, Singh S (2020) Modeling for the use of waste materials (bottom ash and fly ash) in soil stabilization. *Mater Today Proc* 33(3):1610-1614. <https://doi.org/10.1016/j.matpr.2020.05.569>
- Shirsath HA, Joshi SR, Sharma V (2017) Effect of bio-enzyme (terrazyme) on the properties of sub grade soil of road. *Int J Innovative Res Sci Eng Technol* 3(3):231-236
- Tiwari N, Satyam N, Puppala AJ (2021) Strength and durability assessment of expansive soil stabilized with recycled ash and natural fibers. *Transp Geotech* 29:100556. <https://doi.org/10.1016/j.trgeo.2021.100556>
- Vasiya V, Solanki CH (2021) An experimental investigation on black cotton soil using terrazyme. *Int J Eng Trans B Appl* 34(8):1837-1844. <https://doi.org/10.5829/IJE.2021.34.08B.04>

# Experimental Study on Mechanical Properties of Concrete Incorporated with Basalt and Polypropylene Fibers



Sandeep Sathe, Shahbaz Dandin, Shubham Surwase,  
and Alina Kharwanlang

**Abstract** Plain concrete has a very low tensile strength and is susceptible to cracking before the ultimate load. Various types of fibers aid in the resistance of fractures in concrete constructions. The present study aims to understand the engineering properties of M40 grade concrete for the varying percentage of fibers [polypropylene fibers (PF) and basalt fibers (BF)] from 0.2% to 0.8% by 0.2% incrementally for 7 days and 28 days of curing. The optimum percentage of BF and PF were 0.6 and 0.4% by weight of concrete, respectively. Moreover, it was found that BF and PF can potentially increase the compressive strength by 12.90%, split tensile strength by 28.33%, and flexural strength by 16.98%; and the compressive strength by 11.04%, split tensile strength by 18.18%, and flexural strength by 15.47% at optimum percentage on 28 days of curing when compared to plain concrete. Moreover, the optimum percentage of BF and PF decreases the mobility of the concrete in its fresh form by acting as a barrier to the movement of coarse material by 28.57 and 7.14%, respectively, at their optimum percentage.

**Keywords** Polypropylene fiber · Basalt fiber · Split tensile · Flexural · Compressive strength · Mobility

## 1 Introduction

India's population is fast growing, and the construction sector is booming at the same time. Concrete is a highly important part of structure in the construction industry, and there is no substitute for it. Because concrete is brittle by nature, it begins to crack after curing as a result of heat generated through it. After concrete dries, it develops cracks, which might lead to the structure collapsing. Concrete fibers are utilized to

---

S. Sathe (✉) · S. Dandin · S. Surwase · A. Kharwanlang  
School of Civil Engineering, Dr. Vishwanath Karad MIT World Peace University, Kothrud,  
Pune 411038, India  
e-mail: [sandeepsatheresearch@gmail.com](mailto:sandeepsatheresearch@gmail.com)

S. Dandin  
e-mail: [shahbaz.dandin@mitwpu.edu.in](mailto:shahbaz.dandin@mitwpu.edu.in)

© The Author(s), under exclusive license to Springer Nature Singapore Pte Ltd. 2024  
D. Patel et al. (eds.), *Innovation in Smart and Sustainable Infrastructure*, Lecture Notes  
in Civil Engineering 364, [https://doi.org/10.1007/978-981-99-3557-4\\_22](https://doi.org/10.1007/978-981-99-3557-4_22)

275



resist cracks while also increasing durability and tensile strength. As a result, concrete is reinforced with fiber which shows high tensile strength. Added fibers improve the mechanical properties, and it reduces the permeability of concrete significantly. After 28 days, the optimal improvement in flexural, compressive, and split tensile strength was found to be 6.50, 13.09, and 8.13%, respectively (Parashar and Gupta 2021). The compressive strength and modulus of rupture of a 36 mm long chopped basalt filament fiber are both high (Iyer et al. 2015). When compared to the average compressive strength of control specimens, the variation in average compressive strength and split tensile strength containing basalt fibers was found to be 4%, and it improved strain capacity from 4 to 12% (Ayub et al. 2014). Concrete slump values are reduced as fiber lengths and fiber volume fractions increase. A higher fiber volume fraction indicates clumping or balling of the fiber. The compressive strength of concrete mixes increased as the volume fraction and length of basalt fibers increased. The best fiber length and volume fraction were discovered to be 12.0 mm and 0.15%, respectively (Wang et al. 2019a, b). The optimal basalt fiber percentage is found to be between 0.3 and 0.4%. Flexural strength has significantly improved when compared to compressive strength. The concrete containing basalt fiber was found to be non-brittle and to have good bonding properties (Zhou et al. 2020). The use of basalt fiber considerably increased the toughness and crack resistance of the concrete (Elshazli et al. 2022). As basalt fiber content is 0.15% and polypropylene fiber content is 0.33%, compressive strength, flexural strength, and splitting tensile strength increase by 14.1, 22.8, and 48.6%, respectively, when compared to regular concrete without fibers (Wang et al. 2019a, b). The optimal percentage of polypropylene fiber was found to be between 0.25 and 0.5%, resulting in improved compressive and flexural strengths (Ede and Ige 2014). When the total volume fraction of polypropylene fibers (PF) surpasses 0.15%, the fibers have a detrimental influence on compressive strength, and PF reduces compressive strength. As a result, the percentage of fiber in concrete must be closely regulated (Niu et al. 2019). Tensile Strength, flexural strengths, flexural toughness, and ductility both increased significantly. Crack formation in concrete is prevented due to the fiber's bridging ability. While the addition of short polypropylene fiber increases compressive strength significantly, it has only a minor effect on splitting tensile strength. Compressive strength is reduced when long fibers are added to concrete mixtures (Latifi et al. 2022). The PF improved compressive and tensile strengths by increasing axial and perpendicular load resistance. At 0.5% PF by weight of cement, compressive strength increased by 17.8%, and tensile strength increased by 18% (Elkatatny et al. 2020). The compressive and flexural strength values of concrete containing 0 to 0.3% PF are increasing. When the PF was increased to 0.5%, the concrete's compressive and flexural strength began to decline significantly when compared to the control mix (Mashrei et al. 2018). As a result of the studies mentioned, concrete with BF and PF improves the overall performance and effectiveness of concrete. Furthermore, the optimal fiber dosage, length, and aspect ratio all have a significant impact on the performance of concrete. The primary goal of this research is to determine the optimum percentage of BF and PF, as well as their effect on the compressive strength, split tensile strength, and flexural strength of concrete.



## 2 Experimental Program

### 2.1 Material Specifications

In the present experimental study, OPC 53 grade was used as a binding material and tested as per IS Codes: IS: 12,269–1987 (BIS 1987). The density of cement: 2400 kg/m<sup>3</sup>. And relative density of cement is determined by Le Chateliers flask method. Relative density of cement = 3.15. The coarse aggregates were 10 and 20 mm in size, with specific gravity values of 2.7 and 2.8, respectively. The aggregates worked out in the laboratory had a combined fineness modulus of 5.7 accordance with IS: 2386–1963-Part-4 (Reaffirmed 2002) (BIS 1963b), and IS 383–2016 (BIS 2016) coarse aggregates have been tested and confirmed. The fineness modulus values of coarse aggregates 10 and 20 mm were 6.35 and 7.60, respectively. The fine aggregate properties are tested in accordance with the IS: 2386–1963-Part-I-(Reaffirmed 2002) code (BIS 1963a). The fine aggregate used in the study was graded zone II according to IS: 383:2016 (BIS 2016) (Table 1).

Basalt fiber of 12 mm length and diameter of 0.02 mm was used in this experiment. The properties of basalt fiber are presented in Table 2. Polypropylene fiber (Specific gravity = 0.9) is having tensile strength of 350 to 550 MPa, Young's modulus of 7500 MPa, Poisons ratio of 0.2, length of 12 mm, diameter of 0.034 mm, and percentage elongation of 24 to 60%. Also, it shows good resistance to chemical attack and thermal conductivity. It has melting and softening point 166 and 141°C, respectively. BASF Company's Master Glenium SKY 8233 was used as an admixture during the experiment. This admixture is based on modified polycarboxylic ether. This admixture was created for high durability and high-performance concrete. This admixture was used as 1% by the weight cementitious materials (Table 3).

**Table 1** Oxide composition of cement

Oxides	Percentage of oxide in cement
SiO <sub>2</sub>	18.92
Al <sub>2</sub> O <sub>3</sub>	4.55
Fe <sub>2</sub> O <sub>3</sub>	4.95
CaO	66.68
Na <sub>2</sub> O	0.15
MgO	0.87
SO <sub>3</sub>	2.5

**Table 2** Mechanical and engineering properties of BF

Property	Description
Tensile strength in MPa	1650
Aspect Ratio	600
Modulus of elasticity in MPa	89,000
Percentage elongation at break point	3.150
Bulk density in kg/m <sup>3</sup>	2650

**Table 3** Experimental results

Specimen variation	Average compressive strength (N/mm <sup>2</sup> )		Average split tensile strength (N/mm <sup>2</sup> )		Average flexural strength (N/mm <sup>2</sup> )	
	7 days	28 days	7 days	28 days	7 days	28 days
Normal concrete (Group 1)	30.13	44.67	2.80	4.30	2.90	4.40
0.2% BF (Group 2)	32.75	46.91	3.10	4.90	2.95	4.60
0.4% BF (Group 3)	34.51	48.60	3.30	5.38	3.00	4.95
0.6% BF (Group 4)	35.55	51.29	3.60	6.00	3.20	5.30
0.8% BF (Group 5)	33.20	49.42	3.20	5.19	2.95	4.80
0.2% PF (Group 6)	32.20	47.05	3.20	4.50	3.00	4.48
0.4% PF (Group 7)	35.90	52.89	3.50	5.50	3.30	5.30
0.6% PF (Group 8)	34.80	49.23	3.30	5.20	3.00	4.85
0.8% PF (Group 9)	33.95	48.17	3.20	5.10	2.90	4.50

## 2.2 Methodology

The laboratory pan mixer is used for mixing concrete ingredients. Dry mix is prepared in the laboratory in a pan mixer, and then, water is added to maintain water–cement ratio of 0.35. In the present work, IS-10262–2019 is used to prepare the mix design considering medium degree of workability, good quality control, and moderate exposure condition (BIS 2019). M40 grade concrete was made. The experimental investigation consists of determining the strength properties of concrete with basalt and polypropylene fiber at various percentages. Polypropylene and basalt fiber dosages of 0.2, 0.4, 0.6, and 0.8% were finalized for experimental work. Slump cone workability test is performed on fresh concrete as per IS: 7320–1974 and presented in Table 4 (BIS 1974). The workability of concrete decreases as fiber quantity increases.

**Table 4** Test result on workability of fiber-reinforced concrete

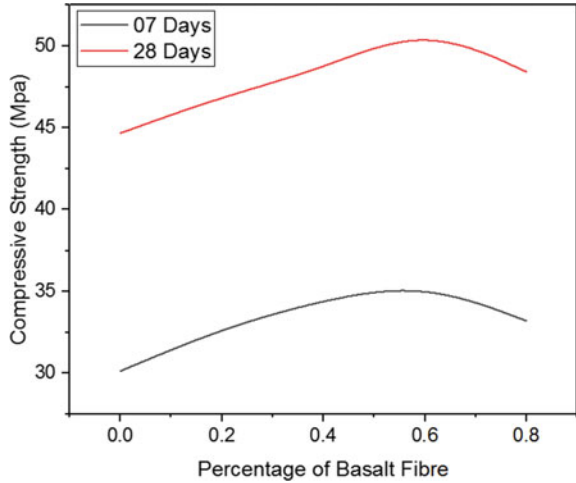
Fiber percentage	Slump cone test result of BF in mm	Slump cone test result of PF in mm
0.0	70	70
0.2	65	68
0.4	55	65
0.6	50	63
0.8	48	60

When a large amount of fiber was added, low slumps were observed. It could be due to the large surface areas of BF accumulating additional cement paste to cover it, causing the viscosity of the mix to increase. As a result, it contributes to slump reductions. Furthermore, the fibers absorb the free water content of the concrete during mixing, and greater amounts of fiber would significantly reduce the workability of the concrete. This makes molding of concrete into the place (or shape) without the use of super plasticizers extremely difficult. The proportion of C:FA:CA = 01:1.88:2.90 was used to cast the cube, cylinder, and beam. The cube of size 150 × 150 × 150 mm, cylinder of 15 mm diameter with 300 mm height, and beam of 150 × 150 × 700 mm was used for casting of specimens of different percentages of basalt and polypropylene fiber. All the cubes, cylinders and beams are filled with the same concrete at times. Materials were sieved before casting the specimens. Batching (by weight) was performed to have the appropriate quantities of the ingredients in the required mix. In this research work, steel molds were used which were cleaned and assembled properly. The inner surfaces of the molds were oiled to avoid the sticking of concrete to the mold surfaces and to achieve easy demolding. The casting was performed by standards. Molds were demolded after 1 day of the casting, and the cubes were properly marked following the curing with the testing age.

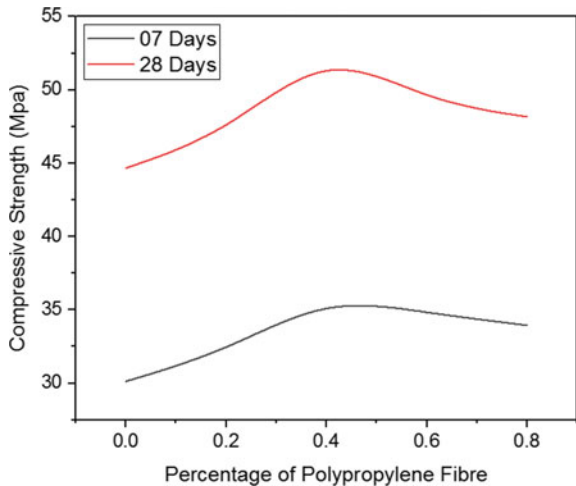
### 3 Tests and Result Discussions

The compression testing machine is needed for analyzing strength of compression of concrete with standard cube size molds after 7 and 28 days curing. Three cubes each with 0, 0.2, 0.4, 0.6, and 0.8% of basalt and polypropylene fiber each were tested as per guideline of IS: 516:1959 (BIS 1959), and individual cube strength and average strength of compression are noted. Also, cylinders were tested on a compression testing machine with capacity 2000 KN. Three cylinders each with 0, 0.2, 0.4, 0.6, and 0.8% of basalt and polypropylene fiber each were tested as per guideline of IS: 5816–1959 (BIS 1999) and individual and average split tensile strength is noted. Beams with various percentages of BF and PF were tested on UTM with capacity 1000 KN for flexure as per guideline of IS: 516–1959 (BIS 1959). The test results of concrete specimens at 7 and 28 days curing periods are presented in Table 3 (Figs. 1 and 2).

**Fig. 1** Compressive strength with varying percentage of basalt fiber

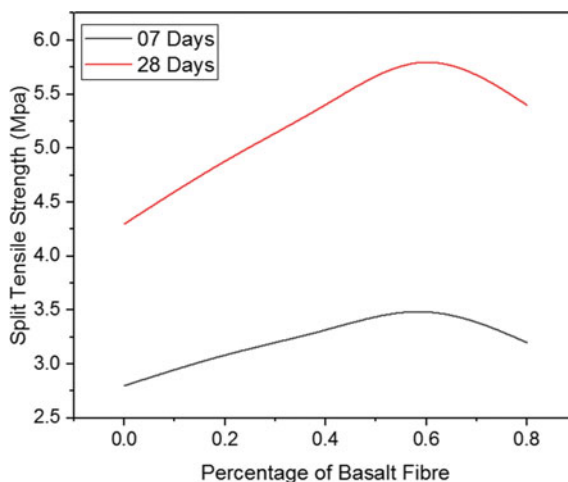


**Fig. 2** Compressive strength with varying percentage of polypropylene fiber



Adding BF percentages of 0.2, 0.4, 0.6, and 0.8% increases compressive strength by 8, 12.63, 15.24, and 9.24% after 7 days, whereas adding PF increases compressive strength by 6.42, 16.07, 13.41, and 11.25% after 7 days. For 28 days of curing, adding a BF percentage of 0.2, 0.4, 0.6, and 0.8% increases compressive strength by 4.77, 8.08, 12.90, and 9.61%, respectively, while adding PF increases compressive strength by 5.05, 15.54, 9.26, and 7.26%. Individual BF and PF fibers significantly improve compressive strength by bridging cracks and providing confinement, thus boosting the composite's strength and reducing transverse deformation of the specimen. Fibers also help to decrease cracking and slightly increase the stiffness of the concrete. The incorporation of fibers avoids the creation of multiscale cracks in concrete at different stress levels, which accounts for the improvement in strength. PF

**Fig. 3** Split tensile strength with varying percentage of basalt fiber

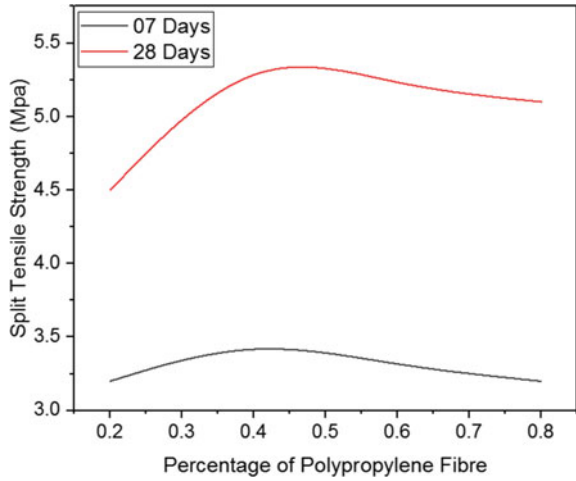


having a low modulus of elasticity improved concrete compressive behavior by minimizing the production of micro-cracks under low stress level. At high levels of stress, PF cannot sustain the loads, whereas BF with a high modulus of elasticity incorporated in cementitious materials improves compressive strength by reducing the development of macro-cracks. Prior research had shown that increasing the amount of fiber added to a relatively large volume has a negative impact on compressive strength (Ayub et al. 2014; Elshazli et al. 2022; Iyer et al. 2015; Wang et al. 2019a, b). This is due to the cement matrix being replaced by a higher volume of fibers, which reduces mechanical characteristics. This decrease could be attributed to the fact that increasing fiber concentration may produce fiber congestion, resulting in balling and improper bonding with concrete. Furthermore, if concrete cannot be compacted effectively due to higher fiber content and lack of workability, it causes negative impact on compressive strength rather than an improvement (Figs. 3 and 4).

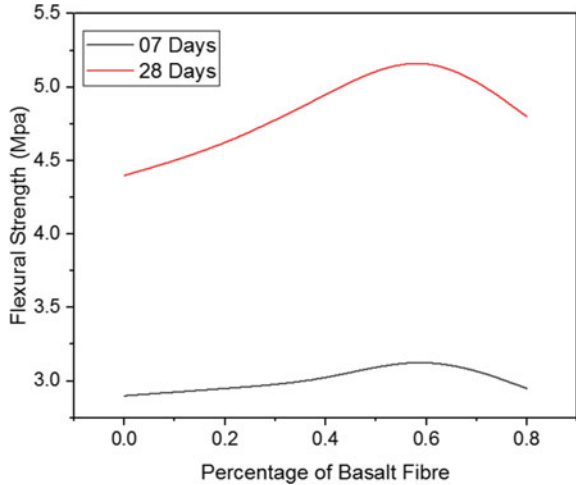
Tensile strength increases by 9.67, 15.15, 22.22, and 12.50% after 7 days of curing when BF percentages of 0.2, 0.4, 0.6, and 0.8% are added, while PF increases tensile strength by 12.50, 20, 15.15, and 12.50% are added. Adding a BF percentage of 0.2, 0.4, 0.6, and 0.8% increases tensile strength by 12.24, 20.07, 28.33, and 17.14%, respectively, after 28 days of curing, whereas adding PF increases tensile strength by 4.44, 21.81, 17.30, and 15.68%. At the failure region, the BF and PF in the concrete bridged micro-cracks. The BF and PF in the concrete restrict the spread of macro-cracks, and the specimen has the highest tensile strength. The findings showed that increasing the BF and PF concentrations over the optimal percentage reduces the tensile strength of concrete specimens. This is due to improper compaction and the presence of additional voids (Figs. 5 and 6).

Adding BF percentages of 0.2, 0.4, 0.6, and 0.8% increases flexural strength by 1.69, 3.33, 9.37, and 1.69% for 7 days of curing, while adding PF increases flexural strength by 3.33, 12.12, 3.33, and 0.0% for 7 days of curing. Adding BF percentages of 0.2, 0.4, 0.6, and 0.8% increases flexural strength by 4.34, 11.11, 16.98, and 8.33%,

**Fig. 4** Split tensile strength with varying percentage of polypropylene fiber

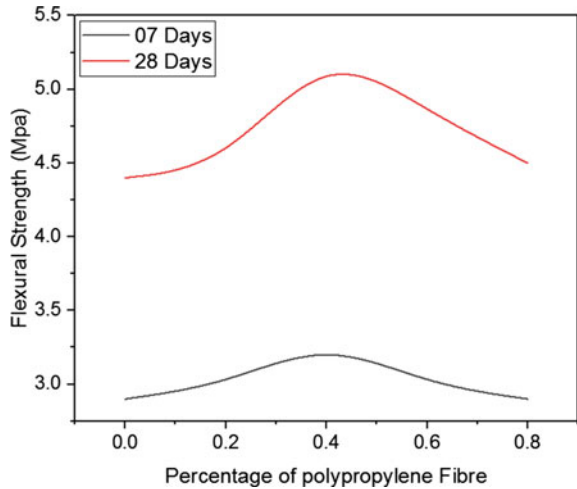


**Fig. 5** Flexural strength with varying percentage of basalt fiber



respectively, after 28 days of curing, while adding PF increases flexural strength by 1.78, 16.98, 9.27, and 2.22%. As the BF and PF content of the concrete increases, it significantly aids in preventing the formation, propagation, and widening of cracks and, as a result, enhances the flexural strength of the concrete. The ductile behavior of a concrete beam was observed as a result of the effective bridging activity of fibers across cracks. Fibers act as a bridge through cracks, increasing the cracking resistance of concrete. Increased fiber content above the optimum percentage produces the balling effect and improper bonding with concrete, resulting in flexural strength loss.

**Fig. 6** Flexural strength with varying percentage of polypropylene fiber



## 4 Conclusions

The experimental study of this work can lead to the following reasonable conclusions. For 7 days and 28 day curing periods, the compressive, split tensile, and flexural strength of concrete increases up to 0.6% for BF and 0.4% PF content, respectively, and then begins to decrease. The concrete with BF shows an increase in compressive strength by 12.90%, split tensile strength by 28.33%, and flexural strength by 16.98% at an optimum percentage on 28 days of curing. The concrete with PF shows an increase in compressive strength by 11.04%, split tensile strength by 18.18%, and flexural strength by 15.47% at optimum percentage on 28 days of curing. The addition of BF and PF to concrete decreases the mobility of the concrete in its fresh form by acting as a barrier to the movement of coarse material by 28.57 and 7.14%, respectively, at their optimum percentage.

## References

Ayub T, Shafiq N, Nuruddin MF (2014) Effect of chopped basalt fibers on the mechanical properties and microstructure of high-performance fiber reinforced concrete. *Adv Mater Sci Eng* 2014(587686):1–14. <https://doi.org/10.1155/2014/587686>

BIS (1959) IS 516 (1959): method of tests for strength of concrete

BIS (1963a) IS 2386–1 (1963a): methods of test for aggregates for concrete. Part I: particle size and shape

BIS (1963b) IS 2386–4 (1963b): methods of test for aggregates for concrete. Part 4: mechanical properties

BIS (1974) IS 7320 (1974): specification for concrete slump test apparatus

BIS (1987) IS 12269 (1987): 53 grade ordinary Portland cement

BIS (1999) IS 5816 (1999): method of test splitting tensile strength of concrete

- BIS (2016) IS 383 (2016): coarse and fine aggregate for concrete-specification. In: Bureau of Indian Standards, New Delhi
- BIS (2019) IS 10262 (2019): concrete mix proportioning-guidelines, 2nd revision. Retrieved from <https://www.standardsbis.in/>
- Ede AN, Ige A (2014) Optimal polypropylene fiber content for improved compressive and flexural strength of concrete. *IOSR J Mech Civ Eng (IOSR-JMCE)* 11(3):129–135. Available at <http://www.iosrjournals.org/>. e-ISSN: 2278-1684, p-ISSN: 2320-334X
- Elkatatny S, Gajbhiye R, Ahmed A, Mahmoud AA (2020) Enhancing the cement quality using polypropylene fiber. *J Petrol Explor Prod Technol* 10(3):1097–1107. <https://doi.org/10.1007/s13202-019-00804-4>
- Elshazli MT, Ramirez K, Ibrahim A, Badran M (2022) Mechanical, durability and corrosion properties of basalt fiber concrete. *Fibers* 10(2):10-1–10-30. <https://doi.org/10.3390/fib10020010>
- Iyer P, Kenno SY, Das S (2015) Mechanical properties of fiber-reinforced concrete made with basalt filament fibers. *J Mater Civ Eng* 27(11):04015015. [https://doi.org/10.1061/\(ASCE\)MT.1943-5533.0001272](https://doi.org/10.1061/(ASCE)MT.1943-5533.0001272)
- Latifi MR, Biricik Ö, Aghabaglou AM (2022) Effect of the addition of polypropylene fiber on concrete properties. *J Adhes Sci Technol* 36(4):345–369. Taylor and Francis Ltd. <https://doi.org/10.1080/01694243.2021.1922221>
- Mashrei MA, Sultan AA, Mahdi AM (2018) Effects of polypropylene fibers on compressive and flexural strength of concrete material. *Int J Civ Eng Technol (IJCIET)* 9(11):2208–2217
- Niu D, Huang D, Fu Q (2019) Experimental investigation on compressive strength and chloride permeability of fiber-reinforced concrete with basalt-polypropylene fibers. *Adv Struct Eng* 22(10):2278–2288. <https://doi.org/10.1177/1369433219837387>
- Parashar AK, Gupta A (2021) Investigation of the effect of bagasse ash, hooked steel fibers and glass fibers on the mechanical properties of concrete. *Mater Today Proc* 44(1):801–807. <https://doi.org/10.1016/j.matpr.2020.10.711>
- Wang D, Ju Y, Shen H, Xu L (2019a) Mechanical properties of high-performance concrete reinforced with basalt fiber and polypropylene fiber. *Constr Build Mater* 197:464–473. <https://doi.org/10.1016/j.conbuildmat.2018.11.181>
- Wang X, He J, Mosallam AS, Li C, Xin H (2019b) The effects of fiber length and volume on material properties and crack resistance of basalt fiber reinforced concrete (BFRC). *Adv Mater Sci Eng* 2019(7520549):1–17. <https://doi.org/10.1155/2019/7520549>
- Zhou H, Jia B, Huang H, Mou Y (2020) Experimental study on basic mechanical properties of basalt fiber reinforced concrete. *Materials* 13(6):1362-1–1362-20. <https://doi.org/10.3390/ma13061362>



# Soil Properties Modification Using PET waste—An Experimental Study



Alka Shah  and Tejas Thaker

**Abstract** In recent years, change in lifestyle mainly due to overuse of different products for personal use, cleaning, packaging, etc., which majority made from the various types of plastics like PET, HDPE and LDPE affected the living organism on the planet earth directly or indirectly. Currently, entire world is finding tangible solution to minimize the use of plastic materials and also recycling or reuse of such materials. This paper presents the reuse of the plastic waste for modification of properties of clayey soil. In this study, PET types of plastic were utilized to analyse the properties of soil. Used plastic water bottles were collected and converted in to form of stripes. Series of experiments were conducted with different percentage of PET waste (0, 0.2, 0.4, 0.8, and 1%) and aspect ratio (2 and 4). The observation of the study shows the significant change in behaviour of clayey soil with inclusion of PET type of waste. This methodology can be use potentially for the construction of pavements having bed subgrade soil.

**Keywords** Soil · Modification · Plastic waste · PET

## 1 Introduction

In recent years, living standard of human being increased the demand of all types of packaged product. Moreover, due to COVID-19 pandemic, the use of well protected and packaged product increases at a great extent. Out of such all the product, majority of the product uses different types of plastics like polyethylene terephthalate (PET), high-density polyethylene (HDPE), polyvinyl chloride (PVC), high-density

---

A. Shah (✉) · T. Thaker  
Pandit Deendayal Energy University, Gandhinagar, Gujarat, India  
e-mail: [alkamurarishah@gmail.com](mailto:alkamurarishah@gmail.com)








T. Thaker  
e-mail: [Tejas.Thaker@sot.pdpu.ac.in](mailto:Tejas.Thaker@sot.pdpu.ac.in)

A. Shah  
Nirma University, Ahmedabad, Gujarat, India

polyethylene (LDPE), polypropylene (PP), polystyrene (PS) and others. Table 1 presents the products generally made from the different types of plastic with example. Out of these, PET, HDPE and LDPE are the type of plastic which are widely used for day-to-day products. It was reported that out of all the types of plastic only 5% goes to recycle and remaining 95% plastics are directly dumped in the land, oceans and anywhere (Ojuri et al. 2022). Littering of plastic in to the ocean creates the life threat for the ocean animals. Waste materials like waste tyre, PP, natural waste fibres, etc., utilization in soil improvement carried out by many researchers (Abbaspour et al. 2020; Ahmad et al. 2010; Ammar et al. 2019; Santoni et al. 2001; Consoli et al. 2002, 2007). Polypropylene was used in many studies to investigate the behaviour of soils (Santoni et al. 2001; Consoli et al. 2002, 2007; Abuel-Maaty 2010; Fatahi et al. 2012; Olgun 2013; Ibraim et al. 2010; Wang et al. 2017; Kaniraj and Havanagi 2001; Estabragh et al. 2011). Very few studies exist in which PET type of plastic waste was used for the improvement of soil, especially problematic soil. PET is the type of plastic used for the manufacturing of single-use plastic water bottles. This study focused on the PET type of plastic looking towards the extensive use of plastic water bottles usage. As per the statistics, 1500 bottles are dumped and discarded in landfills every second. Used PET water bottles is contributing significantly for littering Fathi et al. (2020).

Study was reported by Choudhary et al. (2010) using plastic waste HDPE. Author investigated effect of plastic waste HDPE stripes and effect of different aspect ratio in sandy soil through CBR test. Results shows that the significant improvement in CBR ratio Choudhary et al. (2010). Series of proctor compaction, unconfined compression and triaxial compression tests were carried out using PET bottle strips again with different aspect ratio by Acharyya et al. (2013). Study shows the significant change in properties of sand. Babu and Jaladurgam (2014) carried out the consolidation, CBR and Cu test to investigate the mixture of only fly ash and plastic waste. CBR values of fly ash mixed with waste found more than the plain fly ash Abukhettala and Fall (2021). Akinwumi et al. (2019) used shredded PET plastic bottle waste for affordable compresses earth brick for affordable housing. Compressive strength and erosion parameter were studied with 0, 1, 3 and 7% content of waste Tafreshi et al. (2021). First study was carried out on the different type of plastic waste to study the behaviour of soil with different plastic waste by Abbaspour et al. (2020). Four types of plastic, i.e. HDPE, LDPE, PET and PP, and different form of plastic waste like ground, pellet and flake were considered to study the behaviour of soil. Compaction, CBR, strength, resilient modulus and permeability properties of sand were investigated with the inclusion of waste Shah and Modha (2020). Fathi et al. (2020) conducted shake table tests to investigate the dynamic properties of the sand–PET mixtures. Study shows that addition of the plastic waste strips to the sand could change the soil brittle behaviour. Damping ration of mixture increased and shear modulus decreased with the increase of the plastic waste strips content Solanki et al. (2021). Tafreshi et al. (2021) used the full plastic bottle filled with sand as a bed below the foundation. Results showed that the bottle bed performed well at the higher pressure Fathi et al. (2020). Shah and Modha (2020); Solanki et al. (2021) studied the effect of plastic waste on the properties of soil by converting plastic waste in to geogrid, geocell and

**Table 1** Types of plastic with example of day-to-day products

						
<b>PET</b>	<b>HDPE</b>	<b>PVC</b>	<b>LDPE</b>	<b>PP</b>	<b>PS</b>	<b>Others</b>
Single used plastic bottles filled with liquid – Water – Juice – Cooking oil and many more	Day to day products – Detergent – Shampoo – Cosmetics – Motor oil and many more	– Water distribution system – Roof sheet and many more	– Plastic bags – Food wrapping – Electronic product packaging and many more	– Straws – Bottle caps – Medical and many more	– Egg cartoons – Food takeaway carton and many more	– Sunglasses – Cloths and many more

strips. Study shows that inclusion of plastic waste improves the weak soil IS 14534 (1998); IS 1498 (1970). Table 2 presents the type of waste, its content and forms used for the studies on the soil waste mixture. Above all the study carried out on sandy soil or clay with low plasticity. So, looking towards the problematic soil like clay with intermediate and high plasticity, there is always a need to improve such type of soil. So, in the present study, attempt was made to analyse the behaviour of clayey soil with the inclusion of plastic PET water bottles strips. Scope of the study was to investigate the compaction behaviour of clayey soil and PET waste mixture with two parameters, i.e. content of waste and aspect ratio of PET strips.

## **2 Materials and Methodology**

### **2.1 Materials**

Soil was collected from the Chekhla area near to Sanad. Basic characterization of soil was carried out in the laboratory. According to ISC, soil was classified as CI. The properties of soil were presented in Table 3. Post-consumer plastic water bottles with PET symbol were collected from the canteen of Nirma University. These bottles were cleaned and dried for the further use.

### **2.2 Methodology**

Series of standard proctor test were carried out on clay and PET waste mixture. PET water bottles were manually cut in to strips with two aspect ratios 2 and 4. Aspect ratio is defined as the ratio of length to width. The picture of PET stripes is shown in Fig. 1. When any materials used for the study at that time, it is also necessary to find the properties of the material. So properties of PET plastic waste bottle were also determined in the laboratory using tensile testing machine and thickness gauge. Table 4 presents the properties of plastic waste strip.

### **2.3 Compaction Parameters**

Standard proctor test was conducted with different percentage of PET strips, i.e. 0, 0.2, 0.4, 0.8 and 1% as per the IS standard. PET strips of width of 5mm and length 10 and 20 mm used for the study. To carry out the test series, first soil was completely carried out dry and then compaction parameters of virgin soil was tested, with 0% PET strips. Further, testing was carried out on 0.2, 0.4, 0.8 and 1% content of PET strips. The specification of PET strips was selected based on the literature survey. Figure 2 shows the PET-mixed clayey soil.

**Table 2** Type of waste, its content and forms used for the studies on the soil waste mixture

Name of author	Soil type	Waste material	Waste forms	Size of waste	Content of waste (%)
Koohmishi and Palassi (2022)	CL	Plastic waste (PET bottles)	Strips	$L = 30$ mm $B = 3$ mm $D = 5$ mm $T = 0.2$ mm	0.5, 1, 1.5, 2, 3, 5 and 10
Bozyigit et al. (2021)	CH	Plastic waste (PET bottles)	Strips	$L = 10$ mm $B = 4$ mm $T = 0.05$ mm	0, 0.5, 0.1, 1.5 and 2
Tafreshi et al. (2021)	SW	Plastic waste (PET bottles)	Sand filled bottle used as a reinforcement	Full Bottle	–
Fathi et al. (2020)	SP	Plastic waste (PET bottles)	Strips	$L = 10$ and 50 mm $B = 10$ mm $AR = 1$ and 5	0, 0.5, 0.75 and 1
Jaber et al. (2021)	Subbase soil	Plastic waste (PET)	Granules	$D = 2.5$ mm	2.5, 5, 7.5, 10 and 12.5
Abukhattala and Fall (2021)	A-2-7 (silt or clay gravel sand)	HDPE, LDPE, PET and PP	Ground, pellet, and flake	Pellet 3.3 mm Flake 7 mm $\times$ 8.8 mm in diameter and 0.7 mm in thickness	1 to 10
Akinwumi et al. (2019)	CL	Plastic waste (PET bottles)	Shredded	6.3 to 9.6 mm	0, 1, 3, and 7
Acharyya et al. (2013)	CH	Plastic waste (PET)	Strips	$L = 5, 10, 15$ mm $B = 5$ mm $T = 0.5$ mm	0.5, 1, 1.5, and 2
Babu and Jaladurgam (2014)	–	Plastic waste (PET bottles)	Chips	$L = 10$ –20 mm $T = 0.2$ mm $AR = 20$ –40	0.0, 0.50, 0.75 and 1.0
Choudhary et al. (2010)	SP	HPDE	Strips	$B = 12$ mm $L = 12, 24$ and 36 mm $T = 0.40$ mm $AS = L/B = 1, 2$ and 3	0.0, 0.25, 0.50, 1.0, 2.0 and 4.0

### 3 Results and Discussion

Compaction of soil is a great measure for the behaviour of soil. Compaction is directly related to the field behaviour of soil in worst condition like water logging and heavy load. Figure 3 presents the compaction curve with aspect ratio 2. It is the

**Table 3** Properties of soil

SN	Properties	Value
1	Specific gravity	2.66
2	Liquid limit (%)	41
3	Plastic limit (%)	20
4	Shrinkage limit (%)	16
5	Plasticity index	21
6	Soil classification	CI

**Fig. 1** Clay–PET stripes mixture



**Table 4** Properties of PET plastic waste

SN	Properties	Value
1	Tensile strength (MPa)	80–100
2	Strip length (mm)	100
3	Strip width (mm)	5
4	Strip thickness (mm)	0.13
5	Colour	White

**Fig. 2** PET Plastic water bottle strips



first evident from the compaction curve that dry density and water content decrease with increase in PET content which is directly related to the compaction needed on site. Generally due to inappropriate compaction on site, many times potholes occur in monsoon seasons. With the addition of PET, it directly reduces the compaction effort. Figure 4 shows the compaction curve for the aspect ratio 4. The same behaviour is also observed in aspect ratio 4. For the compaction parameters of PET strips with aspect ratio 2, value of OMC and MDD is first increasing and then decreasing after the PET content of 0.4%. The maximum increase is for the content of 0.4% in both the cases of aspect ratio. In case of aspect ratio 2, this increase is around 3%, and in case of aspect ratio 4, this value is 14%, which indicating the good increase in the compaction characteristics. Such behaviour is due to water absorption of clay and PET waste mixture. Figures 5 and 6 represent the comparison of OMC and MMD for the mix of aspect ratio 2 and 4. From this, it is clearly visible that the maximum dry density is also achieved at 0.4% but there is not much difference in the value. As the optimum density for the mix M2 is 1.65 gm/cm<sup>3</sup>, this value for the N2 is 1.67 gm/cm<sup>3</sup>.

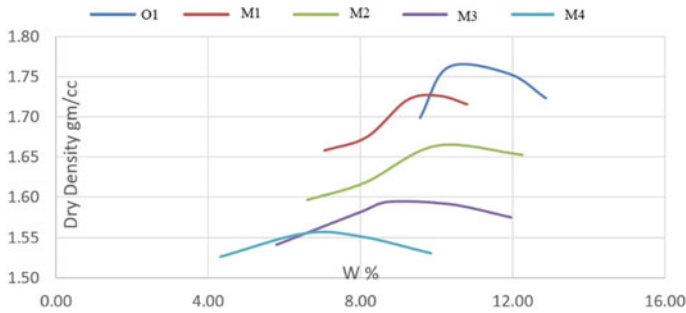


Fig. 3 Compaction curve for aspect ratio 2

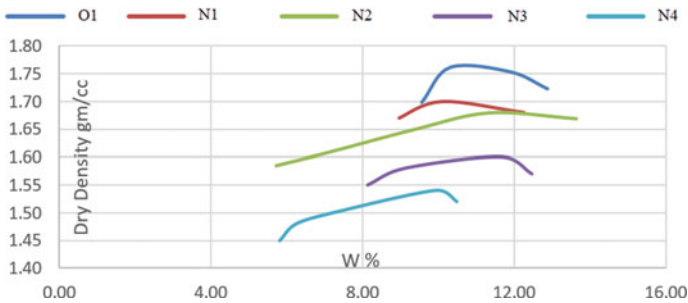


Fig. 4 Compaction curve for aspect ratio 4

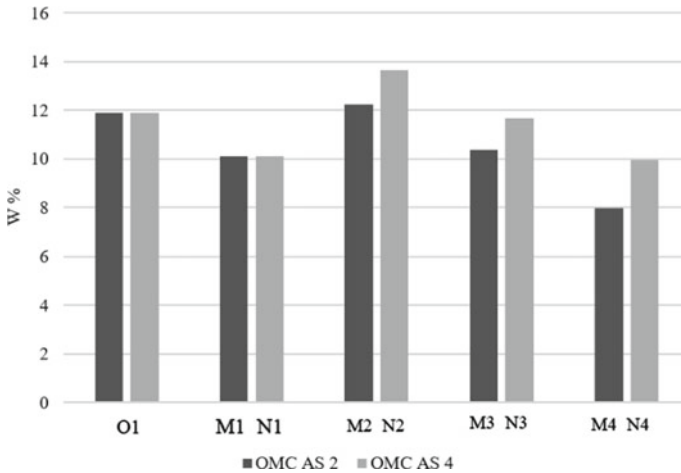
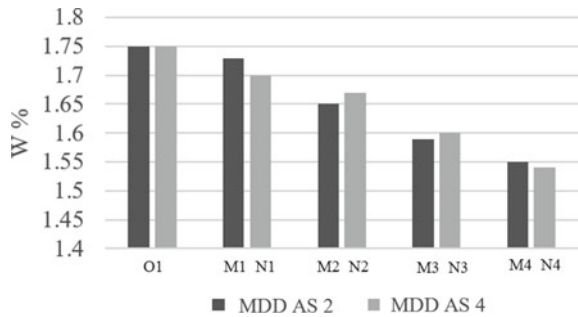


Fig. 5 OMC comparison

Fig. 6 MDD comparison



## 4 Conclusions

Following are the conclusions drawn from the study:

- From the compaction curve, it is evident that dry density and water content decrease with increase in PET content.
- Such behaviour is due to water absorption of clay and PET waste mixture and also the properties of plastic.
- Strips with aspect ratio 4 gives effective result for OMC and MDD with a 0.4% optimum dosage.
- Looking to the PET strips size and results of entire study, it is recommended to use strips of aspect ratio 2 and with 0.4% dosage.
- This systematic and detailed study tried to show the significant reuse of post-consumer water bottle creating litter of the same for the improvement of the properties of clayey soil.



**Acknowledgements** The author is very much grateful to the management of Nirma University for providing facility and financial support to carry out the research work.

## References

- Abbaspour M, Narani SS, Aflaki E, Nejad FM (2020) Behavior of a subgrade soil reinforced by waste tire textile fibers under static and cyclic loading. *J Mater Civ Eng* 32(8):04020208
- Abuel-Maaty AE (2010) Evaluation of characteristics of subgrade stabilized with random polypropylene short fiber. *J Eng Appl Sci* 57(3):167–183
- Abukhettala M, Fall M (2021) Geotechnical characterization of plastic waste materials in pavement subgrade applications. *Transp Geotech* 27:100472
- Acharyya R (2013) Improvement of undrained shear strength of clayey soil with pet bottle strips. In: *Proceeding of Indian geotechnical conference 2013*. Indian Institute of Technology, Roorkee
- Ahmad F, Bateni F, Azmi M (2010) Performance evaluation of silty sand reinforced with fibres. *Geotext Geomembr* 28(1):93–99
- Akinwumi II, Domo-Spiff AH, Salami A (2019) Marine plastic pollution and affordable housing challenge: shredded waste plastic stabilized soil for producing compressed earth bricks. *Case Stud Constr Mater* 11:e00241
- Ammar A, Najjar S, Sadek S (2019) Mechanics of the interface interaction between hemp fibers and compacted clay. *Int J Geomech* 19(4):04019015
- Babu GLS, Jaladurgam MER (2014) Strength and deformation characteristics of fly ash mixed with randomly distributed plastic waste. *J Mater Civ Eng* 26(12):04014093
- Bozyigit I, Bulbul F, Alp C, Altun S (2021) Effect of randomly distributed pet bottle strips on mechanical properties of cement stabilized kaolin clay. *Eng Sci Technol Int J* 24:1090–1101
- Choudhary AK, Jha JN, Gill KS (2012) Utilization of plastic wastes for improving the sub-grades in flexible pavements. In: *Paving materials and pavement analysis*, pp 320–326
- Consoli NC, Vendruscolo MA, Prietto PDM (2002) Behavior of plate load tests on soil layers improved with cement and fiber. *J Geotech Geoenviron Eng* 129(1):96–101
- Consoli NC, Heineck KS, Dal Toé Casagrande M, Coop MR (2007) Shear strength behavior of fiber-reinforced sand considering triaxial tests under distinct stress paths. *J Geotech Geoenviron Eng (ASCE)* 133(11):1466–1469
- Estabragh AR, Bordbar AT, Javadi AA (2011) Mechanical behavior of a clay soil reinforced with nylon fiber. *Geotech Geol Eng* 29:899–908
- Fatahi B, Khabbaz H, Fatahi B (2012) Mechanical characteristics of soft clay treated with fibre and cement. *Geosynth Int* 19(3):252–262
- Fathi H, Chenari RJ, Vafaiean M (2020) Shaking table study on PET strips-sand mixtures using laminar box modelling. *Geotech Geol Eng* 38(1):683–694
- Ibraim E, Diambra A, Wood DM, Russell AR (2010) Static liquefaction of fibre reinforced sand under monotonic loading. *Geotext Geomembr* 28(4):374–385
- IS 1498 (1970): classification and identification of soils for general engineering purposes
- IS 2720–7 (1980) Methods of test for soils. Part 7: determination of water content-dry density relation using light compaction
- IS 14534 (1998) Guidelines for recycling of plastics
- Jaber NH, Radhi MS, Alsaad AJ (2021) Ecological applications of polyethylene terephthalate plastic in producing modified subbase soil. *IOP Conf Ser: Mater Sci Eng* 1067:012006
- Kaniraj SR, Havanagi VG (2001) Behavior of cement stabilized fiber reinforced fly ash soil mixtures. *J Geotech Geoenviron Eng* 127(7):574–584
- Koohmishi M, Palassi M (2022) Mechanical properties of clayey soil reinforced with PET considering the influence of lime-stabilization. *Transp Geotech* 33:100726

- Ojuri OO, Osagie PO, Oluyemi-Ayibiowu BD et al (2022) Eco-friendly stabilization of highway lateritic soil with cow bone powder admixed lime and plastic granules reinforcement. *Cleaner Waste Syst* 2:100012
- Olgun M (2013) Effects of polypropylene fiber inclusion on the strength and volume change characteristics of cement-fly ash stabilized clay soil. *Geosynth Int* 20(4):263–275
- Santoni RL, Tingle JS, Webster SL (2001) Engineering properties of sand-fiber mixtures for road construction. *J Geotech Geoenviron Eng (ASCE)* 127(3):258–268
- Shah A, Modha H (2020) Improving the soil subgrade with plastic waste reinforcement—an experimental study. In: Shukla S, Barai S, Mehta A (eds) *Advances in sustainable construction materials and geotechnical engineering*. Lecture notes in civil engineering, vol 35. Springer, Singapore, pp 153–161
- Solanki Y, Jambudia M, Shah A (2021) Analysis and modification of engineering behavior of soil using plastic waste materials. In: Patel S, Solanki CH, Reddy KR, Shukla SK (eds) *Proceedings of the Indian geotechnical conference 2019*. Lecture notes in civil engineering, vol 136. Springer, Singapore, pp 661–669
- Tafreshi SNM, Omran MP, Rahimi M, Dawson A (2021) Experimental investigation of the behavior of soil reinforced with waste plastic bottles under cyclic loads. *Transp Geotech* 26:100455
- Wang Y-X, Guo P-P, Ren W-X, Yuan B-X, Yuan H-P, Zhao Y-L et al (2017) Laboratory investigation on strength characteristics of expansive soil treated with jute fiber reinforcement. *Int J Geomech* 17(11):04017101

# Use of XRD Technique in Characterising Different Types of Concrete



Diksha, Nirendra Dev, and Pradeep Kumar Goyal

**Abstract** This study investigates the researchers conducted on the microstructure of different types of concrete using the X-ray diffraction technique. Generally, the compressive strength, durability and other properties change due to the changes in the microstructure, and hence, a thorough study on the use of XRD technique were done. A detailed study of the XRD results and findings which are obtained by different researchers was done, and their results were analysed.

**Keywords** Concrete · X-ray diffraction · Compressive strength · Durability · Microstructure

## 1 Introduction

Concrete is a heterogeneous building material that is formed by combining cement, aggregate, and water (and occasionally admixtures) in a proportion that hardens and acquires strength with time on appropriate curing. Admixtures may sometimes be added to concrete as well. Cement undergoes hydration when water is added to it; this hydration results in the production of many phases as well as a change in the chemical make-up of the cement. Additionally, at the current time, researchers are conducting studies for the purpose of replacing traditional ingredients of concrete with industrial by-products and other waste products. This is being done with the goal of lowering both the cost and the amount of carbon emission. As a result of this, it is necessary to do research into the updated chemical composition of the concrete.

---

Diksha (✉) · N. Dev · P. K. Goyal  
Delhi Technological University, Rohini, New Delhi, Delhi, India  
e-mail: [sndiksha7@gmail.com](mailto:sndiksha7@gmail.com)

N. Dev  
e-mail: [nirendradev@dce.ac.in](mailto:nirendradev@dce.ac.in)

P. K. Goyal  
e-mail: [pradeepkgoyal@dce.ac.in](mailto:pradeepkgoyal@dce.ac.in)

Numerous techniques such as Fourier-transform infrared spectroscopy (FTIR), nuclear magnetic resonance (NMR), X-ray powder diffraction (XRD), X-ray fluorescence (XRF), scanning electron microscopy (SEM), differential scanning calorimetry (DSC), thermogravimetric analysis or thermal gravimetric analysis (TGA) are utilised today for the purpose of material characterisation analysis of the composition.

The X-ray diffraction, or XRD, technique is the most helpful of these approaches for determining the identity of crystalline substances that are unknown. The X-ray powder diffraction (XRD) technique is a non-destructive method for analysing the structure of materials, particularly on the atomic or molecular level. It works particularly well with crystalline or partly crystalline substances, although it may also be used to the research of non-crystalline substances. The analysis of crystalline materials' phase composition is the major use of XRD.

The premise of **Bragg's law**, which says that "the path difference between the scattered X-rays is an integral multiple of the wavelength", serves as the foundation for the X-ray diffraction (XRD) technique.

Mathematically,  $2d \sin \theta = n \lambda$ .

where  $d$  represents the interplanar spacing,  $n$  represents a positive integer,  $\theta$  represents the scattering angle and  $\lambda$  represents the de Broglie wavelength of the radiation.

The most conventional method of XRD is single-crystal X-ray diffraction.

During the process of single-crystal XRD, X-rays are sent through a crystal, while it is being held with a goniometer and rotated at various angles. This is done to obtain the scattered rays produced when the atoms of the sample act as a diffraction grating, which results in the appearance of some dark spots on a screen. It is possible to calculate the diffraction grating spacing by using these locations and the scattering angles. In this particular scenario, the grating spacing is identical to the atomic spacing.

Other methods, such as powder diffraction, fibre diffraction and small angle X-ray scattering in the event that the sample in question is amorphous, amongst others, may be used in situations in which it is not feasible to get a crystal of a suitable size (at least 0.1 mm).

In the case of powder XRD, the same method as that used for single-crystal XRD is used; however, in most cases, the powdered sample does not need to be rotated. Because it is presumed that the sample is organised in a random fashion, each particle will have a distinct plane of orientation towards the rays. As a result, rotation is not needed because it is not necessary that the sample be rotated.

Crystal phase identification, the acquisition of lattice parameters, the comprehension of phase transitions and the determination and refining of crystal structures are all areas in which the XRD is very helpful.

## 2 Literature Review

According to Deepty et al. (2019), X-ray diffractometry is an indispensable instrument for the speedy determination of minerals, compounds and other crystalline phases. This method is risk-free, non-blast-furnace destructive and quick for regular automated operation. It finds widespread use in the cement and construction industries for a variety of purposes, including the following:

- Mineralogical and phase analyses of raw materials, completed products and waste products, as well as the by-products of industrial processes,
- Research on the combustibility of cement raw mixtures,
- Polymorphism of clinker phases, as well as the identification of clinker mineral phases and semi-quantitative estimations of those phases,
- The identification of undesirable phases in clinker, such as free lime, periclase and quartz amongst others,
- The composition of cement and the presence of impurities in cement,
- Diagnostic investigations on the factors that lead to scaling and build-ups in cement rotary kilns, coating in cement silos, the factors that lead to the failure of refractory lining, unstable kiln coating, ring formation and kiln shell corrosion,
- Research on the hydration of cement and investigations of a concrete building that has been damaged.

Dhapekar et al. (2015) in this paper, X-ray diffraction (XRD), which is a tried and true method for determining the phase composition of concrete, was used in the authors' experimental research of powder ordinary cement concrete samples, which was presented in their publication. The article was named "Study of Phase Composition of Ordinary Portland Cement Concrete Using X-Ray Diffraction", and it was published in the journal *Cement and Concrete Research* (Ogawa et al. 2011). This research was given the title "Study of Phase Composition of Ordinary Portland Cement Concrete Using X-Ray Diffraction", and it was presented in the publication known as *Cement and Concrete Research*. A laboratory X-ray diffractometer was needed in order to carry out the method in order to perform an XRD study on concrete samples. Through the use of diffraction analysis, it was revealed that the potential cement content in aged traditional hydraulic cement concrete may be increased. Compilation and examination of the results of this inquiry have been completed. They arrived at the conclusion that this approach has the potential to be used in lieu of the traditional analysis of cured concrete, which is a laborious process that takes a considerable amount of time to complete. Throughout the course of this article, an attempt has been made to quantify the phases that are present in conventional Portland cement concrete. This attempt is presented here. This endeavour is going to be brought to a close right now.

Roren et al. (2021) "Controlled Sample Environment for Studying Solid-Gas Interactions by in Situ Powder X-ray Diffraction", ("Controlled Sample Environment for Studying Solid-Gas Interactions") (Kus and Carlsson 2003). In order to undertake X-ray diffraction research, a sample cell with temperature and pressure

control mechanisms is designed. The sample offered consists of a powder. Using the copper plate that is connected to the cell, the temperature may be altered to any value between  $-30$  and  $200^{\circ}\text{C}$ . Using Peltier elements, heat cartridges and a circulating bath chilled by refrigeration, it is feasible to achieve this objective. Throughout the process of constructing a small/wide-angle X-ray diffractometer suited exactly to the client's specifications, different commissioning tests were conducted. This system may be transferred to synchrotron facilities without any difficulty or difficulties.

Dhapekar and Chopkar (2016) in their study "Structural Health Monitoring of Ordinary Portland Cement Concrete Structures Using X-Ray Diffraction" (Narayanan and Ramamurthy 2000) discovered that monitoring the structural health of structures made of ordinary Portland cement concrete has a considerable interest in the life and safety problems it raise. This approach of monitoring the health of structures by utilising XRD has been recognised as a viable alternative to a wide variety of instrumentation methods. This recognition came about as a result of the fact that this method utilises XRD. During the course of this investigation, obtaining reliable data on the phase composition and compressive strength of a cement concrete structure was made entirely possible by making use of a cutting-edge software programme. This was a perfectly doable feat concrete structure (Fig. 1).

The advantages of the method include:

The ease with which samples may be prepared; the ability to determine structures "in situ"; the speed with which measurements can be made; and the capacity to examine mixed phases, such as soil samples.

**Fig. 1** Rigaku's XuLAB X-ray diffraction instrument



### 3 Methodology

One of these three loading methods—front loading, rear loading or side loading—can be used in the preparation of the sample. The front-loading technique, in which the powder is squeezed by a glass slide or by roughening the sample with an emery paper, is the way that is used the vast majority of the time among these techniques. It is acceptable for the mean particle size to be less than 5  $\mu\text{m}$ , and 1–3  $\mu\text{m}$  is the ideal size range.

An X-ray diffractometer is a piece of equipment that is comprised of three primary elements: an X-ray tube, a sample container and an X-ray detector. These elements work together to form the device.

Following their collimation, the X-rays that have been generated will then have their attention focused on the specimen. The intensity of the X-rays that have been reflected is measured and recorded after the sample and the detector have both been spun. This occurs after the rotation of the sample. The Bragg equation must be satisfied for constructive interference to take place, and this is accomplished when the geometry of the X-rays that are incident on the sample. As a direct consequence of this, the intensity reaches its maximum level. A detector captures and processes this X-ray energy. In addition, the detector turns the signal into a count rate, which is then sent to an output device such as a printer or a computer display for further processing. In this method, the presence of a particular crystal may be confirmed by comparing the produced peaks to a standard dataset that is comprised of the peaks of different kinds of crystals.

The geometry of the X-ray diffractometer is designed in such a way that the sample rotates at an angle  $\theta$  in the path of the collimated X-ray beam, while the X-ray detector rotates at an angle  $2\theta$  mounted on the arm to collect the diffracted X-rays. This allows for the maximum amount of information to be gleaned from the experiment. This makes it possible to get a more precise measurement of the diffraction pattern of the material. A goniometer is an instrument that rotates a sample while preserving the original angle at which it was obtained. This may be accomplished by using the goniometer.

Types of grinding the sample for XRD.

#### (a) Hand Grinding

The conventional approach to the preparation of powdered XRD samples is using a mortar and pestle to grind the samples by hand. The mortar and pestle may be made from a variety of stones such as agate, corundum or mullite. Other options include jasper and onyx. The relative hardness of the sample to that of the mortar and pestle as well as the question of whether or not the contamination, i.e. introduced by the grinding medium, will have an influence on how information is interpreted in the future will both play a role in determining the type of material that is used. The majority of the time, samples are ground under a liquid medium like ethanol or methanol in order to reduce the amount of sample that is lost during the grinding process and to reduce the amount of structural damage that

may be caused to the phases in a sample as a result of grinding. This is done for both of these reasons. The grinding of samples may be a lengthy and physically demanding operation, especially if the sample is very hard or has other physical traits that make it difficult to grind. In this case, the grinding of the sample might be particularly challenging. This is particularly true in circumstances in which the sample is of an unusually difficult kind.

#### (b) **Mechanical Grinding**

As was said before, while it is possible to physically grind a sample down to one micrometre, the operation is very lengthy and difficult. Because of its capacity to reduce the material to grain sizes approaching 1  $\mu\text{m}$ , mechanical grinders are a good choice for quantitative XRD research. This ability allows for more accurate results. Shatter boxes and ball mills are two technologies that may be used for this purpose; however, the end effect of using any of these procedures is a very broad range of particle sizes. McCrone Mills is capable of accomplishing the most effective means of creating both very fine grain sizes as well as size distributions that are extremely narrow. In order to aid the cutting back of the lattice stain during the milling process, a liquid media such as ethanol is employed as a medium. The use of this method has a couple of drawbacks, the first of which is that it can only handle a very small number of samples at once, and the second is that there is always a very little amount of contamination (<1 Wt.%).

## **4 Applications**

### **4.1 Autoclaved Aerated Concrete**

#### **4.1.1 To Characterize Tobermorite When Extra Al<sup>1</sup> is Added in AAC<sup>2</sup> (Ogawa et al. 2011)**

XRD using analysis study was done into the hydrothermal process that results in the formation of tobermorite during the manufacturing of aerated concrete. This process leads to the formation of tobermorite. As a starting point for the investigation into the effects of silica source, less reactive quartz obtained from quartz and reactive quartz derived from chart were both employed.

Figure 2, in each and every research, it was found that the compounds C-S-H, katoite and hydroxyllellstadite were all intermediates in the process. It was shown that the incorporation of Al sped up the process of producing tobermorite, as this was seen. There was no discernible change in the rate at which quartz dissolved in the solution as a result of the addition of Al. In the system that also included aluminium,

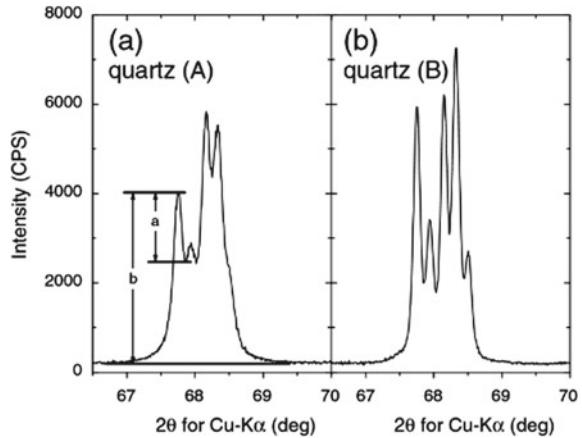
---

<sup>1</sup> Al: aluminium.

<sup>2</sup> AAC: autoclaved aerated concrete.



**Fig. 2** XRD patterns for quartz A and B



two distinct routes, namely the C-S-H route and the katoite route, were found to be present. According to the results, it is essential for the subsequent steps that lead to the synthesis of tobermorite to maintain the structure of the C-S-H that was first formed.

#### **4.1.2 To Investigate the Transformation of Tobermorite Using XRD Due to Changes in Weathering Conditions of Autoclaved Aerated Concrete (Kus and Carlsson 2003)**

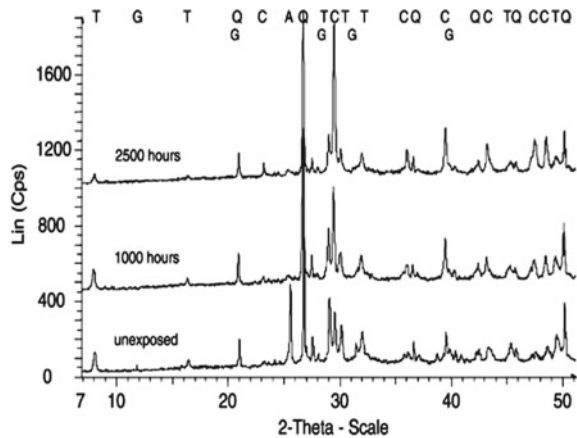
After being exposed to two very different sorts of settings, both natural and artificial, the concrete samples were analysed to see how well they held up. XRD signals (Fig. 3) showed that over the course of time, tobermorite experienced a gradual change into calcium carbonate. This transformation took place in tobermorite. The formation of calcite and gypsum are the two basic types of crystals that occur as a result of the process of weathering.

XRD was unable to determine the presence of gypsum in aged samples, despite the fact that SEM and EDS investigations were able to identify its presence. However, after thirty-six months of natural exposure, XRD analysis showed strong peaks, indicating the existence of gypsum in the sample.

Several reasons for XRD unable to detect gypsum were given as:

The peaks were relatively weak, which made it difficult to establish that gypsum was present in AAC owing to the fact that the amount of gypsum, i.e. typically present, is typically fairly low. As a result of this, it was difficult to demonstrate that gypsum was present in AAC. During the process of artificial weathering, the gypsum initially recrystallised and then proceeded to build brittle layers, which produced an envelope over the air voids. As a result, there is a chance that the powdered sample that was analysed did not include any of these recrystallised layers. There was some

**Fig. 3** XRD patterns of artificially weathered AAC [tobermorite (T), quartz (Q), calcite (C), anhydrite (A), and gypsum (G)]



overlap between the peaks of calcite, quartz and tobermorite and a few of the gypsum peaks.

The sensitivity of XRD towards detection of gypsum is low.

XRD patterns demonstrated the decreased concentration of tobermorite but increased the concentration of calcite with exposure time.

#### 4.1.3 Microstructural Investigations on Aerated Concrete Using XRD When Fly Ash is Used as Filler (Narayanan and Ramamurthy 2000)

As the filler, the AAC samples that were cast either include sand or fly ash. A study was carried out in which a comparison of the two samples' microstructural composition was carried out. In contrast to the wet-cured samples, the AAC samples that included sand revealed (Fig. 4) the presence of tobermorite, which is a C-S-H gel, as well as  $\text{Ca}(\text{OH})_2$  crystals that had a hexagonal shape. These findings contradict with the findings of the wet-cured samples. It was found that the AAC samples that included fly ash did not have full crystallinity; nonetheless, there were observations of needles and plates of ettringite as well as  $\text{Ca}(\text{OH})_2$ .

The sample of AAC fly ash gained some crystallinity after being autoclaved for a period of twelve hours. The interlocking was damaged as a direct consequence of the scattered way in which these crystals were positioned, which led to a loss of structural integrity. In light of this fact, the AAC manufactured with fly ash exhibited a higher drying shrinkage in comparison with the AAC manufactured using sand as the filler.

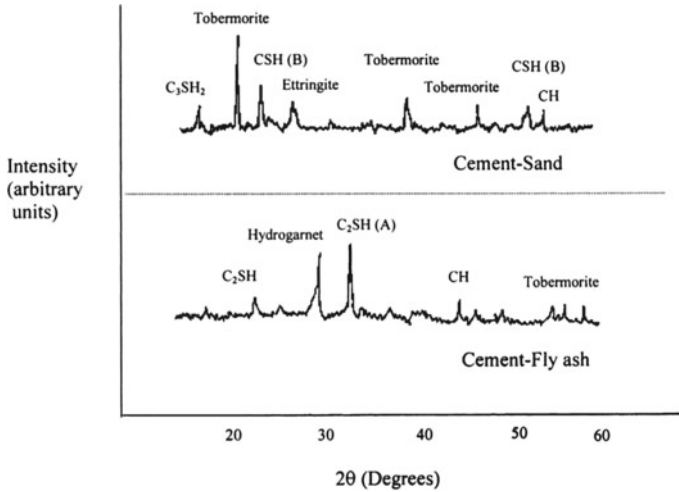


Fig. 4 XRD patterns of AAC

**4.1.4 Investigation of the Influence of Carbonation Depth on the Microstructure of MgO Cement and PC Mixes (Pu and Unluer 2016)**

Here, M10H represents 10% MgO content and 0% cement, while P10H represents 10% cement content and 0% MgO content.

The following results were found for M10H samples after one day curing:

It has been established that HMC is present (Fig. 5). It was calculated that the presence of aggregates in high quantities, comprising over 90% of the whole mix by weight, was the cause for low intensities of these HMCs in each sample. This was determined by analysing the data. There was some overlap between the peaks of the HMCs and the peaks of the quartz. It was discovered that the intensities of HMC peaks decreased as the depth of the sample increased. This was one of the findings. There was a peak of magnesium oxide present as a result of inadequate hydration, and the presence of brucite suggested that carbonation was also incomplete.

After a period of 14 days of curing, the following findings were discovered for M10H samples: (Fig. 6) a greater boost in strength may be attributed to the higher HMC concentration that was found in M10H. After 14 days, there was no longer any brucite peak, which showed that the carbonation process had been completed. In the meanwhile, the XRD data showed the presence of MgO that had not been hydrated, indicating that hydration had not been completed.

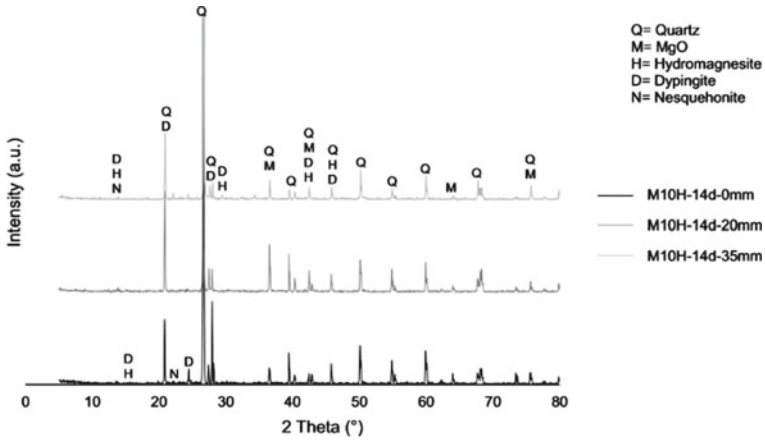


Fig. 5 XRD patterns of M10H samples after 1 day of curing

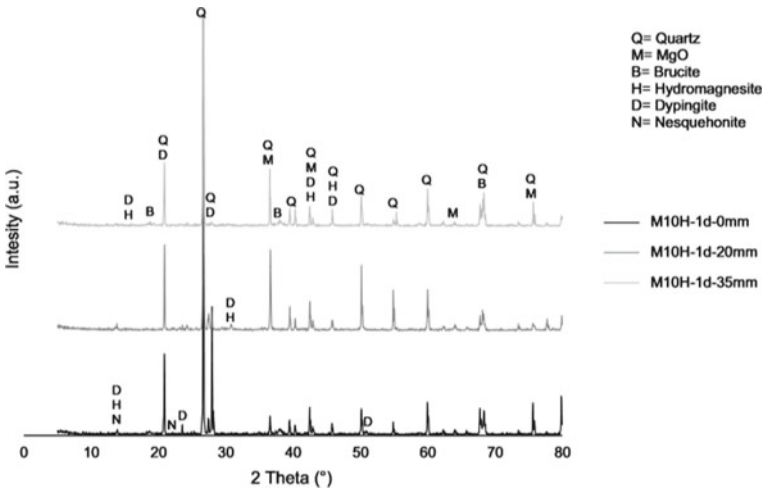


Fig. 6 XRD patterns of M10H samples after 14 days of curing

### 4.1.5 To Understand the Carbonation Process of Brucite by Introducing Seeds (Dung and Unluer 2018)

Figure 7 displays the XRD patterns that were produced by all of the samples after carbonation over a period of 14 days. The carbonation process was shown to result in the development of a variety of HMC phases in all of the samples. In addition to HMCs, the presence of unhydrated MgO and uncarbonated brucite (central peak at 38.1° 2θ) was seen in all of the samples, regardless of whether they included HA (hydration agent) and seeds or not.

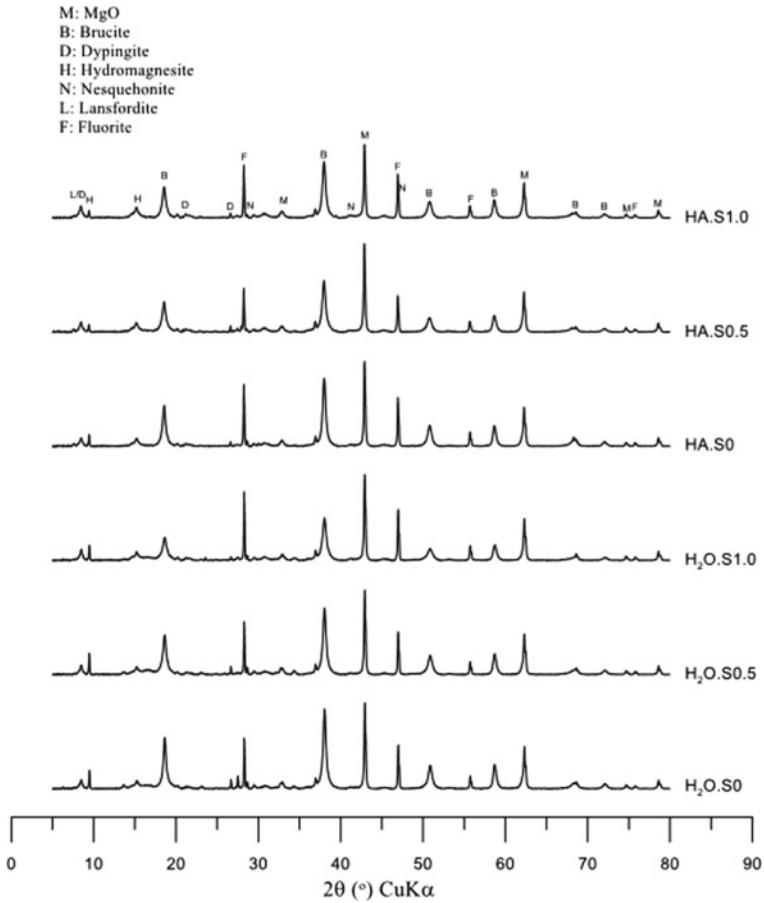
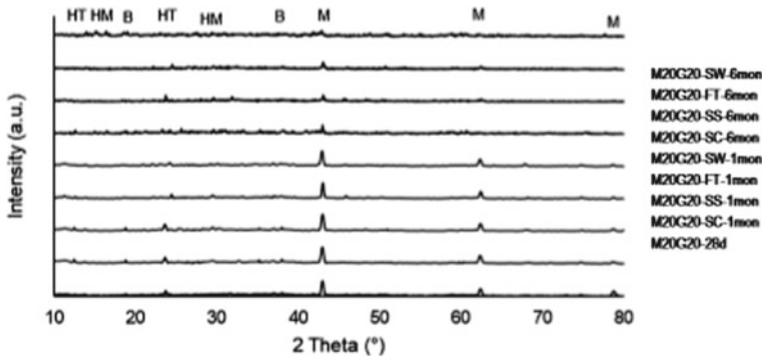


Fig. 7 XRD pattern of all the samples after 14 days of carbonation

Brucite was able to develop not only on the surface of the MgO grains but also on the seed surfaces as a result of the spread of nucleation seeds (Hubler et al. 2011) in the pore space, which led to an increase in the quantity of brucite’s reactive surface area that was accessible for carbonation. Although the introduction of seeds sped up the nucleation process in the HA samples, this did not result in an increase in the surface area of the bulk brucite that was open to carbonation. Instead, this made it possible to achieve a higher level of carbonation efficiency. As a result of this, seeds did not play a significant role in lowering the uncarbonated brucite contents of HA.S0.5 and HA.S1.0, which resulted in values that were comparable to those of HA.S0 (in HA.S0.5, 0.5 denotes the seed % of the sample). This was the case because seeds did not have an effect on the amount of brucite that was carbonated.



**Fig. 8** XRD patterns of different samples M: MgO, B: brucite, HM: hydromagnesite, HT: hydrocalcite, Mu: mullite, Q: quartz

#### 4.1.6 To Study the Influence of Fly Ash and GGBS Addition on the Durability of MgO Cement Concrete (Pu and Unluer 2018)

Figure 8 indicated that its hydration was incomplete due to the presence of a peak for magnesium oxide (MgO), and the presence of peaks for brucite and carbonate (brucite and brucite peaks) suggested that its carbonation was also incomplete. The intensities of the brucite peaks were lower than those that were detected in the M40 samples. This was the case because the concentration of MgO was lower, and the hydration process was slower due to the presence of FA/GGBS. This occurred because of the lower size of the brucite crystals, which was tied to the previous point.

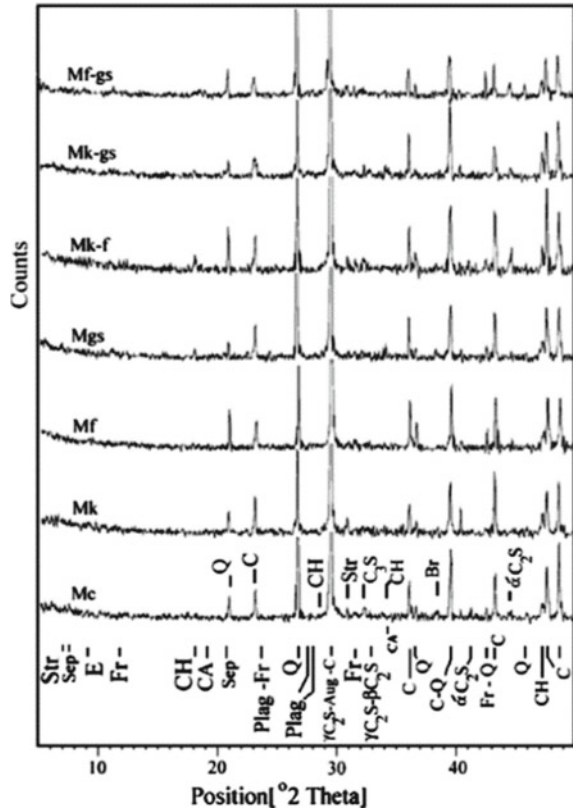
## 4.2 Marine Concrete

### 4.2.1 Influence of Seawater on the Amount of CH<sup>3</sup> Formation on the Concrete Used in Marine Structures (Seleem et al. 2010)

The diffraction patterns of the samples that were taken from the core (the inner) of the specimens after they had been exposed to artificial saltwater for a period of one year are shown in Fig. 9. The decrease in CH may now be seen, which was not the case before to exposure. There is a modest increase in the amount of the produced cementing phases (C2S and C3S). The mineral known as brucite, which is magnesium hydroxide, has been identified in the control mixture. The analysis of the diffractograms of the various mixes indicated that CH virtually completely vanished from all of the mixtures, with the exception of the ones that included GGBS. Friedel's salt, which is represented by the formula  $C_3ACaC_{12}.10H_2O$ , was also generated in almost all of the mixes. The findings of the XRD show that pozzolans are effective

<sup>3</sup> CH: calcium hydroxide.

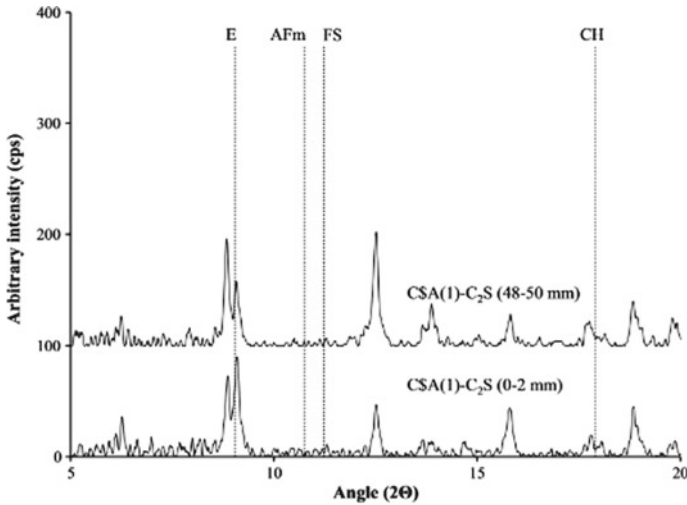
**Fig. 9** XRD patterns of concrete mixtures after 1 year of exposure to seawater



at consuming free lime, which is a primary cause of instability, and also at forming stable favourable compounds.

**4.2.2 Formation of Friedal Salt in Concrete in an Aggressive Marine Environment (Moffatt and Thomas 2017)**

The capacity of these systems to bind externally applied chlorides was shown by XRD analysis (Fig. 10), which was performed on CA(2)-PC, HEPC and PC. This ability was a direct outcome of the creation of Friedel’s salt within millimetres of the exposed surface of the material. Even though C\$A(1)-C2S was unable to bind chlorides, the creation of Friedel’s salt is believed to have been caused by the presence of 70% PC in the binary C\$A(2)-PC system. Friedel’s salt was also produced as a by-product of the reaction that led to the creation of HEPC and PC.



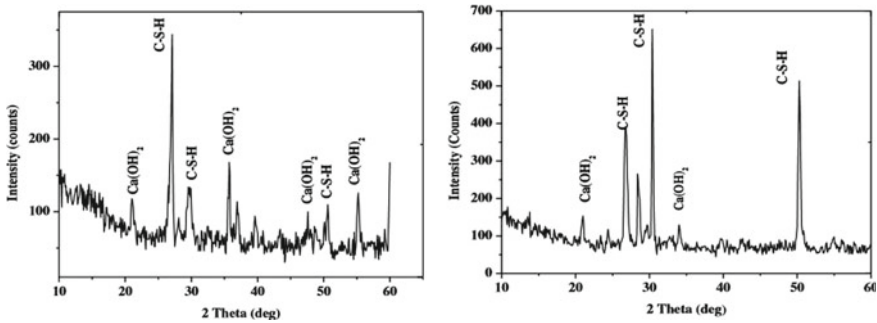
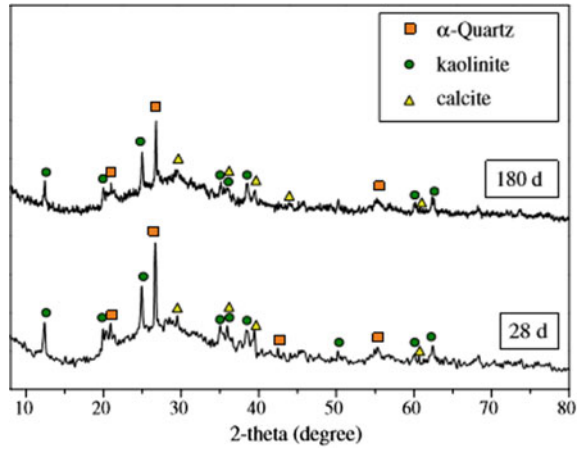
**Fig. 10** XRD pattern of CSA(1)-C<sub>2</sub>S relative to depth; E: ettringite, FS: friedals salt and C: calcite

#### 4.2.3 Influence of Using Geopolymers as Protection Coatings on the Rate of Carbonation in Marine Concrete (Zhang et al. 2012)

Calcite was present in both the 28 day and 180 day products, as shown in Fig. 11. On the other hand, sulphate was not discovered; this might be because the amount was lower than the threshold for detection set by the XRD. Although the magnesium and sulphate ions were seen in the fly-ash-based geopolymer matrix when the specimens were submerged in saltwater, these ions do not seem to have any significant impact on the mechanical strength of the material. It has been observed that alkali-activated slag/metakaolin blends have quicker carbonation when more metakaolin has been employed, and the amount of slag that is utilised in this system makes up 12 weight percent of the total solid content. In exchange for this, a negligibly small quantity of calcite silicate hydrates C-S-H was produced.



**Fig. 11** XRD patterns of the geopolymer coating on samples at ages of 28 d and 180 d



**Fig. 12** XRD analysis of M1 and M3 mix at 28 d

### 4.3 Self-Compacting Concrete

#### 4.3.1 Impact of Blending MK<sup>4</sup> with SCC<sup>5</sup> (Kavitha et al. 2015)

Based on the results of the XRD study (Fig. 12), the primary compounds that were found were C-S-H and CH. It was clear that the inclusion of MK raises the strength of the C-S-H peaks while simultaneously lowering the intensity of the CH peaks. In comparison with the control SCC mix, the C-S-H concentration in the MK blended SCC was much higher. Through a process known as pore size refinement, the creation of C-S-H was successful in filling the capillary pores, which resulted in a reduction in permeability.

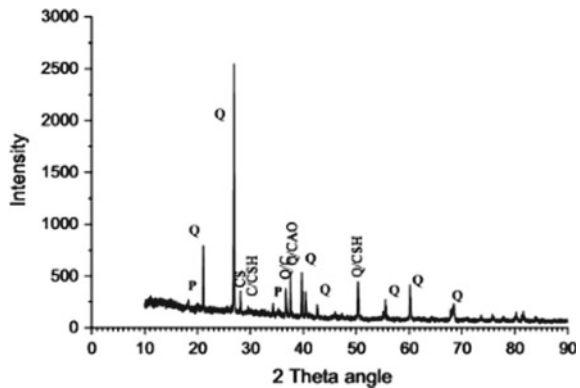
<sup>4</sup> MK: metakaolin.

<sup>5</sup> SCC: self compacting concrete.

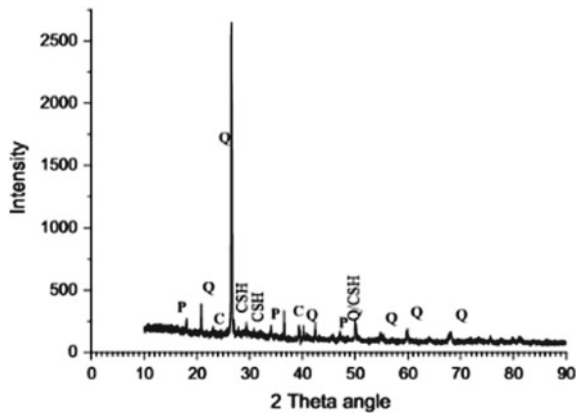
### 4.3.2 Studying the Phase Transition When SCC is Made with Iron Slag as a Replacement of Fine Aggregates (Singh and Siddique 2016)

At the age of 28 days, X-ray diffraction was used to do an analysis on the SCC control combination that did not include any iron slag as well as the SCC that had 40% iron slag. Quartz, calcium silicate hydrates, calcium hydroxide, calcium silicates and calcite have all been identified by XRD as being present in the sample (see Fig. 13). The overlapping of diffraction peaks was one of the most significant challenges that arose during the qualitative investigation of each and every SCC combination. The XRD results for all of the mixes demonstrated that there was not a qualitative shift in the phases that were present (Fig. 14).

**Fig. 13** XRD spectra of SCC control mix (P: calcium hydroxide, CSH: calcium silicate hydrates, Q: Quartz, CS: calcium silicates, CAO: calcium oxide)



**Fig. 14** XRD spectra of SCC mix with 40% iron slag



### 4.3.3 Influence of CSH Gel on the Strength of SCC Blended with Rice Husk Ash (Chopra et al. 2015)

At the age of 28 days, the XRD pattern and analysis (Fig. 15) of both the reference mix and the RHA mixes were carried out on the concrete mixtures. Analyses using XRD and SEM showed that there was an increase in the production of a CSH gel for all mixtures, which helps to explain the improved compressive strength of the concrete that included 15% RHA. The control mixture had a greater number of pores and cracks in comparison with the other mixture. It was found that 15% RHA substitution produced the most dense structure, which in turn led to the best possible compressive strength for the mix.

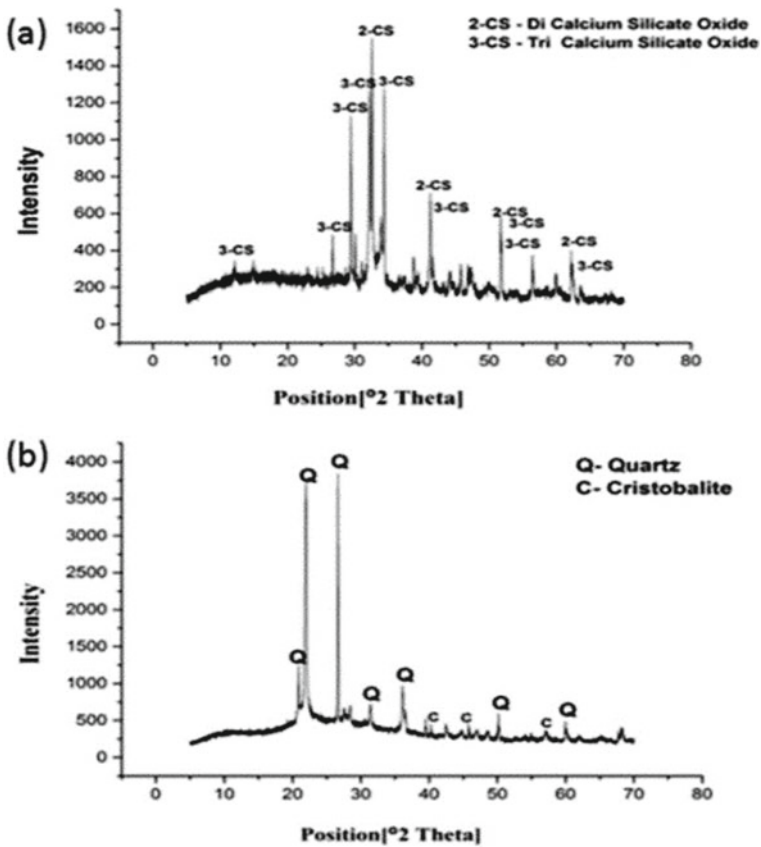


Fig. 15 XRD pattern of a OPC b rice husk ash

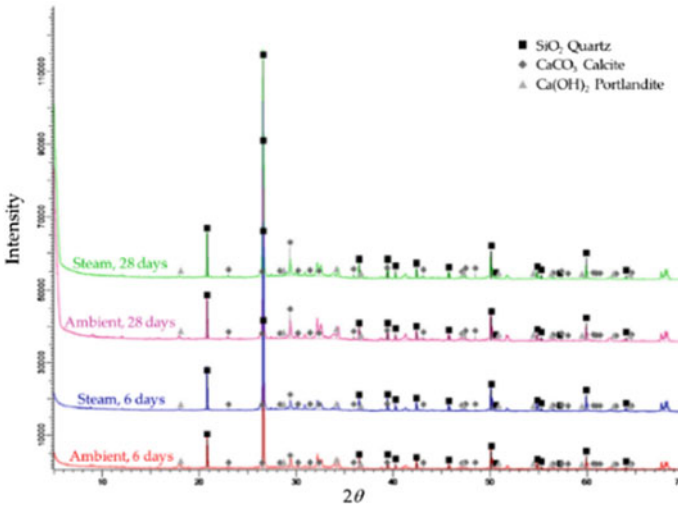


Fig. 16 XRD pattern of FRC cured at different temperatures

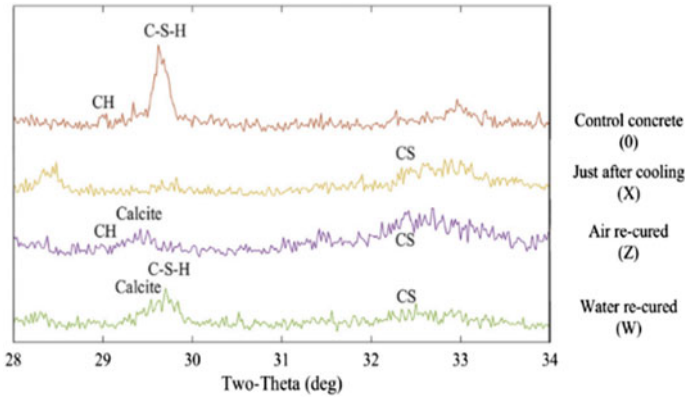
## 4.4 Fibre-Reinforced Concrete

### 4.4.1 To Study the Effect of Heat Curing on the CSH and Portlandite Formation in FRC (Yoo et al. 2018)

The amount of portlandite,  $\text{Ca}(\text{OH})_2$ , was much lower in the samples that were steam-cured as compared to those that were cured in an ambient environment (Fig. 16). This is because, as a result of the acceleration of the pozzolanic reaction that occurred during heat curing, a significant portion of the portlandite was consumed and transformed to high levels of strong C-S-H at an early age. This is the root cause of the problem. After 6 days, the samples that were cured with steam had a larger amount of C-S-H than the samples that were cured in an ambient environment, which led to the steam-cured samples having a higher strength. After the completion of the heat curing process, however, there was only a little variation in the amount of the portlandite that was discovered in the samples that were steam cured. This suggests that the pozzolanic reaction was very close to finishing up while the heat curing procedure was taking place.

### 4.4.2 To Study the Quantitative Behaviour of the CS Content by Heat Curing and Re-Curing in the Air (Akca and Özyurt 2018)

According to the findings shown in Fig. 17 of the XRD analysis, the mineral  $\text{CaCO}_3$  (calcite) was not present in the sample of freshly cooled concrete that was analysed, but it was discovered in samples that were re-cured with either water or air. The



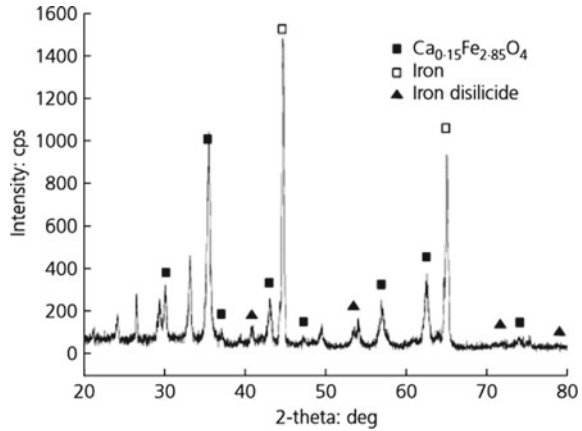
**Fig. 17** XRD analyses conducted on the samples taken from the surface of concretes (CAP)

results of the XRD and SEM investigations were compatible with one another and revealed that the content of C-S-H and  $\text{CaCO}_3$  (XRD) in concrete rose after water re-curing, but the content of  $\text{CaCO}_3$  and  $\text{CaOH}_2$  (slightly) in concrete increased after air re-curing. In addition to this, the content of CS (both C2S and C3S) rose after being heated, and this trend maintained throughout the process of air re-curing. In addition to this, the quantity of CS that was present reduced because the C-S-H gel was regenerated while the substance was being re-cured in water.

**4.4.3 To Reveal the Composition of the White Layer and Its Effect on the Strength of FRC (Yan et al. 2013)**

According to an X-ray diffraction (XRD) investigation, the primary components of the white layer are shown in Fig. 18. These components include iron di-silicide and C-S-H iron. The dense-clustered C-S-H phase, also known as the transition zone, forms linkages with the white composite layer to produce the weave shape and to keep the surface layer of the steel fibre in place. At high temperatures, the nano-silica fine particles fill the area between the transition zone to form or replicate new C-S-H gel. This takes place because the particles are so small. The transition zone is strengthened, and its adherence to the surface of the steel fibre is improved because to the intimate connection that exists between the clustered C-S-H phase and the white composite layer.

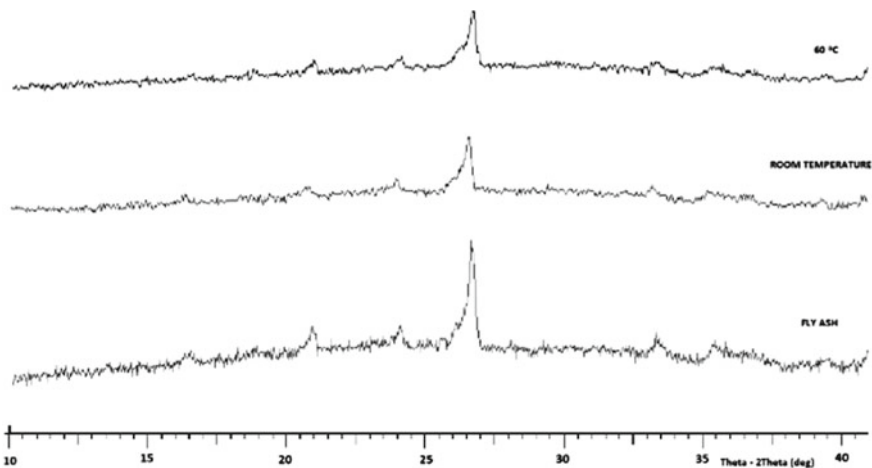
**Fig. 18** XRD pattern of the permeable diffusion layer in the steel fibre surface at 400°C



### 4.5 Geopolymer Concrete

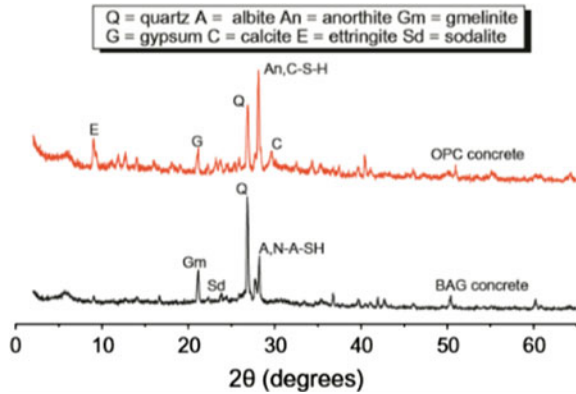
#### 4.5.1 To Study the Geopolymerisation Reaction When a Foaming Agent is Used (Abdullah et al. 2012)

Figure 19 shows the foamed geopolymer concrete, which consisted mostly of amorphous content. The crystalline phases that existed in the fly ash originally (quartz and mullite) have not been altered by the activation reactions in the hardened geopolymer. The broad hump registered between  $2\theta = 20$  and  $30^\circ\text{C}$  indicated the presence of an amorphous phase in the fly ash.



**Fig. 19** XRD pattern of class C fly ash, foamed geopolymer concrete at different temperatures

**Fig. 20** XRD data for OPC and BAG concretes after sulphuric acid exposure



The foamed geopolymer concrete can be seen in Fig. 19, and it is composed almost entirely of amorphous material. The activation events that took place in the hardened geopolymer did not have any effect on the crystalline phases that were initially present in the fly ash. These phases included quartz and mullite. The existence of an amorphous phase in the fly ash was suggested by the presence of a wide hump that was observed between  $2\theta = 20$  and  $30^\circ\text{C}$ . In addition, the large hump that appeared between  $2\theta = 20$  and  $40^\circ\text{C}$  pointed to the presence of amorphous geopolymer gels and C-S-H gels. This demonstrates that the geopolymer reaction and the hydrate reaction took place simultaneously.

#### 4.5.2 Detection of NASH<sup>6</sup> Type Gels in Geopolymer Blended with Fly Ash (Ariffin et al. 2013)

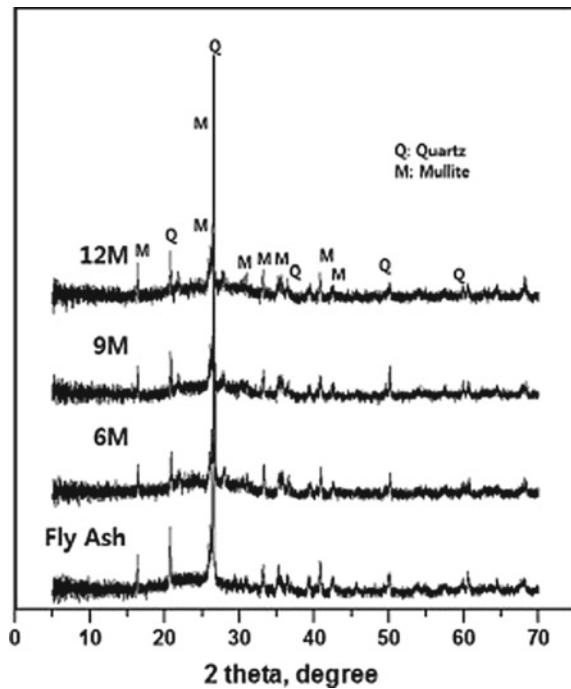
Figure 20 displays the XRD patterns that were produced by the OPC and BAG concrete after being exposed to sulphuric acid for a period of 18 months. The BAG concrete samples still had the primary phases that had been discovered in earlier investigations. On the other hand, gypsum was produced, most likely as a consequence of reactions involving ambient  $\text{CO}_2$ ; nonetheless, there was no ettringite found in geopolymer, which is consistent with the low Ca/Si ratio of these systems. It was anticipated that the Al would take part in the creation of gels of the N–A–S–H type, making it less accessible for the synthesis of ettringite than it would be in Portland cement.

<sup>6</sup> NASH gel: Sodium aluminosilicate hydrate gel.

### 4.5.3 Influence of the Number of Crystals on the Compressive Strength of Geopolymer Concrete (Ryu et al. 2013)

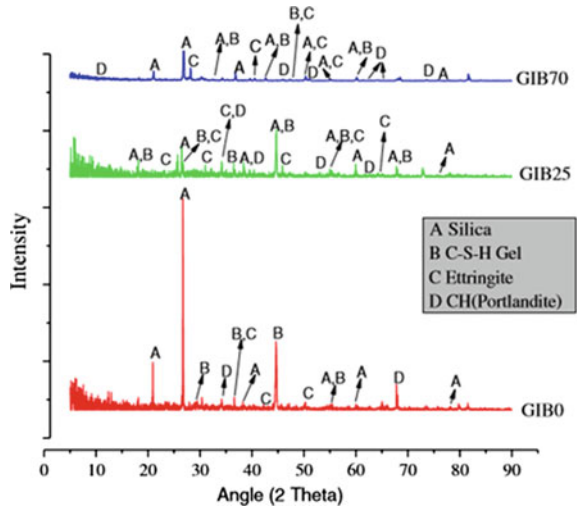
The findings of the XRD examination that were performed on the specimens after 28 days are shown in Fig. 21 according to the molarity of NaOH. The specimens were created using a paste that was based on fly ash, and they were cured for a period of 24 h at a temperature of 60°C. Polymerisation achieved by the alkali-activation method resulted in the production of alumina-silicate compounds with an amorphous structure as the primary products. In the crystalline phase, the findings of the study show that there are several peaks of mullite ( $3\text{Al}_2\text{O}_3\text{SiO}_2$ ) and quartz ( $\text{SiO}_2$ ). The impact that the fly ash components had on the situation may be attributed for this result. In addition, a larger molarity may be associated with a stronger intensity at a temperature of 27°C. It was discovered that the number of crystals grows with increasing compressive strengths.

**Fig. 21** XRD pattern of geopolymer concrete for different values of molarity





**Fig. 22** XRD analyses of control mix and GIB25



### 4.6 Ordinary Portland Cement and Miscellaneous Concretes

#### 4.6.1 Investigating the Effect of Using Granite Industry By-Product in Concrete (Singh et al. 2017)

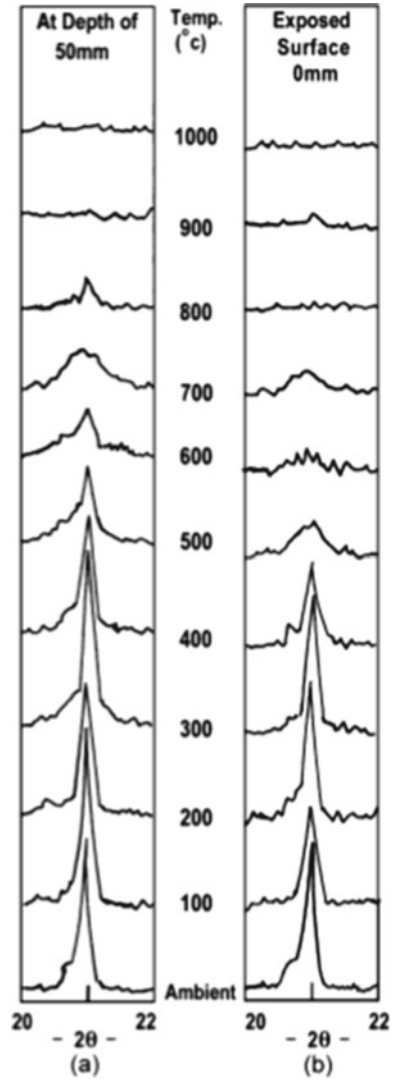
The best compressive strength and the highest packing density of the concrete matrix may both be attributed to the optimal presence of silica and C-S-H gel, as shown by the findings of the XRD analysis (Fig. 22). The thick packing of the concrete that GIB concrete produces is directly attributable to the size and form of the GIB, which is one of the primary reasons why GIB concrete produces such positive outcomes. In addition, the micro-filler activity of the replacement material, which was granite fines, combined with the optimal hydration of cement particles led to GIB concrete with strong compressive and flexural strengths.

#### 4.6.2 Effect of High Temperature on the CH Crystals and CSH Gel (Handoo et al. 2002)

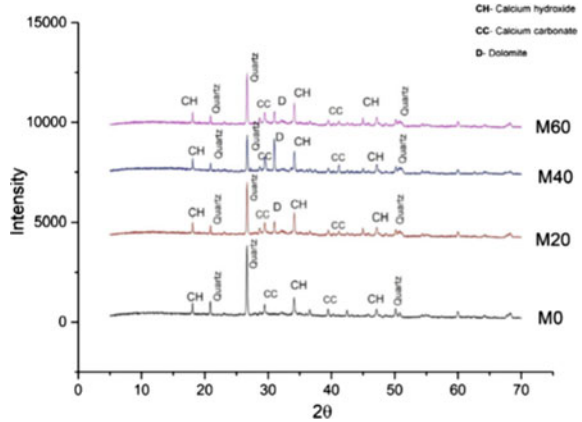
Morphological investigations show that well-developed calcium hydroxide crystals and C-S-H gel undergo evident deformation at temperatures over 600°C. Figure 23 illustrates how there is a slow decline in the amount of Ca(OH)<sub>2</sub> present as the temperature rises, which indicates that the quality of the concrete is gradually becoming worse. As can be seen in the image, there is a difference in the concentration of Ca(OH)<sub>2</sub> that exists at the surface and in the centre of concrete samples that have been subjected to a higher temperature. It was discovered that the fluctuation in intensities of diffraction lines with a wavelength of 4.90 Å was more prevalent in the surface sample than it was in the core sample. Negligible carbonation at the

exposed surface owing to atmospheric CO<sub>2</sub> is indicated by a diffraction line with an essentially same intensity ( $d = 3.03 \text{ \AA}$ ) when measured at the temperature of the surrounding air.

**Fig. 23** XRD pattern of the samples fired at different temperatures **a** core **b** surface



**Fig. 24** XRD spectrum of various mixes at 28 days of casting



**4.6.3 To Investigate the Presence of Unreactive Dolomite in Concrete Having Aggregates Replaced with Waste Marble (Vardhan et al. 2019)**

The XRD spectra in Fig. 24 show that the principal phases that are generated by any mix are the same as those created by any other mix. In addition, an extra peak of dolomite is seen in mixtures that include waste marble, followed by a drop in the peak of quartz. This suggests that there is unreacted dolomite in the mixtures that contain waste marble aggregates.

**5 Results**

According to the findings of the study, in addition to its more traditional applications, XRD is useful for inferring a number of significant results, such as the degree of hydration and carbonation, the possibility of replacing material constituents, the reasons for high and low compressive strengths, the reasons for durability and the positive and negative effects of varying the curing conditions. On the other hand, some drawbacks of the technique were also found, such as the fact that the overlapping of peaks makes it difficult to identify the crystal. This problem, however, can be solved by combining the XRD with another technique, such as the scanning electron microscope (SEM), in order to confirm the results.

## 6 Conclusion and Practical Applications

- The qualitative phase composition of a sample may be efficiently analysed using XRD in the laboratory, which identifies the relative quantities of phases in a mixture by reference the respective peak strengths.
- A sample of powder that has been ground to a fine powder displays the crystalline size and the macrostrain by peak broadening. It is also useful in assessing various flaws through the analysis of peak forms and peak width.
- It is possible to use it to determine the parameters of the unit cell lattice, the index locations, and also the symmetry of the Bravais lattice. The lattice parameters are subject to change, which provides statistics about alloying, doping, stresses, and other topics.
- The determination of residual stress as well as residual strain or macrostrains may be accomplished with the use of XRD.
- If the sample is of sufficient quality, the results of the Rietveld refinement of the complete diffraction pattern will be excellent.

## 7 Future Scope

Work of a comparable kind may be carried out for several additional ways (like SEM, EDS, etc.). In addition, it is possible to do quantitative examination of the crystals by combining XRD with one or more other methods.

## References

- Abdullah MMAB, Hussin K, Bnhussain M, Ismail KN, Yahya Z, Razak RA (2012) Fly ash-based geopolymer lightweight concrete using foaming agent. *Int J Mol Sci* 13(6):7186–7198
- Akca AH, Özyurt N (2018) Deterioration and recovery of FRC after high temperature exposure. *Cem Concr Compos* 93:260–273
- Ariffin MAM, Bhutta MAR, Hussin MW, Tahir MM, Aziah N (2013) Sulfuric acid resistance of blended ash geopolymer concrete. *Constr. Build Mater* 43:80–86
- Chopra D, Siddique R, Kunal (2015) Strength, permeability and microstructure of self-compacting concrete containing rice husk ash. *Biosyst Eng* 130:72–80
- Deepty M, Srinivas C, Kumar ER, Mohan NK, Prajapat CL, Rao TC, Meena SS, Verma AK, Sastry DL (2019) XRD, EDX, FTIR and ESR spectroscopic studies of co-precipitated Mn-substituted Zn-ferrite nanoparticles. *Ceram Int* 45(6):8037–8044
- Dhapekar NK, Chopkar DM (2016) Structural health monitoring of ordinary portland cement concrete structures using X-ray diffraction. *Int J App Eng Res* 11(9):6128–6131
- Dhapekar NK, Majumdar AS, Gupta PK (2015) Study of phase composition of ordinary portland cement concrete using X-Ray diffraction. *Int J Sci Eng Res* 6(11)
- Dung NT, Unluer C (2018) Development of MgO concrete with enhanced hydration and carbonation mechanisms. *Cem Concr Res* 103:160–169
- Handoo SK, Agarwal S, Agarwal SK (2002) Physicochemical, mineralogical, and morphological characteristics of concrete exposed to elevated temperatures. *Cem Concr Res* 32(7):1009–1018

- Hubler M, Jennings H, Thomas J (2011) Influence of nucleation seeding on the compressive strength of ordinary Portland cement and alkali activated blast-furnace slag, pp 1–14
- Kavitha OR, Shanthy VM, Arulraj GP, Sivakumar P (2015) Fresh, micro- and macrolevel studies of metakaolin blended self-compacting concrete. *Appl Clay Sci* 114:370–374
- Kus H, Carlsson T (2003) Microstructural investigations of naturally and artificially weathered autoclaved aerated concrete. *Cem Concr Res* 33(9):1423–1432
- Moffatt EG, Thomas MDA (2017) Performance of rapid-repair concrete in an aggressive marine environment. *Constr Build Mater* 132:478–486
- Narayanan N, Ramamurthy K (2000) Microstructural investigations on aerated concrete. *Cem Concr Res* 30(3):457–464
- Ogawa A et al (2011) *In situ* time-resolved X-ray diffraction of tobermorite formation in autoclaved aerated concrete: influence of silica source reactivity and Al addition. *Cem Concr Res* 41(5):510–519
- Pu L, Unluer C (2016) Investigation of carbonation depth and its influence on the performance and microstructure of MgO cement and PC mixes. *Constr Build Mater* 120:349–363
- Pu L, Unluer C (2018) Durability of carbonated MgO concrete containing fly ash and ground granulated blast-furnace slag. *Constr Build Mater* 192:403–415
- Roren PM, Hunvik KW, Josvanger V, Buseth OT, Fossum JO (2021) Controlled sample environment for studying solid–gas interactions by in situ powder X-ray diffraction. *J App Crystallogr* 54(1):371–375
- Ryu GS, Lee YB, Koh KT, Chung YS (2013) The mechanical properties of fly ash-based geopolymer concrete with alkaline activators. *Constr Build Mater* 47:409–418
- Seleem HE-DH, Rashad AM, El-Sabbagh BA (2010) Durability and strength evaluation of high-performance concrete in marine structures. *Constr Build Mater* 24(6):878–884
- Singh G, Siddique R (2016) Strength properties and micro-structural analysis of self-compacting concrete made with iron slag as partial replacement of fine aggregates. *Constr Build Mater* 127:144–152
- Singh S, Nande N, Bansal P, Nagar R (2017) Experimental investigation of sustainable concrete made with granite industry by-product. *J Mater Civ Eng* 29(6):04017017
- Vardhan K, Siddique R, Goyal S (2019) Strength, permeation and micro-structural characteristics of concrete incorporating waste marble. *Constr Build Mater* 203:45–55
- Yan L, Xing Y, Zhang J, Li J (2013) High-temperature mechanical properties and microscopic analysis of nano-silica steel fibre RC. *Mag Concr Res* 65(24):1472–1479
- Yoo D-Y, Kim S, Kim M-J (2018) Comparative shrinkage behavior of ultra-high-performance fiber-reinforced concrete under ambient and heat curing conditions. *Constr Build Mater* 162:406–419
- Zhang Z, Yao X, Wang H (2012) Potential application of geopolymers as protection coatings for marine concrete III. Field experiment. *Appl Clay Sci* 67–68:57–60

# **Innovations in Sustainable Building Construction Materials**

# Experimental Study on Quarry Dust Cement Mortar with Bacteria



Reshma L. Patel , J. R. Pitroda , Rajesh Gujar , and Jaykumar Soni 

**Abstract** As the world's population continues to grow at an alarming rate, cities are being built up at a rate that is detrimental to the environment. Sand, a natural resource, is a key ingredient of cement mortar, the most popular building material. The scarcity of fine aggregate is the primary worry as the demand for sand grows. Quarry dust is a by-product of quarrying. Quarry dust is generally 5–7% per ton crushing quarry aggregate. Before quarry dust is replaced with natural sand in cement mortar, the physical and chemical properties of the two are examined. However, it seems to have virtually the same qualities. Quarry dust and *Bacillus pasteurii* bacteria at various concentrations like  $10^5$ ,  $10^6$ ,  $10^7$ , and  $10^8$  cell/ml are used to substitute natural sand in this study because *Bacillus pasteurii* may form calcium carbonate ( $\text{CaCO}_3$ ) as a filler material and serve as a binding element in cement mortars. Bacterial mortar has a higher compressive strength than ordinary mortar or sustainable mortar, according to this research. A  $10^7$  cell/ml cell concentration yields a compressive strength test result of  $31.01 \text{ N/mm}^2$ . This way, a cost-effective and environmentally friendly cement mortar may be utilized to recycle trash and safeguard the environment.

**Keywords** Bacteria · Bacterial mortar · Cement mortar · Environment · Natural sand · Quarry dust · Waste utilization

---

R. L. Patel · J. R. Pitroda (✉)  
BVM Engineering College, Vallabh Vidyanagar, India  
e-mail: [jayesh.pitroda@bvmengineering.ac.in](mailto:jayesh.pitroda@bvmengineering.ac.in)

R. L. Patel  
e-mail: [rlpatel@bvmengineering.ac.in](mailto:rlpatel@bvmengineering.ac.in)

R. Gujar  
School of Technology, Pandit Deendayal Energy University, Gandhinagar, India  
e-mail: [rajesh.gujar@sof.pdpu.ac.in](mailto:rajesh.gujar@sof.pdpu.ac.in)

J. Soni  
L J Institute of Engineering and Technology, L J University, Ahmedabad, India  
e-mail: [jay.soni\\_ljiet@ljinstitutes.edu.in](mailto:jay.soni_ljiet@ljinstitutes.edu.in)

# 1 Introduction

Nowadays, the worldwide development of construction work and new technology is essential to fulfilling the requirement of urbanization. In most construction materials, fine aggregate is common and must be needed as they are natural resources; the scarcity of sand is a great concern for saving natural resources.

On the other hand, quarry dust, a by-product of quarry plants, is creating disposal problems and reducing the land's fertility. As quarry dust and fine aggregate have similar physical and chemical properties, quarry dust can be replaced by natural sand in construction materials. It is available in large quantities and is also economical.

Mortar fills brick joints, concrete cub joints, and plaster joints. Using this waste instead of sand in mortar improves strength, durability, and workability.

Microorganisms should be added to the mix to increase the mortar's strength. As the name implies, bacterial cement mortar is a mortar that has had several kinds of bacteria added to it. Several species of bacteria may be used to increase certain mortar features, including strength, durability, and permeability (Patel et al. 2017).

This study is focused on a microorganism-rich quarry dust cement mortar. Crushed rock particles less than 4.75 mm diameter are known as quarry dust, a non-volatile waste product. It is common practice to utilize quarry dust as a filler for roadways. Over 200 million tons of quarry dust are produced yearly, creating land-fill disposal issues and environmental dangers. Quarry dust is used instead of natural sand in this research to minimize the amount of natural sand used. Cement mortar is an effort to employ a sustainable and cost-effective building material for rapidly evolving infrastructures. Therefore, a novel bacterial mortar innovation (*Bacillus pasteurii*) also helps improve the final product's strength. Biological mortar is a branch of calcite carbonate ( $\text{CaCO}_3$ ) precipitation science that can repair cement mortar fractures. As a result of this research, a new sustainable cement mortar has been developed that is superior to ordinary cement mortar in durability.

## 1.1 Objectives of the Study

The study's aims are as follows:

1. To determine a different method of using quarry waste in place of natural sand in cement mortar in order to use waste and lessen the consumption of natural resources.
2. To research the material's mechanical and physical characteristics.
3. To research the physical and chemical characteristics of quarry dust in order to substitute natural sand.
4. Researching the effects of quarry dust and bacteria (*Bacillus pasteurii*) on cement mortar.



## 1.2 *Need of Study*

Any building sector requires cement, sand, and aggregate. River sand is becoming scarce as a result of river erosion and environmental concerns. The absence or scarcity of river sand will have an impact on the building sector; hence, a new alternative material to replace river sand is required to avoid excessive river erosion and environmental damage. Many researchers are investigating alternative alternatives to sand, with quarry stone dust being one of the most important. The needed concrete mix may be created by varying the quantities of quarry dust and sand.

## 2 **Quarry Dust Utilization Research**

### 2.1 *Mortar*

The mechanical characteristics of cement mortar were investigated by substituting artificial sand made from scrap bricks for fine aggregate. Scrap bricks to replace 25% of the sand in the mortar increased the compressive strength by the desired amount (Baali et al. 2007). Quarry dust replacement in concrete and mortar was studied and proved viable. Using metakaolin instead of cement and natural sand instead of quarry dust had superior strength and a more regulated water–cement ratio (Anupama et al. 2011). Stone powder concrete’s compressive strength (CS) is 14.7% greater than conventional concrete (Mahzuz et al. 2011). Crushed rock powder (CRP) has been studied as a partial and complete substitute for natural sand in mortar and concrete in various proportions, such as 20, 40, 60, 80, and 100%, and the strength and durability have been researched (Nagabhushana and Bai 2011). When the sand and powdered sand are mixed, the mortar performs better. Concluded that using it to produce mortar and concrete would reduce waste and the cost of concrete (Haque et al. 2012). To create the mortar mixtures, various ratios were used, including 1:2, 1:3, and 1:6, with a water–cement ratio of 0.5 and 0.55. It was determined that replacing 50% of natural sand with stone dust in mortar cube specimens resulted in good compressive strength (Jadhav and Kulkarni 2013). Stone dust mortar has greater compressive strength than regular sand mortar (Hoque et al. 2013). The strength of modified mortar was studied by substituting 20, 30, and 40% of fine aggregates and adding stone dust to replace 5% of the cement. There were no differences in compressive or tensile strength between the stone dust and cement replacement samples after 7 and 28 days. However, there was an increase in tensile strength of 8.7% based on the findings of the tests (Muhit et al. 2014). Crushed stone dust as a fine aggregate in concrete and mortar has been examined. Compressive strength was lower in the mortar containing sand in the flow range of 85–75% than in the mortar containing crushed stone dust (Rajput and Chauhan 2014). M-sand substituted cement mortar with a 1:6 cement-to-sand ratio, and cement mortar was used to compare the product’s strength and workability. Concluded that the substituting sand increases mortar strength and workability to

some extent but decreases it completely (Praveen and Krishna 2015). The mechanical strength of the mortar was improved by adding 40 to 50% crushed sand as a substitute (Maza et al. 2016). Quarry waste may be recycled in various ways, one of which is by adding it to cement mortar formulations. The findings support the design approach and point to the feasibility of using waste silt in cement mortar formulations in place of up to 20% of natural sand (Solouki et al. 2021).

## 2.2 Concrete

Using limestone, marble, and marble with granite stone waste instead of cement lowered the compressive strength (CS) because of a weaker binding action. Using sand instead enhanced the strength owing to a filler effect, the CS of hardened concrete specimens was reduced after 28 days when cement was replaced in various quantities. They showed that concrete and mortar constructions might benefit greatly from using stone debris instead of sand in their construction (Lakhani et al. 2014). Quarry dust is a low-cost replacement for sand that meets the original intent of the alternative material. According to the findings of experimental studies, quarry dust may be utilized instead of fine aggregate. The strongest concrete is made when 40% of the FA is replaced with quarry dust, and strength declines at 50% (Rao 2016). Concrete strength may be increased by 50% by using sand instead of quarry dust (Vijayakumar et al. 2015). Using quarry dust and saw dust as a strong substitute for natural river sand with improved strength up to the replacement of S3 (50% natural sand, 40% quarry dust and 10% sawdust) saves concrete costs and reduces sand demand, according to the results of studies on strength and durability (Kumar et al. 2020). QD, instead of sand, provides higher compressive strength than standard concrete when used in a 30% ratio (Aishwaryalakshmi et al. 2017). Powdered sand and sand were shown to function poorly in concrete. Stronger results might be obtained by using higher-quality powder sand. A better outcome may be achieved with the proper gradation of sand and powder sand (Haque et al. 2012). Crushed stone dust may be utilized instead of natural sand in cement concrete building projects, saving both money and the environment in the process (Rajput 2018). Stone dust for 45% of the sand in concrete would save a significant amount of natural sand and help prevent pollution caused by dumping this stone dust on otherwise important arable land (Dubal 2018). Quarry dust and GGBS are waste materials; thus, using them helps maintain effective and sustainable development. Quarry dust-based concrete has increased its compressive strength by 30% when GGBS and cement replace fine aggregate is replaced by 20%, and by combining 20% GGBS with 30% quarry dust after 28 days compared to conventional concrete (Bhavana and Madhavi 2016). Quarry dust is partially replaced with sand in the concrete mix, increasing the compressive strength (Sankh et al. 2014).

### 3 Bacteria Utilization Research

#### 3.1 Mortar

Anaerobic bacteria were used in cement mortar at various proportions. According to the findings of the tests, adding an anaerobic hot spring bacteria to mortar/concrete increases compressive strength by 25–30%. They added  $10^5$  cells/ml of anaerobic microbe (*Shewanella* sp.) mixed with water to mortar after 28 days of curing, enhancing its strength by 25%. However, they found no significant improvement in mortar strength when utilizing *Escherichia coli* bacteria (Ghosh et al. 2005). Chemically modified *B. subtilize* (CMBS) has been examined in mortar. A 28% increase in strength over control concrete was claimed by him when utilizing CMBS at an optimal concentration of  $10^6$  cells/ml (Afifudin et al. 2011). An alternative and high-quality cement mortar sealer with cost-effectiveness are based on a microbiological approach, which improves the durability of construction materials over time (Senthilkumar et al. 2014b). After adding *Enterococcus* sp. bacteria and causing  $\text{CaCO}_3$  precipitation in cement mortar. They concluded that there was an impressive 45% increase in compressive strength in the *Enterococcus* sp. treated bio-curing specimens compared to the controls the researcher found (Senthilkumar et al. 2014a). For the experimental examination on cement mortar, utilized varying cell concentrations of *Bacillus cereus* and *Bacillus pasteurii*. Test findings indicated that compressive strength increased by 38% when employing *B. cereus* and by 29% when using *B. pasteurii* (Maheswaran et al. 2014). *Bacillus subtilis* spores added to the mortar mixture increased the compressive strength, notably at a cell concentration of  $10^5$  cells/ml. When crushed fly ash medium was mixed with *Bacillus subtilis* spores, calcium acetate, and urea, the compressive strength improved, notably at a  $10^5$  cells/ml concentration. Compressive strength increased by 25.38, 21.40, and 17.97% compared to the control mortar after 3, 7, and 28 days, respectively, at that concentration (Nugroho et al. 2015). A microenvironment was created on the surface of cement mortar specimens utilizing *Enterobacter* (EB) and *Serratia* bacteria (SB) as nutriment, allowing for the development and reproduction of bacteria. During this period, a calcite layer developed on the surface of the untreated cement mortar specimens, limiting capillary water absorption in the treated specimens by up to 13 times. A cost-effective and ecologically safe alternative cement mortar sealant is now possible thanks to the microbial approach, which also improves the long-term durability of construction materials (Senthilkumar et al. 2014a, b, c).

#### 3.2 Concrete

Microorganisms for carbonate precipitation may cure surface cracks in building materials like concrete and mortar. Concluded that bio-decomposition improves the specimen's durability.  $\text{CaCO}_3$  crystals' intrinsic porosity reduced the sample's water

absorption, reducing the carbonation rate by 25–30% (De Muynck et al. 2008). Ureolytic bacteria like *Bacillus spaericus* have been employed to repair cementitious materials biologically. The microbiological  $\text{CaCO}_3$  precipitation improves concrete's compressive strength (Van Tittelboom et al. 2010). Cement mortar may benefit from the precipitation of calcium by using Ureolytic-type bacteria like *Bacillus sphaericus*. It was discovered that as the number of bacteria increased, so did the CS of a mortar cube after 28 days of curing. At a bacterium dose of  $10^7$  cells/ml, he found that the compressive strength increased by 58% after seven days and 23% after 28 days compared to the control specimen (Sahoo et al. 2016). The strength of bacterial concrete is higher than conventional concrete at all concentrations. At  $10^5$  cells/ml, the greatest strength rise may be seen. Bacterial concrete is cost effective since it requires less repair and maintenance over time. Using bacterial concrete saves money in the long run by reducing the need for repair and maintenance (Sable et al. 2019).

### ***3.3 Outcomes Based on Quarry Dust and Bacteria Utilization Research***

Based on quarry dust and bacteria utilization research, the following outcomes are drawn:

1. Alternatives to using natural sand to make sustainable mortar have been discovered.
2. Using garbage and conserving natural resources was both taken into consideration.
3. Stone dust, a by-product of the quarrying process, is cheap and readily accessible.
4. The fine aggregate used in mortar may be substituted with stone dust sieved via IS sieve no. 100.
5. Different percentages of the previously used quarry dust are being replaced with newer materials. These percentages range from 20 to 100%. At 40–70% replacement, the greatest outcomes were seen.
6. Compressive strength and durability are both improved by substituting sawdust for the original.
7. This environmentally friendly mortar provides superior qualities to regular mortar and is cost effective.
8. Bacteria that precipitate calcite and protect the mortar from acid assaults may be added to the mortar to increase its overall strength.
9. The findings showed that cement mortar with *B. pasteurii* bacteria had a 29% higher strength than cement mortar without it.
10. Maximum compressive strength improves by 58% (after 7 days) and by 23% (after 28 days) when the bacterium dose is set to  $10^7$  cells/ml.

**Table 1** Physical requirement of quarry dust and fine aggregate

Property	Quarry dust	Fine aggregate	Standards
Specific gravity	2.54–2.60	2.60	IS2386 (Part III)–1963
Bulk density (kg/m <sup>3</sup> )	1720–1810	1460	IS2386 (Part III)–1963
Absorption (%)	1.20–1.50	Nil	IS2386 (Part III)–1963
Moisture content (%)	Nil	1.50	IS2386 (Part III)–1963
Sieve analysis	Zone-II	Zone-II	IS383–1970

**Table 2** Chemical requirement of quarry dust and fine aggregate

Compounds	Quarry dust (% by weight)	Fine aggregate (% by weight)
CaO	3.28	02.93
SiO <sub>2</sub>	64.84	88.25
Al <sub>2</sub> O <sub>3</sub>	0.12	00.71
Fe <sub>2</sub> O <sub>3</sub>	0.94	00.93
K <sub>2</sub> O	00.07	00.30
Na <sub>2</sub> O	00.15	00.01
Sulfite	00.22	00.08
MgO	8.49	00.17

## 4 Experimental Materials

Research experiments included using the following items.

### 4.1 Quarry Dust

Quarry dust was collected at the Sahjanand quarry works in Sevaliya, Gujarat, India, and used in this study. This particular QD comes in a powder with a particle size of less than 4.75 mm. Quarry dust was subjected to testing to determine its physical and chemical characteristics. Quarry dust has qualities similar to those of FA (natural sand). The qualities of FA and QD are contrasted in Tables 1 and 2, illustrated.

### 4.2 Fine Aggregate

Rock and mineral fragments are finely separated to form fine aggregate, naturally as a granular substance in soil, rock, or rock dust. Fine aggregate includes fractions ranging from 4.75 mm to 150 microns.

**Fig. 1** *Bacillus pesteurii*  
NCIM 2477



### ***4.3 Bacteria***

*Bacillus* species are rod-shaped bacteria that are aerobic, sporulating, and found in abundance throughout nature. The vast majority of *Bacillus* species are completely harmless. Cement mortar may benefit from using *Bacillus*, a bacterium that can create calcium carbonate ( $\text{CaCO}_3$ ) as a filler ingredient and binding element. Concrete's increased durability and compressive strength may be achieved using calcium carbonate ( $\text{CaCO}_3$ ) to minimize capillary holes. *Bacillus pesteurii* NCIM 2477 is seen in Fig. 1.

### ***4.4 Cement***

For the current investigation, OPC 53 grade was used as the building material for the cement. It complies with the requirements of Indian Standard Specification BIS 12269–1987.

## **5 Design Mix**

Table 3 shows the cement mortar mix design. Materials needed for cube casting for 1 cube size  $70.7 \times 70.7 \times 70.7$  mm.

**Table 3** Design mix of cement mortar

Materials	Cement (gm)	Fine aggregate/quarry dust (gm)	Water (ml)
Weight	190	640	90

## 6 Experimental Methodology

### 6.1 Compressive Strength Test

Casting procedure: combine the sand and cement to the desired weight on a non-porous surface until mixed. Add water and continue mixing until the color is consistent. In bacterial mortar, varying concentrations of bacteria are introduced to distilled water, which is then mixed with sand and cement in a mortar mixer to create the mortar. Compaction takes place by vibrating the paste for two minutes after being placed into the mortar mold. Then, after 24 h, remove the mortar cube from the mold when it has hardened, and let it cure in a transparent container of water for 28 days before using it.

Cubes were removed after 7, 14, or 28 days and evaluated under a machine designed for compressive strength testing. Table 4 and Fig. 2 show the compression tests performed after 7, 14, and 28 days.

For example, as shown in Fig. 3, the compressive strength of cement mortar increases as bacterial concentration increases. However, it decreases at  $10^8$  cells/ml (B4). The former has a higher rating when comparing the strength of conventional cement mortar with that of quarry dust-based mortar. In contrast, the latter's maximum strength is  $31.01 \text{ N/mm}^2$  after 28 days at a bacterial concentration of B3 ( $10^7$  cells/ml).

**Table 4** Comparative experimental results for compressive strength test

Cement mortar mixes	Notation	Compressive strength (N/mm <sup>2</sup> )		
		7 days	14 days	28 days
Fine aggregate based	A	8.14	10.8	17.87
Quarry dust based	B	11	12.4	17.87
Quarry dust + bacteria based ( <i>Bacillus pasteurii</i> )	B1 ( $10^5$ cells/ml)	12	14.27	24.41
	B2 ( $10^6$ cells/ml)	20.27	23.54	28.81
	B3 ( $10^7$ cells/ml)	22.81	24.14	31.01
	B4 ( $10^8$ cells/ml)	19.34	22.27	23.54



Fig. 2 Casting and curing of cement mortar cube

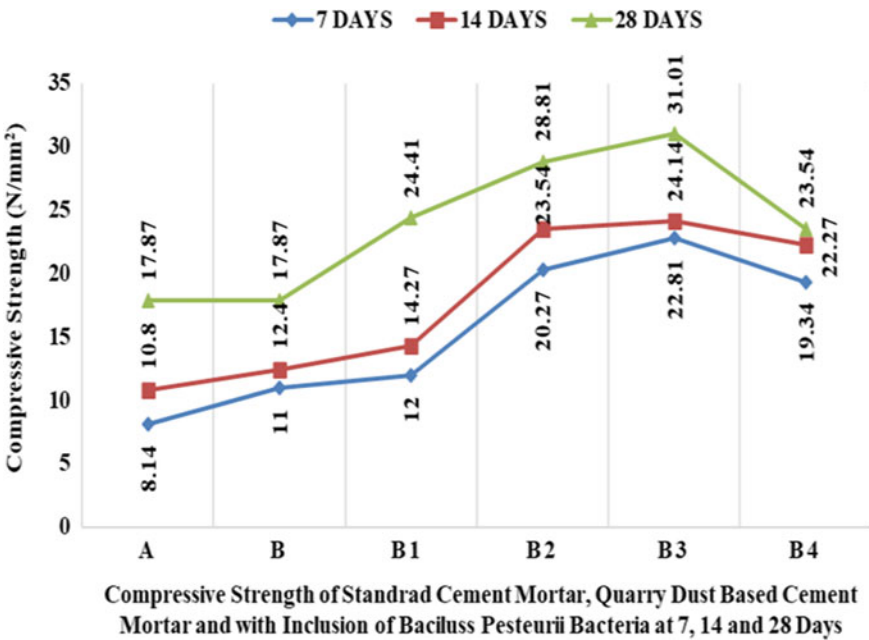
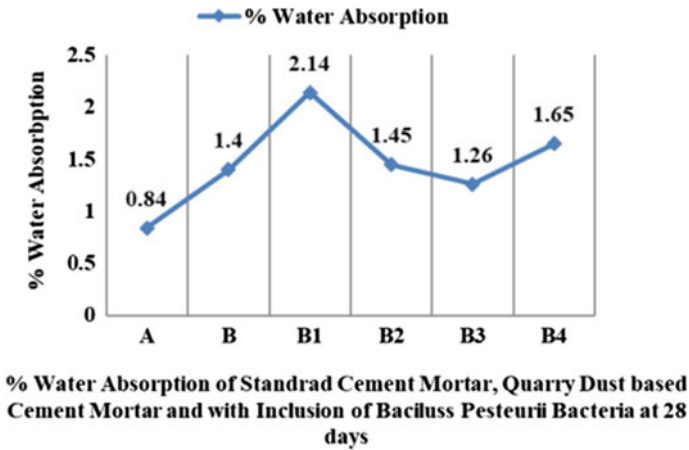


Fig. 3 Experimental results of compressive strength

### 6.2 Water Absorption Test

After curing for 28 days, place the cubes in an oven at 85°C for 24 h to dry them out and increase their water absorption capacity. Weigh the dry cubes and place them back in the water for another 24 h. Take the wet weight of the cubes the next day. Figure 4 depicts the results of the water absorption test after 28 days. The findings of the water absorption test are shown in Table 5 and Fig. 4.





**Fig. 4** Experimental results of water absorption

**Table 5** Average water absorption test results

Cement mortar mixes	Notation	Water absorption (%) at 28 days
Fine aggregate based	A	0.84
Quarry dust based	B	1.40
Quarry dust + bacteria based (Bacillus pesteurii)	B1 ( $10^5$ cells/ml)	2.14
	B2 ( $10^6$ cells/ml)	1.45
	B3 ( $10^7$ cells/ml)	1.26
	B4 ( $10^8$ cells/ml)	1.65

According to the data in the preceding Fig. 4, water absorption is relatively high compared to ordinary mortar. However, it is less at B3 ( $10^7$  cells/ml) concentration, 1.26 times lower.

## 7 Conclusions

The following conclusions may be derived from this research:

1. Bacteria mortar is a more sustainable, cost-effective, and long-lasting alternative to normal mortar cubes because of its superior compressive strength.
2. In places with increased compressive strength, water absorption is minimized.
3. Furthermore, it can be concluded that the B3 kind of mortar has been developed as an innovative product due to its high compressive strength ( $31.01 \text{ N/mm}^2$  and 1.26 water absorption) and low water absorption of 1.26. It is also the strongest kind of mortar out there.

## 7.1 Future Scope

The different prospective scopes of the experimental effort are listed below.

1. To explore the calcite precipitation performance in mortar, more sophisticated tests such as XRD and FESM might be done.
2. Bacterial mortar in different proportions, such as 1:4, 1:3, might be used.
3. Bacterial concrete, using quarry dust as a substitute, might be a new research avenue for creating environmentally friendly building technology.
4. Quarry dust and bacteria might potentially be introduced into the rubber mold paver block.

## References

- Afifudin H, Nadzarah W, Hamidah MS, Hana HN (2011) Microbial participation in the formation of calcium silicate hydrated (CSH) from bacillus subtilis. *Procedia Eng* 20:159–165. <https://doi.org/10.1016/j.proeng.2011.11.151>
- Aishwaryalakshmi V, Kumar N, Prathap MG, Haribabu S (2017) Experiment study on strength of concrete by partial replacement of fine aggregates with quarry dust. *Int J Civ Eng Technol (IJCIET)* 8(9):12–17
- Anupama PS, Nazeer M, Nizad A, Suresh S (2011) Strength studies on metakaolin modified cement mortar with quarry dust as fine aggregate. In: *Proceedings of the international conference on advances in civil engineering*, pp 54–59. 02.ACE.2010.01.42
- Baali L, Naceri A, Mehamed R (2007) Mechanical response of mortar made with natural and artificial fine aggregates. *Asian J Civ Eng (Build Hous)*: 9(1):85–92
- Bhavana TD, Madhavi E (2016) Strength and workability properties of concrete replaced by quarry dust and GGBS. *Int J Eng Res Technol (IJERT)* 5(3):23–27. <https://doi.org/10.17577/ijertv5is030067>
- De Muynck W, Debrouwer D, De Belie N, Verstraete W (2008) Bacterial carbonate precipitation improves the durability of cementitious materials. *Cem Concr Res* 38(7):1005–1014. <https://doi.org/10.1016/j.cemconres.2008.03.005>
- Dubal AC (2018) The utilization of crushed stone dust as a replacement of sand in cement concrete. *Int J Eng Res Appl (IJERA)* 8(9):11–14. <https://doi.org/10.9790/9622-0809031114>. Available at [www.ijera.com](http://www.ijera.com). ISSN: 2248-9622
- Ghosh P, Mandal S, Chattopadhyay BD, Pal S (2005) Use of microorganism to improve the strength of cement mortar. *Cem Concr Res* 35(10):1980–1983. <https://doi.org/10.1016/j.cemconres.2005.03.005>
- Haque M, Ray S, Mahzuz HMA (2012) Use of stone powder with sand in concrete and mortar: a waste utilization approach. *ARNP J Sci Technol* 2(7):613–618
- Hoque T, Rashid MH, Hasan MR, Mondol EF (2013) Influence of stone dust as partially replacing material of cement and sand on some mechanical properties of mortar. *Int J Adv Struct Geotech Eng* 2(2):54–57
- Jadhav PA, Kulkarni DK (2013) Effect of replacement of natural sand by manufactured sand on the properties of cement mortar. *Int J Civ Struct Eng* 3(3):621–628. <https://doi.org/10.6088/ijcsr.2>
- Kumar KH, Shabarish KCV, Bhanu G, Prasad KDV, Kumar CS (2020) An experimental study on effect of replacing natural sand by quarry dust and saw dust on properties of concrete. *Int J Emerg Trends Eng Res* 8(5):1906–1915. <https://doi.org/10.30534/ijeter/2020/71852020>

- Lakhani R, Kumar R, Tomar P (2014) Utilization of stone waste in the development of value added products: a state of the art review. *J Eng Sci Technol Rev* 7(3):180–187. Available at [www.jestr.org](http://www.jestr.org)
- Maheswaran S, Dasuru SS, Murthy ARC, Bhuvaneshwari B, Kumar VR, Palani GS, Iyer NR, Krishnamoorthy S, Sandhya S (2014) Strength improvement studies using new type wild strain bacillus cereus on cement mortar. *Curr Sci* 106(1):50–57. <https://doi.org/10.18520/cs/v106/i1/50-57>
- Mahzuz HMA, Ahmed AAM, Yusuf MA (2011) Use of stone powder in concrete and mortar as an alternative of sand. *Afr. J Environ Sci Technol* 5(5):381–388
- Maza M, Naceri A, Zitouni S (2016) Physico-mechanical properties of mortar made with binary natural fine aggregates (dune sand and crushed sand) with and without chemical admixture. *Asian J Civ Eng (BHRC)* 17(5):663–682
- Muhit IB, Raihan MT, Nuruzzaman M (2014) Determination of mortar strength using stone dust as a partially replaced material for cement and sand. *Adv Concr Constr* 2(4):249–259. <https://doi.org/10.12989/acc.2014.2.4.249>
- Nagabhushana K, Bai HS (2011) Use of crushed rock powder as replacement of fine aggregate in mortar and concrete. *Indian J Sci Technol* 4(8):917–922. <https://doi.org/10.17485/ijst/2011/v4i8/30896>
- Nugroho A, Satyarno I, Subyaktio S (2015) Bacteria as self-healing agent in mortar cracks. *J Eng Technol Sci* 47(3):279–295. <https://doi.org/10.5614/j.eng.technol.sci.2015.47.3.4>
- Patel F, Patel RL, Pitroda J (2017) Parametric study on quarry dust and bacteria in cement mortar for next generation: a review. *IJTE special issue for ICRISSET 2017*, pp 18–22
- Praveen KK, Krishna R (2015) Strength and workability of cement mortar with manufactured sand. *Int J Res Eng Technol (IJRET)* 4(1):186–189. <https://doi.org/10.15623/ijret.2015.0413030>
- Rajput SPS, Chauhan MS (2014) Suitability of crushed stone dust as fine aggregate in mortars. *Int J Emerg Technol Adv Eng* 4(3):87–89. Available at [www.ijetae.com](http://www.ijetae.com). ISSN 2250-2459, ISO 9001:2008 Certified Journal
- Rajput SPS (2018) An experimental study on crushed stone dust as fine aggregate in cement concrete. *Mater Today Proc* 5(9, Part 3):17540–17547. <https://doi.org/10.1016/j.matpr.2018.06.070>
- Rao BK (2016) Study on marble powder as partial replacement of cement in normal compacting concrete. *IOSR J Mech Civ Eng (IOSR-JMCE)* 13(4):1–5. <https://doi.org/10.9790/1684-1304030105>. e-ISSN: 2278-1684, p-ISSN: 2320-334X
- Sable K, Mahadik K, Bhadale V, Mandhare P, Shaikh SKA (2019) Experimental study on bacterial concrete. *J Emerg Technol Innovative Res (JETIR)* 6(4):281–286. [https://doi.org/10.1007/978-981-15-1404-3\\_20](https://doi.org/10.1007/978-981-15-1404-3_20)
- Sahoo KK, Sathyan AK, Kumari C, Sarkar P, Davis R (2016) Investigation of cement mortar incorporating *Bacillus sphaericus*. *Int J Smart Nano Mater* 7(2):91–105. <https://doi.org/10.1080/19475411.2016.1205157>
- Sankh AC, Biradar PM, Naghathan SJ, Ishwargol MB (2014) Recent trends in replacement of natural sand with different alternatives. *IOSR J Mech Civ Eng (IOSR-JMCE)*. International conference on advances in engineering and technology–2014 (ICAET-2014), pp 59–66. Available at [www.iosrjournals.org](http://www.iosrjournals.org). e-ISSN: 2278-1684, p-ISSN: 2320-334X
- Senthilkumar V, Palanisamy T, Vijayakumar VN (2014a) Comparative studies on strength characteristics of microbial cement mortars. *Int J ChemTech Res* 6(1):578–590
- Senthilkumar V, Palanisamy T, Vijayakumar VN (2014b) Fortification of compressive strength in Enterococcus microorganism incorporated microbial cement mortar. *Int J ChemTech Res* 6(1):636–644
- Senthilkumar V, Palanisamy T, Vijayakumar VN (2014c) Enrichment of compressive strength in microbial cement mortar. *Adv Cem Res* 26(6):353–360. <https://doi.org/10.1680/adcr.13.00053>
- Solouki A, Viscomi G, Tataranni P, Sangiorgi C (2021) Preliminary evaluation of cement mortars containing waste silt optimized with the design of experiments method. *Materials* 14(528):1–16. <https://doi.org/10.3390/ma14030528>

- Van Tittelboom K, De Belie N, De Muynck W, Verstraete W (2010) Use of bacteria to repair cracks in concrete. *Cem Concr Res* 40(1):157–166. <https://doi.org/10.1016/j.cemconres.2009.08.025>
- Vijayakumar A, Revathi K, Bharathi C (2015) Strength and durability studies on concrete using quarry dust as fine aggregate. *Int Res J Eng Technol (IRJET)* 2(7):383–387. Available at [www.irjet.net](http://www.irjet.net). e-ISSN: 2395-0056; p-ISSN: 2395-0072. ISO 9001:2008 Certified Journal

# Reclaimed Sand Dust Waste as Eco-Friendly Green Construction Materials



Reshma L. Patel , J. R. Pitroda , Rajesh Gujar , and Jaykumar Soni 

**Abstract** This sector represents one of India's oldest and most widely dispersed economic activities. Most of the metal casting processes in this business used a method called sand-casting molding, which resulted in a substantial amount of sand waste. Sand dust that has been reclaimed is produced in the industry as part of the reclamation process. These take place in the cyclone separator and the bag filter. The waste produced due to the sanding process is disposed of at landfills and other disposal sites. The disposal of waste sand dust causes the poisoning of the surrounding environment. As a result, it has developed into an issue for the environment. This paper presents a complete examination of the use of industrial waste as a construction material that is ecologically acceptable. The topic of the inquiry is offered. In place of fly ash, recycled sand dust waste, also known as RSDW, was used to produce fly ash bricks (FABs). Various percentages of RSD waste are used in place of fly ash, including 20, 40, 60, 80, and 100%, respectively. The paper devotes considerable space to analyzing and discussing the results of compressive strength and water absorption testing.

**Keywords** Compressive strength · Eco-friendly · Environmental preservation · Environmental pollution · Fly ash brick · Green brick · Hazardous waste · Industrial waste · Resource conservation · Reclaimed sand dust waste · Waste utilization

---

R. L. Patel · J. R. Pitroda (✉)  
BVM Engineering College, Vallabh Vidyanagar, India  
e-mail: [jayesh.pitroda@bvmengineering.ac.in](mailto:jayesh.pitroda@bvmengineering.ac.in)

R. L. Patel  
e-mail: [rlpatel@bvmengineering.ac.in](mailto:rlpatel@bvmengineering.ac.in)

R. Gujar  
School of Technology, Pandit Deendayal Energy University, Gandhinagar, India  
e-mail: [rajesh.gujar@got.pdpu.ac.in](mailto:rajesh.gujar@got.pdpu.ac.in)

J. Soni  
L. J. Institute of Engineering and Technology, L. J. University, Ahmedabad, India  
e-mail: [jay.soni\\_ljiet@ljinstitutes.edu.in](mailto:jay.soni_ljiet@ljinstitutes.edu.in)

## 1 Introduction

Sand-casting molding systems were favored by the majority of the metal casting industry for metal casting. Metal casting waste, such as reclaimed sand dust, is a by-product. Waste sand is a big issue for the Indian small and medium-sized metal casting sector. RSD waste is the primary waste generated during the metal casting process. Because this sector uses much sand as a significant raw material, regenerating that sand is an essential part of achieving sustainable growth in terms of environmental performance. As is the general population, small and medium-sized metal casting industries in India are unaware of this. Ever since the turn of the century, they have been disregarding issues. However, focusing on sand regeneration, recycling, reuse, and disposal for metal casting companies is critical today if the industry remains viable in the long term (Andodariya et al. 2017a). Reclamation of system sands has recently become more popular within the metal casting sector. Every company has the challenge of processing an appropriate supply of sand with the characteristics necessary to fulfill the many molding and core-forming requirements. The sheer amount of sand waste produced poses a significant management challenge. Putting large amounts of waste in the ground is becoming more problematic from an environmental standpoint. Various government organizations and departments are interested in learning what chemicals are present in all garbage and how much it may seep into the sand throughout the decade. This concern extends to the industry's land and public landfills. Also, since reclaimed sand dust waste is a particle substance, it poses health problems for those near the trash disposal site.

The improper disposal of metal-casting sand dust waste has caused environmental issues. Simultaneously, green, low-cost, and lightweight building materials are becoming more popular in the construction sector. Therefore, it is necessary to look at how this may be accomplished while keeping material needs within industry standards while also helping the environment. Construction materials made from industrial and agricultural waste are a potential option for designing an economic structure. The ecosystem is also benefited from trash management and hazardous waste disposal. Industrial waste may be recycled and reused to reduce the amount of waste we produce and dispose of more ecologically. The brick industry may absorb solid waste effectively because of the large amount of raw materials and finished products generated (Alonso-Santurde et al. 2012).

Metal casting is one of India's oldest and most widespread industries. A significant quantity of sand is used in the casting system for metal casting to recycle the sand. As a result, a significant amount of sand dust trash is generated during the reclamation process. Due to its enormous volume, managing this sand dust waste is a significant challenge for the casting industry. Because sand dust is a particle material, it is not easy to dispose of. The disposal of sand, dust, and debris from the reclamation process is causing environmental problems due to haphazard methods. At the same time, as the population grows, the building sector expands and develops, driving up the price of raw materials. Industrial solid waste may substitute expensive raw materials in

**Fig. 1** Reclaimed sand dust waste



building material manufacturing while reducing the environmental damage from manufacturing those materials. Refer to Fig. 1. Reclaimed sand dust waste.

Using ecologically friendly, low-cost, and lightweight building materials is becoming more popular in construction. Therefore, it is necessary to look at how this may be accomplished while still keeping material needs within industry standards while also helping the environment to be an economically feasible alternative for building design and waste management from an environmental standpoint, using industrial and agricultural waste as raw material for construction is a logical choice (Shakir et al. 2013).

Brick has been a necessary building material for decades. It is also widely utilized in the building business for wall masonry units. In addition, because of the enormous amount of raw materials used in manufacturing and the wide range of products used in building, the brick sector is well-suited to handle solid waste (Zhang 2013).

To foster a circular economy, it is critical to implement end-of-waste (EoW) decrees for WFS that allow reuse while also protecting the environment and human health (Cioli et al. 2022).

In construction, brick is a popular building material. Fly ash bricks are quickly becoming the most popular green construction material. The basic materials utilized in its production are fly ash and lime. Their existence affects the quality and pricing of the final product. Over 70% of the brick's bulk is made up of fly ash. Having fly ash onsite makes a big difference in building costs. Fly ash consumption has skyrocketed along with building and growth. As a result of the scarcity of fly ash, the cost of producing fly ash bricks is rising. The focus has switched to low-cost or waste construction materials to solve this problem (Shakir et al. 2013; Weng et al. 2003). As a result, industrial solid waste creation and disposal issues are rising. Other parties recycle and reuse industrial waste as raw material in the building sector (Andodariya et al. 2017b).

## 2 Eco-Friendly Green Construction Materials' Utilization Research

Following are the eco-friendly green construction materials' utilization research in brick production:

### 2.1 *Stone Powder*

Replacing cotton waste with limestone powder waste gave better flexural strength, higher energy absorption capacity, and lower labor costs. In addition, it was 60% lighter than conventional concrete brick (Algin and Turgut 2008). Concrete bricks can be made by replacing pebbles with slurry powder from waste marble and granite (Hamza et al. 2011a, b). Therefore, marble clay sustainable bricks with a marble powder composition of 5–20% are recommended for sustainable building material use (Sufian et al. 2021).

### 2.2 *Foundry Sand*

Increasing the amount of leftover foundry sand in concrete increased CS. The highest CS was achieved by replacing fine aggregate with waste foundry sand at 60%, demonstrating a 3.5% cost reduction (Bhimani et al. 2013). Foundry sand is the most common kind of waste generated by metal casting. Because foundries utilize sand as an essential direct material, regenerating this sand is critical to achieving sustainable development. Small and medium-sized foundries in India are unaware of this. They have been ignoring difficulties for a decade. However, today's foundry companies must concentrate on sand regeneration, recycling, reuse, and disposal. Thermal reclamation systems have potential in India's small and medium-sized foundries. They produce more robust molds and cores with fewer chemical additives, better surface quality, reduced porosity, and more dimensionally precise castings. Less chemical additives and better sand grain prevent casting flaws like fining and burn-in (Patange et al. 2013). Belgaum foundry waste sand is used in brick making. The method entailed making bricks in a fully operational brick factory with a monthly output of about 50,000 bricks. Clay–sand combinations were combined, formed into bricks, dried, and fired locally. With little processing, up to 50%, WFS may be added to clay bodies to generate attractive bricks. Wet compression resistance was 3.3 MPa, and WA was 21.6% for 50% WFS bricks burnt at 900°C. WA and the specific gravity of WFS bricks are identical to commercial bricks. However, WFS reduced the bricks' bulk density and compressive strength (Hossiney et al. 2018).



### **2.3 Glass Waste**

The material was dried at 100°C before being torched at 900°C. The inclusion of 2% glass waste in the clay body had no discernible influence on the technical performance of burned bricks. Adding more than 5% trash may affect mechanical characteristics and efflorescence. The leaching test revealed no significant pollutant emissions (Dondi et al. 2009). It was found that the properties of clay bricks depended on wasted glass content and firing temperature; to make clay bricks with good physical and mechanical qualities, use discarded glasses and a fire. About 15–30 Wt% glass bricks burnt at 1100°C had a CS of 26–41 MPa and 2–3% WA. The observed porosity and water absorption of 45% weight glass waste have been found to be higher (Loryuenyong et al. 2009).

### **2.4 Recycle GGBS**

Brick of unfired clay was manufactured from recycled GGBS and clay soil. The durability and mechanical properties tests were promising (Oti et al. 2009).

### **2.5 Natural Fiber**

They added 0.5% jute and banana fiber to the fly ash brick mix to improve CS. Using fly ash and natural fiber helps to save the environment (Salla et al. 2015). A clay–water combination containing oil palm fruit (OF) and pineapple eaves (PF) was tested mechanically. BS3921:1985. CS, WA, and efflorescence were tested. The findings indicated that the average brick's CS was 5.2 MPa (Chan 2011).

### **2.6 Demolition Waste**

Replacing natural sand with fine recycled aggregates from building demolition debris increased compressive strength in cement bricks by 50 and 75% but decreased flexural strength by 50%. So, fine recycled aggregates from demolition debris may be used in brick combinations as a suitable alternative for natural sand (Ismail and Yaacob 2010). The different quantities of the mix were used. The ratio of 2:3:2 consisting of fly ash, cement, and demolition debris at 30% sludge is shown to be the best for brick block manufacture. Greater compressive strength of 14.5 MPa was obtained with a ratio of 2:3:2 (Vaithiyasubramanian et al. 2022).

## 2.7 Agricultural Waste

These waste materials include paper processing residues, cigarette butts, fly ash–lime gypsum, cotton wastes, limestone powder wastes, textile effluent treatment plants, organic residues, and recycled materials' sludge welding flux. The WA and CS of discarded bricks were studied. The bricks made from paper processing and paper pulp waste have a compressive strength 12 times higher than the minimum suggested by Indian Standard IS1007:1992 (Raut et al. 2011). These are higher than the CS of orange peel trash and paper mill leftover waste (Arshad and Pawade 2014). When sludge is added to sugarcane sludge bricks at 20%, the CS decreases, and the water absorption capacity increases. Another disadvantage is the CS of the clay brick (Sumathi and Ambiga 2015). Adding 2% rice husk to standard clay brick increased compressive strength by 6.59 MPa and reduced density by 14.01% (Watile et al. 2015). Sustainability problems are becoming more appealing to green construction raw materials. It is a revolutionary waste disposal technology using agricultural waste as natural components in developing alternative construction goods. They examine clay bricks' physical–mechanical characteristics and microstructure when 50% sludge from water treatment facilities is substituted for clay. An untreated control combination was also created. Each group had three mixes with 5, 10, and 15% SWTP by weight. These clay bricks showed lower CS than non-RSA, SBA, and WSA clay bricks. A lower dosage of RSA, SBA, and WSA (i.e., 5% SWTP weight) in brick samples reduces environmental pressure while increasing efficiency and economy (Heniegal et al. 2020). Mechanical characteristics of earthen bricks, consisting of soil, coarse sand, and straw fibers were studied. Ten alternative compositions of the fundamental elements were initially tested on bricks and blocks. The block displacement control experiments determined the strain performances after the maximum stress (Piattoni et al. 2011). Fly ash production is likely to increase as coal remains a key energy source for 25 years. Unmanaged fly ash, a resource item, may cause environmental issues. At the same time, the global agricultural footprint is rapidly expanding, with huge agricultural lands and bustling agro-based companies. Agricultural wastes generated are not always effectively handled or used. These wastes, such as discarded leaves, fruit bunches, and brick construction, may be recycled. Rice husk and ground nut shells were introduced to the list as agricultural waste. The CS of brick improves with the proportion of rice husk in the brick. After 21 days, a brick with 1% fiber has maximum strength of 7.861 N/mm<sup>2</sup>. Shelled nuts after 21 days, the brick has a maximum strength of 7.826 N/mm<sup>2</sup>. As the brick's CS grows, so does its water absorption. After 21 days, the rice husk fly ash brick has a maximum CS of 7.861 N/mm<sup>2</sup> and a minimum WA of 10.147%. As the brick's CS grows, so does its WA. After 21 days, the maximum CS is 7.826 N/mm<sup>2</sup>, and the lowest WA is 10.256% in ground nut shell fly ash brick. In addition, the utilization of fly ash and agro-waste helps to preserve the environment and agricultural land (Salla et al. 2013). To improve thermal insulation and decrease the compressive strength of the body clay, sewage sludge, brewing sludge, and bagasse were added (Eliche-Quesada et al. 2011). They discussed on the impact of SCBA on the characteristics of burnt

clay bricks. They manufactured clay bricks by 0, 2.5, 5, 7.5, and 10% replacement of SCBA. SCBA might be used to make burnt clay bricks. SCBA does reduce compressive strength. However, with 2.5% SCBA burned at 1000°C and 2.5, 5.0, and 7.5% SCBA fired at 1100°C, excellent strength bricks of 17.2 MPa could be achieved. The SCBA-clay bricks had a lower density than the control bricks owing to SCBA's pore-forming properties. The lower density of heated clay and lightweight bricks was a plus (Phonphuak and Chindaprasirt 2018). The optimal waste material replacement ratio for the greatest brick performance is 5% rice straw ash, sugarcane bagasse ash, and wheat straw ash. Agriculture waste may be used to generate a sustainable supply of raw materials for the brick industry (Heniegal et al. 2020). The best brick parameters are 6.80 MPa compressive strength and 16.30% water absorption when 10% rice husk ash is added by weight (Damanhuri et al. 2020).

## 2.8 Quarry Dust

The sand quarry dust cement bricks have enough CS to be used as an in-filled frame structure. Likewise, sand-rice husk cement bricks absorb enough water as an in-filled masonry wall (Kartini et al. 2012).

## 2.9 Textile Wastewater Sludge/Tannery Sludge/Paint Sludge/Paper Sludge

Creating bricks for civil construction with 20% (mass) sludge may make convenient bricks with good mechanical properties. All bricks were extruded, dried at 100°C, and then fired at 900°C. Ceramics' flexural strength and WA capabilities met Brazilian standards (Herek et al. 2012). Textile mill sludge may be used up to 15% without compromising CS of 3.5 N/mm<sup>2</sup> and WA of 20% as per IS codes (Jahagirdar et al. 2013b). About 10% of treatment plant sewage in clay burnt brick offered compressive strength of 230 kg/cm<sup>2</sup>, which is desirable and advantageous to the environment (Mahajan and Husain 2016). The amount of tannery sludge, quarry dust, and cement used in cement bricks produced good compressive up to 6 N/mm<sup>2</sup> and flexural strength, which may be used for structural applications (Swarna and Venkatakrishnaiah 2014). They discussed on the impact of waste sludge on the characteristics and microstructure of brick clay. Wastewater treatment facilities generate much sludge. Replacing clay in a ceramic body with varying quantities of sludge may save money while helping the environment. Wet waste sludge was added to body clay in percentages of 1, 2, 5, 7, 10, 15, and 20%. Clay bricks benefit from containing up to 5% sludge. Adding more than 5% sludge reduces the mechanical qualities, resulting in inferior bricks (Martínez-García et al. 2012). Textile mills, India's second-biggest sector, confront sludge disposal issues. The goal is to use the

waste from textile mills to make burned clay bricks. Chemical analysis shows that up to 35% of primary material can be replaced with textile mill sludge. Bricks made with sludge are burnt at 6000–8000°C for 8, 16, and 24 h. Textile sludge may be added up to 15% for CS over 3.5 N/mm<sup>2</sup> and WA below 20%. Thus, reusing textile mill waste in burned clay bricks is a preferable method to reduce the issue of final disposal (Jahagirdar et al. 2013a). Nowadays, sewage sludge disposal is a significant issue. However, alternative dumping techniques lead to ground-water pollution and other socio-economic effects. Automobile wastewater treatment plant sludge may be used to replace brick. The compressive strength research found that brick strength decreased with sludge content. Water adsorption measurements showed sludge to be less water-absorbing. The sludge bricks had no efflorescence (Mahajan and Husain 2016). Novel lightweight bricks were created by sintering dried water treatment sludge and rice husk. Lightweight brick sintered at 1100°C with less than 15% rice husk addition meets the applicable construction standard. Sintered goods' CS dropped when rice husk content increased at 1000°C (Chiang et al. 2009). Cotton influences the water absorption of the brick, and up to 40% of cotton waste with soil is beneficial. The brick's water absorption and compressive strength rise as the amount of cotton waste increases, while the bulk of the brick decreases. It produces a strong, lighter-weight composite that has the potential to be used for walls, as a hard-wood board replacement, as a cost-effective alternative to concrete blocks, and as sound barrier panels (Teklehaimanot et al. 2021). Compared to regular brick paint sludge brick, it is lighter in weight and easier to carry. Bricks manufactured from paint waste have been proven to have higher compressive strength than normal bricks. When the strength is proportional to the particle size, decreasing the particle size increases the strength (Naik and Shirodkar 2020). Compressive strength is maintained when sludge is added up to 20%; increasing the quantity of sludge in bricks results in a drop in compressive strength (Bhushan et al. 2019). During loading, the strength increased by 3% as the proportion of hypo-sludge increased. Hypo-sludge bricks absorb 9% of their weight in water, while lime bricks absorb 12.5–15%. Hypo-sludge brick costs less than 10% of the price of regular brick (Suresh et al. 2018). It has been suggested that textile sludge wastes may be mixed up to 5% by weight of clay materials for the construction of bricks, with 5% by weight of clay providing stronger bonding, greater compressive strength, and reduced water absorption (Priyadharshini and Kavisri 2018).

## **2.10 Crumb Rubber**

Crumb rubber-concrete composites are used for low-cost, high-performance thermal insulation. They assembled compressive and splitting strengths, flexural strengths, unit weight, freezing–thawing resistance, and WA values. The experimental findings reveal that replacing sand aggregate with high-level crumb rubber does not cause rapid brittle fracture beyond failure stresses, decreases unit weight, and produces a smoother surface than standard concrete bricks. The thermal insulation properties of

standard cementitious mixtures may be increased by adding crumb rubber (Turgut and Yesilata 2008). The compressive strength of bricks is greatly influenced by recycled concrete aggregate (RCA) and crumb rubber (CR) at values of 30 and 3.0% as sand replacement ratios, respectively (Khalid et al. 2020).

### ***2.11 Fly Ash***

Replacing 10% of fly ash with bagasse ash improves compressive strength and decreases the density and cost of bricks. Reduce the seismic weight of buildings using bagasse ash bricks, so that it may help prevent environmental damage by reducing trash disposal problems (Kulkarni et al. 2013). About 25% of fly ash, cement, and phosphor–gypsum bricks had adequate strength up to 23.56 N/mm<sup>2</sup>. As a result, this brick is employed in locations like curtain walls where water absorption is not an issue (Naik et al. 2014). Adding fly ash 15%, lime 30%, gypsum 2%, and quarry dust 53% to fly ash brick increased compressive strength by 7.91 N/mm<sup>2</sup> and decreased particle air pollution (Sumathi and Mohan 2014). Adding fly ash and granite dust to clay bricks increased compressive strength. However, it decreased water absorption capacity compared to clay bricks (Prasad et al. 2014).

### ***2.12 Alumina Filler Waste***

Unfired bricks made from alumina filler waste have a somewhat better CS than unfired bricks made from clay (Miqueleiz et al. 2013).

### ***2.13 Eggshell Powder***

Burnt clay bricks with 3% eggshell powder offered compressive strength of 5.26 N/mm<sup>2</sup>. In contrast, 3% granite powder bricks gave compressive strength 6.73 N/mm<sup>2</sup> (Nithiya et al. 2016).

Table 1 shows the eco-friendly green construction materials' utilization research in brick production and its comparison.

**Table 1** Eco-friendly green construction materials' utilization research in brick production and its comparison

Author	Utilization area	Material used	Addition/replacement	Tests	Increase (I)/desirable (D)
Nithiya 2016	Clay burnt brick	Egg shell powder	Addition	Compressive strength (CS)	D
Watile 2015	Clay burnt brick	Rice husk	Replacement	CS Water absorption (WA)	D D
Chee Ming 2011	Clay burnt brick	Natural fibre	Addition	CS	D
Prasad 2014	Clay burnt brick	Fly ash granite dust	Addition	WA	D
Miqueleiz 2013	Clay burnt brick	Alumina filler waste	Replacement	CS	I
Luciana 2012	Clay burnt brick	Textile sludge	Addition	CS WA	D D
Jahagirdar 2013	Clay burnt brick	Textile sludge	Addition	CS WA	D D
Martínez-García 2012	Clay brick	Wastewater treatment plants sludge	Addition	CS WA	I
Henegal 2020	Clay brick	RSA SBA WSA	Replacement	CS	Lower
Swarna 2014	Cement brick	Tannery sludge	Addition	CS FS	D I
Kulkarni 2013	Fly ash brick	Bagasse ash	Replacement	CS	D

(continued)

**Table 1** (continued)

Author	Utilization area	Material used	Addition/replacement	Tests	Increase (I)/desirable (D)
Salla 2013	Fly ash brick	Rice husk and ground nut shell	Addition	CS WA	D
Pitroda 2013	Concrete	Foundry sand	Replacement	CS	I
Rania 2011	Concrete	Marble waste granite waste	Replacement	CS	D

## **2.14 Outcomes Based on Eco-Friendly Green Construction Materials Utilization Research**

Based on the eco-friendly green construction materials' utilization research in brick production, the following conclusions are drawn:

1. Brick made using natural fiber like jute fiber, coconut fiber, orange peels, and banana fiber show favorable compressive strength.
2. Replacement of rice husk by weight of brick gives good compressive strength and favorable water absorption to standard clay brick.
3. Up to 10% addition of treatment plant sludge gives desirable compressive strength, and sludge disposal is better for the environment.
4. Clay brick made with the inclusion of fly ash gave excellent resistance to sulfate attack and was 10% lighter brick compared to standard clay brick.
5. The maximum compressive strength was found in bricks made from paper mill waste and waste paper pulp.
6. The percentage of tannery sludge, quarry dust, and cement was 20, 50, and 30, respectively, used in cement bricks that gave favorable compressive and flexural strength.
7. Based on utilization research on eco-friendly green construction materials, fly ash cost increases and alternative industrial waste material reclaimed sand dust is used.

## **3 Experimental Materials**

The essential ingredients are fly ash, water, and quicklime. In addition, the following research supplies are required to experiment:

### **3.1 Fly Ash**

Fly ash Class F is used to make fly ash bricks. It improves the hardened brick's pozzolanic properties. Table 1 lists the chemical parameters of fly ash for investigation.

### **3.2 Reclaimed Sand Dust Waste**

This research requires recovered sand dust, roughly 400 kg of waste collected from Anand. Table 1 lists the chemical parameters of recovered sand dust waste for investigation.



### 3.3 *Sludge Lime*

High calcium fly ash has higher pozzolanic reactivity. The higher the pozzolanic activity, the stronger the fly ash brick. Therefore, we employ sludge lime in our fly ash brick project.

### 3.4 *Quarry Dust*

Quarry dust is used as a binder material collected from the local distributors for fly ash brick production.

### 3.5 *Chemical Composition of Fly Ash and RSD Waste*

Table 2 lists the chemical makeup of the research materials utilized in this study.

## 4 **Brick Mixes**

Bricks made from fly ash and recycled sand dust waste have been completed. Using the ingredients in Table 3, several batches of brick were prepared to replace fly ash with reclaimed sand dust waste. Table 3 displays the proportions of the various brick mixtures.

Afterward, quantities of reclaimed sand dust waste are substituted with fly ash waste. To do so, we made eight batches of bricks, each with 20% of the typical fly ash (A) replaced with 15% quarry dust (B1), 40% replaced with 15% fly ash (B2), 60% with 15% quarry dust (C3), and 75% replaced with 15% fly ash (C4) without the inclusion of the quarry dust (C1).

**Table 2** Chemical composition of fly ash and RSD waste

Chemical composition (% by mass)	Fly ash	RSD waste
Al <sub>2</sub> O <sub>3</sub>	4.38	16.64
SiO <sub>2</sub>	57.69	38.7
MgO	5.90	30.57
SO <sub>3</sub>	0.25	2.67
Na <sub>2</sub> O	0.36	0.63

Source GEO Test House, Gorwa Estate, Vadodara, Gujarat

**Table 3** Replacement of fly ash by RSD waste in fly ash bricks

Brick mixes	Fly ash (kg)	Reclaimed sand dust waste (kg)	Quarry dust (kg)	Sludge lime
A (00%)	60.00	0.00	15.00	25.00
B1 (20%)	40.00	20.00	15.00	25.00
B2 (40%)	20.00	40.00	15.00	25.00
B3 (60%)	0.00	60.00	15.00	25.00
C1 (00%)	75.00	0.00	0.00	25.00
C2 (25%)	50.00	25.00	0.00	25.00
C3 (50%)	25.00	50.00	0.00	25.00
C4 (75%)	0.00	75.00	0.00	25.00

## 5 Experimental Methodology

Material for intimate mixing is manually inserted into a pan mixer with water in the proper amount. The ingredients are combined in a pan and heated to a simmer. The homogenized mortar, which has been mixed using a roller mixer, is then carefully placed into molds. The product is compressed under vibration or hydraulic compression, depending on the machine type. The bricks must be cured in the sun for 24–48 h. To cure the dried-up bricks, water is sprayed on them once or twice a day for seven to twenty-one days, depending on the environment. Seven-day, fourteen-day, and twenty-day compressive strength tests are performed on the bricks. A water absorption test is also performed after the first twenty-one days.

### 5.1 Compressive Strength Test Results [IS 3495:1992 Part I]

Brick samples were compressed and tested for strength using compression testing equipment. This study examined the average strength of three samples from each batch. The unevenness in the bed faces may be removed by grinding the brick sample into two smooth and parallel surfaces. For the last 24 h, the sample has been kept in water at room temperature. After that, make a 1:1 cement mortar and fill the frog with it. Clean water should be used to store the produced sample for three days. Make sure that there is not even a speck of moisture left. Next, calculate the surface area of two parallel planes. Placing the specimen between two pieces of plywood, mortar-filled side up, with flat sides horizontal, and the specimen precisely centered between the machine's plates will provide the best results. To find the maximum load at failure, the load is applied axially at a rate of 14 N/mm<sup>2</sup> per minute until it fails. Refer to Fig. 2 for the machine setup for compressive strength testing and experimental results of compressive strength test, Refer Table 4.

It may be concluded from Fig. 3 that the CS of brick mixtures has increased steadily over time. Additionally, CS at 21 days improves with replacing RSD waste

**Fig. 2** Compressive strength testing machine



**Table 4** Experimental results of compressive strength test

Brick mixes	Compressive strength (N/mm <sup>2</sup> )		
	7 days	14 days	21 days
<i>Fly ash brick</i>			
A (00%)	12.35	12.70	12.87
<i>Fly ash bricks with RSD waste and quarry dust</i>			
B1 (20%)	11.32	13.14	21.82
B2 (40%)	10.96	11.30	18.38
B3 (60%)	6.24	6.80	12.66
<i>Fly ash bricks with only RSD waste</i>			
C1 (00%)	10.57	11.42	11.94
C2 (25%)	12.60	13.14	14.90
C3 (50%)	9.60	11.42	15.29
C4 (75%)	5.39	7.03	10.43

by 20% rather than decreasing by 40 and 60% replacement of RSD waste. However, for 40 and 60% replacement of RSD waste, CS is equivalent to that of typical fly ash brick. As a result, the optimal RSD waste replacement for maximum CS was found to be 20%. The CS of a 20% B1 mix is 58.98% higher than a standard A mix. A B1 mix with 20% replacement showed a maximum CS of 21.82 N/mm<sup>2</sup> after 21 days at the 20% replacement rate.

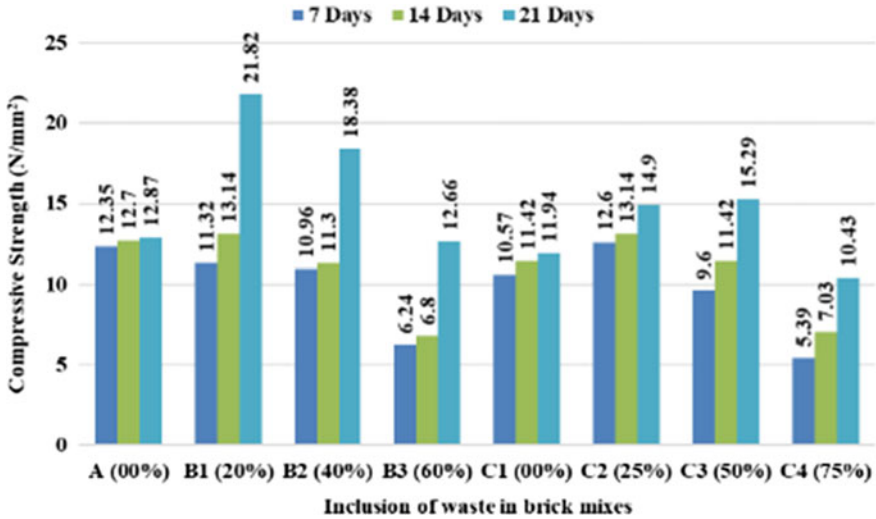


Fig. 3 Compressive strength of brick mixes

### 5.2 Water Absorption (IS 3495:1992 Part II)

Dry the specimen using a vented oven until its mass is practically consistent, between 105 and 115°C. Cool the specimen to room temperature and weigh it to determine its mass (dry weight). Specimens that are warm to the touch are not permitted to be utilized for this purpose. Next, immerse the specimen in clean water at 27 ± 2°C for 24 h after being dry. Remove the specimen from the container and wipe away any traces of water with a wet towel before weighing it. Three minutes have passed since the specimen was withdrawn from the water, so finish weighing it (wet weight). The percentage of water absorbed by mass following a 24 h immersion in cold water is calculated using a formula (Table 5).

Table 5 Experimental results of water absorption test

Brick mixes	Water absorption (%) (by mass)
A (00%)	10.10
B1 (20%)	8.10
B2 (40%)	8.20
B3 (60%)	9.50
C1 (00%)	10.60
C2 (25%)	9.10
C3 (50%)	8.50
C4 (75%)	12.10

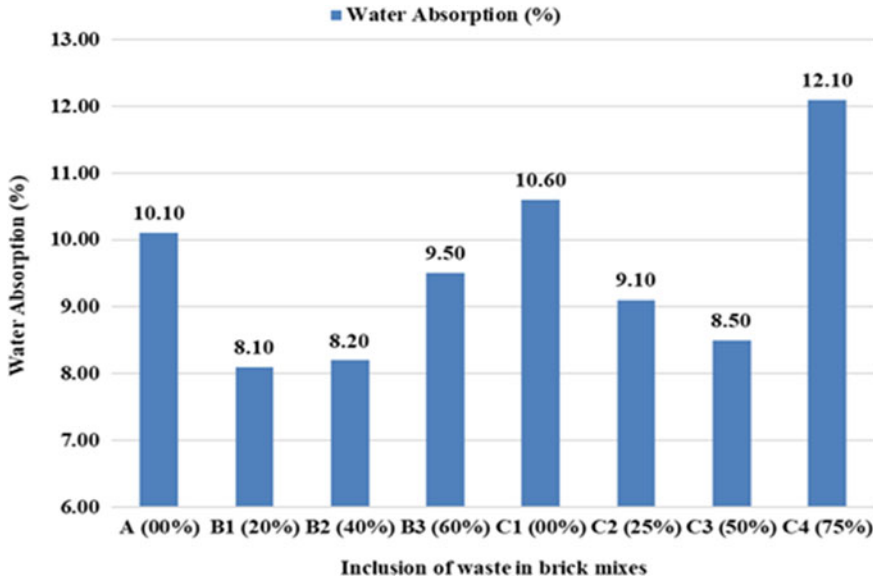


Fig. 4 Water absorption of brick mixes

From Fig. 4, it can be concluded that the percentage of water absorbed by brick mixes rises with an increase in the substitution of RSD waste with fly ash, but that the percentage of water absorbed by every mix is within permissible limits. The best result for WA was observed in the B1 batch, which included a 20% substitution of fly ash with RSD waste. The batch C4 yielded the best results in terms of water absorption. The findings of the WA test revealed that the B2, B3, C2, and C3 batches performed much worse than the standard fly ash brick.

## 6 Conclusions

The following is the conclusion:

1. The compression strength (CS) of brick was increased by substituting RSDW in varied proportions for fly ash compared to the usual fly ash brick.
2. As a result of the study, it was discovered that the optimal RSDW replacement for the maximum CS is 20%. The CS declines by replacing fly ash with RSDW and quarry dust waste.
3. Although total water absorption (WA) capacity improves with the percentage substitution of RSDW, all bricks constructed using RSDW have reduced WA capacity compared to a conventional brick.
4. The CS of the B1 batch of brick created with 20% replacement is 21.82 N/mm<sup>2</sup>. 76.68% higher than the CS of traditional fly ash brick compared to the latter.

5. Additionally, the B1 batch of brick has an 8.10% WA by mass compared to conventional fly ash brick, which is a good result.

## References

- Algin HM, Turgut P (2008) Cotton and limestone powder wastes as brick material. *Constr Build Mater* 22(6):1074–1080. <https://doi.org/10.1016/j.conbuildmat.2007.03.006>
- Alonso-Santurde R, Coz A, Viguri JR, Andrés A (2012) Recycling of foundry by-products in the ceramic industry: green and core sand in clay bricks. *Constr Build Mater* 27(1):97–106. <https://doi.org/10.1016/j.conbuildmat.2011.08.022>
- Andodariya A, Patel RL, Pitroda J (2017a) Feasibility study of using fly ash brick made from reclaimed sand dust waste and quarry dust waste. *MOJ Civ Eng* 3(3):1–5. <https://doi.org/10.15406/mojce.2017.03.00071>
- Andodariya A, Patel RL, Pitroda J (2017b) Techno economical study eco-friendly green brick production using reclaimed sand dust waste: a review. *IJTE special issue for ICRISSET 2017b*, pp 28–32
- Arshad MS, Pawade PY (2014) Reuse of natural waste material for making light weight bricks. *Int J Sci Technol Res* 3(6):49–53
- Bhimani DR, Pitroda J, Bhavsar JJ (2013) A study on foundry sand: opportunities for sustainable and economical concrete. *GRE—Glob Res Anal* 2(1):60–63
- Bhushan B, Kanwar VS, John S (2019) Development of bricks by utilizing waste from paper industry. *Int J Innovative Technol Explor Eng* 9(2):377–386. <https://doi.org/10.35940/ijitee.B6365.129219>
- Chan C-M (2011) Effect of natural fibres inclusion in clay bricks: physico-mechanical properties. *World Acad Sci Eng Technol Int J Civ Environ Eng* 5(1):7–13. <https://doi.org/10.5281/zenodo.1331783>
- Chiang K-Y, Chou P-H, Hua C-R, Chien K-L, Cheeseman C (2009) Lightweight bricks manufactured from water treatment sludge and rice husks. *J Hazard Mater* 171(1–3):76–82. <https://doi.org/10.1016/j.jhazmat.2009.05.144>
- Cioli F, Abbà A, Alias C, Sorlini S (2022) Reuse or disposal of waste foundry sand: an insight into environmental aspects. *Appl Sci (switzerland)* 12(6420):1–13. <https://doi.org/10.3390/app12136420>
- Damanhuri AAM, Lubis AMHS, Hariri A, Herawan SG, Roslan MHI, Hussin MSF (2020) Mechanical properties of rice husk ash (RHA) brick as partial replacement of clay. *J Phys Conf Ser* 1529(4):1–8. <https://doi.org/10.1088/1742-6596/1529/4/042034>
- Dondi M, Guarini G, Raimondo M, Zanelli C (2009) Recycling PC and TV waste glass in clay bricks and roof tiles. *Waste Manage* 29(6):1945–1951. <https://doi.org/10.1016/j.wasman.2008.12.003>
- Eliche-Quesada D, Martínez-García C, Martínez-Cartas ML, Cotes-Palomino MT, Pérez-Villarejo L, Cruz-Pérez N, Corpas-Iglesias FA (2011) The use of different forms of waste in the manufacture of ceramic bricks. *Appl Clay Sci* 52(3):270–276. <https://doi.org/10.1016/j.clay.2011.03.003>
- Hamza R, El-Haggar S, Khedr S (2011a) Utilization of marble and granite waste in concrete bricks. In: 2011a International conference on environment and bioscience IPCBEE, vol 21, pp 115–119. Retrieved from <http://www.ijbbb.org/show-25-312-1.html>
- Hamza RA, El-Haggar S, Khedr S (2011b) Marble and granite waste: characterization and utilization in concrete bricks. *Int J Biosci Biochem Bioinform* 1(4):286–291
- Heniegall AM, Ramadan MA, Naguib A, Agwa IS (2020) Study on properties of clay brick incorporating sludge of water treatment plant and agriculture waste. *Case Stud Constr Mater* 13:e00397. <https://doi.org/10.1016/j.cscm.2020.e00397>

- Herek LCS, Hori CE, Reis MHM, Mora ND, Tavares CRG, Bergamasco R (2012) Characterization of ceramic bricks incorporated with textile laundry sludge. *Ceram Int* 38(2):951–959. <https://doi.org/10.1016/j.ceramint.2011.08.015>
- Hossiney N, Das P, Mohan MK, George J (2018) In-plant production of bricks containing waste foundry sand—a study with Belgaum foundry industry. *Case Stud Constr Mater* 9:1–25. <https://doi.org/10.1016/j.cscm.2018.e00170>
- Ismail S, Yaacob Z (2010) Properties of bricks produced with recycled fine aggregate. *World Acad Sci Eng Technol* 43(7):878–882. <https://doi.org/10.5281/zenodo.1059994>
- Jahagirdar SS, Shrihari S, Manu B (2013a). Reuse of textile mill sludge in burnt clay bricks. *Int J Adv Technol Civ Eng* 2(1):96–99
- Jahagirdar SS, Shrihari S, Manu B (2013b) Utilization of textile mill sludge in burnt clay bricks. *Int J Environ Prot* 3(5):6–13
- Kartini K, Ernida NZA, Fazilla NB, Farhan AH (2012) Development of lightweight sand-cement bricks using quarry dust, rice husk and kenaf powder for sustainability. *Int J Civ Environ Eng (IJCEE-IJENS)* 12(6):1–7. Retrieved from [http://www.ijens.org/Vol\\_12\\_I\\_06/126806-5858-IJCEE-IJENS.pdf](http://www.ijens.org/Vol_12_I_06/126806-5858-IJCEE-IJENS.pdf)
- Khalid FS, Aminuddin MYA, Shahidan S, Irwan JM, Ibrahim MHW (2020) The mechanical properties of brick containing recycled concrete aggregate and crumb rubber as sand replacement. *IOP Conf Ser Mater Sci Eng* 917(012020):1–6. <https://doi.org/10.1088/1757-899X/917/1/012020>
- Kulkarni A, Raje S, Rajgor M (2013) Bagasse ash as an effective replacement in fly ash bricks. *Int J Eng Trends Technol* 4(10):4484–4489
- Loryuenyong V, Panyachai T, Kaewsimork K, Siritai C (2009) Effects of recycled glass substitution on the physical and mechanical properties of clay bricks. *Waste Manage* 29(10):2717–2721. <https://doi.org/10.1016/j.wasman.2009.05.015>
- Mahajan SA, Husain M (2016) Utilization of waste sludge in brick making. In: International conference on global trends in engineering, technology and management, pp 274–278
- Martínez-García C, Eliche-Quesada D, Pérez-Villarejo L, Iglesias-Godino FJ, Corpas-Iglesias FA (2012) Sludge valorization from wastewater treatment plant to its application on the ceramic industry. *J Environ Manage* 95(Suppl):S343–S348. <https://doi.org/10.1016/j.jenvman.2011.06.016>
- Miqueleiz L, Ramirez F, Oti JE, Seco A, Kinuthia JM, Oreja I, Urmeneta P (2013) Alumina filler waste as clay replacement material for unfired brick production. *Eng Geol* 163:68–74. <https://doi.org/10.1016/j.enggeo.2013.05.006>
- Naik NS, Bahadure BM, Jejurkar CL (2014) Strength and durability of fly ash, cement and gypsum bricks. *Int J Computational Eng Res (IJCER) Open Access J* 4(5):1–4. Available at [www.ijcero.nline.com](http://www.ijcero.nline.com). ISSN (e): 2250–3005
- Naik P, Shirodkar V (2020) The use of solid waste in making eco-friendly bricks. *IOSR J Mech Civ Eng (IOSR-JMCE)*, pp 7–12
- Nithiya R, Anto LC, Vinodh KR, Anbalagan C (2016) Experimental investigation on bricks by using various waste materials. *Int J Latest Trends Eng Technol (IJLTET)* 6(3):395–402
- Oti JE, Kinuthia JM, Bai J (2009) Engineering properties of unfired clay masonry bricks. *Eng Geol* 107(3–4):130–139. <https://doi.org/10.1016/j.enggeo.2009.05.002>
- Patange GS, Khond MP, Rathod HJ, Chhadva KB (2013) Investigation of foundry waste sand reclamation process for small and medium scale Indian foundry. *Int J Ind Eng Technol (IJJET)* 3(1):1–6
- Phonphuak N, Chindaprasirt P (2018) Utilization of sugarcane bagasse ash to improve properties of fired clay brick. *Chiang Mai J Sci* 45(4):1855–1862
- Piattoni Q, Quagliarini E, Lenci S (2011) Experimental analysis and modelling of the mechanical behaviour of earthen bricks. *Constr Build Mater* 25(4):2067–2075. <https://doi.org/10.1016/j.conbuildmat.2010.11.039>
- Prasad HNR, Prasad HGV, Hamsagar C, Gowda DY, Lobo NM, Gowda SPUS (2014) An approach for alternative solution in brick manufacturing. *Int J Sci Environ Technol* 3(3):1105–1114

- Priyadarshini B, Kavisri M (2018) Utilization of textile sludge in manufacturing e-bricks. *Int J Civ Eng Technol* 9(11):2266–2273
- Raut SP, Ralegaonkar RV, Mandavgane SA (2011) Development of sustainable construction material using industrial and agricultural solid waste: a review of waste-create bricks. *Constr Build Mater* 25(10):4037–4042. <https://doi.org/10.1016/j.conbuildmat.2011.04.038>
- Salla S, Pitroda J, Shah BK (2013) Comparative study on rice husk and ground nut shell in fly ash bricks. *Int J Inventive Eng Sci (IJIES)* 1(7):5–8
- Salla SR, Pitroda J, Shah BK (2015) Comparative study jute fibre and banana fibre in fly ash bricks. *Int J Eng Trends Technol (IJETT)* 2(2):850–856. Available at <http://www.ijettjournal.org>. Retrieved from <http://edupediapublications.org/journals/index.php/ijr/article/view/1428>. ISSN: 2231-5381
- Shakir AA, Naganathan S, Mustapha KNB (2013) Development of bricks from waste material: a review paper. *Aust J Basic Appl Sci* 7(8):812–818
- Sufian M, Ullah S, Ostrowski KA, Ahmad A, Zia A, Śliwa-Wieczorek K, Siddiq M, Awan AA (2021) An experimental and empirical study on the use of waste marble powder in construction material. *Materials* 14(3829):1–17. <https://doi.org/10.3390/ma14143829>
- Sumathi A, Mohan KSR (2014) Compressive strength of fly ash brick with addition of lime, gypsum and quarry dust. *Int J ChemTech Res* 7(1):28–36
- Sumathi R, Ambiga K (2015) Utilization of sludge in the production of bricks. *Int J Sci Technoledge* 3(1):54–56. ISSN 2321-919X
- Suresh C, Tamilselvi M, Dasarathy AK, Ilango SP (2018) An experimental investigation on hypo sludge bricks. *AIP Conf Proc* 2039(11):1–9. <https://doi.org/10.1063/1.5079038>
- Swarna MA, Venkatakrishnaiah R (2014) Manufacturing of bricks using tannery effluent sludge. *Int J Recent Dev Eng Technol* 3(4):33–36
- Teklehaimanot M, Hailay H, Tesfaye T (2021) Manufacturing of ecofriendly bricks using microdust cotton waste. *J Eng* 2021(8815965):1–10. <https://doi.org/10.1155/2021/8815965>
- Turgut P, Yesilata B (2008) Physico-mechanical and thermal performances of newly developed rubber-added bricks. *Energ Build* 40(5):679–688. <https://doi.org/10.1016/j.enbuild.2007.05.002>
- Vaithiyasubramanian R, Srinivasan D, Kanagarajan AK (2022) Study on preparation of brick blocks by using construction waste and sludge. *Environ Sci Pollut Res* 29:72528–72544. <https://doi.org/10.1007/s11356-022-20968-7>
- Watile RK, Deshmukh SK, Durge PV, Yawale AD (2015) Utilization of rice husk for production of clay brick. In: *International journal of research in advent technology, special issue 1st international conference on advent trends in engineering, science and technology “ICATEST 2015”*, pp 199–203
- Weng C-H, Lin D-F, Chiang P-C (2003) Utilization of sludge as brick materials. *Adv Environ Res* 7(3):679–685. [https://doi.org/10.1016/S1093-0191\(02\)00037-0](https://doi.org/10.1016/S1093-0191(02)00037-0)
- Zhang L (2013) Production of bricks from waste materials—a review. *Constr Build Mater* 47:643–655. <https://doi.org/10.1016/j.conbuildmat.2013.05.043>



# Innovative Sustainable Solution for High-Strength Quaternary Cement Concrete with Lime Powder



Niragi Dave

**Abstract** An experimental study was conducted to regulate the impact of the mechanical behaviour of quaternary concrete made with additional cementitious ingredients. In predetermined ratios, fly ash (FA), lime powder (LP), and silica fume (SF) were combined by swapping out 30–50 per cent of the weight of regular Portland cement (OPC). For all mixtures, water-to-binder ratio and the total amount of cementitious ingredients were held constant at 0.35 and 402 kg/m<sup>3</sup>, respectively. At 7, 28, 56, 90, 180, and 365 days, tests were conducted to evaluate the mechanical behaviour of quaternary concretes, and the results were compared to those obtained for controlled concrete (100% OPC). According to the normal code of practise in India, the complete exercise was prepared, cured, and tested. In addition, durability properties were investigated in terms of permeability and chemical attack. In some permutations of mixes, it was discovered that the strength of the concrete with quaternary binders was greater than that of the controlled concrete because of the cement's synergistic activity with the addition of additional cementitious materials. According to the test results, optimal mixes of FA, SF, and LP as a partial replacement for OPC as quaternary concrete would be a better choice than 100% controlled concrete.

**Keywords** Supplementary cementitious material · Ordinary Portland cement · Fly ash · Silica fume · Lime powder

## 1 Introduction

Using mineral admixtures as a partial substitute for Portland cement in concrete is a better step in the direction of sustainable growth due to its benefits in terms of technology, economy, and the environment. Concrete's physical and chemical characteristics are impacted by the inclusion of inert and pozzolanic components because they promote the filling of micropores, heterogeneous nucleation, and pozzolanic

---

N. Dave (✉)

Department of Civil Engineering, School of Technology, Pandit Deendayal Energy University, Gandhinagar 382426, Gujarat, India  
e-mail: [Niragi.Dave@sot.pdpu.ac.in](mailto:Niragi.Dave@sot.pdpu.ac.in)

reactions, all of which depend on the amount and solubility of amorphous silica. The filling operation involves incorporating additional materials that are finer than the OPC. The microscopic holes between the components are filled by these substances. Hydration of cement paste is accompanied by liberation of heat that raises the temperature of concrete (Pipilikaki and Katsioti 2009). Pozzolanic action occurs between the amorphous silica of the cement additive and the calcium hydroxide/portlandite (calcium hydrate) produced by cement hydration processes to produce non-water-soluble calcium silicate hydrates (calcium-silicate-hydrate). Since calcium-silicate-hydrate has a lower density than calcium hydrate and pure silica, this reaction will cause the reaction products to swell. Studies of concrete's mechanical characteristics, durability, and microstructure should be taken into consideration if concrete is to be resistant to all weathering processes (Pipilikaki and Katsioti 2009; Githachuri and Alexander 2013; Elkhadiri et al. 2002; Vance et al. 2013; Pipilikaki et al. 2008). Mineral additions like limestone fillers, ground granulated blast furnace slag, and natural pozzolana increase the resistance of concrete to the attack of aggressive agents (sulfuric acid) because they reduce the amount of calcium hydroxide, the component of concrete that is most vulnerable to acid attacks (Makhloufi et al. 2013, 2014a). A low heat of hydration, resistance to acids and sulphates, increased workability, and a greater ultimate strength are further advantages (Chang et al. 2005; Monteny et al. 2003; Georgescu et al. 2008). To increase the volume of hydrates and produce a dense structure, pozzolanic materials are added to concrete (Dave et al. 2016; Githachuri and Alexander 2013; Vance et al. 2013b; Makhloufi et al. 2013). Permeability is decreased by using additional cementitious materials, which result in pore refinement as a result of their pozzolanic reaction happening concurrently with cement hydration (Person 1988; Kamann 2004; Yu et al. 1993).

The main objective of the current study is to obtain information on the effects of combining fly ash (FA), silica fume (SF), and lime powder (LP) as a partial replacement for ordinary Portland cement (OPC) on the durability and strength of concretes. An appropriate quaternary mix ratio will be proposed in light of the results.

## 2 Materials and Methods

### 2.1 Materials

The basic materials for concrete utilised in the current study are regular Portland cement, angular coarse aggregates (Sp. Gr. 2.68 and size of aggregate in between 10 and 20 mm), and river sand as fine aggregates (Sp. Gr. 2.62 and maximum size of 4.75 mm). Each of these materials complies with IS: 456–2000. The additional cementitious ingredients used as a partial replacement for OPC to create quaternary mixtures include fly ash, lime powder, and silica fume. The physical traits and chemical composition of cement and other supporting components are listed in Table 1. Table 2 displays various ratios and concrete mix designs for controlled and quaternary

combinations that contain fly ash, lime powder, and silica fume. In order to generate the mix combinations incorporating additional components, these additions were employed to replace 30 and 50% of the weight of OPC, respectively, in quaternary mode. Table 2 displays the slump test results for each mix combination. A total of 100 concrete examples were cast, including specimens for tensile strength tests that were 300 mm high and 150 mm in diameter, specimens for compressive strength tests that were 1503 mm<sup>3</sup> cubes, and specimens for flexural strength tests that were beams 500 mm in length, 100 mm in width, and 100 mm in depth. For the sulphate attack, RCPT, and ultrasonic pulse velocity (UPV) investigations, three additional beam specimens for each mix type were also cast. All of the samples were demoulded and cured in a water curing tank after 24 h.

Utilising industry-standard 150 mm<sup>3</sup> cubes, compressive strength was evaluated in accordance with I.S. 516–1959 utilising a universal testing equipment with a 300 T capacity. Approximately 14 N/mm<sup>2</sup> of stress was applied each minute. The average of three specimens served as a representation of the compressive strength of each batch of concrete. It was tested for split tensile strength in line with IS: 516–2004. The

**Table 1** Properties of materials

Description	OPC	FA	SF	LP
<i>Physical characteristics</i>				
Specific gravity	3.13	2.27	2.24	2.22
Fineness, cm <sup>2</sup> /gm	2285	3720	16,018	4387
<i>Chemical characteristics</i>				
Calcium oxide	66.82	1.42	1.55	57.64
Silicon oxide	17.63	62.32	86.39	0.03
Aluminium oxide	9.83	25.79	0.85	0.05
Ferric oxide	2.29	3.4	1.63	0.07
Manganese oxide	0.03	0.03	0.00	0.00
Magnesium oxide	1.25	2.62	0.14	0.12
Potassium oxide	0.49	0.97	2.00	0.04
Sodium oxide	0.23	0.06	0.38	0.035
Loss of ignition, %	0.9	3.20	2.01	5.52

**Table 2** Slump test results for the workability study of fresh concrete

Mix	Slump (mm)
C Control	122
L1 5SF + 5LP + 70OPC + 20FA	168
L2 7.5SF + 7.5LP + 70OPC + 15FA	185
L3 10SF + 10LP + 50OPC + 30FA	128
L4 15SF + 15 LP + 50OPC + 20FA	117
L5 20SF + 15LP + 50OPC + 15FA	105

concrete was formed into cylinders that were 300 mm tall and 150 mm in diameter. During casting, a table vibrator mechanically vibrated the cylinders. After 24 h, the samples were taken out of the mould, then left to soak in water for 28 days to cure. The concrete cylinders underwent a split tensile test utilising a universal testing device after the required curing period. The average split tensile strength was calculated after testing three identical specimens.

The flexure strength was assessed using standard beam specimens with dimensions of 500 mm long, 100 mm wide, and 100 mm deep after 365 days of curing, supported on an effective span of 400 mm and loaded at the third locations. To measure the ultrasonic pulse velocity, utilised two transducers in touch with the specimen via a coupling medium. It may be used for many different activities, component of the measurement of fracture depth, surface velocity, uniformity, and pulse velocity. SEM was used to examine the morphological features of the concrete mix that were created from OPC, FA, LP, and SF (Scanning Electron Microscopy). A RCPT test was performed in accordance with American Standard Code 1202 (ATM 2005).

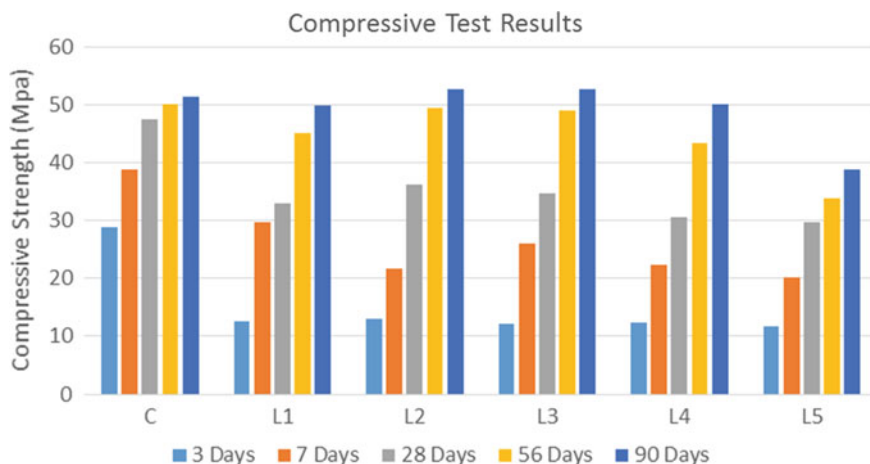
### **3 Results and Discussion**

#### ***3.1 Fresh Properties of Concrete***

For the concrete to be properly positioned and compacted in structural parts, it must have decent workability. By maintaining the water-to-cement ratio or by adding admixtures, high workability can be attained. All of the mixes' new concrete slump values, as shown in Table 2, fall between 100 and 185 mm, which are regarded as a good level of workability. These workability values were achieved using 1% superplasticizer (Glenium 51) to improve workability at a water–cement ratio of 0.40. Fly ash's inclusion (30%) enhances the mix's workability despite the fact that it has a lower specific surface than OPC. This is because the fly ash particles are spherical. The test revealed that adding SF makes concrete sticky and impairs its use.

#### ***3.2 Compressive Strength Test***

At 3, 7, 28, 56, and 90 days after curing, concrete cube specimens from each batch underwent tests to determine their average compressive strength. The findings are shown in Fig. 1. It was demonstrated that six mix combinations' compressive strength increased with time. The quaternary mix combinations L1, L2, and L3 have shown the highest performance over longer ages. Concretes with more cementitious ingredients have stronger concretes due to the interaction of mineral admixtures' silicates with the released lime to produce additional C-S–H. Fly ash along with cement initially



**Fig. 1** Compressive strength test results

makes little contribution to strength, but after 56 days, due to its pozzolanic reaction, it starts to provide some strength.

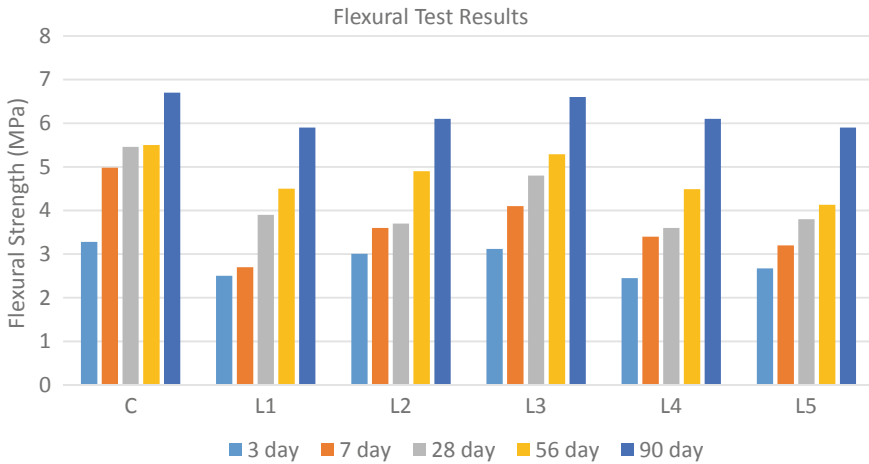
The 20% SF addition to concrete mix was found to make the mixture sticky, reducing the workability of the concrete and impeding the mixing and compaction processes. It causes the compressive strength to decrease. These findings were from Mix L4 and Mix L5.

### 3.3 Flexural Strength

Figure 2 displays the outcomes of the flexural strength tests performed on all quaternary concretes on certain test days. FA, SF, and LP quaternary mix combinations have fared roughly as poorly as control concrete. Mix L3 is shown to have the maximum flexural strength of all the ratios. It was observed that the flexural strength appeared to be significantly affected by the addition of cementitious materials. Observations reveal that the flexural strength grows consistently as the amount of additional cementitious materials in the mix increases.

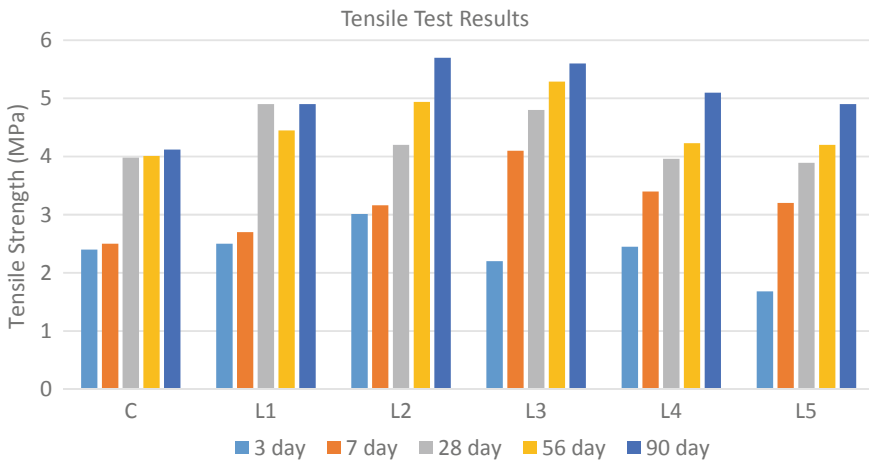
### 3.4 Tensile Strength

Furthermore, as seen in Fig. 3, it was discovered that the tensile strength of all mix combinations grows over time. Split tensile strength increases according to (Yazici and Arel's 2012) research, when fly ash % level rises in concrete examination into the effect of fly ash percentage level on the tensile strength of concrete. After 28 days, it



**Fig. 2** Flexural strength test results

was discovered that the high silica content quaternary binders from SF and LP did not considerably improve in tensile strength, but they still contributed to good strength when compared to control. As compared to 50% replacement level, 30% substitution of cement in quaternary concrete displays a significant increase in tensile strength. For this, less silica content is to blame. According to the test results, it is clear that adding more cementitious materials to quaternary mixes affects the tensile strength; a virtually same pattern of behaviour was observed when OPC was 30% substituted by supplemental cementitious materials. With 30 and 50% OPC replacement, the L2 and L3 combination showed the highest tensile strength.



**Fig. 3** Tensile strength test results

### 3.5 Rapid Chloride Permeability Test

Figure 4 displays the outcomes of the Rapid Chloride Permeability Tests of concrete. Quaternary combinations result in significant reductions in the rapid chloride permeability. Figure 4 illustrates how the RCPT values have dropped with testing age. An increase in resistance to chloride ion penetration is indicated by a decrease in chloride permeability, according to published studies. When cement was used in place of pozzolanic material, the concretes' rapid chloride permeability was dramatically decreased (Li and Roy 1986; Ahmed et al. 2009; Massazza 1993). Due to its denser microstructure, the concrete with large volume pozzolans has decreased chloride permeability. The reduced capillary pore density caused by the pozzolanic process may reduce the chloride permeability of concrete (Thomas 2007; Ahmed et al. 2009). A ternary mixture with 25% fly ash and 10% silica fume showed decreased chloride permeability when compared to binary concrete (Massazza 1993). The recent experiment has shown that quaternary concrete yields better outcomes. The total charge passing through the quaternary concrete, which consists of FA, SF, and LP in L1, L2, L3, L4, and L5, decreases by up to 75% between 28 and 90 days compared to control. It demonstrates that when FA, SF, and LP percentage levels increase, the passing rate at age is decreasing. Finer fineness SF performs well as the fraction of SF in quaternary concrete increases. The results show that OPC with three extra cementitious elements offers improved resistance to chloride permeability.

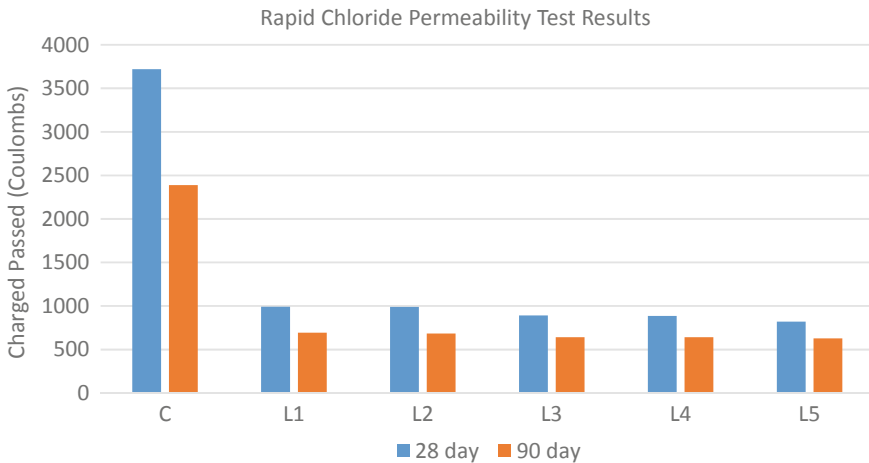


Fig. 4 Charged passed in different quaternary concretes

## 4 Conclusions

In this work, the behaviour of quaternary concrete that has been mixed with FA, SF, and LP is examined. The experimental findings showed that the properties of concrete are affected by the addition of supplemental cementitious ingredients including FA, SF, and LP in cement. The test findings can be used to draw the following conclusions:

1. The addition of pozzolanic materials increased the compressive strength in quaternary concrete, because of its fine fineness as well as pozzolanic reactivity significantly improves the quality of cement paste and the micro-structure of the transition zone between the binder matrix and the aggregates. With regard to strong compressive strength, quaternary concrete with mix L3 has produced the greatest results.
2. The tensile and flexural strengths of quaternary concrete have consistently shown satisfactory results. At the age of 90 days, the ideal Mix L2 and Mix L3 demonstrated stronger flexural strength in comparison to the control mix and higher tensile strength than the control mix.
3. Because the cementitious material used as the binder has a larger surface area, with time and an increase in additional cementitious elements, chloride permeability of concrete decreases. This raises the density of the concrete, as seen by the microstructure. At 90 days old, concrete made using quaternary L1 to Mix L5 showed a 75% lower charge than 100% OPC.
4. The general end drawn from this examination is that quaternary concrete of 10%SF + 10%LP + 50%OPC + 30%FA includes a superior blend than OPC concrete because of financial reasons, better protection from chemical resistance.
5. The greatest OPC cement substitute might be quaternary cement. Its usage in construction could reduce the need for ordinary crude materials used in OPC and increase the utilisation of waste resources in construction.

## References

- Ahmed MS, Kayali O, Anderson W (2009) Evaluation of binary and ternary blends of pozzolanic materials using the rapid chloride permeability test. *J Mater Civ Eng ASCE* 21(9) 446–453
- Chang Z-T, Song X-J, Munn R, Marosszeky M (2005) Using limestone aggregates and different cements for enhancing resistance of concrete to sulphuric acid attack. *Cem Concr Res* 35(8):1486–1494
- Dave N, Mishra AK, Srivastava A, Kaushik SK (2016) Experimental analysis of strength and durability properties of quaternary cement binder and mortar. *Constr Build Mater* 107:117–124
- Elkhadiri I, Diouri A, Boukhari A, Aride J, Puertas F (2002) Mechanical behaviour of various mortars made by combined fly ash and limestone in Moroccan Portland cement. *Cem Concr Res* 32(10):1597–1603
- Georgescu M, Saca N, Voicu G (2008) Hydration–hydrolysis processes in blended cements with limestone filler and fly ash content. *Rom J Mater* 38(4):260–270
- Githachuri K, Alexander MG (2013) Durability performance potential and strength of blended Portland limestone cement concrete. *Cem Concr Compos* 39:115–121



- Kamann PJ (2004) Porosity and permeability in sediment mixtures. Masters thesis, Department of Geological Sciences, Wright State University, Dayton, OH
- Li S, Roy DM (1986) Investigation of relations between porosity, pore structure and  $\text{Cl}^-$  diffusion of fly ash and blended cement pastes. *Cem Concr Res* 16(5):749–759
- Makhloufi Z, Bederina M, Bouziani T, Kadri EH, Bouhicha M (2013) Formulation of superplasticized limestone concrete of Turonian. *Int Rev Mech Eng* 7(6):1103–1114
- Makhloufi Z, Bouziani T, Hadjoudja M, Bederina M (2014a) Durability of limestone mortars based on quaternary binders subjected to sulfuric acid using drying-immersion cycles. *Constr Build Mater* 71:579–588
- Makhloufi Z, Bouziani T, Bederina M, Hadjoudja M (2014b) Mix proportioning and performance of a crushed limestone sand concrete. *J Build Mater Struct* 1(1):10–22
- Massazza F (1993) Pozzolanaic cements. *Cem Concr Compos* 15(4):185–214
- Monteny J, De Belie N, Taerwe L (2003) Resistance of different types of concrete mixtures to sulfuric acid. *Mater Struct* 36(258):242–249
- Person BSM (1988) Shrinkage of high performance concrete. In: Proceedings of international workshop on autogeneous shrinkage of concrete, Hiroshima, Japan, E&FN Spon, London, pp 105–115
- Pipilikaki P, Papageorgiou D, Teas C, Chaniotakis E, Katsioti M (2008) The effect of temperature on the thaumasite formation. *Cem Concr Compos* 30(10):964–969
- Pipilikaki P, Katsioti M (2009) Study of the hydration process of quaternary blended cements and durability of the produced mortars and concretes. *Constr Build Mater* 23(6):2246–2250
- Thomas M (2007) Optimizing the use of fly ash in concrete. Retrieved from [https://www.cement.org/docs/default-source/fc\\_concrete\\_technology/is548-optimizing-the-use-of-fly-ash-concrete.pdf](https://www.cement.org/docs/default-source/fc_concrete_technology/is548-optimizing-the-use-of-fly-ash-concrete.pdf). Accessed on 30 Jan 2017
- Vance K, Aguayo M, Oey T, Sant G, Neithalath N (2013) Hydration and strength development in ternary Portland cement blends containing limestone and flyash or metakaolin. *Cem Concr Compos* 39:93–103
- Yazici S, Arel HŞ (2012) Effects of fly ash fineness on the mechanical properties of concrete. *Sadhana* 37(3):389–403. © Indian Academy of Sciences
- Yu A-B, Standish N, McLean A (1993) Porosity calculation of binary mixtures of nonspherical particles. *J Am Ceram Soc* 76(11):2813–2816

# Effect of Incorporation of Nano-Silica on Mechanical Properties of Mortar and Concrete



Patel Karan and Thakkar Sonal

**Abstract** There are a number of applications of nanotechnology, particularly in concrete. The addition of nano-silica improves both the mechanical and durability properties of concrete. During the hydration process, the reaction of nano-silica with calcium hydroxide creates an additional calcium silicate hydrate bond, which improves the mechanical characteristics of concrete. The effect of the inclusion of nano-silica on the mechanical properties of paste, mortar and concrete is investigated in this study. Nano-silica was introduced as a replacement of cement from 1 to 5% with an increase of 1%. Various mechanical properties and setting time of different mixes were evaluated and compared with the control mix. The cement paste's consistency increased while the setting time of the paste was reduced by 8 and 47%, respectively, due to the inclusion of nano-silica. The optimum dosage of the addition of nano-silica was 3%. At 3% of nano-silica, the compressive strength of the mortar specimen was higher than control mortar by 15 and 28% at 7 and 28 days, respectively. Above three percentages of nano-silica, the strength will be reduced. Similarly, in concrete, the inclusion of nano-silica by 3% led to an increase in compressive strength by 15 and 20%, respectively, at 7 days and 28 days over control concrete. Flexural and split tensile strength was also increased by 3% nano-silica by 15 and 22%, respectively. Nano-silica did not produce a significant change in the modulus of elasticity of concrete.

**Keywords** Nano-silica · Compressive strength · Tensile strength · Split tensile strength

---

P. Karan (✉) · T. Sonal  
Civil Engineering Department, Institute of Technology, Nirma University, Ahmedabad, Gujarat, India  
e-mail: [karanpatel520163@gmail.com](mailto:karanpatel520163@gmail.com)

T. Sonal  
e-mail: [sonal.thakkar@nirmauni.ac.in](mailto:sonal.thakkar@nirmauni.ac.in)

## 1 Introduction

ISO defines nanomaterials as any material having internal or outward dimensions in the nanoscale. Nanomaterials are widely used in various areas, including the medical, pharmaceutical and construction industries. There are many ways of modifying concrete properties and one of the ways is to add nanomaterials to it. Nanomaterials like nano-titania, nano-silica, nano-alumina, nano-zirconium dioxide, carbon nanotubes and carbon nanofibers are widely used. These materials have a very high surface area which is directly related to high reactivity.

Carbon nanotubes have the ability to improve ductility and resist the formation of cracks at the nanoscale, while graphene nano-platelet's inclusion lowers the permeability of water and chloride ions. Nano-kaolinite has anti-microbial and self-cleaning properties when incorporated into concrete (Abhilash et al. 2021; Singh et al. 2013).

Nanomaterials have shown a remarkable effect on cement hydration through a nucleation process that acts as a seed for calcium silicate hydrate hydration. As nano-silica has a high surface area, hydration process gets accelerated resulting in a more compact microstructure and denser mixture. The addition of nano-silica in concrete reduces water absorption, permeability and chloride penetration due to dense packing (Abhilash et al. 2021; Singh et al. 2013). Rupasinghe et al. (2017) observed that 8% nano-silica incorporated cement paste gives higher strength by 18% compared with control cement paste. The incorporation of nano-silica in mortar showed a high torque value during the testing period because of increasing plastic viscosity and yield stress. 2.5% dosage of nano-silica reduces the spread of mortar on the flow table and reduces the setting time of the paste (Senff et al. 2009). Ng et al. (2020) suggested that 3% of nano-silica gives maximum positive results in cement mortar. In twenty-eight days, compressive and flexural strength increased by 38 and 18%, respectively. 20% compressive strength increased with 3% nano-silica, and 50% cement was replaced with GGBS (Said et al. 2021). Total porosity was reduced for all concentrations of nano-SiO<sub>2</sub> concerning the control mix (without nano-SiO<sub>2</sub>). 2% containing nano-SiO<sub>2</sub> mix shows the lowest porosity (Ng et al. 2020). Isfahani et al. (2016) observed that the concrete consisting of 1.5% NS developed 20% more compressive strength compared to concrete without nanomaterial at 0.5 water to binder ratio.

According to the authors (Mukharjee et al. 2020), as nano-SiO<sub>2</sub> has very high specific area, pozzolanic activity increases at early age resulting in early strength in cement. Therefore, even a small amount of nano-silica significantly increased the compressive strength. However, the maximum compressive strength at 28 days was obtained at 2 to 3% dosage of nano-silica, indicating that the nano-silica's optimum dosage was within this range (Behzadian and Shahrajabian 2019; Elkady et al. 2013; Kumar et al. 2019). Compressive strength reduces at higher dosages of nano-silica due to more voids and agglomeration (Elkady et al. 2013). 3% of nano-silica replacement led to increased flexural strength due to less void and the formation of the greater interfacial transition zone in the concrete matrix. The addition of 3% nano-silica increased flexural strength by 15% in both recycled and natural aggregate concrete

**Table 1** Cement's physical properties

Consistency	Setting time (min)		Specific gravity	Fineness (m <sup>2</sup> /kg)
	Initial	Final		
28	80	170	3.12	290.5

(Mukharjee et al. 2020). Kumar et al. 2019 reported that 3% nano-silica improves the tensile strength of concrete by 22%.

Materials like nano-silica redefine the fresh and hardened properties of concrete and also help in enhancing the durability of concrete. Therefore, the use of nanomaterials is likely to revolutionize bulk material properties by controlling the properties at the nano-level by providing an accelerated hydration mechanism and reducing the porosity of concrete. Nano-silica when used in concrete will give high strength, better durability and sustainability and will be an environmentally friendly cementitious composite. As nanomaterial is costly, it is to be used in judicious quantity since an excess of nanomaterials incorporated in concrete does not produce the desired effect; hence, experimental investigation was performed to determine the percentage of nano-silica to be incorporated and its effect on mechanical properties of concrete.

A small increase in initial cost will avoid undue distress in the structure due to particle packing and increase the durability leading to lesser repair and maintenance costs to users of the structures (Rupasinghe et al. 2017).

## 2 Materials and Methods

### 2.1 Materials

Ordinary Portland Cement used was OPC 53, as classified by the IS 269:2015 standard (IS: 12269 2013). Table 1 shows the physical properties of cement (Indian Standard: IS 4031-5 1988): Methods of Physical Tests for Hydraulic Cement of Indian Standards. Nano-silica (NS) particles have an average size of 12 nm. Specification of nano-silica is given in Table 2. Fine aggregate (FA) consisted of river sand. Results of tests conducted on fine and coarse aggregate (CA) are illustrated in Table 3 (IS 2386 (PartIII) 1963b; of Indian Standards). BASF Master Polyheed 8305 superplasticizer (SP) was used, and the specific gravity is 1.07.

### 2.2 Mortar Specimen Preparation

Mortars specimens were prepared with one part cement to two-part aggregate (1:2) ratio and a water/cement ratio of 0.4. Nano-silica was added in various proportions of 0, 1, 2, 3 and 5% by weight of cement. Superplasticizer named BASF Master

**Table 2** Specification of nano-silica

Specific surface area (m <sup>2</sup> /g)	175–225
Avg. particle size (Nm)	12
Tamped density (g/l)	Approx. 50
Specific gravity	2.2
Moisture (Wt%.)	≤ 1.5
pH	3.7–4.5
Purity (Wt%.)	> 99.8

**Table 3** Properties of aggregates

Aggregates	Specific gravity	Water absorption (Wt%.)	Fineness modulus
Fine aggregate	2.6	0.4	2.74
Coarse aggregate (10 mm)	2.6	0.81	6.028
Coarse aggregate (20 mm)	2.77	0.74	7.378

Polyheed 8305 was used in a range of 0.7 to 1%. For each type of mortar mixture, three samples of 75 mm × 75 mm × 75 mm were cast for the compressive strength test. Mortar specimens were prepared by the following procedure: (1) weighing of the dry materials, (2) mixing of cement and sand for one minute, (3) adding nano-silica and superplasticizer in water, (4) adding the solid materials into water and mixing for 3 min. Once the uniform mortar mixture was achieved, take out the mortar to the bowl. A vibrator was used for the compaction of the mortar. Oiled moulds were kept on the vibrator and filled the mould. Because of the less w/c ratio, continuous vibration was given till the finishing of the moulds. After 24 h demoulding was carried out and the mortar cubes were water cured. The mixture design of mortar is shown in Table 4.

**Table 4** Mortar formulations

Mix	Cement (g)	Nano-silica (g)	Sand (g)	Water (ml)	*SP (ml)
Control	200	0	600	80	0
NS1	198	2	600	80	1.2
NS2	196	4	600	80	1.3
NS3	194	6	600	80	1.5
NS5	190	10	600	80	1.6

\* SP: superplasticize

**Table 5** Concrete mixture designs (kg/m<sup>3</sup>)

Mix	Cement	NS	FA	CA	Water	SP
*CO	380	0	790	1197	152	3.8
NS3	369	11.4	790	1197	152	3.8
NS4	365	15.2	790	1197	152	3.8

\* CO: control

### 2.3 Concrete Specimen Preparation

This experimental work used a mixture design of M30 grade concrete. Two dosages of nano-silica of 3 and 4% are considered as cement replacement by weight. Table 5 shows the mixture proportion of concrete mixes. Compressive strength was evaluated on a 150 mm cube specimen. Beams size of 100 mm × 100 mm × 500 mm were used for evaluation of flexural strength while for split tensile test and also for modulus of elasticity 150 mm dia. and 300 mm height cylinders were cast. First, all the dry materials were weighed, and then NS was stirred manually after adding to water. Then superplasticizer was added to the combination. A mixture of cement and aggregates was then added to it.

### 2.4 Test Methods

#### Compressive Strength

The compressive strength (C) test was performed according to (IS 516 1959) on mortar and concrete cubes at an age of 7, 14 and 28 days. All the compression tests are performed using a compression testing machine (CTM). An average of three samples for each combination gave compressive strength of mortar and concrete mix.

$$\text{Compressive strength (MPa)} = P / A \quad (1)$$

where

$P$  Peak load (N).

$A$  Contact surface area (mm<sup>2</sup>).

#### Flexural Strength

The test procedure was used to evaluate flexural strength (IS 516 1959). Concrete specimens were tested at 28 days. A flexural testing machine was used for testing concrete specimens.

$$\text{Flexural strength (MPa)} = (P \times L) / (B \times D^2) \quad (2)$$

where

$P$  Maximum load (N).

$B, D$  Lateral dimension of the specimen (mm).

$L$  Length of span on which the specimen is supported (mm).

### Split Tensile Strength

IS 516 (1959) was used to evaluate the split tensile strength. The peak load has been considered as a failure load for the cylinder.

$$\text{Split tensile strength (MPa)} = 2P / \pi ld \quad (3)$$

where

$P$  Maximum load applied on specimen (N).

$l$  Length of cylinder (mm).

$d$  c/s dim. of cylindrical specimen (mm).

### Modulus of Elasticity

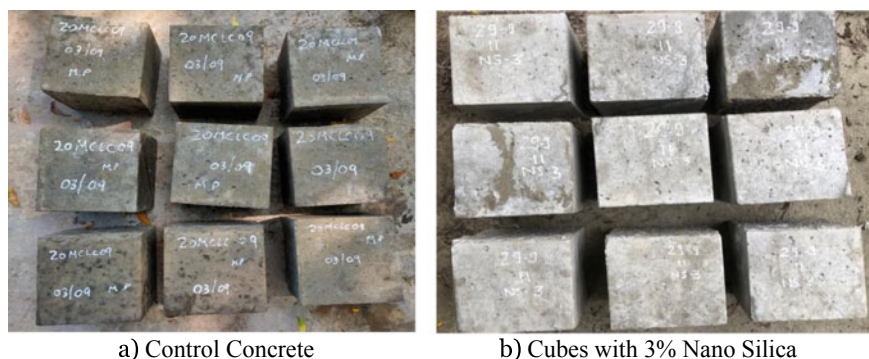
IS 516 has been used to measure the modulus of elasticity of concrete. In this method, the extensometer is attached to the cylinder and placed in UTM, and the load is applied. The load on the cylinder increased to 1/3 of the cube strength. Now, this load is maintained for 1 min. After one minute, the load is gradually released. The extensometer reading is noted and reloaded in the second step until the load reaches 1/3 of the cube strength. The reading from the extensometer is noted, and the load is slowly released.

## 3 Results and Discussion

### 3.1 Compressive Strength

Figure 1 shows the control concrete and cubes with nano-silica.

Table 6 showed the average compressive strength of mortar. It was observed that there was an increase in the compressive strength of mortar with an increase in the dosage of nano-silica up to 3% (NS3) and at 3% maximum strength was observed. For 5% nano-silica (NS5), there is a reduction in compressive strength due to the high surface energy of NS particles causing accumulation and uneven dispersion in the mortar matrix which results in a decrease in strength. Figure 2 shows the compressive



**Fig. 1** a Control concrete; b Cubes with 3% nano-silica

**Table 6** Average compressive strength of mortar

Mixture	Compressive strength (MPa)		
	7 days	14 days	28 days
Control	35.23	45.83	54.2
NS1	38.13	50.56	56.5
NS2	38.43	52.2	59.04
NS3	41	52.8	69.23
NS5	35.7	48.3	57.33

strength comparison at 7, 14 and 28 days for mortars. The optimum dosage of nano-silica for concrete is also 3%. Table 7 shows the compressive strength of concrete. For a greater nano-silica dose, it was difficult to produce uniform dispersion of nano-silica particles in water, which results in a decrease in the compressive strength of mortar and concrete at larger nano-silica dosages. Figure 3 shows comparison of compressive strength of concrete at different curing age.

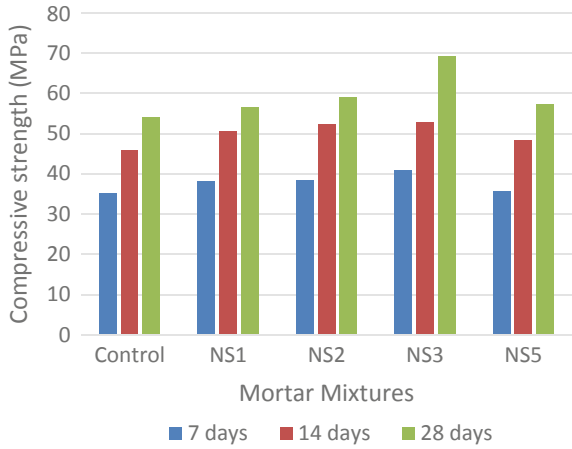
### 3.2 Flexural Strength

Figure 4 shows the beams of control concrete and mixture incorporating 3% nano-silica.

Test results show that NS3 concrete has higher flexural strength than control concrete. Further increasing the dosage of nano-silica flexural strength was reduced. The flexural strength of NS4 concrete is nearly similar to that of control concrete. The average 28-day flexural strength of concrete mixtures is shown in Table 8. Figure 5 shows the comparison of the flexural strength of concrete.



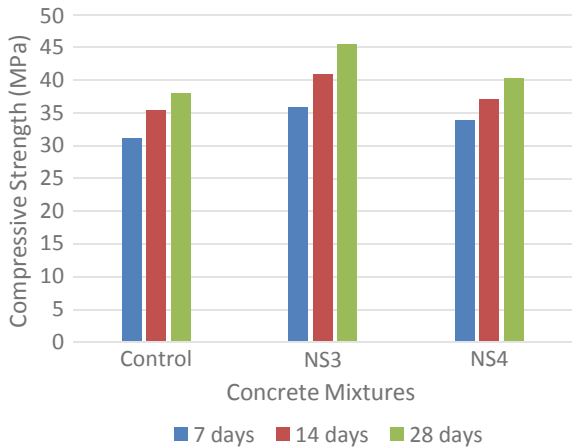
**Fig. 2** Compressive strength of mortar



**Table 7** Average compressive strength of concrete

Mixture	Compressive strength (MPa)		
	7 days	14 days	28 days
Control	31.2	35.4	38.06
NS3	35.92	40.86	45.53
NS4	33.9	37.1	40.23

**Fig. 3** Compressive strength of concrete



### 3.3 Split Tensile Strength

At 3% dosage of NS, maximum split tensile strength is obtained. The split tensile strength of concrete mixtures is given in Table 8. Above 3% nano-silica split tensile

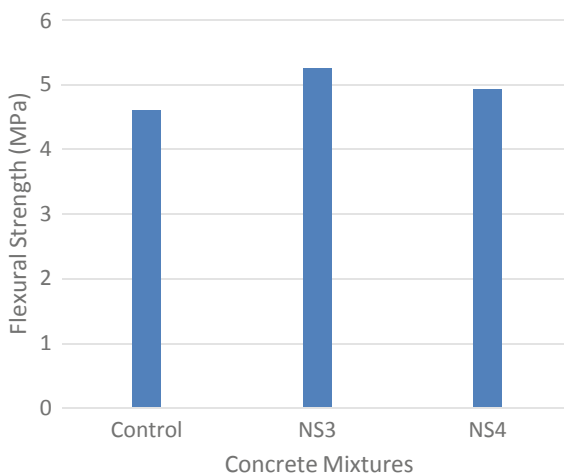


**Fig. 4** Control and 3% nano-silica beams for flexure

**Table 8** Average flexural and split tensile strength of concrete

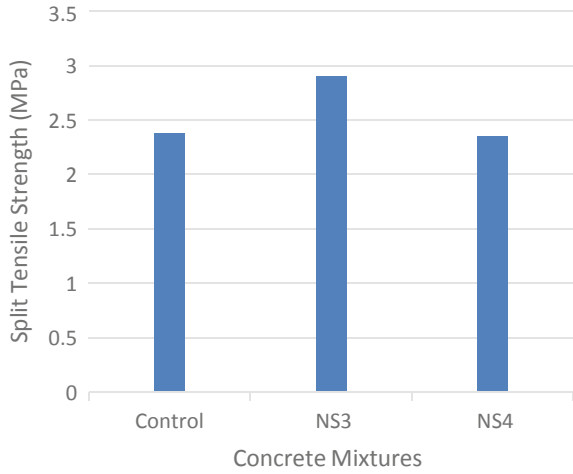
Mixture	Flexural strength (MPa)	Split tensile strength (MPa)
	28 days	28 days
Control	4.6	2.38
NS3	5.26	2.9
NS4	4.93	2.35

**Fig. 5** Flexural strength of concrete



strength was decreased. NS4 concrete shows lower 28 days split tensile strength than the control concrete. A comparison of split tensile strength is mentioned in Fig. 6.

**Fig. 6** Split tensile strength of concrete

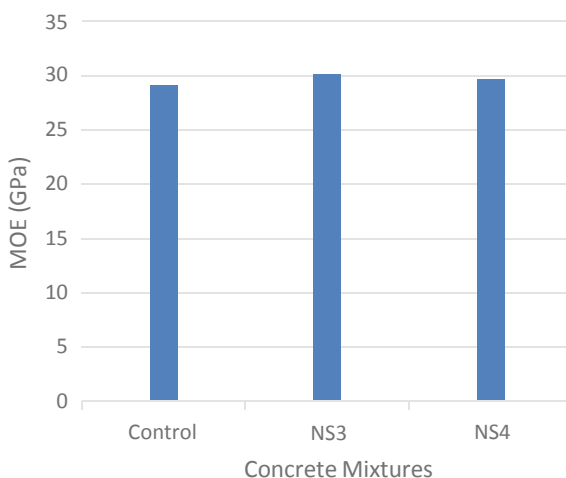


**Table 9** Average MOE of concrete mixtures

Mixture	Modulus of elasticity (GPa)
	28 days
Control	29.102
NS3	30.13
NS4	29.639

### 3.4 Modulus of Elasticity

Table 9 shows the average 28 days modulus of elasticity of concrete. It was observed that there was a slight increase in the modulus of elasticity of NS3 concrete. Figure 7 mentioned a comparison of the MOE of concrete.

**Fig. 7** Modulus of elasticity

## 4 Conclusion

The current study's findings have led to the following conclusions.

- The setting time of cement was decreased with increasing nano-silica dosage. This is because of nano-silica has a very fine particle size so, it has large specific surface area and required more water for wetting.
- It was observed that by incorporating 3% nano-silica in mortar mix, the compressive strength increased by 28%. In concrete incorporating 3% nano-SiO<sub>2</sub> in concrete mix, the compressive strength increased by 20%.
- Above the optimum dosage, the compressive strength was decreased; this may be due to uneven dispersion of nanoparticles and agglomeration leads to weak zone in concrete matrix.
- Flexural strength test reveals that 3% nano-silica increased the flexural strength by 15%.
- Split tensile strength was also increased by 22% for 3% nano-silica.
- The addition of nano-silica did not significantly alter the concrete's modulus of elasticity. It was noticed that the elastic modulus of concrete had slightly increased.

Thus, it can be observed that inclusion of 3% of nano-silica in concrete will lead to 20% increase in compressive strength, 15% increase in flexural strength and 22% increase in split tensile strength. Besides this due to dense particle packing durability of material also increases. Thus, for high rise buildings, we can optimize the use of materials by using nano-silica. Thus, overall entire construction industry will be benefited and saving of materials can be done. Nanomaterials will lead to sustainable and durable structures.

Initial cost of incorporation of nanomaterials may be higher, which may hinder into application at large scale level. Durability properties can be evaluated in future to highlight more benefits of use of nano-silica.

**Acknowledgements** Authors would like to thank Nirma University and Civil Department for providing with funds and facilities to carry out the work.

## References

- Abhilash PP, Nayak DK, Sangoju B, Kumar R, Kumar V (2021) Effect of nano-silica in concrete: a review. *Constr Build Mater* 278:122347. Elsevier Ltd. <https://doi.org/10.1016/j.conbuildmat.2021.122347>
- Behzadian R, Shahrajabian H (2019) Experimental study of the effect of nano-silica on the mechanical properties of concrete/PET composites. *KSCE J Civ Eng* 23(8):3660–3668. <https://doi.org/10.1007/s12205-019-2440-9>
- Elkady H, Serag MI, Elfeky MS (2013) Effect of nano silica de-agglomeration, and methods of adding super-plasticizer on the compressive strength, and workability of nano silica concrete. *Civ Environ Res* 3(2):21–34. ISSN 2222-1719 (Paper) ISSN 2222-2863 (Online). Available at [www.iiste.org](http://www.iiste.org)
- IS 516 (1959) Methods of tests for strength of concrete
- IS 2386–1 (1963a) Methods of test for aggregates for concrete. Part I: particle size and shape
- IS 2386–3 (1963b) Methods of test for aggregates for concrete. Part 3: specific gravity, density, voids, absorption and bulking
- IS 4031–4 (1988) Methods of physical tests for hydraulic cement. Part 4: determination of consistency of standard cement paste
- IS 4031–5 (1988) Methods of physical tests for hydraulic cement. Part 5: determination of initial and final setting times
- IS 4031–2 (1999) Methods of physical tests for hydraulic cement. Part 2: determination of fineness by specific surface by Blaine air permeability method
- IS 12269 (2013) 53 grade ordinary Portland cement
- Isfahani FT, Redaelli E, Lollini F, Li W, Bertolini L (2016) Effects of nanosilica on compressive strength and durability properties of concrete with different water to binder ratios. *Adv Mater Sci Eng* 2016(8453567):1–16. <https://doi.org/10.1155/2016/8453567>
- Kumar S, Kumar A, Kujur J (2019) Influence of nanosilica on mechanical and durability properties of concrete. *Proc Inst Civ Eng Struct Build* 172(11):781–788. <https://doi.org/10.1680/jstbu.18.00080>
- Mukharjee BB, Barai SV (2020) Influence of incorporation of colloidal nano-silica on behaviour of concrete. *Iran J Sci Technol Trans Civ Eng* 44(2):657–668. <https://doi.org/10.1007/s40996-020-00382-0>
- Ng DS, Paul SC, Anggraini V, Kong SY, Qureshi TS, Rodriguez CR, Liu Q-feng, Šavija B (2020) Influence of SiO<sub>2</sub>, TiO<sub>2</sub> and Fe<sub>2</sub>O<sub>3</sub> nanoparticles on the properties of fly ash blended cement mortars. *Constr Build Mater* 258:119627. <https://doi.org/10.1016/j.conbuildmat.2020.119627>
- Rupasinghe M, Nicolas RS, Mendis P, Sofi M, Ngo T (2017) Investigation of strength and hydration characteristics in nano-silica incorporated cement paste. *Cement Concr Compos* 80:17–30. <https://doi.org/10.1016/j.cemconcomp.2017.02.011>
- Said AM, Islam MS, Zeidan MS, Mahgoub M (2021) Effect of nano-silica on the properties of concrete and its interaction with slag. *Transp Res Rec* 2675(9):47–55. SAGE Publications Ltd. <https://doi.org/10.1177/0361198120943196>

- Senff L, Labrincha JA, Ferreira VM, Hotza D, Repette WL (2009) Effect of nano-silica on rheology and fresh properties of cement pastes and mortars. *Constr Build Mater* 23(7):2487–2491. <https://doi.org/10.1016/j.conbuildmat.2009.02.005>
- Singh LP, Karade SR, Bhattacharyya SK, Yousuf MM, Ahalawat S (2013) Beneficial role of nanosilica in cement-based materials—a review. *Constr Build Mater* 47:1069–1077. <https://doi.org/10.1016/j.conbuildmat.2013.05.052>

# Ecobricks—A Sustainable Solution to Plastic Waste



Vaishali Sahu, Abhishek, Yash Vats, and Niragi Dave

**Abstract** The present work focused on the use of plastic bottles and plastic wrappers to make ecobricks which can be used as a building material. PET bottle of sizes, 250 ml (cylindrical), 750 ml (cylindrical) and 1 L (cubical) has been used in the present study and were filled with shredded and compacted plastic wrappers to prepare an ecobrick. These ecobrick can accommodate 170 to 350 gm of plastic wrappers waste. Plain ecobricks and ecobricks with mortar have been tested for compressive strength and then prototypes have been created using both types of ecobricks. Plain ecobrick showed strength in the range of 25–45 MPa, however with mortar the strength in the range of 27–31 MPa was noted. The strength of plain ecobrick and with mortar has been found to be more than the first-class brick and thus can be used as construction building blocks. It can be concluded that ecobrick is an economical construction material for social projects in region where litter and informal dumpsites are a common problem and industrial recycling might not be yet available. Using ecobrick as plastic disposal measures shall help in achieving the sustainable development goals 2030, namely SDG:11 Sustainable cities and communities, SDG13: Climate action, SDG14: Life below water and SDG15: Life on land.

**Keywords** Plastic waste · Ecobrick · Compressive strength · Recycling

---

V. Sahu (✉) · Abhishek · Y. Vats  
The NorthCap University, Gurgaon, India  
e-mail: [vaishalisahu@ncuindia.edu](mailto:vaishalisahu@ncuindia.edu)

Abhishek  
e-mail: [abhishek18cvu001@ncuindia.edu](mailto:abhishek18cvu001@ncuindia.edu)

Y. Vats  
e-mail: [yash18cvu007@ncuindia.edu](mailto:yash18cvu007@ncuindia.edu)

N. Dave  
Pandit Deendayal Energy University, Gandhinagar, Gujarat, India  
e-mail: [Niragi.Dave@sat.pdpu.ac.in](mailto:Niragi.Dave@sat.pdpu.ac.in)

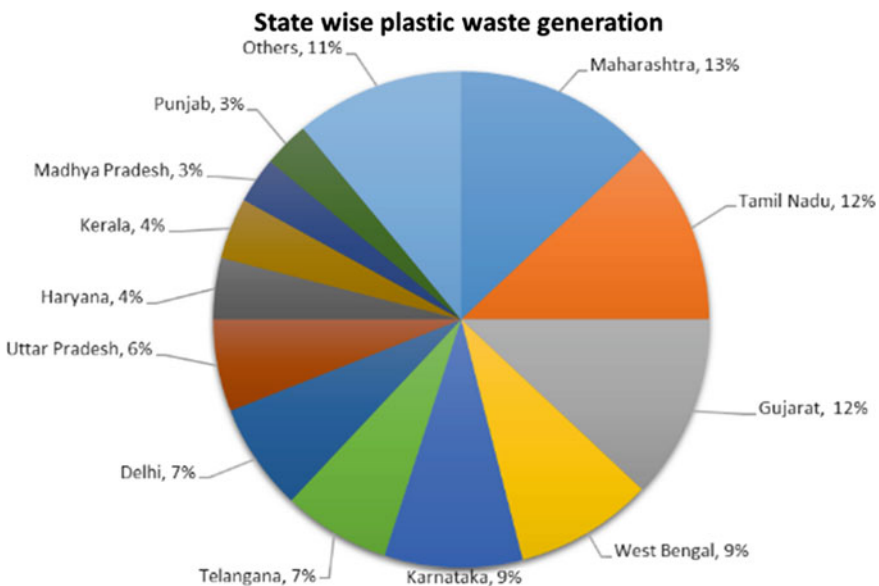
## 1 Introduction

Plastic pollution is among the most persistent environmental issues with speedily growing production and use of plastic items, like, bottles, wrapping plastic, disposables, etc. Out of the daily waste generation in Indian cities, 92% is the waste generated due to thermoplastic, PET, and PVC. They can be recycled for 7–9 times, after which they have to be disposed of (CPCB Report 2015).

Bulk generation and accumulation of plastic waste represent a growing threat to environmental and public health. Nearly 6.5 billion tonnes of plastic wastes are produced each year worldwide (Jnr et al. 2018). Plastic waste disposal in the environment has caused extreme environmental concerns for centuries due to the prolonged degradation of plastics. Other than its impact on the landfill sites, plastic waste has become so dominant that marine habitats, biomes, and human health are now under a significant threat (Singh and Ruj 2015).

The total plastic waste generated in India during 2019–20 was approximately 34,69,780 TPA as per the annual report of central pollution control board. According to the generation rate data collected from 35 states/UT, the percentage distribution of plastic waste generation is illustrated in Fig. 1. It is noted that maximum quantity of plastic waste is generated in Maharashtra followed by Tamil Nadu and Punjab in that order (CPCB annual report 2020–21).

In general, plastic waste is a mixture of different types of plastics; thus, it is difficult to recycle these materials and ultimately ending at the landfill sites or through some treatment methods (Hopewell et al. 2009).



**Fig. 1** State-wise plastic waste generation



The plastic waste disposal and treatment methods are also increasing carbon footprints and the emission of hazardous atmospheric pollutants (Aragaw and Mekonnen 2021). The rising plastic-waste footprint is a huge challenge that requires substantial advances in recycling and upcycling to ensure sustainability and environmental resilience (Sharma et al. 2020).

The need of the hour is to manage the plastic waste and provide a sustainable solution to this ever-increasing waste stream through sustainable recycling. Recycling is the method to convert the waste materials into environmental, economic and social resource (Afroz et al. 2017).

Recycling PET waste plastic bottles to produce brick/building block is an environmentally friendly way to manage the plastic waste and save the environment from the degradation. Among many recyclable alternatives researched to manage plastic waste, ecobricks seem to be very promising solution (Wahid et al. 2015).

Ecobrick is a building block made from the waste PET plastic bottles and filled with materials like packaging waste, foams, cellophanes, inorganic waste material, soil, etc. (Hopewell et al. 2009).

Ecobricks are a low-cost building material and is an effective recycling method to reduce waste disposal in areas where industrial recycling is not yet available. It prolonged the time period of the plastic waste by utilizing it and recycling it when required resources are available in that area (Antico et al. 2017).

Ecobricks are themselves a great recycle of the waste plastic with a valuable output as building material. The so developed ecobrick utilizing recycled concrete aggregate and waste plastic bottles consume zero-energy, are emission-less, cheap, and also eliminate the need for disposal of plastic bottles and concrete waste materials. Even after demolition of the buildings those bottle bricks will be a usable item at other alternate places. Recycling avails the opportunities to minimize the consumption of oil, CO<sub>2</sub> emission and the waste that needs to be disposed of (Edike et al. 2020).

Ecobricks provides numerous short-term and long-term benefits. An ecobrick can easily be used in construction and set there for many years. Many ecobrick building ideas have been researched in recent past where ecobricks have been used as green building blocks.

In the present work, engineering properties of ecobrick made with PET bottles and filled with plastic packaging materials have been studied. An attempt has been made to study the effect of shape, size and density of the PET bottles on the strength.

## 2 Material and Methods

The materials used in the present study and the tests performed have been discussed in this section.

**PET Bottles:** PET bottles of 250 ml (bottle A), 750 ml (bottle B) and 1 L (cubical shaped, bottle C) capacity have been used to prepare ecobricks. Apart from different sizes, shapes, like regular circular and rectangular has been selected to study the effect of shape and size of bottle on the strength and durability of prepared ecobricks.

**Filling Material** Packaging plastic wrappers have been used as the filling material in the ecobrick to cater maximum amount of plastic in it. Wrappers from packets of atta, bread, chocolate, biscuits, snacks, etc. are used to fill the PET bottles to a desired density. Packaging plastic is been cut into small pieces using scissors so that it can be filled into the PET bottles easily and will increase the weight of the bottle. Plastic waste is shown in Fig. 2.

**Preparation of Ecobrick** Empty capped bottles of different sizes were collected, washed with water and then dried in the air. The shredded plastic wrappers were filled in three layers. Each layer was compacted through a tamping rod so that maximum amount of plastic waste can be filled in the bottle. After the three compacted layers have been filled, the cap of the bottle was tightly fixed. The prepared ecobricks are shown in Fig. 3.

**Physical Testing** Physical tests like dimensioning of the bottles, initial weight and final weight, thermal shrinkage test has been performed on the empty PET bottles. Through initial and final weight, the amount of plastic filling has been determined.

**Fig. 2** Plastic waste used for filling PET bottles



**Fig. 3** Ecobricks

Demarcation on the bottles have been marked for measurement and is shown in Fig. 4.

Demarcation has been made on the bottle and the dimensions were measured. The bottles after initial measurement have been kept in oven for 24 h at 50°C with the cap opened. Final measurements have been noted after 24 h. Figure 5 shows the bottles for shrinkage test. Shrinkage percentage has been determined using the following formula and given in Table 1.

$$\frac{\text{Initial dimension} - \text{Final dimension}}{\text{Initial dimension}} \times 100$$

**Compressive Strength** The prepared ecobricks were tested for the compressive strength test on the compression testing machine. As the cylindrical bottles have

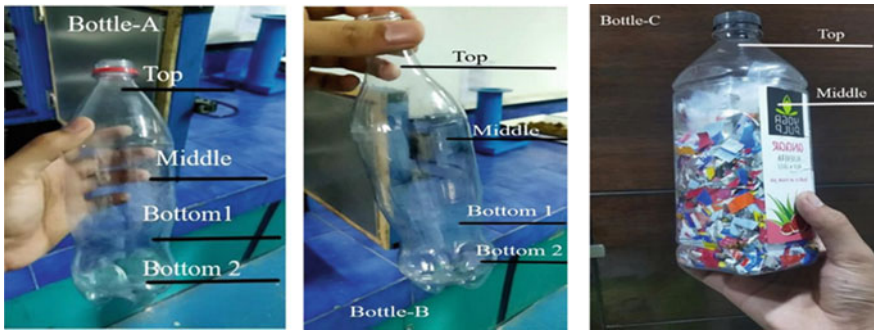


Fig. 4 Demarcation on the bottles

Fig. 5 Bottles for thermal shrinkage



**Table 1** Physical parameters of the bottles

Demarcations	Bottle A	Bottle B	Bottle C
Top (mm)	26.5	26.5	46
Middle (mm)	28	73	79
Bottom 1 (mm)	45	57	82
Bottom 2 (mm)	60	75	82
Height (mm)	155	247	252
Initial weight (gm)	20	29	32
Final weight (gm)	190	290	378

curved surface a steel disc has been placed at the top and bottom for the uniform distribution of the applied load. Figure 6 shows the cylindrical and the cubical shaped bottles under the compressive load. Further, attempt has been made to study the strength of ecobrick along with mortar. Cubical and cylindrical specimens using 1:3 mortar and ecobrick has been casted for compressive strength test. A wooden cubical mould of dimension  $22 \times 22 \times 22 \text{ cm}^3$  has been prepared and a cylindrical mould of height 30 cm and diameter 15 cm has been used in the present study. Figure 7 shows the moulds used in the study.

Four ecobricks of 250 ml size were placed in cubical mould in two layers whereas 1 each of 750 and 1000 ml, respectively, have been used in cylindrical mould. Mortar was filled inside the moulds in three layers and each layer was compacted with the help of a tamping rod to achieve desired density. Orientation of the bottle in the mould is shown in Fig. 8 and the process of preparation is shown in Fig. 9.

Five moulds of each specimen type were prepared and kept in ambient environment for 24 h. The specimens were demoulded and were cured for 7, 14 and 28 days. Compressive strength test has been conducted after each curing period.

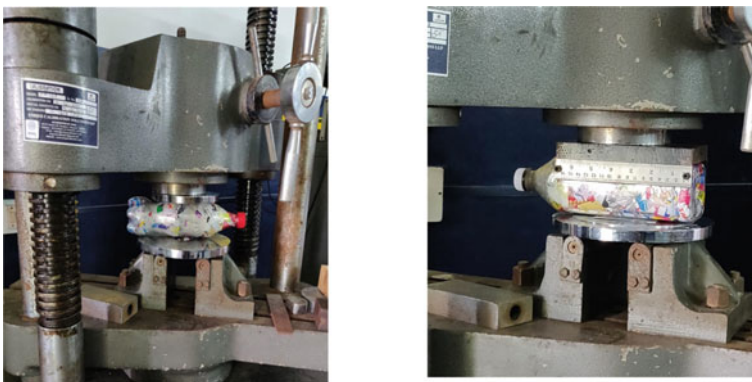
**Fig. 6** Ecobricks under the compressive load



Fig. 7 Cubical and cylindrical mould



Fig. 8 Ecobrick in mortar mould



Fig. 9 Process of cubical mould formation



### 3 Result and Discussion

The initial and final dimensions of the PET bottles were measured and the shrinkage percentage was calculated as given in Table 2. It can be observed that the top and bottom of the bottle has experienced maximum shrinkage. Further the shrinkage % is within 5% at all sections. The shrinkage has been resulted as the empty bottles were used. However, when the ecobricks shall be used at field they will be filled with infill materials that will reduce the shrinkage percentage. It has been reported that inorganic material, like sand, bagasse can restrict the shrinking of the ecobrick (Antico et al. 2017).

Ecobricks have been prepared with 250 ml (sample A) and 750 ml (sample B) cylindrical bottles and 1000 ml (sample C) cubical shaped bottle. The initial and final weight of the bottles shows that nearly 170 g of plastic wrappers was used in 250 ml bottle, 260 gm in 750 ml bottle and 350 gm in the cubical 1000 ml bottle. These sample A, B, C were tested for compressive strength and the results are given in Table 3.

It can be seen from here that the strength increases with the size of the bottles and the amount of plastic filling. Further, the cubical bottle showed better strength owing to the uniform shape and more amount of filled plastic. Moreover, these ecobricks shall be used along with mortar in the field that may further improve the strength. To analyze the bonding of mortar with the ecobricks, the cubical moulds with 4 bottles A and cylindrical moulds with 1 bottle B and C, respectively, were casted, cured and tested for compressive and tensile strength. The results of cylindrical moulds are given in Table 4 and of cubical mould are given in Table 5.

It can be observed from here that ecobrick provides lesser strength with mortar but higher than plain mortar after 28 days of curing. This shows that ecobricks improved the performance of mortar. Split tensile strength of cylindrical specimens were observed higher than the compressive strength, owing to the inclusion of the

**Table 2** Shrinkage in PET bottles

Demarcations	Shrinkage percentage (%)		
	Bottle A	Bottle B	Bottle C
Top dimension	3	3.7	3.66
Middle dimension	2.2	2.5	2.8
Bottom 1 dimension	2.5	2.85	1.5
Bottom 2 dimension	4.5	4.8	1.5

**Table 3** Ultimate strength of ecobrick

Sample	Ultimate compressive strength (N/mm <sup>2</sup> )
A	25
B	35
C	43

**Table 4** Strength of cylindrical moulds

Curing period	Compressive strength, MPa	Splitting strength, MPa
<i>B—750 ml bottle</i>		
14 days	20	23
28 days	27	31
<i>C—1 L cubical bottle</i>		
14 days	21	28
28 days	30	39

**Table 5** Strength of cubical moulds

Curing period	Compressive strength, MPa	Splitting strength, MPa
14 days	20	10.5
28 days	31	12

ecobrick within the mortar specimen. However, the split tensile strength of cubical mould with 250 ml bottles was less.

The strength is observed to be much higher than the first-class brick (17–20 MPa). These ecobricks (plain and with mortar) can be used to replace the conventional brick. The authors propose the use of ecobrick as a building construction material for marginal structures like, animal shelter, boundary wall of gardens, stools and benches in community parks, etc.

Pilot models of ecobrick (plain and with mortar) have also been created. A small stool which contains a 16 number of ecobricks of 750 ml was prepared and binded with plastic cellophane tape. The total amount of plastic used in making complete stool (16 ecobrick) was 3.520 kg (220 \* 16). Similar stools can not only provide recycle alternative to the plastic waste but also save plastic waste going to the landfill sites, sea and water bodies and open burning. The stool is shown in Fig. 10.

Ecobrick along with mortar was used to prepare a wall unit and is shown in Fig. 11. The use of plastic bottles in the wall unit also saves the amount of mortar to be used. This is an attractive alternative to be used as building material.

Ecobrick is proved to be a fast and useful method to utilize that plastic waste. This will benefit our society by cleaning the environment. Ecobrick concept will also benefit stray dogs and cows as animals in cities are often found to eat plastic which choke their throat and eventually lead to death. Plastic bags and packets are burnt by people in winters which generates an enormous number of toxic gases but if we utilize all that waste in making ecobricks these activities will end or be reduced to a large extent.

**Fig. 10** Stool from plain ecobrick



**Fig. 11** Wall unit with ecobrick



## 4 Conclusion

Ecobrick prepared with plastic wrappers as filling material can use up to 350 gm of shredded and compacted plastic wrappers and resulted into a good density material. Shrinkage of the PET bottles was found to be within 5% and can be reduced by the use of non-combustible material like sand in the bottles. Strength of an ecobrick increases with the size of the bottle used as the amount of the plastic infill also increases with the size. Further, cubical-shaped bottle resulted to a much higher strength. Strength of an ecobrick depends on the materials that have been used for filling the PET bottles. If the amount of plastic fill is increased the strength of ecobrick can be enhanced. Therefore, based on the strength requirement and the application area, the ecobrick can be customized by choosing appropriate size, shape and the amount of the infill material. Ecobrick with mortar resulted into reduced strength



when compared with plain ecobrick, however, the 28 days strength was more than plain mortar and first-class brick.

## 5 Limitation and Future Scope

The present study was focused on using maximum amount of waste plastic and thus plastic infill has been used to prepare the ecobrick. It can be extended by using different types of filling materials to prepare ecobrick. Large-scale pilot model of stool and a wall unit has been created in the present study. It is proposed to prepare a large prototype and real-time loading can be tested on the same.

**Acknowledgements** We acknowledge the faculty and staff of Civil and Environmental Engineering Department for their motivation and support to complete this work.

## References

- Afroz R, Rahman A, Masud MM, Akhtar R (2017) The knowledge, awareness, attitude and motivational analysis of plastic waste and household perspective in Malaysia. *Environ Sci Pollut Res* 24:2304–2315. <https://doi.org/10.1007/s11356-016-7942-0>
- Annual Report (2020-21) Implementation of plastic waste management rules, 2016. In: Central Board of Pollution Board (CPCB)
- Antico FC, Wiener MJ, Araya-Letelier G, Retamal RG (2017) Eco-bricks: a sustainable substitute for construction materials. *Rev Construcción* 16(3):518–526. <https://doi.org/10.7764/RDLC.16.3.518>
- Aragaw TA, Mekonnen BA (2021) Current plastics pollution threats due to COVID-19 and its possible mitigation techniques: a waste-to-energy conversion via pyrolysis. *Environ Syst Res* 10(8):1–11
- Central Pollution Control Board (CPCB) (2015) Assessment and characterization of plastic waste generation in 60 major cities. In: Central Pollution Control Board (CPCB), Ministry of Environment, Forest and Climate Change
- Edike UE, Ameh OJ, Dada MO (2020) Production and optimisation of eco-bricks. *J Cleaner Prod* 266:121640
- Hopewell J, Dvorak R, Kosior E (2009) Plastics recycling: challenges and opportunities. *Philos Trans R Soc B Biol Sci* 364:2115–2126. <https://doi.org/10.1098/rstb.2008.0311>
- Jnr AK-L, Yunana D, Kamsouloum P, Webster M, Wilson DC, Cheeseman C (2018) Recycling waste plastics in developing countries: use of low-density polyethylene water sachets to form plastic bonded sand blocks. *Waste Manage* 80:112–118
- Sharma HB, Vanapalli KR, Cheela VRS, Ranjan VP, Jaglan AK, Dubey B, Goel S, Bhattacharya J (2020) Challenges, opportunities, and innovations for effective solid waste management during and post COVID-19 pandemic. *Resour Conserv Recycl* 162:105052
- Singh RK, Ruj B (2015) Plastic waste management and disposal techniques—Indian scenario. *Int J Plast Technol* 19(2):211–226
- Wahid SA, Rawi SM, Desa NM (2015) Utilization of plastic bottle waste in sand bricks. *J Basic Appl Sci Res* 5(1):35–44

# Development of Rubber Mould Paver Blocks Using Textile Effluent Treatment Plant Sludge



Reshma L. Patel , J. R. Pitroda , Rajesh Gujar , Jaykumar Soni ,  
Bansari N. Dave , and Vismay Shah 

**Abstract** An important and long-standing sector in India is the textile industry. Its numerous operations result in an enormous quantity of liquid waste being produced. During textile wastewater treatment, sludge is generated in the effluent treatment plant (ETP). The government has designated a specific location for its waste disposal. The majority of the generated sludge is disposed of in landfills or dumped in designated locations by the government. The improper disposal of textile sludge contributes to environmental damage. As a result, the disposal of textile sludge has become a major environmental concern. An extensive overview of the literature review on the utilization of textile effluent treatment plant sludge as concrete, blocks, paver blocks and bricks is discussed. Using textile ETP sludge as a cement replacement in M30 grade rubber mould paver blocks (RMPB) is the goal of this work. As a cement replacement material, rubber mould paver blocks made from textile sludge may be used at a weight percentage of 0, 5, 10, 15, 20, 25, 30, 35, and 40%. Compressive and abrasion resistance decreases with increasing sludge concentration. When ETP sludge replaces cement to a greater or lesser extent, it falls short of the desired esteem.

---

R. L. Patel · J. R. Pitroda (✉)  
BVM Engineering College, Vallabh Vidyanagar, India  
e-mail: [jayesh.pitroda@bvmengineering.ac.in](mailto:jayesh.pitroda@bvmengineering.ac.in)

R. L. Patel  
e-mail: [rlpatel@bvmengineering.ac.in](mailto:rlpatel@bvmengineering.ac.in)

R. Gujar  
School of Technology, Pandit Deendayal Energy University, Gandhinagar, India  
e-mail: [rajesh.gujar@sot.pdpu.ac.in](mailto:rajesh.gujar@sot.pdpu.ac.in)

J. Soni · V. Shah  
L J Institute of Engineering and Technology, L J University, Ahmedabad, India  
e-mail: [jay.soni\\_ljiet@ljinstitutes.edu.in](mailto:jay.soni_ljiet@ljinstitutes.edu.in)

V. Shah  
e-mail: [vishmay.shah\\_ljiet@ljinstitutes.edu.in](mailto:vishmay.shah_ljiet@ljinstitutes.edu.in)

B. N. Dave  
Nobel Engineering College, Junagadh, India  
e-mail: [bansaridave389@gmail.com](mailto:bansaridave389@gmail.com)

**Keywords** Cement · Construction materials · Rubber mould textile sludge paver blocks (RMTSPB) · Sludge disposal · Solid waste management · Textile effluent treatment plant (ETP) sludge

## 1 Introduction

The Indian textile industry is regarded to be one of the country's biggest and oldest industries. Many operations and procedures in textile companies need large quantities of water, resulting in hazardous waste. The treatment of textile wastewater generates a large amount of sludge. A by-product of 240 dyeing plants is 70–80 million tonnes of textile sludge per day or more (Lekshmi and Sasidharan 2015). A total of 20 million metric tonnes of textile sludge may be stored at each plant. Sludge management in textile and wastewater treatment has become a major issue because of the huge volume. Chemical sludge due to pollution, disposal, and dumping is prohibited by the pollution control board.

There is a shortage of materials in India's building sector. One way to reduce the cost of construction is to utilize the sludge from textile effluent treatment plants instead of traditional building materials. Using ETP sludge as construction and building materials reduces disposal and dumping problems in addition to turning waste into sustainable products (Patel et al. 2017b). India's textile industry is one of the country's most significant and oldest industries. Large quantities of water are used in textile manufacturing operations, resulting in hazardous waste. The treatment of textile wastewater generates a large amount of sludge. Sludge management in textile and wastewater treatment has become a major issue because of the huge volume.

As a result, there is a market for a substance that can substitute cement to some extent, and textile effluent treatment plant sludge can do just that if it is cost-effective to do so instead of cement. The sludge contains more harmful elements and serves as a source of new ideas since appropriate disposal methods are seldom utilized. Sludge management alternatives are becoming more important. This article suggests that textile sludge added to a rubber mould paver block is studied for its effects (Patel et al. 2017a). In addition to converting waste into manageable goods, textile effluent plant sludge as cement eliminates disposal and dumping concerns. Researchers are trying to figure out how strong rubber mould textile sludge paver blocks are in this research (RMTSPB).

## 2 Sludge Utilization Research

### 2.1 Concrete

The use of textile sludge as a fine aggregate replacement impacts the workability and density of the concrete. The compressive strength of M20 grade concrete, which contains 32% of textile sludge and 22% of fly ash, is 20.22 N/mm<sup>2</sup> and may be used in construction (Kulkarni et al. 2012). Fly ash bricks are made in Phase-I using synthetic sludge aggregate (SSA), and concrete mix is made in Phase-II using sludge. The results showed that Phase-I bricks produced had compressive strengths comparable to class-B bricks and are more affordable. In concrete grades M20, M30, and M40, sludge replaces sand starting in Phase-II. If sludge concentration increases, concrete's compressive strength decreases. They concluded that 5% of the sand in concrete could be substituted with SSA (Raghunathan et al. 2010). Textile ETP sludge contains little silica and calcium, which may be substituted with cement. It was necessary to follow the code requirements while testing the textile ETP sludge as a binder (IS 1727–1967). Compressive and tensile strength seems to diminish as the amount of ETP sludge substantial increases. The textile ETP sludge might replace up to 5% of cement without causing any problems (Sandesh et al. 2014). Concrete may have a textile sludge content of 0 to 10% by substituting the cement in the mix. Textile sludge replaces 10% of the cement to produce a compressive strength of 29.33 N/mm<sup>2</sup> at a 0.4 w/c ratio (Lekshmi and Sasidharan 2015). Textile waste is termed ETP sludge (ETP). This toxic sludge harms our environment in many ways. TMS concrete was mixed with a plasticizer solution containing 1% cement. Sludge reduces concrete strength and workability. In concrete containing textile mill sludge and a plasticizer concentration over 35%, tiny particles lose compressive strength (CS) and workability. Textile mill sludge of concrete may minimize the negative effects of sludge waste. Concrete needs extra water due to the textile mill sludge. Textile mill sludge floats. The M20 has a compressive strength of 23.55 N/mm<sup>2</sup> when fine particles replace 35% of the sludge (Kaur et al. 2017). Cremated textile sludge ash was combined with 10% of cement in concrete blocks to test CS, leaching, and water absorption. Its use instead of cement speeds up hydration and improves CS. Increased cement replacement affects concrete properties, including CS and WA, with a limit of 20% replacement deemed sound. The cube samples only discharged a small number of heavy metals compared to what is needed to cause cellular cytotoxicity. Consequently, heavy metal contamination of sludge ash concrete cubes is eliminated. If textile waste is dumped outdoors, it might pose a risk to human health and the environment. This important problem may be resolved by using textile sludge to make great concrete and recycling it (Kasaw et al. 2021). Toxic chemicals and colours are found in textile treatment plant sludge. A lot of it ends up in landfills after textile water treatment. TMS applied more than 25% of the intended plasticizer amount reduces compressive strength. It teaches us how to recycle textile mill waste into building materials. Sludge waste concrete volume impacts compressive strength. Textile mill sludge is hygroscopic. Concrete's compressive strength decreased when textile mill

waste surpassed 25% (Kaur and Singh 2019). Automobile ETP sludge may be used to make cement concrete products. Cement can be replaced by automobile sludge up to 35%. Drying specimens from various hydration periods increased the strength of cement-automobile ETP sludge binders. The flexural strength, compressive strength, and wear resistance of flooring tiles decreased and water absorption increased with increase of the percentage of automobile sludge. Brick CS and bulk density decreased as the amount of soil replaced by vehicle sludge increased. Above 900°C, bricks increase strength and WA by producing gehlenite ( $\text{Ca}_2\text{Al}_2\text{SiO}_7$ ). Testing on car muck revealed that 35% might be recycled into construction materials. Auto sludge usage is expected to save energy and help to healthier air and water (Garg et al. 2014). Incineration is one method of disposing of sludge. Burning may decrease sludge, but it generates ash that must be dealt with later. Due to its properties, sewage sludge ash has been used to replace natural aggregate in concrete partly. Untreated ash was used as an aggregate because it was light. Up to 25% of natural aggregate volume may be substituted with synthetic aggregate to meet structural requirements. Compaction and water absorption were acceptable when up to 25% of sludge ash was used. Due to the ash's latent pozzolanic activity, concrete containing SSA exhibited properties comparable to concrete with just natural aggregate when filled. The product may also be utilized for non-structural applications without requiring high strength and a waste aggregate dose exceeding 25% of aggregate volume (Kosior-Kazberuk 2011).

## 2.2 Blocks

Industrial waste like 30–45% of sludge content may be used to make concrete blocks (Senthilkumar et al. 2008). Textile plant sewage was used to produce cement foundation solid blocks. Compressive strength decreases when cement content rises to 80%.

Cement content increases block density, whereas sludge content decreases it. Fly ash may replace 30% of the cement in cement-fly ash blocks to reduce the cost of the construction blocks. Increase in fly ash content leads to an increase in solid block compressive strength. It turns out that the ideal mixture is 30% of sludge, 30% of cement, and 40% of fly ash. The density of the blocks decreases as the amount of fly ash increases (Jahagirdar et al. 2012). Sludge is a common wastewater treatment waste product that India's largest industry struggles to dispose of. Sludge from wastewater treatment plants may replace up to 15% of the base material. After drying at temperatures ranging from 3000 to 6000°C for 8, 16, and 24 h, sludge is applied. Compressive strength of more than 8.33 N/mm<sup>2</sup> and water absorption (WA) ratio of less than 0.50% may be increased up to 15%. Consequently, reusing solid wastewater sludge from conventional effluent treatment is a better solution to the ultimate disposal problem (Dhinesh et al. 2014). Water treatment sludge's primary goals are to enhance its value and provide a cost-effective disposal option. Solid waste from the water treatment facility was used as a fine aggregate in the concrete mix to make hollow blocks. Developing nations erect barriers out of concrete blocks.

Combinations of water treatment sludge were successful for hollow non-load-bearing concrete blocks. In contrast, mixes of 10 and 20% of water treatment sludge were successful for hollow load-bearing concrete blocks. Water treatment sludge mixes containing 10% and 20% save about Rs. 64 and 105 per block, respectively. Hollow concrete blocks made from 50% water treatment sludge are non-load-bearing and cost Rs. 5.0 less per block. Hollow concrete blocks made from treated sludge may prove to be an effective long-term disposal option (Kaosol 2010).

### **2.3 Paver Blocks**

Sludge is used as a cement substitute up to 40% in casting the M50 grade concrete paver block. For each of the aforementioned paver block combinations, additional fly ash (up to 40%) and silica fume (2.5%) were applied. Compressive strength was more than 30 MPa, and water absorption was less than 6% when cement was replaced with sludge up to 30% of the time (Kulkarni et al. 2012). Polypropylene fibre was also mentioned as a possible addition to improve the performance of paver blocks. They found that the compressive strength decreased when partial sludge-cement substitution in paver blocks increased. Cement substitution with sludge up to 30% improves the compressive strength of paver blocks by up to 0.5%. The study's findings showed that adding quarry dust and textile sludge to concrete improved its compressive strength (Sudheesh et al. 2015). More than 300 million tonnes of industrial waste produced annually in India are chemical and industrial waste. Hypo sludge is a paper industry waste. So it is the disposal of this garbage. Using hypo sludge in place of cement and fine aggregate in the casting of M30 grade paver blocks, which fulfils IS standards for medium traffic, showed encouraging results in this research. Concrete paver blocks with replacement percentages of 0, 10, 20, 30, 40, 50, and 60% had their compressive strength evaluated. In order to evaluate compressive strength, hypo sludge is entirely replaced with fine aggregate. The compressive strength was increased by 10% to replace hypo sludge. Hypo sludge may therefore replace up to 10% of cement in a building (Mithun 2016).

### **2.4 Brick**

The physico-chemical characteristics of textile ETP sludge were partially substituted clay in traditional bricks production. A variety of measurements were made on the solid to understand its physico-chemical and thermogravimetric characteristics better. Bricks having a sludge content ranging from 0 to 30% met shrinkage and weight loss standards, which was confirmed by adding up to 30% of sludge content. A brick sludge mix with less than 9% of sludge content burned at 800°C for at least 8 h met quality bricks requirements. They found, even with up to 9% of sludge replacement, compressive strength was increased (Baskar et al. 2006). Textile ETP

sludge recycling in building materials investigated the engineering characteristics of a South Indian textile sludge compound. Sludge substitution in structural and non-structural applications of up to 30% of cement was assessed for sustainability. They find that textile sludge may replace cement to a maximum of 30% in the casting of structural and non-structural buildings (Balasubramanian et al. 2006). Fly ash has been strengthened using silica fume, which was also utilized in this research for strengthening purposes. Textile sludge is used instead of fly ash to produce fly ash bricks. In addition, they found that when sludge concentrations rose, the compressive strength of the bricks decreased. Minimum required brick compressive strength and water absorption may be achieved by mixing up to 20% of other materials such as sludge and fly ash with cement and quarry dust, for example (Palanisamy 2011). Industrial waste may be used to make bricks, concrete, and other building materials. They deduced from the findings that 25–30% of the sludge was suitable for use in the manufacture of bricks (Senthilkumar et al. 2008). Reusing textile ETP sludge in building materials is investigated via solidification/stabilization treatment of sludge, where 30 to 70% of sludge was used to substitute cement fractionally. According to the results, sludge mix bricks may meet BIS class C to class K brick requirements and have a strength of 25 N/mm<sup>2</sup> (Patel and Pandey 2009). Created energy-efficient bricks by utilizing dry sludge obtained from a textile wastewater treatment plant. Using sludge as raw material and casting them at 500°C produced the most energy-efficient bricks. The bricks may have up to 6.66% of sludge injected into them and meet IS standards for compressive strength when fired at 500°C. Because of their lower fire temperature, sludge mix bricks can be an energy-efficient alternative to regular bricks (Lissy and Sreeja 2014). The sludge may be recycled into an energy-efficient brick by combining it with clay. To make bricks, textile waste was used in various quantities (10–40%) and temperatures (600, 900, and 1200°C). The results revealed that 10 and 20% of sludge bricks fulfilled Ethiopian class “A” brick criteria, with compressive strengths of 30.43 and 29.10 Mpa at 1200°C, respectively. Fired sludge-containing bricks containing 10–20% of sludge consumed between 26 and 50% less energy than pure clay bricks. Aside from that, the burnt clay bricks stabilized certain heavy metals found in the brick leachate, which displays the sludge. Textile sludge in various amounts and temperatures was used to make energy-efficient bricks. Making sludge-to-energy-efficient bricks may help reduce energy use and reduce the final brick weight, which reduces transportation costs (Beshah et al. 2021). The sludge created by the facility was put to good use in the brick-making process, reducing waste generation. The sludge had a specific gravity of 1.53 and a moisture content of 162%. Sludge content increased water demand and brick absorption, which was shown to be inversely proportional. The brick’s compressive strength, on the one hand, declined. Cement and fly ash, on the other hand, enhanced the bricks’ characteristics. Shearing resistance increased, while water absorption and compressive strength remained unaffected. As a result, it is safe to say that only sludge may be utilized in brick production. However, the bricks’ qualities improved significantly when stabilizers such as cement and fly ash were added (Nair et al. 2013). Using dredged soil and ETP waste for compressed adobe brick manufacturing was explored. XRF and chemical methods were used to analyse elements of the ETP sludge and



dredged soil. Various dredging soil to ETP sludge ratios was employed to produce the specimens (bricks) for testing, using a sodium hydroxide/sodium silicate solution combination as a binder (ratios of 1:1, 1.15, 1:2, 1.25, and 1.3). Hand-operated CINVA-RAM machines were used to shape the bricks. Three hours of baking at 60°C followed by 28 days of curing at room temperature were used to cure the test specimens (bricks). After 28 days at 60°C heat curing for three hours, the compressive strength of 1:2 ETP sludge and dredged soil specimen reached 4.41 MPa, the modulus of rupture was 2.59 MPa, and the water absorption rate was 0.3% (Islam et al. 2015). Textiles, India's second-largest sector after sugar, have sludge disposal problems. ETP sludge may be used to substitute clay soil in brick-making partly. The industry has produced emerald-green clay bricks. Using unburned bricks reduces pollutants. The GREEN bricks created have strength more than the necessary 3.5 N/mm<sup>2</sup>. The M3 sample has a compressive strength of 5.27 N/mm<sup>2</sup>, greater than the mix percentage. In comparison, typical good quality burnt clay bricks may absorb up to 20% of their weight in water. Water absorption is improved by ETP sludge waste percentage. However, it was found that 10% of this sludge waste gave the greatest bonding and compressive strength while absorbing less water. The ETP sludge may be used to create paver blocks and walkway constructions. Using ETP sludge reduces pollutants on land and in the atmosphere and is environmentally beneficial (Ravikrishnan and Senthilselvan 2014). Tannery effluent treatment facilities receive tannery wastewater. Tannery effluent sludge is difficult to dispose of due to its high solid content. Untreated dewatered sludge may be dumped on land or buried. Landfilling may not be an option for big, well-organized communities owing to sludge disposal. Cement bricks may include up to 20% of tannery sludge or 100% of quarry dust instead of sand. The best approach to produce sludge brick was to add 20% of sludge to the mix, according to an experimental programme limited by the materials and testing procedures employed (Swarna and Venkatakrishnaiah 2014). Historically, bricks were the preferred construction material. Clay was used as a binder, along with natural and industrial waste materials. Textile sludge waste bricks represent the city's dedication to solid waste management. In regions where clay is limited, these wastes are used to minimize the quantity of clay required. The sludge concentration varied from 5 to 15% depending on sample weight. The temperature and duration of exposure to fire are varied to study burnt bricks. The quantity of sludge in bricks affects density, compressive strength, ringing sound, water absorption, and efflorescence. Textile sludge waste and its absorption into the clay material used in brick manufacturing suggest that textile sludge may partially replace clay soil in brick production. The strength of the burnt bricks generated surpassed the necessary 3.5 N/mm<sup>2</sup>. Its compressive strength is higher than the manufacturer's. Part charred brick absorbs more water than good quality burned clay bricks. Technical investigations show that up to 5% of textile sludge waste may be used with clay materials for brick-making, providing better bonding, CS, and decreased WA. Textile sludge may be enlarged and used to create paver blocks and sidewalk constructions. Thus, using textile sludge reduces both land and air pollutants, making it eco-friendly (Priyadharshini and Kavisri 2018). Efflorescence and water absorption rise as sludge concentration in bricks increases, while brick density, compressive strength, and



ringing sound decrease. In terms of compressive strength, higher firing temperatures and longer firing times, such as 8000°C and 24 h, provide better results than other temperature and firing time combinations. Compressive strength higher than 3.5 N/mm<sup>2</sup> may be achieved by adding up to 15% of textile mill sludge. (Jahagirdar et al. 2013).

The following Table 1 shows the sludge utilization research and its comparison.

## ***2.5 Outcomes Based on Sludge Utilization Research***

The following conclusions are derived from sludge use research:

1. Recycling textile ETP sludge into an innovative material could be a practical solution to the problem of landfilling and reduce its impact on the environment.
2. Reduction in the cement requirement results in less CO<sub>2</sub> emission from cement manufacturing Industry.
3. Compressive strength and workability of concrete decrease with increase in the sludge proportion as substitute for cement.
4. In concrete production, sludge may replace cement up to a maximum of 30%.
5. Bricks produced with up to a quarter mix percentage met quality-brick standards. Strength and water absorption may be improved by decreasing the sludge proportion and increasing other additives.
6. Textile ETP sludge fulfils the basic characteristics of cement and may thus be utilized as a binder in concrete.
7. For non-traffic and light-traffic areas, sludge mix paver blocks may be utilized.

## **3 Experimental Materials**

Research experiments included using the following items.

### ***3.1 Textile Sludge***

The textile ETP sludge was collected from Surat, Gujarat state, India. The sludge had a moisture level of 9.66%. Sun drying the sludge at an average temperature of 32°C for 66 h dried the waste material. The textile ETP waste is shown in Table 2 using chemical analysis. CaO and silica are found in textile ETP sludge (Patel et al. 2017a).

**Table 1** Sludge utilization research and its comparison

Authors	Utilization area	Material used	Test	Results
Kulkarni et al. (2012)	Concrete	Textile sludge (TS)	CS	32% sludge can be used
Sandesh et al. (2014)	Concrete	Textile ETP sludge (T ETP S)	Compressive strength (CS) Split tensile strength (STS) Flexural strength (FS)	5% cement can be replaced
Lekshmi and Sasidharan (2015)	Concrete	T ETP S	CS STS Modulus of elasticity	0 to 10% sludge can be used
Kaur et al. (2017)	Concrete	Textile mill sludge (TMS)	CS	35% sludge can be used
Baskar et al. (2006)	Clay bricks	TS	CS	6 to 9% sludge can be used
Patel and Pandey (2009)	Cement bricks	TS	CS Density	Up to 30% sludge can be used
Raghunathan et al. (2010)	Fly ash brick Concrete	T ETP S	CS	5% sludge can be used
Palanisamy (2011)	Fly ash brick	TS	CS Water absorption (WA)	20% sludge can be used
Jahagirdar et al. (2013)	Burnt clay Bricks	TMS	CS Density WA efflorescence Ringing sound	15% sludge can be used
Lissy and Sreeja (2014)	Bricks	TS	CS	7% sludge can be used
Kishore (2012)	Paver blocks	TS	CS WA	Up to 30% sludge can be used
Sudheesh et al. (2015)	Paver blocks	TS	CS	30% sludge can be used
Jahagirdar et al. (2012)	Solid blocks	TS	CS Density	30% sludge can be used
Balasubramanian et al. (2006)	Construction materials	T ETP S	CS WA Block density Wet transverse Effloresces	Maximum 30% sludge can be used

**Table 2** Chemical composition of textile ETP sludge

Chemical composition	Result (%)
SiO <sub>2</sub>	2.56
Fe <sub>2</sub> O <sub>3</sub>	43.806
Al <sub>2</sub> O <sub>3</sub>	0.179
CaO	39.613
MgO	0.204
SO <sub>3</sub>	10.272

**Table 3** Physical properties of cement

Physical properties	Results
Fineness (m <sup>2</sup> /kg)	326
Initial setting time (min)	120
Final setting time (min)	190

**Table 4** Chemical composition of cement

Chemical composition	Result (%)
SiO <sub>2</sub>	21.04
Fe <sub>2</sub> O <sub>3</sub>	3.77
Al <sub>2</sub> O <sub>3</sub>	6.02
CaO	62.93
MgO	2.49
SO <sub>3</sub>	1.72

### 3.2 Cement

The cement used in this experiment was OPC Grade 53, which is a common Portland cement. It complies with the Indian Standard IS 456: 2000 standard. Tables 3 and 4 show the composition's physical and chemical properties.

### 3.3 Fine Aggregate

This granular substance comprises finely split rock and mineral particles and may be found in nature as fine aggregate. Fine aggregate includes fractions with a size range of 4.75 mm to 150 microns.

### 3.4 Coarse Aggregate (Semi-Grit)

Compared to fine sand, coarse aggregate is much heavier, making it ideal for a wide range of applications. As a bedding material for pavement, semi-grit is an excellent choice for construction as one of the building sands used by construction firms. Semi-grit is less than 12 mm in size.

### 3.5 Water

The water must be safe to drink and devoid of harmful contaminants. IS 456:2000 stipulates the specifications to be followed.

## 4 Design Mix

Cement was substituted with textile ETP sludge in the design mix of M30 grade with 60-mm-thick rubber mould paver block (IS 456–2000, IRC SP 63–2004) indicated in Table 5. Table 6 depicts the combination of design elements.

**Table 5** Design mix of M30 grade 60-mm-thick RMTSPB

Cement	Fine aggregate	Coarse aggregate	Admixture	Water
410	685	1160	7	155
1	1.67	2.83	0.017	0.38

**Table 6** Replacement of cement with textile ETP sludge in RMTSPB

Paver block mixes	Cement	Textile sludge (kg)	Fine aggregate (kg)	Coarse aggregate (kg)	Water	Admixture (lit)
A–0%	24.60	0.00	41.10	69.60	9.30	0.42
B1–5%	23.37	1.23	41.10	69.60	9.30	0.42
B2–10%	22.14	2.46	41.10	69.60	9.30	0.42
B3–15%	20.91	3.69	41.10	69.60	9.30	0.42
B4–20%	19.68	4.92	41.10	69.60	9.30	0.42
B5–25%	18.45	6.15	41.10	69.60	9.30	0.42
B6–30%	17.22	7.38	41.10	69.60	9.30	0.42
B7–35%	15.99	8.61	41.10	69.60	9.30	0.42
B8–40%	14.76	9.84	41.10	69.90	9.30	0.42

Where A is without replacing cement RMPB, B1 to B8 is the replacement of cement by textile ETP sludge in RMPB.

## 5 Experimental Methodology

### 5.1 Testing Methodology

Cement, textile ETP sludge, fine aggregate, semi-grit, and admixture are used in RMTSPB. This RMTSPB uses textile ETP sludge to replace cement in the amount of 5, 10, 15, 20, 25, 30, 35, and 40%, depending on the weight of the cement used in the mix. Four paver blocks were cast for the compressive strength and abrasion resistance tests. After around 24 h, the specimens were moved to a secure location. Water curing proceeded until the samples were examined after 28 days for both tests.

### 5.2 Compressive Strength Test [IS 15658:2006]

Paver block samples were tested for compressive strength using compression testing equipment. The average strength values were evaluated on four samples from each batch. Water at a constant temperature of 20°C has been used to keep the block cool for the whole  $24 \pm 4$  h storage. The testing machine's bearing plates need to be cleaned. The specimens are placed in place using the bearing plates as a reference. A constant load of  $15 \pm 3$  N/mm<sup>2</sup>/min would be applied without shock, and the load would be raised continually until the specimen could no longer support any more load or delamination took place. The specimen was subjected to a variety of stresses and strains. Table 7 summarizes the compressive strength data. Refer to Fig. 1, which compressive strength of RMPB and RMTSPB with textile sludge in different proportions.

Because of this, a higher sludge percentage results in decreased compressive strength of the RMTSPB mixtures of grade M30. For optimal compressive strength, the textile sludge content was optimized at 20% of cement replacement. The compressive strength of a 20% of B4 mix is 28.02 N/mm<sup>2</sup>.

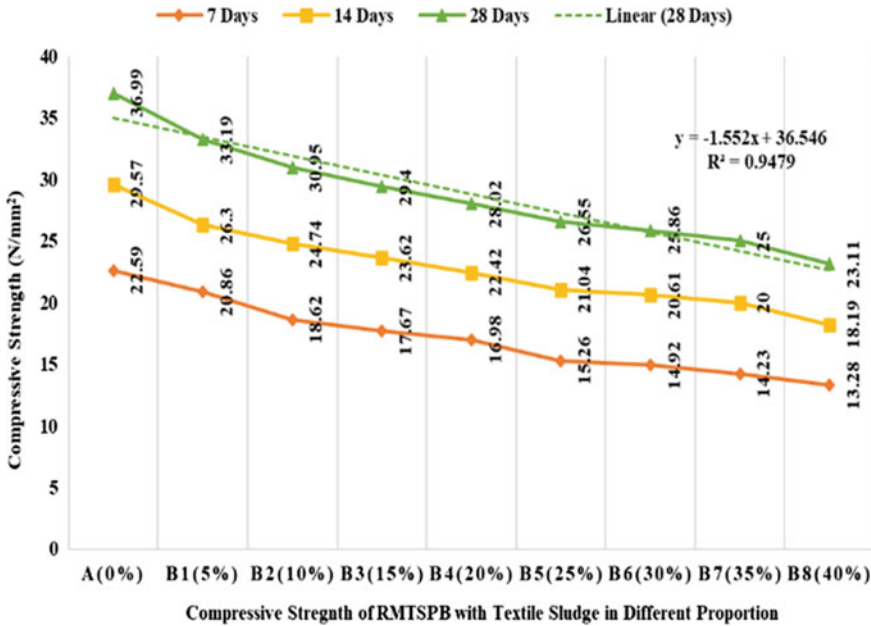
### 5.3 Abrasion Resistance Test

The abrasion resistance test results are compiled in Table 8.

Based on Fig. 2, it can be concluded that when sludge percentage increases, abrasion resistance of M30 grade RMTSPB mixes decreases. Textile sludge content

**Table 7** Comparative experimental results for compressive strength test of RMTSPB

Description	Rubber mould paver block mixes	Average compressive strength (N/mm <sup>2</sup> )		
		7 days	14 days	28 days
Standard RMPB	A-0%	22.59	29.57	36.99
Rubber mould textile sludge paver blocks (RMTSPB)	B1-5%	20.86	26.30	33.19
	B2-10%	18.62	24.74	30.95
	B3-15%	17.67	23.62	29.40
	B4-20%	16.98	22.42	28.02
	B5-25%	15.26	21.04	26.55
	B6-30%	14.92	20.61	25.86
	B7-35%	14.23	20.00	25.00
	B8-40%	13.28	18.19	23.11

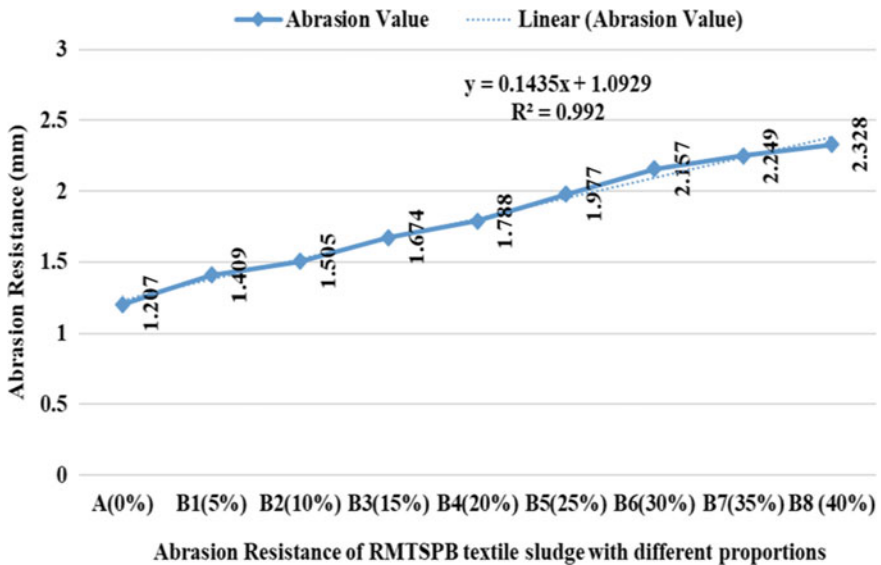


**Fig. 1** Compressive strength of RMPB and RMTSPB with different proportions of textile sludge

was optimal at 20% of cement replacement for the greatest abrasion resistance. The thickness is reduced by 1.788 mm when B4 is used as a percentage of the mix.

**Table 8** Abrasion resistance test results for all paver block mixes at 28 days

Description	Rubber mould paver block mixes	Average abrasion resistance for all rubber mould paver block mixes with/without textile sludge at 28 days (mm)
Standard RMPB	A-0%	1.207
Rubber mould textile sludge paver blocks (RMTSPB)	B1-5%	1.409
	B2-10%	1.505
	B3-15%	1.674
	B4-20%	1.788
	B5-25%	1.977
	B6-30%	2.157
	B7-35%	2.249
	B8-40%	2.328



**Fig. 2** Abrasion resistance of RMPB and RMTSPB with different proportions of textile sludge

## 6 Conclusion

From these experimental results, the following conclusions have been drawn:

1. RMTSPB compressive strength declines with an increasing proportion of textile ETP sludge after 28 days. Using textile ETP sludge up to 20% may provide CS closer to 30 N/mm<sup>2</sup>.

2. The abrasion resistance of the RMTSPB diminishes with an increase in textile ETP sludge percentage after 28 days and after 22 rotations of the block. A sludge concentration of 20% reduces the abrasion resistance by 1.788 mm.
3. Textile ETP waste may thus replace up to 20% of the cement in research.

## References

- Balasubramanian J, Sabumon PC, Lazar JU, Ilangovan R (2006) Reuse of textile effluent treatment plant sludge in building materials. *Waste Manage* 26(1):22–28. <https://doi.org/10.1016/j.wasman.2005.01.011>
- Baskar R, Begum KMMS, Sundaram S (2006) Characterization and reuse of textile effluent treatment plant waste sludge in clay bricks. *J Univ Chem Technol Metall* 41(4):473–478
- Beshah DA, Tiruye GA, Mekonnen YS (2021) Characterization and recycling of textile sludge for energy-efficient brick production in Ethiopia. *Environ Sci Pollut Res* 28(13):16272–16281. <https://doi.org/10.1007/s11356-020-11878-7>
- Dhinesh A, Karthikeyan R, Dinesh S, Karthik PR, Karthik S (2014) Preliminary studies of common effluent treatment waste sludge in manufacturing of solid block. *Sch J Eng Technol* 2(2A):161–167
- Garg M, Singh LP, Maiti S, Pundir A (2014) Characterization of automobile effluent treatment plant sludge: its utilization in construction materials. *Constr Build Mater* 73:603–609. <https://doi.org/10.1016/j.conbuildmat.2014.09.115>
- Islam MS, Begum R, Salam A (2015) Alternative building bricks using dredged soil and ETP sludge. *Int J Innovative Sci Eng Technol (IJISSET)* 2(9):761–769. Available at [www.ijiset.com](http://www.ijiset.com). ISSN 2348–7968
- Jahagirdar S, Shrihari S, Manu B (2012) Reuse of textile mill sludge in cement based solid blocks. *Int J Eng Res Ind Appl (IJERIA)* 5(3):213–224
- Jahagirdar SS, Shrihari S, Manu B (2013) Utilization of textile mill sludge in burnt clay bricks. *Int J Environ Protect* 3(5):6–13
- Kaosal T (2010) Reuse water treatment sludge for hollow concrete block manufacture. *Energy Res J* 1(2):131–134. <https://doi.org/10.3844/erj.2010.131.134>
- Kasaw E, Adane Z, Gebino G, Assefa N, Kechi A, Alemu K (2021) Incineration of textile sludge for partial replacement of cement in concrete production: a case of Ethiopian textile industries. *Adv Mater Sci Eng* 2021(9984598):1–6. <https://doi.org/10.1155/2021/9984598>
- Kaur H et al (2017) The workability and compressive strength of concrete using textile mill sludge and plasticizer. *Int J Civ Struct Environ Infrastructure Eng Res Dev (IJCSEIERD)* 7(4):1–8. <https://doi.org/10.24247/ijcseierdaug20171>. ISSN(P): 2249-6866; ISSN(E): 2249-7978
- Kaur H, Singh J (2019) Compressive strength of concrete by partial replacement of cement with textile mill sludge. *Int J Recent Sci Res (IJRSR)* 10(7A):33384–33387. <https://doi.org/10.24327/IJRSR>. Available at <http://www.recentscientific.com>. CODEN: IJRSFP (USA)
- Kishore KV (2012) Utilisation of sludge concrete in paver blocks. *Int J Emerg Trends Eng Dev* 4(2):509–516
- Kosior-Kazberuk M (2011) Application of SSA as partial replacement of aggregate in concrete. *Pol J Environ Stud* 20(2):365–370
- Kulkarni GJ, Dwivedi AK, Jahgirdar SS (2012) Textile mill sludge as fine aggregate in concrete. *Glob J Res Eng Ind Eng* 12(2):21–25. Global Journals Inc. (USA). Online ISSN: 2249-4596; Print: ISSN: 0975-5861
- Lekshmi S, Sasidharan S (2015) Experimental investigation on the use of textile sludge in concrete. *Int J Adv Eng Technol (IJAET)* 8(4):559–565



- Lissy PNM, Sreeja MS (2014) Utilization of sludge in manufacturing energy efficient bricks. *IOSR J Mech Civ Eng (IOSR-JMCE)* 11(4):70–73. Available at [www.iosrjournals.org](http://www.iosrjournals.org). e-ISSN: 2278-1684, p-ISSN: 2320-334X
- Mithun CKNT (2016) Hypo sludge paver blocks. *Int J Adv Technol Eng Sci* 4(7):224–228
- Nair KP, Vivek JM, Shibu K (2013) Suitability of sludge as a building material. *Int J Sci Eng Res (IJSER)* 4(5):23–28
- Palanisamy V (2011) Utilization of textile effluent waste sludge in brick production. *Int J Sci Basic Appl Res (IJSBAR)* 4(1):1–10
- Patel H, Pandey S (2009) Exploring the reuse potential of chemical sludge from textile wastewater treatment plants in India—a hazardous waste. *Am J Environ Sci* 5(1):106–110. <https://doi.org/10.3844/ajes.2009.106.110>
- Patel K, Patel RL, Pitroda J (2017a) Technical feasibility study on utilization of textile sludge as a cement substitute in rubber mould paver block. *Int J Constr Res Civ Eng (IJCRCE)*, 3(1):19–25. <https://doi.org/10.20431/2454-8693.0301003>
- Patel K, Patel, Patel RL, Pitroda J (2017b) Environmental and technical feasibility study on utilization of textile effluent treatment plant sludge as a construction material: a review. In: *International conference on research and innovations in science, engineering and technology (ICRISET—2017)*, *IJTE special issue for ICRISET 2017b*, pp 5–9
- Priyadharshini B, Kavisri M (2018) Utilization of textile sludge in manufacturing e-bricks. *Int J Civ Eng Technol* 9(11):2266–2273
- Raghunathan T, Gopalsamy P, Elangovan R (2010) Study on strength of concrete with ETP sludge from dyeing industry. *Int J Civ Struct Eng* 1(3):379–389
- Ravikrishnan S, Senthilselvan S (2014) Novel green bricks manufactured from textile ETP sludge. *Int J Sci Eng Res (IJSER)* 5(6):76–81
- Sandesh NU, Varun K, Prashanth VP (2014) A study on engineering properties of textile ETP sludge based cement concrete. *Int J Innovations Eng Technol (IJJET)* 4(4):324–330. ISSN: 2319–1058
- Senthilkumar K, Sivakumar V, Akilamudhan P (2008) Experimental studies on disposal of various industrial solid wastes. *Mod Appl Sci* 2(6):128–132. <https://doi.org/10.5539/mas.v2n6p128>
- Sudheesh C, Kumar TRP, Kumar SS (2015) Effect of compressive strength on concrete by partial replacement of cement with textile sludge and polypropylene fibres. *Int J ChemTech Res* 8(4):2219–2226
- Swarna MA, Venkatakrishnaiah R (2014) Manufacturing of bricks using tannery effluent sludge. *Int J Recent Dev Eng Technol (IJRDET)* 3(4):33–36. Available at [www.ijrdet.com](http://www.ijrdet.com). ISSN 2347–6435(Online)

# Sustainable Method for Construction and Demolition Waste: A Review



Mitali Mistry, Hetvi Chaudhari, and M. A. Shabiimam

**Abstract** India's construction industry plays a vital role in our country's economy. Over the past few decades, development in infrastructure has been a boon but has also led to serious environmental issues. Development in infrastructure has a dark side in the generation of an enormous amount of construction and demolition waste due to the construction, renovation, or demolition of a structure. This article discusses the status of C&D waste, sustainable methods to reduce environmental impacts, challenges, and current scenarios around the world. This review study also discusses implementing a zero-waste strategy in the construction industry to reduce and optimize C&D waste. Mishandling and mismanagement of the waste have been done for a long time, and the potential in terms of materials recovery is realized. Also, the article discusses about the reuse of various materials available as recycled materials. Government of India also implied various rules and regulations for a zero-waste strategy and motivated the public to use recycled materials. Recycled materials have some specific characteristics other than normal raw materials so more reliable and more economical. The recycled materials have 10% less price than the normal materials.

**Keywords** Construction and demolition waste · Recycling · Waste recovery · Sustainability · Waste management

---

M. Mistry · H. Chaudhari · M. A. Shabiimam (✉)  
Department of Civil Engineering, SOT, Pandit Deendayal Energy University,  
Gandhinagar 382007, India  
e-mail: [shabiimam.ma@sot.pdpu.ac.in](mailto:shabiimam.ma@sot.pdpu.ac.in)

M. Mistry  
e-mail: [mitali.mmtne21@sot.pdpu.ac.in](mailto:mitali.mmtne21@sot.pdpu.ac.in)

H. Chaudhari  
e-mail: [hetvi.cmtne21@sot.pdpu.ac.in](mailto:hetvi.cmtne21@sot.pdpu.ac.in)

# 1 Introduction

“Every year, around 400 million tonnes of material are used in the construction sector” observed by the UK Green Building Council. Some activities of construction and demolition works like roads, industrial structures, flyovers, buildings, highways, subways, etc. created major pollutants. C&D increases from time to time which impacts the environmental system (Weber et al. 2002). Due to construction and demolition waste the various impacts occur in environment like landfill depletion, energy and non-energy resource computation, air pollution, noise pollution, water pollution, and resource depletion. Various research found that the construction and demolition sectors have contributed to climate change, drinking water pollution, air pollution, and landfills to around 50%, 40%, 23%, and 50%, respectively (Bokarde 2021). The change in the environment depends on the materials used in construction and demolition activities. Inert and non-biodegradable materials like concrete, metal, plaster, plastic, wood, glass, etc. are used in construction and demolition activities. Some of the materials are inert and non-hazardous but non-inert and hazardous waste. Approximately, 85% of C&D is concrete, masonry, and ceramics that are reused as inert materials (Gálvez-Martos et al. 2018). The other waste has high density, high volume, bulky, weight, hazardous metals, etc.

Construction and delimitation waste is reused in different ways; some of them are effective and others are harmful to nature. Considering the usage of construction and delimitation waste (C&D) as landfill work should present three aspects. The construction and delimitation waste (C&D) occupied a large area of landfills and reduced the soil’s capacity (Jim 1998). There is a high risk for groundwater and surface water due to the leachate from unlined landfills. Some of the non-inert materials in C&D waste like lead, asbestos, tar, preservative residues, and paint may have hazardous effects over time (Fatta et al. 2003). Recycling means not only contributing a large amount of rebuilding the resources such as aggregate (Li et al. 2003). Also needs to treat materials with traditional methods like landfills (Lease et al. 2002).

## 1.1 C&D Waste Quantity

The world considers construction and demolition waste to be precedence because it constitutes one of the large wastes. Construction, demolition, and renovation work generated the C&D waste. Table 1 has the same data about waste generation in the country. Major countries generate around 10 billion tonnes of construction and demolition. The US generated approximately 700 million tonnes (Nowak and Crane 2002). China produced around 3 million tonnes because of the renewal program and development of large-scale urbanization (Zheng et al. 2017). China uses various methods for C&D waste which helps to reduce the value of annual generation. C&D waste was treated, disposed, and prevented by China government (Aslam et al. 2020).

**Table 1** Information about the country

Sr. no.	Country	Waste generation (million tonnes)	References
1	EU	850	EC (2016), Wu et al. (2019)
2	US	600	EC (2016), Wu et al. (2019)
3	Germany	218.8	Net source ( <a href="http://www.stonecycling.com">www.stonecycling.com</a> )
4	India	150	Net source (wiki)
5	UK	67.8	Net source (UK statistics on waste department for environment food and rural affairs)
6	Canada	35.6	Net source ( <a href="http://www.canada.ca">www.canada.ca</a> ) government of Canada
7	Netherland	25.12	Net source ( <a href="http://www.clo.nl-1990-2018">www.clo.nl-1990-2018</a> )
8	China	3	Zheng et al. (2017)

Around 30–40% of waste is generated in urban areas (Wang et al. 2016). India produced 150 million tonnes of C&D waste.

## 1.2 Sustainability of C&D Waste

Sustainability means wasting material cutting down on resources, reusing the waste and recovering the materials from the C&D of waste in organized ways. C&D waste is still unsophisticated stage in many countries and landfilling is the most beneficial method for it (Hahladakis et al. 2020; Marzouk and Azab 2014; Silva et al. 2017). The various agencies introduce the idea of a sustainable method of use of C&D waste. If at least 50% of the total mass of the C&D wastes were used as recycled and reused, then it makes a minimum impact on the environment as said by the LEED-ND (Kamino et al. 2019). C&D waste materials are considered as relatively low environmental impact materials, which can be divided into two categories the statement given by the BREEAM. Sustainable materials were calculated as having a low impact on the environment as per the document on green guide to specification. Other materials are called road construction materials which are considered constituted and reclaimed materials. Here is the step for C&D waste in the aspect of environmental impacts.

Sustainability means the life cycle of various materials which gives the minimum impact on the environment. The first step for C&D waste was a collection of the material from the various sites which was the disposal at the site. Then separate the waste material with specifications as rules of the different agencies and characteristics of the materials. Recover the waste material which comes out during separation process. For C&D waste, recycled material is the better option that affects the social, economic, and environment (Yuan et al. 2011). Recycling the waste material based on their characteristics helps to utilize the waste effectively. Recycle waste material used as new construction material or products which was less impact on the

**Fig. 1** Process of waste materials sustainability



environment. It also reduced waste and avoids the toxic material that impacts the environment. All steps will help the environment and easily utilize the C&D waste.

Figure 1 understands the process of waste materials sustainability. Also considered is the guideline for treating waste (Alsheyab 2022).

## 2 Characteristics/Source of C&D Waste

The different complex materials were used during the construction and demolition work. These materials generate highly polluted waste. Waste is classified into two categories for better understanding. Here are some of the different materials and their characteristics.

### 2.1 Major Components

Major components are considered as the main part of the construction which are not easily reused. Here some of the materials are recycling coarse aggregate, brick, fine recycled concrete aggregate, metals, rubble/stone, and timber/wood.

**Table 2** Property of recycled coarse aggregate

Sr. no.	Materials	Water absorption (%)	Bulk-specific gravity (kg/dm <sup>3</sup> )	References
1	BCRA	0–20.6	1.7–3	Angulo et al. (2004)
2	RCA	2.35	2.55	Ryou and Lee (2014)
3	RAC	2.03	1.25	Shahidan et al. (2017)
4	RAC	5.03	2.43	Thomas et al. (2013)

*BCRA* Brazilian coarse recycled aggregate

*RCA* recycled coarse aggregate

*RAC* recycled aggregate concrete

*RA* recycled aggregate

### 2.1.1 Recycled Coarse Aggregate (Cement/Concrete/Aggregate)

The characteristics of aggregates are relevant to three aspects which are chemical, physical, and mineralogical. Mainly recycled aggregates are tested by sieved, sampled, and separated into four types of heavy media classes based on mineralogical and physical characteristics. Ceramic and cement-based particles have physical aggregates properties that were conflicting. Using different methods, the preferable method is the homogeneity of physical properties. The efficient method for separation of recycled aggregates are using water absorption and bulk-specific gravity properties techniques (Angulo et al. 2004). The recycled coarse and fine aggregates were based on cement materials. Table 2 mentions the different properties of C&D material of cement-concrete (aggregate).

Bulk-specific gravity means the ratio of the weight of the given volume of aggregate.

The various study of recycled coarse aggregate depends upon the constitution of silicates. Portland cement is a secondary option for recycled coarse aggregate.

### 2.1.2 Brick (Masonry Work)

Brick is the key material of construction. C&D waste has a major part from brick, but another type of brick waste is considered waste. Another type was the bricks that were broken, damaged, and had excessive cutting. Overburnt brick is also considered waste. Bricks have higher durability throughout life, which helps environmental properties (Bansal and Singh 2007; Bansal et al. 2014). Bricks have a cooler surface which helps with hot temperatures. The recycled bricks have some amount of cement and concrete materials, so that effect the various properties. The recycled bricks aggregated depend on major properties that have physical and mechanical properties. Recycle bricks have a more excellent shrinkage value. The study has found that it has a 10–12% lower cost than regular brick (Paul et al. 2018). Table 3 mentions the properties of recycled brick with cement, concrete, and aggregate (Paul et al. 2018).

**Table 3** Properties of recycled brick

Sr. no.	Properties	Depending upon	Comment
1	Compressive strength	AOS	Increased with age increased
2	Workability	AOS	Lower workability compared to normal brick
3	Elastic modulus	–	Better result than normal brick
4	Young modulus	–	Range of 17–24 GPa
5	Resistance	–	Better resistance compared to normal brick

AOS age of the structure

### 2.1.3 Fine Recycled Concrete Aggregate

Break the concrete chunk into smaller pieces and remove the mortar layer from the brick or aggregate then crush it. FRCA depended upon the water absorption and specific gravity. Treated fine RCA and crushed fine RCA have a specific gravity of 2.35 and 2.04 and water absorption of 5.39% and 9.38%, respectively (Shrivastava and Gettu 2020). The crushed fine RCA has been treated thermo-mechanically, and treated RCA has been normally recycled fine aggregate. The study has shown that natural fine aggregate with crushed brick and pozzolanic admixture which partially replaces up to 50% gives 40% higher strength concrete (Olofinnade and Ogara 2021).

### 2.1.4 Metals

Steel and aluminium were generally major components during construction work. The source of metals in C&D waste was from RCC, railing, doors, staircase, windows, etc. It was easily collected from the waste. The characteristics of steel never affect making the reused product. Aluminium is recycled multiple times which helps the environment. Recycling aluminium required very less energy than the new aluminium.

### 2.1.5 Rubble/Stone

The rubble and stone were used in the construction work. Marble, sandstone, and granite are easily reused due to their attraction and characteristics.

### 2.1.6 Timber/Wood

The old buildings were made from wood/timber and soil materials. C&D waste has a major part of wood from the demolition of old buildings. There are no significant characters that were changed in the timber.

## 2.2 Minor Components

Minor components are considered subparts of the construction which are easily reused. Here, some of the materials are conduits, pipes, tiles, electrical fixtures, and panels.

### 2.2.1 Conduits, Pipes, Tiles, Electrical Fixtures, Panels

The minor materials were plastic, iron, wires, glass, laminated panels, etc. The minor components have no effect on the inter-life span which contained 15% of all C&D waste. Irons are getting corroded over a period of time. Recycled glass waste aggregates have a specific gravity of 2.49 and water absorption of 0.06% (Meddah 2014).

## 3 Process of C&D

The government of India implemented a zero-waste strategy for construction and demolition waste that reduced and optimized the waste (Liyanage et al. 2019). Here are some steps for reusing construction and demolition waste. The first collection of the waste from different sites. Then separated the materials based on inert and non-inter waste.

Figure 2 shows the process of C&D waste; this process collected the waste material from sources and also mentioned the classification of waste (Islam et al. 2019).

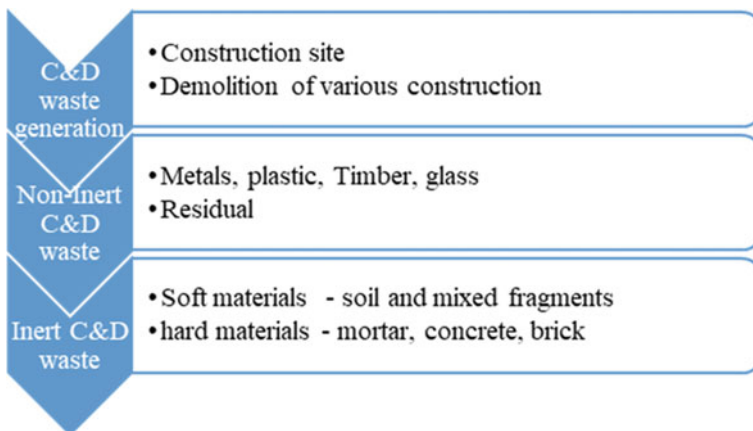


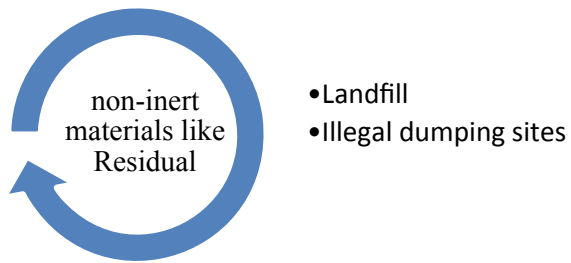
Fig. 2 Process of C&D waste





**Fig. 3** Processes of non-inert materials like metal and timber

**Fig. 4** Processes of non-inert material like residuals



Materials are reduced in different ways which helps to recycle the waste and reused it. Some inert materials are used in a landfill as covering material, and some are recycled with various techniques.

Figures 3 and 4 both mention the non-inert materials which have different processes as per materials (Islam et al. 2019).

Inert C&D waste is based on soft and hard materials. Soft materials are used for landfills and illegal dumping sites. The remaining material is used for recycling with on-site recycling and recycling facilities in the plant and made the mortar and concrete products with recycled aggregates. For hard materials used the same method as soft materials.

#### 4 Recycled and Reused C&D Waste

Reusing and recycling were totally different processes for construction and demolition waste. Reusing means not transforming into phenomena. The waste materials do not dumped in landfill before they need to be recycled and converted into a particular product that helps the environment. Globally in Japan, Korea, Norway, Singapore, etc., waste materials enclosed under this segment are concrete, bricks, tiles, metals, and plastics. The same study has shown that construction and demolition waste materials were reused as landfilling or made into recycled products which are helpful to new construction, creative work, road construction, etc. Table 4 shows the same components with recycled and totally reused efficiently.

The disposal of construction and demolition waste required a large landfill area. If the waste generated was 7.5 billion m<sup>3</sup> for their dumping, the height will set 20 m,

**Table 4** Recycled and efficient

Sr. no.	Component	Recyclable	Efficiency (%)	References
1	Recycled coarse aggregate	Landfill recyclable in plants	13.5%	Córdoba et al. (2019)
			13.52	Córdoba et al. (2019)
2	Bricks (masonry waste)	Landfill or recyclable in plants	–	–
3	Fine recycled concrete aggregate (mortar)	Landfill or recyclable in plants	–	–
4	Metals	Non-recyclable in plant	0.98%	Córdoba et al. (2019)
5	Timber/wood	Non-recyclable in plant	–	–

so the area required is 375 million m<sup>2</sup> which occupies half of Singapore's area. 90% volume of landfills could be cut by recycling the product (Zheng et al. 2017).

#### 4.1 Recycled Coarse Aggregate

The recycled coarse aggregates were directly used in landfills or needed some treatment like crushing. The RA has lesser compressive strength, so it was not perforable to be used as new concreting. It is used in limited ways like road bases, paving stones, concrete blocks, concrete pipes, etc. (Bansal and Singh 2007). RA is used with silica fume, fly ash, etc. Then it is used for the normal structure (Rao et al. 2007). RA was used as secondary raw material (Özalp et al. 2016). As several studies have shown that recycled aggregate is treated by the TSMA method because properties are improved by surface treatment (Mistri et al. 2020), the RCA was crushed into the machine as per a specific size. As mentioned above that the RCA has high water absorption, we need to treat the RCA with epoxy resin (Shahidan et al. 2017).

#### 4.2 Bricks (Masonry Work)

Bricks were easily reused materials. It has high durability and is easily cursed. It will reuse on new sites if it was not reused then we recycled it for another usage (Bokarde 2021). During the demolition work, the bricks were separated with the mortar by using the chiselled. If the mortar was removed, then it was used in a new project without any processes. It was also used for artistic creation, small particle aggregates, landfilling, precast materials like interlocking tiles, brick pavers, kerb

stones, and landscaping. Brick converted into brick paver is the best option. Recycled bricks were used as a lightweight material. Recycled brick aggregate is mixed with fly ash and cement by crushing, screening, and blending for made various materials.

### ***4.3 Fine Recycled Concrete Aggregate (Mortar)***

There was no guideline about the use of fine recycled concrete aggregate. Various methods and research were found on how to reuse the fine recycled concrete aggregate. FRCA used as concrete in construction work is a better option than cement because the FRCA gives higher quality compared to cement (Nedeljkovic et al. 2021). 20% and 30% FRCA particles were added to concrete which gives similar compressive strength as compared to natural fine aggregate (Zega and Maio 2011).

### ***4.4 Metals***

Steel that came from the C&D waste can be resized by the customers' requirement, which was a better option than remelting and rolling in the new steel (Bansal and Singh 2007). It saves energy that helps the environment. Steel waste has good durability so that is easily used for made products like steel furniture and fire hydrants. The solid bonding process can be used for the Aluminium scrap.

### ***4.5 Rubble/Stone***

The rubbles were collected from the C&D waste and processed into the fine and coarse aggregate that will be applied to the concrete blocks (Sabai et al. 2013).

### ***4.6 Timber /Wood***

Timber waste that lay hold from the knockdown bridges and unnecessary power poles is also can be reused instead of throwing out in landfills. Reusing waste of timber is right on as some solid wood timber furnishes are decreasing.

## 5 C&D Plant in Various Countries

The various industries, government organizations, and other non-government organizations solve the problem of C&D waste. They have started some programs for better management of C&D waste. Many projects are implemented for C&D waste across various locations in India, Korea, and Japan which can be reviewed and analysed. The various treatment plants with the efficiency shown below (Table 5).

Various plants were used in the different methods that depended upon which type of waste was used. Burari is India's first plant for the generation of products with the help of C&D waste. Now, the plant has the capacity to treat the 2000TPS. Most of the plants were working under the public-private partnership (PPP). C&D waste is crushed in the plant and made into bricks, drainage slabs, concrete blocks, paving blocks, etc. The cost of recycled materials is 10–12% less than that of normal materials (Paul et al. 2018). The cost of recycled brick, fly ash brick, and red brick is 5.5–6, 5–6, and 7–8 Rs, respectively.

**Table 5** Information about recycled plant

Sr. no.	Location	Treatment of materials	Efficiency	Component produced	References
1	Burari, Delhi	500 TPD	95%	Brick, blocked, kerb stones	del Río Merino et al. (2010)
2	Korea	67 million	51.2%	–	del Río Merino et al. (2010)
3	Ahmedabad	300 TPD	–	Paver block, suitability tiles, park seats	Huovila et al. (2019)
4	Enzyme India Pvt. Ltd	150 TPD	–	Concrete block	Kolaventi et al. (2021)
5	Telangana	500 TPD	–		Kolaventi et al. (2021),
6	Thane	600 TPD	–	Bricks, paver block, kerb stone, tiles	Roychowdhury et al. (2020)
7	Bengaluru	750 TPD		Recycled concrete aggregate	Roychowdhury et al. (2020)
8	Jaipur	300 TPD		Kerb stone, paver block, concrete brick	Roychowdhury et al. (2020)
9	Gurugram	300 TPD		Paver block	Roychowdhury et al. (2020)
10	Chandigarh	180 TPD		Kerb, channel, tiles, paver block	Roychowdhury et al. (2020)
11	Vijayawada	200 TPD		Recycled sand and aggregate	Roychowdhury et al. (2020)

## 6 Steps by GOI

The government organization has made some steps for construction and demolition work. The steps were notified by the Ministry of Environment, Forests, and Climate Changes (MoEF&CC) in the year 2016. Ministry of Housing and Urban Affairs drafted report in 2018 that disposable the construction and demolition waste (C&D) can be used as recycled products. Promoting usage of recycling products made from construction and demolition waste is essential. Here are some steps which are the main initiatives of the 2016 C&D waste management.

- In the contract of municipal and government for construction, it was compulsory for all the local bodies to use 10–20% recycled products.
- It is proposed to assess the conditions together with a change in the compensation fee for the supply of construction and demolition waste and reduced the recycled products price to 20% as per conventional products.
- The collection and disposal of the construction and demolition waste were the responsibility of the large developers.
- We recommend that waste generators be provided with the necessary incentives for on-site waste collection, disposal, and recycling.
- The database is maintained by the recycled products from various government contracts and the utilization of waste generators.

## 7 Conclusion

We can conclude that C&D waste has contributed to air pollution, noise pollution, water pollution, and resource depletion, and to mitigate its impact, zero-waste strategy is implemented by reusing and recycling materials obtained from waste such as concrete and bricks. Landfilling was the convent option for all the agencies, but it required more land area that will impact groundwater and soil quality. On the other hand, recycled products were used in concrete as new construction and made the new product that is used in the construction. Several techniques were helping to recycle the C&D waste and several research will help to reduce the C&D. The better option for C&D waste was to recycle and then reuse that product. Various steps taken by India's government and local bodies have also helped the cause. Various similar steps taken by different countries are also helpful in accessing the situation of C&D waste.

## References

- Alsheyab MAT (2022) Recycling of construction and demolition waste and its impact on climate change and sustainable development. *Int J Environ Sci Technol*. Springer Science and Business Media Deutschland GmbH, pp 2129–2138

- Angulo SC, Ulsen C, Carrijo PM, Silva RM, John VM, Kahn H (2004) Characterization of Brazilian construction demolition waste coarse recycled aggregate
- Aslam MS, Huang B, Cui L (2020) Review of construction and demolition waste management in China and USA. *J Environ Manage* 264(February):110445
- Bansal S, Singh SK (2007) A sustainable approach towards the construction and demolition waste status of health and sanitation in rural communities view project waste management view project a sustainable approach towards the construction and demolition waste. *Int J Innov Res Sci Eng Technol An ISO 3297(2)*
- Bansal S, Singh Head SK, Kurian J (2014) In: The fourth International Fib Congress
- Bokarde K (2021) Sustainable management of construction and demolition waste. *Int J Res Appl Sci Eng Technol* 9(12):250–257
- Córdoba RE, Marques JD, Santiago CD, Pugliesi E, Schalch V (2019) Alternative construction and demolition (C&D) waste characterization method proposal. *Engenharia Sanitaria e Ambiental* 24:199–212
- del Río Merino M, Gracia PI, Azevedo ISW (2010) Sustainable construction: construction and demolition waste reconsidered. *Waste Manage Res*, pp 118–129
- European Commission Directorate - General (2016) EU construction & demolition waste management protocol. *Off J Eur Union*
- Fatta D et al (2003) Generation and management of construction and demolition waste in Greece—an existing challenge. *Resour Conserv Recycl* 40(1):81–91
- Gálvez-Martos JL, Styles D, Schoenberger H, Lahl Barbara Z (2018) Construction and demolition waste best management practice in Europe. *Resour Conserv Recycl* 136:166–178
- Hahladakis JN, Purnell P, Aljabri HMSJ (2020) Assessing the role and use of recycled aggregates in the sustainable management of construction and demolition waste via a mini-review and a case study. *Waste Manage Res* 38(4):460–471
- Huovila P, Iyer-Raniga U, Maity S (2019) Circular economy in the built environment: supporting emerging concepts. *IOP Conf Ser Earth Environ Sci* 297:012003
- Islam R, Nasifa TH, Yuniarto A, Uddin ASMS, Salmiati S, Shahid S (2019) An empirical study of construction and demolition waste generation and implication of recycling. *Waste Manage* 95:10–21
- Jim CY (1998) Urban soil characteristics and limitations for landscape planting in Hong Kong. *Landsc Urban Plan*
- Kamino G, Gomes S, Bragança L (2019) Improving the sustainability assessment method SBTool urban—a critical review of construction and demolition waste (CDW) indicator. *IOP Conf Ser Earth Environ Sci* 225:012004
- Kolaventi SS et al (2021) Implementing site waste-management plans, recycling in India: Barriers, benefits, measures. *Proc Inst Civ Eng Eng Sustain* 175(1):30–51
- Lease K, Anthony R, Seldman N (2002) Zero waste: replacing waste management with discards management in the Hong Kong Special Administrative Region
- Li WX, Tang XX, Yu Z (2003) On regeneration and recycle utilization of construction waste. *29(15):130–131*
- Liyanage KLAKT, Waidyasekara KGAS, Mallawaarachchi H (2019) Adopting the zero waste concept for eliminating C&D waste in the construction industry. *MATEC Web Conf* 266:02008
- Marzouk M, Azab S (2014) Environmental and economic impact assessment of construction and demolition waste disposal using system dynamics. *Resour Conserv Recycl* 82:41–49
- Meddah MS (2014) Recycled aggregates in concrete production: engineering properties and environmental impact
- Mistri A, Bhattacharyya SK, Dhami N, Mukherjee A, Brai SV (2020) A review on different treatment methods for enhancing the properties of recycled aggregates for sustainable construction materials. *Constr Build Mater*
- Nedeljković M, Visser J, Savija B, Valke S, Schlangen E (2021) Use of fine recycled concrete aggregates in concrete: a critical review. *J Build Eng*

- Nowak DJ, Crane DE (2002) Carbon storage and sequestration by urban trees in the USA. *Environ Pollut*, pp 381–389
- Olofinnade O, Ogara J (2021) Workability, strength, and microstructure of high strength sustainable concrete incorporating recycled clay brick aggregate and calcined clay
- Özalp F, Yılmaz HD, Kara M, Kaya Ö, Şahin A (2016) Effects of recycled aggregates from construction and demolition wastes on mechanical and permeability properties of paving stone, kerb and concrete pipes. *Constr Build Mater* 110:17–23
- Paul SC, Babafemi AJ, Angraini V, Rahman MM. (2018) Properties of normal and recycled brick aggregates for production of medium range (25–30 MPa) structural strength concrete. *Buildings* 8(5)
- Rao A, Jha KN, Misra S (2007) Use of aggregates from recycled construction and demolition waste in concrete. *Resour Conserv Recycl* 50(1):71–81
- Roychowdhury A, Somvanshi A, Verma A (2020) Another brick off the wall: improving construction and demolition waste management in Indian Cities, p 146
- Ryou J, Lee YS (2014) Characterization of recycled coarse aggregate (RCA) via a surface coating method. *Int J Concr Struct Mater* 8(2):165–172
- Sabai MM, Cox MGD, Mato RR, Egmond ELC, Lichtenberg JJN (2013) Concrete block production from construction and demolition waste in Tanzania. *Resour Conserv Recycl* 72:9–19
- Shahidan S, Mohammad Asmi MA, Kupusamy K, Mohd Zuki SS, Ali N (2017) Utilizing construction and demolition (C&D) waste as recycled aggregates (RA) in concrete. *Procedia Eng*, pp 1028–1035. Elsevier Ltd.
- Shrivastava V, Gettu R (2020) Characterisation of recycled aggregates and mortar studies using recycled fine aggregate.
- Silva RV, De Brito J, Dhir RK (2017) Availability and processing of recycled aggregates within the construction and demolition supply chain: a review. *J Clean Prod* 143:598–614
- Thomas C, Setien J, Polanco J, Alaejos P, De Juan MS (2013) Durability of recycled aggregate concrete. *Const Build Mater* 40:1054–1065
- Wang J, Wu H, Duan H, Zillante G, Zuo J, Yuan H (2016) Combining life cycle assessment and building information modelling to account for carbon emission of building demolition waste: a case study. *J Clean Prod* 172:3154–3166
- Weber WJ, Jang YC, Townsend TG, Laux S (2002) Leachate from land disposed residential construction waste. *J Environ Eng* 128(3):237–245
- Wu H, Zuo J, Yuan H, Zillante G, Wang J (2019) A review of performance assessment methods for construction and demolition waste management. *Resour Conser Recycl*. Elsevier B.V.
- Yuan F, Shen LY, Li QM (2011) Emergy analysis of the recycling options for construction and demolition waste. *Waste Manage* 31(12):2503–2511
- Zega CJ, di Maio AA (2011) Use of recycled fine aggregate in concretes with durable requirements. *Waste Manage* 31(11):2336–2340
- Zheng L, Wu H, Zhang H, Duan H, Wang J, Jiang W, Dong B, Liu G, Zuo J, Song Q (2017) Characterizing the generation and flows of construction and demolition waste in China. *Constr Build Mater* 136:405–413

# **Innovations in Climate Change Assessment**



# An Enhanced Bottom-Up Approach to Assess the Catchments' Vulnerability to Climate Change



Vishal Rakhecha and Ankit Deshmukh

**Abstract** Managing water resources is becoming difficult due to projection uncertainty in the future climate. Traditional top-down modeling paradigms do not provide sufficient information to water resource managers for proper decision-making in the present uncertainties. It is due to huge uncertainty in the future projection of GCM and uncertainties in GCM downscaling techniques parameterization of hydrological models. We built upon a recently developed bottom-up approach to estimate the catchments' vulnerability to climate change. The framework identifies the vulnerable combination of climate (temperature and precipitation) that causes adverse conditions for an indicator of vulnerability, such as depletion of water or less water availability. In this work, we specify the vulnerability of the catchment by the reduction in the mean annual runoff by 50% of its historical flow. We simulate synthetic climate scenarios using historical data of the past few decades with three techniques, Synthpop, KNN-CAD, and Maximum Entropy Bootstrap Weather Generator (MEBWG), which can best simulate the frequency and extrema event of the future climate. Synthetic climate data were used to compute the indicators that we divided into the vulnerability classes. A data mining algorithm [classification and regression tree (CART)] is used to associate the vulnerability classes with the synthetic climate combinations. We use a total of 77 US catchment data in the study and compute the critical threshold for each catchment for climatic variables (precipitation, temperature, and land use). The critical threshold provides an estimation of catchments' vulnerability to climate change and can be used for critical decision-making under uncertainties for water policies.

**Keywords** Catchments' vulnerability · Classification and regression tree · Global climate model · Climate change

---

V. Rakhecha · A. Deshmukh (✉)  
Pandit Deendayal Energy University, Gandhinagar, India  
e-mail: [deshmukh.acad@gmail.com](mailto:deshmukh.acad@gmail.com)

V. Rakhecha  
e-mail: [vishal.rcv18@sof.pdpu.ac.in](mailto:vishal.rcv18@sof.pdpu.ac.in)

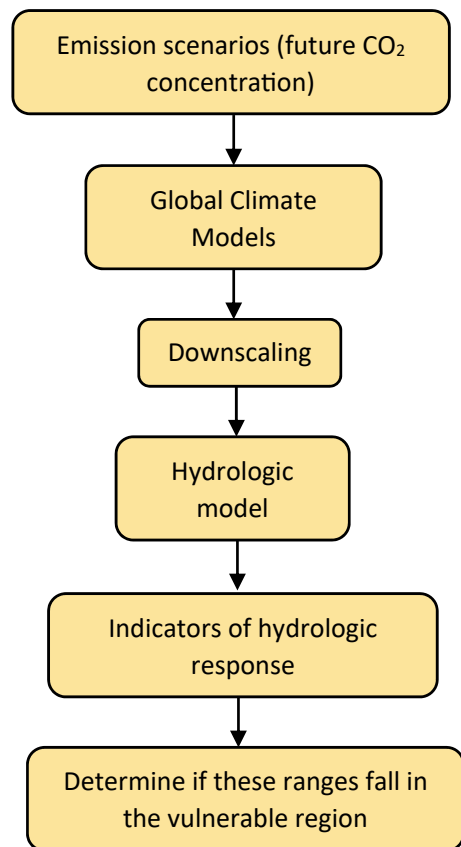
# 1 Introduction

## 1.1 Top-Down Approach

The top-down hydrological modeling approach utilizes the general climate models (GCM) projected climatic variables (i.e., precipitation and temperature) to predict streamflow. The uncertainty in the GCM makes reliable streamflow projection challenging (Mujumdar and Ghosh 2008). The steps involved in the implementation process for obtaining a hydrologic projection with a top-down approach are shown in (Fig. 1).

Top-down methodology forces a hydrologic model to use available GCMs' environmental change information for smaller regions/areas with many uncertainties (Keller et al. 2022). The uncertainties occur due to downscaling of GCM, which generates information about a country/ larger region to a small region on which we use a hydrological model. A second criticism is that GCMs and regional climate

**Fig. 1** Top-down modeling approach



model (RCMs) resolutions are still not fine enough to perfectly understand and simulate catchment response. A third criticism of the top-down model is that they are likely to ignore or at least underestimate detailed data of smaller regions, i.e., extremes of precipitation and temperature variations of the region, which ultimately lead to error in determining vulnerable region/area (Mujumdar and Ghosh 2008).

### 1.2 Bottom-Up Approach

The Bottom-up approach starts from policymakers and focuses on the extent to which its objectives (determining the vulnerable range for smaller regions/areas) are attained over time and first we defining vulnerability definition of indicators (identifying the indicators at which vulnerable cases occurs such as mean annual runoff, drought, flood, etc.). The bottom-up approach is independent of future climate change projections; therefore, this vulnerability-based bottom-up approach is helpful for deciding factors under larger uncertainty. The bottom-up, vulnerability-based approach is useful for decision-makers and water policymakers who are working in a smaller region or who have difficulty finding precise or accurate data. This provides a mechanism for moving from the bottom level (determining the vulnerable range) to top policymakers (vulnerable environment) (Sabatier 1986). The bottom-up modeling framework processes are shown in Fig. 2.

Our focus will be on the 'inspect environmental change space' with the bottom-up framework, in which we will explore different climatic scenario generators using multiple algorithm/weather generators. We use three algorithm generators

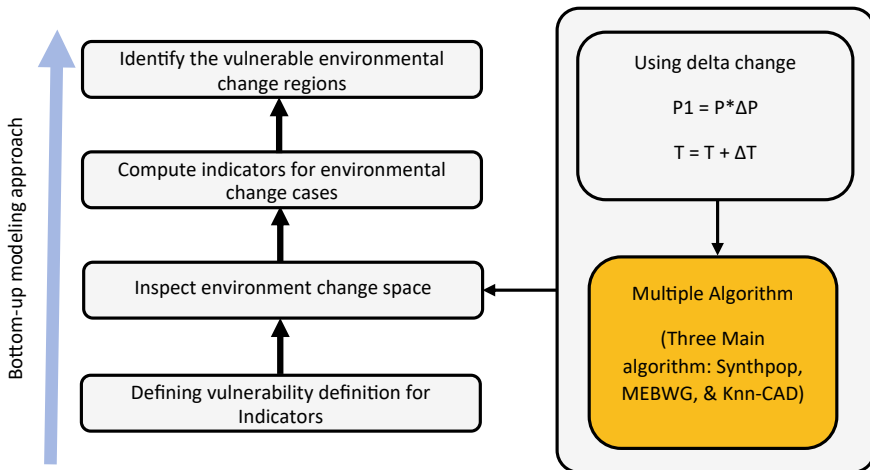


Fig. 2 Bottom-up modeling approach

to generate climates samples—Synthpop, KNN-CAD, and Maximum Entropy Bootstrap Weather Generator (MEBWG).

### 1.3 Weather Generator

In order to produce synthetic repetitions of climatic variables of the same duration while maintaining the essential statistical properties of the actual weather data, such as mean and standard deviation, we employ theoretical simulation tools called ‘weather generators’ (Machado et al. 2014).

There are several classes of random weather generators; such classes can be categorized into (1) parametric, (2) non-parametric, and (3) semi-parametric. Parametric models are the most often used techniques for modeling temperature and precipitation probability distributions using Markov chains. Some examples of parametric models are SIMMETEO (Soltani and Hoogenboom 2003; Elshamy et al. 2006), GEM (Hanson and Johnson 1998), WGENK (Kuchar 2004), AAFC-WG (Qian et al. 2004, 2008), WGEN (Craigmile and Guttorp 2011).

By using the bottom-up approach to assess catchments’ vulnerability, we are exploring a large number of climatic scenarios with three weather generators and a delta change method to improve our approach. In the delta change method, we are changing temperature and precipitation by their historical mean, which amplifies the scope of our climate scenario. Then we try to identify how these changes in the input of precipitation and temperature will produce a change simulation of runoff using a hydrological model. After this, we calculate indicators and define indicators in classes for runoff scenarios. Ultimately, we are finding the combination of precipitation and temperature, which define our final indicator’s vulnerable cases using the classification and regression tree (CART).

## 2 Methodology

The bottom-up approaches focus on the past and present vulnerability for estimating the catchment’s vulnerability to climate change. In this work, we specify the vulnerability of the catchment by the reduction in mean annual runoff (MAR) by 50% of its historical flow. MAR is an indicator used in this study, and we can add other indicators of interest, such as drought and flooding. Here, we examine different climate combinations of precipitation and temperature. We employ three distinct synthetic climate generators to create various climatic scenarios, preserving statistical properties like mean, standard deviation, geographical and terrestrial correlation, and generalizing historical extremes. Here, we are showing Synthpop (Nowok et al. 2016), KNN-CAD (King et al. 2015), and Maximum Entropy Bootstrap Weather Generator (MEBWG) (Srivastav and Simonovic 2015). We are using the delta change method to explore the different environmental space combinations. And we simulate streamflow with

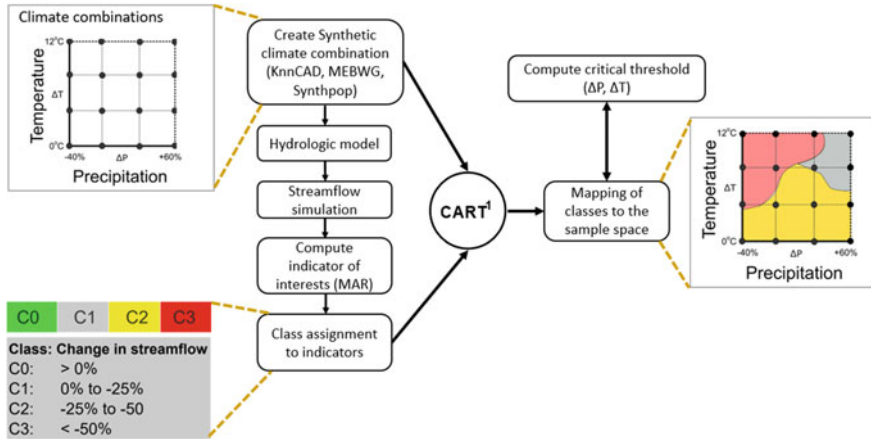


Fig. 3 Bottom-up-based framework is used to compute the critical threshold for an indicator

these climatic combinations with our hydrological model. For each climatic case, we compute streamflow and then compute MAR. We follow a similar procedure to simulate climate change with the weather generator. However, along with delta change, we generate a new climate combined with the aforementioned weather generator, compute streamflow, and then MAR. We compare the original indicator values (generated without any weather generator input) with weather generator simulated MAR. In the end, we found the combination of precipitation and temperature change threshold with the classification and regression tree (CART) (Fig. 3).

### 2.1 Parameter Generator

Our parsimonious hydrological model has 13 parameters (See Deshmukh and Singh 2016). To calibrate the model, we generate 7500 parameter sets using the feasible ranges specified in Table 1 for each catchment. Later, we simulated the streamflow of each parameter set and compared it with ten-year historical observed streamflow data from 1959 to 1968. To identify behavioral parameter sets, we use Nash–Sutcliffe efficiency (NSE) > 0 and volume % bias range between ±25%. Fifty parameters (behavioral parameter sets) were identified to simulate the climate change scenarios.

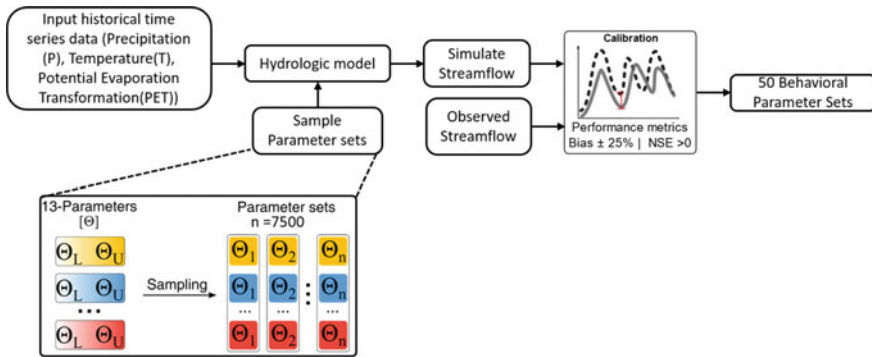
### 2.2 Model Calibration

See Fig. 4.

**Table 1** Behavioral parameter sets are computed with the parameter ranges

	Parameter	Description	Feasible range		Units
			Lower	Upper	
Soil	Sb	Maximum depth of soil store	0	2000	mm
	B	Shape factor of distribution bucket	0	7	
	Fc	Threshold storage parameter	0	1	
	Kd	Deep recharge coefficient	0	0.5	
Vegetation	M	Fraction of deep-rooted vegetation	0	1	
	LAI <sub>max</sub>	Maximum leaf area index	0	6	mm
	LAI <sub>min</sub>	Minimum leaf area index	0	6	mm
	Cei	Maximum canopy interception	0	0.49	mm
Routing	A <sub>ss</sub>	Recession coefficient for saturated soil	0.05	0.5	day
	A <sub>bf</sub>	Recession coefficient for groundwater	0.001	0.05	day
Snow	Ddf	Degree day factor	0	20	mm°C <sup>-1</sup> d <sup>-1</sup>
	Tth	Threshold factor for snow formation	-5	5	°C
	Tb	Base temperature for snow melt	-5	5	°C

Adopted from Deshmukh and Singh (2016)



**Fig. 4** Model calibration process and identification of behavioral parameter sets

**2.2.1 Nash–Sutcliffe Efficiency (NSE)**

The Nash–Sutcliffe efficiency (NSE) is calculated as the ratio of the residual variance to the observed variance is subtracted from on. How closely the experimental vs simulated data plot matches the 1:1 line is determined by the Nash–Sutcliffe efficiency. An ideal match between the model and the actual data is indicated by  $NSE = 1$ .  $-\infty < NSE < 0$ , shows that the experimental mean is a better predictor than the model.  $NSE = 0$  denotes that the model predictions are equally accurate to the observed Data mean (Waseem et al. 2017).

$$\text{NSE} = 1 - \frac{\sum_{i=1}^n (\text{OBS}_i - \text{SIM}_i)^2}{\sum_{i=1}^n (\text{OBS}_i - \overline{\text{OBS}})^2} \quad (1)$$

Here,

$\text{OBS}_i$  observed streamflow  
 $\text{SIM}_i$  simulated streamflow  
 $\overline{\text{OBS}}$  mean streamflow

## 2.3 Generating Synthetic Data

Three weather generators are used to create synthetic climates from available historical data—Synthpop, KNN-CAD, and MEBWG.

### 2.3.1 Synthpop Weather Generator

Synthpop replicates the initial observed data and keeps the variable associations. The core behind synthetic data is to substitute some or all of the observed values with samples from suitable probability distributions to retain the original data's fundamental statistical properties. The Synthpop package is available for R; for more information, read this check (Nowok et al. 2016).

### 2.3.2 KNN-CAD Weather Generator

We are using K nearest neighbor (KNN-CAD) weather generator algorithm. It utilizes the block resampling method for preserving temporal correlations of temperature variables and the perturbation method to enhance the generation of extreme temperature and precipitation values. This model reshuffles the observed daily data, keeping information on all sites that refer to their corresponding day's weather to preserve climate variables. For a detailed explanation, check (King et al. 2015).

### 2.3.3 Maximum Entropy Bootstrap Weather Generator (MEBWG)

As part of MEBWG, three main components are applied: (1) orthogonal transformations are applied to spatially correlated weather variables at multiple sites; (2) MEB generates synthetic replicates of decorrelated transformed variables; and (3) inverse orthogonal transformations are applied to the weather variables at multiple sites to restore their spatial correlations. In addition to the time-dependent structure, the MEB model can also capture other statistical characteristics. Additionally, it ensures effective smoothing and limited extrapolation past extremes (Srivastav and Simonovic 2015).

## 2.4 *Compute Indicator of Interests*

We generate the different climate scenarios for each catchment using historical discharge, 50 best parameters, and synthetic climatic data (rain, PE, minimum temperature, maximum temperature, and average temperature) generated through synthetic data generators (Synthpop, KNN-CAD, and MEBWG). Furthermore, we use the delta change method for extreme climatic ranges. The delta change method is used to adjust the mean of a series of observed climatic data and then use the changed data to simulate the discharge with the model (Räty et al. 2014). We change the precipitation from 40 to 160% in the increment of 10% and temperature from 0 to 12 in the increment of 1 °C.

Later, we calculate the indicator (MAR) and assign the classes for each runoff scenario. We use CART to relate climate combinations with indicator classes for each catchment for the weather generator case.

## 2.5 *Class Assignment to Indicators*

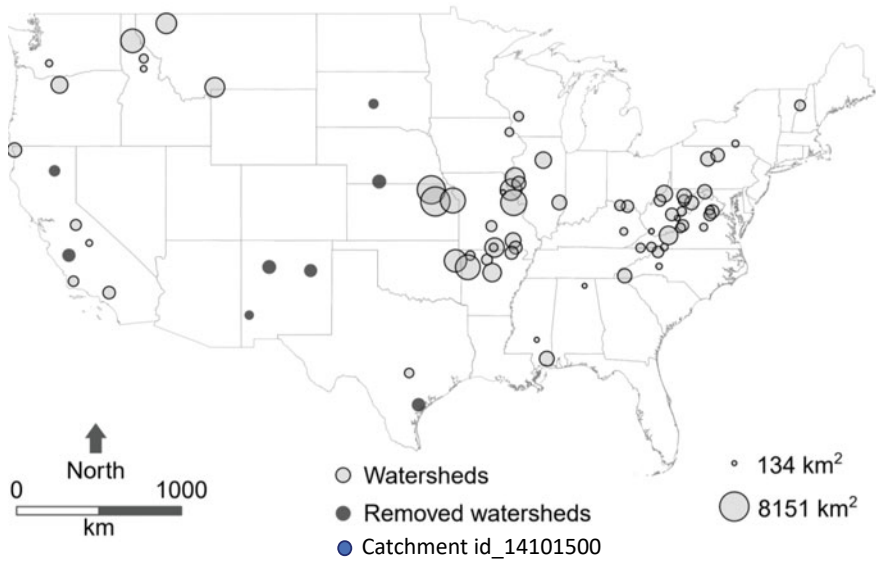
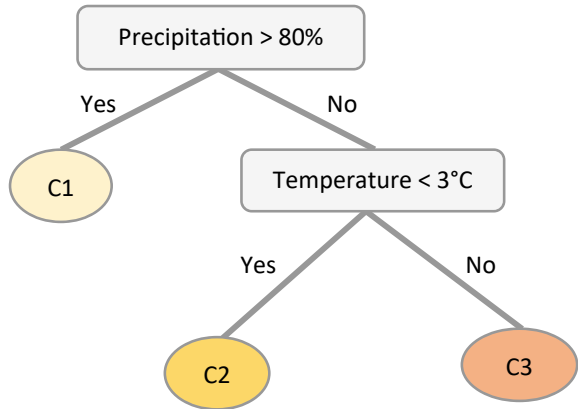
Classification and regression tree (CART) is the most straightforward algorithm for decision tree modeling. It has been used to forecast outcomes using a set of predictor factors. Because they require very minimal data pre-processing, they are ideal for data mining jobs (Breiman 1984; Therneau et al. 2013). Decision tree models have a substantial advantage over other analytical models in terms of ease of learning and use (<http://CRAN.R-project.org/package=rpart>). CART is used to relate environment change combinations with vulnerability classes. For example, the vulnerability class is predicted based on precipitation and temperature. We have defined four classes for indicator MAR (C0, C1, C2, C3). C0 is classified as an increase in MAR, C1 is decreased by 25% of its historical mean, C2 is decreased by 25%–50%, and C3 is decreased by more than 50%. We can see that C3 is the most vulnerable case for the indicator MAR (Fig. 5).

## 3 *Study Area and Data*

We use 77 catchments in the conterminous USA (Fig. 6). Gagged stations are selected according to the uninterrupted historical data series length. Precipitation and temperature values can be found for ten years, from 1959 to 1968. Consequently, each catchment considered in this study had 3653 data entries for each weather variable. Earlier studies carried out for the catchments are classified as minimally impacted in the Falcone database (Falcone 2011). In this paper, we will discuss Catchment id\_14101500 in Fig. 6.



**Fig. 5** Classification and regression tree (CART)



**Fig. 6** Location of the catchments used in the study. Each circle on the map represents the centroid of the catchment, and the size of each circle represents the catchment area. Adopted from Deshmukh and Singh (2016)

## 4 Result and Discussion

We simulate 8450(=13 Precipitation cases × 13 Temperature cases × 50 Parameter cases) streamflow scenarios, and the MAR indicator is computed. Climate cases and indicator classes are computed with CART, and a sample output CART is shown in Fig. 7.

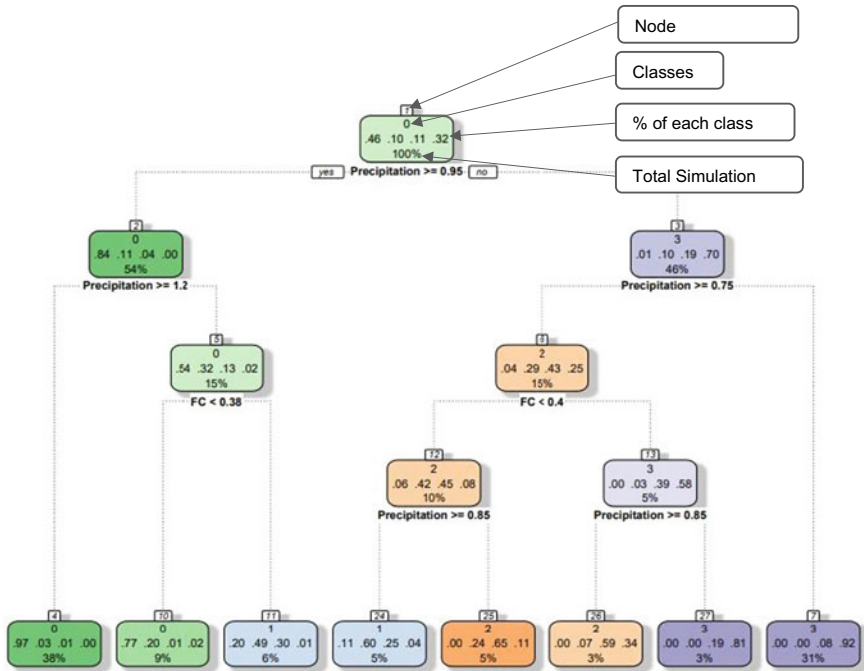


Fig. 7 KNN-CAD classification and regression tree (CART) of 14101500 catchment

To understand the CART output, (a) ‘node’ means the order of calculating branches one after another. (b) ‘Classes’ is defined based on the ‘% of each class’ available in that branch, the class with the highest percentage represents the whole branch (there are four classes 0, 1, 2, and 3, refer to Fig. 3 for vulnerability classes definition). (c) ‘% of each class’, the total simulation available in the branch is divided into four classes, each carrying a certain simulation from the total simulation. All values add up to 1 (classes are arranged in increasing order from left to right, i.e., Class0, Class1, Class2, and Class3). (d) ‘Total simulation’ is the percentage of overall simulations available in that branch.

To compute the critical threshold for a climatic variable such as precipitation, we use the weightage average of all the critical classes for precipitation ending nodes with the samples on the branch. In Fig. 7, we have two end notes, 0.85 and 0.75; we will compute the weightage average with the number of samples (climatic combinations) in the branch to get the average threshold. Similarly, we compute the critical threshold for all 77 catchments for every method and found that the precipitation is a dominant control for the indicator mean annual runoff. Temperature appears to be the second dominant control here.

We observed that the most dominating factor is precipitation for most catchments from where the tree starts. Vulnerability is specified as a reduction in the mean annual runoff by 50% of its historical streamflow. After that, temperature and other variables

come into the picture. From (Fig. 10), we can see that from a total of  $13 \times 13 \times 50$  samples, that is, 8450 samples (100%), around 2600 samples (31%) are coming under vulnerable cases due to precipitation, while 247 (4%) are due to change in secondary characteristic, i.e., threshold storage parameter (FC). In Fig. 8, we can see that vulnerable cases occur during a 35% ( $= (1 - 0.65) * 100$ ) reduction in precipitation; the pattern is different. In Fig. 9, node-1 already comes in the critical class, with higher precipitation than other cases. According to the Synthpop weather data generator, at normal precipitation (i.e., 1), almost 60% of overall simulation already comes in the vulnerable case. Here, a vulnerable case occurs even when there is an increase in precipitation by 20%, and vulnerable simulations are more than the other two. Figure 10 is CART for MEBWG and is similar to Fig. 7. This result is for only one catchment, while vulnerability occurs in a different scenario for others. For some catchments, the vulnerable class starts at a reduction of 15% in precipitation; for others, it starts at a 35% reduction. Other than precipitation, the temperature is also a dominating factor in finding vulnerable cases of the catchment. After temperature, other parameters like soil depth, field capacity, threshold storage, and vegetation play a minor role in vulnerable cases. Very few catchments are similar to the Fig. 9 case, where the vulnerable class occurs at normal precipitation. Other than finding vulnerable cases, we can also see how to overcome them.

We are showing a comparison of all three weather generators (Synthpop, KNN-CAD, MEBWE) and original (delta change only) in Fig. 11. We found that using weather generators along with delta change provides a higher critical threshold, which suggests that only using delta change might be underestimating the catchments' vulnerability. Using a weather generator can improve the accuracy of a bottom-up-based framework to assess the catchments' vulnerability to climate change.

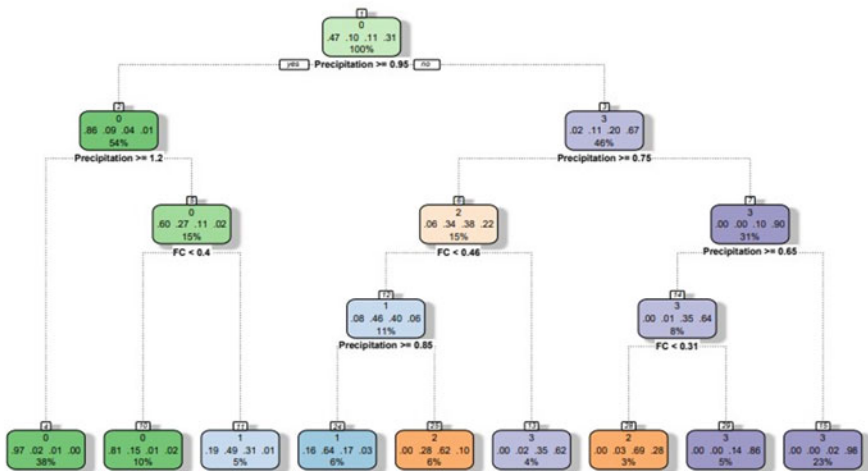


Fig. 8 Original (BASE) classification and regression tree (CART) of 14101500 catchment

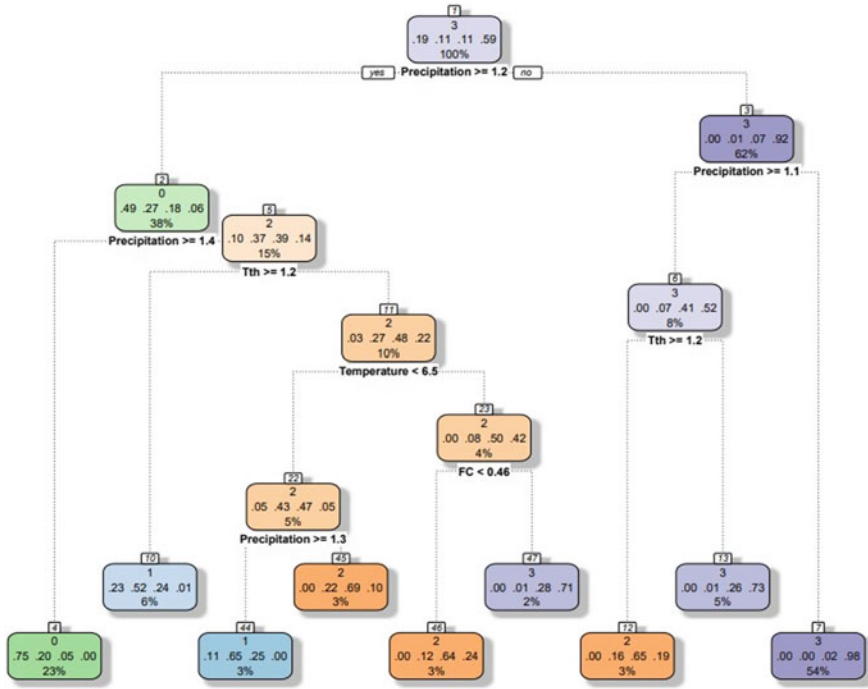


Fig. 9 Synthpop classification and regression tree (CART) of 14101500 catchment

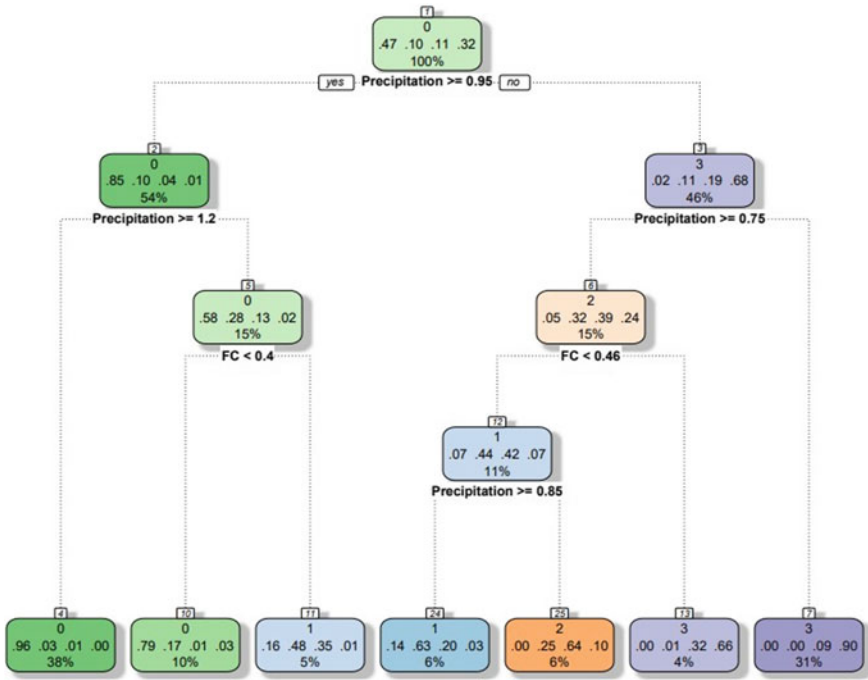


Fig. 10 MEBWG classification and regression tree (CART) of 14101500 catchment

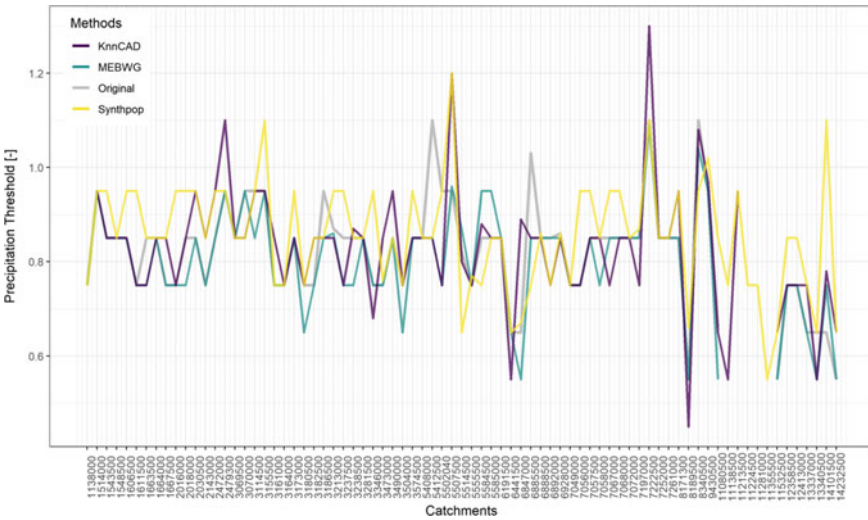


Fig. 11 Precipitation change threshold comparison

## 5 Conclusion

This study presents different methods for finding vulnerable cases of present catchments based on historical data of 13 parameters corresponding to hydrologic and physio-climatic characteristics. Our study provides an approach to understanding the impact of climate change on watersheds independent of future projections, thus aiding the policymaker's intake decisions in the presence of significant uncertainties. We also explored whether data generators are in the presence of extreme conditions.

Our analysis indicates that precipitation has the most significant impact on catchments' vulnerability due to climate change. We also find that most vulnerable cases occur during a threshold value of 0.75 or 25% reduction in average precipitation, and other characteristics have a minor impact. In the case of precipitation change threshold (Fig. 11), we found some extreme threshold values by KnnCAD and Synthpop method for some catchments. During analysis, we also found that KNN-CAD has shown the most extreme events, while Synthpop's average has remained near 80% of the original threshold value. We also find that every catchment has the capability to control vulnerable cases based on the CART diagram.

## References

- Breiman L (1984) Classification and regression trees, 1st edn. Routledge. <https://doi.org/10.1201/9781315139470>
- Craigmile PF, Guttorp P (2011) Space–time modelling of trends in temperature series. *J Time Ser Anal* 32:378–395. <https://doi.org/10.1111/j.1467-9892.2011.00733.x>
- Deshmukh A, Singh R (2016) Physio-climatic controls on vulnerability of watersheds to climate and land use change across the U. S.: controls on vulnerability. *Water Resour Res* 52(11):8775–8793. <https://doi.org/10.1002/2016WR019189>
- Elshamy ME, Wheeler HS, Gedney N, Huntingford C (2006) Evaluation of the rainfall component of a weather generator for climate impact studies. *J Hydrol* 326:1–24. <https://doi.org/10.1016/j.jhydrol.2005.09.017>
- Falcone JA (2011) GAGES-II: geospatial attributes of gages for evaluating streamflow. Report. Reston, VA. USGS Publications Warehouse. <https://doi.org/10.3133/70046617>
- Hanson CL, Johnson GL (1998) GEM (generation of weather elements for multiple applications): its application in areas of complex terrain. *Hydrol Water Resour Ecol Headwaters IAHS* 248:27–32 <http://CRAN.R-project.org/package=rpart>
- Keller A, Garner K, Rao N, Knipping E, Thomas J (2022) Downscaling approaches of climate change projections for watershed modeling: review of theoretical and practical considerations. *PLOS Water* 1:e0000046. <https://doi.org/10.1371/journal.pwat.0000046>
- King LM, McLeod AI, Simonovic SP (2015) Improved weather generator algorithm for multisite simulation of precipitation and temperature. *JAWRA J Am Water Resour Assoc* 51(5):1305–1320. <https://doi.org/10.1111/1752-1688.12307>
- Kuchar L (2004) Using WGENK to generate synthetic daily weather data for modelling of agricultural processes. *Math Comput Simul* 65:69–75. <https://doi.org/10.1016/j.matcom.2003.09.009>
- Machado N, Ventura T, Danelichen VH, Biudes M (2014) Performance of neural network for estimating rainfall over Mato Grosso State, Brazil

- Moisen GG (2008) Classification and regression trees. *Encyclopedia Ecol* 1:582–588. <https://doi.org/10.1016/B978-008045405-4.00149-X>
- Mujumdar P, Ghosh S (2008) Modeling GCM and scenario uncertainty using a possibilistic approach: application to the Mahanadi River, India. *Water Resour Res* 44. <https://doi.org/10.1029/2007WR006137>
- Nowok B, Raab GM, Dibben C (2016) synthpop: bespoke creation of synthetic data. *R J Stat Softw* 74(11). <https://doi.org/10.18637/jss.v074.i11>
- Qian B, Gameda S, Hayhoe H, De Jong R, Bootsma A (2004) Comparison of LARS-WG and AAFC-WG stochastic weather generators for diverse Canadian climates. *Clim Res* 26:175–191. <https://doi.org/10.3354/cr026175>
- Qian B, Gameda S, Hayhoe H (2008) Performance of stochastic weather generators LARS-WG and AAFC-WG for reproducing daily extremes of diverse Canadian climates. *Climate Res* 37:17–33. <https://doi.org/10.3354/cr00755>
- Räty O, Räisänen J, Ylhäisi J (2014). Evaluation of delta change and bias correction methods for future daily precipitation: intermodel cross-validation using ENSEMBLES simulations. *Clim Dyn* 42. <https://doi.org/10.1007/s00382-014-2130-8>
- Sabatier PA (1986) Top-down and bottom-up approaches to implementation research: a critical analysis and suggested synthesis. *J Publ Policy* 6(1):21–48. <https://doi.org/10.1017/S0143814X00003846>
- Soltani A, Hoogenboom G (2003) Minimum data requirements for parameter estimation of stochastic weather generators. *Clim Res* 25:109–119
- Srivastav RK, Simonovic SP (2015) Multi-site, multivariate weather generator using maximum entropy bootstrap. *Clim Dyn* 44(11–12):3431–3448. <https://doi.org/10.1007/s00382-014-2157-x>
- Therneau T, Atkinson B, Ripley B (2013) Rpart: recursive partitioning. R Package Version 4.1-3
- Waseem M, Mani N, Andiego G, Usman M (2017) A review of criteria of fit for hydrological models

# Identification of Best CMIP6 Climate Models for Offshore Wind Energy Assessment



Deepjyoti Basak, Nagababu Garlapati, and Jaydeep Patel

**Abstract** Offshore wind harvesting has grown vividly in recent decades, as it is recognized as a promising source in many parts of the world. The less interaction of landmasses makes it more efficient when compared with onshore winds. The impact of climate change on the energy sector, especially changes in wind energy output, is gaining traction. As a result, determining the future of offshore wind energy is critical for developing an effective energy plan. However, how offshore wind generation will respond to rapidly intensifying global warming remains inconclusive. Wind energy is an integral part of India's energy mix. Therefore, it is essential to know how it changes as the climate changes. Consequently, global climate models (GCMs) can simulate climate change and effectively evaluate atmospheric circulation patterns. However, GCMs have systematic errors leading to improper output. Hence, the selected CMIP6 models have been evaluated with RAMA buoy data using five statistical parameters in this paper. Furthermore, the weighted multi-model ensemble is produced by the MCDM technique using the parameter's output. The model's performance is then compared to ERA5 data, which shows that when compared to uniform weighted MME, the weighted MME developed in this study for predicting future wind energy over the Indian offshore region has more notable outcomes.

**Keywords** Offshore wind harvesting · Climate change · Global climate models · CMIP6

---

D. Basak (✉) · N. Garlapati · J. Patel  
Pandit Deendayal Energy University, Gandhinagar, India  
e-mail: [deepjyoti.bphd20@sot.pdpu.ac.in](mailto:deepjyoti.bphd20@sot.pdpu.ac.in)

N. Garlapati  
e-mail: [Nagababu.Garlapati@sot.pdpu.ac.in](mailto:Nagababu.Garlapati@sot.pdpu.ac.in)

J. Patel  
e-mail: [jaydeep.patel@sot.pdpu.ac.in](mailto:jaydeep.patel@sot.pdpu.ac.in)



## 1 Introduction

The harvesting of offshore wind for power generation has globally increased (International Energy Agency 2019). On the other hand, climate change indubitably influences the provincial wind pattern and intensity which in turn affects the wind farms' future viability. Therefore, assessment of wind resource is an important step before taking any engineering infrastructure decisions (Masson-Delmotte et al. 2019). Climate models are the most effective technique for predicting the wind resource influence by climate change. Climate models or general circulation models (GCMs) are numerical models, capable to portray three-dimensional Earth system, and project the future climate subjected to specific emission scenarios governed by the Intergovernmental Panel on Climate Change (IPCC). The World Climate Program (WCRP) released its sixth phase of the Coupled Model Intercomparison Project (CMIP6) in 2015, governed by five possible Shared Socioeconomic Pathways (SSPs) (Lupo et al. 2013).

However, uncertainties about environmental interaction, approximations during climate modeling, spatio-temporal resolution, and different perspectives, lead to overestimate or underestimate the calculate values when compared with observed values. As a result, various GCMs produce different outcomes for the same forcing (Jain et al. 2019). The disparity in results is related to many uncertainties, including selection of GCMs, emission scenarios, and RCM downscaling technique. These levels of uncertainty associated with GCM become critical for persisting their impact on climate change (Mandal et al. 2019). Quantile mapping (QM) proven as an effective technique to remove the bias due to the imperfect knowledge of physics underpinning many atmospheric processes (Enayati et al. 2021). Likewise downscaling the spatial resolution is another technique to minimize the errors. A study shows that the downscaled wind speed (WS) spatial patterns are mostly similar with reference data, and the method introduce in study greatly reduces biases, especially over offshore locations (Zhang and Li 2021).

Researchers used ensemble of climate model (CMIP6, CMIP5 and earlier version) to comprehend the changes in wind characteristics worldwide under various emission conditions, which yielded better results than individual models (Xuan et al. 2017). Multi-modal ensemble (MME) avoids individual GCM errors and limiting the bias w.r.t reference model for future climate predictions (Yan et al. 2016). Hence, GCMs selection for MME that reflected the current climate more exactly, and can assist the effects of climate change forecasts efficiently is a critical task (Basharin et al. 2016). Even though the GCMs independently misinterpret the information at any grid point, MME does not examine the positive and negative characteristics of each model because it is automatically optimized (Bannister et al. 2017).

The use of uniform weighted MME explored the evolution of Europe's wind energy supply under the effects of climate change. Both intermediate (SSP2-4.5) and extreme scenarios (SSP 5-8.5) shows large reduction in wind power density in northern Continental Europe and the Central Mediterranean, as well as an increase in West Finland (Martinez and Iglesias 2021). The future European large-scale wind

energy resource is expected to rise in Northern-Central Europe (Baltic Sea and neighboring areas) and decline in the Mediterranean region by the end of century. There is also likely to be an increase in intra-annual variability in the Baltic Sea and neighboring areas and a decrease in Mediterranean areas, but no substantial changes in interannual variability in Europe (Carvalho et al. 2017). However, all other European locations will expect a significant decline (up to 20%) by the end of the century. Changes in wind resource are highly unknown, however, SSP2-4.5 predicts a rise over Iberia and eastern Ukraine (Carvalho et al. 2021). Similar trend of projection along the Guinea coast can be viable on temporal characteristics and increases at the far future period (2070–2099) with a larger magnitude than mid-century (2040–2069) (Akinsanola et al. 2021).

The appraisal of wind potential for Indian offshore under climate change is examined for three places, with Jakhau being identified as having a high potential (Kulkarni et al. 2016). Krishnan et al. (Krishnan and Bhaskaran 2020) evaluated the wind potential across the western offshore region of India (Bay of Bengal) using both CMIP5 and CMIP6 ensemble. Under the extreme scenario, WS drops over central and southern BoB region. In the first place, results notified that CMIP6 simulation outperformed the CMIP5 models. Furthermore, model data is validated with in-situ RAMA buoy data associated with same time intervals at buoy locations. Outcome of the study shows, the values of few GCMs either underestimate or overestimate the observation data for certain potential locations. Author extended the study and calculated the statistical biases to evaluate the credibility of individual models with reference data—ERA-interim and scatterometer data.

The benefits of multi-model ensemble for future wind resource estimates are generally demonstrated in the literature. However, it was also reported that the ensemble models either overpredict or underestimate the projections for the climate. So, utilizing CMIP6 simulation models, we comprehend a novel multimodal ensemble (MME) technique in this study. Each GCM model employed in MME's for current investigation to pinpoint the shifting characteristics of wind potential over the Indian offshore region is given a certain weight depending on statistical criteria—mentioned in Sect. 2.1. Here, the individual weights are determined using the well-known multi-criteria decision methods (MCDM), which has already demonstrated its effectiveness (Nagababu et al. 2022). The results of the weighted MME are compared to earlier research as well as to a uniform ensemble of comparable GCMs. We also evaluate the credibility of weighted MME by examining the agreement over the historical period of 25 years using ERA5 reanalysis (reference) dataset.

## 2 Data and Methodology

### 2.1 Data Acquisition

The data required for this study is acquired from a previous study executed for the eastern part of Indian offshore region (Krishnan and Bhaskaran 2020) BCC-CSM2-MR, CanESM5, EC-EARTH3, GFDL-ESM4, GISS-E21-G, GISS-E21G-CC, GISS-E21-H, MPI-ESM12-HR, MRI-ESM2 were the identified GCMs for the present study having the positive NSE (Nash–Sutcliffe efficiency), Index of Agreement (IA), and Pearson correlation coefficient (CC) values closer to 1. Maximum values (near to 1) indicate the effective match with reference data, and lower root mean square error (RMSE) value and bias (B) values indicate the better fit to reference data. The numerical value of evaluated quantities of selected GCMs are mentioned in Table 1.

The monthly temporal resolution of near surface wind (10 m) from selected GCMs imposed with intermediate and extreme scenarios were obtained from ESGF Portal (<https://esgf-node.llnl.gov/search/cmip6/>). In this study, simulation models projected the wind potential over the entire Indian offshore region, including the other adjacent areas. The WS data during 1990–2014 (historical), and the two future periods–near future and far future of (2021–2045) and (2075–2099) years respectively are considered for this study. The typical lifespan of a high-quality, modern wind turbine is 20 years, though this can be increased to 25 years or beyond depending on the environment and the suitable maintenance practices being used. Hence, the span of 25 years for historical and future was divided by considering the maximum life of horizontal axis wind turbine (HAWT) (Pakenham et al. 2021).

**Table 1** CMIP6 products used to inspect the climate change

Models	NSE	IA	CC	B	RMSE
BCC-CSM2-MR	0.26	0.84	0.73	0.35	1.7
CanESM5	0.27	0.85	0.83	0.93	1.69
EC-EARTH3	0.5	0.88	0.78	0.19	1.4
GFDL-ESM4	0.14	0.81	0.72	0.79	1.83
GISS-E21-G	0.32	0.84	0.72	0.13	1.63
GISS-E21G-CC	0.29	0.83	0.71	0.02	1.66
GISS-E21-H	0.27	0.83	0.70	0.23	1.68
MPI-ESM12-HR	0.54	0.9	0.81	0.1	1.33
MRI-ESM2	0.35	0.85	0.76	0.51	1.59

### 2.2 Multi-model Ensemble for Resource Evaluation

Figure 1 shows the graphical representation of the methodology adopted for the present work. Initially, all simulations have different spatial resolutions which must re-grid at a common resolution. Also, before studying the effects of climate change, climate simulations must free from errors (i.e., bias corrected). Hence, bilinear interpolation is used as it is the best-found technique in literature when compared to other (Kulkarni et al. 2015). The methodology is divided into two techniques: (1) Uniform ensemble and (2) Weighted ensemble.

In the first technique the re-grid models are used to form uniform weighted ensemble where weights of individual GCMs is similar. Then the effectivity of the model is check by observing the difference with ERA5. However, the traditional approaches of bias correction do not distinguish the errors from the various inconsistencies in climate simulations. For instance, in the case of MME simulations rectifying each member individually would conflate the errors of simulation with its internal variability (Vaithinada Ayar et al. 2021). Subsequently, for the second technique we used weighted MME by implying selected model, as discussed in previous section. The weights for ensemble are evaluated by (Shannon entropy)–a multi-criteria decision analysis (MCDA) using the statistical values as inputs, evaluated in the study (Krishnan and Bhaskaran 2020), listed in Table 1.

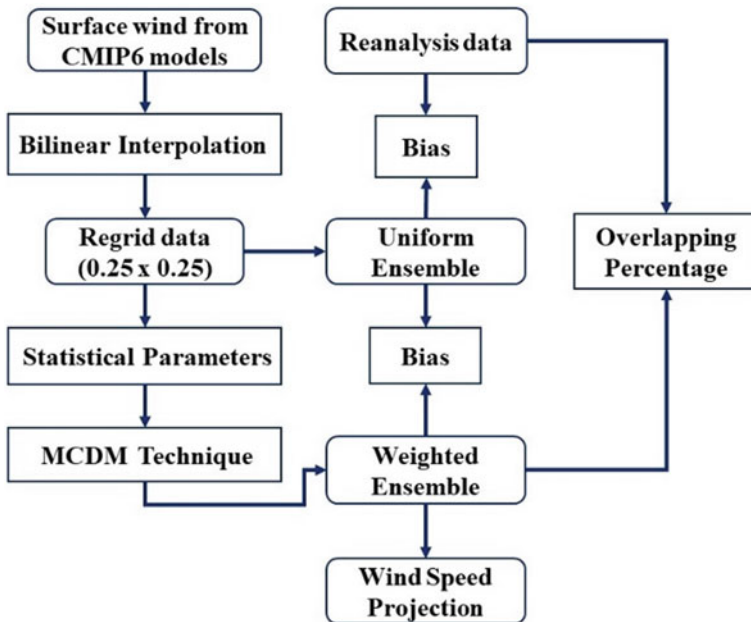


Fig. 1 Flowchart of methodology adopted for present study

The accuracy of weighted MME is also validated grid-wise by comparing the historical period with ERA5 data. It can be noticed in the result section that majority of grid points experience minimum bias with reference data, and maximum grid points are overlapping with the reference data. The reanalysis data used for the study is the updated version from ECMWF with  $0.25^\circ \times 0.25^\circ$  spatial resolution, including 10 m surface wind. The credibility of ERA5 reference was previously evaluated by various researchers (Li et al. 2020). Finally, the WS at 100 m hub heights is evaluated using WEM.

### 2.3 Extrapolation

The vertical extrapolation of surface wind to turbine hub height at 100 m is carried out using Power law. This law is the most convenient method for predicting WS at a turbine hub elevation using observations taken at a reference level. The mathematical relationship of wind at two elevation is given as:

$$\left(\frac{X1}{X2}\right)^n = \frac{U1}{U2} \quad (1)$$

where  $U1$  is the WS (m/s) at height  $X1$  (in meters) and  $U2$  is the known WS at a reference height  $X2$ . Furthermore,  $X2 > X1$  and  $U2 > U1$  and  $n$  is the coefficient of friction coefficient. It represents the local climate, atmospheric conditions, stability of weather, and land topography. In the case of lack of information about the terrain the value of  $n = 1/7$  (used for present study) can be assumed. However, if the wind information is available for two distinguish height, then value of  $n$  is calculated by curve fitting. Also, it is apparent that impacts of all these components are imbedded in the wind velocity time records, and hence the entire reflections should be on exponent value prediction (Şen et al. 2012).

### 2.4 Climate Change Impact of Future WS

Majorly, the concern about the climate change effects have been an important concern behind the expansion of wind energy projects. The Intergovernmental Panel on Climate Change, claims the long-term changes in the large-scale atmospheric circulation, such as a poleward shift and strengthening of the westerly winds,” and that these changes will most likely continue.

For the projections over the Indian offshore, the median difference between historical and future time period according to Eq. (2) was calculated by comparing monthly average WS (WS) of historical period (1990–2014) with future WS for both the emission scenarios. This study looked at how climatic changes would affect WS across the Indian offshore region in the future.

$$C = \frac{X - Y}{Y} \times 100 \tag{2}$$

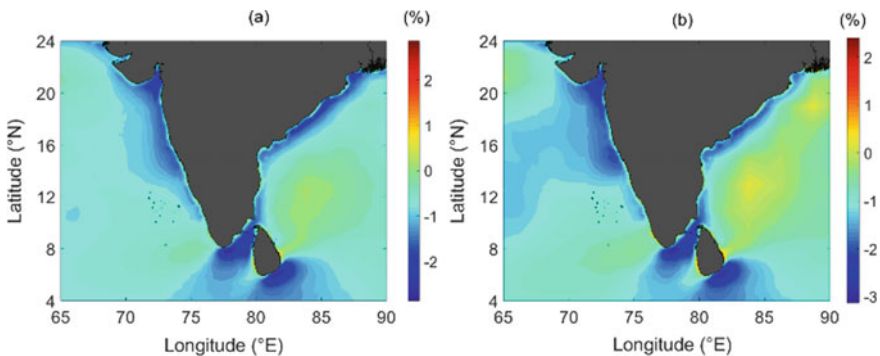
In Eq. (2), X represents the median of the WS data for future period, while Y represents the same parameter but for the historical time period.

### 3 Results

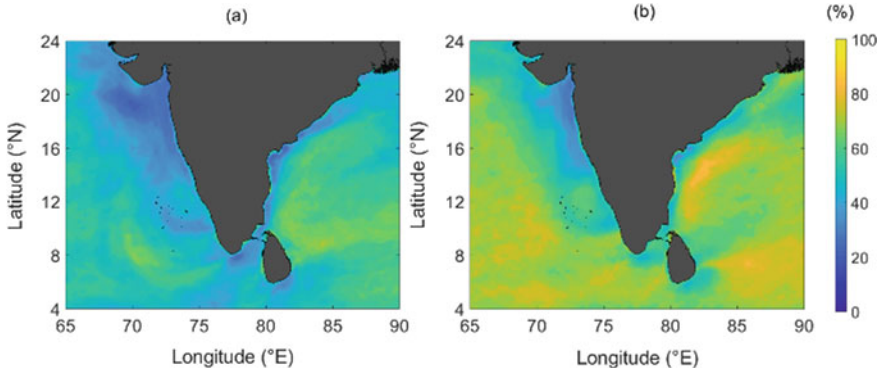
#### 3.1 Bias Correction

GCM products are well recognized for systematic mistakes or bias due to imperfect information of the physics underpinning many atmospheric interactions. We employed weighted ensemble approach, which is based on Shannon entropy, to reduce the bias or errors. The difference between the uniform MME and ERA5 is shown in Fig. 2a, whereas the difference between the weighted ensemble and the reanalysis database is shown in Fig. 2b. It is apparent that the method used to form ensemble can remove bias and reduce the inaccuracy on both the positive and negative ends.

ERA5 reanalysis data is well tested in previous literatures. Therefore, it can be considered as the prominent data for validating the simulation models. To validate the weighted MME model, the overlapping percentage (OP) is calculated. Figure 3a shows the OP values between uniform ensemble and ERA5 while Fig. 3b notified the OP values between weight MME and reanalysis dataset. Results depicted that approximately 90% of grid points overlap with reference data, while the percentage is very for uniform ensemble.



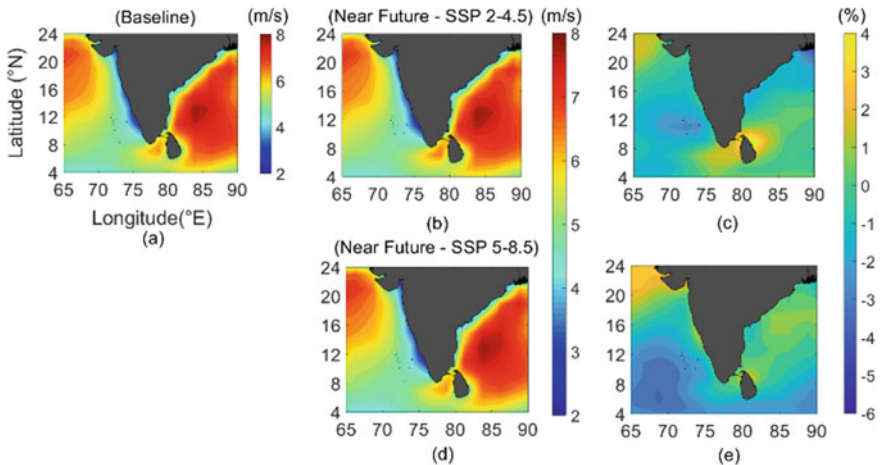
**Fig. .2** Annual bias between uniform weights (a) and variable weights with ERA5 reanalysis data (b)



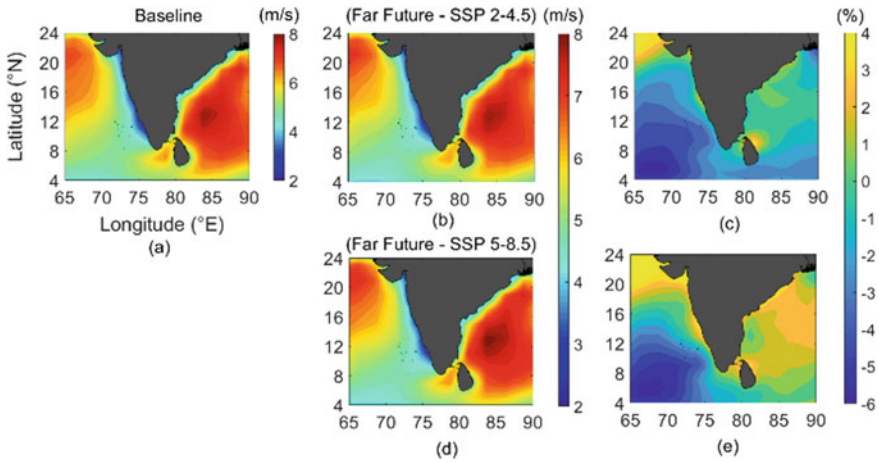
**Fig. 3** Difference between the overlapping percentage (OP) of uniform MME (a) and weighted MME (b) with ERA5 dataset

### 3.2 Annual Wind Speed Projections

Wind speed is the prerequisite parameter for the performance and safety of wind generators in any wind farms. In such condition when wind speed value exceed the cut off range, it may compromise the safety of current wind farms, also may imply the possibility of bearing high construction costs in the maintenance and future planning of wind farms (Zhang et al. 2018). Figures 4 and 5 represents the comparison of the difference in wind speed values between the historical and future was performed in order to determine the uncertainties of climate on wind speed values.



**Fig. 4** Mean WS forecast for near future at Indian offshore region. For intermediate scenario (upper row–b) and extreme scenario (lower row–d), mean WS of the baseline (m/s)–(a) and % change compared to the baseline for near future (c) and far future (e)



**Fig. 5** Mean WS forecast for far future at Indian offshore region. For intermediate scenario (upper row–b) and extreme scenario (lower row–d), mean WS of the baseline (m/s)–(a) and % change compared to the baseline for near future (c) and far future (e)

### 3.2.1 Projections for Near Future

Figure 4 illustrates the percentage change of wind speed values from past to near future at standard hub height of 100 m. The calculation methods is already mentioned in Sect. 2.4. The maximum values of WS in Fig. 4c remained relatively constant in the early twenty-first century when compared to historical levels, but several grid sites (mostly in the Bay of Bengal region) have shown the increment approximately by 1–3%.

Under SSP2–4.5, wind speeds are often similar to the early stage in the near future–Fig. 4b, while a slight rise in magnitude can viable in Fig. 4c, between 80- and 85-degree longitude. However, Fig. 4dconveys the WS values under SSP5-8.5 have increased slightly over Arabian Sea’s (between 12 and 24-degrees north latitude) and a few coordinates of BoB as well, when compared to the intermediate GHG scenario. Overall results shows that certain grid points over BoB may experience the rise in wind characteristics by 1 to 2%–Fig. 4e, compared to the historical stage, under SSP2-4.5.

### 3.2.2 Projections for Far Future

Projected changes of wind speed for far future with respect to historical under both scenarios are depicted in Fig. 5. If no intervention is made to reduce greenhouse gas emissions, then number of grid points in the eastern offshore of the country will increase marginally compared to the historical stage under SSP5-8.5.



Comparing to near future values of SSP5-8.5, more intense wind speed values can be expected from Fig. 5d, at the mid coordinates of BoB. While the near future values of entire shoreside in Fig. 5b are moreover similar to the intermediate pathway. Furthermore, the coastal region in Fig. 5e (primarily concentrated in the east between 80- and 90-degrees longitude and 16 to 20 degrees latitude) would grow by approximately 4%, which may significantly resolve the obstacles of wind energy projects. It can also be noticed in Fig. 5c, that the entire Arabian sea will experience significant reduction of WS during far future under both the socio-economic pathways.

## 4 Discussion

In this study it is clearly notified that climate change may impact on electricity generation derived from wind energy in coming years. It is clearly visible in results that under the intense emission scenario (SSP 5–8.5), wind speed at hub height over Bay of Bengal may increase by  $\geq 4\%$ , which is higher than intermediate greenhouse scenario (SSP 2–4.5). On one hand it can be stated that electricity generation can be increase if the harnessing of offshore is planned suitably. And on other hand, predicting such developments in advance is crucial too. The pertinent research findings in this paper can be used in designing present and future wind farm projects over the Indian offshore region. It is worth mentioning that CMIP6 climate models are performing well in future upgrades. The outcomes of the study may consider as preceding evaluation for long-term changes in wind resources under GHG scenarios. In upcoming work, we will explore the future wind potential to better guide and planning for the same study area.

## 5 Conclusion

This work evaluated the simulation capabilities of weighted MME of surface winds, generated using the score values of statistical parameters. This study also showcases the methodology for generating the weighted ensemble model, which may beneficial for similar studies like this. The major outcomes can be concluded as:

- The results show that the weighted MME performs substantially better in simulation than the uniform ensemble. Additionally, it has been observed that the bias is lessened over a significant portion over BoB, which is roughly between  $+0.5$  and  $-1$  m/s from both ends.
- The implications of weights to individual GCMs, derived using innovative Shannon's entropy, exhibit similar values and coincide with the ERA5 reanalysis data approximately over  $\geq 90\%$  of grid sites, showing that the method used in the study is effective at predicting future wind generation.

- The evaluation of WS from past and future period under the consideration climate change impact depicted a significant rise by the end of century. Under the higher emission scenario (SSP 5–8.5), several coordinated across the Bay of Bengal may experience the growth by approximately 4%, posing to overcome many obstacles in the expansion of wind projects in the affected areas. Whereas the wind speed under SSP 2–4.5 the windspeed may increases between 1 and 2 m/s during both the future periods.

## References

- Akinsanola AA, Ogunjobi KO, Abolude AT, Salack S (2021) Projected changes in wind speed and wind energy potential over West Africa in CMIP6 models. *Environ Res Lett* 16(4):044033. <https://doi.org/10.1088/1748-9326/abed7a>
- Bannister D, Herzog M, Graf HF, Hosking JS, Short CA (2017) An assessment of recent and future temperature change over the Sichuan Basin, China, using CMIP5 climate models. *J Clim* 30(17):6701–6722. <https://doi.org/10.1175/JCLI-D-16-0536.1>
- Basharin D, Polonsky A, Stankūnavičius G (2016) Projected precipitation and air temperature over Europe using a performance-based selection method of CMIP5 GCMs. *J Water Clim Change* 7(1):103–113. <https://doi.org/10.2166/wcc.2015.081>
- Carvalho D, Rocha A, Gómez-Gesteira M, Santos CS (2017) Potential impacts of climate change on European wind energy resource under the CMIP5 future climate projections. *Renew Energy* 101:29–40. <https://doi.org/10.1016/j.renene.2016.08.036>
- Carvalho D, Rocha A, Costoya X, DeCastro M, Gómez-Gesteira M (2021) Wind energy resource over Europe under CMIP6 future climate projections: What changes from CMIP5 to CMIP6. *Renew Sustain Energy Rev* 151:111594. <https://doi.org/10.1016/j.rser.2021.111594>
- cmip6 Data Search | cmip6 | ESGF-CoG. <https://esgf-node.llnl.gov/search/cmip6/>. Accessed 29 Sept 2022
- Enayati M, Bozorg-Haddad O, Bazrafshan J, Hejabi S, Chu X (2021) Bias correction capabilities of quantile mapping methods for rainfall and temperature variables. *J Water Clim Change* 12(2):401–419. <https://doi.org/10.2166/wcc.2020.261>
- International Energy Agency (2019) Offshore wind outlook 2019: world energy outlook special report. [Online]. Available: [www.iea.org/t&c/](http://www.iea.org/t&c/)
- Jain S, Salunke P, Mishra SK, Sahany S (2019) Performance of CMIP5 models in the simulation of Indian summer monsoon. *Theor Appl Climatol* 137(1–2):1429–1447. <https://doi.org/10.1007/s00704-018-2674-3>
- Krishnan A, Bhaskaran PK (2020) Skill assessment of global climate model wind speed from CMIP5 and CMIP6 and evaluation of projections for the Bay of Bengal. *Clim Dyn* 55(9–10):2667–2687. <https://doi.org/10.1007/s00382-020-05406-z>
- Kulkarni S, Deo MC, Ghosh S (2015) Comparison of wind speeds derived by alternative statistical downscaling techniques at the Indian offshore sites
- Kulkarni S, Deo MC, Ghosh S (2016) Evaluation of wind extremes and wind potential under changing climate for Indian offshore using ensemble of 10 GCMs. *Ocean Coast Manag* 121:141–152. <https://doi.org/10.1016/j.ocecoaman.2015.12.008>
- Li D, Feng J, Dosio A, Qi J, Xu Z, Yin B (2020) Historical evaluation and future projections of 100-m wind energy potentials over CORDEX-East Asia. *J Geophys Res Atmos* 125(15):e2020JD032874. <https://doi.org/10.1029/2020JD032874>
- Lupo A, Kininmonth W, Armstrong JS, Green K (2013) Global climate models and their limitations

- Mandal S, Arunkumar R, Breach PA, Simonovic SP (2019) Reservoir operations under changing climate conditions: hydropower-production perspective. *J Water Resour Plan Manag* 145(5):04019016. [https://doi.org/10.1061/\(asce\)wr.1943-5452.0001061](https://doi.org/10.1061/(asce)wr.1943-5452.0001061)
- Martinez A, Iglesias G (2021) Wind resource evolution in Europe under different scenarios of climate change characterised by the novel shared socioeconomic pathways. *Energy Conv Manage* 234:113961. <https://doi.org/10.1016/j.enconman.2021.113961>
- Masson-Delmotte V et al (2019) Global warming of 1.5°C an IPCC special report on the impacts of global warming of 1.5°C above pre-industrial levels and related global greenhouse gas emission pathways, in the context of strengthening the global response to the threat of climate change, sustainable development, and efforts to eradicate poverty Edited by Science Officer Science Assistant Graphics Officer Working Group I Technical Support Unit. [Online]. Available: [www.environmentalgraphiti.org](http://www.environmentalgraphiti.org)
- Nagababu G, Puppala H, Pritam K, Kantipudi MP (2022) Two-stage GIS-MCDM based algorithm to identify plausible regions at micro level to install wind farms: a case study of India. *Energy* 248:123594. <https://doi.org/10.1016/j.energy.2022.123594>
- Pakenham B, Ermakova A, Mehmanparast A (2021) A review of life extension strategies for offshore wind farms using techno-economic assessments. *Energies (Basel)* 14(7):1936. <https://doi.org/10.3390/en14071936>
- Şen Z, Altunkaynak A, Erdik T (2012) Wind velocity vertical extrapolation by extended power law. In: *Advances in meteorology*, vol 2012. <https://doi.org/10.1155/2012/178623>
- Vaittinada Ayar P, Vrac M, Mailhot A (2021) Ensemble bias correction of climate simulations: preserving internal variability. *Sci Rep* 11(1):3098. <https://doi.org/10.1038/s41598-021-82715-1>
- Xuan W, Ma C, Kang L, Gu H, Pan S, Xu YP (2017) Evaluating historical simulations of CMIP5 GCMs for key climatic variables in Zhejiang Province, China. *Theor Appl Climatol* 128(1–2):207–222. <https://doi.org/10.1007/s00704-015-1704-7>
- Yan R, Huang J, Wang Y, Gao J, Qi L (2016) Modeling the combined impact of future climate and land use changes on streamflow of Xinjiang Basin, China. *Hydrol Res* 47(2):356–372. <https://doi.org/10.2166/nh.2015.206>
- Zhang S, Li X (2021) Future projections of offshore wind energy resources in China using CMIP6 simulations and a deep learning-based downscaling method. *Energy* 217:119321. <https://doi.org/10.1016/j.energy.2020.119321>
- Zheng CW, Xiao ZN, Peng YH, Li CY, Du ZB (2018) Rezoning global offshore wind energy resources. *Renew Energy* 129:1–1. <https://doi.org/10.1016/j.renene.2018.05.090>

# Analysis of Rainfall Using Family of Innovative Trend Methods for Climate Change Detection



Anishka Priya Suresh, Celina Thomas, Aiswarya K. Ajith, A. V. Amalenthu, and Adarsh Sankaran

**Abstract** Trend analysis of hydro-meteorological data is one of the essential procedures in climate change detection studies. Innovative Trend Analysis (ITA) methods are relatively new graphical procedure for determining the trends of time series datasets. This paper proposes the applications of two recent variants of ITA method namely Innovative Polygonal Trend Analysis (IPTA) and Innovative Trend Pivot Analysis (ITPA) method for analysing the temporal trend along with the trend propagation of monthly and seasonal rainfall data of (1871–2016) period of All India main land and North East (NE) region, to capture the signature of climatic changes. The mean-based and standard deviation-based IPTA could capture the progression in the trend. More complex polygons and presence of two or more cycles indicating difference in climatic conditions are obtained for standard deviation in comparison with mean-based analysis. The trend length and slope are computed which depicted the amount as well as transition associated with the rainfall in between the months. A decreasing trend is obtained for the series of months as well as seasons from standard deviation analysis and the highest magnitude of rainfall transition is observed from May to June. To examine the presence of sub trends and risks, ITPA method is applied. Positive trend slope indicates an increase in rainfall from month to month and season to season. From IPTA analysis there is no month or season in which there is a significant change between the first and second half of the datasets of the study period. Thus, the risk factor is low for All India region, which conclude that the

---

A. P. Suresh (✉) · C. Thomas · A. K. Ajith · A. V. Amalenthu · A. Sankaran  
Department of Civil Engineering, TKM College of Engineering, Kollam 691005, India  
e-mail: [anishkaponnu99@gmail.com](mailto:anishkaponnu99@gmail.com)

C. Thomas  
e-mail: [celinathomas2000@gmail.com](mailto:celinathomas2000@gmail.com)

A. K. Ajith  
e-mail: [aishuka2000@gmail.com](mailto:aishuka2000@gmail.com)

A. V. Amalenthu  
e-mail: [amalenthuvassanth@gmail.com](mailto:amalenthuvassanth@gmail.com)

A. Sankaran  
e-mail: [adarsh1982@tkmce.ac.in](mailto:adarsh1982@tkmce.ac.in)

climatic change impacts have more visible changes at local spatial scales than very large spatial domain like All India.

**Keywords** Rainfall · Trend · Climate change · India

## 1 Introduction

Trend analysis of hydrological and meteorological data is an essential procedure in climate change impact assessment studies. Several statistical and graphical procedures are available for trend analysis of hydro-meteorological data (Sonali and Kumar 2013). The non-parametric Mann–Kendall (MK) method is perhaps the most popular method for trend analysis study (Mann 1945; Kendall 1975). Sen's Innovative Trend Analysis (ITA) method (Sen 2012) is identified to be one of the graphical methods which gained wide popularity within short span of its introduction. ITA method and its piece-wise variants was applied in the past for analysing temperature, rainfall, and streamflow data at different temporal scales (Cui et al. 2017; Ali et al. 2019; Sen et al. 2019; Wang et al. 2020; Şişman and Kizilöz 2021).

Several improvisations were proposed in the recent past and it includes Innovative Polygonal Trend Analysis (IPTA) (Sen et al. 2019), Trend Polygon Star Concept methods (Ceribasi et al. 2021a), Innovative Triangular Trend Analysis (ITTA) (Güçlü et al. 2020), Innovative Trend Pivot Analysis Method (ITPAM) (Ceribasi et al. 2021b), etc. Unlike the traditional ITA and its probabilistic variant (Sen 2012, 2021) the above methods consider multiple datasets simultaneously (like time series of different, months, seasons), which helps in capturing the trend propagation and eventually help for detecting the climatic changes or non-stationary behaviour. Even though such methods were applied for some regions like Turkey, China, and Vietnam (Ceribasi et al. 2021a, b; Ceribasi and Ceyhunlu 2021; San et al. 2021), its applications for hydro-meteorological data from other parts of the globe is still at infant stage. This study proposes the application of IPTA and ITPA methods of ITA family for the detection of climate changes in Indian main land and the climatically sensitive NE region, considering rainfall datasets of different temporal scales.

## 2 Data

Monthly rainfall data of All India spatial scale and North East region of 1871–2016 period was collected from Indian Institute of Tropical Meteorology (IITM), Pune. The rainfall time series of different months and seasons was compiled and used for the trend analysis.

### 3 Methodology

#### 1. Innovative Trend Analysis (ITA)

This method is used to analyse the trend associated with the data series. Here the time series is divided into two equal halves (first half and second half) and is represented on X and Y axis, respectively, as in Fig. 1. If data points are on 45° line, it indicates no trend. Data points appearing above and below 45° line indicates increasing and decreasing trend, respectively. Magnitude of trend can be obtained by the distance of the data point from the 45° line. Trend obtained can be monotonic or non-monotonic. Trends are divided into categories as low, medium, and high.

#### 2. Family of ITA Methods

Different methods that have evolved from ITA are:

##### (a) Innovative Polygonal Trend Analysis (IPTA)

In IPTA method, for, e.g. in case of monthly data, the data is written in a matrix format as shown

$$\begin{pmatrix} x_{1,1}, x_{1,2}, \dots, x_{1,12} \\ x_{2,1}, x_{2,2}, \dots, x_{2,12} \\ \dots \\ x_{i,1}, x_{i,2}, \dots, x_{i,12} \\ \dots \\ x_{n,1}, x_{n,2}, \dots, x_{n,12} \end{pmatrix} \tag{1}$$

First the data is divided into two equal halves and their arithmetic mean (AM) or standard deviation (SD) is computed. Then, a plot between first half mean (or SD) vs second half mean is done in a 2D plane to get a polygon, known as IPTA graph as shown in Fig. 2.

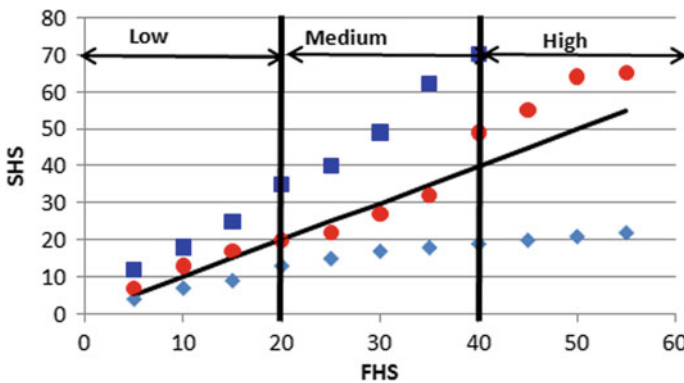


Fig. 1 Illustration of ITA method with data class. FHS—first half series; SHS—second half series

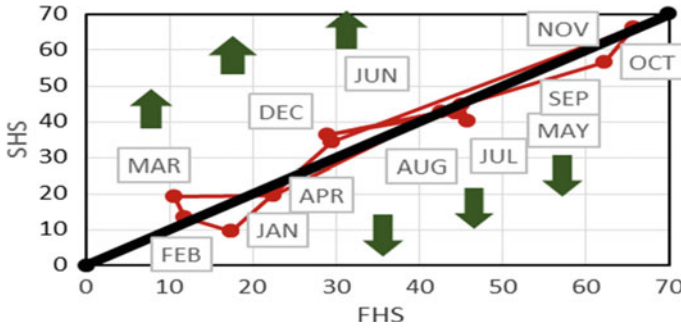


Fig. 2 Illustration of IPTA method. FHS—first half series; SHS—second half series

From the graph it is clear that those months which are appearing above the 45° line shows an increasing trend and vice versa. Depending upon the data, the polygon may differ and based on the nature of polygon obtained we can ensure whether the data homogenous or not. Trend slope (TS) and Trend length (TL) associated with the data can also be calculated from this method and based on that many other interpretations also can be made.

(b) **Innovative Trend Pivot Analysis (ITPA)**

This method is an improved variant of Sen’s (Sen et al. 2019) IPTA. By this method, the risk classes showing variations can also be understood. In this method, the trend regions are divided into five classes, which thus help in classifying the trend with better clarity. When the datasets were analysed with this method, two different graphs can be developed—the ITPA graph and the risk graph as shown in Fig. 3.

The graph on the left side in Fig. 3 is the improved IPTA graph (ITPA graph). Here the trend regions are divided into five classes like Very High Degree (VHD), High Degree (HD), Medium Degree (MD), Low Degree (LD), and Very Low Degree (VLD). Here the data length on both axes is divided into three equal parts along with 45° lines. If a data point is falling on 45° line, then there exists no trend.

In the risk graph, the region is divided into five equal parts indicated by different colours as in Fig. 3. This graph helps to identify the risk associated with the points. For example, of a point fall in medium degree increasing trend, this point may be in the first-degree risk class, as per the risk graph. This infers that there exist considerable differences between the two halves of the series.

## 4 Results and Discussion

### a. Results of MK Test

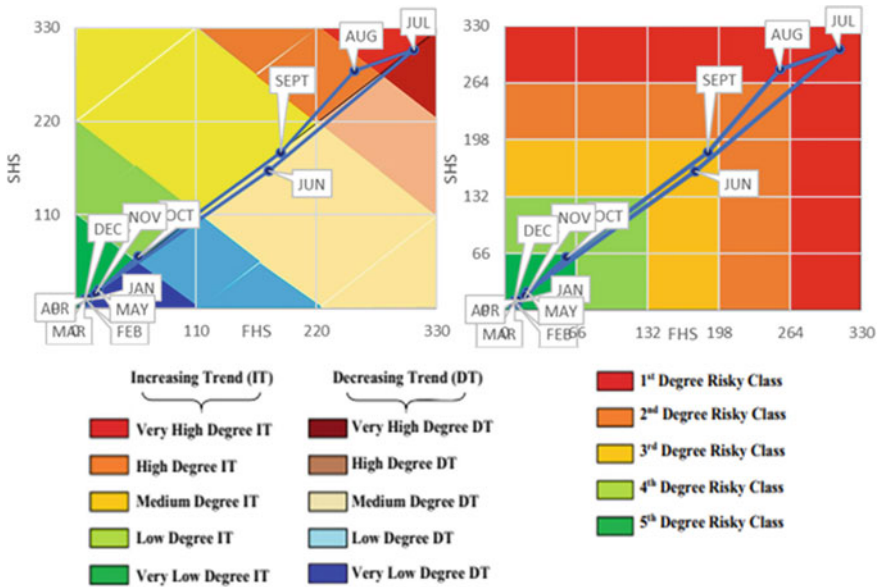


Fig. 3 IPTA method of trend analysis. Left panel is the IPTA graph and right panel is the risk graph

Firstly, the classical MK method is used to find trend of rainfall data of All India and NE region and the results obtained are presented in Table 1. MK trend results give valuable information regarding the nature as well as the significance of trends associated with the data. In the case of All India (AI), a significant decreasing trend is observed in the months of June and July at 90% level whereas seasonal data doesn't show any significant trend. In case of NE region, significant decreasing trend is observed in months of March and August at 95% level. A decreasing trend is observed in seasons of winter and monsoon.

**b. IPTA Results**

In this study, IPTA method is applied to rainfall time series of different months and seasons. Mean-based and SD-based analyses were done separately and results are summarized in Tables 2 and 4. IPTA plots for monthly and seasonal data are presented in Fig. 4. Figure 4 shows that the polygons are narrow so the data is inferred to be homogenous in mean. From the graph of AI region, it can be seen that there exists no significant trend in most of the months as well as seasons.

August and October rainfall shows an increasing trend whereas June rainfall shows a decreasing trend. Increasing trend is noted during July, October, November, December months and also during winter season in NE region of India. The SD-based graphs resulted in more visible polygons compared to AM-based graphs. As observed from the graph, the polygon obtained may have two or more cycles associated with it, which clearly depicts multiple cycles of climatic variations exist in association with the data. From the AI graph it is observed that most of the months show a decreasing



**Table 1** MK test results of AI and NE regions

January	-0.690	-1.199
February	-0.419	-1.360
March	0.318	<b>-2.286*</b>
April	1.570	0.027
May	0.181	-0.304
June	<i>-1.665*</i>	-1.570
July	<i>-1.694*</i>	0.069
August	0.890	<b>-2.822*</b>
September	-0.920	-1.313
October	0.594	0.905
November	0.128	0.049
December	-0.258	-0.005
WINT	-0.575	<i>-1.879*</i>
PREM	0.739	-0.917
MONS	-1.282	<b>-2.897*</b>
POSTM	0.570	1.076

\*The bold figures shows statistically significant trend at 5% level and the figures in italics shows the trend at 10% level

**Table 2** Arithmetic mean and standard deviation results of seasonal rainfall data

	Months											
	JAN	FEB	MAR	APR	MAY	JUN	JUL	AUG	SEP	OCT	NOV	DEC
AI-AM												
Trend	▼	▼	▲	▲	▲	▼	▼	▲	▼	▲	▼	▲
AI-SD												
Trend	▼	▼	▲	▼	▼	▼	▼	▼	▼	▼	▲	▲
NE-AM												
Trend	▼	▼	▼	▼	▼	▼	▼	▼	▼	▲	▲	▲
NE-SD												
Trend	▲	▼	▼	▲	▲	▼	▼	▼	▲	▲	▲	▲

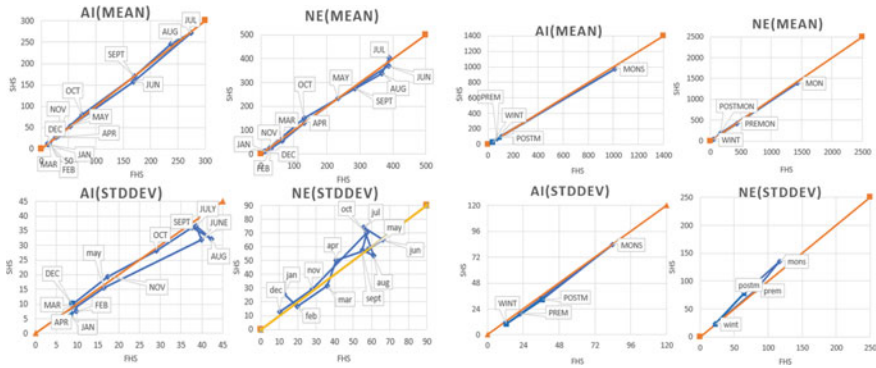
**Table 3** Arithmetic mean and standard deviation-based results of seasonal rainfall data

Seasons	W	PRM	M	PSM
AI-AM				
Trend	▼	▲	▼	▲
AI-SD				
Trend	▼	▼	▼	▼
NE-AM				
Trend	▼	▼	▼	▲
NE-SD				
Trend	▲	▲	▲	▲

W—winter, PRM—pre-monsoon, M—monsoon, PSM—post monsoon

**Table 4** Trend slope and trend length values obtained from IPTA for monthly data (mean and standard deviation results)

Mon.	Jan.-Feb.	Feb.-Mar.	Mar.-Apr.	Apr.-May	May-June	June-Jul.	Jul.-Aug.	Aug.-Sep.	Sep.-Oct.	Oct.-Nov.	NOV-DEC	DEC-JAN
<i>AI-mean</i>												
TS	0.516	3.668	0.998	0.992	0.905	1.078	0.689	1.136	0.939	1.144	0.967	4.76
TL	2.495	4.531	15.857	37.187	<b>156.213</b>	<b>154.933</b>	43.573	101.881	131.31	66.16	26.1	1.692
<i>AI-SD</i>												
TS	0.737	-2.704	-2.141	0.974	0.701	-3.385	-1.198	-0.839	0.92	0.756	1.115	9.567
TL	1.708	2.246	0.981	9.737	<b>28.574</b>	4.895	5.856	6.092	11.548	14.78	12.643	3.413
<i>NE-mean</i>												
TS	0.649	0.957	1.118	1.003	0.886	<b>10.004</b>	2.728	0.806	0.804	1.178	0.944	0.752
TL	20.02	45.595	99.901	146.08	<b>203.554</b>	34.595	68.52	103.398	198.81	159.6	27.388	48.316
<i>NE-SD</i>												
TS	-1.306	0.893	3.871	0.486	0.811	-0.898	<b>-3.844</b>	-0.649	<b>5.214</b>	1.387	0.916	0.792
TL	11.297	21.924	19.102	19.122	10.44	13.904	21.364	7.308	12.741	<b>50.32</b>	24.188	15.679



**Fig. 4** IPTA plots for monthly and seasonal data (mean and standard deviation-based analysis)

trend (except March, November, and December) whereas no significant variation is observed in the case of seasonal plots.

From IPTA method, the trend length (TL) as well as trend slope (TS) can also be computed. The values of TS and TL obtained for AI and NE monthly and seasonal data are given in Tables 4 and in 5. In the case of AI, largest value of trend length is observed from May to June and from pre-monsoon to monsoon season, indicating the highest transition in rainfall magnitude. All the trend slopes are positive hence the variation from month to month and season to season is increasing. In NE, trend slope obtained is positive and its increase is the highest in the month of June and July and from post monsoon to winter. Highest transition in the magnitude of rainfall is observed from May to June, September to October and from monsoon to post monsoon. In the case of SD-based analysis of AI data, both negative and positive values are obtained for trend slope in between the months. So, the variation is irregular and as a result more than one climatic variation can be experienced. Highest magnitude of rainfall is observed from May to June and from pre-monsoon to monsoon in case of seasons. A comparative result is obtained for monthly as well as seasonal data. Highest value for trend slope is obtained in between the months of December and January so the transition is high in between these months. In NE region, trend slope exhibits a negative value from July to August, which shows a decreasing transition in between these two months and a corresponding high transition (increasing) from September to October. Maximum change in rainfall magnitude is noted from October to November and from winter to pre-monsoon. Similarly, from months of March to May as well as from pre-monsoon to post-monsoon, amount of rainfall observed is quite similar in this region.

**c. ITPAM Results**

In the ITPAM method, the IPTA developed graph and risk graph as indicated in Figs. 5 and 6 for AM and SD-based analysis. From the developed IPTA graphs, the nature of trend, i.e. increasing (low, medium, high) and decreasing (low, medium, high) can be obtained. Also from the risk graph, the risk associated with the data,

**Table 5** Trend slope and Trend length values obtained from IPTA for seasonal data (mean and standard deviation results)

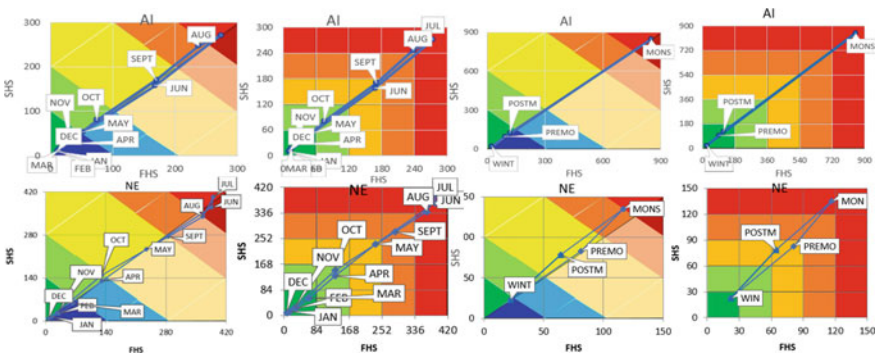
Trend characteristics/Season	PRM	M	PSM a
AI			
Trend (region-class)	DT VLD	DT VLD	DT VHD
Symbolic trend type	↓	↓	↑
Risk class	5 <sup>TH</sup>	5 <sup>TH</sup>	1 <sup>ST</sup>
Risk range	0-180	0-180	720-900
NE			
Trend (region-class)	IT LD	IT MD	IT HD
Symbolic trend	↘	→	↗
Risk class	5 <sup>TH</sup>	3 <sup>RD</sup>	1 <sup>ST</sup>
Risk range	0-30	60-90	120-150

i.e. whether it is a 1st, 2nd, 3rd, 4th or 5th can be obtained, based on which, the management decisions can be made for future. A comparison between IPTA graph and risk graph can also be made from the analysis, i.e. trend is obtained in medium region and the risk is of first-degree class, and it is said that some climatic variability exists. But here no such cases are noticed in the present study.

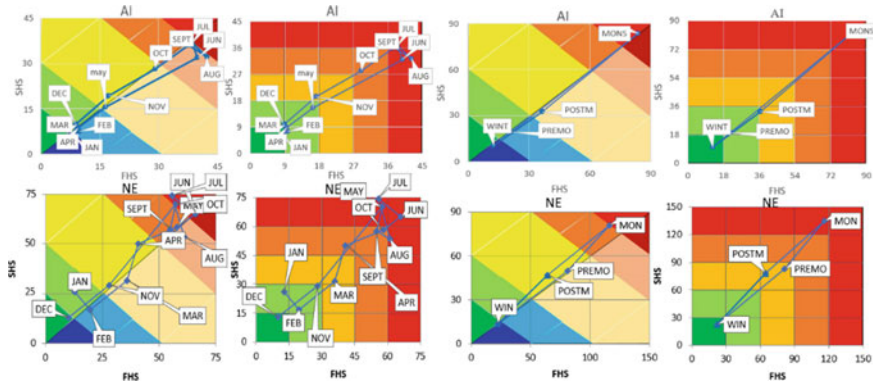
The following conclusions are obtained from Tables 6 and 7.

- The August rainfall falls on the high degree trend class and it is also in the first-degree risk class.
- All the results are satisfactory in between the developed IPTA graph as well as risk graph.
- For seasonal data the changes are highlighted in Table 7.

The following conclusions are obtained from Tables 8 and 9.



**Fig. 5** Developed IPTA and risk plots for monthly and seasonal data (mean-based analysis)



**Fig. 6** Developed IPTA and risk plots for monthly and seasonal data (standard deviation-based analysis)

**Table 6** ITPAM results for monthly data (mean-based analysis)

Trend Characteristics \Months	JAN	FEB	MAR	APR	MAY	JUN	JUL	AUG	SEP	OCT	NOV	DEC
<b>AI</b>												
Trend (region-class)	DT VLD	DT VLD	IT VLD	IT VLD	IT LD	DT MD	DT VHD	<b>IT HD</b>	DT MD	IT LD	DT VLD	NT VLD
Symbolic trend	↓	↓	↓	↓	↘	→	↑	↗	→	↘	↓	↓
Risk class	5 <sup>TH</sup>	5 <sup>TH</sup>	5 <sup>TH</sup>	5 <sup>TH</sup>	5 <sup>TH</sup>	3 <sup>RD</sup>	1 <sup>ST</sup>	1 <sup>ST</sup>	3 <sup>RD</sup>	4 <sup>TH</sup>	5 <sup>TH</sup>	5 <sup>TH</sup>
Risk range	0-60	0-60	0-60	0-60	0-60	120-180	240-360	240-360	120-180	60-120	0-60	0-60
<b>NE</b>												
Trend (region-class)	DT VLD	DT VLD	DT VLD	DT LD	DT MD	DT VHD	IT VHD	<b>DT HD</b>	DT HD	IT LD	IT VLD	IT VLD
Symbolic trend type	↓	↓	↓	↘	↗	↑	↑	↗	↗	↘	↓	↓
Risk class	5 <sup>TH</sup>	5 <sup>TH</sup>	5 <sup>TH</sup>	4 <sup>TH</sup>	3 <sup>RD</sup>	1 <sup>ST</sup>	1 <sup>ST</sup>	1 <sup>ST</sup>	2 <sup>ND</sup>	4 <sup>TH</sup>	5 <sup>TH</sup>	5 <sup>TH</sup>
Risk range	0-84	0-84	0-84	84-168	168-252	336-420	336-420	336-420	252-336	84-168	0-84	0-84

For All India data of monsoon months (June, July August, and September), the rainfall falls on the high degree trend class and it is also in the first-degree risk class. Rainfall of May falls on medium degree trend class and fourth degree risk class

- August rainfall of North East region falls on high degree trend class and also on the first-degree risk class.

**Table 7** ITPAM results for seasonal data (mean analysis)

Seasons	W-PRM	PRM-M	MON-PSM	PSM-W
<i>AI-mean</i>				
TL	1.086	0.992	0.988	1.093
TS	100.764	<b>1065.997</b>	<b>1029.59</b>	137.233
<i>AI-SD</i>				
TL	1.015	1.03	1.077	0.931
TS	12.87	<b>89.33</b>	69.609	32.65
<i>NE-mean</i>				
TL	0.997	0.966	0.95	<b>1.24</b>
TS	541.566	1389.113	<b>1741.218</b>	190.925
<i>NE-SD</i>				
TL	1.028	1.476	1.089	1.33
TS	<b>84.328</b>	62.794	76.98	69.76

W—winter, PRM—pre-monsoon, M—monsoon, PSM—post-monsoon. The changes are marked in bold

**Table 8** ITPA results for monthly data (standard deviation-based analysis)

Trend	Months											
	JAN	FEB	MARCH	APRIL	MAY	JUNE	JULY	AUG	SEPT	OCT	NOV	DEC
Trend (region – class)	DT-VLD	DT-LD	IT-LD	IT-LD	DT-MD	<b>DT-HD</b>	<b>DT-HD</b>	<b>DT-HD</b>	<b>DT-HD</b>	DT-MD	IT-MD	IT-LD
Symbolic trend type	⬇	↘	↘	↘	➡	↗	↗	↗	↗	➡	➡	↘
Risk class	5 <sup>th</sup>	4 <sup>th</sup>	4 <sup>th</sup>	4 <sup>th</sup>	4 <sup>th</sup>	1 <sup>st</sup>	1 <sup>st</sup>	1 <sup>st</sup>	1 <sup>st</sup>	2 <sup>nd</sup>	3 <sup>rd</sup>	4 <sup>th</sup>
Risk range	0-9	9-18	9-18	9-18	9-18	36-45	36-45	36-45	36-45	27-36	18-27	9-18
<i>NE</i>												
Trend(region – class)	IT-LD	DT-LD	DT-MD	<b>IT-MD</b>	IT-HD	DT-VHD	IT-VHD	<b>DT-HD</b>	IT-HD	IT-VHD	IT-MD	IT-VLD
Symbolic trend type	↘	↘	➡	➡	↗		⬆	↗	↗	⬆	➡	⬇
Risk class	4 <sup>th</sup>	4 <sup>th</sup>	3 <sup>rd</sup>	2 <sup>nd</sup>	2 <sup>nd</sup>	1 <sup>st</sup>	1 <sup>st</sup>	1 <sup>st</sup>	2 <sup>nd</sup>	1 <sup>st</sup>	4 <sup>th</sup>	5 <sup>th</sup>
Risk range	15-30	15-30	30-45	45-60	45-60	60-75	60-75	60-75	45-60	60-75	15-30	0-15

- In the case of seasonal analysis, only in monsoon rainfall of North East India, change is noted. It falls on high degree trend class and also on the first-degree risk class.

If a point in the ITPA graph is not in high class but it falls on first-degree risk class, then it indicates a significant change between the first and second half datasets of that point. Thus, the risk factor associated with that point is high. The two graphical procedures of ITPA and IPTA applied in the study are capable to give overall

**Table 9** ITPA results for seasonal data (standard deviation analysis)

Trend	Seasons			
	W	PRM	M	PSM
Trend(region –class)	DT-VLD	DT-LD	DT-VHD	DT-MD
Symbolic trend type	⬇	↘	⬆	➡
Risk class	5 <sup>th</sup>	4 <sup>th</sup>	1 <sup>st</sup>	3 <sup>rd</sup>
Risk range	0-18	18-36	72-90	36-54
NE				
Trend(region –class)	IT-VLD	IT-MD	<b>IT-HD</b>	IT-MD
Symbolic trend type	⬇	➡	↗	➡
Risk class	5 <sup>th</sup>	3 <sup>rd</sup>	1 <sup>st</sup>	3 <sup>rd</sup>
Risk range	0-30	60-90	120-150	60-90

W—winter; PRM—pre-monsoon, M—monsoon, PSM—post-monsoon

insight on the changing climate, seasonal changes and on mean/SD non-stationarity of rainfall datasets of AI and NE regions.

## 5 Conclusions

ITA methods are relatively new graphical procedure for useful for determining the trends of hydro-meteorological datasets. The two recent variants of ITA methods namely Innovative Polygonal Trend Analysis (IPTA) and Innovative Trend Pivot Analysis (ITPA) are applied to monthly and seasonal rainfall data of (1871–2016) for All India and NE regions. Trend lengths and Trend slopes are extracted from IPTA graphs. Two different graphs-improved IPTA and risk graphs are obtained from ITPA analysis to identify the risk factor in the region during a particular time period. The important observations made from the study are:

- Since the polygon is narrow and slopes of straight lines are identical, the data homogeneity in mean is noticed for AI and NE regions.
- More complex polygons and presence of two or more cycles indicating differences in climatic conditions captured via standard deviation-based analysis in comparison with mean-based analysis.
- In the case of AI, largest value of trend length hence the largest transition of rainfall is observed from May to June, both by mean and standard deviation analyses.
- The largest increase in the magnitude of rainfall is observed in the North Eastern region from monsoon to post monsoon season

- For both the regions, the SD-based analysis is giving a more visible polygon than mean-based analysis indicating SD–Non-stationarity is critical over mean stationarity.
- Both AM and SD-based ITPA methods, the risk factor is low for All India as well as North Eastern region.

## References

- Ali R, Kuriqi A, Abubaker S, Kisi O (2019) Long-term trends and seasonality detection of the observed flow in Yangtze River Using Mann-Kendall and Sen's Innovative Trend Method. *Water* 11:1855. <https://doi.org/10.3390/w11091855>
- Ceribasi G, Ceyhunlu AI (2021) Analysis of total monthly precipitation of Susurluk Basin in Turkey using innovative polygon trend analysis method. *J Wat Clim Chang* 12(5):1532–1543
- Ceribasi G, Ceyhunlu AI, Ahmed N (2021a) Analysis of temperature data by using innovative polygon trend analysis and trend polygon star concept methods: a case study for Susurluk Basin, Turkey. *Acta Geophys*. <https://doi.org/10.1007/s11600-021-00632-3>
- Ceribasi G, Ceyhunlu AI, Ahmed N (2021) Innovative trend pivot analysis method (ITPAM): a case study for precipitation data of Susurluk Basin in Turkey. *Acta Geophys* 69:1465–1480
- Cui L, Wang I, Lai Z, Tian Q, Liu W, Li J (2017) Innovative trend analysis of annual and seasonal air temperature and rainfall in the Yangtze River Basin, China during 1960–2015. *J Atmos Solar-Terr Phys* 164:48–59
- Güçlü YS, Şişman E, Dabanlı I (2020) Innovative triangular trend analysis. *Arab J Geosci* 13:27. <https://doi.org/10.1007/s12517-019-5048-y>
- Kendall MG (1975) Rank correlation methods, 4th edn. Charles Griffin, London
- Mann HB (1945) Non-parametric tests against trend. *Econometrica* 13:163–171
- San M, Akacay F, Linh NTT, Kankal M, Pham QB (2021) Innovative and polygonal trend analyses applications for rainfall data in Vietnam. *Theoret Appl Climatol* 144:809–822
- Sen Z (2021) Probabilistic innovative trend analysis (PITA). *Int J Global Warming* 20(2): 93–105
- Şen Z, Şişman E, Dabanlı I (2019) Innovative polygon trend analysis (IPTA) and applications. *J Hydrol* 575:202–210
- Sen Z (2012) Innovative trend analysis methodology. *J Hydrol Engng* 17(9) [https://doi.org/10.1061/\(ASCE\)HE.1943-5584.0000556](https://doi.org/10.1061/(ASCE)HE.1943-5584.0000556)
- Şişman E, Kizilöz B (2021) The application of piecewise ITA method in Oxford, 1870–2019. *Theoret Appl Climatol* 145:1451–1465. <https://doi.org/10.1007/s00704-021-03703-z>
- Sonali P, Kumar DN (2013) Review of trend detection methods and their application to detect temperature changes in India. *J Hydrol* 476:212–227
- Wang Y, Xu Y, Tabari H, Wang J, Wang Q, Song S, Hu Z (2020) Innovative trend analysis of annual and seasonal rainfall in the Yangtze River Delta, eastern China. *Atmos Res* 231:104673. <https://doi.org/10.3390/w11091855>



# Review on Statistical Post-processing of Ensemble Forecasts



Rashmi Yadav and Sanjaykumar M. Yadav

**Abstract** Statistical post-processing of the ensemble outputs of meteorological and hydrological forecasts is essential to address the errors and uncertainty introduced in the forecasting. Post-processing (PP) generates well-calibrated predictions by analyzing the statistical relationship among the historical predictions and their corresponding observations. In the scientific communities of statistical, meteorological, climatological, hydrological, and engineering many recent developments are now thriving. These techniques range from simple to complex from straightforward bias corrections to quite complex procedures for modifying the distribution that take correlations between the prognostic factors considered. The foremost activities working out in the area of statistical post-processing from statistical advancements to functioning applications, focusing on different methods available and their comparison is summarized in the paper. The review shows good performance of the logistic regression in several studies for the PP of numerical weather forecasts.

**Keywords** Ensemble forecasts · Post-processing · Parametric methods · Non-parametric methods

## 1 Introduction

Flood forecasting plays a critical role in the reduction of economic as well as life losses and is considered a challenging task in hydrology (Kumar et al. 2020). Considering the real-time flood forecasting systems (FFS) in India, most of the cast-off techniques are based on either a statistical or deterministic approach (Jain et al. 2018). The reliability of the FFS is based on highly accurate weather forecasts (Nanditha and Mishra 2021). Operational and research FFS over the globe are progressively

---

R. Yadav (✉) · S. M. Yadav  
Sardar Vallabhbhai National Institute of Technology, Surat, Gujarat 395007, India  
e-mail: [rashmiy276@gmail.com](mailto:rashmiy276@gmail.com)

S. M. Yadav  
e-mail: [smy@ced.svnit.ac.in](mailto:smy@ced.svnit.ac.in)

succeeding in the direction of probabilistic forecasting by incorporating the perturbed members of ensemble prediction systems (EPS), in spite of a deterministic forecasts (Cloke 2008).

Predicting the exact state of the atmosphere is not possible as the Earth's atmosphere is a complex and non-linear system. Weather forecasts remain limited because of the complexity of the numerical illustration of physical processes and sensitivity in outcomes of the pattern of initial conditions (Cloke and Schaake 2018). Numerical Weather Predictions (NWP) by the ensemble prediction systems are thus used as the meteorological input to hydrological models. Ensemble Prediction system forecasts a high-rate product output with higher potential to extend the lead time and superior predictability. Ensemble methods allow the user to incorporate a set of predictions instead of using a single prediction (Murray 2018). The fundamental characteristics that an ensemble should possess are: reliability and accuracy, and its skills should be evaluated taking both into consideration (Buizza 2018).

The two approaches for that can be (i) combining various models to advance a single model preferably can be called a multi-model ensemble, and (ii) using a single model but perturbing the initial conditions to give multiple inputs and produce multiple results. The basic ideology is to characterize the range of possible outcomes using these perturbed forecasts (Wu et al. 2020). Then, it is assumed that large ensemble spreads represent higher forecast uncertainty and narrower spreads represent truncated uncertainties. Nevertheless, in training the initial ensemble members do not signify initial-condition uncertainty (Hamill et al. 2008; Hu et al. 2016). Furthermore, perturbed forecasts show similar model errors as single integration predictions. Therefore, to attain bias-corrected and calibrated uncertainty predictions, PP of the ensemble forecasts is required.

The methods for creating ensemble prediction forecasts are rather simple. Numerous functioning ensemble prediction systems operate on the Monte Carlo basis (Abaza et al. 2014; Yu et al. 2016) of numerical weather predictions with a realization initiated from a central investigation (the control member forecast) and the rest are produced by disturbing the initial parameters (ensemble members or perturbed forecast). An EPS enumerates the uncertainty that results from the dual aspects described as first making slight changes to the initial conditions and second being the repeated operation of the NWP model several times. An ensemble prediction is a subset of the forecasted variable's distribution that takes into account uncertainty in initial variables and predictor variables.

These methodologies use previous predictions and observations (as well as presumably auxiliary parameters) to determine the parameters of a statistical model, which is then used in real-time to evaluate the "true" (unbiased) probability distribution of the prediction parameter, conditional on the raw prediction (and any other predictors). Statistical modification of NWPs necessitates a lengthy historic dataset of weather predictions and observations that is used for the prediction of distribution with plausible sampling uncertainty and bias.

Over the last few decades, at least 2 categories of statistical methods have emerged: analogs methods and ensemble model output statistics. One of those is completely non-parametric and involves locating comparable atmospheric conditions in the past

and then using them to enhance the current predictions. In contrast, ensemble model output statistics fit to the group of parametric regression systems. If  $y$  signifies the considered meteorological variable and  $(x_1, x_2, \dots, x_n)$  are the equivalent  $n$  perturbed forecasts, then the ensemble model output statistics predictive distribution is basically a distribution whose parameters subject to the values of  $(x_1, x_2, \dots, x_n)$ .

Instead of single point values, ensemble PP produces a complete predictive distribution or a discrete collection of modified perturbed members that serve as a sample from an amended predictive distribution. For predictable non-probabilistic dynamical predictions, model output statistics purposes to rectify the mean. Because dispersion errors also exist for NWP, ensemble-MOS offers a more challenging issue. Most PP approaches may be divided into two categories statistically: first that presume the predictive distribution fits a group of known probability distribution functions and other that do not. Comprehensively such categories are termed parametric and non-parametric statistical PP methods. Recent advances for these two classes will be addressed distinctly and then the comparison of these methods is carried out of the literature considered in this review study.

## 2 Parametric Ensemble Post-processing Methods

On the basis of the variable taken into consideration, distribution-based PP methods stipulate a parametric model for the predictive distribution by identifying an appropriate probability distributions family (Raftery et al. 2005). To rectify systematic errors, the forecast distribution variables are associated with the predictors from the NWP model mostly through regression equations. The regression coefficients are calculated by fine-tuning appropriate loss functions for distribution predictions.

Messner et al. (2016) exhibited square-root transformed meteorological data using non-homogeneous regressions with logistic predictive distributions, where the regression parameters were assessed by employing maximum likelihood. On the transformed scale the probabilities are computed as:

$$P\{y_t \leq q\} = \begin{cases} \frac{\exp\left[\frac{(q-\mu_t)}{\sigma_t}\right]}{1+\exp\left[\frac{(q-\mu_t)}{\sigma_t}\right]}, & q > 0 \\ 0, & \text{otherwise} \end{cases} \quad (1)$$

where  $\mu_t$  is logistic distribution mean, and  $\sigma_t$  is the ensemble standard deviation of logistic predictive distribution, and  $q$  is the quantile threshold.

In spite of postulating a continuous predictive distribution for the vectors of verification (denoting  $V$ ), as with Bayesian Model Average and Non-homogeneous Gaussian Regression, a substitute is to predict just the probability,  $p$ , of the event  $\{V \leq q\}$ . Amongst some of the models used to accomplish this is logistic regression. (Williams et al. 2014). The two-predictor logistic regression can be employed for specifying

the probability that verification ( $V$ ) or future observation will be then or equal to the quantile ( $q$ ).

Extended logistic regression (ELR) (Messner et al. 2014; Schmeits and Kok 2010)–Logistic regression is a regression model from the generalized linear model framework to model the conditional probability of binary events. For the binary predictands Model Output Statistics method is a compatible technique (Messner 2018). For the adjustment of the spread in the predictive distribution in the ELR method, the ensemble spread is taken as the scale parameter. For an instance, the probability of a continuous variable  $y$  falling lower than a certain threshold quantile can be projected with Eq. 2 as

$$P[(h(y) < h(q)|X)] = \left[ \frac{\exp\left[\frac{h(q)-\mu}{\sigma}\right]}{1 + \exp\left[\frac{h(q)-\mu}{\sigma}\right]} \right] \quad (2)$$

where  $y$  is the variable,  $h$  designates the function,  $q$  is the quantile thresholds, ensemble mean ( $\mu$ ) is the location factor and ensemble standard deviation ( $\sigma$ ) is the scale factor. ELR is capable of avoiding the issue of intersecting regression lines and also permits, evaluating the probabilities for any threshold value.

Ordered logistic regression (Messner et al. 2014) is a prevalent regression model from statistics and econometrics for ordinal input, that has not been acknowledged considerably in meteorology till date. It is an enhancement of conventional logistic regression for multi-category and ordered predictands, much the same as ELR. Differs from ELR in the way that distinct intercepts are fitted for particular thresholds as an alternative to modeling them as a linear function of the (transformed) thresholds.

Furthermore, the commonly compared methods are Bayesian Model Averaging (Raftery et al. 2005) and the non-homogeneous regressions (NHR), particularly bearing in mind that ELR is understood as a non-homogeneous regression with logistic-distributed errors (Messner et al. 2014). Non-homogenous regression approach has the capability of representing and correcting both bias and dispersion errors while necessitating the estimate of a small number of parameters, especially if the only predictor variable is the ensemble mean.

Additionally, the classic LR's performance for extreme events is limited because it can only forecast the likelihood of crossing a few discrete thresholds. In contrast, the ELR works well even for exceptional occurrences and offers predictions of the entire distribution (Wilks 2018). Additionally, standard LR has many more parameters than ELR, making it more sensitive to the size of the training window, whereas ELR is not significantly impacted by sample size.

Other parametric methods of PP methods are Truncated non-homogeneous regression (Messner et al. 2016), non-homogeneous Gaussian regression (Williams et al. 2014), Ensemble MOS (Wilks 2018), Kernel dressing, and Neural network.

### 3 Non-parametric Ensemble Post-Processing Methods

Bremnes (2004) suggests using quantile regression techniques, which consider only a subset of the predictive distribution's quantiles. Traditionally, the quantiles are computed individually, which can result in unenforceable crossing quantiles. This difficulty, though, can be avoided by summing up the constraints to the estimate or merely rearranging the quantiles at last.

The quantile-to-quantile transform (also acknowledged as Quantile Mapping), (Madadgar et al. 2012; Verkade et al. 2013) is an unequivocal strategy in the sense that the forecasts' unequivocal climatology is re-mapped to the observations' unequivocal climatology. The quantile-to-quantile transform is not supposed to produce post-processed ensembles as skilled as those produced by conditional correction. An enhancement in prediction climatology may, however, account for a considerable portion of the skill of a conditional correction, and an unconditional correction offers a useful starting point for a conditional improvement that is more intricate. Quantile Mapping is a statistical methodology that is frequently used PP technique in streamflow forecasting that modifies model predictions using cumulative density functions from recorded observed data and model simulations.

Other non-parametric PP approaches use numerous straight transformations of ensembles, developing from simple bias correction or variance inflation measures. Flowerdew (2014) straightly plots the forecast probability to observed event frequency for a sequence of thresholds, for making the predictions consistent while conserving the resolution. Each threshold is calibrated using the most local region consistent with attaining a quantified sample size, and the algorithm only requires perceiving each set of training data once, dipping the storing necessities for bulky gridded datasets.

Other non-parametric methods are Rank histogram calibration, Ensemble dressing (Williams et al. 2014), Individual ensemble member adjustment, Member by member (Vannitsem and Hagedorn 2011), and Neural network.

Various proposed methods of the statistical PP of the ensemble forecasts make it essential to study the comparison, which method performs better and will be more appropriate. A few researchers have showed the comparison of the PP methods and their performances. Table 1 summarizes the parametric and non-parametric methods of PP, and the results reflected in selected literature based on the comparisons of different PP methods. Here + indicates the outperformance of the method over others, ± shows moderate performance, and – represents the relatively poor performance of the adopted post-processing method. Van Schaeybroeck and Vannitsem (2015) inspected member-by-member PP methods and Taillardat and Vannitsem et al. (2021) concluded that quantile regression forests (QRF) methods performance is good for temperatures and wind speed datasets.

One of the demerits of QM is poor performance in the case when the raw NWP's agonize from issues of reliability or coherence. A subtler drawback is faced in the case of shorter training periods. Parametric methods are able to evade the issue (Zhao et al. 2017) (the performance may get hindered in case of extreme events that

**Table 1** Comparison of the method used in the literature referred (Non-Homogeneous Regression–NHR, Bayesian Model Averaging–BMA, Logistic Regression–LR, Extended Logistic Regression–ELR, Ordered Logistic Regression–OLR. Non-parametric Quantile Regression–QR, Other Ensemble Dressing Method–OED, Forecast Assimilation–FA, Member by Member–MBM)

Authors	Data type	Parametric					Non-parametric			
		NHR	BMA	LR	ELR	OLR	QR	OED	FA	MBM
Velthoen et al. (2019)	Precipitation						+			+
Verkade et al. (2013)	Temperature precipitation			+			+			
Messner et al. (2014)	Precipitation Wind			±	+	+				
Bentzien and Friederichs (2012)	Precipitation	±		+			+			
Wilks (2006)	Precipitation Wind	+	±	±				+	±	
Williams et al. (2014)	Precipitation Wind	+	+	–				+		
Schmeits and Kok (2010)	Precipitation		+		+					
Wilks and Hamill (2007)	Temperature precipitation	+		±				±		
Stephane and Hagedorn (2011)	Temperature	+								+

Here + indicates relatively good performance by the method mentioned in the column, – represents poor performance, and ± shows the moderate performance of the PP method

occurred not very often in historical archives while performing non-parametric PP) by extrapolating the statistical relationship that is developed by the datasets of ordinary events with extreme events as long as the statistical conventions are justifiable. In such cases of higher percentiles, the QM estimates become highly unstable and can result in more harm than good.

## 4 Conclusion

The paper summarizes different post-processing approaches to address the bias and uncertainty in the meteorological forecasts generated by the perturbations in the initial conditions. The review shows good performance of the logistic regression in several studies for the PP of ensemble forecasts.

## References

- Abaza M, Anctil F, Fortin V, Turcotte R (2014) Sequential streamflow assimilation for short-term hydrological ensemble forecasting. *J Hydrol* 519:2692–2706. <https://doi.org/10.1016/j.jhydrol.2014.08.038>
- Bentzen S, Friederichs P (2012) Generating and calibrating probabilistic quantitative precipitation forecasts from the high-resolution NWP Model COSMO-DE. *Weather Forecast* 27(4):988–1002. <https://doi.org/10.1175/WAF-D-11-00101.1>
- Bremnes JB (2004) Probabilistic forecasts of precipitation in terms of quantiles using NWP model output. *Mon Weather Rev Am Meteorol Soc* 132(1):338–347. [https://doi.org/10.1175/1520-0493\(2004\)132%3c0338:pfopit%3e2.0.co;2](https://doi.org/10.1175/1520-0493(2004)132%3c0338:pfopit%3e2.0.co;2)
- Buizza R (2018) Ensemble forecasting and the need for calibration. In: *Statistical postprocessing of ensemble forecasts*. Elsevier Inc. <https://doi.org/10.1016/b978-0-12-812372-0.00002-9>
- Cloke HL, Schaake JC (2018) *Handbook of hydrometeorological ensemble forecasting*. <https://doi.org/10.1007/978-3-642-40457-3>
- Cloke HL (2008) A review of ensemble techniques. *J Hydrol*
- Flowerdew J (2014) Calibrating ensemble reliability whilst preserving spatial structure. *Tellus A: Dyn Meteorol Oceanogr* 66(1):22662
- Hamill TM, Hagedorn R, Whitaker JS (2008) Probabilistic forecast calibration using ECMWF and GFS ensemble reforecasts. Part II: precipitation. *Mon Weather Rev* 136(7):2620–2632. <https://doi.org/10.1175/2007MWR2411.1>
- Hu Y, Schmeits MJ, van Andel SJ, Verkade JS, Xu M, Solomatine DP, Liang Z (2016) A stratified sampling approach for improved sampling from a calibrated ensemble forecast distribution. *J Hydrometeorol* 17(9):2405–2417. <https://doi.org/10.1175/JHM-D-15-0205.1>
- Jain SK, Mani P, Jain SK, Prakash P, Singh VP, Tullos D, Kumar S, Agarwal SP, Dimri AP (2018) A Brief review of flood forecasting techniques and their applications. *Int J River Basin Manage* 16(3):329–344. <https://doi.org/10.1080/15715124.2017.1411920>
- Kumar S, Jain SK, Gurrappu S (2020) Challenges and recent developments in flood forecasting in India. In: *Roorkee water conclave*
- Madadgar S, Moradkhani H, Garen D (2012) Towards improved post-processing of hydrologic forecast ensembles. *Hydrol Process* 28:104–122
- Messner JW, Mayr GJ, Wilks DS, Zeileis A (2014) Extending extended logistic regression: extended versus separate versus ordered versus censored. *Mon Weather Rev* 142(8):3003–3014. <https://doi.org/10.1175/MWR-D-13-00355.1>
- Messner JW, Mayr GJ, Zeileis A (2016) Heteroscedastic censored and truncated regression with crch. *R J* 8(1):173–181. <https://doi.org/10.32614/rj-2016-012>
- Messner JW (2018) Ensemble postprocessing with R. In: *Statistical postprocessing of ensemble forecasts*. Elsevier Inc. <https://doi.org/10.1016/B978-0-12-812372-0.00011-X>
- Murray SA (2018) The importance of ensemble techniques for operational space weather forecasting. *Space Weather* 16(7):777–783. <https://doi.org/10.1029/2018SW001861>
- Nanditha JS, Mishra V (2021) On the need of ensemble flood forecast in India. *Water Secur* 12:100086. <https://doi.org/10.1016/j.wasec.2021.100086>

- Raftery AE, Gneiting T, Balabdaoui F, Polakowski M (2005) Using Bayesian model averaging to calibrate forecast ensembles. *Mon Weather Rev* 133(5):1155–1174. <https://doi.org/10.1175/MWR2906.1>
- Schmeits MJ, Kok KJ (2010) A comparison between raw ensemble output, (modified) Bayesian model averaging, and extended logistic regression using ECMWF ensemble precipitation reforecasts. *Mon Weather Rev* 138(11):4199–4211. <https://doi.org/10.1175/2010MWR3285.1>
- Stephane V, Hagedorn R (2011) Ensemble forecast post-processing over Belgium: comparison of deterministic-like and ensemble regression methods. *Meteorol Appl* 18:94–104. <https://doi.org/10.1002/met.217>
- Van Schaeybroeck B, Vannitsem S (2015) Ensemble post-processing using member-by-member approaches: theoretical aspects. *Q J R Meteorol Soc* 141(688):807–818. <https://doi.org/10.1002/qj.2397>
- Vannitsem S, Bremnes JB, Demaeyer J, Evans GR, Flowerdew J, Hemri S, Lerch S, Roberts N, Theis S, Atencia A, Ben Bouallègue Z, Bhend J, Dabernig M, Cruz LD, Hieta L, Mestre O, Moret L, Plenković IO, Schmeits M, Taillardat M, Van den Bergh J, Van Schaeybroeck B, Whan K, Ylhaisi J (2021) Statistical postprocessing for weather forecasts. *Am Meteorol Soc*, pp E681–E699
- Vannitsem S, Hagedorn R (2011) Ensemble forecast post-processing over Belgium: comparison of deterministic-like and ensemble regression methods. *Meteorol Appl* 104:94–104. <https://doi.org/10.1002/met.217>
- Velthoen J, Cai JJ, Jongbloed G, Schmeits M (2019) Improving precipitation forecasts using extreme quantile regression. *Extremes* 22(4):599–622. <https://doi.org/10.1007/s10687-019-00355-1>
- Verkade JS, Brown JD, Reggiani P, Weerts AH (2013) Post-processing ECMWF precipitation and temperature ensemble reforecasts for operational hydrologic forecasting at various spatial scales. *J Hydrol* 501:73–91. <https://doi.org/10.1016/j.jhydrol.2013.07.039>
- Wilks DS (2006) Comparison of ensemble-MOS methods in the Lorenz '96 setting. *Meteorol Appl* 13(3):243–256. <https://doi.org/10.1017/S1350482706002192>
- Wilks DS, Hamill TM (2007) Comparison of ensemble-MOS methods using GFS reforecasts. *Mon Weather Rev* 135(6):2379–2390. <https://doi.org/10.1175/MWR3402.1>
- Wilks DS (2018) Univariate ensemble postprocessing. In: *Statistical postprocessing of ensemble forecasts*. <https://doi.org/10.1016/B978-0-12-812372-0.00003-0>
- Williams RM, Ferro CAT, Kwasniok F (2014) A comparison of ensemble post-processing methods for extreme events. *Q J R Meteorol Soc* 140(680):1112–1120. <https://doi.org/10.1002/qj.2198>
- Wu W, Emerton R, Duan Q, Wood AW, Wetterhall F, Robertson DE (2020) Ensemble flood forecasting: current status and future opportunities. *Wires Water* 7(3):1–32. <https://doi.org/10.1002/wat2.1432>
- Yu W, Nakakita E, Kim S, Yamaguchi K (2016) Improving the accuracy of flood forecasting with transpositions of ensemble NWP rainfall fields considering orographic effects. *J Hydrol* 539:345–357. <https://doi.org/10.1016/j.jhydrol.2016.05.047>
- Zhao T, Bennett JC, Wang QJ, Schepen A, Wood AW, Robertson DE, Ramos MH (2017) How suitable is quantile mapping for postprocessing GCM precipitation forecasts? *J Clim* 30(9):3185–3196. <https://doi.org/10.1175/JCLI-D-16-0652.1>



# Statistical Downscaling Model (SDSM) for Long Term Prediction of Rainfall and Maximum Temperature



Himanshukumar Babuji Thakor and Falguni P. Parekh

**Abstract** Climate change is a biggest threat that has impacted hundreds of millions of people. It is critical to calculate the severity of rainfall and temperature in locations prone to hydro meteorological disasters in transitional climatic patterns. As a result, the primary goal of this research is to evaluate the severity of rainfall and maximum temperature under three Representative Concentration Pathways (RCPs) using CanESM2 data from the Global Climate Model. The historic data of 40 years (1981–2021) of the Vadodara district are used which is considered as base period. Our findings were based on CanESM2 scenarios, specifically RCP8.5, which is modelled in the SDSM to determine decade wise future rainfall and maximum temperature from the years 2021–2100 under various carbon emission scenarios. The results reveal that due to the climate change, the general amount of rainfall and temperature in this region of Vadodara District shows increasing trend from 2021 to 2100 when compared to the base period. It is observed that decade wise monthly maximum temperature is increasing in every month. The maximum increasing rate of maximum temperature is 10.22% for the month of July and minimum increasing rate is 1.27% for the month October is observed from 2021 to 2100 compared to base period. It is observed that decade wise monthly rainfall is increasing in each month. For the month of July, rainfall is increasing at the average rate of 9.47% from 2021 to 2100 with respect to base period. Similarly for the month September, rainfall is increasing at the average rate of 3.28% from 2021 to 2100 with respect to base period. The maximum increasing rate of rainfall is 64.72% for the month of June and minimum increasing rate is 3.28% for the month September is observed compared to base period.

**Keywords** Downscaling · Rainfall · Statistical · Temperature

---

H. B. Thakor · F. P. Parekh (✉)

Water Resources Engineering and Management Institute, Faculty of Technology & Engineering,  
The Maharaja Sayajirao University of Baroda, Vadodara, India  
e-mail: [fpparekh-wremi@msubaroda.ac.in](mailto:fpparekh-wremi@msubaroda.ac.in)

H. B. Thakor

e-mail: [himanshuthakor97@gmail.com](mailto:himanshuthakor97@gmail.com)

## 1 Introduction

Climate change is considered to be the biggest challenge facing the mankind in the twenty-first century. Unusual or extreme weather and climate-related events are very important for human being. Climate plays very important role in agricultural productivity and vegetative growth. Climate change can be considered as change in average weather conditions, or in the time variation of weather around longer term average conditions. The impact of climate change on the various meteorological parameters has drawn attention of the entire world. Rainfall and temperature are crucial parameters that have both positive and negative impacts on agriculture. Vadodara district is surrounded by industrial areas as well as agricultural area. The climate change impact at local level is also equally important to study. The rationale behind the selection of this topic is to implement SDSM model to know the effect of climate change at local level.

Temperature and rainfall are the main factors in the hydrological cycle, which influences climate change. The continuous increase of greenhouse gas concentration in the atmosphere leads to climate change and to estimate that Global Climate Models (GCMs) are used. GCMs output are of coarse spatial resolution which cannot be used directly for hydrological assessment. Downscaling is a technique to convert the coarse spatial resolution of the GCMs output into a fine resolution. It includes generating point/station data of a specific area by using the GCM climatic output variables.

Statistical Downscaling Model (SDSM) is a combination of regression-based and stochastic-based weather originator methods. SDSM is often used in research to downscale weather parameters such as precipitation and temperature in order to forecast future hydrological conditions. Most scientists and researchers have utilised a variety of statistical models to arrive at the conclusion that SDSM is one of the most reasonable and trustworthy approaches available. The Canadian global climate model predictor, for example, was used to assess three different types of models and conclude that SDSM is a more dependable and robust method than Long Ashton Research Station Weather Generator (LARS-WG) and the mathematical approach Artificial Neural Network (ANN).

The objective of this paper is to investigate the adaptability of SDSM for downscaling maximum temperature, and precipitation and to generate. As a result, the primary goal of this research is to evaluate the intensity of rainfall in three different scenarios. RCPs derived from CanESM2 data from the Global Climate Model in the Vadodara District.

For the span of 40 years (1981–2021), historical data of the Vadodara district were used, as well as global climate model data from CanESM2 under RCP8.5 for the year 2022–2101. The model was calibrated between 1981 and 2000, and then validated between 2001 and 2015.

The programme SDSM 4.2 was used in this work, which is a decision support tool for estimating local climate change consequences using a robust statistical downscaling technique. Dawson and Wilby created this software, which is written in Visual Basic 6.0.

The important aim is to see if the SDSM can be used to downscale the maximum temperature and precipitation in the Vadodara District at the same time.

SDSM can be used to apply the results of this work based on local-scale data to future emission scenarios.

Hassan and Harun (2011) describe the application of statistical downscaling method (SDSM) to downscale rainfall and temperature. Results of downscaling show that during the calibration and validation stage, the SDSM model can be well acceptable regard its performance in the downscaling of daily precipitation and temperature.

Soltani et al. (2016) studied changes in the spatial and temporal patterns of climate extreme indices were analyzed. Daily maximum and minimum air temperature, precipitation, and their association with climate change were used as the basis for tracking changes at 50 meteorological stations in Iran over the period 1975-2010.

Touseef et al. (2020) predict the climate change impacts on long-term precipitation trends. It deals with the analysis of observed historical (1960–2010) and arithmetic mean method in assembling precipitation from CMIP5 Global Climate Models (GCMs) datasets for a future period (2020–2099) under four emission scenarios.

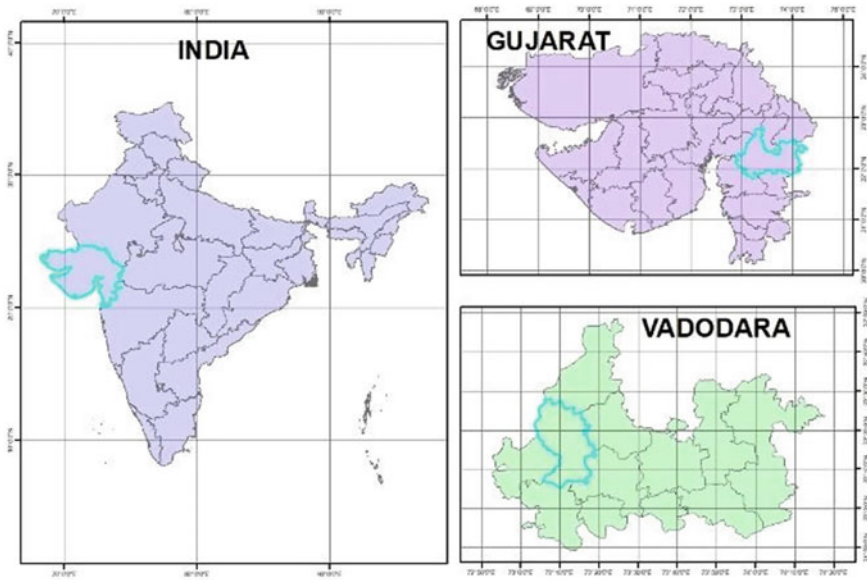
Tahir et al. (2017) studied historical data from nine weather stations and were collected for a period of 30 years (1976–2005) and global climate model data from CanESM2 for the period 2071–2100 under RCPs of RCP2.6, RCP4.5, and RCP8.5. The generated future rainfall data from 2071 to 2100 was then compared to the rainfall from 1976 to 2005, which served as a baseline. During the years 2071–2100, the RCP2.6 scenario showed an increase of 8.13 percent, whereas the RCP4.5 scenario showed a 14.7 percent increase. Under the RCP8.5 robust scenario, an abrupt increase of around 40.6 percent was recorded. As a result, it is concluded that, as a result of climate change, the future pattern of rainfall in the Limbang River basin is steadily increasing under all scenarios.

According to a study conducted by Hussain et al. (2015) the performance of the Statistical Downscaling Model (SDSM) constructed by annual and monthly sub-models for rainfall downscaling from Global Climate Models (GCMs) over two districts in Sarawak. According to the HadCM3 H3A2 and H3B2 scenarios, both stations show an increasing trend in future annual rainfall. By 2074, the annual rainfall in Belaga and Limbang is anticipated to increase by 37.8% and 22.7 percent, respectively, according to SDSM.

## 2 Material and Methods

### 2.1 Study Area

The study area is located in Gujarat's Vadodara District as shown in (Fig. 1). Vadodara District, also known as Vadodara District, is a district in Gujarat, India. It is located in the eastern section of the state. The administrative headquarters are in Vadodara,



**Fig. 1** Location of study area

which is located in the western half of the district. The district of Vadodara has a total area of 7,794 km<sup>2</sup>. The district has a population of 4,165,626 people in 2011, with 49.6 percent living in cities, 50.4 percent in rural areas, 5.3 percent belonging to scheduled castes, and 27.6 percent belonging to scheduled tribes. After Ahmadabad and Surat, it is Gujarat's third most populous district (out of 33) as of 2011. The climate in the Vadodara district is dry, with three distinct seasons: summer, winter, and monsoon.

## 2.2 Data Collection

For the years 1981 to 2021, NASA POWER was used to collect daily precipitation data. Before the analysis, the daily data were transformed to monthly, seasonal, and annual time scales.

The National Centre for Environmental Prediction (NCEP) provided the daily observed predictor dataset, which was mostly made up of reanalysis data made up of atmospheric variables, on a grid-scale of 22.2065 N latitude X 73.1822 longitude over a 40-year period (1981–2021). (Source: <http://www.cics.uvic.ca/scenarios/sdsm/select.cgi>).

There have been numerous initiatives taken to downscale for the present and future. To begin, the SDSM's inputs are predicted, and predictors are defined and

screened. Temperature and rainfall are employed as predictand datasets, and NCEP reanalysis predictors are used.

SDSM use multi-linear regression to alter predictands and predictors, a process known as calibration. Each station's present and prospective daily precipitation (rainfall) and temperature are being generated by the model. Daily rainfall and temperature series are used to determine monthly and annual rainfall and temperature.

SDSM is a downscaling tool for rainfall and temperature. The most important stage in SDSM is to establish a quantitative link between the predicted (observed) and the predictor. SDSM is further broken down into three sub-models: yearly, seasonal, and monthly. A regression equation is driven by all of these models. However, the annual sub-model produces a single equation for the entire year, whereas the seasonal sub-model derives the equation independently for each season. Monthly sub-model, on the other hand, develops the equation for each month separately. Furthermore, depending on the type of parameter to be downscaled, the sub-models may be conditional or unconditional. For example, the conditional model is suitable for downscaling rainfall while the unconditional model is appropriate for temperature downscaling.

The data utilised in this work for rainfall calibration is for 20 years (1981–2000), and the model was validated using data from 2001 to 2020. SDSM is used to construct a model for daily rainfall downscaling. In all eight stations, a regression equation is applied monthly, and the conditional sub-model is used. Ordinary Least Square (OLS) and Dual Simplex are two strategies for optimising the model in SDSM (DS).

Because OLS is faster than DS, it is being used. During the calibration and validation periods, the coefficients of correlation ( $r$ ) was utilised to assess the model's performance using historical and simulated data.

### **3 Results and Analysis**

#### ***3.1 Model Calibration and Validation***

In this study, observed data of 40 years are collected and divided into two time periods. 20 year of data are used for calibration of model and 20 years of data are used for validation of model. For validation process, Weather Generator SDSM 8.5 is used. It produces synthetic current daily weather data based on inputs of the observed time series' data, and the multiple linear regression parameters produced. 20 years of observed data, will be used in Weather Generator as independent observe data and not used during calibration procedure. (Fig. 2) shows a validation result of SDSM model downscaling of monthly rainfall during model validation period and (Fig. 3) depicts monthly maximum temperature during model validation period.

The rainfall validation results give a very close estimation of the monthly rainfall with observed rainfall. The coefficient of correlation is 0.99 which reveals that model is very good and can be used for future scenario generation.

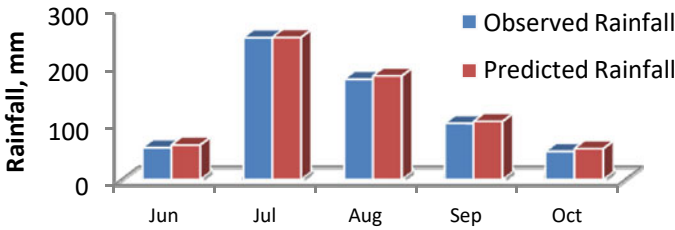


Fig. 2 Monthly rainfall during model validation period

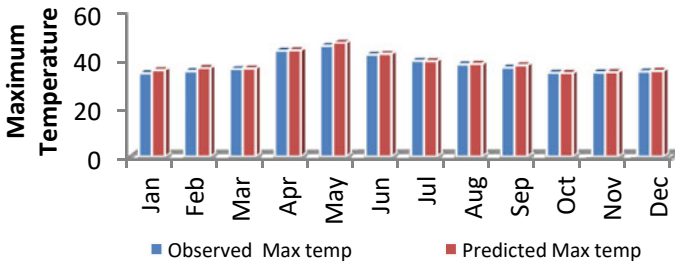


Fig. 3 Monthly maximum temperature during model validation period

Similarly the estimation of maximum temperature results are very close to the observed maximum temperature. The coefficient of correlation is 0.99 which reveals that model is very good and can be used for future scenario generation.

**Downscaling future maximum Temperature under climate change scenarios**

The SDSM software’s scenario generator was used to create ensembles of synthetic daily weather time series given a daily atmospheric predictor variable to downscale future emission scenarios. Decade wise scenarios are generated starting from 2021 to 2100. Our findings are based on CanESM2 scenarios, specifically RCP8.5, which were modelled in the SDSM to determine future rainfall for the years 2022–2101 under varied carbon emissions. Monthly maximum temperature is increasing in every month. The rate of increase is varying for each month. Figure 5 shows decade wise rate of increase of maximum temperature of January and May month. For the month of January maximum temperature is increasing at the average rate of 9.47% from 2021 to 2100 with respect to base period. Similarly for the month May, maximum temperature is increasing at the rate of 6.29% from 2021 to 2100 with respect to base period. The maximum increasing rate of maximum temperature is 10.22% for the month of July and minimum increasing rate is 1.27% for the month October is observed compared to base period.

Figure 4 shows maximum temperature generated decade wise from Year 2021–2100. It is observed that decade wise monthly maximum temperature is increasing in every month. The rate of increase is varying for each month. Figure 5 shows decade wise rate of increase of maximum temperature of January and May month.

For the month of January maximum temperature is increasing at the average rate of 9.47% from 2021 to 2100 with respect to base period. Similarly for the month May, maximum temperature is increasing at the rate of 6.29% from 2021 to 2100 with respect to base period. The maximum increasing rate of maximum temperature is 10.22% for the month of July and minimum increasing rate is 1.27% for the month October is observed compared to base period.

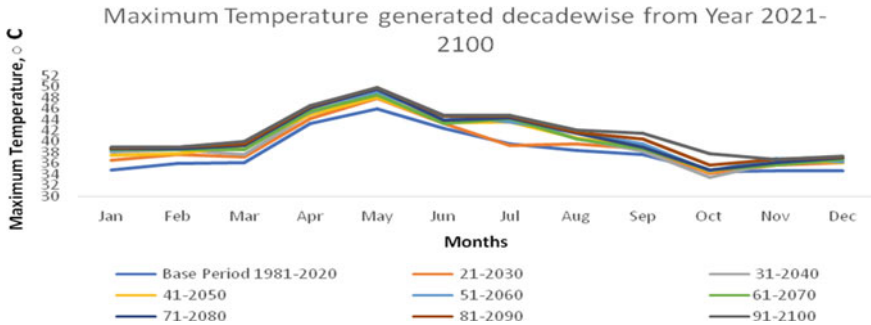


Fig. 4 Maximum temperature generated decade wise from Year 2021–2100

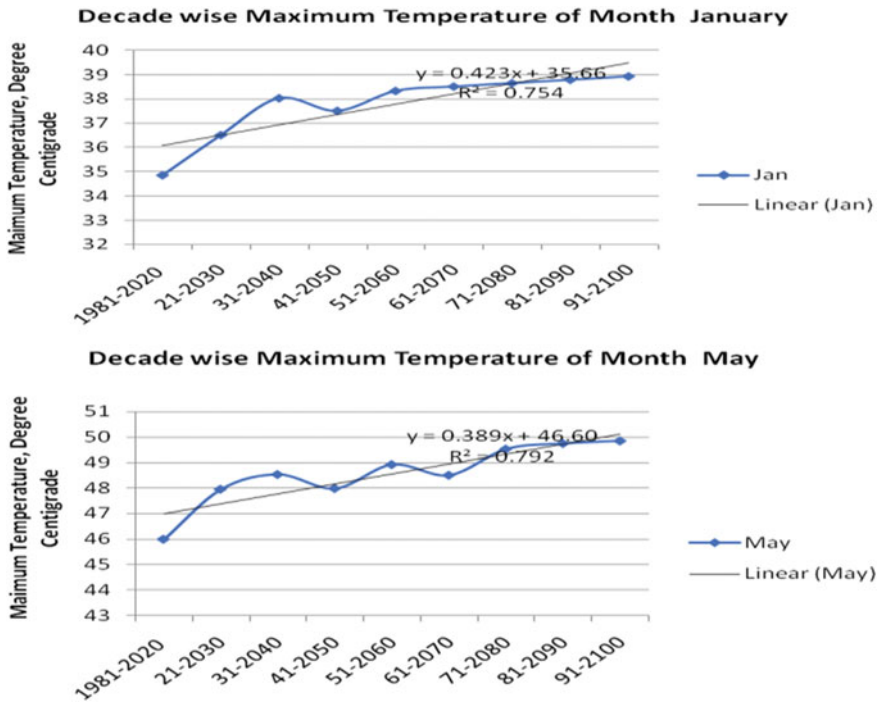
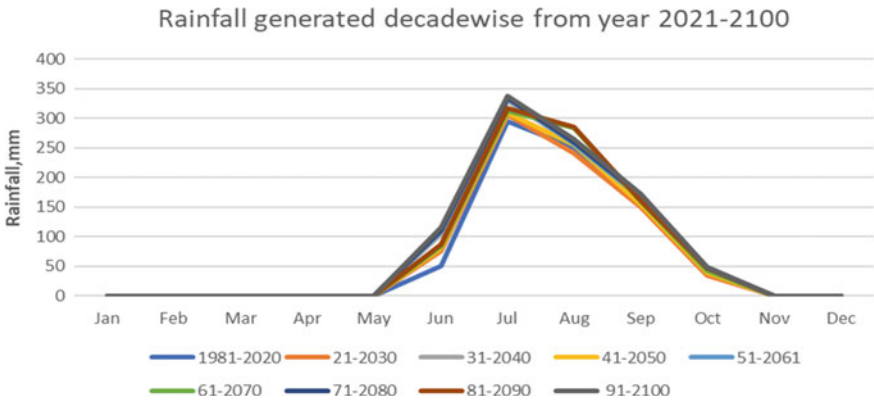


Fig. 5 Decade wise maximum temperature scenario generated



**Fig. 6** Rainfall generated decade wise from year 2021–2100

In (Fig. 5), the trend line shows that maximum temperature is increasing over a period of 1981 to 2100.

**Downscaling future Rainfall under climate change scenarios**

In Vadodara, the season with the most rainfall is from June to September, whereas the season with the least rainfall is from January to May.

Figure 6 shows rainfall generated decade wise from year 2021–2100. It is observed that decade wise monthly rainfall is increasing in each month. The rate of increase is varying for each month. Figure 7 shows decade wise rate of increase of rainfall of June and September month. For the month of June, rainfall is increasing at the average rate of 9.47% from 2021 to 2100 with respect to base period. Similarly for the month September, rainfall is increasing at the rate of 3.28% from 2021 to 2100 with respect to base period. The maximum increasing rate of rainfall is 64.72% for the month of June and minimum increasing rate is 3.28% for the month September is observed compared to base period. For September, it is observed that during 1981–2020, rainfall was decreasing but after 2021 rainfall is increasing for Vadodara.

In (Fig. 7), the trend line shows that rainfall is increasing over a period of 1981 to 2100.

This study’s findings may aid policymakers and responsible authorities in better planning water management and drainage systems in the future transition climate.

**4 Conclusions**

The SDSM generates the maximum temperature and rainfall very well during the calibration and validation period, as coefficient of correlation is 0.99 for both. The correlation between observed and forecasted maximum temperature and rainfall are very



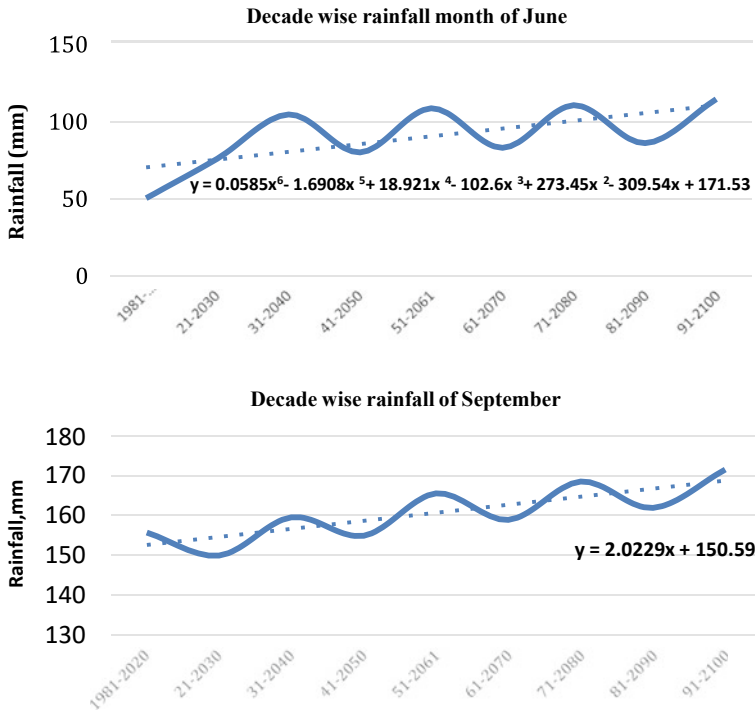


Fig. 7 Decade wise rainfall scenario generated

close, so it is concluded that SDSM can be efficiently used for the future prediction of weather parameters.

The scenario generated for maximum temperature indicates increase in maximum temperature for all Months but maximum increase is found for the month of July for Vadodara.

Rainfall scenario generated for rainfall reveals that compared to base period, there is overall increase in rainfall in all months, i.e. June, July, August, and September for the study area. The maximum increase of rainfall is in month June.

Vadodara is city which is surrounded by industrial areas as well as agricultural area. The increase in maximum temperature may increase crop water requirement. The policy makers or irrigation department needs to arrange more water for irrigation. Similarly, increase in rainfall may lead to flood situation in study area. Mitigation measures can be planned accordingly.

## References

- Hassan Z, Harun S (2011) Statistical downscaling for climate change scenarios of rainfall and temperature
- Hussain M, Yusof KW, Mustafa MR, Afshar NR (2015) Application of statistical downscaling model (SDSM) for long term prediction of rainfall in Sarawak, Malaysia
- Soltani M, Laux P, Kunstmann H, Stan K, Sohrabi MM (2016) Assessment of climate variations in temperature and precipitation extreme events over Iran
- Tahir T, Hashim AM, Yusof KW (2017) Statistical downscaling of rainfall under transitional climate in Limbang River Basin by using SDSM
- Touseef M, Chen L, Yang K, Chen Y (2020) Long-term rainfall trends and future projections over Xijiang River Basin, China

# A Non-parametric Test-Based Trend Analysis of the Rainfall and Temperature Pattern in the District of Bharuch, Gujarat



Khushboo A. Jariwala and Prasit G. Agnihotri

**Abstract** Rapid urbanization is a factor in climate change, which has negative effects on the environment. Change must occur as much as feasible in order to lessen the effects. Understanding the climatic conditions over years, if not decades, is necessary to analyze the shift. The temperature and rainfall patterns for a certain site are the most frequently researched climate change factors, however it differs from place to place. Therefore, both long-term trends and recent variations in rainfall and temperature in the Bharuch district are examined in this study. Researchers examined data on precipitation and temperature from 1981 to 2020. Statistical trend analysis methods like the Mann–Kendall test and Sen’s slope estimator were used to examine and analyze the problems. The annual maximum and minimum temperatures have showed a growing trend, whereas the monsoon’s maximum temperature has shown a falling trend, according to a thorough analysis of the statistics over the past 39 years. Throughout the monsoon season, rainfall is gradually increasing (Sen’s slope = 0.76). The lowest temperature trend was modestly warming or growing over the study period, while the maximum temperature trend was declining (Sen’s slope =  $-0.13$ ). The lowest temperature trend analysis result, however, is statistically significant at the 95 percent level of confidence, but the highest temperature trend analysis result is not.

**Keywords** Climate variability · M–K Test · Sen’s slope estimator · Trend analysis

## 1 Introduction

The climate is a crucial component of the earth’s system. Temperature, precipitation, air pressure, and humidity are only a few of the factors that affect the weather and climate. The term “climate is frequently used to describe the weather on a specific

---

K. A. Jariwala (✉) · P. G. Agnihotri  
Sardar Vallabhbhai National Institute of Technology, Ichchhanath, Surat 395007, India  
e-mail: [khushboojariwala247@gmail.com](mailto:khushboojariwala247@gmail.com); [pga@ced.svnit.ac.in](mailto:pga@ced.svnit.ac.in)

P. G. Agnihotri  
e-mail: [pga@ced.svnit.ac.in](mailto:pga@ced.svnit.ac.in)

day. It is, broadly speaking, the statistical evaluation of relevant features in terms of their mean and variability over time scales ranging from months to hundreds or millions of years (Solomon 2007). A major obstacle in the study of climate change detection is analyzing long-term changes in climatic variables. Several dataset extensions and improvements, as well as more difficult data analyses, have allowed for a greater understanding of past and present climate change throughout the world. Global climate change may cause long-term rainfall patterns to change, depleting water supplies and increasing the impact of hydrological extreme events like floods and droughts. Rainfall and temperature are the two main physical aspects of a region's climate that determine its environmental state, which has an impact on agricultural productivity (Singh et al. 2022; Kumar and Raj Gautam 2014; Modarres and Silva 2007). The timely availability of sufficient water supplies and a favorable environment in any location are requirements for the security of food, energy, and related industries. The amount of rainfall that an area receives impacts how much water is available to support a variety of needs, including those for agriculture, industry, home water supply, and hydroelectric power generation. Rainfall patterns and levels are the most significant factors that affect agriculture because agriculture is very important to India's economy and people's livelihood (Kumar and Raj Gautam 2014; Gajbhiye et al. 2016). Millions of India's numerous citizens still rely on agricultural products for their livelihood despite recent technological improvements. For millions of people, agriculture provides their primary source of income, and the majority of their crops depend on seasonal rainfall. Due to the lack of analysis in this region and the current data analysis is not sufficient to overcome the water scarcity for different purposes and to maintain the environmental balance. This analysis will ensure that how much amount of water management will help to use available water and to maintain the water levels below the ground for future needs without damaging environmental conditions.

The temperature and rainfall, two essential climate study variables, are examined in-depth in this article. Temperature and temperature variations have an effect on a number of hydrological processes, including rainfall (Smadi 2006; Tabari and Talae 2011). These processes then influence temperature. Trend study of temperature, rainfall, and other climatic variables on various geographical scales can aid in the creation of future climate scenarios (Arora et al. 2005; Addisu et al. 2015; Wanishsakpong et al. 2016). As a result, this study's objective is to examine how frequently it rains and how hot it gets in Bharuch, one of Gujarat's poorest districts. The monthly swings were typically forecast with the monsoon season (June–September) in mind after looking at the seasonal tendencies of both parameters on an annual basis. Knowing the local weather and rainfall patterns is necessary for this. The targeted region might handle agricultural, irrigation, and other water-related operations more skillfully if it understood the uncertainties connected to rainfall and temperature trends.

## 1.1 Materials and Methods

### Bharuch District

Bharuch district is one of the oldest districts in India located in west and in south-east region in Gujarat as shown in Fig. 1. Bharuch district lies between north latitudes 21.4399 N to 22.2354 N and east longitudes 72.5377 E to 73.4826 E and is typically 15 m above sea level. Vadodara is located in the north, Narmada Vadodara is in the east, and Surat Vadodara is in the south. Its western border is formed by the Gulf of Khambhat as shown in Figs. 1 and 2.

In Bharuch, which has a tropical savanna environment, the Arabian Sea has a significant role in controlling the weather. Early March through the end of June mark the start of the summer season. With maximum average temperatures of roughly 40 °C, April and May are the warmest months.

The monsoon season, with an average rainfall of 800 mm, begins in late June and lasts until September (31 inches). During these months, the highest temperature is typically around 32 °C (90 °F). Up until late November, when winter officially starts, the temperature starts to rise again in October. December to late February is considered winter, when temperatures often hover around 23 °C (73 °F).



**Fig. 1** Location map of Bharuch in Gujarat State



Fig. 2 Administrative Map of Bharuch District. Source Maps of India

### 1.2 Data Collection

From 1980 to 2017, the India Meteorological Department in Pune provides monthly average observed station data for rainfall, maximum and lowest temperatures for the district of Bharuch (37 years). The “Imputation (most frequent)” strategy, a statistical technique for substituting missing data with the most common values within each column, was used to impute the missing values.

Trend is characterized as the long-term change in the dependent variable or the overall movement of a series over a significant amount of time. Trend is influenced by the temporal resolution of rainfall and its relationship to temperature. To evaluate the importance of temperature and rainfall patterns, statistical techniques like regression analysis and the coefficient of determination  $R^2$  are applied. The MKT trend test was used to identify and assess the trend, and the least squares approach was used to determine the slope of the regression line. To analyze the link, the average, standard deviation, and coefficient of variation (CV) of rainfall and temperatures were calculated.

### 1.3 Mann-Kendell Test

A nonparametric statistical test called the M–K test is used to analyze trends in time series data from climatology and hydrology (Mann 1945). Since Mann first established the test in 1945, environmental time series have routinely employed it. The decision to take this test has two benefits. The data does not have to be evenly distributed because it is a nonparametric test. Due to inhomogeneous time series, the test is less sensitive to unexpected breakdowns. The null hypothesis H0 states that there is no trend in this test (the data is independent and randomly ordered). Comparing this to alternative hypothesis H1, which asserts that a trend exists, The M–K statistic is calculated using the formula shown below:

$$S = \sum_{k=1}^{n-1} \sum_{j=k+1}^n \text{sgn}(x_j - x_k)$$

The trend test is performed on a time series  $X_k$ , which is ranked from  $k = 1, 2, 3, \dots, n_1$  and  $j = i + 1, i + 2, i + 3, \dots, n$ . As a reference point, each of the data points  $x_j$  is used.

$$\begin{aligned} \text{sgn}(x_j - x_k) &= 1 \text{ if } x_j - x_k > 0 \\ &= 0 \text{ if } x_j - x_k = 0 \\ &= -1 \text{ if } x_j - x_k < 0. \end{aligned}$$

This particular test was computed using the XLSTAT 2017 application. Indicating an upward tendency is a very high positive S number, while a very low negative value suggests a downward trend. In order to establish if a trend is statistically significant, the Z value is utilized.

### 1.4 Sen’s Slope Estimator Test

A nonparametric technique for determining the size of a time series trend is Sen’s estimate (Sen 1968). Sen’s nonparametric method was used in the test to establish the true slope of an existing trend, such as the rate of change over time, using the XLSTAT 2017 program. A positive Sen’s slope value denotes an upward or developing trend in the time series, whereas a negative value denotes a downward or declining trend.

## 2 Results and Discussion

### 2.1 Results

According to a trend analysis of numerous studies (Jain and Kumar 2012), nonparametric approaches are widely employed, with the M-K test (Mann 1945) being one of the finest of them and chosen by many researchers. The descriptive statistics for rainfall, including mean, SD, coefficient of variation, kurtosis, and skewness, are discussed in Table 1. The research region has the maximum rain during the monsoon season, which lasts from June to September, as seen by the monthly rainfall pattern shown in Fig. 3. Figure 6 shows the seasonal rainfall distribution in the study region. According to the collected figures, the monthly average rainfall's coefficient of variation (CV) runs from 55 to 358%. The highest kurtosis coefficient, at 29.47, and the highest skewness, at 5.45, were both found in the month of February.

Tables 2 and 3 contain the recorded temperature data as well as descriptive statistics for the highest and lowest temperatures, including mean, standard deviation, coefficient of variation, skewness, and kurtosis, respectively. Even while the CV for the highest and lowest temperature is less than that for rainfall, the skewness and kurtosis values show more extreme variation. The findings from the analysis of the observed data for the years 1981 to 2020 are displayed in Figures 4 and 5. Both of these numbers unequivocally demonstrate that the highest and lowest temperatures are greater in the months preceding monsoons and lower during monsoon seasons. The maximum and lowest temperature data from 1981 to 2020 were analyzed for seasonal changes, although these trends are not very important in terms of temperature. The examination of the highest and lowest temperature trends is shown in Figures 7 and 8, respectively (Fig. 6).

The M-K test is also used in trend analysis. The M-K test is a nonparametric technique for determining if a variable displays a monotonic upward or decreasing trend over time. The statistics (Table 1) show that there is no trend in any of the research areas' seasonal rainfall patterns. Over the period 1981–2019, rainfall patterns are not statistically significant, and the finding is not significant at the 95% confidence level. Averaged over all of the recorded period, the greatest temperature trend demonstrated a slight warming or increasing tendency (Sen's slope =  $-1.621$ ), whilst the lowest temperature trend showed a cooling tendency (Sen's slope =  $0.1498$ ). However, the lowest temperature trend analysis result, as opposed to the highest temperature trend analysis result, is not statistically significant at the 95% level of confidence.

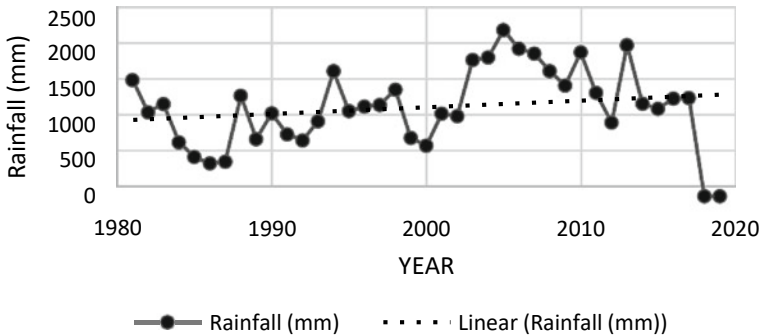
### 2.2 Discussion

Since rainfall has such a big impact on how water is used in different places, researchers and legislators must consider the unpredictable nature of meteorological circumstances when making decisions. Box and whisker plots were initially



**Table 1** Descriptive statistics for rainfall

Statistic	Jan	Feb	Mar	Apr	May	Jun	Jul	Aug	Sep	Oct	Nov	Dec
Nbr. of observation	39.00	39.00	39.00	39.00	39.00	39.00	39.00	39.00	39.00	39.00	39.00	39.00
Minimum	0.00	0.00	0.00	0.00	0.00	6.77	18.45	5.46	1.58	0.13	0.00	0.00
Maximum	13.76	37.59	23.26	12.10	63.38	962.19	1007.06	793.96	491.63	172.81	69.72	32.27
1st Quartile	0.01	0.01	0.01	0.08	0.22	81.31	253.75	169.39	74.61	14.54	0.08	0.01
Median	0.07	0.08	0.07	0.62	1.50	157.96	476.77	265.18	176.39	24.21	0.71	0.04
3rd Quartile	1.02	0.93	0.64	1.94	5.37	355.69	651.18	384.50	295.46	66.27	4.13	0.67
Mean	1.34	1.70	1.39	1.53	7.67	240.91	455.32	296.65	189.63	42.64	7.74	1.68
Variance ( $n-1$ )	8.99	37.17	15.96	6.37	216.79	45,682.55	63,848.68	34,537.99	19,385.95	1999.07	278.68	28.62
Standard dev	3.00	6.10	4.00	2.52	14.72	213.73	252.68	185.84	139.23	44.71	16.69	5.35
Skewness (P)	2.97	5.45	4.55	2.76	2.47	1.40	0.09	0.89	0.35	1.52	2.78	5.03
Kurtosis (Pearson)	8.24	29.47	21.58	7.96	5.29	1.92	-0.78	0.55	-0.95	1.82	7.09	25.95



**Fig. 3** Trend analysis for rainfall (mm)

used to show changes in monthly rainfall. Box and whisker plots (Tukey 1977) have a compact structure that allows for side-by-side comparisons of multiple datasets, in contrast to more thorough representations like the histogram (Banacos 2011). The statistical distribution is shown visually in these graphs in a way that is simple to comprehend.

The median of the box and whisker figure is shown by a horizontal line, while the top and bottom horizontal lines illustrate the interquartile range (shown by the box). The 25th and 75th percentiles are shown by the horizontal lines at the bottom and top of the boxes, respectively. Vertical lines display outside ranges (as shown by the whiskers). If the median line is stretched outside significantly from the center, the distribution may be skewed. The interquartile range (box), which indicates the dataset's middle 50% relative dispersion, is shown by the length of each whisker, which represents the dataset's outer range (10th to 25th percentiles and 75th to 90th percentiles) (Banacos 2011). Since the vast majority of the values are in the top whisker, or fourth quartile, it is obvious that the dataset is not normally distributed.

Low ( $CV < 20\%$ ), moderate ( $20\% < CV < 30\%$ ), high ( $CV > 30\%$ ), extremely high ( $CV > 40\%$ ), and  $CV > 70\%$  are the categories used to categorize the degree of variability.  $CV > 70\%$  indicates exceptionally high inter-annual variability of rainfall. According to the data, it was discovered that every month had a  $CV$  of at least 30%, emphasizing the region's substantial precipitation variability. According to the statistics, the amount of rainfall in the area varies greatly.

Since the kurtosis values and the skewness value are lower in the monsoon months, it is evident from the kurtosis values analysis that the dataset is light tailed and exhibits a symmetric pattern (July, August, and September). In other words, the area under investigation experiences symmetrical patterns of rainfall throughout the monsoon season. The post- and pre-monsoon months, however, exhibit a high kurtosis value in the dataset, showing that rainfall during these months is strongly tailed, reflecting the occurrence of outliers or extreme values. The studied area's rainfall is fundamentally uneven before and after the monsoon season. Understanding the behavior of surface air temperature, which can change geographically and temporally on local, regional, and global scales, is essential for understanding climatic variability. One of

**Table 2** Descriptive statistics for maximum temperature

Statistic	No. of observations	Minimum	Maximum	1st Quartile	Median	3rd Quartile	Mean	Variance (n)	Standard deviation (n)	Variation coefficient (n)	Skewness	Kurtosis (Pearson)
Jan	40.0	26.2	29.7	27.3	27.7	28.2	27.8	0.6	0.8	0.0	0.4	0.4
Feb	40.0	27.2	31.3	28.2	28.8	29.2	28.8	0.7	0.8	0.0	0.4	0.4
Mar	40.0	30.0	33.4	31.0	31.4	32.1	31.5	0.6	0.8	0.0	0.3	-0.4
Apr	40.0	31.7	35.3	33.1	33.4	33.8	33.4	0.5	0.7	0.0	-0.3	1.1
May	40.0	32.0	35.0	33.3	33.6	34.0	33.6	0.4	0.6	0.0	-0.2	0.6
Jun	40.0	30.0	33.0	31.2	31.7	32.1	31.6	0.5	0.7	0.0	-0.3	-0.3
Jul	40.0	27.9	30.6	28.7	29.1	29.4	29.1	0.3	0.5	0.0	0.3	0.7
Aug	40.0	27.3	29.8	27.9	28.3	28.6	28.3	0.2	0.5	0.0	0.5	0.8
Sep	40.0	28.1	30.9	28.7	29.0	29.4	29.1	0.3	0.6	0.0	0.8	0.8
Oct	40.0	29.1	33.7	30.1	30.9	31.6	31.0	1.3	1.2	0.0	0.6	-0.4
Nov	40.0	28.6	32.8	29.9	30.7	31.7	30.7	1.2	1.1	0.0	0.0	-0.8
Dec	40.0	26.6	30.5	28.6	29.1	29.5	29.0	0.7	0.8	0.0	-0.7	0.3
Winter	40.0	27.4	29.4	27.9	28.4	28.7	28.4	0.3	0.6	0.0	0.1	-0.8
Spring	40.0	28.7	31.3	29.6	30.2	30.6	30.2	0.4	0.6	0.0	-0.1	-0.7
Summer	40.0	31.8	33.9	32.4	32.9	33.2	32.9	0.2	0.5	0.0	-0.1	-0.5
Monsoon	40.0	27.8	30.2	28.4	28.6	28.9	28.7	0.2	0.5	0.0	0.6	1.5
Autumn	40.0	28.9	32.4	29.6	30.2	30.8	30.3	0.7	0.8	0.0	0.6	-0.1

**Table 3** Descriptive statistics for minimum temperature

Statistic	No. of observations	Minimum	Maximum	1st Quartile	Median	3rd Quartile	Mean	Variance (n)	Standard deviation (n)	Variation coefficient (n)	Skewness (Pearson)	Kurtosis (Pearson)
Jan	39.0	16.9	20.7	18.4	18.9	19.5	18.9	0.7	0.8	0.0	-0.1	-0.2
Feb	39.0	17.4	21.6	19.5	19.8	20.5	19.9	0.9	0.9	0.0	-0.4	0.3
Mar	39.0	21.1	23.7	22.2	22.6	23.0	22.6	0.4	0.6	0.0	-0.1	-0.4
Apr	39.0	23.7	26.5	25.0	25.3	25.6	25.3	0.3	0.6	0.0	-0.3	0.4
May	39.0	26.5	28.6	27.0	27.4	27.7	27.4	0.2	0.5	0.0	0.3	-0.3
Jun	39.0	27.2	28.6	27.8	28.0	28.3	28.0	0.1	0.3	0.0	-0.2	-0.9
Jul	39.0	26.2	27.6	26.6	26.9	27.2	26.9	0.1	0.4	0.0	0.0	-1.0
Aug	39.0	25.2	27.2	25.8	26.0	26.2	26.0	0.2	0.4	0.0	0.3	0.4
Sep	39.0	24.7	26.8	25.6	25.9	26.2	25.9	0.2	0.5	0.0	-0.5	0.0
Oct	39.0	23.5	26.4	24.5	25.0	25.4	25.0	0.4	0.7	0.0	0.0	-0.6
Nov	39.0	19.9	24.7	21.9	22.8	23.6	22.6	1.3	1.1	0.1	-0.3	-0.5
Dec	39.0	18.6	21.8	19.6	20.4	20.9	20.3	0.6	0.8	0.0	-0.2	-0.9
Winter	39.0	18.4	20.8	19.2	19.6	19.9	19.6	0.3	0.5	0.0	0.0	-0.3
Spring	39.0	19.7	22.5	21.0	21.2	21.8	21.2	0.4	0.7	0.0	-0.4	-0.1
Summer	39.0	26.1	27.9	26.7	26.8	27.2	26.9	0.1	0.4	0.0	0.2	-0.1
Monsoon	39.0	25.8	27.4	26.2	26.4	26.7	26.4	0.1	0.4	0.0	0.2	-0.5
Autumn	39.0	23.4	25.7	24.2	24.4	24.9	24.5	0.3	0.5	0.0	0.1	-0.6

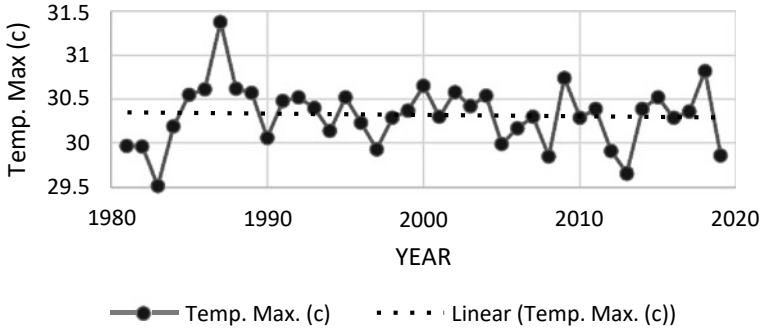


Fig. 4 Trend analysis for maximum temperature

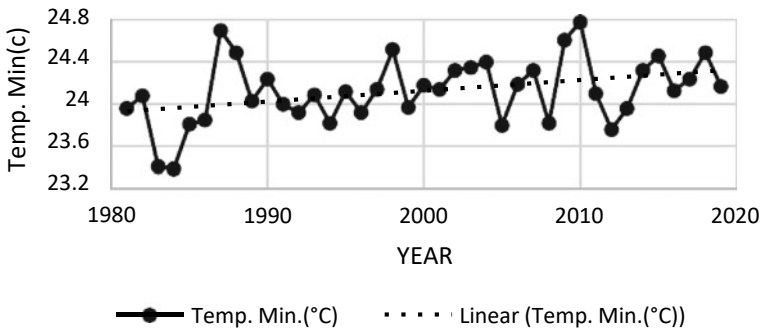


Fig. 5 Trend analysis for minimum temperature

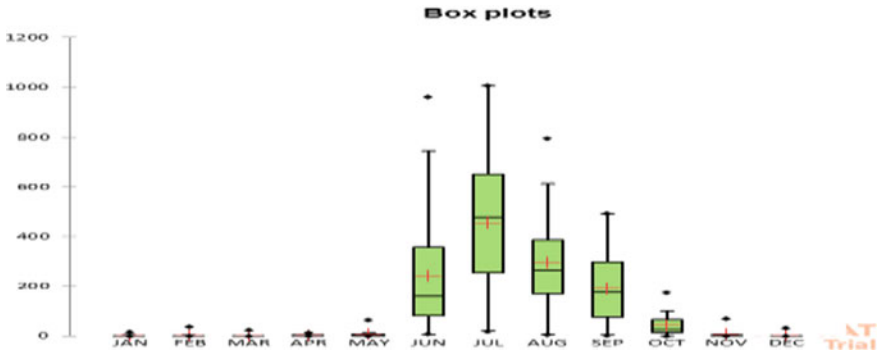


Fig. 6 Boxplot diagram for rainfall

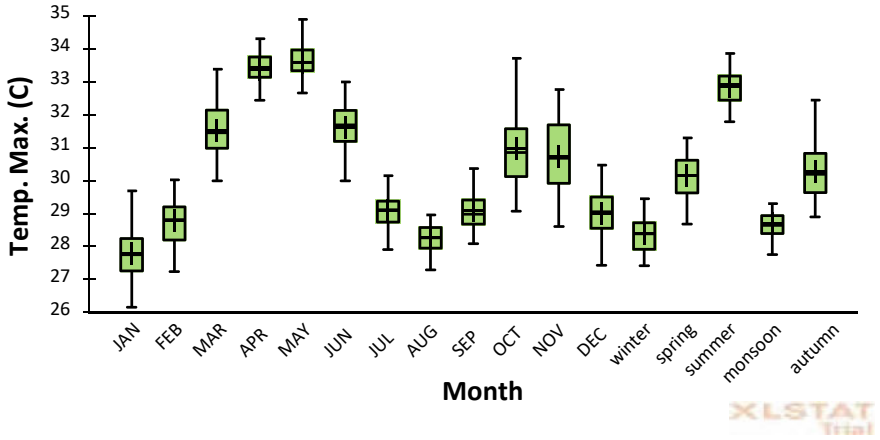


Fig. 7 Boxplot diagram for maximum temperature

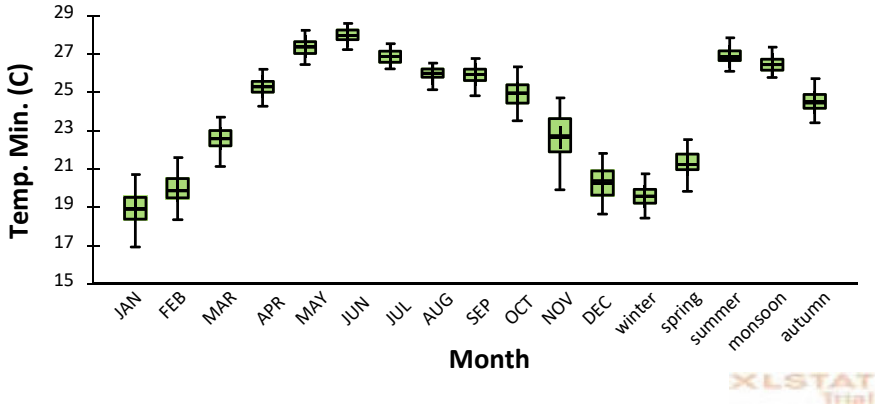


Fig. 8 Boxplot diagram for minimum temperature

the most crucial variables in forecasting weather and climate is surface air temperature (Ghasemi 2015). Despite the plethora of evidence for rising global temperatures, precise temporal trend forecasting remains difficult (Gil-Alana 2018). Similar to how air temperature impacts the water cycle in the research area, a thorough investigation of the nature of its occurrence is necessary. The monthly maximum and lowest temperatures show a falling tendency even though the study region experiences its highest rainfall in July, August, and September. Additionally, the temperature rises both before and after the monsoon season. Figure 6 displays the seasonal mean maximum temperature and its trend over the time period under consideration.

### 3 Conclusions

Gujarat has a long history of climatic change and unpredictability, and the Bharuch region is no exception. In the study locations, there are frequent climatic variations or shifts. Climate change exacerbates already existing social and economic problems in this region since communities there rely mostly on resources that are climate-sensitive, particularly wet agriculture. Reduced societal, economic, and personal losses may result from improved ability to adjust to severe future climatic unpredictability. Since more than 80% of agriculture depends on rain, rainfall, and temperature are the two primary climatic variables in the area. The current study looked at weather data for the Gujarati city of Bharuch. The time series was examined using Sen's slope estimator and the nonparametric M–K test, two well-known methods for trend analysis. The variability analysis, monthly rainfall, maximum temperature, and minimum temperature are all represented using box and whisker graphs.

The plots show that the monsoonal months, from June through September, receive the most rainfall, despite the fact that the variation in maximum and minimum temperatures is roughly the same for all months. To suggest that because rainfall is the main factor driving agricultural growth in the studied region, its extreme occurrence during monsoon, as well as post- and pre-monsoon months, is crucial to growth. An underdeveloped region, such as Bharuch district, is particularly vulnerable to significant influences of climate variability, particularly rainfall variability.

The inquiry has shown that the maximum and lowest temperatures in the research region do not vary much over the course of the year, and as a result, temperature variations are not anticipated to have an impact on agricultural output. The parties involved should consider rainfall variability and general temperature variance in order to plan for climate change.

**Acknowledgements** The India Meteorological Department in Pune provided the information we needed for our study, and we appreciate their quick response. The tutorials and user-friendliness of programs like ArcGIS 10.2, R, and XLSTAT, which were used to make the graphs in this piece, deserve praise. The resources and responsiveness of the library and computer center of the Sardar Vallabhbhai National Institute of Technology, Surat, would definitely be lauded.

### References

- Addisu S, Selassie YG, Fissaha G, Gedif B (2015) Time series trend analysis of temperature and rainfall in lake Tana Sub-basin, Ethiopia. *Environ Syst Res* 4(1):1–2
- Arora M, Goel NK, Singh, P (2005) Evaluation de tendances de température en Inde. *Hydrol Sci J* 50(1):81–93
- Banacos PC (2011) Box and whisker plots for local climate datasets: interpretation and creation using excel 2007/2010
- Gajbhiye S, Meshram C, Singh SK, Srivastava PK, Islam T (2016) Precipitation trend analysis of Sindh River basin, India, from 102-year record (1901–2002). *Atmos Sci Lett* 17(1):71–77

- Ghasemi AR (2015) Changes and trends in maximum, minimum and mean temperature series in Iran. *Atmos Sci Lett* 16(3):366–372
- Gil-Alana LA (2018) Maximum and minimum temperatures in the United States: Time trends and persistence. *Atmos Sci Lett* 19(4)
- Jain SK, Kumar V (2012) Trend analysis of rainfall and temperature data for India
- Kumar R, Raj Gautam H (2014) Climate change and its impact on agricultural productivity in India. *J Climatol Weather Forecast* 2(1)
- Mann HB (1945) Nonparametric tests against trend
- Modarres R, da Silva VD (2007) Rainfall trends in arid and semi-arid regions of Iran. *J Arid Environ* 70(2):344–355
- Sen PK (1968) Estimates of the regression coefficient based on Kendall's tau. *J Am Stat Assoc* 63(324):1379–1389
- Singh U, Agarwal P, Sharma PK (2022) Meteorological drought analysis with different indices for the Betwa River basin, India. *Theoret Appl Climatol* 148(3–4):1741–1754
- Smadi MM (2006) Observed abrupt changes in minimum and maximum temperatures in Jordan in the 20th century. *Am J Environ Sci* 2(3):114–120
- Solomon S (2007) *Climate change 2007: the physical science basis : contribution of working group I to the fourth assessment report of the intergovernmental panel on climate change*. Cambridge University Press
- Tabari H, Talaei PH (2011) Analysis of trends in temperature data in arid and semi-arid regions of Iran. *Glob Planet Change* 79(1-2):1–10
- Tukey (1977) *Exploratory data analysis*
- Wanishakpong W, McNeil N, Notodiputro KA (2016) Trend and pattern classification of surface air temperature change in the Arctic region. *Atmos Sci Lett* 17(7):378–383



# Role of Changing Atmospheric Temperature and Radiation on Sea Ice Conditions Over Laptev and Greenland Seas for the Recent Decade



Dency V. Panicker, Bhasha H. Vachharajani, and Rohit Srivastava

**Abstract** The recent climate change coupled with extreme anthropogenic activities which enhance greenhouse gases has highly impacted the existence of sea ice over the Northern Poles. The temperature rise has a first-order impact on sea ice conditions over the Arctic. Analyses of seas, namely the Laptev and Greenland seas give a general understanding of the influence of these atmospheric parameters (air temperature, sea surface temperature and outgoing longwave radiation) on the cryosphere (sea ice area, sea ice extent and sea ice concentration) for the recent time scales; 2012–16 and 2017–21. Laptev being a marginal sea of the Arctic shows high variability in sea ice area compared with the Greenland Sea which is only an outlying portion of the Arctic Ocean. While classifying the life cycle of sea ice into the growth and decay phase, it is observed that the temperatures are high during 2017–21 compared with those during 2012–16. During the growth phase of sea ice, over Laptev, 2012–16  $r^2_{(SIA, SST)} = 0.69$  and  $r^2_{(SIA, T2M)} = 0.74$  is lower compared to  $r^2_{(SIA, SST)} = 0.92$  and  $r^2_{(SIA, T2M)} = 0.76$  during 2017–21. Similarly over Greenland Sea,  $r^2_{(SIA, SST)} = 0.88$  and  $r^2_{(SIA, T2M)} = 0.70$  during the time frame: 2012–16 and  $r^2_{(SIA, SST)} = 0.89$  and  $r^2_{(SIA, T2M)} = 0.84$  during the period: 2017–21. Since outgoing longwave radiation positively influences both the seas during both spans;  $r^2_{(SIA, OLR)} = 0.76$  for Laptev and  $r^2_{(SIA, OLR)} = 0.37$  for the Greenland Sea show positive trend. The sea ice extent and area trends vary widely by month depending on region and season. For both Laptev and Greenland Seas, the influence of temperatures is seen more during the growing season than the melt, indicating the recent hike in winter warming causing

---

D. V. Panicker (✉) · R. Srivastava  
Department of Physics, School of Energy Technology, Pandit Deendayal Energy University,  
Gandhinagar, Gujarat, India  
e-mail: [vpanickerdency@gmail.com](mailto:vpanickerdency@gmail.com)

R. Srivastava  
e-mail: [rohit.prl@gmail.com](mailto:rohit.prl@gmail.com)

B. H. Vachharajani  
Department of Mathematics, School of Technology, Pandit Deendayal Energy University,  
Gandhinagar, Gujarat, India  
e-mail: [bhasha.vachharajani@sot.pdpu.ac.in](mailto:bhasha.vachharajani@sot.pdpu.ac.in)

Arctic amplification. This work demonstrates the importance and the extent of influence of atmospheric temperatures and outgoing longwave radiation on the sea ice conditions over the two geographically distinct seas of the Arctic.

**Keywords** Sea ice concentration · Sea ice area · Sea ice extent · Laptev Sea · Greenland Sea

## 1 Introduction

A small change in the atmospheric condition over a long time (climate) has always altered the sea ice condition over the poles (Alekseev et al. 2001). The existence of these, so-called refrigerators of the globe (poles) are very vital for the proper sustenance of Earth's ecosystem (Gawor et al. 2016). The atmospheric circulation; mainly polar cells highly play a role in maintaining the Earth's global temperature (Qian et al. 2015). In Antarctica, it is the ice or the glaciers that are formed over the land, while over the Arctic it is the seawater which freezes to form sea ice (Hellmer, 2004). In the Arctic, these ice are highly delicate as small changes in the atmospheric-oceanic interaction can alter their existence altogether. Some of the factors like temperature, wind and current highly weigh a major responsibility in causing variation in the formation and decay process of sea ice conditions (Laidler et al. 2008). On the contrary, over Antarctica, it is only the interaction with the atmosphere that needs to be considered. However one cannot overlook the fact that this continent has ice anchored to its shores—known as fast ice (Fraser et al. 2012). But the distinct characteristics of these ice are that they cannot be moved by winds or currents (Heil 2006). Therefore in the case of Antarctica, the oceanic factors influencing the condition of ice/glaciers can be neglected at least to a small extent. Due to the aforementioned concerns raised over the Arctic region as a whole, the regions over this circle are considered due to the scientific and potential attention it demands.

Therefore to understand the interaction of developing sea ice with the atmosphere above it, parameters like sea surface temperature (SST), temperature above 2 m (T2M) and outgoing longwave radiation (OLR) are considered throughout this paper. The Arctic climatic condition has already taken a one-eighty-degree turn due to the increase in greenhouse gases which are emitted by various human intervening anthropogenic activities (Wang and Overland 2012). As the amount of ice cover over the sea deteriorates, more appearance of open water enhances the warming effect by absorbing more heat into the system (Bintanja et al. 2011). The latent heat capacity of water is higher, it holds on to this heat for a prolonged period of time causing the openings to widen further. This is one of the reasons for the rise in winter warming and the weakening of the seasonal cycle (Bintanja and Van der Linden 2013). Such changes also attribute to the concurrent anomaly patterns of SST. SST over the Arctic are highly influenced by the formation of the North Atlantic oscillation (NAO) (Singh et al. 2013). This oscillation basically develops due to the pressure difference between

the Azores and Iceland (Chepurin and Carton 2012). These NAO have the potential to alter the temperature at the surface to a great extent.

Further, the change in air temperature is also seen to impact the melting of sea ice to a greater extent. The rate of change in temperature above 2 m is often governed by the horizontal advection and diabatic heating of the atmosphere (Hurrell et al. 2003). Such horizontal advection is even likely to aggravate extratropical cyclones which may cause the transport of heat and energy in a poleward direction. Apart from the heat that prevails over the surface, it is vital to look into the radiative processes which also govern the atmosphere. The atmospheric energy budget is often maintained by the emission of longwave radiation back into the atmosphere (Serreze et al. 2011). A series of moisture and heat advection into the atmosphere alters the longwave fluxes of the Arctic (Hartmann 1994; Shah et al. 2020) causing large-scale variability in atmospheric circulation and thereby influencing the radiation budget over the region (Kapsch et al. 2016).

Considering all the changes in the atmosphere which are evidently visible, the study attempts to understand the influence of these parameters on the sea ice condition. Therefore the two seas, namely the Laptev Sea and the Greenland Sea are taken and their sea ice conditions are associated with the atmospheric variables to understand the degree of influence during both; the growth stage and decay stage of sea ice for the spans; 2012–16 and 2017–21 (five years each). The study yields a general understanding of the current state of these seas with respect to their cryospheric entities.

## 2 Study Domain

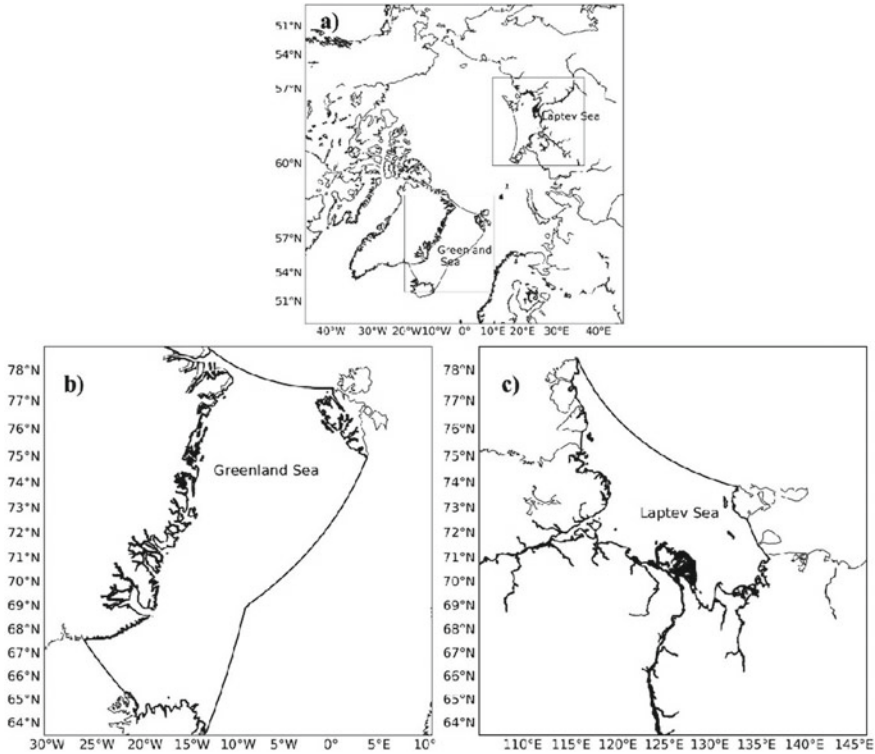
Detailed topography of the two considered marginal seas; the Laptev Sea and the Greenland Sea is mentioned in the upcoming section.

### 2.1 Laptev Sea

Laptev Sea is a marginal sea of the Arctic Ocean off the coast of Northern Siberia bounded by the Taymyr Peninsula and the islands of Severnaya Zemlya on the west and by the New Siberian Islands and Kotelnny Island on the east (Cox et al. 2016), with coordinates 105–150°E and 63–79°N (Fig. 1). Laptev Sea is known as the birthplace of ice<sup>1</sup> and is, therefore, the chief source of Arctic sea ice. The sea has an average outflow of 483,000 km<sup>2</sup>/year (estimated during the period 1979–95) (Ghosh 2021). It is therefore considered one of the significant regions of net ice production and

---

<sup>1</sup> Alarm as Arctic Sea ice not yet freezing at latest date on record (25 August 2021). The Guardian. <https://www.theguardian.com/world/2020/oct/22/alarm-as-arctic-sea-ice-not-yet-freezing-at-latest-date-on-record>.



**Fig. 1** Region of interest **a** Location of Laptev and Greenland Sea over the Arctic Circle, **b** Laptev Sea and **c** Greenland Sea

export (Itkin and Krumpfen 2017, Zakharov 1966). Laptev is extremely shallow, with water depths between 15 m and 200 m (Dethleff et al. 1998), and comprises an area of  $\sim 500 \times 10^3 \text{ km}^2$ . The sea ice over the sea is formed towards the coast during early winter, later it drifts west across the Arctic, before breaking up in the spring into the Fram Strait located between Greenland and Svalbard.

If ice is formed after winter then it will be thinner compared with the previous one (during winter) and thus is more likely to melt before it reaches the Fram Strait. The topography of the sea is also seen to have an intense impact. The sea experiences heat waves from its neighbouring part of Siberia. During this phase, the surface air temperature was reported to be  $38 \text{ }^\circ\text{C}^2$  over the south of Laptev Sea. Often this heat was an aftermath of the winds that predominantly brought hot continental air towards the sea<sup>3</sup> further making the sea ice push itself north.

<sup>2</sup> Reported new record temperature of  $38 \text{ }^\circ\text{C}$  north of Arctic Circle. (8 July 2020). World Meteorological Organization. <https://public.wmo.int/en/media/news/reported-new-record-temperature-of-38%C2%B0c-north-of-arctic-circle>.

<sup>3</sup> Arctic Sea ice. (n.d.). Copernicus. <https://climate.copernicus.eu/esotc/2020/arctic-sea-ice>.

## 2.2 Greenland Sea

The Greenland Sea is the outlying portion of the Arctic Ocean. It has an area of 1,205,000 km<sup>2</sup> and a depth of 1450 m. The sea is surrounded by Greenland in the west, Svalbard Island in the east, the Arctic Ocean in the north and the Norwegian Sea and Iceland in the south,<sup>4</sup> with coordinates 30°W–10°E and 63–79°N (Fig. 1). Greenland Sea has an acute role in deep ocean convection (Timokhov 1994). The intensity of these convections is often governed by the heat and freshwater fluxes contributing to buoyancy and the buoyancy advection of the region (Brakstad et al. 2019). The aftermaths of such processes are the release of brine during the formation of ice from water, causing the salinity of the underlying water to increase (Rudels, 1990). The freezing process may indirectly cause water to sink into deeper layers, which is a precondition since the fresher water at the surface requires higher density to penetrate the denser water below (Visbeck et al. 1995).

## 3 Data and Methods

To understand the ocean—atmospheric coupled with cryospheric conditions of the two seas—the Laptev Sea and the Greenland Sea, certain atmospheric and cryospheric parameters are considered for the span of 2012–21. The data acquisition sources along with the methodology adopted are described in subsequent sections.

### 3.1 Data Sources

#### 3.1.1 Sea Ice Data

The sea ice parameters used for the current study are: sea ice area (SIA), sea ice extent (SIE) and sea ice concentration (SIC). The timeline of 2012–21 is divided into two spans, i.e. 2012–16 and 2017–21. This is in order to compare the latter time period with the former one. Additionally, the recent decade is selected to understand the current influence of temperature on sea ice growth and decay, as it is already recorded by the scientist that a significant incline in temperature is observed during the selected span compared with the past 40 years. All three variables are retrieved from Near-Real-Time DMSP SSMIS Daily Polar Gridded Sea Ice Concentrations (NSIDC)<sup>5</sup> having a spatial resolution of 25 × 25 km.

---

<sup>4</sup> Britannica, the Editors of Encyclopaedia. “Greenland Sea”. Encyclopedia Britannica, 1 May. 2017, <https://www.britannica.com/place/Greenland-Sea>. Accessed 27 March 2022.

<sup>5</sup> NSIDC scientific data search. (n.d.). National Snow and Ice Data Center I. <https://nsidc.org/data/search/>.

- SIA: It is the percentage of sea ice within each data cell and is added up to report how much of the Arctic is covered by ice; the area typically uses a threshold of 15%,<sup>6</sup> measured in km<sup>2</sup>.
- SIE: It defines a region as ice-covered or not ice-covered. For each satellite data cell, the cell is said to either have ice or to have no ice, based on a threshold. The most common threshold used by NSIDC is 15%, meaning that if the data cell has greater than 15% SIC, the cell is considered ice-covered; less than that is considered to be ice-free.<sup>7</sup>
- SIC: This describes the relative amount of area covered by ice, compared with some reference area. Thus, concentration describes how much of a 25 × 25 km box is covered by sea ice. Ice concentration typically is reported as a percentage (0% to 100% ice).

### 3.1.2 Atmospheric Reanalyses

The reanalyses atmospheric data of SST, T2M and OLR are downloaded from ERA-5 at a spatial resolution of 27.75 × 27.75 km for the spans 2012–16 and 2017–21.

- SST: It is the temperature of seawater near the surface. In ERA-5, SST is given by two external providers. Before September 2007, SST is from HadISST2 and from September 2007 onwards, it is from OSTIA. This parameter has units in kelvin (K).<sup>8</sup>
- T2M: This parameter is the temperature of the air at 2 m above the surface of the sea. 2 m temperature is calculated by interpolating between the lowest model level and the Earth's surface, taking account of the atmospheric conditions. This parameter is also measured in kelvin (K) (See Footnote 8).
- OLR: The thermal (longwave) radiation emitted to space at the top of the atmosphere is commonly known as outgoing longwave radiation (OLR). This parameter is accumulated over a particular time period which depends on the data extracted. For the reanalysis, the accumulation period is over 1 h ending at the validity date and time. The unit of the data at the time of retrieval is J m<sup>-2</sup> (See Footnote 8). But for the current study, it is converted to Wm<sup>-2</sup>.

---

<sup>6</sup> National snow and ice data center. (n.d.). National Snow and Ice Data Center I. <https://nsidc.org/data/g02135>.

<sup>7</sup> Data: Terminology | National snow and ice data center. (3 April 2020). National Snow and Ice Data Center I. <https://nsidc.org/cryosphere/seaiice/data/terminology.html>.

<sup>8</sup> Copernicus climate data store. (n.d.). Copernicus Climate Data Store | Copernicus Climate DataStore. <https://cds.climate.copernicus.eu/cdsapp#!/dataset/reanalysis-era5-single-levels?tab=overview>.

## 3.2 Methodology

After the acquisition of cryospheric (SIA, SIE and SIC) and atmospheric (SST, T2M and OLR) datasets from the above-mentioned domains, the method of interpolation and extrapolation is done to bring each dataset to one spatial resolution, in this case, 27.75 km. Data are only retrieved for the specific latitude–longitude of Laptev and Greenland seas using shape files of these regions. NaN values are removed, and the void pixels are assigned 0 value for the prompt averaging of data points. The daily data are averaged to obtain monthly data for each variable. The time frame 2012–21 is divided into two spans as; 2012–16 and 2017–21. Splitting the time domain into two gives a better understanding of the trend of events happening in five years each. Researchers in the past have already contributed a lot to the decline of sea ice over the entire region of the Arctic. It is established that ~13% is the rate of decline every decade (Meehl et al. 2018; Simon et al. 2022; Zhang et al. 2016). Further, the differences between the two periods are taken for the parameters, SIA and SIE to understand the significant rise/fall in sea ice conditions prevailing over the seas. Later, regression analyses of these parameters with the atmospheric parameters are done, to understand the influence of temperature and radiation in sea ice growth/decay. The decay phase consists of months from April–September and the growth phase consists of months from October–March. Separate analyses of these two seasons help one understand the life cycle of sea ice better.

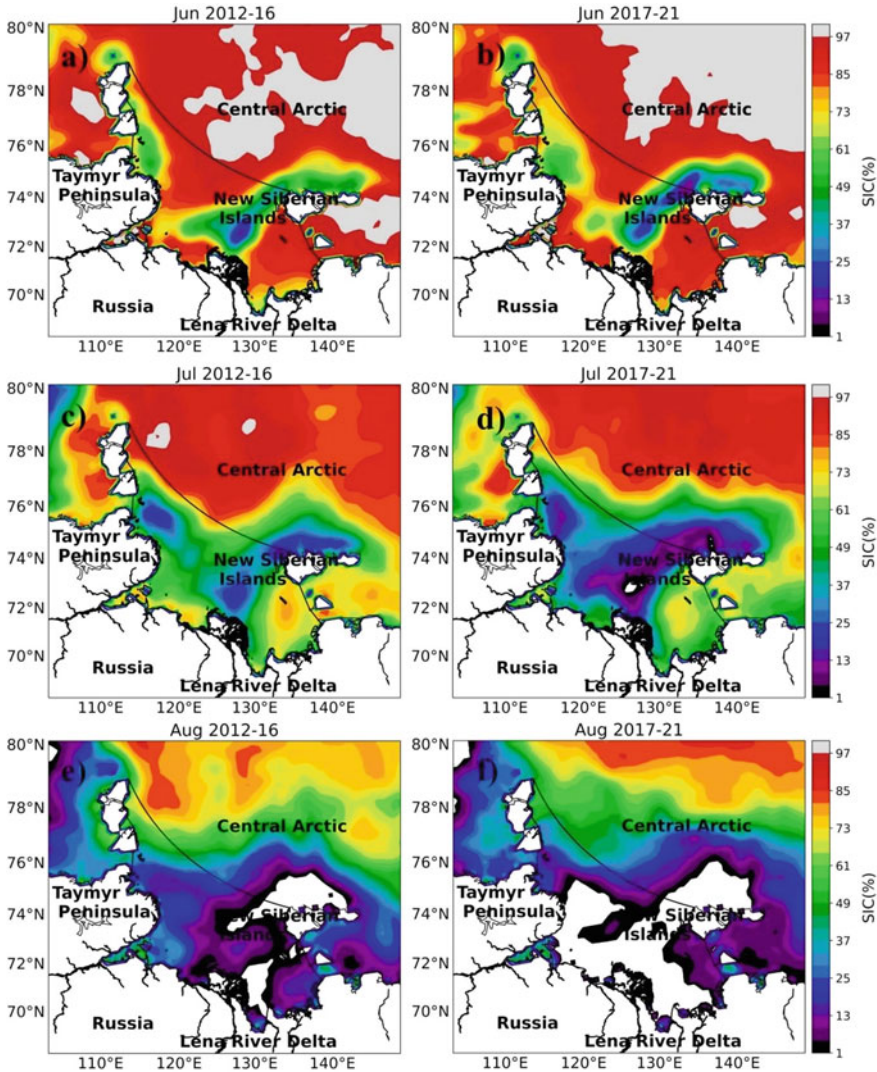
## 4 Results and Discussion

### 4.1 Spatial Variability in Sea Ice Condition

#### 4.1.1 Laptev Sea

The spatial plot (Fig. 2) shows SIC over Laptev during the decay phase (April–September). For the months from June to August, SIC steadily decreases. In June, the sea is seen to experience SIC greater than 61%. However, in July the sea shows SIC smaller than 73%. Ultimately in August, the SIC is found to be less than 25% and open waters are also seen appearing. This pattern of melt in sea ice is quite normal because only during these months, summers are seen intensifying with the rise in temperatures (rise in both SST and T2M). While comparing the two time zones, i.e. 2012–16 with 2017–21, it is understood that SIC during the latter period is less than that during the former years. While comparing the month of June (Fig. 2a, b) shown in the two timelines, it is found that during 2012–16 (Fig. 2a), the concentration of sea ice is above 85% at a majority of the locations. However, only a small area at the centre of the sea has a concentration below 37%. Even at locations above Taymyr Peninsula (78–76°N, 110°E), denser sea ice is formed.





**Fig. 2** Spatial variation of sea ice concentration (SIC) over Laptev Sea during a June, 2012–16, b June, 2017–21, c July, 2012–16, d July, 2017–21, e August, 2012–16 and f August, 2017–21

On the contrary, for the year 2017–21 (Fig. 2b) in June, higher latitudes exceeding 76°N have denser and homogenous SIC with 97% SIC. But over the sea, SIC of less than 37% is abundantly present when compared with that in June 2012–16. The greater decline in SIC values in June 2017–21 is due to two reasons. Firstly, the SST value in 2012–16 (June) is 271.95 K and that during 2017–21 is 272.24 K, showing a significant rise in the latter period. Therefore rise in SST can cause a decline in SIC. Secondly, there exists ~ 1 K rises in T2M values. T2M in 2012–16 is



280.03 K and that during 2017–21 is 281.87 K. The warmth evolved at the surface of the sea will definitely cause the air above it to heat up, ultimately contributing to the rise in T2M. By July 2012–16 (Fig. 2c), majority of sea ice have come down to concentrations below 85%. While comparing it with the past month (June), the concentration has significantly decreased over the entire sea which is as expected during the melt. Some locations within the sea show SIC dropping down even below 25%, regions such as south of Severnaya Zemlya, north of New Siberian Islands and to the north of Lena River Delta (LRD). While comparing this span with the recent years 2017–21 (Fig. 2d) it is visible that the sea has tremendously lost ice. Regions east of LRD however remain somewhat similar (which is an exceptional case). An arc-like contour (connecting the LRD and the New Siberian Islands) which is also found during the former span has considerably lost a huge amount of ice, which has caused SIC to fall below 13%. Similar is the situation with sea ice located towards the east of Taymyr Peninsula. During this month the south part of the sea shows a temperature of 279 K and the north part exhibits temperature almost above the freezing point. Additionally, during this season, the shores observe temperatures of 295–297 K, due to which sea ice towards the land region (Russia) is less dense than the portions above it. However, July which is the primary month of the decay season is demarcated for bringing in excessive fog and snow squalls, which may contribute to the development of sea ice at times.

Further in August 2012–16 (Fig. 2e), the entire SIC of the sea drops to range below 25%. The region around New Siberian Islands is found to be completely ice-free, even when the location is close to the central Arctic. Additionally, the region around LRD also shows a slight reduction of sea ice and a gradual bend towards ice-free conditions. August being very close to September (which is demarcated as the month with Arctic sea ice minimum condition), such a large decline in SIC can be anticipated. Much more alarming is the state of sea ice during the latter span, 2017–21 for the month of August. From the spatial plot (Fig. 2f) it is clearly visible that the entire sea is absent of any concentrations above 13%. Researchers in the past have observed low-pressure systems getting developed over the Arctic during this month. Due to the existence of such low-pressure systems, the ice tends to move towards the southward direction. When this ice gets too low to come in contact with the waters which have water temperatures below the freezing point, the prevailing sea ice tends to melt contributing more to ice-free regions. This may be the causative factor attributing to the decline in sea ice conditions. Apart from the spatial comparison of sea ice during the decay phase for the two spans; 2012–16 and 2017–21, quantitative calculations are also made and are visible in Table 1. Table 1 displays the difference in SIA and SIE for each month. Here, both SIA and SIE are represented in million square kilometres. Therefore, when the differences are zero (or null), it does not indicate that the values of these parameters in both spans are the same. Instead, it shows that the difference is not quite significant.

Further in August 2012–16 (Fig. 2e), the entire SIC of the sea drops to range below 25%. The region around New Siberian Islands is found to be completely ice-free, even when the location is close to the central Arctic. Additionally, the region around LRD also shows a slight reduction of sea ice and a gradual bend towards

ice-free conditions. August being very close to September (which is demarcated as the month with Arctic sea ice minimum condition), such a large decline in SIC can be anticipated. Much more alarming is the state of sea ice during the latter span, 2017–21 for the month of August. From the spatial plot (Fig. 2f) it is clearly visible that the entire sea is absent of any concentrations above 13%. Researchers in the past have observed low-pressure systems getting developed over the Arctic during this month. Due to the existence of such low-pressure systems, the ice tends to move towards the southward direction. When this ice gets too low to come in contact with the waters which have water temperatures below the freezing point, the prevailing sea ice tends to melt contributing more to ice-free regions. This may be the causative factor attributing to the decline in sea ice conditions. Apart from the spatial comparison of sea ice during the decay phase for the two spans; 2012–16 and 2017–21, quantitative calculations are also made and are visible in Table 1. Table 1 displays the difference in SIA and SIE for each month. Here, both SIA and SIE are represented in million square kilometres. Therefore, when the differences are zero (or null), it does not indicate that the values of these parameters in both spans are the same. Instead, it shows that the difference is not quite significant.

The highest difference between the two is observed in the month of July and October with values of  $1.11 \times 10^5 \text{ km}^2$  and  $1.17 \times 10^5 \text{ km}^2$  respectively. SIE during 2012–16 is almost seen to be steady with a value of  $8.72 \times 10^5 \text{ km}^2$  throughout winter. The lowest value in SIE is observed during September ( $1.19 \times 10^5 \text{ km}^2$ ). Similar to 2012–16, in 2017–21 also the highest value remains static. An understanding of this steadiness is that in millions this might appear constant, but there might be very slight differences if we lower the place values. The minimum value

**Table 1** Monthly variation in SIA, SIE along with the difference in the two parameters for the two spans; 2012–16 and 2017–21 over Laptev Sea

Laptev sea months	SIA ( $\times 10^5$ ) km <sup>2</sup>			SIE ( $\times 10^5$ ) km <sup>2</sup>		
	2012–16	2017–21	Difference in SIA	2012–16	2017–21	Difference in SIE
Jan	8.49	8.49	0.00	8.72	8.72	0.00
Feb	8.47	8.46	0.01	8.72	8.72	0.00
Mar	8.47	8.44	0.03	8.72	8.72	0.00
Apr	8.33	8.31	0.02	8.72	8.72	0.00
May	7.82	7.79	0.02	8.66	8.62	0.03
Jun	6.19	5.44	0.76	8.09	7.45	0.63
Jul	3.60	2.49	1.11	5.75	4.18	1.57
Aug	1.52	0.89	0.63	2.68	1.64	1.04
Sep	0.64	0.60	0.04	1.19	1.05	0.13
Oct	3.59	2.42	1.17	5.09	3.53	1.55
Nov	7.95	7.77	0.18	8.71	8.56	0.15
Dec	8.50	8.43	0.07	8.72	8.72	0.00

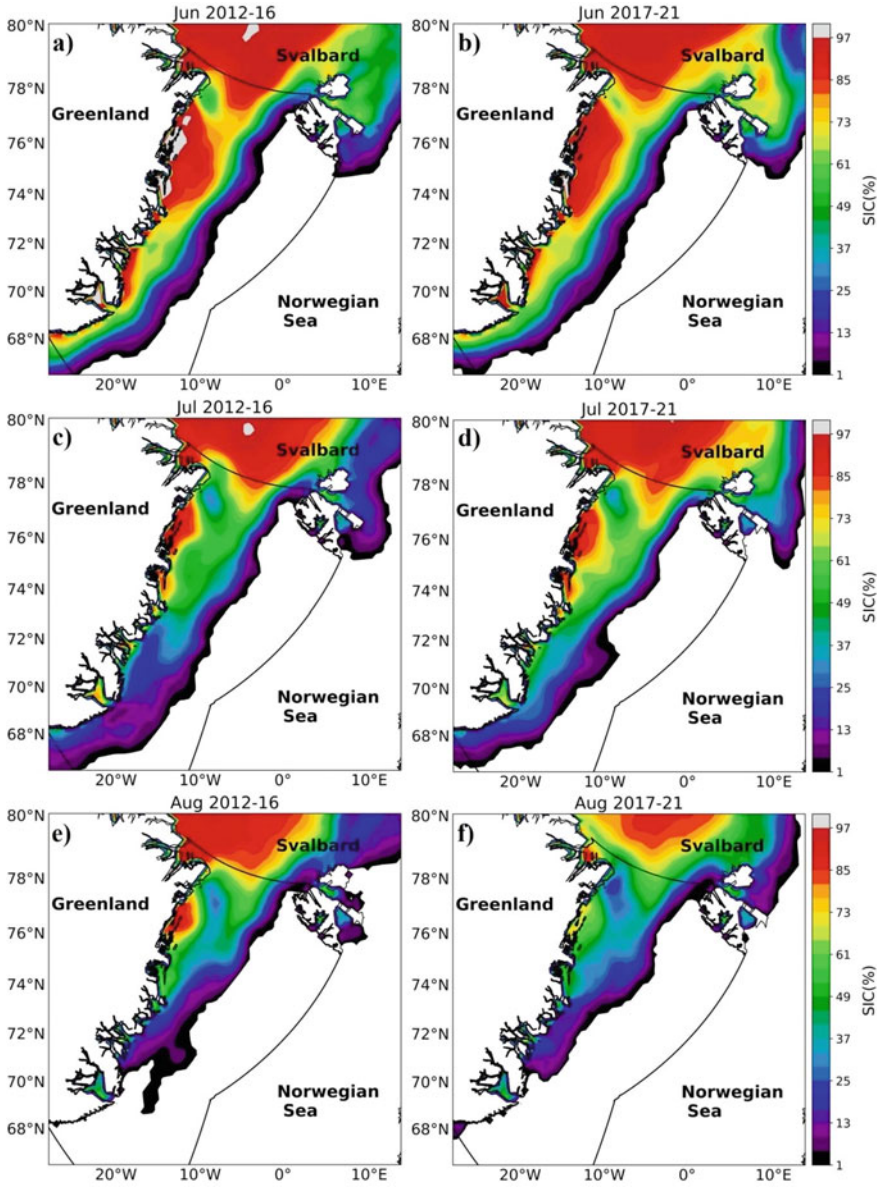
is during September ( $1.05 \times 10^5 \text{ km}^2$ ). While comparing the difference in SIE, it remains almost insignificant during DJFMA. Here also the highest difference in SIE is observed in July and October with values of  $1.57 \times 10^5 \text{ km}^2$  and  $1.55 \times 10^5 \text{ km}^2$  respectively.

#### 4.1.2 Greenland Sea

The Greenland Sea is extremely further away from the Central Arctic region and closer to the North Atlantic Ocean, the Atlantic waters with temperatures  $\sim 287.85 \text{ K}$  are seen to greatly influence the sea ice conditions over the region compared with the Arctic waters. In Fig. 3 the SIC is found to exhibit a layering effect with locations closer to the Norwegian Sea showing low SIC and the region near Greenland showing higher SIC. During June 2012–16 (Fig. 3a), starting from the north near Svalbard, the sea is devoid of SIC above 65%. However as one moves towards the south, the region of sea closer to Greenland experiences higher SIC than compared with those near the Norwegian Sea (Table 2).

The Greenland region excessively rich in snow and glaciers would have facilitated the sea ice to develop at least to a few magnitudes. Again in June 2017–21 (Fig. 3b) the concentrations are seen to be greater in the north; towards the south, the decline is visible.

The locations near Iceland have SIC of less than 49% and the width of the trail is also seen to be low. Overall during June, some regions show high SIC during the recent span compared with that during the latter span, but this does not suffice that the number of pixels during 2017–21 is considerably less compared with that during 2012–16. By July 2012–16 (Fig. 3c), SIC has significantly deteriorated from higher SIC values by June 2012–16 and this trend is obvious as we have considered the decay process of sea ice. Here SIC greater than 85% is confined to the northern locations. The area closer to Arctic Circle might add to an advantage for the growth in sea ice towards the north of the Greenland Sea. Towards the south and close to the Iceland region, the SIC is always found to be less than 37%. Comparing this with the latter span of 2017–21 (Fig. 3d), the area of spread of SIC in the south of the Greenland Sea has noticeably decreased. However, the region around Svalbard is showing slight development of SIC in the recent span than in the previous span. By August 2012–16 (Fig. 3e), the entire sea is devoid of any sea ice over the south. In the north, near the Arctic, SIC is greater than 85%. However with time, by 2017–21 (Fig. 3f), it has significantly decreased.



**Fig. 3** Spatial variation of sea ice concentration (SIC) over Greenland Sea during **a** June, 2012–16, **b** June, 2017–21, **c** July, 2012–16, **d** July, 2017–21, **e** August, 2012–16 and **f** August, 2017–21

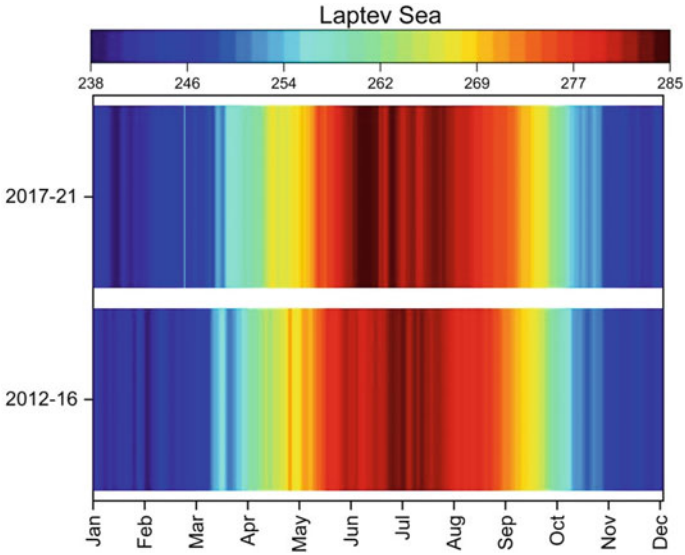
**Table 2** Monthly variation in SIA, SIE along with the difference in the two parameters for the two spans; 2012–16 and 2017–21 over Greenland Sea

Greenland Sea	SIA ( $\times 10^5$ ) km <sup>2</sup>			SIE ( $\times 10^5$ ) km <sup>2</sup>		
	2012–16	2017–21	Difference in SIA	2012–16	2017–21	Difference in SIE
Jan	4.54	4.54	0.00	6.17	6.07	0.11
Feb	4.93	4.63	0.30	6.66	6.17	0.49
Mar	5.19	5.11	0.08	6.82	6.77	0.05
Apr	5.54	5.27	0.27	7.22	7.10	0.12
May	5.11	4.73	0.38	6.89	6.61	0.28
Jun	4.02	3.75	0.26	6.29	5.72	0.57
Jul	2.20	2.12	0.09	4.17	3.89	0.27
Aug	1.36	0.95	0.41	2.59	2.08	0.51
Sep	1.45	0.91	0.54	2.53	1.71	0.82
Oct	2.70	2.27	0.43	3.96	3.35	0.61
Nov	3.67	3.49	0.19	5.12	4.78	0.33
Dec	4.29	4.29	0.00	5.83	5.77	0.06

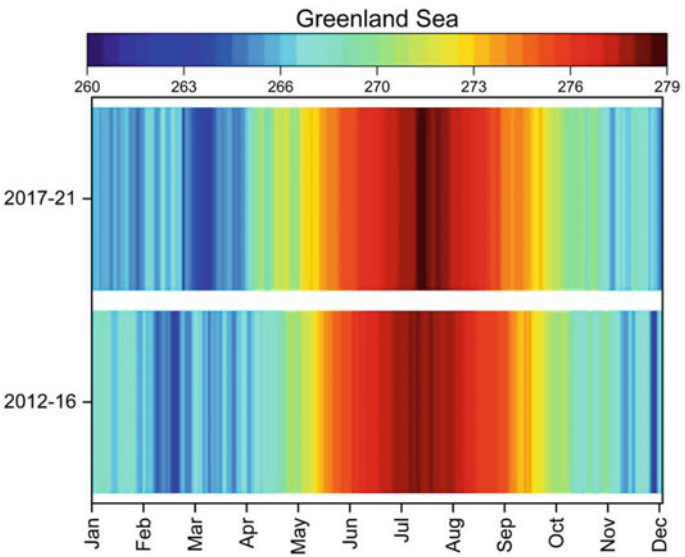
## 4.2 Daily Variability in Temperature (T2M) Over Laptev and Greenland Seas

As we now know how sea ice condition over Laptev and Greenland Seas prevails, therefore it is vital to look into the behaviour of T2M over the considered seas. Figures 4 and 5 show the daily temperature variation for the considered years; 2012–16 and 2017–21 over the Laptev Sea and Greenland Sea. Over Laptev (Fig. 4), from a glance at the plot, one can highlight that the summers during 2017–21 are much hotter than those during 2012–16. June, July and August are found to show extremely high temperatures.

Overall the range of T2M over Laptev lies within the range of 238–285 K. By the end of June in 2012–16, T2M starts to rise from 280 to 281 K. Soon 9th July onwards, the value again increases to 282 K and further increases on 18th July to 283 K after which, a gradual decline to subsequent values are observed. Apart from July, the hike in the value of T2M is also observed during June, but here the T2M values are limited to 281 K. While comparing these temperatures with those during 2017–21, it is evident that the values during this span are significantly higher than those of the former span. When the temperature reaches 280 K by the end of June 2012–16, the value has already reached 284 K in 2017–21. The highest fluctuation in the value of T2M here in the latter span is also observed during June–July like that of the former span. Sea ice decay is usually from April to September. Here in the temperature profile, it is distinctly visible that during these months of the year, the air above the sea is extremely warm when compared with other months. The heat exchange between the atmosphere and the sea further contributes to the melt away



**Fig. 4** Daily variability profile of temperature (T2M) over Laptev Sea during 2012–16 and 2017–21



**Fig. 5** Daily variability profile of temperature (T2M) over Greenland Sea during 2012–16 and 2017–21

of the newly formed sea ice over the region. It is also understood that the latent heat capacity of water is much higher than that of soil/land, therefore the water molecules over the sea hold up the heat for a longer duration and gradually emit it in the form of ice-albedo feedback or longwave infrared radiation into the atmosphere which again facilitates the air above it to gain more and more heat (Meehl et al. 2018). This cyclic exchange of heat between the two systems hampers not only the formation of new ice but also causes the melt away of multiyear ice contributing to the appearance of more open water over the region.

While understanding the variation of T2M over the Greenland Sea (Fig. 5) it is found that the range of T2M is significantly higher than those of the Laptev Sea. The lower range of T2M over the Laptev Sea is about 238 K, but over the Greenland Sea, it has increased to 260 K, however when observing the highest boundary limit, it is found that the temperature is confined to 279 K. During 2012–16, the summer T2M lies between 270 and 279 K. A seasonal cyclic pattern is observed for T2M with the temperature slowly building up in July–August and further subsiding. In 2017–21, the summer is seen to exist for a prolonged period, this can be justified by the higher values (above 273 K) that exist in May and October which is quite absent in the previous years; 2012–16. Also during July–August the temperatures are seen to be higher than that in other months during 2017–21 when compared with 2012–16. Rest the cyclic pattern of T2M with highs and lows are also visible during this period as that of 2012–16. Similar to the Laptev Sea, the Greenland Sea has higher values of T2M during 2017–21 which is a reason for the low values of SIC, SIA and SIE.

### **4.3 Linear Regression Analyses of Sea Ice Area (SIA) with Sea Surface Temperature (SST), Temperature at 2m (T2M) and Outgoing Longwave Radiation (OLR)**

#### **4.3.1 Laptev Sea**

Monthly variability in temperatures during the summers for the considered years over the Laptev Sea provides the need to extend the study quantitatively to establish the role of these in the sea ice retreat process. Therefore linear regression analyses are performed between SIA and atmospheric entities such as; SST, T2M and OLR and are displayed in Table 3. Also the byproducts of the regression analyses such as; the slope, intercept and correlation coefficient values are all mentioned in Table 3, which gives one valid grounds to associate the two parameters quantitatively. From the previous section (Sect. 4.1), the spatio-temporal pattern of SIC clearly shows the recent stratification which is happening over the sea around the year. The stratification is primarily due to the gush of fresh waters from the Lena River and the sea ice melt waters. Additionally, the presence of an ice shelf inhibits the exchange of energy and momentum between the ocean and the atmosphere (Simon et al. 2022). It is also known that the deep shelf region of the sea consists of low temperature saline waters

which are not significantly affected by seasonal changes/fluctuations. However, the interaction of the temperature above the surface and the air above it with the sea ice can be understood by associating SST and T2M with SIA.

During the growth of sea ice in both periods, SST lies within the range between 271–275 K. Majority values are seen highly concentrated around lower SST and higher SIA values. Regression analyses of SST with SIA yields  $r^2 = 0.69$  ( $p < 0.05$ ) during 2012–16 and  $r^2 = 0.92$  ( $p < 0.05$ ) during 2017–21, showing SST has a greater influence on sea ice during the recent span (however the  $p$  values state that the two  $r$  values are statistically insignificant). Further during the decay stage of sea ice decrease in SIA is found with an increase in SST for all the years. Here, the range of SST is found to be slightly higher than that during winters, which also adds to the excess decay of sea ice during summers. The correlation coefficient ( $r^2$ ) values are 0.92 ( $p > 0.05$ ) and 0.89 ( $p > 0.05$ ) for 2012–16 and 2017–21, respectively. During winters, it is found that the impact of SST on SIA is greater in 2017–21 than in 2012–16, however during summers, it is the opposite, i.e. the influence of SST on SIA is more in 2012–16 than in 2017–21. The results directly point out the recent winter amplification which is prevailing over the Arctic as a whole.

While understanding the relationship of SIA with T2M during winters, it is found that the area remains almost constant ( $8-9 \times 10^5 \text{ km}^2$ ) with a decrease in T2M from

**Table 3** Results of regression analyses of SIA with SST, T2M and OLR during the growth and decay of sea ice for the two spans; 2012–16 and 2017–21 over Laptev Sea

Laptev sea				
	Growth		Decay	
Period	2012–16	2017–21	2012–16	2017–21
Equation	$y = a + b*x$			
<i>SIA with SST</i>				
Intercept	1422.02 ± 176.94	877.02 ± 47.85	504.40 ± 26.19	340.61 ± 21.71
Slope	-5.20 ± 0.65	-3.20 ± 0.17	-1.83 ± 0.09	-1.22 ± 0.07
$r$	-0.83	-0.96	-0.96	-0.94
$r^2$	0.69	0.92	0.92( $p > 0.05$ )	0.89( $p > 0.05$ )
<i>SIA with T2M</i>				
Intercept	57.41 ± 5.49	68.93 ± 6.37	76.14 ± 17.59	88.62 ± 16.26
Slope	-0.20 ± 0.02	-0.24 ± 0.02	-0.25 ± 0.06	-0.30 ± 0.05
$r$	-0.86	-0.87	-0.60	-0.70
$r^2$	0.74	0.76	0.37	0.49
<i>SIA with OLR</i>				
Intercept	35.05 ± 3.27	42.31 ± 3.71	27.46 ± 8.81	32.25 ± 7.38
Slope	0.18 ± 0.02	0.22 ± 0.02	0.12 ± 0.04	0.14 ± 0.03
$r$	0.84	0.87	0.43	0.58
$r^2$	0.71 ( $p > 0.05$ )	0.76 ( $p > 0.05$ )	0.19	0.34



235 to 255 K. This trend is the same for all the considered periods. The regression analyses performed between the two quantities show  $r^2 = 0.74$  ( $p < 0.05$ ) and  $r^2 = 0.76$  ( $p < 0.05$ ) for the years 2012–16 and 2017–21, respectively. Further, during summer (decay of sea ice), an exact fit of these parameters is not found, which is validated by the correlation coefficient values mentioned in Table 3.

For the years 2012–16 and 2017–21,  $r^2 = 0.37$  and  $0.49$  ( $p < 0.05$ ), respectively. In the case of OLR, SIA is seen to increase with the increase in OLR during the growth stage and during decay, SIA is found to decrease with a decrease in OLR, indicating that both the parameters are directly associated; as one increases the other also increases. Correlation coefficient values are  $r^2 = 0.71$  and  $0.76$  ( $p > 0.05$ ) during growth and  $r^2 = 0.19$  and  $0.34$  ( $p < 0.05$ ) during decay, for years 2012–15 and 2017–21, respectively.

Overall the parameters SST and T2M are inversely associated with SIA while OLR is positively related. The high degree of influence among SIA with SST and T2M is observed during winter months; precisely the influence is more during the recent span than the previous years. Similarly larger influence of OLR on SIA is also found during the decay period than in the growth stage.

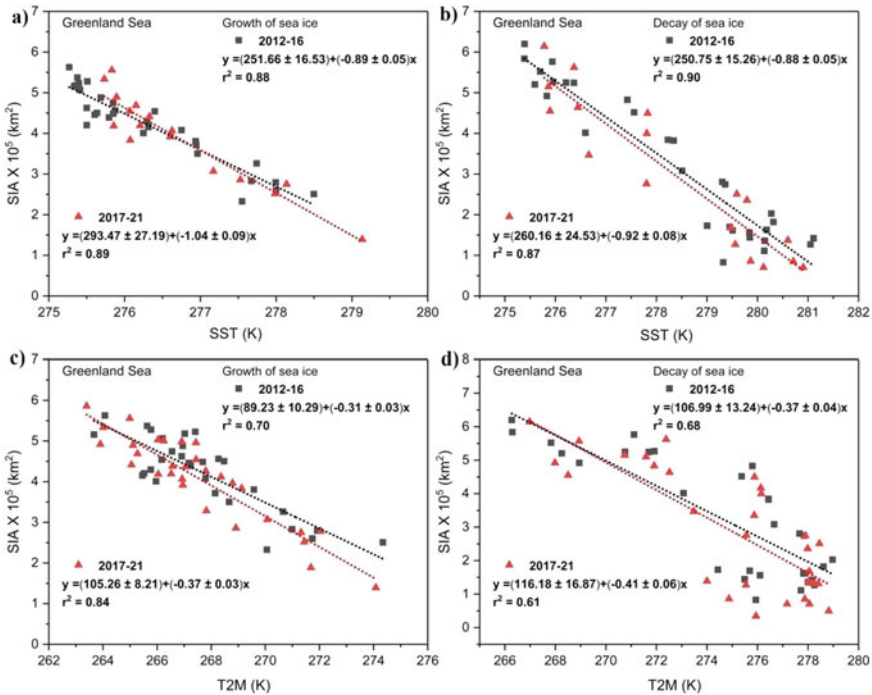
### 4.3.2 Greenland Sea

Greenland Sea located towards the south of Arctic Circle is greatly influenced even by a slight hike in temperature. Additionally, over this region, the NAO is observed to show high impact. One of the reason by which the oscillation is developed is through the pressure difference which originates between the Azores Island and locations closer to Iceland. Azores Island shows high pressure when Iceland observes low pressure or vice versa. The other causative factors may be associated with wide range of physical and biological responses including; the variation in sea ice cover, wind speed, sensible heat flux, latent heat flux, temperatures, OLR, etc. After 1990s it is known that SST is highly correlated with NAO. It is also believed that the determination of NAO helps one know the Arctic atmospheric condition to one third extent (Panicker et al. 2021).

Here, Fig. 6 regression analyses are performed between SIA and atmospheric variables; like SST, T2M and OLR during both the decay and the growth months of sea ice for all the considered spans; 2012–16 and 2017–21. During the growth of sea ice, gradual development of sea ice is observed in Fig. 6a (as one moves from right to left). When the temperature falls from 279 to 275 K, the plot clearly shows the inverse relationship between the two variables. SST and SIA are negatively correlated for both the timelines; 2012–16 and 2017–21 ( $r = -0.94$ ). The value  $r^2 = 0.88$  ( $p > 0.05$ ) and  $r^2 = 0.89$  ( $p > 0.05$ ) during the aforementioned periods clearly demonstrates that the two quantities are highly negatively correlated (as;  $r^2 > 0.5$ ). The information related to intercept, slopes, etc. are clearly addressed in Table 3. However during the decay stage of sea ice, primarily when it is summers, the range of SST is seen to be noticeably high than that during winters. Here the highest point in the range reaches up to 282 K additionally, the observed slope in Fig. 6b is much

steep than those in winters. During 2012–16,  $r^2 = 0.90$  and 2017–21,  $r^2 = 0.87$ , which shows that during the former span the sea ice is vastly influenced by the change in SST than during the latter years. While relating T2M with SIA (Fig. 6c and d), the concentration of higher SIA values are observed in places where the temperature is low. The relationship between the two entities is again expected to be strongly opposite with  $r^2 = 0.70$  and  $r^2 = 0.84$  ( $p > 0.05$ ) in 2012–16 and 2017–21, respectively. Further relating SIA with OLR gives new insight to the study.

Even though OLR is a function of temperature, it can yield the amount of radiation emitted by ice or snow when treated as a black body (Zhang et al. 2016; Shah and Srivastava 2020). The correlation coefficient value clearly demonstrated that the existence of sea ice is directly related with OLR. As one increases, the development of the other also occurs. During sea ice growth the range of OLR lies between  $-180 \text{ Wm}^{-2}$  and  $-152 \text{ Wm}^{-2}$  and SIA between  $1 \times 10^5 \text{ km}^2$  and  $6 \times 10^5 \text{ km}^2$ . When OLR increases the growth of sea ice also occurs. The correlation coefficient values of OLR and SIA are not strong which are visible from the values in Table 4,  $r^2 = 0.37$  for the both the periods. However, during the decay phase of sea ice the range of OLR has dropped down from  $-204 \text{ Wm}^{-2}$  to  $-168 \text{ Wm}^{-2}$ . During 2012–16,  $r^2$



**Fig. 6** Regression analyses of Sea Ice Concentration (SIA) with Sea Surface Temperature (SST) during **a** growth phase, **b** decay phase of sea ice, Sea Ice Concentration (SIC) with Temperature at 2m (T2M) during **c** growth phase and **d** decay phase over Greenland Sea during the years 2012–16 and 2017–21

= 0.20 and during 2017–21,  $r^2 = 0.16$ , which states that the relationship between the two parameters are not exceedingly strong.

Overall it can be stated that over Greenland Sea, SIA holds negative correlation between SST and T2M and positive correlation with OLR (at least to a small extent). The notable feature is that better correlation values are observed more during the growth phase when compared with that during the decay phase. SST and T2M highly show negative influence on SIA during winter than in summers. This relation suggests Greenland Sea experiences more warming during winter, than in summer. This occurrence is not unique to this sea, but there exists a well-known concept termed as Arctic Amplification (AA), which is experienced by majority of the seas in the Arctic Circle.

The results represented in the paper demonstrates the spatio temporal variation in sea ice conditions over the two seas of Arctic, namely Laptev Sea and Greenland Sea for the spans; 2012–16 and 2017–21. Laptev being a marginal sea of the Arctic shows high variability in SIC, SIA and SIE compared with Greenland Sea which is only an outlying portion of the Arctic Ocean. Even while quantitatively comparing the amount of sea ice over Laptev Sea and Greenland Sea, the range of SIA and SIE is noticeably high for Laptev when compared with Greenland Sea. The differences between the two seas in SIA and SIE are  $\sim 3 \times 10^5 \text{ km}^2$  and  $\sim 1 \times 10^5 \text{ km}^2$ ,

**Table 4** Results of regression analyses of SIA with SST, T2M and OLR during the growth and decay of sea ice for the two spans; 2012–16 and 2017–21 over Greenland Sea ( $r^2$  value have  $p < 0.05$ )

Greenland sea				
	Growth		Decay	
Period	2012–16	2017–21	2012–16	2017–21
Equation	$y = a + b*x$			
<i>SIA with SST</i>				
Intercept	251.66 ± 16.53	293.47 ± 27.19	250.75 ± 15.26	260.16 ± 24.53
Slope	-0.89 ± 0.05	-1.04 ± 0.09	-0.88 ± 0.05	-0.92 ± 0.08
$r$	-0.94	-0.94	-0.95	-0.93
$r^2$	0.88	0.89	0.90	0.87
<i>SIA with T2M</i>				
Intercept	89.23 ± 10.29	105.26 ± 8.21	106.99 ± 13.24	116.18 ± 16.87
Slope	-0.31 ± 0.03	-0.37 ± 0.03	-0.37 ± 0.04	-0.41 ± 0.06
$r$	-0.84	-0.91	-0.82	-0.78
$r^2$	0.70	0.84	0.68	0.61
<i>SIA with OLR</i>				
Intercept	19.39 ± 3.67	21.05 ± 4.13	20.97 ± 6.52	19.02 ± 6.85
Slope	0.09 ± 0.02	0.10 ± 0.02	0.09 ± 0.03	0.08 ± 0.03
$r$	0.61	0.61	0.45	0.40
$r^2$	0.37	0.37	0.20	0.16

respectively. Additionally when comparing the recent span with the former span, over all the considered seas the decrease in sea ice condition is evidently visible with the passage of time. Over Laptev the highest difference in SIA between the two periods; 2012–16 and 2017–21 is observed in the month of July and October with values  $1.11 \times 10^5 \text{ km}^2$  and  $1.17 \times 10^5 \text{ km}^2$ , respectively. Here also the minimum value is during September ( $1.05 \times 10^5 \text{ km}^2$ ). The difference in SIE is also found to be in July and October with values  $1.57 \times 10^5 \text{ km}^2$  and  $1.55 \times 10^5 \text{ km}^2$ , respectively. However the difference in SIA/SIE over Greenland Sea is less than that over Laptev Sea. The highest difference in SIA is observed during September,  $0.54 \times 10^5 \text{ km}^2$ . The SIE trend is similar to that of SIA. The difference in SIE is highest in September and lowest in March.

While associating SIA with atmospheric parameters (SST, T2M and OLR), over both the regions, SST and T2M are inversely associated with SIA while OLR is positively related with SIA. The high degree of influence among SIA with SST and T2M is observed during winter months; precisely the influence is more during the recent span than the previous years. Similarly larger influence of OLR on SIA is also found during the decay period than in the growth stage. This clearly makes the sea suspicious of have been experiencing winter warming more than summer warming. This is not only in this case; this effect of Arctic Amplification (AA) is a known concept which is already being experienced by majority of the seas over the Arctic Circle. Over Laptev, in 2017–21  $r_{(\text{SIA}, \text{SST})} = -0.96$  and  $r_{(\text{SIA}, \text{T2M})} = -0.87$  which is higher compared with  $r_{(\text{SIA}, \text{SST})} = -0.83$  and  $r_{(\text{SIA}, \text{T2M})} = -0.86$  during 2016–21. Similarly over Greenland Sea,  $r_{(\text{SIA}, \text{SST})} = -0.94$  and  $r_{(\text{SIA}, \text{T2M})} = -0.91$  during 2017–21 and  $r_{(\text{SIA}, \text{SST})} = -0.94$  and  $r_{(\text{SIA}, \text{T2M})} = -0.84$  during 2012–16. Since outgoing longwave radiation has a positive influence on both the seas during both the spans;  $r_{(\text{SIA}, \text{OLR})} = 0.85$  for Laptev and  $r_{(\text{SIA}, \text{OLR})} = 0.61$  for Greenland Sea.

Given the relationship of SIC, SIA and SIE with atmospheric conditions over Laptev and Greenland Sea, it is now understood that small change in these entities may be impacting the ice condition in inverse manner causing more warming of the region as this feedback mechanism moves in a cyclic manner. Additionally, there is extensive change experienced in the sea ice condition over both the seas during the recent decade.

## 5 Conclusions

The results represented in the paper demonstrate the spatio temporal variation in sea ice conditions over the two seas of Arctic, namely Laptev Sea and Greenland Sea for the spans; 2012–16 and 2017–21. Laptev being a marginal sea of the Arctic shows high variability in SIC, SIA and SIE compared with Greenland Sea which is only an outlying portion of the Arctic Ocean. Even while quantitatively comparing the amount of sea ice over Laptev Sea and Greenland Sea, the range of SIA and SIE is noticeably high for Laptev when compared with Greenland Sea. The differences between the two seas in SIA and SIE are  $\sim 3 \times 10^5 \text{ km}^2$  and  $\sim 1 \times 10^5 \text{ km}^2$ , respectively.

Additionally when comparing the recent span with the former span, over all the considered seas the decrease in sea ice condition is evidently visible with the passage of time. Over Laptev the highest difference in SIA between the two periods; 2012–16 and 2017–21 is observed in the month of July and October with values  $1.11 \times 10^5 \text{ km}^2$  and  $1.17 \times 10^5 \text{ km}^2$ , respectively. Here also the minimum value is during September ( $1.05 \times 10^5 \text{ km}^2$ ). The difference in SIE is also found to be in July and October with values  $1.57 \times 10^5 \text{ km}^2$  and  $1.55 \times 10^5 \text{ km}^2$ , respectively. However the difference in SIA/SIE over Greenland Sea is less than that over Laptev Sea. The highest difference in SIA is observed during September,  $0.54 \times 10^5 \text{ km}^2$ . The SIE trend is similar to that of SIA. The difference in SIE is highest in September and lowest in March.

While associating SIA with atmospheric parameters (SST, T2M and OLR), over both the regions, SST and T2M are inversely associated with SIA while OLR is positively related with SIA. The high degree of influence among SIA with SST and T2M is observed during winter months; precisely the influence is more during the recent span than the previous years. Similarly, larger influence of OLR on SIA is also found during the decay period than in the growth stage. This clearly makes the sea suspicious of have been experiencing winter warming more than summer warming. This is not only in this case; this effect of Arctic Amplification (AA) is a known concept which is already being experienced by majority of the seas over the Arctic Circle. Over Laptev, in 2017–21  $r_{(\text{SIA}, \text{SST})} = -0.96$  and  $r_{(\text{SIA}, \text{T2M})} = -0.87$  which is higher compared with  $r_{(\text{SIA}, \text{SST})} = -0.83$  and  $r_{(\text{SIA}, \text{T2M})} = -0.86$  during 2016–21. Similarly, over Greenland Sea,  $r_{(\text{SIA}, \text{SST})} = -0.94$  and  $r_{(\text{SIA}, \text{T2M})} = -0.91$  during 2017–21 and  $r_{(\text{SIA}, \text{SST})} = -0.94$  and  $r_{(\text{SIA}, \text{T2M})} = -0.84$  during 2012–16. Since outgoing longwave radiation has a positive influence on both the seas during both the spans;  $r_{(\text{SIA}, \text{OLR})} = 0.85$  for Laptev and  $r_{(\text{SIA}, \text{OLR})} = 0.61$  for Greenland Sea.

Overall, the paper demonstrates how the variability of atmospheric temperature inherently affects the condition of sea ice over the two seas of the Arctic. Knowing the relationship and the extent of the effect of one on the other variable helps the scientific community to predict and make necessary changes at the global level to limit the excess melt away of sea ice over the seas of the Arctic. Additionally, further scientific studies are required to understand other atmospheric variables which hamper the pace and rate of sea ice melt and growth over the region.

## References

- Alekseev G, Johannessen O, Kovalevskii D (2001) Development of convective motions under the effect of local perturbations of sea-surface density. *Izv Atmos Ocean Phy* 37:341–350
- Bintanja R, Graverson RG, Hazeleger W (2011) Arctic winter warming amplified by the thermal inversion and consequent low infrared cooling to space. *Nat Geosci* 4(11):758–761. <https://doi.org/10.1038/ngeo1285>
- Bintanja R, Van der Linden EC (2013) The changing seasonal climate in the Arctic. *Sci Rep* 3(1). <https://doi.org/10.1038/srep01556>

- Brakstad A, Våge K, Håvik L, Moore GW (2019) Water mass transformation in the Greenland sea during the period 1986–2016. *J Phys Oceanogr* 49(1):121–140. <https://doi.org/10.1175/jpo-d-17-0273.1>
- Chepurin GA, Carton JA (2012) Subarctic and Arctic Sea surface temperature and its relation to ocean heat content 1982–2010. *J Geophys Res Oceans* 117(C6):n/a–n/a. <https://doi.org/10.1029/2011jc007770>
- Cox CJ, Uttal T, Long CN, Shupe MD, Stone RS, Starkweather S (2016) The role of springtime Arctic clouds in determining autumn sea ice extent. *J Clim* 29:6581–6596. <https://doi.org/10.1175/JCLI-D-16-0136-1>
- Dethleff D, Loewe P, Kleine E (1998) The Laptev Sea flaw lead—detailed investigation on ice formation and export during 1991/1992 winter season. *Cold Reg Sci Technol* 27(3):225–243. [https://doi.org/10.1016/s0165-232x\(98\)00005-6](https://doi.org/10.1016/s0165-232x(98)00005-6)
- Fraser AD, Massom RA, Michael KJ, Galton-Fenzi BK, Lieser JL (2012) East Antarctic Landfast sea ice distribution and variability, 2000–08. *J Clim* 25(4):1137–1156. <https://doi.org/10.1175/jcli-d-10-05032.1>
- Gawor J, Grzesiak J, Sasin-Kurowska J, Borsuk P, Gromadka R, Górniak D, Świątecki A, Aleksandrak-Piekarczyk T, Zdanowski MK (2016) Evidence of adaptation, niche separation and microevolution within the genus *Polaromonas* on Arctic and Antarctic glacial surfaces. *Extremophiles* 20(4):403–413. <https://doi.org/10.1007/s00792-016-0831-0>
- Ghosh D (2021) Laptev Sea. *WorldAtlas*. <https://www.worldatlas.com/seas/laptev-sea.html>
- Hartmann DL (1994) *Global physical climatology*. Acad. Press, San Diego, 411 pp
- Heil P (2006) Atmospheric conditions and fast ice at Davis, east Antarctica: a case study. *J Geophys Res* 111(C5). <https://doi.org/10.1029/2005jc002904>
- Hellmer HH (2004) Impact of Antarctic ice shelf basal melting on sea ice and deep ocean properties. *Geophys Res Lett* 31(10):n/a–n/a. <https://doi.org/10.1029/2004gl019506>
- Hurrell JW, Kushnir Y, Ottensen G, Visbeck M (2003) An overview of the North Atlantic oscillation. *The North Atlantic Oscillation. Clim Sig Environ Impact*, pp 1–35. <https://doi.org/10.1029/134gm01>
- Itkin P, Krumpen T (2017) Winter sea ice export from the Laptev Sea preconditions the local summer sea ice cover and fast ice decay. *Cryosphere* 11(5):2383–2391. <https://doi.org/10.5194/tc-11-2383-2017>
- Kapsch M-L, Graverson RG, Tjernström M, Bintanja R (2016) The effect of downwelling longwave and shortwave radiation on arctic summer sea ice. *J Clim* 29:1143–1159. <https://doi.org/10.1175/JCLI-D-15-0238.1>
- Laidler GJ, Ford JD, Gough WA, Ikummaq T, Gagnon AS, Kowal S, Qrunnut K, Irngaut C (2008) Travelling and hunting in a changing Arctic: assessing Inuit vulnerability to sea ice change in Igloodik, Nunavut. *Clim Change* 94(3–4):363–397. <https://doi.org/10.1007/s10584-008-9512-z>
- Meehl GA, Chung CT, Arblaster JM, Holland MM, Bitz CM (2018) Tropical decadal variability and the rate of Arctic Sea ice decrease. *Geophys Res Lett* 45(20). <https://doi.org/10.1029/2018gl079989>
- Panicker DV, Vachharajani B, Ram Rajak D (2021) Evolution of sea ice thickness over various seas of the Arctic Region for the years 2012–13 and 2018–19. In: Sahni M, Merigó JM, Jha BK, Verma R (eds) *Mathematical modeling, computational intelligence techniques and renewable energy. Advances in intelligent systems and computing*, vol 1287. Springer, Singapore. [https://doi.org/10.1007/978-981-15-9953-8\\_21](https://doi.org/10.1007/978-981-15-9953-8_21)
- Qian W, Wu K, Chen D (2015) The Arctic and polar cells act on the Arctic Sea ice variation. *Tellus a: Dyn Meteorol Oceanogr* 67(1):27692. <https://doi.org/10.3402/tellusa.v67.27692>
- Rudels B (1990) Haline convection in the Greenland sea. *Deep Sea Res Part A Oceanogr Res Papers* 37(9):1491–1511. [https://doi.org/10.1016/0198-0149\(90\)90139-m](https://doi.org/10.1016/0198-0149(90)90139-m)
- Serreze MC, Barrett AP, Cassano JJ (2011) Circulation and surface controls on the lower tropospheric air temperature field of the Arctic. *J Geophys Res* 116(D7). <https://doi.org/10.1029/2010jd015127>

- Shah R, Srivastava R, Patel J (2020) Study of regional heterogeneity of cloud properties during different rainfall scenarios over monsoon-dominated region. *J Water Clima Change* 12(4):1086–1106. <https://doi.org/10.2166/wcc.2020.178>
- Shah R, Srivastava R (2020) Effect of ocean warming on cloud properties over India and adjoining oceanic regions. *Pure Appl Geophys* 177(12):5911–5925. <https://doi.org/10.1007/s00024-020-02607-9>
- Simon A, Gastineau G, Frankignoul C, Lapin V, Ortega P (2022) Pacific decadal oscillation modulates the Arctic sea-ice loss influence on the midlatitude atmospheric circulation in winter. *Weather Clim Dyn* 3(3):845–861. <https://doi.org/10.5194/wcd-3-845-2022>
- Singh RK, Maheshwari M, Oza SR, Kumar R (2013) Long-term variability in Arctic Sea surface temperatures. *Polar Sci* 7(3–4):233–240. <https://doi.org/10.1016/j.polar.2013.10.003>
- Timokhov LA (1994) Regional characteristics of the Laptev and the East Siberian seas: climate, topography, ice phases, thermohaline regime, circulation. *Berichte zur Polarforschung* 114: 15–32. <http://epic.awi.de/26322/1/BerPolarforsch1994144.pdf>
- Visbeck M, Fischer J, Schott F (1995) Preconditioning the Greenland sea for deep convection: ice formation and ice drift. *J Geophys Res* 100(C9):18489. <https://doi.org/10.1029/95jc01611>
- Wang M, Overland JE (2012) A sea ice free summer Arctic within 30 years: an update from CMIP5 models. *Geophys Res Lett* 39(18). <https://doi.org/10.1029/2012gl052868>
- Zakharov VF (1966) The role of flaw leads off the edge of fast ice in the hydrological and ice regime of the Laptev Sea. *Oceanology* 6:815–821
- Zhang J, Tian W, Chipperfield MP, Xie F, Huang J (2016) Persistent shift of the Arctic polar vortex towards the Eurasian continent in recent decades. *Nat Clim Chang* 6(12):1094–1099. <https://doi.org/10.1038/nclimate3136>

# **Innovations in Sustainable Infrastructure Development**



# Performance Evaluation of Control Variables for the Development of a Blockchain Model for Construction Projects



Debasis Sarkar and Purvesh Raval

**Abstract** Many factors affect the progress and life cycle of a real-estate project. Therefore, evaluating such factors has become an indispensable and fundamental component of every firm operating in the real-estate industry. This paper aims at identifying and evaluating the control variables associated for the development of blockchain model applicable to construction projects. When a cutting-edge technology like blockchain is applied to this kind of job, it has the potential to become far more efficient. As a result, the purpose of this research is to develop a preliminary process framework that can direct users who are interested in utilising blockchain technology as a tool, as well as to identify the factors that influence the use of blockchain technology as a smart contract, supply chain management, and financing instrument tool by presenting them in the form of key performance indicators (KPIs). Eight major project factors like technology, organisation, finance, environment, BIM, data management and security, input–output, and project-process related have been identified. Subsequently significant KPIs have been identified under each category. Multi-criteria decision-making (MCDM) tool analytic network process (ANP) is used to establish the weights of the criterion based on the replies from three-stage questionnaire surveys performed among industry professionals working for prominent construction businesses in Ahmedabad, Gujarat, India. This study will reduce the possibility of time and cost overrun and enhance the probability of successful completion of a project within stipulated time and cost frame.

**Keywords** Building information modelling (BIM) · Key performance indicator (KPI) · Analytic network process (ANP) · Blockchain

---

D. Sarkar (✉) · P. Raval  
Pandit Deendayal Energy University, Gandhinagar, India  
e-mail: [debasis.sarkar@sot.pdpu.ac.in](mailto:debasis.sarkar@sot.pdpu.ac.in)

P. Raval  
e-mail: [purveshraval24@gmail.com](mailto:purveshraval24@gmail.com)

# 1 Introduction

The integrity and dependability of data may be significantly improved with blockchain technology, a system that links blocks of information. The industrial landscape is undergoing a rapid transformation due to the fourth industrial revolution (4IR), which is defined by the convergence of developing technologies. The construction industry is not an exception, and numerous convergence activities have taken place due to the integration of various emerging technologies. Some examples of these technologies include building information modelling (BIM), drones, augmented reality (AR), 3D printing, enterprise resource planning (ERP), virtual reality (VR), the Internet of Things (IoT), and blockchain technology, among others (Kim et al. 2020). This investigation focuses on the performance evaluation of control variables for developing the BIM-integrated blockchain model for construction projects. This new technology integration is one of the topics covered in this investigation.

Information together like links in a chain. The article “Blockchain Technology Development Strategy” (Korea Institute of Science and Technology Information 2018) identifies blockchain technology as one of the emerging technologies that ensure data reliability and security while increasing efficiencies. Blockchain technology is one of the technologies expected to have a significant impact in the future. The technology behind blockchain makes it possible for members in a network to work together to record, validate, store, and extract information without the need for a centralised data middleman. Which of the following best describes a distributed ledger system that encourages decentralisation, openness, and data integrity? (Seo 2017). Blocks are connected in order of their creation sequence, and within each block is a collection of transaction records that each has their unique hash value. When opposed to a centralised database system, the fact that the identity of each block is determined by its hash value and that of the block that came before it makes it far more difficult for the data to get corrupted. Using blockchain technology has several significant benefits, such as lowering transaction costs, making it harder to fake or change data, and giving people more freedom.

In their research, Tezel et al. (2020) observed that the construction sector receives criticism for moving slowly to adopt new technologies. Real-time asset tracking, smart contracts, and crypto-currencies may improve commercial transactions in the construction sector. The major issues of construction sector are the lack of motivation to adopt and implement new technologies. Undergoing digital transformation by construction industry is also the need of the hour. There are lot of issues in the traditional procurement system, lack of coordination among the various hierarchy levels of the construction industry, lack of cooperation between the various stakeholders, poor management of resources, unhealthy competition and also very less profit margins are real concerns of the construction industry. The proposed blockchain model would definitely take care of most of these concerns of the construction sector.

## 2 Background

The technology behind blockchain is one of the most revolutionary developments of the past ten years. Its ability to record, enable, and secure a vast number of different types of transactions raises an intriguing question: can the same distributed ledger technology that powers bitcoin also enable better execution of strategic projects in a traditionally conservative industry like construction, which involves large teams of contractors and subcontractors as well as an abundance of building codes, safety regulations, and standards? According to David Bowcott, global director of development, innovation, and intelligence in Aon's Global Construction and Infrastructure Department, "Increasingly, we are thinking more carefully about when and where we need to compete and what can we share and collaborate on." Saving money, freeing up significant resources, and accelerating the completion of these complicated projects might all be accomplished by using blockchain technology to automate the contractual processes and paperwork that underpins them. (Quotes are taken, unless otherwise specified, from interviews that we did as part of our research). Genuine estate construction and development projects enabled by blockchain in the commercial real-estate sector, HerenBouw, based in Amsterdam, is utilising blockchain technology for an expansive development project in the city's harbour. According to Marc Minnee, the founder of Propulsion Consulting, HerenBouw's goal was to establish a project management system enabled by blockchain technology to make the building construction life cycle more efficient. The application Minnee developed for HerenBouw to employ blockchain technology focuses on registering transactions at legally critical moments, an area where precision and an audit trail are critical. "Blockchain provides a platform for visibly cascading work items down the chain and holding everyone accountable for accomplishing essential tasks," said Minnee. "Blockchain has the potential to revolutionise the way work gets done." Information prompt, clear communication, and fewer errors are some of the benefits offered by the system. According to Minnee, "Stakeholders have a clear and evenly distributed motivation to register these facts on-chain: Either you will not get what you purchased or get paid." They also build trust with one another, which helps to make their respective business processes run more smoothly. "Stakeholders spend more time exploring creative design and building process possibilities," according to the report. Launch of blockchain project pilots are currently under construction (Tapscott et al. 2019).

According to estimates provided by Aon, a worldwide risk adviser to the construction industry, 95% of the building construction data is lost when the building is handed over to the first owner. Briq, a blockchain company based in California, showcases the potential to capture and secure the documentation of a construction project in a blockchain ledger. This ledger is accessible to all parties involved in the project, and it can be given to the owner as a deliverable. Briq, a company based in Minneapolis, was hired by Gardner Builders to create a "Digital Twin" of a newly constructed office building. This "Digital Twin" included an inventory of every asset, broken down by room. According to Bassem Hamdy, CEO of Briq, "when a product or

specification has to be discovered in a building, there is finally a location to search for what is actually in that building.

When a product or standard needs to be found in a structure," the specs stored in blockchain are very comprehensive. They include paint colours, ceiling fittings, LED bulbs, and door hardware. Additionally, they include user manuals, warranties, and a countdown clock that building owners can monitor. "Any improvements and refurbishments to the building can be documented, and the whole repository can be transferred to new owners if the asset is put up for sale," said Ellis Talton, Briq's director of growth marketing. "If the asset is put up for sale, the repository can be transferred to the new owners," said Talton. To put it another way, the building owners are provided with a living ledger that details everything that has occurred with the building, overcoming cultural obstacles (Tapscott et al. 2019).

Established procedures in the building industry may slow down the general deployment of blockchain technology. "The construction business is technologically advanced in many facets of it does," said Talton. "The industry as a whole is very innovative." However, a strong emphasis is placed on personal connections in this field. Many businesses are privately held and owned by families. Relationships that have existed for decades can be considered when choosing general contractors and subcontractors. Talton further mentioned that very little money, less than one percent of revenues, is put into up-front contracting and IT infrastructure for managing complicated building projects (whereas in aerospace and automotive, this amount ranges from 3.5% to 4.5%). According to him, "the building process, including the people and materials, accounts for the great majority of the costs associated with the project." According to Scott Nelson, CEO of Sweetbridge, blockchain-based project management might work particularly well in the construction industry: "Projects are well-structured, and their foundation is in contracts". The goals are crystal clear: complete the task on schedule, according to specification, and without rework. Traditional project management methods are still effective, but some projects could benefit from a more decentralised and agile approach. In such an approach, transparency is prioritised, and participants can be reimbursed for labour performed and for results achieved. The potential applications of blockchain technology in project management has been explored and implemented by Tapscott et al. 2019).

Blockchain technology will eventually have game-changing applications in the field of project management. We strongly recommend that organisations investigate and make the most of this potential. Here are a few steps that come next. Determine the various applications that could benefit from using blockchain. Look for places where the endeavour's success depends on mobilising resources outside the organisation's limits, where identities, contracts, and payments must be audited and protected, and where the provenance and ownership of assets must be tracked.

Build prototypes and get the first feedback from pilot programmes. Carry out a first investigation: Audit the systems that are now being used to talk to the people who are already utilising them, and think about who would need to be engaged in determining feasible solutions, selecting one to prototype, creating the pilot, and engaging in testing. Develop a rationale for why investing in blockchain will benefit your company. Find ways how blockchain can improve project success, such

as increasing procedures and organisational ability to identify and exchange vast volumes of data with specified persons and entities. According to David Bowcott of Aon, “Collectively, we are all better off if we encourage data collaboration and use blockchain and machine learning to help us establish longer-term industry road maps for investments and technologies that can boost productivity and efficiency and lessen risk.” Even while project management principles will continue to be essential, blockchain technology makes it possible for managers to concentrate their efforts on finding solutions to challenges and improving the quality of the project’s deliverables (Tapscott et al. 2019).

### 3 Objectives and Problem Statement

The primary objectives of the research are as follows:

1. To perform bibliometric analysis for significant keywords of this research.
2. To study the control variables for the development of a blockchain model and to evaluate the performance variables through a multi-criteria decision-making (MCDM) tool for construction projects.

## 4 Literature Review

### 4.1 *Performance Evaluation of Control Variables for the Development of a Blockchain Model*

There is a chance that the model for the information flow computation of seven key performance indicators will be able to eliminate the slowdowns in project performance caused by the wrong structure and measurement of information (Bapat et al. 2021).

According to Coates et al. (2010), it has come to light that key performance indicators (KPIs) make it possible to organise and display information in a systemic manner, which is necessary for reliable assessment and monitoring of business benefits brought about by BIM adoption. As a consequence of this, KPIs can serve as a method for comparing the success of various BIM adoptions about the following objectives: measuring the quality of projects; standardising information and measurement processes throughout the community; setting appropriate benchmarking targets, and recording the effectiveness of action. (Demediuk et al. 2021).

To prioritise KPI using factor analysis, Sarkar (Tapscott et al. 2019) conducted a questionnaire survey with 69 different respondents. There are 41 KPIs, and 15 of them have been determined to be the most important. Additionally, the process flow for effectively using BIM in facility management has been outlined in a sequence that makes logical sense. Since only a few years ago, the use of BIM in the offsite

building has been increasing significantly, a barrier that prevents the varied output formats of BIM software from being interoperable has emerged due to the lack of widespread adoption of universal BIM standards. In order to facilitate the dissemination of information, Nawari (2012) produced the “Model View Definition” handbook. According to Becerik-Gerber et al. (2012), traditional construction engineering and management have been unsuccessful in resolving the challenges that have arisen due to incorrect communication flows between members of the project team and inefficient management in the AEC industry. They have also implemented a remote construction monitoring system in addition to the virtual collaboration technique that they are using for this project. Sarkar (2011) created the conceptual framework for incorporating risk management into BIM. Because of this integration, risk can be evaluated stage-by-stage throughout the project (Becerik-Gerber et al. 2012).

Additionally, BIM is in charge of risk management on the floor above it, which can improve project performance through planning the project and monitoring it at a more granular level. A safety risk management strategy may be valuable to a project if the project manager can properly combine safety management with building information modelling (BIM). According to Sarkar (Tapscott et al. 2019), early clash detection of MEP services can acquire the targeted project performance increase for urban transportation projects in India, such as mass rapid transit systems (MRTS). This research has also helped the architecture, engineering, and construction (AEC) industry by making an excellent framework for integrating BIM and risk management (Sarkar and Gujar 2021).

The analytic hierarchy process (AHP) and the analytic network process (ANP) are two similar decision-making multi-criteria decision-making (MCDM) procedures that Saaty first presented in 1980, 1996, and 2006.

## 5 Bibliometric Analysis

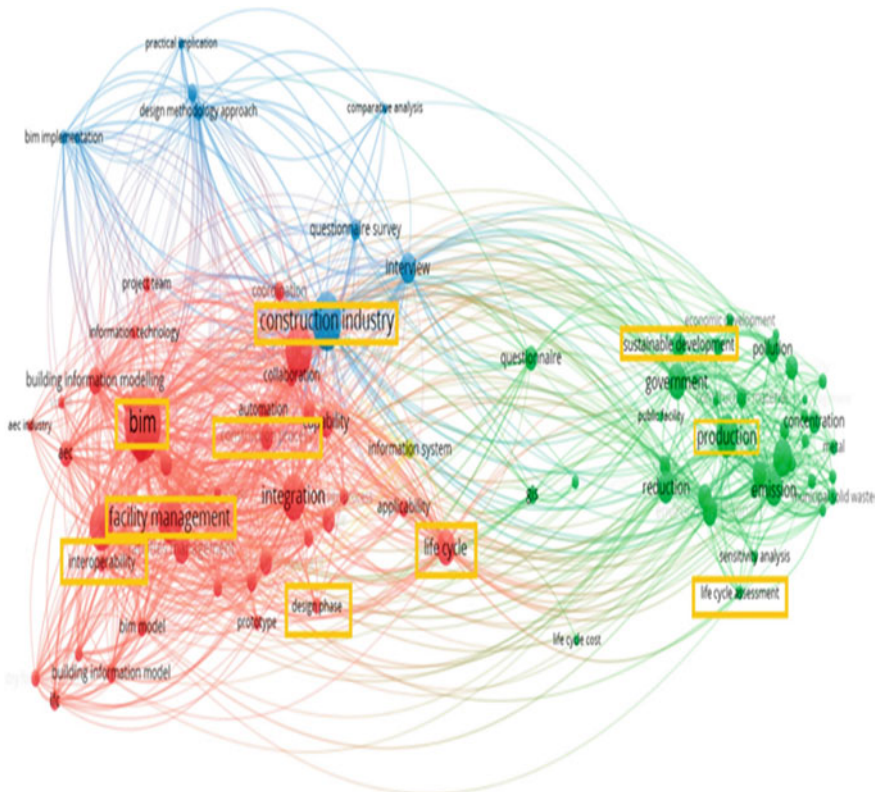
The VOS viewer incorporates not one, not two, but three distinct methods of analysis: network visualisation, overlay visualisation, and density visualisation. The magnitude of each circle depicts the significance of the corresponding term. The proximity of two circles represents the connection that exists between the two circles. When the affinity is more robust, the distance between the two places is shorter, and when the affinity is weaker, the distance between the two places is greater. The circle's colour indicates the cluster that the circle is a part of, and there are several different clusters, each of which is represented by a unique hue.

A representation of a network is shown in Fig. 1. Within the red region, BIM serves as the central focus, and the degree to which the phrases “facility management (FM),” “construction process,” and “design phase” are related to one another begins to recede. The majority of the publications are focused on facilities management (FM), whereas the construction and design sections are lacking. The phrase “life cycle” serves as a bridge between the red and green sides. According to the study of the data visualisation, the terms in the green region have “production” at their

centre, with “Sustainable Development” and “life cycle assessment” related to it. However, the phrases “construction industry” and “BIM” are located at a significant distance from the phrase “Sustainable Development,” which indicates that it is of lower relevance. The association with the entire life cycle is also meaningless to consider. This circumstance, or the lack of progress in the construction sector, is mirrored in the development of sustainable building practices (Nawari 2012).

The depiction of the research trend with time as the criterion is shown in Fig. 2. The terms related to BIM as the core are highlighted since this has been the primary focus of study over the last five years. As a result, the following present picture of the field may be disclosed based on the bibliometric study, which is described in Figs. 1 and 2.

It is currently in the preliminary and intermediate stage, but the integration of BIM and network systems can support the improvement of the construction and operation phases of the architecture, engineering, and construction (AEC). This integration makes it easier to retrieve and manage information, and it is currently taking place.



**Fig. 1** Visualisation of research hotspot or major cluster sets and keywords in the construction industry via VOS viewer



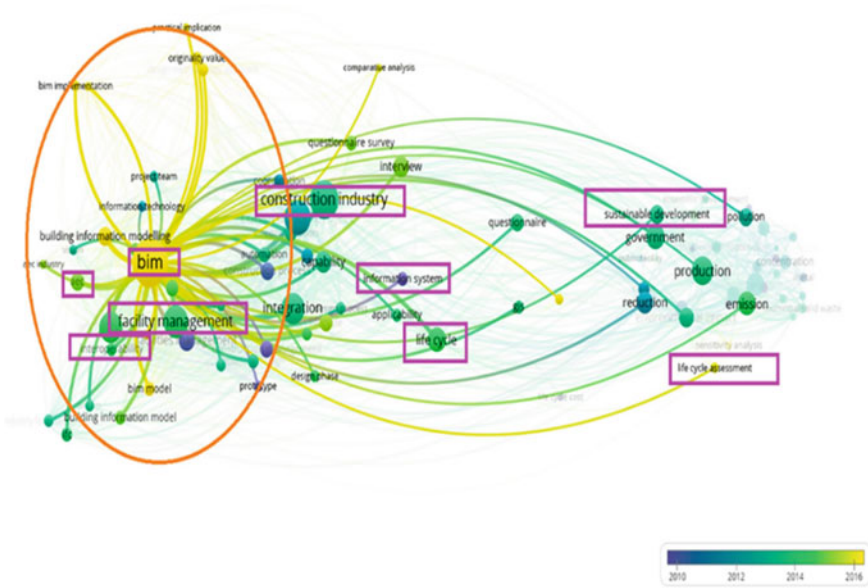


Fig. 2 Visualisation of research hotspots in the construction industry

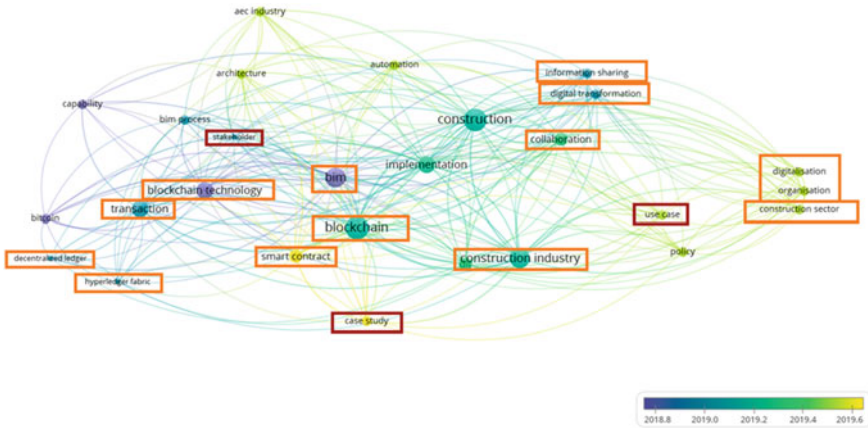
The utilisation of BIM over the entirety of a building’s life cycle presents both opportunities and challenges. There is still more work to ensure the interoperability of data information across the building life cycle.

The facility management phase attracted more attention than the building design, construction, and maintenance stages throughout the study into the construction industry and BIM. The concept that problems with the life cycle should be addressed early on has received much attention in recent years.

As shown in Fig. 3, the construction sector has undergone a digital transition in recent years, which may be considered an emerging trend. This will become the dominant development trend in the construction business in the foreseeable future, and it is worthwhile to investigate the application of blockchain technology in the construction sector (Nawari 2012).

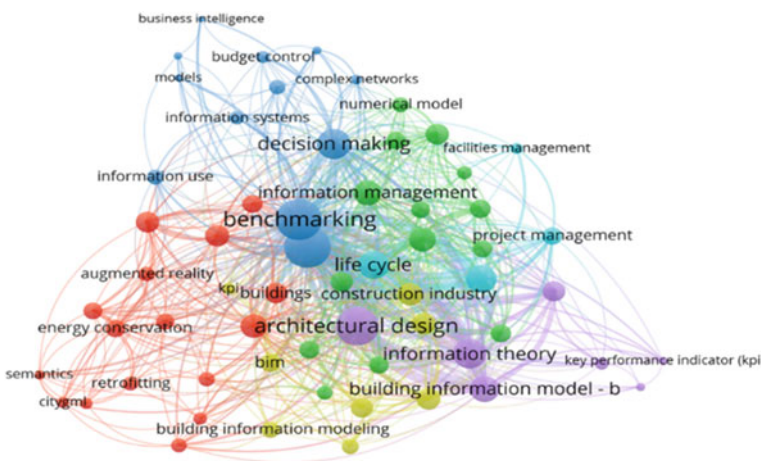
The Scopus database was searched to get the articles that were analysed. Scopus provides a more diverse selection of articles (Echchakoui 2020) In addition, Scopus is among the most exhaustive databases of journals that have been subjected to peer review. In April of 2022, a search for published works on the Internet was carried out using the terms “building information modelling” (BIM) and “blockchain” as the beginning keywords. It was determined to search for certain types of literature, including journals, conference proceedings, title terms, and years. During the preliminary investigation, 127 publications about scientific literacy were discovered, 89 of which were engineering-related. The Scopus database’s indexed copies of the articles that matched the criteria were culled. This data does not contain newspaper articles, books, book references, or book chapters. A total of 89 items were selected from the





**Fig. 3** Visualisation of research hotspots in the application of blockchain in the construction industry

total of 127 that were mentioned. The paper had been downloaded in CSV format before it could be processed using the VOS viewer. This would allow for the patterns in the bibliometric form to be shown and analysed (Jan et al. 2009). The number of keywords utilised may be changed according to one’s preferences, and less important keywords can be eliminated. Using the VOS viewer programme, it is possible to mine data, create maps, and organise the articles that have been obtained from the database. The overlay of BIM and blockchain in Fig. 4, made with the VOS viewer, shows how important both are in the real world. (Echchakoui 2020).



**Fig. 4** Overlay visualisation of BIM and KPIs

For a more in-depth bibliometric study, see here. KPIs have been substituted for the blockchain term. A total of 82 papers have been recognised as having some study on KPIs associated with BIM. This term has been used a total of 141 times in research articles, and it is used three times in each study. It provides an overlay representation of BIM and KPIs-related papers studied in the VOS viewer programme, as seen in Fig. 2. This demonstrates how vital key performance indicators are about building information modelling (BIM).

As part of the ongoing bibliometric research, the term “blockchain” was included in the list of keywords alongside “BIM” and “KPIs.” This returns the result that there were no documents discovered. This suggests that most academics are attempting to connect BIM with other types of technology but that no one has begun research to determine key performance indicators for the integration of BIM with blockchain. Based on these data, identifying key performance indicators (KPIs) for any new technology is shown to be significant. Also, this kind of identification is essential for the future of realistic development and to help researchers work in this direction so that BIM and blockchain can be used together (Nawari 2012) (Fig. 5).

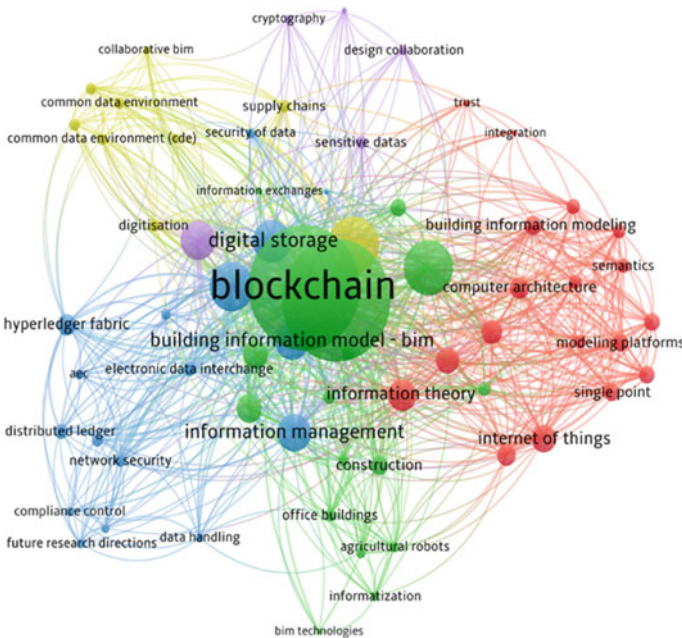
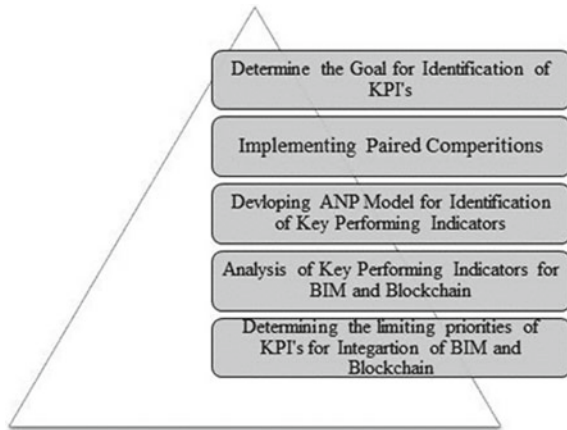


Fig. 5 Overlay visualisation of BIM and blockchain

**Fig. 6** Algorithm of ANP model for identification of control variables



## 6 Conceptual Framework

It is necessary to evaluate various control variables to develop the blockchain model by identifying the key performance indicators (KPIs). Because of this, it is first necessary to list out all potential variables related to the development of integrated BIM and blockchain technology. This will allow for improved performance of construction projects that use blockchain technology. The fundamental framework, which Gongbo and Shun (2011) made effective use of, has been chosen. Based on these essential control variables, which comprise 201 in total, the process of determining key performance indicators (KPIs) will be carried out to construct a complete framework. The key performance metrics were generally broken down into eight different categories, which are (i) associated with technology; (ii) associated with organisations; (iii) associated with finances; (iv) associated with the environment; (v) associated with building information modelling; (vi) associated with data management and security; (vii) associated with input and output, and (viii) associated with projects and processes (Gongbo and Shun 2011) (Fig. 6).

## 7 Methodology

This section describes the process taken to perform the systematic literature review and describes its results, including the extensive list of challenges and opportunities compiled from the literature that informed the development of the framework and bibliometric indicators that describe the body of literature reviewed. In addition, the remaining research methods used to develop the framework are explained, namely a focus group discussion, an in-depth interview, and the socio-technical systems approach adopted.

A preliminary survey was carried out with the use of these possible markers. A well-structured questionnaire was developed to investigate the use of BIM and blockchain technologies once the building phase is complete. The questionnaire was divided into three distinct parts when it was constructed. In the initial part of the survey, we gathered some basic information about the respondents, and we also asked them a few questions to better determine their level of technological savvy. In the second and third sections of the pilot survey, the respondent is asked to rate the significance of the indicators that have been discussed thus far on a scale that ranges from five (extremely important), four (very strongly important), three (strongly important), two (moderately critical), and one (not at all important). In Ahmedabad, Gujarat, those individuals who had some kind of direct or indirect connection to the building information modelling (BIM) business were the focus of the inquiry. The group of people who used BIM comprised professionals from various fields, such as architects, structural engineers, electrical engineers, plumbing experts, HVAC experts, project management consultants, and other BIM service providers. Around 15 industry people from Ahmedabad and the surrounding area in Gujarat who were directly or indirectly involved with BIM technology were handed the questionnaire. There were 12 “yes” answers from these people who were asked to be respondents.

In Annexure 1, the key performance indicators (KPIs) associated with the performance evaluation of control variables for the development of the blockchain model are listed, beginning with F1 and ending with F201, together with the reference.

## 8 Case Study and Analysis

Building information modelling (BIM) is one of the most exciting innovations to emerge in recent years in design, engineering, and construction. Even though its use is still relatively new and there is much to learn about it, it is altering how contractors and engineers conduct business. Observing the implementation of BIM by other companies and their successes and failures along the road is one method for gaining knowledge in this area. BIM was initially developed more than a decade ago to differentiate the information-packed architectural 3D modelling from the conventional 2D sketch. It is being lauded as a saviour for complex projects by those who support it due to its capacity to repair problems early on in the design stage and precisely schedule construction. This ability is the primary reason for this praise.

BIM has seen a surge in popularity in recent years, there is still no consensus over how to define it. “BIM is the virtual representation of the physical and functional aspects of a facility from its origin onward,” said Patrick Suermann, PE, a testing team leader for the National Building Information Model Standard (NBIMS). As such, it functions as a shared information repository for cooperation across the whole life cycle of a facility. According to the National Institute of Building Sciences (NIBS), it is “a digital representation of physical and functional characteristics of a facility and a shared knowledge resource for information about a facility forming a reliable basis

for decisions during its life cycle, defined as existing from its earliest conception to its demolition.” [citation needed] In general, however, building information modelling (BIM) technology enables the digital construction of an accurate virtual model of a structure. The finished computer-generated models contain precise and well-defined geometry and relevant data required to aid the construction, manufacturing, and procurement processes necessary to materialise the final building. These models may be found on the computer (Nawari 2012).

BIM is a desktop computer environment that includes 3D modelling concepts, information database technology, and interoperable software. This environment can be used by architects, engineers, and contractors to design a facility and simulate its construction. BIM is the primary component of building information modelling (BIM). Because of this technology, members of the project team can develop a virtual model of the building and all of its systems in three dimensions, which can communicate the information they have generated. The building geometry, spatial linkages, quantitative characteristics of building components, and geographic information are some of the aspects that are included in the model. Similarly, the drawings, specifications, and construction details are vital to the model. The project team can swiftly identify design and construction concerns and find solutions to those issues in a virtual environment far before the construction phase in the physical world.

Therefore, BIM is a procedure that you use to collect and manage building data throughout the life cycle of a project. Building design and construction often benefit from utilising three-dimensional, real-time, and dynamic software. This helps to control and improve overall efficiency. The process results in the production of the building information model, which incorporates all of the pertinent data relating to the geometry of the building, the spatial relationships within the building, the geographic information, and the quantities and properties of the building components. Contractors, architects, engineers, and others in the construction industry are continually looking for new methods to enhance the BIM process, causing construction technology to continue to advance over time. According to Chuck Eastman, director of Digital Building Laboratory, one of the many significant advantages that may be gained from making use of modern BIM design tools is that it: at this point, they define objects using parameters. That is to say, and the objects are described in terms of parameters and relations to other objects so that if a change is made to a related object, this one will likewise be updated to reflect the new state. Objects that use parameters can automatically re-build themselves by the rules that are inherent in them. The requirements may be straightforward, such as requiring a window to be entirely contained within a wall and moving the window along with the wall, or they may be intricate, specifying size ranges and addressing aspects such as the actual link between a steel beam and column (Nawari 2012).

The questionnaire includes two essential topics: blockchain technology and BIM. Participants were asked to rate how interested they were in adopting blockchain technology for supply chain management and smart contracts on a scale from one to five. This was part of the inquiry that asked respondents about their interest in using blockchain technology (from extremely interested to not at all interested). The outcome was dominated by weighting (3) being interested, at 44.44% of the

total. Other rank distributions were as follows: (4) highly interested for 29.63% of respondents; (2) moderately interested for 22.22% of respondents; (1) somewhat interested for 3.7% of respondents; and (0) not at all interested for 0% of respondents. This demonstrates that individuals are interested in using blockchain for BIM, even though there is not currently a substantial available framework.

## 9 Result Interpretation

The findings of the ANP as a whole demonstrate that technologically linked aspects have gotten the highest amount of attention out of all of the KPIs. This is measured in terms of the relative relevance of each KPI compared with the others. The following is a list of the additional aspects in descending order of how important they are: BIM, the environment, data management and security, organisation, project-process, financial considerations, and input–output relationships. This result is supported by the fact that the weight given to the technology-related factor is 0.265, which is much higher than the weights given to any of the other factors when those factors are evaluated to make an integrated model that combines BIM and blockchain (Table 1).

**Table 1** Ranking of major factors based upon normalisation

Sr. No	KPIs	Normalised	Idealised	Rank based on the calculated weight from the study
1	Technology related factors	0.265	1.000	1
2	Organisation related factors	0.125	0.472	5
3	Finance related factors	0.048	0.181	7
4	Environment related factors	0.143	0.540	3
5	BIM related factors	0.182	0.687	2
6	Data management and security related factors	0.137	0.517	4
7	Input–Output related factors	0.039	0.147	8
8	Project–Process related factors	0.061	0.230	6

## 10 Discussion

The findings of this study demonstrate how well the ANP approach works for examining the KPIs for the use of blockchain technology in the construction sectors. It has been noted that eight important components have been grouped together from the 201 discovered KPIs. The most crucial aspects may be determined by prioritising and ranking these eight factors using the various MCDM approaches. For effective project implementation without significant schedule and expense overruns, the project authorities might apply corrective and preventative mitigation measures.

By integrating blockchain and building information modelling (BIM), a construction project may have a single source of truth for all of its details (Kim et al. 2020). A trustworthy digital twin of the asset, such a model may assist with its design, development, operation, and maintenance throughout its existence, to make a model of the blockchain and building information model used in the infrastructure project that is being studied right now.

## 11 Conclusion

Following the completion of this research work, it is possible to conclude that, according to the ranking of significant factors based upon normalisation, the technological related factors weightage of 0.265 and the building information modelling related factors weightage of 0.182 are, among other factors, the highest and second-highest, respectively, in terms of importance when it comes to the development of a blockchain model for use in construction projects. It is possible to conclude from this that the significance of technology and BIM will play a key part in creating a blockchain model for the construction sector, while the finance related factors weightage of 0.048 and the input–output related factors weightage of 0.039 don't add much to building a blockchain model for construction projects based on these ANP-based results.

**Disclosure Statement** The authors reported no potential conflict of interest.

## Annexure 1

See Table 2.



**Table 2** Key performance indicators (KPIs) related to performance evaluation of control variables for the development of the blockchain model

Sr. no.	Description of KPIs	References
<i>Technology-related</i>		
F1	Complexity in development of integration of building information modelling with blockchain technology	Li et al. (2018)
F2	Complexity in the selection of specific blockchain platform	Hamledari and Fischer (2021)
F3	Compatibility of building information modelling with blockchain technology	Li et al. (2018)
F4	Compatibility of the integrated model with the existing market	Shojaei et al. (2019)
F5	Cost of development of blockchain technology	Hamledari and Fischer (2021)
F6	Cost of implementation of an integrated model	Ye et al. (2020)
F7	Operational and maintenance cost of blockchain technology	Shojaei et al. (2019)
F8	Relative advantages of blockchain technology	Hamledari and Fischer (2021)
F9	Privacy of data exchange between stakeholders	Hamledari and Fischer (2021)
F10	Scalability of blockchain tool	Akhavan et al. (2021)
F11	Availability of specific blockchain tool	Li et al. (2018)
F12	Trialability of an integrated model	Hargaden et al. (2019)
F13	Observability of data in blockchain model	Hamledari and Fischer (2021)
F14	Immutability of information stored in blockchain	Li et al. (2018)
F15	The perceived novelty of the integrated model	Ye et al. (2020)
F16	Level of integration of the Internet of things and cloud computing	Li et al. (2018)
F17	Disintermediation of existing centralised banking	Ye et al. (2020)
F18	Perceived benefits of payment automation	Hamledari and Fischer (2021)
F19	Computability of devices used in integrated model	Sarkar et al. (2015)
F20	Infrastructural facility	Alizadeh Salehi and Yitmen (2018)
F21	Increase in data availability	Pradeep et al. (2020)
F22	Reduction of information asymmetry	Akhavan et al. (2021)
F23	Reliability of blockchain technology	Hamledari and Fischer (2021)
F24	Exclusion of false information from contractual information	Kim et al. (2020)
F25	Hacking attempts system denials	Ye et al. (2020)
F26	High-security encryption	Li et al. (2018)
F27	Contract conclusion with a reasonable fee	Hargaden et al. (2019)

(continued)



**Table 2** (continued)

Sr. no.	Description of KPIs	References
F28	Transparency of payment process	Li et al. (2018)
F29	The integrity of blockchain technology	Hunhevicz and Hall (2020)
F30	Confidentiality of data shared in the developed model	Sarkar et al. (2015)
F31	Interoperability of blockchain with other technology	Akhavan et al. (2021)
F32	Perceived challenges for adopting blockchain in the payment process	Li et al. (2018)
F33	The hype of the developed model	Li et al. (2018)
F34	Trust in the blockchain technology	Pradeep et al. (2020)
F35	Storage capacity of computers	Pradeep et al. (2020)
F36	Decentralisation of the existing banking system	Shojaei et al. (2019)
F37	Inclusiveness of blockchain tool	Kim et al. (2020)
F38	Maturity of blockchain technique in the market	Hamledari and Fischer (2021)
<i>Organisation related</i>		
F39	Top management support	Iyer and Jha (2004)
F40	Top management knowledge/awareness	Lokshina et al. (2019)
F41	Firm size in terms of staff	Hamledari and Fischer (2021)
F42	The capability of human resources	Hamledari and Fischer (2021)
F43	Financial resources of the company	Iyer and Jha (2004)
F44	Presence of training facilities	Shojaei et al. (2019)
F45	Organisational culture	Hargaden et al. (2019)
F46	Supportive technological environment	Akhavan et al. (2021)
F47	Perceived risk of vendor lock-in	Kim et al. (2020)
F48	Perceived efforts in collaboration	Hamledari and Fischer (2021)
F49	Organisation learning capability	Iyer and Jha (2004)
F50	Organisation innovativeness	Lokshina et al. (2019)
F51	Information technology governance	Hunhevicz and Hall (2020)
F52	Enormous resources (energy, infrastructure)	Iyer and Jha (2004)
F53	High need for process harmonisation	Ye et al. (2020)
F54	Well-defined scope of organisation	Hunhevicz and Hall (2020)
F55	Existing infrastructure for the adoption of blockchain and BIM	Li et al. (2018)
F56	Learning culture of nontechnical staff	Akhavan et al. (2021)
F57	Data management of organisation	Hamledari and Fischer (2021)
F58	Organisational security	Hamledari and Fischer (2021)
F59	Privacy of organisation	Hargaden et al. (2019)

(continued)

**Table 2** (continued)

Sr. no.	Description of KPIs	References
F60	Coordination problem	Hamledari and Fischer (2021)
F61	Specific guidelines for BIM and Blockchain adoption	Kim et al. (2020)
F62	Organisational relationship	Iyer and Jha (2004)
F63	Organisational readiness	Das et al. (2021)
F64	Training and skill development policy	Hunhevicz and Hall (2020)
F65	The reputation of the blockchain platform provider	Das et al. (2021)
F66	The social network of organisation	Pradeep et al. (2020)
F67	Customer response	Akhavan et al. (2021)
F68	The demand of clients to use BIM and blockchain	Lokshina et al. (2019)
F69	The leadership of the BIM manager	Iyer and Jha (2004)
F70	Availability of initial investment	Iyer and Jha (2004)
<i>Finance related</i>		
F71	Transaction's speed	Hamledari and Fischer (2021)
F72	Comprehensibility of the transactions	Hargaden et al. (2019)
F73	Easy verification of transactions	Hamledari and Fischer (2021)
F74	Transparency in transaction	Hamledari and Fischer (2021)
F75	Capitalisation—Ease of the conversion of income or assets into capital	Ye et al. (2020)
F76	Ease in money usage	Shojaei et al. (2019)
F77	Reduction of usage of currency	Hamledari and Fischer (2021)
F78	Removal of economic barriers	Das et al. (2021)
F79	Reduction in inventory problems	Ye et al. (2020)
F80	Increase in sales of real estate	Shojaei et al. (2019)
F81	Ease invalidation of transaction	Hamledari and Fischer (2021)
F82	Increase in net income	Hamledari and Fischer (2021)
F83	Peer-to-peer transaction	Hamledari and Fischer (2021)
F84	Reduction in corruption	Hamledari and Fischer (2021)
F85	Immutability of transactions—It cannot be altered once inserted into the blockchain	Hamledari and Fischer (2021)
F86	Permanent availability of the transactions data	Hamledari and Fischer (2021)
F87	Chronological order of transactions data	Lokshina et al. (2019)
F88	Decreased delays and errors in transactions	Ye et al. (2020)
F89	Instant and digitally recorded money transfer	Akhavan et al. (2021)
F90	Increased revenue in procurement by secured loans	Pradeep et al. (2020)

(continued)

**Table 2** (continued)

Sr. no.	Description of KPIs	References
F91	Real-time tracking of transaction and decreased costs	Kim et al. (2020)
F92	Auditing system which examines and evaluates the financial statement of organisation	Hamledari and Fischer (2021)
F93	Accountability structure serves as the foundation for establishing effective financial processes	Hamledari and Fischer (2021)
F94	Level of financial awareness in stakeholders	Shojaei et al. (2019)
F95	Type of currency utilised in project especially in foreign direct investment	Ye et al. (2020)
F96	Level of dependency on centralised banking system	Hamledari and Fischer (2021)
F97	Type of financial model for cash-in and cash-out flow	Hamledari and Fischer (2021)
<i>Environment related</i>		
F98	Regulations regarding new technology	Li et al. (2018)
F99	Competitive pressure	Shojaei et al. (2019)
F100	Government policy	Shojaei et al. (2019)
F101	Government support	Akhavan et al. (2021)
F102	Stakeholder pressure	Li et al. (2018)
F103	Customer pressure	Hunhevicz and Hall (2020)
F104	Trading partner readiness	Li et al. (2018)
F105	Legal/standards uncertainties	Lokshina et al. (2019)
F106	Institutional-based trust	Hargaden et al. (2019)
F107	Technology progress in the industry	Alizadeh Salehi and Yitmen (2018)
F108	Support from the community	Kim et al. (2020)
F109	Professional consultation	Das et al. (2021)
F110	Expert assistance	Akhavan et al. (2021)
F111	Perceived constraint of infrastructure	Sarkar et al. (2015)
F112	Market turbulence	Ye et al. (2020)
F113	Market power	Ye et al. (2020)
F114	Market dynamics	Sarkar et al. (2015)
F115	Customer readiness	Shojaei et al. (2019)
F116	Consensus among trading partners	Hargaden et al. (2019)
F117	Characteristics of industry	Li et al. (2018)
F118	Industry standards for BIM and blockchain	Shojaei et al. (2019)
F119	Environmentally friendly system	Pradeep et al. (2020)
F120	Ease in operating environment	Pradeep et al. (2020)

(continued)

**Table 2** (continued)

Sr. no.	Description of KPIs	References
<i>BIM related</i>		
F121	Man, hours spent per project	Das et al. (2021)
F122	Speed of development	Chin et al. (2008)
F123	Revenue per head	Pradeep et al. (2020)
F124	IT investment per unit of revenue	Hamledari and Fischer (2021)
F125	Cash flow monitoring	Ye et al. (2020)
F126	Better architecture	Li et al. (2018)
F127	A better product	Chin et al. (2008)
F128	Reduced costs, travel, printing, document shipping	Ye et al. (2020)
F129	Bids won or win percentage	Shojaei et al. (2019)
F130	Client satisfaction and retention	Pradeep et al. (2020)
F131	Employee skills and knowledge development	Shojaei et al. (2019)
F132	Ease of usability/BIM interface	Chin et al. (2008)
F133	Parametric nature of BIM elements	Lokshina et al. (2019)
F134	Feature of “customizable schedule” and “shared parameters”	Chin et al. (2008)
F135	Coordinated 2D (plan) views, 3D views, data attributes and schedules in BIM	Shojaei et al. (2019)
F136	Ease of navigation, search, and highlight elements within BIM	Chin et al. (2008)
F137	Type of software used for 2D-3D modelling and structural modelling	Hamledari and Fischer (2021)
F138	Dependency on service provider of software	Hamledari and Fischer (2021)
F139	Cost of adoption of building information modelling	Hamledari and Fischer (2021)
F140	Cost of implementation of building information modelling along with progress monitoring	Chin et al. (2008)
F141	Operation and maintenance cost of building information modelling	Sarkar et al. (2015)
<i>Data management &amp; Security related</i>		
F142	Data accuracy in integrated model	Shojaei et al. (2019)
F143	Level data security in building information modelling	Hamledari and Fischer (2021)
F144	Complexity of data available at site	Lokshina et al. (2019)
F145	Data transparency in blockchain	Hamledari and Fischer (2021)
F146	Data processing and exploration system	Das et al. (2021)
F147	Data transparency in computer aided design	Akhavan et al. (2021)

(continued)

**Table 2** (continued)

Sr. no.	Description of KPIs	References
F148	System for modification of entered data in blockchain	Das et al. (2021)
F149	Extensive data exchange through wireless technology	Lokshina et al. (2019)
F150	Data storage facility and its implementation cost	Chin et al. (2008)
F151	System for data collection from deployed sensors	Alizadeh Salehi and Yitmen (2018)
F152	Data acquisition system for BIM	Alizadeh Salehi and Yitmen (2018)
F153	System of data auditing and modification	Das et al. (2021)
F154	Method of data communication	Ye et al. (2020)
F155	Internet protocol selection	Hamledari and Fischer (2021)
F156	Data backup and recovery	Shojaei et al. (2019)
F157	System for checking accuracy of collected data of progress	Sarkar et al. (2015)
<i>Input–output related</i>		
F158	Collection of as-built data for the facility	Sarkar et al. (2015)
F159	Data accuracy of collected data for progress monitoring	Hamledari and Fischer (2021)
F160	Availability of infrastructural facility for proper implementation of progress tracking	Sarkar et al. (2015)
F161	Availability of specific progress monitoring tool	Alizadeh Salehi and Yitmen (2018)
F162	Complexity in selection of progress monitoring system	Alizadeh Salehi and Yitmen (2018)
F163	Cost of information gathering	Sarkar et al. (2015)
F164	Cost of information improvisation	Shojaei et al. (2019)
F165	Cost of development of progress monitoring system	Alizadeh Salehi and Yitmen (2018)
F166	Cost of implementation of input devices for progress monitoring	Alizadeh Salehi and Yitmen (2018)
F167	Operational and maintenance cost of progress monitoring system	Sarkar et al. (2015)
F168	Availability of as-built BIM (model) from consultants	Das et al. (2021)
F169	Clarity of facility management (FM) functions to be accomplished using BIM	Sarkar et al. (2015)
F170	Standardisation of formats for collected data	Hamledari and Fischer (2021)
F171	Defined required attributes for each discipline and element of facility	Ye et al. (2020)
F172	Reliability of collected as-built data	Chin et al. (2008)

(continued)

**Table 2** (continued)

Sr. no.	Description of KPIs	References
F173	Quick / in advance decision-making	Sarkar et al. (2015)
F174	Complexity in selection of data analysis and improvisation tool for collected data from site	Hamledari and Fischer (2021)
F175	Potentiality of direct and indirect cost savings in using BIM as FM tool	Shojaei et al. (2019)
F176	Reduced response time to user complain	Sarkar et al. (2015)
F177	Reduced error/improved quality of FM service	Shojaei et al. (2019)
F178	Facilitating access to real-time data	Sarkar et al. (2015)
F179	Improved and standardised record keeping	Hamledari and Fischer (2021)
F180	Asset management and data tracking	Sarkar et al. (2015)
F181	Emergency performance planning	Sarkar et al. (2015)
F182	Improved space management and reduced vacancy	Akhavan et al. (2021)
F183	Analysing and reporting energy efficiency	Sarkar et al. (2015)
F184	Accelerated decision-making for preventive and corrective maintenance	Lokshina et al. (2019)
F185	Better visualisation of design options for retrofit, renovation, or demolition of existing facility	Sarkar et al.(2015)
<i>Project process related</i>		
F186	Size of the project/facility	Hamledari and Fischer (2021)
F187	Type of the project/facility	Sarkar et al. (2015)
F188	Complexity (no. of utilities) of the project/facility	Sarkar et al. (2015)
F189	Duration of project	Das et al. (2021)
F190	Availability of resources at site	Shojaei et al. (2019)
F191	Location of project	Sarkar et al. (2015)
F192	Existing facilities of project	Sarkar et al. (2015)
F193	Access to the database	Hamledari and Fischer (2021)
F194	Standardisation of process and frequency of updating the BIM and database	Sarkar et al. (2015)
F195	Standardisation of data in blockchain	Hamledari and Fischer (2021)
F196	Interoperability of BIM, facility management systems and other database tools	Hamledari and Fischer (2021)
F197	Interoperability of BIM, blockchain and progress monitoring tool	Sarkar et al. (2015)
F198	Effective collaboration between project stack holders	Chin et al. (2008)

(continued)

**Table 2** (continued)

Sr. no.	Description of KPIs	References
F199	Involvement of expertise person in design phase and other strategic decisions	Sarkar et al. (2015)
F200	Existing process for approval of bills	Hamledari and Fischer (2021)
F201	Project management process at site and at office	Hamledari and Fischer (2021)

## References

- Alizadeh Salehi S, Yitmen I (2018) Modeling and analysis of the impact of BIM-based field data capturing technologies on automated construction progress monitoring. *Int J Civ Eng* 16(12):1669–1685
- Akhavan P, Ravanshadnia M, Shahrayini A (2021) Blockchain technology in the construction industry: Integrating BIM in Project Management and IOT in Supply Chain Management, Proceedings of 2nd International Conference on Knowledge Management, Blockchain and Economy, Tehran, 1–7
- Bapat, H, Sarkar D, Gujar R (2021) Evaluation of key performance indicators of integrated project delivery and BIM model for infrastructure transportation project in Ahmedabad, India through decision-making approach. *J Inst Eng (India) Ser A* 102(4):995–1011
- Becerik-Gerber B, Jazizadeh F, Li N, Calis G (2012) Application areas and data requirements for BIM-enabled facilities management. *J Constr Eng Manag* 138(3):431–442
- Chin S, Yoon S, Choi C, and Cho C (2008) RFID+ 4 D CAD for progress management of structural steel works in high-rise buildings. *J Comput Civ Eng* 22(2):74–89
- Coates P, Arayici Y, Koskela K, Kagioglou M, Usher C, and O'Reilly K (2010) The key performance indicators of the BIM implementation process. In: International Conference on Computing in Civil and Building Engineering, vol 30, Nottingham UK, 157–162
- Das M, Tao X, and Cheng J C (2021) BIM security: A critical review and recommendations using encryption strategy and blockchain. *Autom Constr* 126:103682, 1–22
- Demediuk S, Kokkinakis A, Patra MS, Robertson J, Kirman B, Coates A, Chitayat A, Hook J, Nolle I, Olarewaju O, Slawson D, Ursu M, Block F, Drachen A (2021). Performance index: a new way to compare players. In: Atthe 2021 MIT sloan sports analytics conference. IEEE
- Echchakoui S (2020) Why and how to merge Scopus and Web of Science during bibliometric analysis: the case of salesforce literature from 1912 to 2019. *J Mark Anal* 8(3):165–184
- Gongbo Y, Shun L (2011) Analytical study on the protective price of water trading for Valley City. *Energy Procedia* 5:241–249
- Hamledari H, and Fischer M (2021) Role of blockchain-enabled smart contracts in automating construction progress payments. *J Legal Aff Dispute Resolut Eng Constr* 13(1):04520038
- Hargaden V, Papakostas N, Newell A, Khavia A, Scanlon A (2019) The role of blockchain technologies in construction engineering project management. IEEE International Conference on Engineering, Technology and Innovation (ICE/ITMC), Valbonne Sophia-Antipolis, France, 1–6
- Hunhevciz J J, and Hall D M (2020) Do you need a blockchain in construction? Use case categories and decision framework for DLT design options. *Adv Eng Inform* 45:101094, 1–14
- Iyer KC, Jha KN (2004) Factors affecting cost performance: evidence from Indian construction projects. *Int J Proj Manage* 23(4):283–295
- Jan N, Ludo V E (2009) Software survey: VOSviewer, a computer program for bibliometric mapping. *Conf Scientometric Informetrics* 84:523–538
- Kim H, Anderson K, Lee S, Hildreth J (2013) 'Generating construction schedules through automatic data extraction using open BIM (building information modeling) technology. *Autom Constr* 35:285–295

- Kim K, Lee G, Kim S (2020) A study on the application of blockchain technology in the construction industry. *KSCE J Civ Eng* 24(9):2561–2571
- Korea Institute of Science and Technology Information (2018) Blockchain technology development strategy. KISTI Publication, Seoul, Korea
- Li J, Greenwood D, and Kassem M (2018) Blockchain in the built environment and construction industry: A systematic review, conceptual models and practical use cases. *Automat Construct* 102:288–307
- Lokshina IV, Greguš M, Thomas WL (2019) Application of Integrated building information modeling, IoT and blockchain technologies in system design of a smart building. *Procedia Comput Sci* 160:497–502
- Nawari (2012) BIM standard in off-site construction. *J Arch Eng* 18(2), [https://doi.org/10.1061/\(ASCE\)AE.1943-5568.0000056](https://doi.org/10.1061/(ASCE)AE.1943-5568.0000056)
- Pradeep ASE, Amor R, Yiu TW (2020) Blockchain improving trust in BIM data exchange: A case study on BIMCHAIN. In *Construction Research Congress 2020: Computer Applications*, 1174–1183. Reston, VA: American Society of Civil Engineers
- Sarkar D (2011) Simulation application in project risk management for infrastructure transportation project. *Int J Proj Org Manage* 3(3-4):374–392
- Sarkar D, Raghavendra H B, and Ruparelia M (2015) Role of key performance indicators for evaluating the usage of BIM as tool for facility management of construction projects. *Int J Civ Struct Eng* 5(4):370–378
- Seo Y, Song J, and Kong Y (2017) Blockchain technology: prospect and implications in perspective of industry and society. Software Policy and Research Institute (SPRI) Issue Report, Seoul, Korea (2017–004)
- Shojaei A, Flood I, Moud HI, Hatami M, and Zhang X (2019) An implementation of smart contracts by integrating BIM and blockchain. In *Proceedings of the Future Technologies Conference (FTC) 2019: vol 2:519–527*. Springer International Publishing, Cham, Germany
- Tapscott D, Vargus RV (2019) How blockchain will change construction
- Tezel A, Papadonikolaki E, Yitmen I, Hilletoft P (2020) Preparing construction supply chains for blockchain technology: an investigation of its potential and future directions. *Front Eng Manage* 7(4):547–563
- Ye X, Sigalov K, König M (2020) Integrating BIM-and cost-included information container with Blockchain for construction automated payment using billing model and smart contracts. In *ISARC. Proceedings of the International Symposium on Automation and Robotics in Construction*, vol 37, 1388–1395 IAARC Publications, Kitakyushu, Japan



# Examining Different Job-Site Layout Strategies and Their Effects on Construction Productivity



Vismay Shah , Jaykumar Soni , Devang Shah, Dhruvi Shah, Rajesh Gujar , and J. R. Pitroda 

**Abstract** After the bid wins and the contractors receive the notice to continue or a letter of commencement, the job-site layout is routinely established and designed for construction project delivery. Temporary offices, sanitary facilities, worker rest spaces, crane sites, storage and workshop areas, access points and access roads, utilities, and other key characteristics are all considered while planning the layout of the job site. These worksite design decisions have an impact on the site's operational capabilities and, through productivity, have a direct impact on cost and schedule. This study will look at several worksite layout design and optimization methodologies that have been used in practice and proposed through research. The influence on worksite productivity and contract delivery is examined and evaluated using the factors and variables considered in the identified methodologies. Through a survey of working professionals in India important elements for job-site layout are investigated further. The results of the survey are reported, analyzed, and discussed in connection to the factors, and essential parameters identified, as well as their impact on job-site

---

V. Shah

L J Institute of Engineering and Technology, L.J University, Ahmedabad 382210, India  
e-mail: [vishmay.shah\\_ljiet@ljinstitutes.edu.in](mailto:vishmay.shah_ljiet@ljinstitutes.edu.in)

J. Soni (✉)

Highways and Water, SAI Consulting Engineers Pvt. Limited - SYSTRA Group, Ahmedabad, India  
e-mail: [jsoni@systra.com](mailto:jsoni@systra.com)

D. Shah

DJMIT, Mogar, Anand, Gujarat 388340, India  
e-mail: [devang.shah@djmit.ac.in](mailto:devang.shah@djmit.ac.in)

D. Shah · R. Gujar

Pandit Deendayal Energy University, Gandhinagar, Gujarat 382007, India  
e-mail: [dhruvi.smtcl21@dot.pdpu.ac.in](mailto:dhruvi.smtcl21@dot.pdpu.ac.in)

R. Gujar

e-mail: [rajesh.gujar@dot.pdpu.ac.in](mailto:rajesh.gujar@dot.pdpu.ac.in)

J. R. Pitroda

BVM Engineering College, Vallabh Vidyanagar 388120, India  
e-mail: [jayesh.pitroda@bvmengineering.ac.in](mailto:jayesh.pitroda@bvmengineering.ac.in)

performance and contract success. A discussion of potential directions for job-site perks concludes the study.

**Keywords** Job-site layout · Productivity · Construction Industry

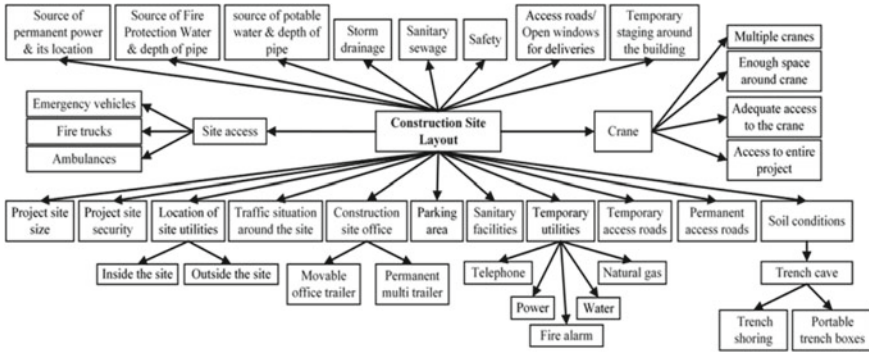
## 1 Introduction

Construction is a distinctive endeavor manufacturing industry in which general contractors provide prototype buildings based on the specifications of property owners. The drawings, requirements, and other contractual terms generated by professional engineers, which form the basis for competing and bidding, include these criteria. After the bidding process is completed, the chosen general contractor is responsible for performing the work to the specified quality within the contractually enforced time and cost restrictions. While managing the integration and delivery of a wide variety of supplies and equipment as well as huge capital expenditures, the project must be completed under unforeseeable environmental circumstances. The involvement of many industry stakeholders and opposing interests makes putting successful programs in place considerably more challenging.

One of the most important tasks a construction site manager must accomplish to ensure the project's success is planning the construction site's layout. The application of tools and procedures supplied by the discipline of construction project management has resulted in the concept of a successful construction site layout. As a result of the application of tools and methods given by the discipline of construction project management, the concept of a successful construction site layout is emerging at this moment (Muhammad et al. 2020).

Planning the site plan for construction projects is an important phase that can impact the project's efficacy and profitability and its, performance and success (Hammad et al. 2017). Due to the complexity of decision considerations, facility layout design is a complicated effort for a number of construction tasks, including the identification, size, position, and synchronization of facilities, plants, equipment, and personnel inside the perimeter of a building site (Alanjari et al. 2014). Because of the organizational diversity of construction operations—project design, time limitations, work areas, environmental circumstances, and facility locations—each construction project's site layout design is unique. Site plan designs are typically the responsibility of the contractors that are awarded the job. These designs are designed to ensure that work on the construction site is completed quickly and efficiently to maximize resource and space use. A rational and effective approach to designing an optimal site plan maximizes available space, saving money, and time while fostering a safe working environment and permitting safe access and exit.

Contractors may secure their productivity and profit by proactively developing sites, using lean construction practices, and a variety of other factors that affect on-site project delivery (Small and Baqer 2016). This study first examines previously



**Fig. 1** Construction site layout variables (Zolfagharian and Irizarry 2014)

established methodologies for site layout planning and then discusses future developments in site layout planning. According to (Zolfagharian and Irizarry 2014), the construction site Layout consists of various features as described in Fig. 1.

This study focuses on elements that the general contractor may directly influence. The analysis undertaken by Naoum (2016) in the U.K. identified more than a hundred scholarly journal articles on building work performance. In this study, practitioners analyzed 46 elements that directly influence construction worker productivity, including “preconstruction, activities during construction, management-related factors, organization factors, and motivational and social aspects.” This inquiry focuses on process flow features such as site congestion, poor site design, and inadequate design of site layouts.

The layout of the construction site and design of the site layout is essential and have a significant impact on almost all operations required to create a project. The cost of constructing the site plan must take into consideration the number of construction-related facilities, the area’s size and form, and the construction timeline. (Memarian 1967). The placement of tower cranes, entry and exit gates, labor colonies, temporary contractor and client offices, sanitary facilities for laborers, general material storage areas, steelyard and binding yards, access roads, medical areas, and security cabins are all examples of temporary facilities. Changing site layout decisions may be difficult or costly as the project progresses; therefore, a proper site layout plan is essential for effective production and efficiency. With an intelligent and effective job-site plan, unnecessary material movement is eliminated, labor efficiency increases, costs and durations are reduced, worker safety is enhanced, and construction quality is improved.

There are several methods that may be used to construct the job-site layout and optimize the site. Each strategy must take into account the elements and aspects that contribute to worksite efficiency and contract fulfillment. (Zhang et al. 2019) in their study for an agent-based modeling approach for understanding the effect of worker–management interactions on construction workers’ safety-related behaviors provided a model for designing the job-site layout. This study presents a summary

of methodologies reported in the literature and investigates crucial worksite layout design considerations. The significance of the highlighted parameters was investigated further via an India-based survey of professionals. When possible, survey results are matched to literature-based tasks and priorities.

## 2 Laying Out the Job Site: Different Approaches to Site Design

As noted in the beginning, the layout of the construction site is crucial to the success of the project. The site architecture must successfully meet several competing factors, including as:

- Limitations on space usage, such as established regions of operation on the job site.
- Automobile access to the construction site and to work areas within the construction site.
- Several more temporary facilities, including sanitary facilities, drinking water, and medical facilities, were provided for the workforce.
- Material mobility and the worker and public security/safety precautions that go with it.

A variety of methodologies can be utilized for project site layout design, and a literature study was conducted to examine the current state and best practices. A detailed synopsis of previous research on this topic was generated by identifying several strategies, including heuristics, rule-of-thumb, optimization, and artificial intelligence approaches (Sadeghpour and Andayesh 2015), who analyzed approximately 100 technical journal papers from 1987 to 2015. Knowledge-based techniques (including heuristics), mathematical optimization methods (which include linear and non-linear optimization), and AI techniques were mentioned, among other methods and techniques like genetic algorithms, neural networks, etc. The great majority of techniques emphasized the construction of static site layouts, and all approaches incorporated efficiency and geographical proximity objectives.

Out of the numerous existence of site layout techniques, (Muhammad et al. 2020) said that using virtual reality (VR) for job-site organization is a valuable and modern management phenomenon for site layout planning.

The construction technology industry is very competitive and difficult to navigate owing to the high level of risk associated with the use of digital technology in building projects and the traditionally conservative nature of construction businesses. This level of complexity has an effect on the process of job-site technology diffusion and adoption, which is the procedure by which construction organizations decide whether or not to buy and use the latest technology (Sepasgozar and Davis 2019).

In terms of site space, predefined, grid-system, and continual area paradigms were recognized. A dimension-less representation, estimated dimensions, or actual

dimensions were used to assign items to space models. Approximate dimensions were used more often than real dimensions to determine object dimensions using various knowledge-based, heuristic, and mathematical optimization techniques. All other options are sub-optimal in nature for mathematical optimization methodologies since there will be an ideal solution. By definition, the heuristic techniques yielded sub-optimal solutions that may be implemented in reality.

Regardless of the methodologies used, (Sadeghpour and Andayesh 2015) discovered that choice variables might be classified using definitions of six distinct structures. These include (1) Approaches to locate the spaces, (2) How objects are defined (in terms of area, typologies, and movement), (3) Time consideration (Are they static or dynamic), (4) Objectives and goals, (5) How to plan and optimize, and (6) Which techniques are employed (neural network, algorithm, model, etc.)?

- Temporary Facilities
- Equipment and supplies for the construction industry
- Areas for storing materials, tools
- Workplaces for contractors, clients, etc.
- Exit and Entry point
- Other site objects.

Ray and Raju (2009) studied heuristic techniques in further depth, including three possible ways for allocating places to items on the worksite:

- An ad hoc method or
- A first-come, first-served strategy based on a thumb rule or
- The contractor's experience.

The ad hoc method was rule-based and included more precise design needs to meet the specific demands of activities on a given location, whereas the thumb rule-based approach was completely reliant on judgment. The third method, called first-come, first-served, identified and placed commodities on the site in the order that they were planned. Each method has its own set of advantages and disadvantages. This technique allows contractors to build and produce cost-effective site plans quickly, and the ad hoc and first-come techniques were excellent for resolving urgent task-related difficulties. During construction, however, the ideas caused confusion and/or considerable inefficiencies. To complete the layout for execution, more considerations are required for each, and procedures must be increased, upgraded, or adjusted as a result.

The alternative ways discussed place a greater emphasis on the process than on the technique or methodology. According to the literature, building site usage planning is one of these strategies (Nanaware 2017). Design decisions are supported by a decision-making process involving the entire project team of stakeholders, and collective proposals are accepted by consensus. The proof-of-concept was based on locating temporary facilities and determining when they will be required. An alternative philosophical viewpoint was presented (Kim 2002). This project focused on subcontracting options based on the operational needs of independently operating subcontractors assigned to a specific project. The workplace is structured to meet

subcontractor needs while eliminating subcontractor disputes caused by space allocation, which has impacted job-site productivity, introduced and worsened delays, and lowered worker morale in prior projects. (Cooke and Williams 1988). Also recognized (Russ 2002) are site layout techniques that include health and safety considerations when the layout design is established.

### **3 Survey Regarding the Current Practices When It Comes to Job-Site Layout**

In examining the various methods of job-site planning, several factors and considerations were used. This covered the placement of entrances, temporary facility needs, workplace safety, health precautions, workers utilized, and other aspects. All of these factors influence site activities and, by consequence, the worksite's efficiency.

A survey was designed and conducted on the construction companies and working professionals on a building site in India in order to explain and establish which productivity-related factors are significant. Respondents were asked to select who should be in charge of designing the layout of a worksite-based on basic demographic information. The importance of several variables in designing an efficient job-site layout was appraised using a 5-point Likert scale. The following aspects were evaluated:

- Access Points: Vehicle and crew entrance and exit points.
- Cranes/Lifts/Support Equipment: Locations of tower cranes, people lifting equipment, generator, and temporary power sources.
- Warehouse/Workshop Spaces: Locations for material storage, workshops, tool sheds, and equipment storage.
- WC and bathroom facilities, worker restrooms, and food and foodservice locations are examples of worker support facilities.
- Offices of general contractors, subcontractors, and owners/consultants.

The poll was delivered through email and other media platforms. A total of 55 replies were collected, with involvement from engineers, consultants, real-estate developers, project managers, subcontractors, and regulators being approximately equal. On the basis of the ranking derived from the average Likert answer data, any counterintuitive patterns were identified.

## 4 Responsibility for Site Planning and Layout Design, According to Survey Responses

Tables 1 and 2 illustrate the survey results in terms of the elements evaluated and their respective importance for job-site layout design. Table 1 shows how engineers and construction professionals are rated by occupation and whether or not they have prior worksite layout experience.

Table 2 summarizes the employer rankings. The results are compared to the total number of responders in both tables, which are ranked. The highest priority rankings go to cranes, vehicle access points, and material storage places, demonstrating the

**Table 1** Variables are ranked according to their profession and experience with site layout design

Variables	Ranking	As per profession		Past experience	
	All respondents	Engineer	Construction	Yes	No
Locations of tower cranes	1	1	1	1	2
The locations of vehicle entrance and exits	2	3	2	2	2
Locations for storing materials	3	2	5	3	5
Locations for personnel to enter and exit	4	9	5	5	4
Lifts and hoists for personnel	5	5	8	4	4
Portable power sources and generators	6	5	4	2	8
Areas for workshops	7	7	4	8	9
Facilities for WC/ Toilet	8	8	9	7	8
Site of a general contractor	9	9	8	5	10
Rest areas for workers	10	11	12	12	10
Equipment storage areas	11	12	8	12	7
Locations for food and food service	12	8	9	12	13
Toolsheds	13	9	11	12	13
Owner/consultant site offices	14	13	14	13	11
Subcontractor site offices	15	14	15	14	15

**Table 2** Employer’s ranking of variables

Variables	Ranking	Employer			
	All respondents	Sub or G/C	Owner	Designer/consultant	Regulators
Locations of tower cranes	1	2	1	2	1
The locations of vehicle entrance and exits	2	2	3	4	3
Locations for storing materials	3	3	3	6	9
Locations for personnel to enter and exit	4	8	3	5	4
Lifts and hoists for personnel	5	5	10	4	4
Portable power sources and generators	6	5	4	6	5
Areas for workshops	7	6	6	9	7
Facilities for WC/ Toilet	8	8	7	9	5
Site of a general contractor	9	8	11	4	11
Rest areas for workers	10	10	6	14	4
Equipment storage areas	11	8	6	10	9
Locations for food and food service	12	15	11	10	10
Toolsheds	13	13	11	11	13
Owner/consultant site offices	14	14	12	10	12
Subcontractor site offices	15	14	13	12	14

relevance of the components. Owner/consultant and subcontractor site offices are given the least weight in overall rankings.

When the data was broken down by background and profession, individuals who identified as engineers pointed to the growing relevance of food/food service facilities for employees and tool sheds, regardless of their employer or direct involvement in the building. Engineers underestimated the need of personnel hoists and elevators. Those who identified themselves as construction specialists prioritized the workshop and equipment storage facilities. The many perspectives of people who have had previous



experiences are fascinating. Respondents with prior experience ranked the necessity of locating generators and temporary power facilities, as well as general contractor work site offices, much higher. Those without expertise gave less importance to the location of electricity and generators, while those with knowledge gave more importance to the location of equipment storage.

The employer rankings are summarized in Table 2. Employees of general contractors prioritize equipment storage while downplaying people’s entrances and exits. Owners, on the other hand, value staff entrances and exits more than autos, tower cranes, or material storage facilities. Both regulators and consultants under-value material storage rooms, and their views on worker rest areas are starkly opposed. Consultants ranked this as the least important variable, despite regulators emphasizing its significance.

Generalizations about the importance of different aspects can be derived based on the results of this poll. Overall, the patterns and rankings are acceptable and logical, and any inconsistencies can be explained properly. A useful technique for generalizing the data is to look at the average relevance and ranking of the categories (access points, cranes/lifts/support equipment, storage/workshops, worker help, and offices). Table 3 illustrates this.

The patterns are mostly the same. Cranes, lifts, and support equipment are given first priority by general contractors and subcontractors, followed by access points. Consultants and designers are becoming increasingly aware of the importance of workplace surroundings, as they directly impact their work. Regulators have placed a greater emphasis on worker support variables, which reflect concern for the workforce’s well-being, as one might expect.

Tower crane layout planning, the procedure that determines the number, location, and kind of tower cranes to be used, greatly influences the efficiency and economy

**Table 3** Ranks by categories

Ranks	All respondents	Table 1		Table 2			
		Profession: Subcontractors & Engineers	Non-Experienced & Experienced	sub or G/C	Owner	Designer/ Consultant	Regulators
Access points	1	2	2	1	2	2	1
Cranes, lifts, and other support equipment	2	2	4	2	1	3	1
Offices	5	4	4	6	4	2	4
Workshops for storage	3	3	3	5	6	5	4
Worker support	4	4	5	4	2	4	2

**Table 4** Different methodologies adopted

Research	Optimization method	Objective
Marzouk and Abubakr (2016)	BIM modeling and genetic algorithm	Multiple
Wang et al. (2015)	BIM modeling	Multiple
Tam et al. (2002)	Genetic algorithm	Multiple
Abdelmegid et al. (2015)	Genetic algorithm	Multiple
Lien and Cheng (2014)	BIM modeling & GIS	Multiple

of building projects. And for the same reason (Younes and Marzouk 2018) provided an agent-based model to prepare tower crane layout.

When it comes to preparation of tower crane layout planning Table 4 represent the different approach used by various authors in their studies.

## 5 Summary and Conclusion

As previously indicated, the construction industry is experiencing a productivity crisis, and there are numerous areas where major contributions might be made to—and drive change. The link between job-site planning and construction productivity is one of the essential factors for a general contractor. Over the last few decades, many different ways for giving decision aid to encourage effective and successful job-site layout design have been developed and researched. Among the strategies employed are heuristic and knowledge-based processes, mathematical optimization, resource assignment systems, and artificial intelligence. In this study, the methods for leading collaborative teams to drive job-site design through consensus decision making are also examined and reviewed. The bulk of techniques provide proofs of concept and consider a wide range of constructs with varied degrees of complexity. Consider temporary structures, construction equipment, storage areas, workshops, access routes, and site artifacts. A study was conducted to determine which specific site layout design elements are emphasized by Indian practitioners. The findings enabled a more in-depth examination of differences in variables such as the respondent's profession, whether or not they had prior experience with site layout design and their workplace. The most important priority was determined to be the tower crane site, vehicle access points, and material storage places. Depending on the respondent's point of view, the relevance of worker support features such as rest areas versus working locations differs. The findings allow for a re-examination of the priority of job-site items, given the variety of techniques presented.

## References

- Abdelmegid MA, Shawki KM, Abdel-Khalek H (2015) GA optimization model for solving tower crane location problem in construction site s. *Alex Eng J* 54(3):519–526. <https://doi.org/10.1016/j.aej.2015.05.011>
- Alanjari P, Razavialavi S, Abourizk S (2014) A simulation-based approach for material yard laydown planning. *Autom Constr* 40:1–8. <https://doi.org/10.1016/j.autcon.2013.12.010>
- Cooke B, Williams P (1988) Construction planning, programming and control. In: *Urban land economics and public policy*. <https://doi.org/10.1007/978-1-349-19444-5>
- Hammad AWA, Rey D, Akbarnezhad A (2017) A cutting plane algorithm for the site layout planning problem with travel barriers. *Comput Oper Res* 82:36–51. <https://doi.org/10.1016/j.cor.2017.01.005>
- Kim D (2002) Exploratory study of lean construction: assessment of lean implementation
- Lien LC, Cheng MY (2014) Particle bee algorithm for tower crane layout with material quantity supply and demand optimization. *Autom Constr* 45:25–32. <https://doi.org/10.1016/j.autcon.2014.05.002>
- Marzouk M, Abubakr A (2016) Decision support for tower crane selection with building information models and genetic algorithms. *Autom Constr* 61:1–15. <https://doi.org/10.1016/j.autcon.2015.09.008>
- Memarian B (1967) Development of high reliability construction work systems: lessons from production practices of high performance work crews. *Gastronomía Ecuatoriana y Turismo Local*. 1(69):5–24
- Muhammad AA, Yitmen I, Alizadehsalehi S, Celik T (2020) Adoption of virtual reality (VR) for site layout optimization of construction projects. *Teknik Dergi/Tech J Turk Chamber Civ Eng* 31(2):9833–9850. <https://doi.org/10.18400/TEKDERG.423448>
- Nanaware MR (2017) Application of inventory control technique in construction. *Int J Eng Res General Sci* 5(4)
- Naoum SG (2016) Factors influencing labor productivity on construction sites. A state-of-the-art literature review and a survey. *Int J Prod Perf Manage*
- Ray PS, Raju DAS (2009) On-site construction productivity. In: *IIE annual conference. Proceedings*, pp 108–112. <http://gateway.library.qut.edu.au/login?url=http://search.proquest.com/docview/192457902?accountid=13380>
- Russ T (2002) *Site planning and design handbook*. McGraw-Hill. <https://doi.org/10.1036/0071377840>
- Sadeghpour F, Andayesh M (2015) The constructs of site layout modeling: an overview. *Can J Civ Eng* 42(3):199–212. <https://doi.org/10.1139/cjce-2014-0303>
- Sepasgozar SME, Davis S (2019) Digital construction technology and job-site equipment demonstration: modelling relationship strategies for technology adoption. *Buildings* 9(7):1–33. <https://doi.org/10.3390/BUILDINGS9070158>
- Small EP, Baqer M (2016) Examination of job-site layout approaches and their impact on construction job-site productivity. *Procedia Eng* 164(June):383–388. <https://doi.org/10.1016/j.proeng.2016.11.634>
- Tam CM, Tong KL, Chan KW (2002) Genetic algorithm for optimizing supply locations around tower crane. *J Constr Eng Manage* 127(4):315–321
- Wang J, Zhang X, Shou W, Wang X, Xu B, Kim MJ, Wu P (2015) A BIM-based approach for automated tower crane layout planning. *Autom Constr* 59:168–178. <https://doi.org/10.1016/j.autcon.2015.05.006>
- Younes A, Marzouk M (2018) Tower cranes layout planning using agent-based simulation considering activity conflicts. *Autom Constr* 93(May):348–360. <https://doi.org/10.1016/j.autcon.2018.05.030>

- Zhang P, Li N, Jiang Z, Fang D, Anumba CJ (2019) An agent-based modeling approach for understanding the effect of worker-management interactions on construction workers' safety-related behaviors. *Autom Constr* 97:29–43. <https://doi.org/10.1016/j.autcon.2018.10.015>
- Zolfagharian S, Irizarry J (2014) Current trends in construction site layout planning. *Samaneh*, pp 1723–1732. <https://doi.org/10.1061/9780784413517.fm>

# Comparative Study of Prospective PPP Models for Highway Projects of India



Naimish Bhatt and Debasis Sarkar

**Abstract** Infrastructure is necessary for any development, and for development, finance is required. Therefore, the government introduced the public–private partnership in infrastructure development to fulfill the need for finance. Generally, in India, three basic models, namely EPC, BOT (toll), and BOT (annuity), are adopted to fulfill infrastructure needs using private investment. As a result, they will get a good return on investment. However, due to specific terms and conditions of finance and a few government loopholes, the private firms interest is declining in PPP infrastructure development, particularly in the road sector. Therefore, the government introduced a new model in January 2016, the Hybrid Annuity Model (HAM), in the road sector, combining EPC and BOT (annuity). In the present study, a financial study has been carried out for three different PPP models for a case study of Porbandar-Dwarka. HAM is the best suitable model for a financial return on investment and the development of new infrastructure in low traffic, a region having only religious and social importance.

**Keywords** BOT (Toll) · BOT (Annuity) · HAM · IRR · NPV

## 1 Introduction

Over the past few years, Indian road (highway) segments have been experimenting with PPP challenges. However, the policy has reduced the enthusiasm of private investors for road infrastructure development since 2015. With the private sector's subsidized evaporation, the government depended on engineering, procurement, and construction (EPC) (Press Information Bureau 2016). In 2015, the government proposed the Hybrid Annuity Model (HAM) as a mid-way component to

---

N. Bhatt (✉) · D. Sarkar  
Pandit Deendayal Petroleum University, Gandhinagar, Gujarat, India  
e-mail: [naimish.bhatt@sot.pdpu.ac.in](mailto:naimish.bhatt@sot.pdpu.ac.in)

D. Sarkar  
e-mail: [Debasis.Sarkar@sot.pdpu.ac.in](mailto:Debasis.Sarkar@sot.pdpu.ac.in)

renew private sector interests in the roadway portion (Press Information Bureau 2016). The HAM model is supposed to be a mixture of the traditional EPCs and the different long-term concession framework variations that can conceive different risk allocations. The present study will discuss the financial aspects of India's best-adapted three PPP models to develop road infrastructure. Financial aspects of Build, Operate, and Transfer (BOT-Toll), BOT-Annuity, and Hybrid Annuity Model (HAM) are compared, and the best adoption feasibility of the HAM model is discussed.

### ***1.1 Significance of HAM***

- (a) This model is best suitable for attracting private investors where low traffic is observed and a need to develop a particular corridor for some important reason.
- (b) 40% of Bid project cost, as cash support during construction period payable to the concessionaire by authority after achieving different milestones mentioned in the agreement.
- (c) The concessionaire must bear 60 percent of the bid project bill during the construction phase.
- (d) Inflation-indexed project costs are the weighted average of the Wholesale Price Index (WPI) and the Factory Workers' Consumer Price Index at 70:30.
- (e) Toll collection is the responsibility of authority, and O&M payments made by authority as quoted in the agreement shall be inflation-adjusted.
- (f) The concessionaire period consists of two major parts: (i) the Construction period and (ii) fixed one year of operation.

## **2 Methodology**

There is a need for a new model for attracting private investors in road development via PPP mode, which leads to adopting the new model, which gives a better return on investment. Here, we are analyzing the HAM model from the data available. First, we calculate the net present value (NPV) and internal rate of return (IRR). The following methodology was adopted for the analysis:

### **Step 1: Cash Flow Diagram**

Engineers use the cash flow diagram as a guide that displays cash transfers during the project. Initial funding, service, operating costs, project earnings or savings, etc., are included.

### **Step 2: Net Present Value**

The net present value (NPV) of a project is the sum of the actual values of all the cash flows expected to happen over the project's life. The general formula for NPV is

$$NPV = \sum_{t=1}^n \frac{Ct}{(1+r)^t} - \text{Initial investment} \quad (1)$$

$Ct$  = the cash flow at the end of the year  $t$ ,  $n$  = life of the project, and  $r$  = discount rate.

A good NPV means that the investment's gain increases the estimated expense and would be profitable. A negative valuation of the NPV, on the other hand, results in a net investment loss.

### Step 3: Internal Rate of Return

A project's internal rate of return (IRR) is the discount rate, making its NPV equivalent to zero. In other words, the discount rate contrasts the actual value of potential cash flows with the original investment. For example, it is the value of  $r$  in the following equation:

$$\text{Investment} = \sum_{t=1}^n \frac{Ct}{(1+r)^t} = 0 \quad (2)$$

$Ct$  = the cash flow at the end of the year  $t$ ,  $n$  = life of the project, and  $r$  = internal rate of return. The IRR is the value of  $r$ , which satisfies the following equation;

$$\text{Investment} = \frac{P1}{(1+r)} + \frac{P2}{(1+r)^2} + \frac{P3}{(1+r)^3} + \dots + \frac{Pn}{(1+r)^n} \quad (3)$$

In general, to get a higher percentage of return on their savings, investors go for a higher IRR value. But, again, the IRR value depends on the project types, whether they are single or many.

## 2.1 Case Study and Data Collection:

The National Highway Authority of India (NHAI) has taken up the upgrade of the existing two-lane road from Km 356.766 (design chainage km 379.100) to Km 473.000 (design chainage km 496.848) in the State of Gujarat to four lanes with a paved shoulder layout of the Porbandar-Dwarka portion of NH-8E. The length of the project is 117.748 km (Fig. 1).

The present study's main objective is to establish the project's technical, environmental, and social viability and prepare the detailed project report to upgrade the existing two-lane road to 4 lanes configuration. The socio-economic analysis's primary purpose is to provide an overview of the state's socio-economic set up and the related status of the project influence area within the state. The details include the present status, past performance, and the economy, population, and urbanization perspective. In addition, the profile depicts the spatial distribution of



**Fig. 1** Location of road Location of Road-Project Case Study

economic activities. It is observed that over 80 percent of the vehicular traffic on the project corridor originates or terminates in the State of Gujarat. Therefore, the socio-economic analysis of the broad influence area is confined to this state.

### 3 Result and Discussion

It would help assess a project if you calculated the applicable cash flows and the incremental after-tax cash flows associated with the project. Three essential elements form the cash flow stream of a traditional project: (1) Original investment, (2) Operational cash inflow (3) Terminal cash outflow. A diagram noted as cash flow allows the representation of the cash inflow and outflow graphically. Figure 2 shows that the timeline is represented with a horizontal axis and subdivided into duration into days, months, or years. Every cash flow represents payment or receipt against the line at the end of the duration. An upward arrow represents the positive cash flow, and a downward arrow reflects the spending over the projects.

Here, Figs. 3, 4, and 5 show cash flow diagrams for the different cases considered under study. BOT (toll), BOT (annuity), and HAM, three models used for PPP projects, are considered for the case study, and all three are analyzed for cash flow and calculating the values of NPV and IRR of the project. The cash flow diagram for BOT (Toll) is shown in Fig. 3, which shows an initial investment, and after that gradient, the cash inflow demonstrates a gradual increase every year. Similarly, for the case



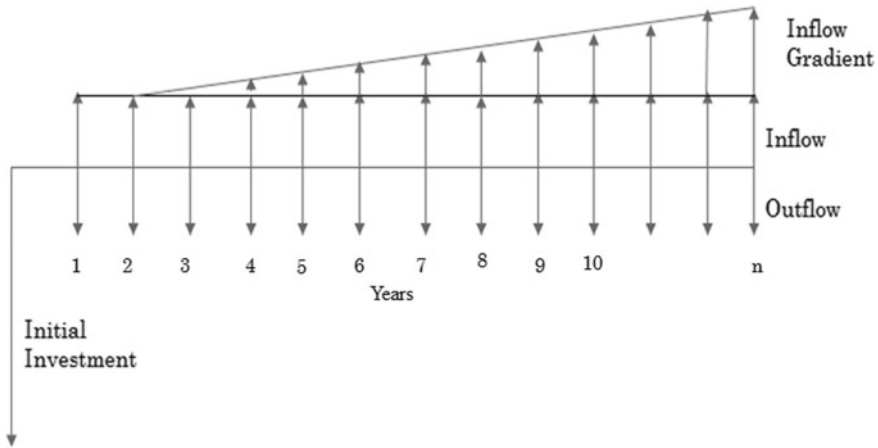


Fig. 2 Cash flow diagram

of BOT (annuity), Fig. 4, annuities are 20%. Therefore, the BOT (annuity) model displays a flat income source and is represented by its cash flow diagram. Figure 5 shows the newly adopted hybrid annuity model (HAM) for PPP road construction and a gradual decrease in the cash inflow, and simultaneously cash outflow is also reduced.

For the evaluation process of the expenditure, NPV and IRR are used. Net present value (NPV) discounts the actual value of the stream of projected cash flows associated with the planned investment and provides the project with a cash surplus or deficit. The internal rate of return (IRR) measures the percentage rate of return at which the net present value of zero will result from the same cash flows. Net present

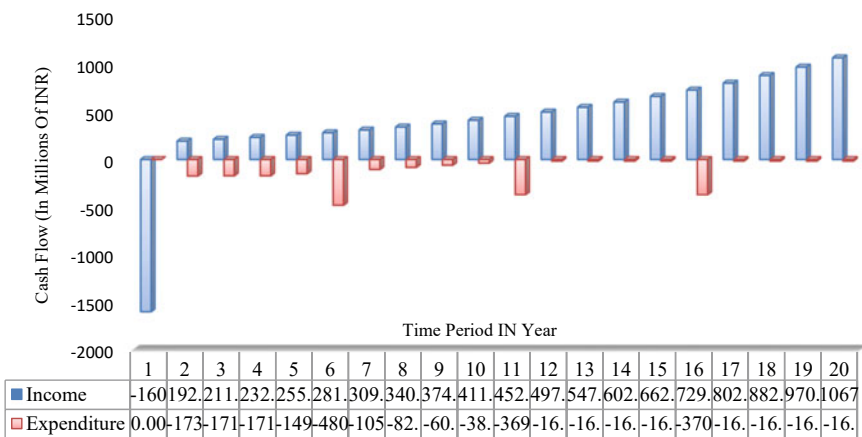


Fig. 3 Cash flow diagram for BOT (Toll)

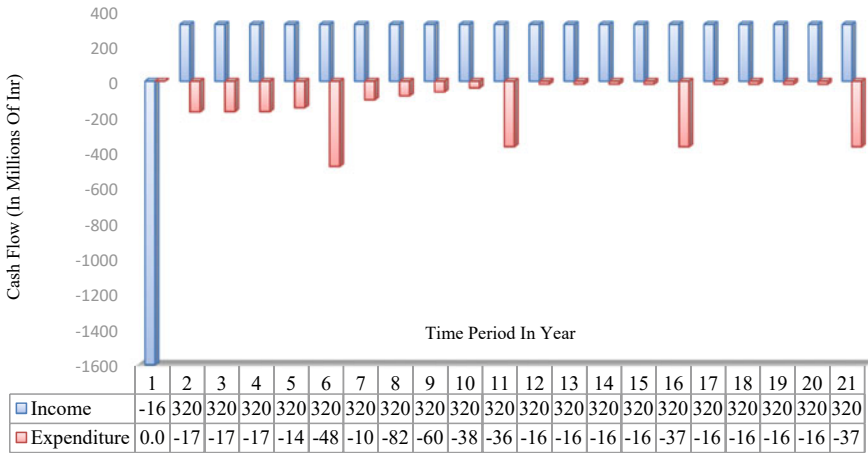


Fig. 4 Cash flow diagram for BOT (annuity of 20%)

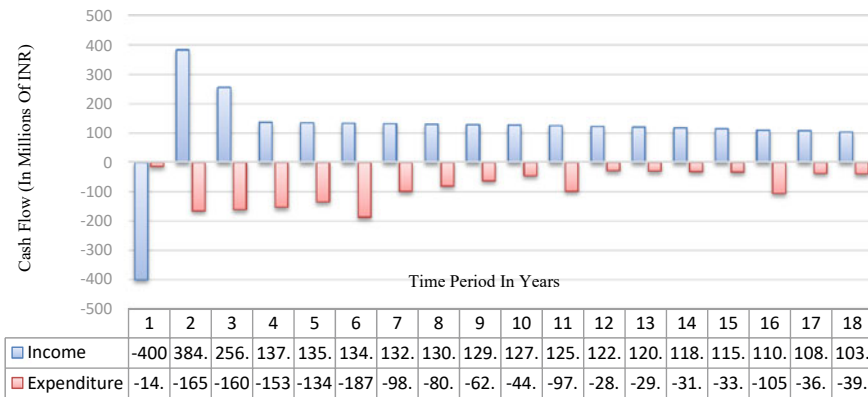


Fig. 5 Cash flow diagram for HAM

value (NPV) for every three cases is calculated before and after-tax consideration. For example, for the first case of BOT (Toll), the value of NPV is around 2395.3 INR in millions for a 5% rate to - 649.5 INR for a 18% rate, and a graph of NPV and IRR is shown for the same in Fig. 6. Then, according to Fig. 6, the NPV becomes zero (0) at the rate of 8.32%, which becomes its internal rate of return (IRR) before tax, and similarly, after tax; the value of IIR is around 11.46%, which is also mentioned in Fig. 6. NPV and IRR are also calculated for the BOT (annuity) case of an annuity of 20% to the concessionaire. In such a case, the NPV and IRR are 577.69 INR in a million at a 5% rate to - 649.5 INR in a million at a 18% rate for an annuity amount of 20% as shown in Fig. 7.

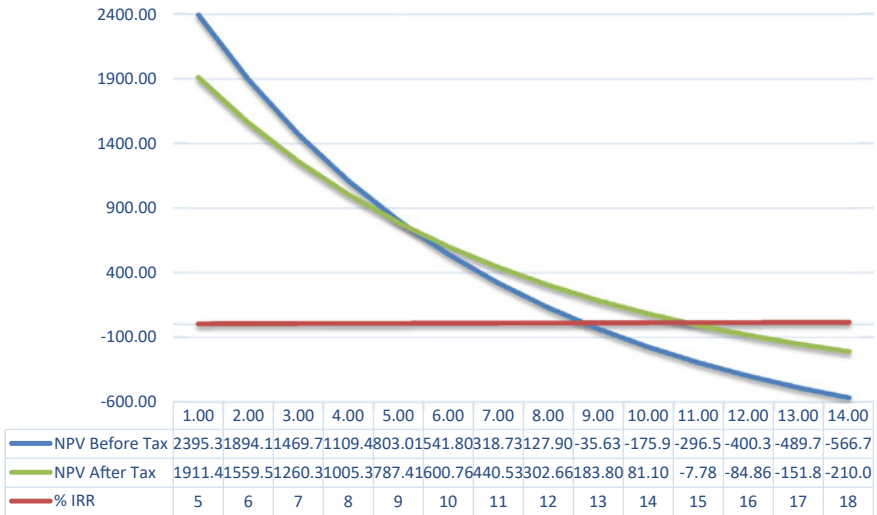


Fig. 6 NPV versus IRR for BOT (Toll)

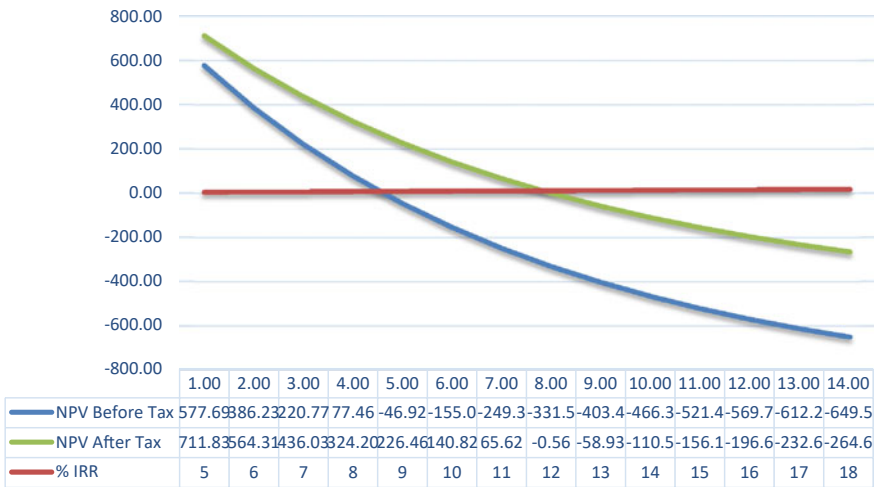


Fig. 7 NPV versus IRR for BOT (annuity of 20%)

HAM is a newly adopted model, and NPV and IRR are also calculated for that model. The graph in Fig. 8 shows details of the NPV and IRR getting for the HAM model. The value of NPV is varied from 53.53 INR in a million to -72.05 INR in a million for a 12% and 23% rate of return.

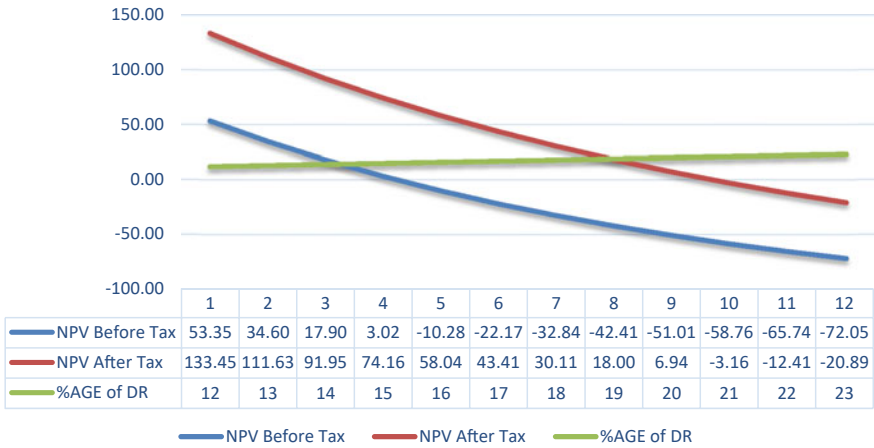


Fig. 8 NPV versus IRR for HAM

### 4 Conclusion

This paper compares the financial aspects of the three different PPP models used for highway construction in India. According to the case study taken, HAM proves a better model than the other two BOT (toll) models (toll) and BOT (annuity). The following points reflect the consideration and adoption of the HAM model are better than any other for the given case study. Porbandar and Dwarka have social and religious critical only and very low traffic census on such a road. Developing road BOT (toll) and BOT (annuity) models do not work correctly. Due to low traffic, private investors will not get a proper return on their investment, and the road remains undeveloped. In such a situation, HAM offers a good return on investment, and the development of roads is also taken care of by the private concessionaire in PPP mode.

As discussed in the result section, the financial analysis of the HAM model shows a lower difference, 53.53 INR in a million to -72.05 INR in a million, of net present value (NPV) for the higher rate of return, which shows that there are significantly fewer chances of inflation due to annuity payment. In comparison, there is a higher difference in the value of NPV for other models with less return on investment. HAM is a combination of the two most attractive models, EPC and Annuity, so as per clause during the construction period, the concessionaire will get 40% of the invested amount, and the remaining 60% will get during the concessionaire period of fix 15 years as an annuity decided by the authority. In BOT (toll), the leading financial risk belongs to the concessionaire only. The return on investment is calculated based on IRR, and as discussed earlier, the value of IRR in the HAM model is around 15% before tax and 21% after tax. IRR in BOT (toll) is around 9% before tax and 12% after tax; similarly, for BOT (annuity), the highest value of IRR is around 14% before tax and 18% after tax. Therefore, HAM gives a good return regarding IRR while comparing it with the other two models.

HAM is the solution for new road infrastructure development for some social and religiously important places where low traffic flow is observed. HAM is the only suitable model to develop road infrastructure in such areas from the case study we discussed.

## References

- Chou J, Pramudawardhani D (2015) Cross-country comparisons of critical drivers, critical success factors and risk allocation for public-private partnership projects. *Int J Project Manage* 33(5):1136–1150. <https://doi.org/10.1016/j.ijproman.2014.12.003>
- Garg S, Mahapatra D (2018) Hybrid annuity model: Hamming risk allocations in Indian highway public-private partnerships. *J Pub Aff*, pp 1–16
- Ismail S, Azzahra Haris F (2014) Rationales for public private partnership (PPP) implementation in Malaysia. *J Fin Manage Prop Constr* 19(3):188–201
- Jain A, Khan F, Gupta P, Gupta K, Yadav SR (2019) Challenges faced in PPP and ham model and the need for an alternative. *J Civ Eng Sci Technol* 10(2):93–104
- Kumar A, Bhosale A, Gujar A, Jadhav V, Chavan G (2017) Study of different public-private partnership (PPP) model for the road infrastructure. *Int Res J Eng Technol* 4(3):2409–2012
- McErlane A, Heaney SG, Haran M, McClements S (2016) The application of stakeholder theory to UK PPP stakeholders. In: Chan PW, Neilson CJ (eds) *Proceedings of the 32nd annual ARCOM conference*, vol 2, pp 863–872, 5–7 Sept 2016, Manchester, UK, Association of Researchers in Construction Management
- Parliament of India (2016) Infrastructure lending in the road sector, two hundred thirty sixth report. Department related Parliamentary Standing Committee on Transport, Tourism and Culture, Rajya Sabha
- Press Information Bureau (2016) Government of India, Cabinet Committee on Economic Affairs (CCEA)
- Shrestha A, Chan T-K, Aibinu AA, Chen C, Martek I (2017) Risks in PPP water projects in China: perspective of local governments. *J Constr Eng Manag* 143(7):05017006
- Treasury HM (2018) Report by the comptroller and auditor general PFI and PF2

# Factors Affecting Improvements in Labour Productivity in Building Construction Projects—India



B. Srikanth, Ashwin Raut, Anuja Charpe, and Rahul Reddy

**Abstract** The construction industry's productivity is mostly determined by three factors: labour factors, management methods, and external challenges. Over the years, various aspects affecting labour productivity in building sector have been identified. It is critical to understand the degree of productivity in order to design innovative methods to improve construction productivity. The objective of this paper is to find the improvement measures in labour productivity. This paper presents a combination of a literature review and a data analysis of questionnaire survey on the aspects of labour productivity. The identified productivity factors have been divided into five groups, i.e., communication, labour management, management factor, supervision and leadership, and use of construction methods. During the data collection, a total of 86 responses has been collected from various contractors, project managers, consultants, and site engineers working in the building construction sector. The analysis of the study provides a better understanding of productivity concerns in India and directs their efforts to enhance productivity for construction professionals.

**Keyword** Labour productivity · Labour utilization · Communication · Team management

---

B. Srikanth (✉) · A. Raut · R. Reddy  
Department of Civil Engineering, Koneru Lakshmaiah Educational Foundation, Vaddeswaram,  
Guntur (Dt.), Andhra Pradesh, India  
e-mail: [srikanthbommisetty2@gmail.com](mailto:srikanthbommisetty2@gmail.com)

A. Raut  
e-mail: [ashwin7588@gmail.com](mailto:ashwin7588@gmail.com)

R. Reddy  
e-mail: [rahul35reddy@gmail.com](mailto:rahul35reddy@gmail.com)

A. Charpe  
Department of Civil Engineering, Velagapudi Ramakrishna Siddhartha Engineering College,  
Vijayawada, Andhra Pradesh, India  
e-mail: [anujacharpe@gmail.com](mailto:anujacharpe@gmail.com)

## 1 Introduction

Construction productivity, which is generally described as the ratio of output to input, is a well-studied issue. The significance of construction productivity comes from the fact that it is a key indicator of a project's success. Organizations must increase construction productivity performance in order to survive in today's highly competitive business climate (Park 2006). Because construction is a labour-intensive business with labour being the most adaptable resource accessible to management, the bulk of scholars and researchers have focused on increasing construction labour productivity.

The construction business is the world's largest and the most difficult industry. In the construction business, human resources play a critical role in increasing productivity. The efficient and effective utilization of human resources can contribute to increased productivity. Construction projects are mostly labour intensive, using just the most basic hand tools and equipment, with labour costs accounting for between 30% to the 50% of overall construction costs. India has one of the world's fastest growing construction industries. After agriculture, the construction industry employs the second-largest number of people (Kumar 2013) When a construction project is completed on schedule and on budget, it is called a success. Productivity must be efficient for this to happen. In strategic and operational planning, productivity forecasting is critical. For many complicated scenarios, quantitative forecasting is employed in the decision-making process (Sherif Mohamed et al. 2005).

Site productivity is a challenging characteristic to evaluate since it varies greatly depending on the dimension of site and the location of measurement. Average labour productivity, one factor input, overall productivity, performance evaluation, changeover time, and other methods of measuring and analyzing site productivity have been determined by some researchers for the purposes of establishing a baseline and improving construction productivity (Agrawal and Halder 2020). Increased productivity results in bigger profits and more investment opportunities. Productivity gains can result in greater compensation and improved working conditions for employees. Increased productivity is also crucial for job generation in the long run. One of the most important factors affecting the physical development of a building project is labour productivity. Construction workers should be knowledgeable with the resources, equipment, and machinery they utilize in order to carry out work effectively (Murodif and Erizal 2016).

The main objective of the paper is to identify the factors which will improve the labour productivity on construction projects in the buildings in India. Based on various literature reviews, it is observed that many studies focus on overall factors of labour productivity, especially factors which decrease the labour productivity. However, not much emphasis is given on strategies which enhance productivity in positive way. The practitioners and researchers emphasize on negative factors and try to find a way to tackle them, but do not realize the potential to improve further ways to make labour efficient. Thus, in this paper our focus is to tap into the areas where there is potential to gain further improvements in productivity. Further, during the

research ranking of the factors affecting positive labour productivity factors. This will provide practitioners the much-needed strategy to carry out work within stipulated time and with better precision.

## 2 Literature Review

Atfal et al. (2016) studied to examine productivity using work sampling approach. They classified worker's activities into three categories, (i.e. effective work, important contributing labour, and inefficient work). The labour utilization rate (LUR) study revealed that formwork had a 47.32% success rate, reinforcing had a 43.17% success rate, and concrete had a 49.76% success rate. LUR was 45.60% of the total value of all three works. They ran a questionnaire survey and received 53 replies out of 60 questionnaires. After that, they conducted a reliability study to determine the average correlation between the data using the split-half approach. According to the findings of the study, there were eight separate categories that influenced labour productivity: (1) Manpower, (2) Management, (3) Environment, (4) Motivation, (5) Material and equipment, (6) Timetable, (7) Safety group, and (8) Quality group.

In another research, authors emphasized on establishing the relation between various factors and productivity of labours involved in masonry works. They investigated productivity based on following criteria such as; (1) What form of productivity is being investigated? (2) What degree of productivity is being reviewed? (3) The strategy to data collecting. The research focused on six categories of improvements: measurement, improvement assessment, factor identification and ranking, influence and relationship (Dolage and Chan 2013). Shoar and Banaitis (2019) compiled a list of investigations carried out by various scholars throughout the Middle East and Africa. Individual elements relative relevance has been observed to differ depending on location. However, certain of the elements, such as labour competence, site manager leadership skill, adequate tools and equipment, and choice of construction technique have consistently been reported in the top 10 factors by different researchers in different places.

In another research conducted by Tangen (2004) categorized the labour productivity in 10 major groups, those are poor site management, lack of communication, improper supervision, poor material planning, tool and equipment issues, improper drawing management, project management incompetency, craftsmen issues, lack of meetings, and poor labour motivation. He identified material waste is the critical factor influencing labour productivity in Kerala, which found that material issues had the greatest impact on productivity. Further to fill the gap of Tangen (2004), Ghate et al. (2016) conducted a questionnaire survey in the Mumbai region, India and discovered that skilled labour, on-site safety, work schedule, availability of material, building method, and other factors impact labour productivity. The most important component in increasing productivity has been stated to be the use of skilled labour. This is due to competent labour that can accomplish more work in the same amount of time with better quality and greater precision. Skilled labour, by definition, may



create more high-quality work than unskilled labour. Productivity will be significantly greater if it is calculated by the number of hours spent working and the value of work generated. This is due to the fact that experienced labour will be able to create more and rework will be reduced. However, if productivity has been measured by the wages paid to workers and the value of the labour they create, it may not be significantly greater skilled labour costs up to 50% more than unskilled labour. Aside from that, competent labour is frequently found to be in limited supply. One of the primary risks in building construction projects is a labour shortage, which may turn a well-performing project into one with cost and schedule overruns (Ghodrati et al. 2018; Attar et al. 2012; Kazaz et al. 2016; Gomez et al. 2015). As a result, hiring specialized labour for all jobs is not always possible or financially practical.

The focus of current research is to establish the relationship between the factors affecting productivity and in what way they correlate with the masonry labour productivity. As the labour lacks knowledge on steps to be adopted for enhancing the productivity, managers need to step up with this analysis and try to overcome the issue of lack of productivity, which affects the project's completion timely.

### 3 Methodology

The research methodology comprises of systematic literature to identify the factors, gathering data from relevant industry professionals and analyzing the data using relative important index (RII) method. For the collection of the data, the industry professionals from various hierarchy levels were chosen. The chosen professionals were selected from Hyderabad region, the professionals were involved in the building construction works. The data was collected from the contractors (8 Nos.), project managers (15 Nos.), planning engineers (32 Nos.), and site engineers (68 Nos.) during the month of February 2022. Factors that improve labour productivity were adopted from the previous studies described from the literature review. A total of 25 factors was grouped into five major groups which will improve the labour productivity. The five major groups are communication, labour management, management team, supervision and leadership, and use of construction methods as shown in Fig. 1.

To generate a reasonable sample of that population, Eq. (1) was used (Alaghbari et al. 2019).

$$n = \frac{m}{1 + \left(\frac{m-1}{N}\right)} \quad (1)$$

where,  $n$  = sample size of limited population,  
 $m$  = unlimited population, and  
 $N$  = available population.

In total 123 responses have been collected from the project managers, contractors, consultants, and site engineers who have experience in building construction projects in India. The questionnaire has design based on considerations of cost, time, and



**Fig. 1** Categories of positive labour productivity factors

quality. The individual’s opinions on the presented inquiries were evaluated using a Likert scale for this study. On a scale of 1—extremely low, 2—low, 3—moderate, 4—high, and 5—very high, respondents were asked to rate the factors impacting the productivity in building construction projects. For ranking factors, the relative importance index (RII) technique was used which is well-known statistical technique used to understand the importance of parameters (Agrawal and Halder 2020). The RII method is used to determine and understand the criticality of factors based on quantification of factors using weightages, for this technique Likert Scale is used. RII can be calculated by using the following equation.

$$RII = \frac{\sum_{i=1}^n [w_i x_i]}{AN} = \frac{5n_5 + 4n_4 + 3n_3 + 2n_2 + 1n_1}{5(n_5 + n_4 + n_3 + n_2 + n_1)} \tag{2}$$

where,

$W$  = weight assigned by the respondents—1 to 5,

$A$  = highest weight,

$N$  = total no. of respondents participated in survey, and

$X$  = frequency of each weightage.

The RII approach is a tried and tested method for assessing employee satisfaction, making it the perfect fit for our study.

## 4 Results and Discussion

The factors improving labour productivity in construction projects have been divided into five major groups, a total of 25 factors (Hamza, et al. 2022; Alaghbari et al. 2019; Hasan et al. 2018; Javed et al. 2018). The factors were ranked using RII values with

**Table 1** Relative important index of labour management

S. No.	Sub-criteria	RII (%)	Rank
1	Using repeating construction crews	66.97	1
2	Increasing the number of laborers	66.27	2
3	Using part-time laborers	64.18	3
4	More number of skilled laborers	61.86	4
5	Creating a sense of ownership for individual tasks	59.76	5

the greatest value indicating the highest rank, positive factors affecting on labour productivity factors were studied.

#### ***4.1 Relative Importance Index (RII) of the Labour Management***

When on a job site, the staff would be working all of the time. That level of output would offer you the more productivity and better profitability. However, the majority of the time, though, you'll observe a group of construction workers sitting about doing nothing. In the majority of situations, they are—awaiting the start-up of a piece of heavy machinery, they are awaiting the arrival of goods at their work area, they're waiting for their work area to be ready for a project, they're waiting for directions from a foreman on what to do next. That's a lot of time spent waiting and all of that waiting is something you want to avoid as much as possible. You want your staff to be actively involved in tasks which need to be completed, rather than waiting for them to begin for whatever reason by using the repeating construction crews the waiting may be reduced. If you can reduce the time spent waiting and motivate your foremen to keep their employees actively engaged in projects, labour productivity will increase (Table 1).

#### ***4.2 Relative Importance Index (RII) of the Communication Factor***

It becomes evident where the firm is now, where it needs to go in the future, and what measures need to be done to get there with the support of effective communication among management and staff. All of this information gives all staff clear directives, which improves productivity and reduces uncertainty. Employees' jobs become less stressful, quicker, more efficient, and happier when they are given specific instructions. Effective communication may help your firm enhance productivity, but you may believe that developing strong internal communication is costly and complicated. There are, however, a few non-expensive options (Table 2).

**Table 2** Relative important index of communication factor

S. No.	Sub-criteria	RII (%)	Rank
1	Giving laborers clear and direct instructions	75.58	1
2	Clear roles and responsibility	73.02	2
3	Regular and effective communication on construction status with project stakeholders	72.79	3
4	Effective site communication	71.62	4
5	There is a better flow of information between workers	66.97	5

When employees in a firm have effective communication skills, they are more likely to hold one another accountable. Because clear instructions are provided via efficient workplace communication, employees know what is expected of them. This enhances responsibility, which in turn increases productivity. There will be no motivation to improve if there is no responsibility in the workplace. When information is not properly passed to the appropriate individuals, there may be miscommunication and misunderstanding, which can lead to a company’s downfall. Confusion is constantly prevalent in the workplace when there has been a lack of good communication. Some employees believe their bosses stated one thing, while others believe they said something quite different. How can everybody work toward the same objective and maximize productivity in this situation? It’s critical to have a robust communication system in place so everyone understands the objectives and can work together to achieve them.

### 4.3 *Relative Importance Index (RII) of the Management Team*

Another factor that affects productivity is management. It’s more efficient to arrange work and establish a priority list for the entire team. It’s also more efficient to use team management software to keep track of what task each person is working on. That isn’t to say that employees can’t communicate with one another. Productivity is accomplished through a top-down strategy in which leadership plays a central role. Leaders must communicate effectively, establish process norms, establish a hierarchy of significance, empower employees, and implement a strong training program. Because materials are such a large part of the building budget, lowering procurement or purchase expenses may save a lot of money. Poor material handling can also lead to significant and needless expenses, as well as a reduction in construction productivity (Table 3).

**Table 3** Relative important index of labour management

S. No.	Sub-criteria	RII (%)	Rank
1	Materials and supply chain management	67.44	1
2	Improvement of equipment and tools	67.20	2
3	Periodic meeting with labour	66.97	3
4	Material management	63.95	4
5	Safety, healthy and, wages	63.02	5

#### ***4.4 Relative Importance Index (RII) of the Supervision & Leadership***

Supervisors may help their staff be more efficient and productive by creating a competitive working atmosphere with clearly stated standards, extensive job training, flexible designs, and performance-based compensation. The primary focus of supervision is on overseeing or measuring the progress of workers within his authority. He is a key part of the managerial structure. He is the one who has direct contact with the employees and serves as a critical connection between management and the employees. At the bottom of the management hierarchy, a supervisor would be a leader. He is a worker's companion, philosopher, and leader. He encourages people to work as a team and to give their all. He is the one who can assist in maximizing workforce use. A supervisor organizes his group's operations and resources in a systematic manner. He delegated power to workers and assigned duties to each of them. When the work they are doing is not adequately organized, workers become frustrated. If labour is not appropriately assigned, some workers may be idle while others may be overburdened. In an organization's structure, that the very first line supervisor has a crucial role. He is personally responsible for upholding an organization's rules and regulations. He can employ both financial and non-financial incentives to improve worker productivity. Any act of disciplinary problems is dealt with quickly and appropriately (Table 4).

**Table 4** Relative important index of supervision and leadership

S. No.	Sub-criteria	RII (%)	Rank
1	Providing project management training for the site supervisors	66.27	1
2	Improving first-line leadership which may include training/coaching/mentoring	64.41	2
3	Enhancing leadership and decision-making for the supervisors	63.95	3
4	For managing workforce there will be sufficient number of supervisors	62.32	4
5	Experienced supervisors	60.93	5

**Table 5** Relative important index of use of construction methods

S. No.	Sub-criteria	RII (%)	Rank
1	Lean construction	74.88	1
2	Building information modelling (BIM)	73.95	2
3	Industrialization	69.76	3
4	Modularization	66.27	4
5	Constructability	58.83	5

#### 4.5 *Relative Importance Index (RII) of Construction Methods*

Once a potential area for increased construction productivity has been identified, management should seek to achieve and maintain the gains over time. In this regard, the current study introduces “lean construction,” an alternative control system with well-defined technologies, to aid in optimizing the building process and increasing productivity. Eliminating waste in such a process, which is a result of interruptions that impair construction productivity, is one of the main concerns in lean construction theory. In addition, a long list of lean theory advantages has been compiled, including the following: a decrease in waste, production costs, production cycle time, labour, and inventory; an improvement in overall, profit, and flexibility; and an increase in cash flow and current facility capacity. Construction is a field where advances in communication and technology have a significant impact. BIM systems are becoming more popular on construction sites, and for good reason. The benefits of increased productivity and organization cannot be overstated, and BIM was included to every project manager’s toolkit (Table 5).

#### 4.6 *RII of Overall Positive Factors Improving Labour Productivity*

The overall factors which will improve the labour productivity are given in Table 6, a total of 25 subfactors was identified and their significant values have been found, the top 10 factors which may improve labour productivity are: Giving laborers clear and direct instructions, Lean construction, Building information modelling (BIM), Clear roles and responsibility, Regular and effective communication on construction status with project stakeholders, Effective site communication, Industrialization, Materials and supply chain management, Improvement of equipment and tools, Using repeating construction crews, There is a better flow of information between workers, Periodic meeting with labour.

Giving laborers clear and direct instructions has ranked first with an RII of 75.58%, while lean construction placed second rank with an RII of 74.88%, building information technology (BIM) placed third rank with an RII of 73.95%, clear roles and

**Table 6** RII of overall positive factors improving labour productivity

Factors	RII	Overall RANK
Giving laborers clear and direct instructions	75.58	1
Lean construction	74.88	2
Building information modelling (BIM)	73.95	3
Clear roles and responsibility	73.02	4
Regular and effective site communication on construction status with project stakeholders	72.79	5
Effective site communication	71.62	6
Industrialization	69.76	7
Materials and supply chain management	67.44	8
Improvement of equipment and tools	67.2	9
Using repeating construction crews	66.97	10
There is a better flow of information between workers	66.97	10
Periodic meeting with labour	66.97	10
Increasing the number of laborers	66.27	13
Providing project management training for the site supervisors	66.27	13
Modularization	66.27	13
Improving first-line leadership which may include training/coaching/mentoring	64.41	16
Using part-time laborers	64.18	17
Material management	63.95	18
Enhancing leadership and decision-making for the supervisors	63.95	18
Safety, healthy, and wages	63.02	20
For managing workforce there will be sufficient number of supervisors	62.32	21
More number of skilled laborers	61.86	22
Experienced supervisors	60.93	23
Creating a sense of ownership for individual tasks	59.76	24
Constructability	58.83	25

responsibility will be placed fourth rank with an RII of 73.02%, regular and effective communication on construction status with project stakeholders ranked fifth with an RII of 72.79%, and effective site communication ranked sixth with an RII of 71.62%, these factors which have RII > 70%, as shown in graph 1, the factors which has less significant value and RII < 60% are creating a sense of ownership or control for individual task with an RII of 59.76% and constructability with an RII of 58.83% has the less significant value among all.

## 5 Conclusion

The study has looked into the factors that improve the labour productivity in the construction industry and found total of 25 factors which will improve the labour productivity positively. These 25 factors have been divided into five major groups, those are communication, labour management, management team, supervision and leadership, and use of construction methods. The data received from respondents using the questionnaire survey technique was further reduced by utilizing the RII approach to rate them. Giving laborers clear and direct instructions, lean construction, BIM, clear roles and responsibility, regular and effective communication on construction status with project stakeholders are the top five factors which may improve labour productivity. The factors which have less significant value are constructability and creating a sense of ownership or control for individual tasks among all the factors. In most Indian construction sites, low labour productivity is a constant issue. However, on building sites, labour productivity is rarely assessed; therefore the losses are never discovered. The research has identified elements that have a positive influence on labour productivity in India, the findings will assist building construction professionals in their attempts to enhance productivity.

## References

- Agrawal A, Halder S (2020) Identifying factors affecting construction labour productivity in India and measures to improve productivity. *Asian J Civ Eng* 21(4):569–579
- Alaghbari W, Al-Sakkaf AA, Sultan B (2019) Factors affecting construction labour productivity in Yemen. *Int J Constr Manag* 19(1):79–91
- Attar AA, Gupta AK, Desai DB (2012) A study of various factors affecting labour productivity and methods to improve it. *IOSR J Mech Civ Eng (IOSR-JMCE)* 1(3):11–14
- Dolage DAR, Chan P (2013) Productivity in construction-A critical review of research. *Eng J Inst Eng Sri Lanka* 46(4)
- Ghate PR, More AB, Minde PR (2016) Importance of measurement of labour productivity in construction. *Int J Res Eng Technol* 5(7):413–417
- Ghodrati N, Wing Yiu T, Wilkinson S, Shahbazpour M (2018) Role of management strategies in improving labor productivity in general construction projects in New Zealand: managerial perspective. *J Manag Eng* 34(6):04018035
- Gomez CP, Raut A, Raji AU (2015) Generating value at preconstruction: minding the gap in lean architectural practice. In: *Proceedings IGLC*, vol 15, pp 1–8
- Hamza M, Shahid S, Bin Hainin MR, Nashwan MS (2022) Construction labour productivity: review of factors identified. *Int J Constr Manag* 22(3):413–425
- Hasan A, Baroudi B, Elmualim A, Rameezdeen R (2018) Factors affecting construction productivity: a 30 year systematic review. *Eng Constr Archit Manag* 25(7):1–22
- Javed AA, Pan W, Chen L, Zhan W (2018) A systemic exploration of drivers for and constraints on construction productivity enhancement. *Built Environ Project Asset Manage*
- Kazaz A, Ulubeyli S, Acikara T, Er B (2016) Factors affecting labor productivity: perspectives of craft workers. *Procedia Eng* 164:28–34
- Kumar Y (2013) Productivity analysis of small construction projects in India. *Asian J Appl Sci*, pp 1–6. ISSN: 1996-3343



- Mohamed S, Srinavin K (2015) Forecasting labor productivity changes in construction using the PMV index. *Int J Ind Ergon* 35(2005):345–351
- Murodif A, Erizal MW (2016) Measurement of productivity using work sampling method at Menara Sentraya building project Jakarta Indonesia. *Scholars J Eng Technol (SJET)* 4(5):244–248
- Park HS (2006) Conceptual framework of construction productivity estimation. *KSCE J Civ Eng* 10(5):311–317
- Shoar S, Banaitis A (2019) Application of fuzzy fault tree analysis to identify factors influencing construction labor productivity: a high-rise building case study. *J Civ Eng Manag* 25(1):41–52
- Tangen S (2004) Professional practice demystifying productivity and performance. *Int J Product Perform Manag* 54(1):34–46

# Systematic Processing Framework for Identifying, Assessing and Overcoming Delays in Construction Projects in India



Chaitanya P. Mali and Ajay P. Shelorkar

**Abstract** For nations and organisations, infrastructure development is considered to be one of the most advantageous activities in renovation and rejuvenation of the society for bringing strategic objectives and goals from merely written plans to reality. Although delays in construction industry has been the focus of extensive investigation over a few decades now, few academics made an attempt to investigate how delays affect both public and private building projects in many countries around the world, particularly in developing and financially struggling nations. The purpose of this work is to close a critical knowledge gap in this area by identifying, assessing and overcoming the major causative factors of delays in construction projects in Nashik, India. The main objective of the study is to develop and construct a systematic processing framework in the form of flowchart for the study area. The procedure for gathering data for the study is carried out by questionnaire survey involving 250 construction industry professionals based on simple random sampling, with 48 critical delay factors that are divided into seven main categories. Relative importance index (RII) analysis was used to rank the respondents' feedback. Using IBM SPSS Statistics, the data's internal consistency and reliability, or Cronbach's alpha, were examined (Version 28) and it was found out to be 0.74. Results showed that disputes in labour and labour strikes (RII = 0.855), poor material management (RII = 0.851) and contractor's incompatibility with new technology (RII = 0.845) were listed as the top three reasons for construction project delays in Nashik, India. The top most factors influencing delay were shown in simplified manner with Ishikawa diagram. The systematic processing framework was developed to overcome the problem on hand. The municipal corporation of Nashik, in order to become successful and efficient, construction employees need to be trained in the necessary technical skills, which requires significant investment from higher education institutions as well as other stakeholders. This study paves the pathway for the future developments of

---

C. P. Mali (✉) · A. P. Shelorkar  
MVPS's KBT College of Engineering, Nashik, India  
e-mail: [mali.chaitanya98@gmail.com](mailto:mali.chaitanya98@gmail.com)

A. P. Shelorkar  
e-mail: [shelorkar.ajay@kbtcoe.org](mailto:shelorkar.ajay@kbtcoe.org)

construction management models to use in residential and infrastructure projects in Nashik as well as in Indian construction industry.

**Keywords** Construction delays · Construction industry · Causes of delay · Systematic processing framework · Relative importance index

## 1 Introduction

### 1.1 General

For nations and organisations, infrastructure development is considered to be one of the most advantageous activities in renovation and rejuvenation of the society for bringing strategic objectives and goals from merely written plans to reality. The effectiveness of a nation's initiatives and its capacity to meet its development goals are gauged by the performance of those projects. Delay can be considered as the amount of time that is spent beyond the agreed-upon delivery date or the contract's expiration date. Delays in building projects can occur for a variety of reasons (variations, low productivity, lack of resources, etc.), and these reasons can differ from one location to another. Additional changes brought about by delays include postponements, higher prices, and even contract termination. The fact that construction project delays are an unavoidable aspect of the project's construction life was also stressed.

Even while modern construction projects use better management practices and very advanced technologies, they still experience delays that push back the project's completion date. Construction project delays and cost escalations are a significant issue in India, as they are in many other developing nations. Despite the sector's expanding importance in India, numerous projects are still not finished on desired schedule or within the allotted budget. This suggests that a project's delays will always have unfavourable effects on the way the contract turns out. These construction project delays stifle economic activity across the globe, causes less work opportunities, also turn off overseas investments in Indian infrastructure development (Hemanta et al. 2012). Additionally, the nature and timeframe of projects (it can last anywhere between couple of months to couple of years.) affect the features of delay causes and the extent of their impact. Construction delays are typically attributed to improperly managed projects that might have been stopped if a productive method of analysing the associated repercussions had been implemented.

Many research works prior to this study have also stated that a rigorous application of project management techniques can significantly lessen the difficulties related to delays in many projects, notably in construction projects. Therefore, a key aspect in this difficulty is the lack of project management techniques for dealing with these delays. However, research has shown that despite implementing different project management techniques, construction projects still confront the issue of project delays in the majority of countries, particularly in low as well as middle-income

countries. Additionally, the repercussions of delays in construction projects extend beyond the construction industry to the entire economies of the affected nations.

Therefore, it's indeed essential for all concerned parties of the organisation or endeavour concerned to put out effort to determine and assess the causes of such occurrences in order to prevent them in future practices. Numerous studies have been conducted recently to pinpoint the primary reasons why construction projects around the world delay. The main goals of these research were to classify the main reasons for delays and to evaluate the benefits of BIM over the conventional method. The main goal of this research activity is to examine the causes of the delays in building projects in India by designing a framework for systematic processing called as a systematic processing framework.

None of these research initiatives have been carried out in Nashik, Maharashtra, India. Furthermore, the plenty of these research activities focus on certain areas, and it is unclear whether they are relevant in the context of Indian construction. This inhibits the resources accessible to industry partners involved to address the many delay issues that are discussed in the research. And because the construction industry in India is currently expanding at an increasing rate, it is necessary to pinpoint those few significant causes that will enable all the interested parties in infrastructure sector to focus their expertise and capital on hand towards addressing the most prominent determinants of construction delays for accomplishing ideal and beneficial results.

Typically, shortcomings in the implementation processes are to blame for most construction projects' inability to reach their goals, which eventually causes the contractor and customer to become unhappy. Numerous significant projects have so far fallen short of their deadlines due to the industry's inability to manage delays in construction projects. The above insinuates towards that the failure to complete the infrastructure project will always have unfavourable effects upon the outcome of the contract. Construction delays are commonly used in reference to poor onsite project management that might have been addressed if a productive method of analysing the associated repercussions had been implemented. Therefore, a key aspect in this difficulty is the lack of project management techniques for dealing with these delays. However, research has shown that despite implementing different project management techniques, construction projects still confront the issue of project delays in the majority of countries, especially in developing and financially struggling countries. Despite the fact that delays in infrastructure ventures and schemes have been a theme for investigation for decades and although several studies have been directed at their effects towards public and private infrastructure programmes in other nations, particularly in developing and financially struggling nations across the world, none of such studies have been carried out in Nashik, Maharashtra, India. Furthermore, most of these investigations concentrate on designated locations, and it is unclear whether or not they are relevant to the global construction industry environment. This restricts the resources industry participants have accessible to address the many delay issues that are discussed in the research. And because the construction industry in India is currently expanding at an increasing rate, it is right time to investigate a few delay factors that will enforce organisations and project participants to channel their efforts

and available resources as well as wealth on addressing the most important causes of construction delays in order to achieve ideal and beneficial results.

The purpose of this research initiative, which only features residential building construction projects in Nashik, India, is to close a critical information gap by examining, classifying, and assessing the factors that affect delays in infrastructure projects. The background information on building project delays is given in the first section of the study, which is followed by a review of previous studies that have been done in various nations that are pertinent. Before examining the study's conclusions, the methodology employed in this research project and the insights gained by using analytical techniques too are highlighted. The study repercussions, final thoughts, and noteworthy suggestions are expressed during this report's closing part. These are focused on using the right management approaches that also serve as a guide for implementing the concrete strategies necessary to handle and reduce the significant delay issues identified, while conducting forthcoming infrastructure projects in India and worldwide.

## ***1.2 Problem Statement***

In “Annual report 2020–21 (Annual Reports—Ministry of Housing and Urban Affairs 2020–21), the Ministry of Housing and Urban Affairs (MHUA) in 4.1/No. 3 of (2020)” addressed the issue of how 75% of public construction projects took longer than expected and were delayed. Due to the contractor's inability to participate in more projects, delays result in a loss of output and income. Therefore, the opportunity cost the predicament that the contractor strives is equivalent to the profit the contractor loses. Due to the aggressive tendering procedure, the contractor with the lowest bid/winning price wins the contract or tender. This is the major reason public construction projects known as PPP project or initiatives frequently perform poorly and are delayed.

## ***1.3 Objectives of Study***

- To identify and assess the major causative factors of delay in building construction project in the study area using RII and SPSS software.
- To find the most impactful delay factors in construction projects in the study area of Nashik, India.
- To develop systematic processing framework to overcome delays in construction projects in Nashik, India.

## 2 Literature Review

It is evident from the literature review's findings that numerous studies have identified and looked into the elements that cause infrastructure project delays in different countries. However, because the jurisdictional and socio-cultural context as well as the motives for delays alter by location and project characteristics, so generalisations made from studies on similar kinds of projects and those undertaken in other countries may not be totally appropriate for the extent and character of the current study. Consequently, by identifying and examining the major causes of delays in Indian road and construction projects, the current investigation aspires to close a huge knowledge gap. This will make it possible for project managers and decision-makers to be aware of the fact that project delays are relatively common, making it crucial to identify them early on.

Construction delay classification:

- Excusable but non-compensable delay—Such delays persist on by events that are not the fault of any of the parties.
- Compensable delay—Such delays persist due to the result of the owner's actions or those of a third party for whose actions the owner is responsible.
- Inexcusable delay—Such delays persist due to the fault of the contractor, his subcontractors, or the material suppliers.

One of the most endemic issues in the global construction sector is noted to be delays (Razek et al. 2008; Alinaitwe et al. 2013; Elhusseiny et al. 2021; Kikwasi 2013). The results of the analysis of the top five most significant delay reasons are given in Table 1 along with a comparison of delay factors across nine randomly chosen Asian nations. It is to be concluded that financial problems faced by owners and contractors in Asian countries (Pakistan Malaysia, Turkey, Vietnam, Jordan, Kuwait, Cambodia, UAE, and Iran; see Table 1) are among other similar findings (Enshassi et al. 2009; Ren et al. 2008; Shirowzhan et al. 2020).

When the data analysis was compared with that of Asian nations, it was discovered that, with the exception of Cambodia, "financial issues" is the most prominent frequently occurring factor that led to building delays in all eight Asian nations. This study's top ranking, "Difficulties in funding projects" by the contractor, illustrates the poor financial standing of contractors (Al-Momani 2000). A contract may have project delays if a project is given to a contractor who is experiencing financial difficulties (Assaf et al. 1995). This is typical in a number of nations, such as Vietnam, Jordan, Turkey, and Iran. Another element, "Dispute on Land Usage", was ranked third in the study. This is a result of the conflict over land compensation between the project owner and the landowner. For instance, project owners only offer government rates while landowners seek market rates. The third-place rating for Cambodian experiences follows the same ranking pattern. In this study, "improper project feasibility study" came in fourth place. Due to unrealistic project timetables, inaccurate estimates, a lack of planning for the project, as well as frequent changes made during the building phase, project owners bear responsibility for poor

**Table 1** Comparison with nine selected Asian Countries

Countries	Top most five ranking causes of delay in construction projects				
	1	2	3	4	5
Kuwait	Change in commands	Financial constraints faced by owners/client	Lack of experience of the owner/client	Unavailability of materials	Weather effects/change
Iran	Progress payment delay	Client requests for modifications during construction	Poorly managed site	Client's decision-making is moving too slowly	Contractors' financial difficulties
Malaysia (Endut et al. 2005)	Incorrect planning by the contractor	Contractor's improper site administration	Finance and payments for completed work	Subcontractor experience is insufficient	Issues/conflicts involving subcontractors
Turkey	Changes in design and materials	Payment delays	Issues with cash flow	Financial issues with the contractor	Inadequate labour productivity
Jordan	Contractor's financial difficulties	Owner issues too many change orders	Contractor's poor scheduling and planning	Availability of low-skilled labour	Shortage of technical experts
Vietnam (Hoai et al. 2008)	Inadequate site monitoring and management	Inadequate project management support	Owner's financial difficulties	Contractor's financial issues/difficulty	Design changes during or after the completion of project
UAE (Faradi and El-Sayegh 2006)	Orders for changes or variations	Owner-caused delay	Owner-issued oral change orders	Owner's late payments	Due to intense competition, the contract price was low
Pakistan (Haseeb et al. 2011; Hussain et al. 2018)	Contractor having trouble financing the project	Progress payments that are late	Land use disagreement	Land use controversy/dispute	Project is awarded at the lowest price
Cambodia	Working through the wet season/monsoon	Flooding of the construction site/work area	Effects of road construction on nearby private property	The lowest-qualified bidder should get the job	Recurring failures of the equipment

project feasibility. The fifth-ranked element in this study—and the same ranking as in the UAE—is “award project to the lowest offer price”. Low bidders win is the conventional contractor selection criterion used in the majority of Asian countries, as evidenced in this situation (Odeh and Battaineh 2002).

### 3 Research Methodology

Current investigation uses a questionnaire survey approach to look into the key elements that significantly affect delay in construction projects in Nashik, India. This research follows quantitative approach for collecting information and data from the study population through field sources. The target population consists of 250 respondents residing in the Nashik city of Maharashtra state which includes contractors, consultants, project owners/clients and subcontractors, site engineers and other key players in the construction industry. Samples for the investigation were chosen using the straightforward simple random sampling procedure to reduce and remove any bias during sample selection. Structured questionnaires are utilised to collect the preliminary source of information in this research study by our own individual administration, allowing the researchers to directly get first-hand information from the respondents. Based on their work experiences and judgement, the respondents were given questionnaires to learn their thoughts and level of knowledge on delays in building projects. In the light of their expertise and professional experiences, the respondents were individually given the questionnaires to get their thoughts and learn what they knew about delays in building projects. The study’s goal and the frequent delay causes that were discovered throughout the literature analysis were taken into consideration when creating the questionnaire survey. This study examined 48 total elements that have been identified as influencing delays in building projects and were grouped into seven key categories. These categories include delays linked to contractors, consultants, owners/clients, labour, and equipment, materials, projects, and delays connected to outside factors. In addition, “the contribution level of each of these elements was evaluated in this study using the Likert’s scale of four ordinal measurements, ranging from 1 to 4 (Allen and Seaman 2007)”. Seven Microsoft Excel sheets representing each of the delay factors mentioned previously were filled out with the data gathered for the study.

The same data was used to calculate Cronbach’s alpha value. Cronbach’s alpha is a measure of internal consistency, i.e. how closely related a set of items are as a group. It is considered to be a measure of scale reliability. Technically speaking, Cronbach’s alpha is not a statistical test but it is a coefficient of reliability (or consistency). It was calculated using **IBM SPSS Statistics (Version 28)**. Table 1 gives the “internal consistency of Cronbach’s alpha Gliem and Gliem (2003)”. SPSS Statistics is a statistical software suite developed by IBM for data management, advanced analytics, multivariate analysis, business intelligence, criminal investigation. SPSS is a widely used programme for statistical analysis in social science. It is also used by market researchers, health researchers, survey companies, government, education



**Table 2** Internal consistency of Cronbach’s Alpha (Gliem and Gliem 2003)

S/N	Cronbach’s alpha, $\alpha$	Internal consistency
1	$\alpha \geq 0.8$	Excellent
2	$0.8 > \alpha \geq 0.7$	Good
3	$0.7 > \alpha \geq 0.5$	Satisfactory
4	$\alpha < 0.5$	Poor

researchers, marketing organisations, data miners, and others. The original SPSS has been described as one of “sociology’s most influential books” for allowing ordinary researchers to do their own statistical analysis.

“In an effort to achieve the objective of the study, a relative importance index (RII) was selected as a suitable analytical method (Doloi et al. 2012)”. “This was used to analyse the ratings received through the questionnaires and establish a mean rating point or rankings of degree of influence that represents the rating for each group contributors (Gebrehiwet and Luo 2017; Taherdoost 2016; Taherdoost and Group 2017). Each calculation was carried out using RII formula in Eq. (1) (Doloi et al. 2012)”:

$$\text{Relative importance index, RII} = \frac{\sum W}{A \times N} \tag{1}$$

where  $W$ , represents the rating given to each factor by the respondents. For factors that cause delay e.g. 4 is for very high contributing factor, 3 is for high contributing factor, 2 is for low contributing factor and 1 is for very low contributing factor.  $A$  is the highest weight (4 for this study) and  $N$  represents the total number of samples (250 for this study). In this study 4 represented strongly agreeing to the delay factor, 3 represented agreeing to the delay factor while 2 represented disagreeing to the delay factor and lastly 1 represented strongly disagreeing to delay factor. The study was conducted according to the ethical codes of Savitribai Phule Pune University and standard ethical practices required of any reputable academic research. Respondents were informed about the research work and its impacts on future measures regarding project delay controls before filling the questionnaires. It was made known to the respondents that their participation in the research survey was an exercise of their choice and were at liberty not to participate. They also were assured of confidentiality (Table 2).

## 4 Results and Discussion

### 4.1 Cronbach’s Alpha Data Reliability Test

Cronbach’s alpha data reliability results were produced after analysing the questionnaire survey results in order to assess the internal consistency of the respondents’ Likert scale responses. According to the study’s research purpose, the reliability test results were obtained for the variables that affect construction delays. Furthermore, using Table 1 and the Cronbach coefficient, the internal consistency of the delay is assessed. The internal consistency is quite good, as evidenced by the Cronbach’s alpha reliability test results for the 48 factors, which indicate a Cronbach’s alpha of 0.746. This shows that the respondents’ answers to the 48 variables that affect construction delay have an outstanding reliability of 74.6%. Table 1: Internal consistency of Cronbach’s alpha shows that (Gliem and Gliem 2003), the results obtained are good and satisfactory. It can be said that the information gathered is valid, reliable, and correlated for each of the seven categories of delay factors.

### 4.2 Analyses of Contractor-Related Delay Factors

According to Table 3, the three most important factors that respondents agreed on with respect to contractors are cited as one of the main reasons for project delays. These were contractor’s incompatibility with new technology (RII = 0.845), contractor’s slowness in site mobilisation (RII = 0.801), and lack of risk analysis and management by contractor (RII = 0.745). Along with significant degree of delay in building projects, respondents selected the contractor’s incompatibility with modern technology far more significant cause than any other building projects that are delayed because of contractors in Nashik (RII = 0.845). Although it is estimated that the following factors contribute significantly to building delays: the three reasons are, in order of decreasing importance, contractor’s paucity in judgement call (RII = 0.623), disagreements with the subcontractor (RII = 0.645), and the contractor’s slowness in document preparation (RII = 0.654).

**Table 3** Classification of RII

Scale	Level of contribution	RII
1	Very low	$0.0 \leq RII \leq 0.2$
2	Low	$0.2 < RII \leq 0.4$
3	Average	$0.4 < RII \leq 0.6$
4	High	$0.6 < RII \leq 0.8$
5	Very high	$0.8 < RII \leq 1.0$

**Table 4** RII ranking for contractor-related delay factor

S/N	Contractor-related causes of delays	RII	RII ranking	Level of contribution
1	Contractor's inadequate planning and scheduling	0.711	5	High
2	Contractor's incompatibility with new technology	0.845	1	Very high
3	Contractor's paucity in judgement call	0.623	8	High
4	The sluggish site mobilization by the contractor	0.801	2	Very high
5	The contractor took too long to prepare the documentation	0.654	6	High
6	The contractor's subpar site monitoring and management	0.732	4	High
7	Disagreements with the subcontractor	0.645	7	High
8	Lack of risk analysis and management by contractor	0.745	3	High

### 4.3 Analyses of Consultant-Related Delay Factors

The findings of an analysis of the project site's causes and associated factors in Table 4. The three most significant delay causes connected to consultants, as perceived by the respondents, are financial difficulties affecting the consultant (RII = 0.827), errors in the consultant's drawings (RII = 0.803), and complexity of project design (RII = 0.763). The three criteria within the consultant-related category utilising the minimal substantial delays have a great degree of participation to construction delays, comparable towards the categorisation of delays linked to contractors. These include: the consultant's lack of experience (RII = 0.650), the contractor's delay in receiving the site (RII = 0.694), and the consultant's slowness in approving the drawing (RII = 0.707), respectively.

### 4.4 Analyses of Owner/Client-Related Delay Factors

The outcomes of a poll's interpretation of the variables that contribute to owner/client-related delays are exhibited in Table 10. Foremost likely, reason for project delays, as reported by the respondents, are delays in owner payments for finished work (RII = 0.832), according to Table 5's analysis of the most significant client-related component. In addition, the owner's poor coordination and communication (RII = 0.805) took second place in this discipline, besides that work is suspended because of the owner (RII = 0.791), third on the list. Despite being the least major owner/

**Table 5** RII ranking for consultant-related delay factors

S/N	Consultant-related causes of delays	RII	RII ranking	Level of contribution
1	The consultant's procrastination in approving the drawings	0.707	6	High
2	Errors in consultant's drawings	0.803	2	Very high
3	Financial difficulties affecting the consultant	0.827	1	Very high
4	Consultant and contractor lack coordination	0.751	4	High
5	A delay in giving the contractor the site	0.694	7	High
6	Communication barriers faced by consultant	0.749	5	High
7	Consultant's inexperience	0.650	8	High
8	Complexity of project design faced by consultant	0.763	3	High

client-related causes of delay, the following three elements, respectively, conflicts between owners in a joint ownership (RII = 0.631), the owner's late revision and approval of pertinent documents (RII = 0.683), and owner contract modifications during construction (RII = 0.735).

#### ***4.5 Analyses of Material Related Delay Factors Related to***

According to Table 6, the three most significant delay reasons connected to materials are inadequate material management (RII = 0.851), materials not being available when needed (RII = 0.814), and an increase in material pricing (RII = 0.791). (RII). Although contributing more to building delays than its equivalents in one of the other subcategories, which contribute significantly more, material management is recognised as is by far the most crucial materials concerning reason of delay in construction projects in Nashik from the respondents' points of view. Building delays are heavily influenced by the two aspects in the materials-related class that have the least relevant delay causes, comparable with any of the other delay classifications. These are, respectively, a material shortage (RII = 0.685) and the market's availability of certainties caused finishing material decisions to be delayed (RII = 0.721).

**Table 6** RII ranking for owner/client-related delay factors

S/N	Owner/client-related causes of delays	RII	RII ranking	Level of contribution
1	The owner's late revision and approval of pertinent documents	0.683	6	High
2	Owner delays in paying for finished work	0.832	1	Very High
3	Owner's poor coordination and communication	0.805	2	Very High
4	Owner disputes when there is joint ownership	0.631	7	High
5	Technical miscommunications with suppliers and contractors	0.786	4	High
6	Suspension of work due to owner	0.791	3	High
7	Owner contract modifications during construction	0.735	5	High

#### ***4.6 Analyses of Labour and Equipment Related Delay***

The findings of a survey analysis of the causes causing consultant-related delays are given in Table 7. According to the respondents' perspectives, disputes in labour and labour strikes (RII = 0.855), poor labour supply and labour productivity (RII = 0.836), and an ineffective safety inspection and accelerated visitation project (RII = 0.806) seem to be the three key reasons for the delay caused by the labour and equipments on the work site. The three aspects that experience the fewest major delays under the equipment and labour-concerning classification does not have that much significance to construction delays, much like the contractor-related delay categories as well as the consultant and owner related delay categories. These are, respectively, failure to use the checklist (RII = 0.666), expensive or time-consuming equipment is not delivered as requested (RII = 0.704), and lack of equipment listings and associated design data (RII = 0.714).

#### ***4.7 Analyses of Project Related Delay Factors***

The findings of an analysis of the project site's causes and associated factors. The three aspects consultant-related delays are provided in Table 8. According to that experience the fewest major delays under the project- to the respondents' perspectives, changes in site concerning classification does not have that much circumstances (RII = 0.768), inadequate data gathering and significance to construction delays, much like the any other survey (RII = 0.812), and accidents on site (RII = 0.840) are

**Table 7** RII ranking for material-related delay factors

S/N	Material-related causes of delays	RII	RII ranking	Level of contribution
1	Shortage of material	0.685	7	High
2	Frequent unexpected modifications in specifications of material during construction	0.774	4	High
3	Poor material management	0.851	1	Very high
4	Escalation of material prices	0.791	3	High
5	Insufficient turnover and start-up resources makes project slow	0.727	5	High
6	Lateness in finalising finishing material due to availability of certainties in market	0.721	6	High
7	Materials not in right place when needed	0.814	2	Very high

**Table 8** RII ranking for labour and equipment-related delay factors

S/N	Labour and equipment-related causes of delays	RII	RII ranking	Level of contribution
1	Poor labour supply and labour productivity	0.836	2	Very high
2	Disputes in labour and labour strike	0.855	1	Very high
3	Shortage of recent technology of equipments	0.732	5	High
4	Unavailability of equipment lists and related design data	0.714	6	High
5	Shortage of equipment operators	0.762	4	High
6	Lack of safety effective inspection and expediting visits on project	0.806	3	Very high
7	Large or long lead-time equipment not received as requested	0.704	7	High
8	No use of checklist	0.666	8	High

the categories presented in this investigation up until now. These three most significant delay reasons connected to are, respectively, issues brought on by pre-existing structures (RII = 0.683), access restrictions on the job site (RII = 0.712), and rework brought on by construction errors (RII = 0.746).

**Table 9** RII ranking for project-related delay factors

S/N	Project- related causes of delays	RII	RII Ranking	Level of contribution
1	Changes in site conditions	0.768	3	High
2	Insufficient data collections and survey	0.812	2	Very high
3	Accidents on site	0.840	1	Very high
4	Problems due to existing structures	0.683	6	High
5	Rework due to error in construction	0.746	4	High
6	Restricted access on site	0.712	5	High

**Table 10** RII ranking for external-related delay factors

S/N	External factors- related causes of delays	RII	RII ranking	Level of contribution
1	Inclement weather effects	0.836	1	Very high
2	Inaccurate cost estimates	0.735	3	High
3	Restriction due to site location	0.696	4	High
4	Changes in government regulation and laws	0.744	2	High

#### **4.8** *Analyses of External Related Delay Factors*

According to the respondents’ points of view, Table 9 gives that inclement or adverse weather effects (RII = 0.836) and modifications and changes to government regulations and legislation (RII = 0.744) seem to be the two key reasons for the delay influenced by outside factors in the same vein as the other delay types, site location restrictions (RII = 0.696), seems to be the least contributing delay causes among external or outside factors, having any significant impact on construction delays (Table 10).

#### **4.9** *Rating the Ten Important Consequences that Influence Infrastructure Project Delays in Nashik*

See Table 11.

**Table 11** RII ranking for the ten most significant factors that causes construction delays in Nashik

S/N	Top ten significant factors	RII	Category
1	Disputes in labour and labour strikes	0.855	Labour and equipment-related
2	Poor material management	0.815	Material-related
3	Contractor’s incompatibility with new technology	0.845	Contractor-related
4	Accidents on site	0.840	
5	Inclement weather effects poor labour supply and labour productivity	0.836 0.836	External factors labour and equipment-related
6	Delays in payments for completed work by owner	0.832	Owner/client-related
7	Financial difficulties affecting the consultant	0.827	Consultant-related
8	Materials not in right place when needed	0.814	Material-related
9	Insufficient data collections and survey	0.812	Project-related
10	Lack of communication and coordination by owner	0.805	Owner/client-related

#### ***4.10 Systematic Processing Framework for Overcoming Delay in Construction Projects***

A schematic representation of a framework often known as a “flowchart”. This study used a systematic processing framework, which frequently follows a particular logical sequence. The schematic is especially helpful in figuring out the rationale of the operation since it permits the presentation of a flow chart flowing from one phase to another. The created framework flowchart, showcased above in Fig. 1, aids in analysing and evaluating the concerns for construction project delays, just as demonstrated by the scenarios provided further in this explanation. The first step served as the framework process’s starting point. The following step was to compile a set of potential project delays for infrastructure projects in Nashik which are intended to be incorporated into the desired questionnaire after carefully examining the relevant prior studies. A questionnaire was created as the next stage. In the section on the survey questionnaire, the structure of the questionnaire and relevant information are covered. The feedback from the questionnaire is considered while selecting further step of flowchart. Throughout this instance, the reasons contributing towards infrastructure project delays were investigated for their importance and their implications on the entire time frame of the endeavour. Choosing whether it is necessary to modify the delay reasons should be the next stage. If the answer is no, move on to the next step; if the response is yes, we need to determine the more likely causes of construction delays; for this purpose, undertake the literature review procedure again. The



next step's objective is to construct a prototype employing the BIM network's functions and functionality. This 3D model should serve as the starting point for future BIM functionalities namely 4D and 5D modelling. After the model is finalised, all functionalities must be recognised and grouped into the proper specialities, e.g. shuttering, concreting, and finishing. The next step is to utilise one of the computerised scheduling software to plan out a timetable for the listed activities. This timetable helps establish approximately how lengthy it is to complete the project by using basic arithmetic and rational thinking to explain the connections, interconnections, and sequencing of all the project's activities. At this point, the 3D BIM model was linked to the project regular schedule to generate a 4D BIM model. The time schedules for the projects typically do not include all the levels of information necessary to do certain process analyses. Additionally, by simulating a hypothetical infrastructure project, 4D modelling offers a number of choices in this field. This relevance of all this stag stems from the fact that the 5D modelling featured the expense component as the fifth dimension, whereas the 4D model featured the fourth dimension of "duration" for enhancement of the appraisal of a development's building potential and operational strategy. At around this juncture, the fifth-dimension incorporation shall make it conceivable to illustrate the value for every operation in the BIM model. This will make it simpler to subtract quantities, rapidly produce cost budgets, and emphasise how the model's economic depictions connect to time. The next step is to design a client-friendly software/application on a computer or mobile device allowing the user/client to input the real start and end dates of the activity as part of the analytical process for construction. The client must then enter the real duration or start and end dates for each of the chosen activities. A decision node was used to symbolise the following step and show the potential for different approaches. The client-friendly software/application will use the user-inputted data to check for delays after the client's inputs. It is possible to establish if there is a delay or not by employing a pragmatic delay evaluation approach. The delays can be overcome by using SCL delay and disruption protocol which helps into this investigation using few delay analytical techniques. The choice of the most reliable delay analysis methodology is influenced by a number of factors, including the accessibility of information, the scope of the study, the technical capabilities, the available time, and other factors. In the light of the findings of the strategy that has been used, two choices were established: most likely a paucity of delay, meaning the schematic process being completed, if not then there must be some existence for the concerning delay in the project for the selected option, resulting the client to move onto the further step.

At this point in time, before moving on to the following decision node, the client will select the reason for the delay using the user/client-friendly software or application. Out among the existing choices concerning delay reasons, the client would be requested to provide us with the delay source for the selected activity. Because it offered various paths, a decision node also represented this stage. The first choice related to the delay reason "change of scope during construction" will be presented to the client. Depending on his or her preference, the second alternative can be tied to other reasons for the delay. The first alternative suggests that the selected reason

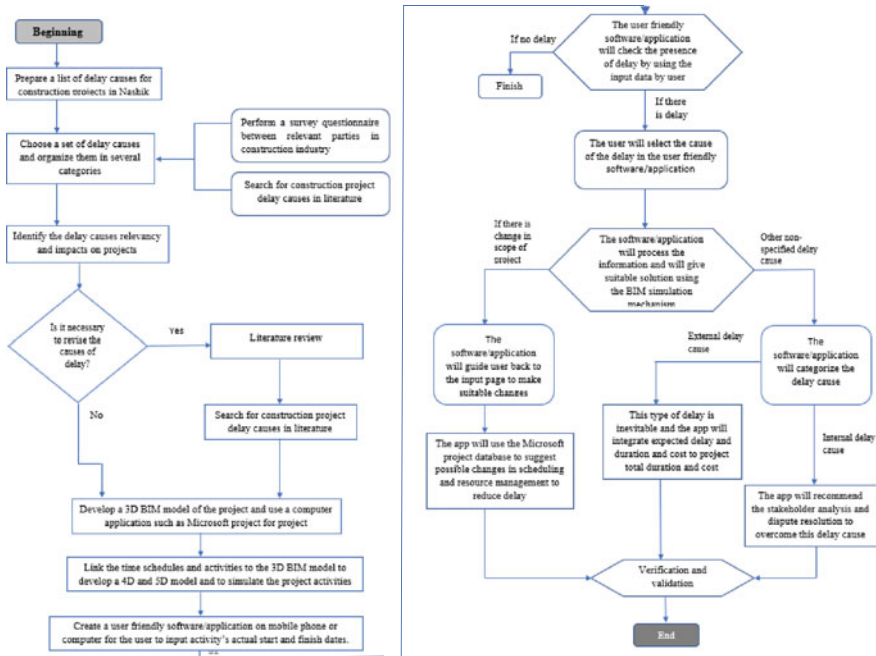


Fig. 1 Systematic processing framework

for the activity’s delay was a change in scope or variation demands during construction. It is evident that the alterations were made after the project paperwork were approved, the bids were opened, and work on the workplace started. This reason for the delay will require more effort on the job site because it isn’t included in the BIM model. The software/application will direct the client back to the input page in this stage so they can make the necessary modifications, and it will utilise the Microsoft project database to recommend potential scheduling and resource management adjustments to minimise delay. Reaching this step in the second alternative, nevertheless, implies that perhaps the event’s specified delay reason was associated to additional delay reasons. It offered two possibilities in conjunction with the delay categorisation, thus a decision node was used to represent it. The two groups utilised to categorise delay reasons were extrinsic and intrinsic. (Intrinsic delay are the ones those inherent to participants involved and managing the particular project such as owner/client, consultant, and/or contractor-subcontractors.) But on the contrary, unforeseen factors like force majeure that impose delays outside of the participants’ control are known as external delay reasons. The client will indeed be prompted to the next level of action again for internal delay reason categorisation in this scenario. Based on the selected delay reason, the user/client-developed model will provide stakeholder analysis and conflict resolution to address it. In contrast, the user will be led through the sub-step for the category of external delay cause. When determining the project’s cumulative timeframe and expenditure, this type of delay reason must

always be put into consideration because, contrary to internal delay reasons, it is often inevitable. A decision node served as a representation for the final stage, which included all of the earlier courses. To demonstrate the integrity of the generated model and, consequently, the framework for systematic processing was to corroborate and validate, which in turn is the key objective of all the data collected. The last phase same as the first, showed the framework process's termination node.

## **5 Research Implications**

The report's distinctiveness aside, the ramifications of its discoveries are very substantial, noteworthy, relevant, and pertaining to socioeconomically, ethical, legislative, and intellectual aspects.

### ***5.1 Socio-Economic Implications***

To lessen or avoid the possible negative consequences of building project delays on the construction sector, legislators, venture owners, authorities, lawmakers and other prominent industry participants certainly are inspired by identifying the key elements that affects the delays in Nashik infrastructure sector. After that, the construction industry's practices and operations will be enhanced, enabling the timely completion of subsequent projects to build homes, offices, hospitals, schools, and other crucial infrastructure for the community.

### ***5.2 Ethical and Legislative Implications***

This study's recommendations will be beneficial towards building owners, suppliers, corporate entities, consultancies, governmental entities, and all other major agencies related to infrastructure sector in Nashik and surrounding districts. The builders and developers can take inspiration from the findings of this study to incorporate into their own worksites and projects resulting in timely and cost-effective project delivery to their respective clients. These could empower such relevant parties to promptly identify the first indications of delays in construction projects. The findings of this research may potentially be used as a guide for developing necessary temporary and lengthy scientifically proven policies and procedures required to drastically decrease or eliminate the effects of building project delays. The study's findings will also allow governments, legislatures, and construction managers comprehend the necessity of first identifying delay reasons when analysing potential dangers in the early stages of building projects, since these delay concerns are typically ubiquitous.

### **5.3 *Research Limitations and Constraints***

A total of 250 respondents have undergone structured questionnaire to provide the necessary input to fulfil this investigation's preliminary objective which was to identify and assess the key delay concerns in building and infrastructure projects in Nashik, India. But it's important to keep in mind that evaluating a larger sample size could be challenging and produce murky results. Nevertheless, this investigation seeks to fulfil a knowledge void regarding the examination of infrastructure project delays in the Indian construction industry. Consequently, it gives a logical and comprehensive report that serves as a benchmark for studies regarding construction delay and management contracting, especially in poor and developing countries. If potential researchers seek to further investigate in the regions surrounding India or any other neighbouring nations, they could be able to corroborate their findings by drawing on the incisive result of this research.

### **5.4 *Significance/Originality of the Research***

This investigation or research work is significant and relevant to the developing country like India and surrounding neighbouring countries because presenting relevant data that could assist aspiring building contractors that try to expand in the construction sector in Nashik, India. This research expands our expertise in the field of infrastructure project delays and concerns related to such endeavours.

## **6 Conclusion**

We hereby summarise that this investigation examined the critical factors that affect infrastructure project delays within the context of the Indian construction industry especially in Nashik district. The intrinsic circuitry and consistency of the factors that impact infrastructure project delays was confirmed and affirmed by Cronbach's alpha test and it was found out to be 0.746. Top three most important concerns that lead to delays in the building industry in Nashik indicates labour disputes and strikes (RII = 0.855), inadequate material management (RII = 0.851), and contractor incompatibility with new technology (RII = 0.845). The highest delay causes containing seven categories were displayed in easier manner in the Ishikawa diagram for reader understanding. To address the delays in building projects with thorough justification, a systematic processing structure was designed.

Through a thorough examination and recorded reports, this study's major objective is to provide a better understanding of delays in the Indian construction sector. Therefore, important players and participants in the worldwide construction business should pay attention to the study's conclusions. This is due to the investigation's

potential to oversee the design and development of scientifically proven strategies helpful in removing the adverse consequences of infrastructure projects' delays and then improve the procedures and activities of the construction industry.

The following suggestions are important according to the results of the research and even to ensure that the handling of such harmful delays in infrastructure projects has enough improvement:

- It's crucial to look into labour disputes, poor material management, and financial weaknesses of the consultant and owner in order to prevent or eliminate the delays from infrastructure projects;
- It's crucial for contractors to effectively apply project management concepts, utilising the right tools and procedures to manage construction projects in order to reduce delays and improve their managerial skills;
- Since consultants work as a liaison between clients and contractors, it is crucial that they provide effective communication and coordination among all parties involved in the project. This would assist in preventing delays brought on by improper communication on building sites;
- The municipal corporation of Nashik should heavily spend on developing the facility to train and instruct construction workers with the required competencies to improve their skillset required for the designated job. This process should be done in collaboration with MNC's partnered NGOs and institutions of higher learning to become beneficial and productive; in other words, the labour force should be examined in order to reduce delays.

## References

- Abd El-Razek ME, Bassioni HA, Mobarak AM (2008) Causes of delays in building construction projects in Egypt. *J Constr Eng Manag* 134(11):831–841
- Alinaitwe H, Apolot R, Tindiwensi D (2013) Investigation into the causes of delays and cost overruns in Uganda's public sector construction projects. *J Constr Dev Countries* 18(2):33–47
- Allen IE, Seaman J (2007) Online nation: five years of growth in online learning. Survey Reports, The Sloan Consortium
- Al-Momani AH (2000) Construction delay: a quantitative analysis. *Int J Proj Manage* 18(1):51–59
- Annual Reports—Ministry of Housing and Urban Affairs (2020–21), Government of India
- Assaf SA, Alkhail M, Al-Hazmi M (1995) Causes of delay in large building construction projects. *J Manage Eng ASCE* 11(2):40–45
- Doloi H, Sawhney A, Iyer KC, Rentala S (2012) Analysing factors affecting delays in Indian construction projects. *Int J Proj Manage* 30. <https://doi.org/10.1016/j.ijproman.2011.10.004>
- Elhousseiny HO, Nosair I, Ezeldin AS (2021) Systematic processing framework for analyzing the factors of construction projects' delays in Egypt. *Ain Shams Eng J* 12(2):1501–1511
- Endut IR, Akintoye A, Kelly J (2005) Cost and time overruns of projects in Malaysia. Unpublished
- Enshassi A, Al-Najjar J, Kumaraswamy M (2009) Delays and cost overruns in the construction projects in the Gaza Strip. *J Fin Manage Prop Constr* 14(2):126–151
- Faradi AS, El-Sayegh SM (2006) Significant factors causing delay in the UAE construction industry. *Constr Manag Econ* 24(11):1167–1176

- Gebrehiwet T, Luo H (2017) Analysis of delay impact on construction project based on RII and correlation coefficient: empirical study. *Procedia Eng* 196
- Gliem JA, Gliem RR (2003) Calculating, interpreting, and reporting cronbach's alpha reliability coefficient for likert-type scales. In: 2003 Midwest research to practice conference in adult, continuing, and community education, Columbus, pp 82–88
- Haseeb M, Bibi A, Rabbani W (2011) Problems of projects and effects of delays in the construction industry of Pakistan. *Austr J Bus Manage Res* 1(5):41–50. <https://doi.org/10.52283/NSWRCA.AJBMR.20110106A05>
- Hemanta D, Anil S, Iyer KC, Sameer R (2012) Analyzing factors affecting delays in Indian construction projects. *Int J Project Manage* 30(4):479–489
- Hussain S, Zhu F, Ali Z, Aslam H, Hussain A (2018) Critical delaying factors: public sector building projects in Gilgit-Baltistan, Pakistan. *Buildings*
- Kikwasi G (2013) Causes and effects of delays and disruptions in construction projects in Tanzania. *Austral J Constr Econ Build Conf Ser* 1:52. <https://doi.org/10.5130/ajceb-cs.v1i2.3166>
- Le-Hoai L, Lee Y, Lee J-Y (2008) Delay and cost overruns in vietnam large construction projects: a comparison with other selected countries. *KSCE J Civ Eng* 12:367–377. <https://doi.org/10.1007/s12205-008-0367->
- Odeh AM, Battaineh H (2002) Causes of construction delay: traditional contracts. *Int J Project Manage* 20(1):67–73
- Ren Z, Atout M, Jones J (2008) Root causes of construction project delays in Dubai. In: Dainty A (ed) Proceedings of 24th annual ARCOM conference, 1–3 Sept 2008, Cardiff, UK, Association of Researchers in Construction Management, pp 749–757
- Shirowzhan S, Tan W, Sepasgozar S (2020) Digital twin and CyberGIS for improving connectivity and measuring the impact of infrastructure construction planning in smart cities. *ISPRS Int J Geo-Inf* 9:240. <https://doi.org/10.3390/ijgi9040240>
- Taherdoost H (2016) How to design and create an effective survey/questionnaire; a step by step guide. *Int J Acad Res Manage (IJARM)* 5. Ffhal-02546800f
- Taherdoost H, Group H (2017) Sampling methods in research methodology; How to choose a sampling sampling methods in research methodology. *SSRN Electron J* 5(2):18–27

# Review of Fire Risk Factors for Fire Risk Assessment in Urban Areas: The Case of Ahmedabad, India



Priyanka Raval and Ronak Motiani

**Abstract** Fire incidents have increased drastically due to rapid urbanization. More than 9000 fire incidents causing large casualties were recorded in 2020, as documented by the India risk survey 2021. Thus, it becomes of utmost necessary to assess the risk associated with urban areas, especially metro cities. The present work critically reviews fire risk assessment studies of urban areas. It involves the review of critical factors affecting the urban fire, Indian standards and code used in practice, factor integration techniques for preparation of risk maps, and optimization of the fire station. The factors affecting fire hazards are bifurcated into satellite data, metrological data, bio-physical data, planning and regulation data, and other ancillary data. Based on the review, the eleven parameters significantly influence the city under consideration are derived. Further, as a case study, the land utilization of Ahmedabad City is studied. The isochrones map is developed for the city, and fire stations are marked. The generated map shows the coverage area by a particular fire station. The map also highlights the area at higher risk where the timely response to calls for service is difficult from the nearest fire stations. This study provides an essential contribution for new researchers, assessing the fire risk of buildings and old structures in urban cities. The study can help administrators, city planners, and civil society organizations plan to provide facilities, minimize fire hazards, and solve related issues to decrease fire risk.

**Keywords** Urban fire · Fire risk factors

---

P. Raval (✉) · R. Motiani  
Department of Civil Engineering, Pandit Deendayal Energy University, Gandhinagar, India  
e-mail: [priyankaraval1411@gmail.com](mailto:priyankaraval1411@gmail.com)

R. Motiani  
e-mail: [ronak.motiani@sot.pdpu.ac.in](mailto:ronak.motiani@sot.pdpu.ac.in)

## 1 Introduction

Inadequate infrastructure planning and construction execution relevant to fire prevention and mitigation considerably increase the potential for fire, fire ignition, and spread. Fire affects people, extends to loss of property and resources, and degrades air quality. Due to burn-related injuries or fire, more than 1,80,000 people die every year across the world. More than 95% of these deaths and injuries happen in developing nations, where risks increase due to rapid urbanization. In developing countries, fire policy and mitigation strategies are constrained due to insufficient or inadequate information. Prime Minister of India warned in April 2022 that the temperature is rising rapidly in India, so the Government of India needs to focus on the urban fire issues. According to the India risk survey 2021, in recent years, the fire risk has increased, specifically in urban areas, as India's urban population improved by 1.34%, from 34.9% in 2020 to 35.4% in 2021. And the population density is 464.1 people per sq. mt. Dense urban clusters mean a higher probability of casualties as fires has a domino effect. The India Risk Surveys 2021 has placed India at 4th position in fire incidents. There were over 9300 reported cases of fire casualties with more than 9000 fatalities in India in the year 2020; it makes the severe cause of consideration for sustainable infrastructure (Kaur et al. 2021). According to a survey, around Rs. one thousand crores are lost per year due to fire.

One of the primary reasons for these fire casualties is fast urbanization and the shortage of fire protection norms and protection protocols. According to National Crime Records Bureau records, residential buildings noticed 58% of fire-related casualties in 2019 in preference to 2% in factories. In 2021, there were at least 15 notable cases of fire regarding incidents in COVID hospitals; due to this Supreme Court directed all states to implement fire protection audits of dedicated COVID hospitals (Kaur et al. 2021). In 2016, National Building Code (NBC) suggested that building residents conduct regular fire protection inspections to ensure they meet their standards. However, for commercial buildings, it is far up to statutory authorities so as the State Factory Inspectorate and various outside entities, depending on their nature, to audit for fire safety purposes. In 2020, the Ministry of Health issued regulations requiring certification of third-party fire protection. In December 2020, the Supreme Court instructed all states to conduct fire audits, and the National Disaster Management Authority (NDMA) has set fire protection standards for hospitals and other public facilities.

These two most highly urbanized states, Maharashtra and Gujarat, account for about 30% of the country's fire accident deaths. Ahmedabad is among the largest city in Gujarat and was formerly Gujarat's capital. Ahmedabad is still the judicial capital, as the Gujarat High Court is located there. The estimated population of Ahmedabad is more than 8.1 million in the city. Thus, Ahmedabad is the fifth-largest city and the seventh-largest metropolitan area in India. It is clear that tall buildings are rising, resulting in a growing volume span. High-rise buildings have diverse structures and functions, as well as a variety of facilities, high-density personnel, and complex fire safety measures (Li et al. 2018). The prediction of fire occurrences depends on



many environmental and human factors, presenting a nonlinear and complex problem (Jafari Goldarag et al. 2016). Each parameter has its significance on the fire described in the particular paper. The fire risk map will be generated based on geographical information system (GIS) (Castro and Chuvieco 1998).

Suggesting the critical urban fire risk factors requires an in-depth review of the existing fire risk factors of wildfires and urban fires to understand the strength and weaknesses of all the risk factors. The study will also describe each fire risk factor to identify the reason for considering the particular factor for the risk assessment. Developing a fire risk assessment method with referred critical risk factors needs a detailed review of existing risk assessment approaches to get the maximum accuracy of the output of the urban risk assessment. Given these objectives, the study of existing critical fire risk factors and risk assessment methods are presented in the review. For the future scope of the study, the review has also included some methods for urban fire optimization to locate the maximum service coverage area with minimum travel time. For completeness, the review has also provided a methodology for urban fire risk assessment. Further, Ahmedabad City, India, is taken for the case study to assess the city's risk, and maps are generated using Landsat data to understand this study better. The primary outcome of this review is to propose several urban fire hazards and vulnerability factors that can be used for the urban fire risk assessment.

## 2 Literature Review & Methodology

The review analysed considerable research on wildfires and urban fires to assess the various fire risk factors and suggested urban fire risk hazards and vulnerability factors. However, the current study has reviewed some methods to assign weightage to the critical risk factors to perform the urban fire risk assessment with the aim of developing of detailed risk map that allows for a better response and mitigation of the effects of urban fires.

### 2.1 *Review of Indian Standards and Codes*

The Indian standards and codes, such as the National Building Code of India, IS: 11460-1985, IS: 1643-1988, for fire safety in building, during construction, while planning, in temporary structures, etc. These documents provide technical information and guidelines to improve fire safety by specifying the fire safety management, operational management, and emergency rescue operations that should be implemented. Part 4 of the National Building Code of India focuses on fire and life safety. The code specifies construction, occupancy, and protective factors required to minimize the fire's danger to the property and life (Bureau of Indian Standards 2016). IS:11460-1985 is a code for fire safety of libraries and archives which gives details regarding the planning, designing, and construction of library buildings and archive

buildings according to the IS: 1553-1976 and IS: 2663-1977, respectively (Bureau of Indian Standards 2005). IS: 1643-1988 is a code of practice for fire safety of buildings (general): exposure hazard covers the necessity regarding the building spacing to provide appropriate protection against the exposure hazard. Exposure hazards express the risk of the spread of fire through the open space in a building (Bureau of Indian Standards 1988). IS: 8758-2013 is a code for fire precautionary measures in constructing temporary structures and pandals. IS: 8758- 2013 focuses on the fire safety of locations, construction, and maintenance of temporary structures and pandals (Bureau of Indian Standards 2013).

Based on the review of referred documents, several fire safety recommendations are provided for temporary structures, permanent structures, technical details, during construction, after construction, etc.

## **2.2 Fire Risk Factors**

Since the primary outcome of this study is to provide urban fire risk factors that can be used to develop a method for urban fire risk assessment. After the extensive literature review, it has been observed that there is a massive necessity for fire risk assessment and the optimization of fire stations in urban areas in India. Also, various primary fire hazard and vulnerability factors affect the fire risk assessment, as described in Table 1.

Table 1 describes the series of fire risk factors that affect the behaviour of wildfires and urban fires. The table also explains how these fire risk factors affect the fire risk and its behaviour. These risk factors are used to analyse the forest and urban areas' fire risk. The fire risk assessment maps are generated based on these critical risk factors.

The review proposes a methodology that needs to be adopted while performing an urban fire risk assessment, as Fig. 1 suggests. The first step is to collect various data that affect fire behaviour. After completing the first step, each parameter should weightage using suitable multi-criteria decision-making techniques. Based on the weightage of the fire risk factors, the risk maps are to be generated using the ArcGIS Desktop software. For the validation of the prepared urban fire risk zone map, the past five years' fire event data can be a map on the fire risk assessment.

## **2.3 Fire Risk Assessment**

Fire risk is the likelihood of the occurrence of fire. Fire incidents are rapidly increasing in the forest as well as in urban areas. Fire causes damage to the environment, people, and valuable property.

The fire risk assessment study has been done for Dhaka city in the GIS framework, which develops the methodology to generate fire hazard factors and risk maps. To

**Table 1** Various fire risk factors are as follows

FRF	Description	Sources
FRF1—wind speed	Influence fire behaviour An increase in wind speed can spread smoke rapidly	Cai and Chow (2012), Nelson (2002)
FRF2—Population	The population is among the primary reasons behind several fire incidents Population data can be used to estimate future demand for fire emergency services	Lamat et al. (2021), Kiran et al. (2018)
FRF3—land use land cover	LULC can be categorized into different classes: water body, built-up area, vegetation, open land, forest land, etc.	Lamat et al. (2021)
FRF4—temperature	High temperature leads to drying moisture and influences the occurrence of fire	Bonora et al. (2013), Peacock et al. (1999)
FRF5—slope	In case a fire occurs at the bottom of a steep gradient or slope, it will spread faster upwards as it can pre-heat the imminent fuels with rising hot air, and upward drafts are much more likely to create spot fires	Kushla and Ripple (1997)
FRF6—road network	Fires are generally ignited close to roads in all LULC classes This impact is consistent with previous studies in several ecosystems, which revealed a high spatial clustering of human-caused fire ignitions around accessibility networks	Ricotta et al. (2018)
FRF7—earthquakes	Fires, frequently associated with broken gas and electrical lines, are a general side effect of earthquakes	Tsukagoshi et al. (n.d.), Zolfaghari et al. (2009)
FRF8—ignition sources	Electric sparks, mechanical sparks, static electrical sparks, and lightning	Syphard (2019), Lautenberger et al. (2015)
FRF9—vegetation type	There is a range of vegetation types across India Vegetation type affects the frequency of ignition and time-to-ignition, duration of flaming, and censurability	Ganteaume et al. (2011)
FRF1—cooking	Fire incidents in Indian homes are verified due to cooking. The existence of cooking oils and appliances used for preparing food, along with the existence of liquefied petroleum gas (LPG) as an origin of energy, make it an ideal combination of fire hazards in the kitchen	Jain et al. (2013)
FRF11- MRTS	A major fire in a metro tunnel can cause damage to the infrastructure in terms of economic and life loss. A large number of users are potentially exposed to these risks	Poon and Lau (2007)

(continued)

**Table 1** (continued)

FRF	Description	Sources
FRF12—structural material	Effects of fire vary with the different structural materials such as concrete, wood, and steel	Gan et al. (2019)
FRF13—infrastructure	Infrastructure includes the position of gas and fuel stations, industrial zone, residential zone, commercial zone in the city, etc.	Gernay et al. (2016)
FRF14—plot area ratio	Floor Space Index or Floor Area Ratio liberalized population density. FSI also plays a role in restricting the height of the structure. It also affects the space around the building	Bureau of Indian Standards (2016)
FRF15—zones	The zone, residential, commercial, industrial, etc., have different fire risks	

establish a method, different fire hazard zones have been categorized based on past fire incidence. A total of five fire zones are categorized from highly hazardous to least hazardous. Electrical faults cause maximum numbers of fire incidence in Dhaka city. In the less hazardous zone, the cause of the fire is gas, and in the least hazardous Zone, the cause is machine heat, cooking, candles, etc. For risk analysis of fire hazards, an expert system is developed which follows the framework of the ‘Fire Risk Assessment Method for Engineering,’ proposed by Erik (1992). The fire risk analysis is defined as the result of the potential risk P by the protection level D and acceptance level A. The Fire Hazard Software is used. The software uses graphical user interfaces (GUI) to ease the analysis. The conclusion says that in highly hazardous areas like industrial areas, warning systems, fire extinguishers, warning systems, and automatic sprinklers should be provided (Alam and Baroi 2004).

Another extensive analysis study on urban fire risk was done, and Haikou city has taken it as a case study. The analysis has been done concerning the risk of fire casualty in urban areas, vulnerability, and urban anti-fire capability. The statistics data on fire accidents between 2000 and 2009 says that fire accidents are about to increase and can be more complicated. The analytical hierarchy process (AHP) method has been implemented to analyse urban fire risk. Also, the gray correlation degree method gives weight to each coefficient of parameter or indicator. The weighted sum can get depending on the weighted coefficient, and evaluation correlates with actual indicators. And finally, values of urban fire risk, urban vulnerability, and urban anti-fire capability can be identified. Thus, the research concludes that the gray correlation degree method can be applied for urban fire risk assessment (Zhang 2013).

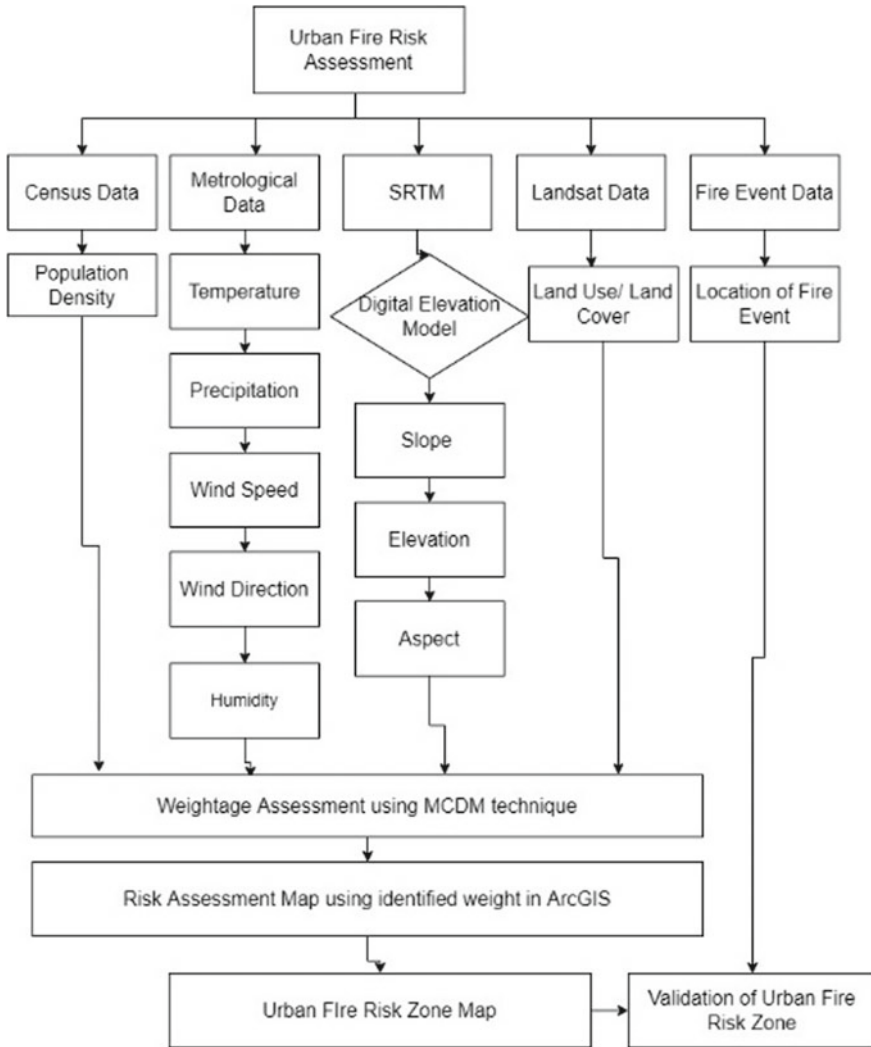


Fig. 1 Critical factors for fire risk assessment

### 2.4 Optimization of the Fire Station

Well-organized formation of urban fire stations is necessary for a timely response for rescue service at the place of the fire accident. Locating urban fire stations is a multi-dimensional issue that includes many parameters, including population, water availability, fire risk, and the preference of decision-makers (Badri et al. 1998; Church and Li 2016; Murray 2013). The problem associated with fire station location has been considerably studied using the geographical information system (GIS) and

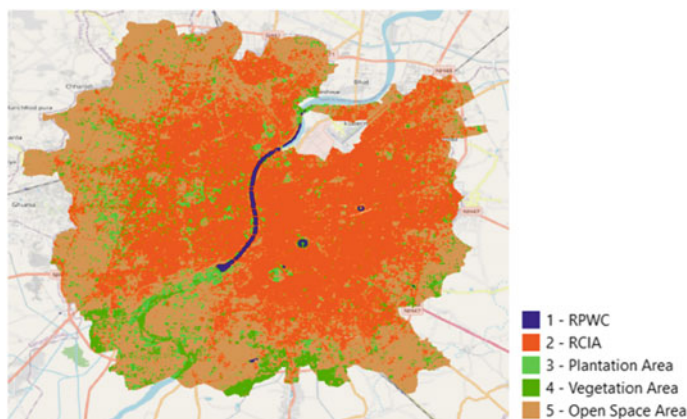
mathematical models (Aktaş et al. 2013; Eiselt and Marianov 2015; Liu et al. 2006; Murray 2013; Aktaş et al. 2013; Liu et al. 2006; Murray 2013). The access may reduce the overall time or distance from the fire station to the risk site; the p-median problem (PMP) is widely used (Hakimi 1964). For service coverage, methods such as location set covering problem (LSCP) and maximal covering location problem (MCLP) have been extensively utilized for analysing the location of existing and new fire stations (Church and Reville 1972; Toregas et al. 1971). Integration of access and service coverage addresses a more extensive range of concerns. Therefore, the bi-objective spatial optimization model develops to consider access and service coverage. The empirical study was done in Nanjing, China, on fire station location planning, and the fire accident data was taken from 2002 to 2013. The proposed spatial optimization model uses the locating set covering problem (LSCP) and p-median problem (PMP). The model aims to decrease the number of fire stations with minimum travel distance or time. The possible location of the fire station is represented in the center of demand areas. In terms of service coverage, various studies have specified that the straight-line distance can be a satisfactory substitute for network travel time, and it has been generally accepted in fire station siting (Cudnik et al. 2012; Eiselt and Marianov 2015; Murray 2013). The conclusion of the research is that the bi-objective optimization model gives the best location of fire station including the access and service coverage.

### 3 Case Study on Ahmedabad

Gujarat's largest city and the seventh-largest metropolis in India, Ahmedabad, was founded on the eastern bank of the river Sabarmati in 1411 AD as a walled city. The city has traditionally been one of the most important trade and commerce centers in western India. Furthermore, it is one of the major industrial and financial centers in India, contributing about 14% of all stock exchange investments and 60% of state productivity. There are several national, regional, and global institutions of scientific and educational excellence in the city. There are many exquisite monuments, temples, and modern buildings that reflect the city's architectural tradition (Doshi n.d.).

As discussed in the introduction, Ahmedabad is one of the fastest-growing cities in India, with a population above 8 million. So, the fire risk to the people and property is high. Therefore, it is a massive requirement to obtain the critical fire risk factors for the city. And further, there is the requirement of fire risk assessment planning and access and service coverage. Hence, for Ahmedabad City, the factors influencing fire are classified under various categories such as Shuttle Radar Topography Mission (SRTM), metrological data, census data, Landsat data, and planning and regulation data (Fig. 2).

The LULC map of Ahmedabad has created using the QGIS software. To create the LULC map, the Landsat images have been used. The Landsat images are taken from the United States Geological Survey. Data processing has been done on the Landsat image in which the five land use classes have classified. These five land use classes are river, pond, water clogged area (RPWC), residential, commercial, and



**Fig. 2** LULC map of Ahmedabad (RPWC: river, pond, water clogged area, RCIA: residential, commercial, industrial area)

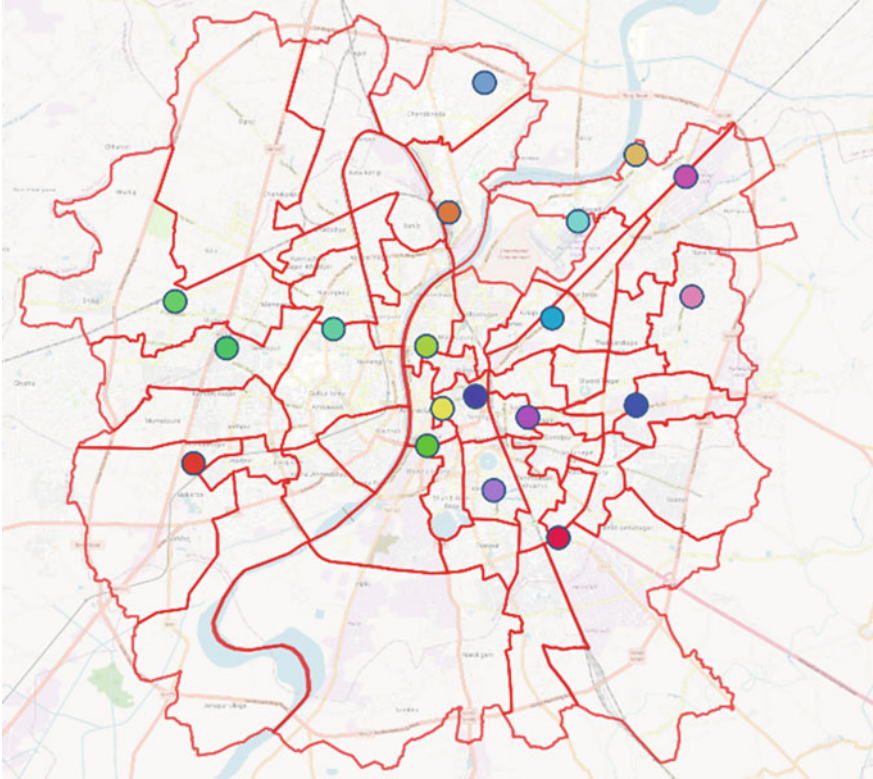
industrial area (RCIA), plantation area, vegetation area, and open space area. Three algorithms are used: minimum, maximum likelihood, and spectral angle mapping. After these, the sieve corrections are done at levels 4 and 8 to get the maximum accuracy of the LULC map. The area under these five different classes is obtained. The map represents that the maximum area of the city is covered by built-up, and the minimum area is under the class of plantation and vegetation area. There are 19 fire stations in Ahmedabad, as shown in Fig. 3.

The data of the fire station is collected from the fire department of the Ahmedabad Municipal Corporation's fire office in Ahmedabad. These 19 fire stations are located using the latitude and longitude of the respective fire station in the geographical information system. And when further analysis has been done on the city, like service coverage area, it has found a massive problem with access to fire risk sites. Also, there is no fire station in the newly developed areas of the city. The purpose of locating these 19 urban fire stations is to identify the service coverage area of each fire station. To map the service coverage area with respect to the optimum time, the review has taken the flash over time.

Figure 4 represents the natural fire growth over time. In the growth phase, first of all, the material is inflamed by the influence of an event and creates tiny flames of fire. These local flames grow step by step, and their thermal reflex causes more consumption of the blazing material or flame enhancement increases and reaches the flaming temperature. It may develop entirely and achieve the conditions of hot flashes point. In the burn step, when the flames of fire reach the roof, the distribution begins under the roof. Subsequently, flammable gases will reach the flame temperature, and the whole closed space will fire in a very short time (Bagheri et al. 2017).

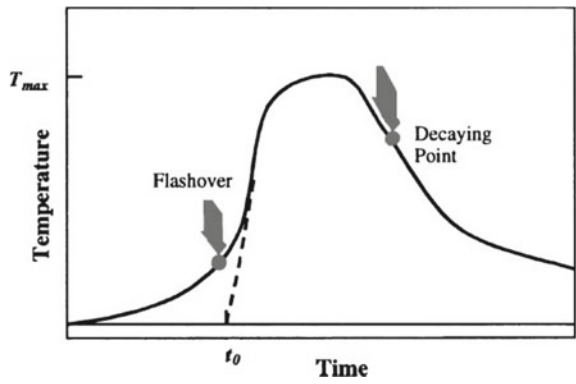
As modernization is increasing day by day, especially in urban areas. Various modernization factors also affect the fire, for example, the material curtain fabric, furniture, floor material, etc. All these modernization factors are responsible for the





**Fig. 3** Location of the fire station

**Fig. 4** Natural fire development (Ma and Ma 2000)





change in fire growth. Therefore, there is a requirement to know the flashover time considering the modernization factors. Hence, the study has reviewed new research performed by the Fire Safety Research Institute (FSRI) that illustrates the difference between natural and synthetic furnished rooms in terms of burn efficiency (Anon 2020). It has been determined that natural and synthetic furnished rooms have similar flashover times since FSRI released the original comparison video in 2009 (Anon 2020). The average optimum time for a natural furnished room is greater than 30 min, whereas the average optimum time for a synthetic furnished room is three minutes and thirty-eight seconds. Therefore, the study has taken three different times for service coverage areas to assess the risk to the city. The time taken to map the service coverage area is 2, 5, and 8 min. The service coverage area concerning the time of each fire station is specified in Fig. 5.

ORS tool is used in QGIS Desktop 3.20.2 software to create the service coverage area map for different times. Figures 6, 7, and 8 show the area not included in the service coverage from the fire station. From Fig. 6, the 2 min service coverage area can be seen. And it also shows that significantly less area is covered in 2 min and the

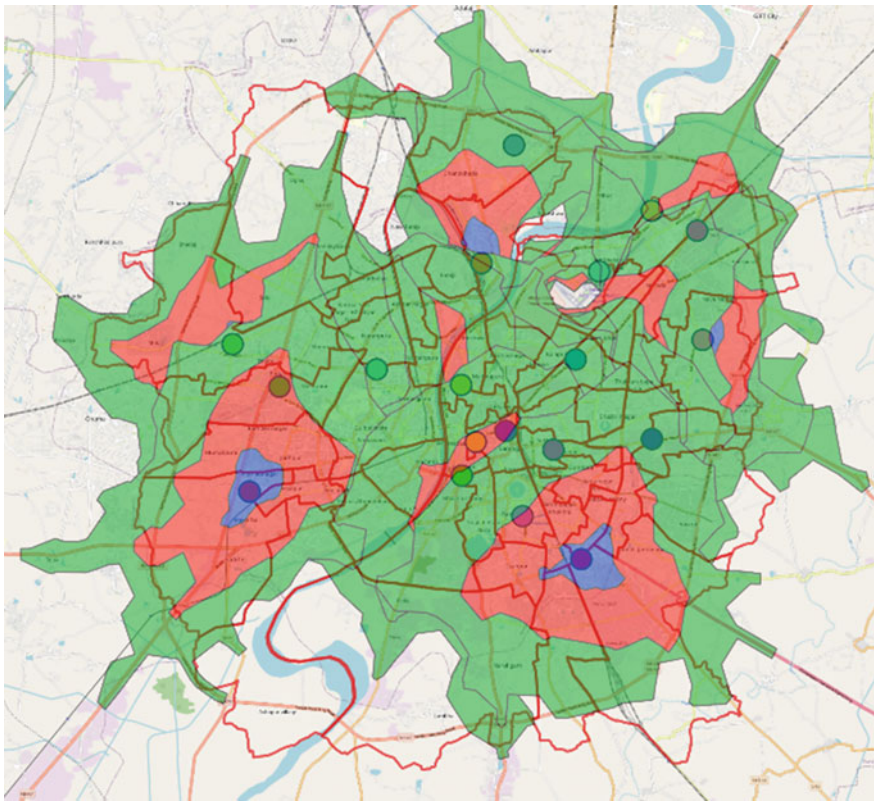
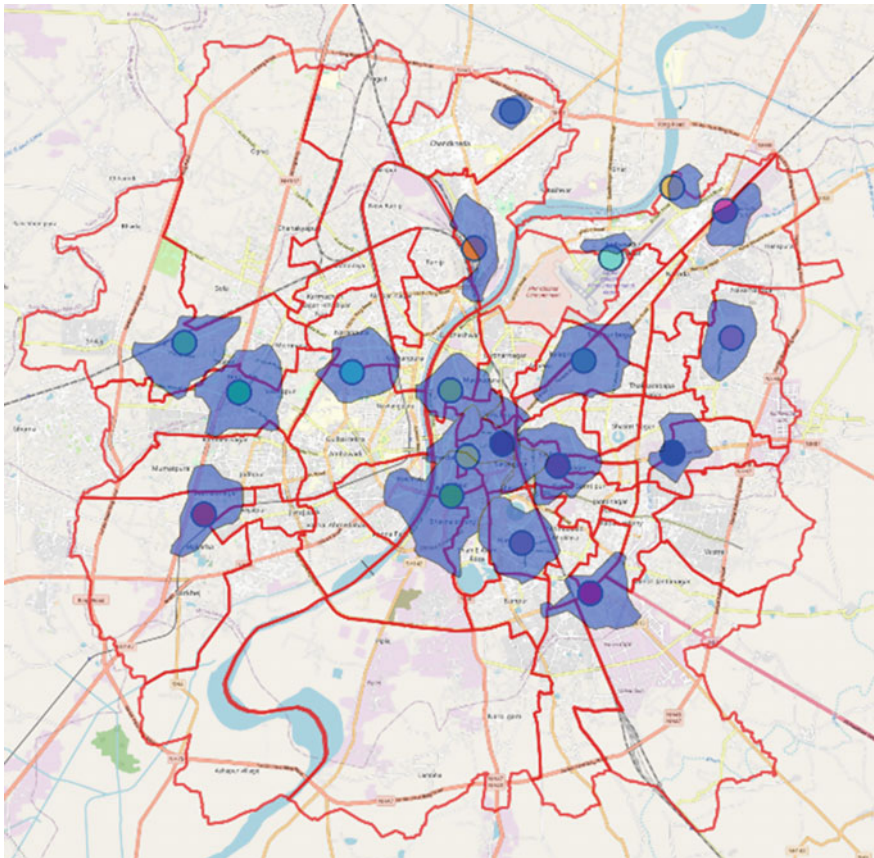


Fig. 5 Service coverage from the fire station

rest of the areas are at risk. Considering the flash over time, a further 5-min service coverage area map is developed. Figure 7 shows that many areas are at risk, such as Sarkhej, Shilaj, Bhadaj, Chanakyapuri, Tragad, Narol Gam, Hanspura, Vastral, and some areas of Vatva GIDC as well. These areas have a very large population, so the people are at high risk. The area also covers historical monuments such as Sarkhej Roja and the most prominent industrial areas like Vatva GIDC, which are at high risk. Further, 8 min is taken as the maximum response time, and it has been observed that the maximum area of the city is covered. However, still, there are uncovered areas such as Ghuma, Lambha, New Ranip, Ognaj, and Adalaj. The population density is also high in these areas, and historical monuments like Adalaj stepwell are at very high risk. Hence, the emergency service cannot reach that area. Therefore, our work focuses on Ahmedabad City to find the optimum location for a fire station with minimum distance, travel time, and maximum service coverage area.



**Fig. 6** 2 min service coverage

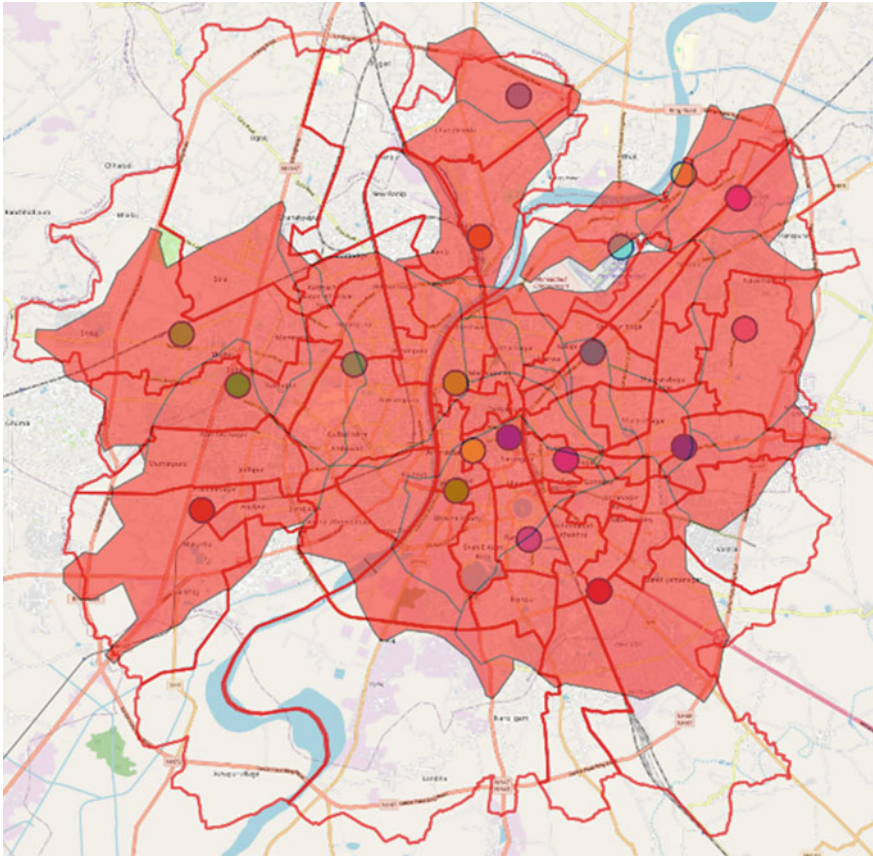
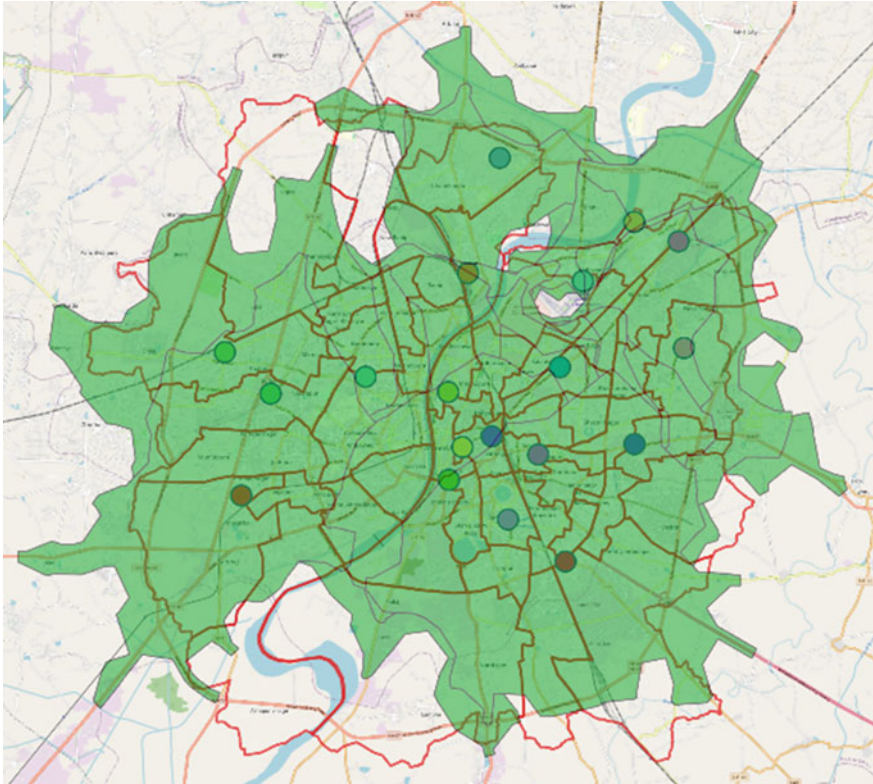


Fig. 7 5 min service coverage

## 4 Conclusions

In order to understand the importance of fire risk assessment and fire station optimization, a comprehensive review has been conducted on fire risk assessment globally, including many cities such as Haikou, Bangladesh, Dhaka, Bangladesh, and Nanjing, China. Existing methods for urban fire risk assessment and fire station optimization were reviewed to understand their importance of it. The present study has examined the critical factors for urban fire risks. The review concludes the critical risk factors with effective factor integration techniques. The study proposes eleven dominant factors contributing to fire risk in Ahmedabad city. As the maximum area of the city is covered by the built-up, thus the primary critical factors that influence the city's fire risk are land use and land cover) and population. The secondary factors are planning and regulation data such as zone and plot area ratio. Further critical factors are temperature, road network, cooking, ignition sources, MRTS, structural material, and





**Fig. 8** 8 min service coverage

city infrastructure. These critical factors are analysed using the factors integration techniques. In the review of the integration method, it has been observed that most researchers have used the analytical hierarchy process to assign weightage to the critical factors. In addition to improving decision-maker learning, AHP utilizes consistency measures to enhance the efficiency of the decision-making process. Whereas the analytical hierarchy process has certain limitations as the weight of certain critical factors also affects the other requirements. Therefore, to overcome this limitation of AHP, Decision Making Trial and Evaluation Laboratory (DEMATEL) can be used to assign the weightage to the critical factors. The weightage given to the parameters can either be in terms of ranges from 1 to 9 or in terms of severity such as low, moderate, high, and very high. Based on these weighted fire risk factors, urban fire risk map can be developed using fire risk assessment methods. Another objective of the review focuses on the optimization of the fire station.

Ahmedabad is a rapidly growing city in Gujarat. Hence, there is a considerable problem with service coverage from a fire station to the risk site. From Fig. 5, it can be seen that most fire stations are located inside the S.P Ring Road. Thus, it is difficult to reach the risk site if the fire occurs outside the S.P. Ring Road. Hence,

Figs. 6, 7, and 8 are developed using the QGIS software. These images represent the service coverage area from the fire station, and it can be seen that there is an area where the emergency service cannot reach even after the 8 min. Therefore, the fire stations must be strategically located to provide maximum service coverage with a minimum possible number of fire stations in Ahmedabad.

## 5 Future Scope

A further extension of this study can involve evaluating the finding of different multi-criteria decision making and machine learning algorithms to determine the best method for assessing the weightage for fire risk factors. Additionally, location optimization techniques can be studied based on a fire risk assessment map.

## References

- Aktaş E, Özeydin Ö, Bozkaya B, Ülengin F, Önsel Ş (2013) Optimizing fire station locations for the Istanbul metropolitan municipality. *Interfaces* 43(3):240–255. <https://doi.org/10.1287/inte.1120.0671>
- Alam JB, Baroi GN (2004) Fire hazard categorization and risk assessment for Dhaka City in GIS framework. *J Civ Eng (IEB)* 32(1):35–45
- Anon (2020) New comparison of natural and synthetic home furnishings. Fire Safety Research Institute. Retrieved <https://fsri.org/research/new-comparison-natural-and-synthetic-home-furnishings#tabs-overview>
- Badri MA, Mortagy AK, Alsayed CA (1998) A multi-objective model for locating fire stations. *Eur J Oper Res* 110(2):243–260. [https://doi.org/10.1016/S0377-2217\(97\)00247-6](https://doi.org/10.1016/S0377-2217(97)00247-6)
- Bagheri H, Shabankareh AA, Safi M (2017) Numerical investigation of the behavior of steel frames under the effect of natural fire condition. Scinzer Scientific Publications. <https://doi.org/10.21634/SJE.3.2.1421>
- Bonora L, Conese CC, Marchi E, Tesi E, Montorselli NB (2013) Wildfire occurrence: integrated model for risk analysis and operative suppression aspects management. *Am J Plant Sci* 04(03):705–710. <https://doi.org/10.4236/ajps.2013.43a089>
- Bureau of Indian Standards (1988) IS 1643 (1988): code of practice for fire safety of buildings (general): exposure hazard. Bureau of Indian Standards, New Delhi, India
- Bureau of Indian Standards (2005) IS 11460 (1985): code of practice for fire safety of libraries and archives. Bureau of Indian Standards, New Delhi, India
- Bureau of Indian Standards (2013) IS 8758 (2013): recommendations for fire precautionary measures in the construction of temporary structures and pandals. Bureau of Indian Standards, New Delhi, India
- Bureau of Indian Standards (2016) National building code part-IV (Fire Safety).Pdf.
- Cai N, Chow WK (2012) Wind effect on spread of fire and smoke. In: *Acem'12*, pp 3197–3207
- Castro R, Chuvieco E (1998) Modeling forest fire danger from geographic information systems. *Geocarto Int* 13(1):15–23. <https://doi.org/10.1080/10106049809354624>
- Church R, ReVelle C (1972) The maximal covering location problem, vol 6, no 6
- Church RL, Li W (2016) Estimating spatial efficiency using cyber search, GIS, and spatial optimization: a case study of fire service deployment in Los Angeles County. *Int J Geogr Inf Sci* 30(3):535–553. <https://doi.org/10.1080/13658816.2015.1083572>

- Cudnik MT, Yao J, Zive D, Newgard C, Murray AT (2012) Surrogate markers of transport distance for out-of-hospital cardiac arrest patients. *Prehosp Emerg Care* 16(2):266–272. <https://doi.org/10.3109/10903127.2011.615009>
- Doshi BV (n.d.) Amdabad municipal corporation. Ahmedabadcity.Gov.In. Retrieved [https://ahmedabadcity.gov.in/portal/jsp/Static\\_pages/introduction\\_of\\_amdavad.jsp](https://ahmedabadcity.gov.in/portal/jsp/Static_pages/introduction_of_amdavad.jsp)
- Eiselt HA, Marianov V (2015) Applications of location analysis, vol 232, pp 1–437. <https://doi.org/10.1007/978-3-319-20282-2>
- Erik DS (1992) Fire risk assessment method for engineering, NFPA, SFPE Spring Seminar, New Orleans, USA
- Gan W, Chen C, Wang Z, Song J, Kuang Y, He S, Mi R, Sunderland PB, Hu L (2019) Dense, self-formed char layer enables a fire-retardant wood structural material. *Adv Funct Mater* 29(14):1807444:1–9. <https://doi.org/10.1002/adfm.201807444>
- Ganteaume A, Marielle J, Corinne LM, Thomas C, Laurent B (2011) Effects of vegetation type and fire regime on flammability of undisturbed litter in Southeastern France. *For Ecol Manage* 261(12):2223–2231. <https://doi.org/10.1016/j.foreco.2010.09.046>
- Gernay T, Selmet S, Tondidni N, Khorasani NE (2016) Urban infrastructure resilience to fire disaster: an overview. *Procedia Eng* 161:1801–1805. <https://doi.org/10.1016/j.proeng.2016.08.782>. Elsevier
- Hakimi SL (1964) Optimum locations of switching centers and the absolute centers and medians of a graph. *Oper Res* 12(3):450–459. <https://doi.org/10.1287/opre.12.3.450>
- Jafari Goldarag Y, Mohammadzadeh A, Ardakani AS (2016) Fire Risk assessment using neural network and logistic regression. *J Indian Soc Rem Sens* 44(6):885–894. <https://doi.org/10.1007/s12524-016-0557-6>
- Jain A, Nyati P, Nuwal N, Ghoroi C, Ansari A, Gandhi PD (2013) UL—IIT Gandhinagar kitchen fire safety system
- Kaur MM, Dayal P, and Sharma V (2021) India risk survey. Pinkerton global headquarters
- Kiran KC, Corcoran J, Chhetri P (2018) Spatial optimisation of fire service coverage: a case study of Brisbane, Australia. *Geogr Res* 56(3):270–284. <https://doi.org/10.1111/1745-5871.12288>
- Kushla JD, Ripple WJ (1997) The role of terrain in a fire mosaic of a temperate coniferous forest. *For Ecol Manage* 95(2):97–107. [https://doi.org/10.1016/S0378-1127\(97\)82929-5](https://doi.org/10.1016/S0378-1127(97)82929-5)
- Lamat R, Kumar M, Kundu A, Lal D (2021) Forest fire risk mapping using analytical hierarchy process (AHP) and earth observation datasets: a case study in the mountainous Terrain of Northeast India. *SN Appl Sci* 3(4):1–15. <https://doi.org/10.1007/s42452-021-04391-0>
- Lautenberger C, Rich D, Zak C (2015) Spot fire ignition of natural fuel beds by hot metal particles, embers, and sparks. Taylor & Francis. <https://doi.org/10.1080/00102202.2014.973953>
- Li SY, Tao G, Zhang LJ (2018) Fire risk assessment of high-rise buildings based on gray-FAHP mathematical model. *Procedia Eng* 211:395–402. <https://doi.org/10.1016/j.proeng.2017.12.028>
- Liu N, Huang B, Chandramouli M (2006) Optimal siting of fire stations using GIS and ANT algorithm. *J Comput Civ Eng* 20(5):361–369. [https://doi.org/10.1061/\(asce\)0887-3801\(2006\)20:5\(361\)](https://doi.org/10.1061/(asce)0887-3801(2006)20:5(361))
- Ma Z, Mäkeläinen P (2000) Parametric temperature–time curves of medium compartment fires for structural design. *Fire Saf J* 34(4):361–375
- Murray AT (2013) Optimising the spatial location of urban fire stations. *Fire Saf J* 62(PART A):64–71. <https://doi.org/10.1016/j.firesaf.2013.03.002>
- Nelson RM (2002) An effective wind speed for models of fire spread. *Int J Wildland Fire* 11(2):153–161. <https://doi.org/10.1071/WF02031>
- Peacock RD, Reneke PA, Bukowski RW, Babrauskas V (1999) Defining flashover for fire hazard calculations. *Fire Saf J* 32(4):331–345
- Poon L, Lau R (2007) Fire risk in metro tunnels and stations. *Int J Performability Eng* 3
- Ricotta C, Bajocco S, Guglietta D, Conedera M (2018) Assessing the influence of roads on fire ignition: does land cover matter? *Fire* 1(2):1–9. <https://doi.org/10.3390/fire1020024>
- Syphard A (2019) Ignition sources. Part of Springer Nature 2018. <https://doi.org/10.1007/978-3-319-51727-8>

- Toregas C, Swain R, ReVelle C, Bergman L (1971) The location of emergency service facilities. *Oper Res* 19(6):1363–1373. <https://doi.org/10.1287/opre.19.6.1363>
- Tsukagoshi I, et al (n.d.) A study on urban fire prevention in case of big earthquake. In: Proceedings of the eighth world conference on earthquake engineering, no. 1, pp 769–776
- Zhang Y (2013) Analysis on comprehensive risk assessment for urban fire: the case of Haikou City. *Procedia Ineering* 52:618–623. <https://doi.org/10.1016/j.proeng.2013.02.195>
- Zolfaghari MR, Peyghaleh E, Nasirzadeh G (2009) Fire following earthquake, intra-structure ignition modeling. *J Fire Sci* 27(1):45-79. <https://doi.org/10.1177/0734904108094516>

# Modelling the Impact of Various Strategies for Improving the Outdoor Thermal Comfort at a City Level



Yash G. Bhavsar and Anurag Kandya

**Abstract** One of the greatest environmental concerns for the long-term viability is to develop sustainability of future cities and to plan heat mitigation techniques for improving human outdoor thermal comfort. In this research work, a case study for Ahmedabad City has been considered which has hot, semi-arid climate-Bsh based on Köppen climate classification and aim of the study is to improve the outdoor thermal comfort and to plan heat mitigation strategies of Ahmedabad City, Gujarat, India, by assessing the outdoor thermal comfort of a city with analysing mean radiant temperature with thermal indices such as PET, PMV/PPD and UTCI with the application of ENVI-met V5.0.2 Software. For conducting the study, an urban canopy of Ahmedabad City has been examined from Maninagar area, and it has an administrative boundary of 7692.33 m<sup>2</sup> was model in ENVI-met (SPACES). The analysis was done during 09 May 2021 a hot summer day and 17 December 2021 a cool winter day to create a challenging environmental situation, and the input data for the simulations process are based on the meteorological station of GPCB located in Maninagar area. Software simulations were performed (for 24 h), and based on simulation of modelling, the four different case scenarios in ENVI-met model result are presented. The simulated results show that the suggested strategies have an effect on OTC, which means adopting case-2 and case-3 in particular location can reduce the temperature around 1.5–2 °C with Tmrt reduce up to 1.02–6.20 °C in summer and also, adopting case-2 and case-3 in particular location can increase the temperature around 0.5–1.0 °C in winter. The study provides better understanding of heat mitigation strategies on human thermal comfort at a city level (Ahmedabad), and the findings of this research provide finer suggestions for improving outdoor thermal comfort environment.

**Keywords** Envi\_met software · Human thermal comfort · Urban microclimate · Residential area · Ahmedabad City India

---

Y. G. Bhavsar (✉) · A. Kandya  
Pandit Deendayal Energy University, Gandhinagar, India  
e-mail: [yash.bmten20@sot.pdpu.ac.in](mailto:yash.bmten20@sot.pdpu.ac.in)

A. Kandya  
e-mail: [Anurag.Kandya@sot.pdpu.ac.in](mailto:Anurag.Kandya@sot.pdpu.ac.in)



## ***Abbreviations***

ASHRAE	American Society of Heating, Refrigerating & AC for Engineers
CPCB	Central pollution control board
EN 16798-1	Basics of Thermal Comfort
GPCB	Gujarat pollution control board
ISO 7730	Ergonomics of the thermal environment
OTC	Outdoor thermal comfort
PET	Physiological equivalent temperature
PMV	Predicted mean vote
PPD	Predicted percentage of dissatisfied
RH	Relative humidity
SVF	Sky view factor
T <sub>a</sub>	Air temperature
T <sub>mrt</sub>	Mean radiant temperature
UHI	Urban heat Island
UTCI	Universal thermal climatic index

## **1 Introduction**

The world is seeing rapid urbanization, as well as global warming and climate change. As a result, the role of urban planning, design and architectural production plays a crucial role to accomplish outdoor thermal comfort. As a result, one of the primary variables that must be addressed in order to achieve outdoor thermal comfort and construct cities that are environmentally friendly and are capable of achieving the highest degree of outdoor thermal comfort is the urban climate. A large number of publications on urban climate have been produced in order to deal with the climate of the city, which can play a significant role in enhancing urban climatology for better designing and mitigating the effects of climate change on the city's rapidly growing population. As a result, sustainable city planning is a step forward in reducing cities harmful effects on the environment.

### ***1.1 Effect of Climate Change***

In weather forecasting, climate change may contribute to heat warnings and medical issues. Many studies have been conducted in recent decades to improve the outdoor thermal comfort, and it has been demonstrated that a comfortable outdoor thermal environment can promote outdoor activity, improve urban climatology, and improve human physical and mental health. The thermal budget of the human body is highly

influenced by the sun's radiation, convection in the surrounding air and sweat evaporation which will cause several of health problems for humans. As a result, extended heat exposure can lead to a range of health problems, including heat rashes, heat cramps and heat exhaustion to potentially fatal heat strokes (Abdollahzadeh et al. 2021; Gajjar 2019).

**Definition of Thermal Budget**—The skin must be around 33 °C to sustain a consistent flow of heat from the human body's core (37 °C) to the surrounding environment.

## ***1.2 What is Thermal Comfort***

The ASHRAE 55 standard thermal comfort is defined as “the mental condition in which a particular situation or a person's satisfaction is expressed with the thermal environment.” It is a subjective opinion varies from individual perception based on the age group, standard of livings, body type, metabolism and the type of clothes worn during every season and also depends on various climatic factors. More than 165 thermal comfort indices have been established to evaluate the thermal environment by taking external factors and the human body's energy balance into account for both indoor as well outdoor thermal environment (Atwa et al. 2020; Kumar et al. 2020).

To proceed with the research study, the paper is divided into five sections. As discussed earlier, the part 1 will be the introduction part of the research study then, the second part will be the methodology with study area which will provide the geographic and climatic context as well as the studied solution methods and model validation, while Sect. 3 contains the results and discussion and lastly, and Sect. 4 contains the conclusions.

The research aims to focus on improving the outdoor thermal comfort and to plan heat mitigation strategies of an Ahmedabad City, Gujarat, India, by assessing the outdoor thermal comfort of a city with analysing mean radiant temperature with thermal indices such as predicted mean vote/predicted percentage of dissatisfied, physiological equivalent temperature and universal thermal climatic index with the application of ENVI-met software and also to investigate the levels of human thermal comfort.

## **2 Methodology**

This section will firstly give the basic information regarding the case study and geographic condition with climate context of the research area. The key focus of this case study is Chaturbhuj colony Kankaria, located in Maninagar area in Ahmedabad City, Gujarat, India, and it is characterized by a hot semi-arid climate. Secondly, it describes a numerical simulation software that can be used to assess the microclimate in outdoor areas. The software considers all environmental characteristics including

the mean radiant temperature, the air temperature, the relative humidity and the wind speed (Barakat et al. 2017; Bruse 1998).

## ***2.1 Case Study: Chaturbhuj Colony, Maninagar, Ahmedabad***

The study area which was selected to conduct the research work is a small urban pocket from Maninagar area of Ahmedabad City has been considered which is located at coordinates of latitude  $23^{\circ} 0' 4''$  and Longitude  $72^{\circ} 35' 45''$ , and it has an administrative boundary of  $7692.33 \text{ m}^2$  to form a better perspective in hot semi-arid climate to assess how different strategies may improve outdoor thermal comfort conditions. Based on simulation of modelling, the four different case scenarios in ENVI-met (SPACES) with the grid size of  $(44*45*38)$  (X\*Y\*Z Grids) as our case study with base case scenario and other three case were model for simulation and evaluated, and then, the plan is to evaluate the area for thermal performance and to plan the various heat mitigation strategies to improve outdoor thermal comfort (Figs. 1 and 2).

Summer, monsoon and winter are the three primary seasons in Ahmedabad. The temperature is high from March to June, where it feels like heatwave with average summer day light savings time of 6:00 AM to 19:15 maximums with high temperature of  $35\text{--}46^{\circ}\text{C}$  and average minimums of  $40.5^{\circ}\text{C}$ . From mid-June to September, the south-west monsoon offers a humid environment with annual average rainfall of roughly 800 mm, while winter lasts from November to February, with December and January being the coldest months. It has a 3 m/s average wind speed and an 8 m/s maximum wind speed.

## ***2.2 Software Selection for Conducting the Study***

The main concern of the study is to selecting best software available to achieve the purpose of the study. Because field measurement takes time and requires a lot of manpower, equipment and expense. It is hard to conduct on field measurement and get the accurate meteorological data. There are various softwares available for evaluating outdoor thermal comfort. To proceed with the study, ENVI-met software was selected based on the literature review and most widely used software to conduct the research on urban microclimate. ENVI-met (Bruse 1998) is a gridded 3D model, and it is a numerical model that simulates of meteorological variables in a gridded domain. It uses a holistic approach in which all the different aspects of a microclimate are linked and simulated together in one model.

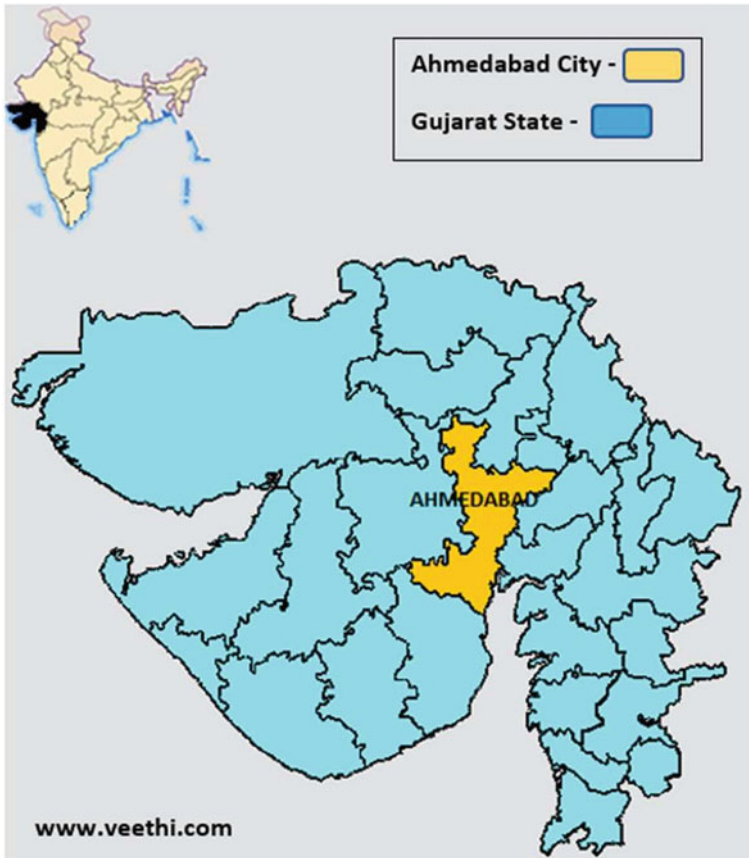


Fig. 1 Map of Gujarat showing Ahmedabad City

### 2.3 Methods

To conduct the study and to perform simulation for better thermal performance, a meteorological data of Maninagar weather station has been collected for performing simulations. The station which records meteorological data is located in Maninagar area itself at a coordinate of  $23.02^{\circ}\text{N}$ ,  $72.58^{\circ}\text{E}$  which has been used for simulation in ENVI-met software. The weather data has been downloaded from CPCB Website (historical data) and used for the best result of simulation.

The software simulation was performed for extreme condition to evaluate the outdoor thermal comfort for the hottest day in summer as well coldest day in winter, and selected day for the hottest day was (09-05-2021), where temperature reaches maximum up to  $44^{\circ}\text{C}$  at 15:00 in afternoon, and the coldest day was (17-12-2021), where the temperature reaches minimum  $7^{\circ}\text{C}$  at 7:00 in morning (Figs. 3 and 4).



Fig. 2 Location of The Study Area (Chaturbhuj Colony, Kankaria Maninagar, Ahmedabad, Gujarat, India) <https://earth.google.com/>

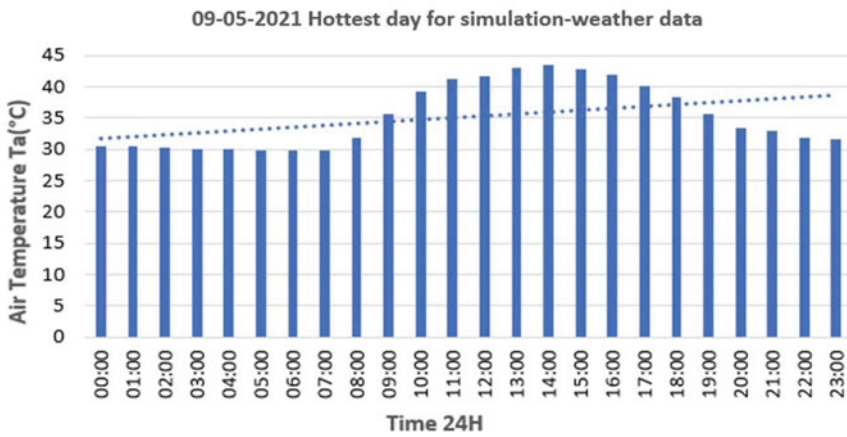


Fig. 3 Graph shows the air temperature for 24 h of 09th May 2021 hottest day

The flow chart of methodology shows that ENVI-met model was applied to conduct this study. The framework of ENVI-met software is shown in below flow chart.

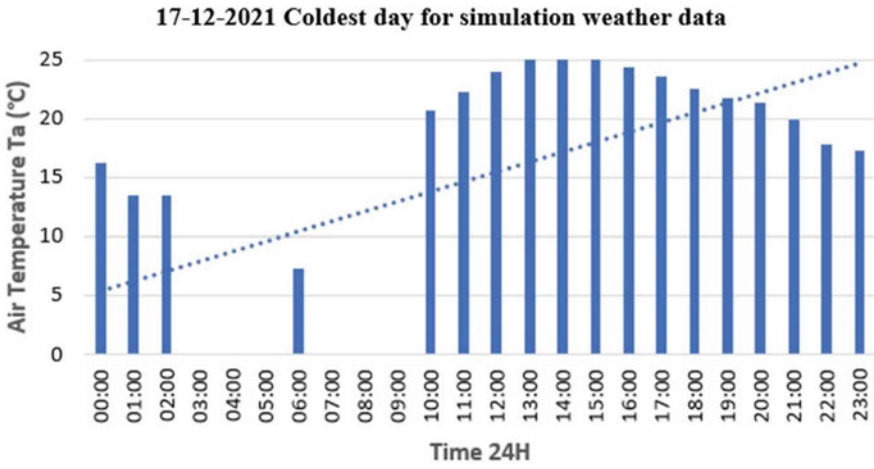
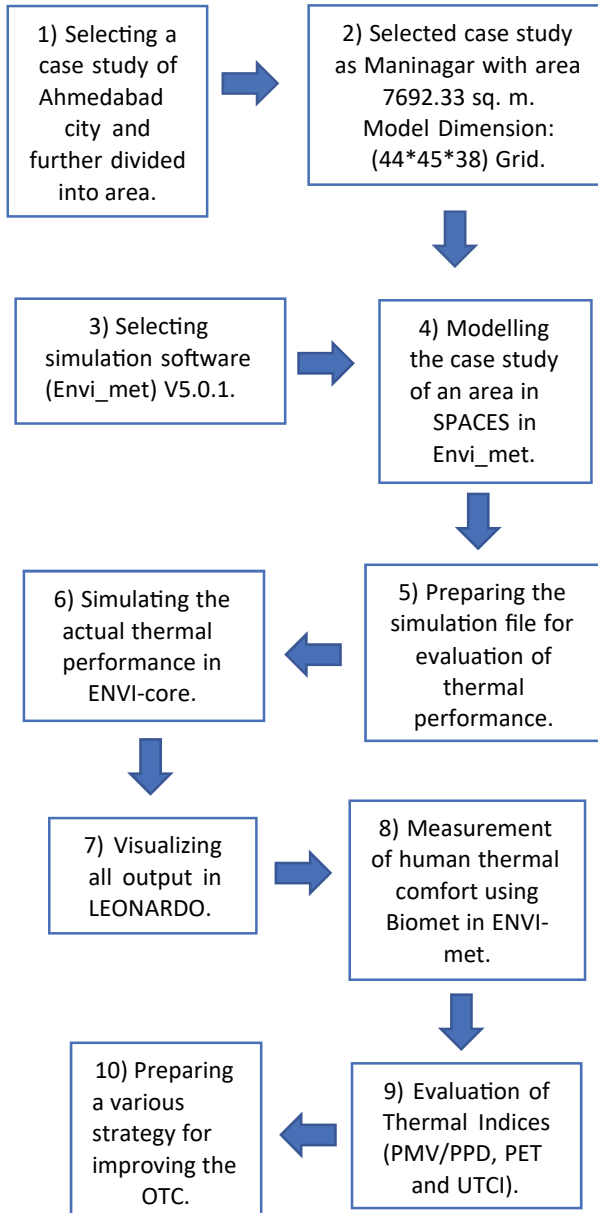


Fig. 4 Graph shows the air temperature for 24 h of 17th Dec 2021 coldest day



The below four different case scenarios were modelled in ENVI-met (SPACES) has a location of Maninagar area of Ahmedabad City, which has 7692.33 sq. km. area and has residential location coordinates of latitude  $23^{\circ} 0' 4''$  and longitude  $72^{\circ} 35' 45''$ . Below, the various cases are mentioned below:

***Four Different Case Scenario:***

1. Base case scenario—It represents the current situation of area.
2. Number of trees at equal interval on all four side of corners—It means all four-side covered with oak tree and hedges on road divider (central verge)) and vegetation cover increased by 20% of the selected area.
3. Random Arrangement of tree near the building area—As mentioned earlier, vegetation cover increased by 20% of the selected area, and trees are arranged near the building area to provide proper shading and cooling effect to the building.
4. Façade and roof greening on building with some water bodies with base case scenario of tree arrangement—It means 100% of the roof and façade greening in the selected area covered with wall greening and roof greening with base case scenario of tree (means tree were same as it in case-1), and it also includes water bodies around 2–5% in this case.

The scaling of model = 1:1 (Actual Area) in ENVI-met model.

### 2.4 Preparing the Simulation file in ENVI-met Guide (.SIMX)

As discussed earlier, software simulations were performed in sunniest month as well as coldest month for the year 2021 which has the (24 h) simulation and below, and Table 1 shows the input details of meteorological parameters with various other parameters.

**For Hottest Day—09-05-2021 Time and Date:**

**Meteorology—By Simple Forcing:**

See Table 2.

**For Coldest Day—17-12-2021 Time and Date:**

See Table 3.

**Meteorology—By Simple Forcing:**

See Table 4.

**Table 1** Shows the input data of time and date for the hottest day simulation

Start date	09-05-2021
Start time	6:00 AM
Total simulations time (h)	24 h



**Table 2** Shows the input data of meteorology for the hottest day simulation

Temperature °C. min. at 08:0	29 °C
Temperature °C. max. at 16:00	44 °C
Relative Humidity %. Min at 18:00	18
Relative Humidity %. Max at 09:00	49
Wind Speed	3.15 m/s
Wind Direction	355.00° (NW/E)
Roughness length	0.010 m
Cloud Cover (low, medium and high)	0, 4, 0

**Table 3** Shows the input data of time and date for the coldest day simulation

Start date	17-12-2021
Start time	6:00 AM
Total simulations time (h)	24 h

**Table 4** Shows the input data of meteorology for the coldest day simulation

Temperature °C. min. at 07:00	7 °C
Temperature °C. max. at 16:00	26 °C
Relative Humidity %. Min at 08:00	6
Relative Humidity %. Max at 12:00	53
Wind Speed	3.15 m/s
Wind Direction	96.95° (NW/E)
Roughness length	0.010 m
Cloud cover (low, medium and high)	0, 4, 6
CPU cores:	Multi core (Parallel)
Dynamic time step management	2 s, 2 s, 2 s

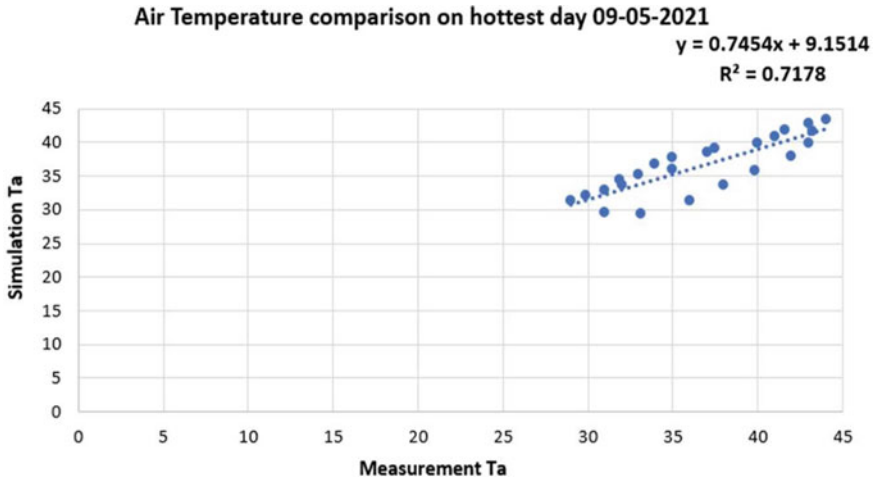
## 2.5 Model Validation

It is to check the accuracy of the model with real scenario. By comparing the outcomes of simulations with field observations, the ENVI-met model was validated. The measurements were done within the Maninagar area itself, where all meteorological data was recorded with an interval of 01:00 h' time and the instrument are located at coordinates of 23.02°N, 72.58°E, and data is download through CPCB Website.

### Comparison of simulation (ENVI-met) results with measurements on 09 May 2021 for the hottest day (Summer)

See Fig. 5.

Here, you can see from the above scatter plot the RMSE value of air temperature between the measured and simulated data on 09 May 2021 for the 24 h was 0.2806



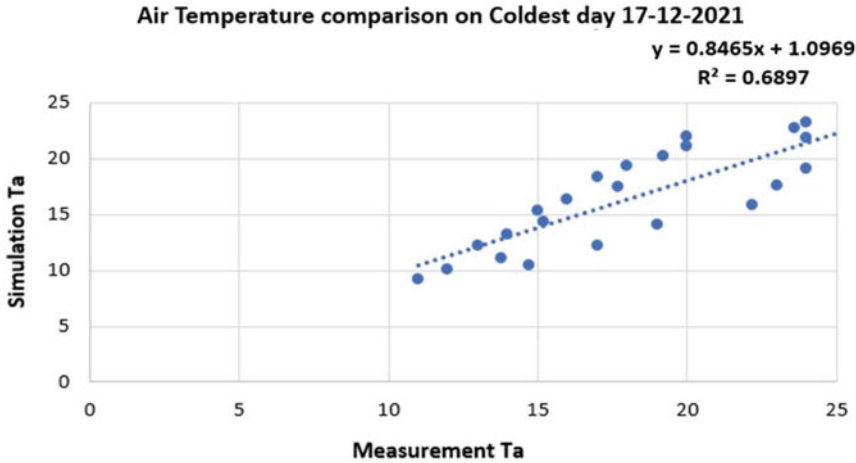
**Fig. 5** Graph represents the scatter plots for the simulated and measured data of air temperature for the validation of model

and  $R^2$  value is 0.71. The correlation coefficient between the two sets of data is 0.84, while the index of agreement between the two data set is 0.91 which is nearly to 1 which indicates the perfect match of the model. The data set which is used to create the scatter plot has only 24 h data and the data from simulations and measurements are compared to show the accuracy of the simulation results. The measured and simulation air temperature during 09th May 2021 are been compared for the 24 h, the patterns of air temperature between the measurement and the simulation are more or less the same, and the peak of Ta according to the measurement is 0.5–2 °C higher than according to the simulations.

**Comparison of simulation (ENVI-met) results with measurements on 17 Dec 2021 for the coldest day (Winter)**

See Fig. 6.

Here, you can see from the above scatter plot the RMSE value of air temperature between the measured and simulated data on 17 Dec 2021 for the 24 h was 0.8728 and  $R^2$  value is 0.68. The correlation coefficient between the two sets of data is 0.83. While the index of agreement between the two data set is 0.86 which is nearly to 1 which indicates the perfect match of the model. The data set which is used to create the scatter plot has only 24 h data, and the data from simulations and measurements are compared to show the accuracy of the simulation results. The measured and simulation air temperature during 17 December 2021 are been compared, the patterns of air temperature between the measurement and the simulation are more or less the same, and the peak of Ta according to the measurement is 0.5–2 °C higher than according to the simulations.



**Fig. 6** Graph represent the scatter plots for the simulated and measured data of air temperature for the validation of model

### 3 Result and Discussion

The results were obtained by extracting raw output data using LEONARDO thematic mapping tools on the outdoor environment on particular location of four different case scenarios that were modelled in ENVI- met (SPACES) for Chaturbhuj colony, Kankaria Maninagar, Ahmedabad (Lat = 23.02 & Long = 72.60). The average air temperature and other environmental parameters for the particular site have been evaluated at 1.5 m height above ground level. There are total eight times simulations were performed in ENVI-core for four different case scenarios for coldest day in winter as well hottest day in summer for year 2021. (Means 4 times simulation performed for summer and 4 times simulation performed for winter) to get the better idea regarding how thermal comfort can affect for both the seasons. Each simulation takes times around 10–12 h for evaluating of the result.

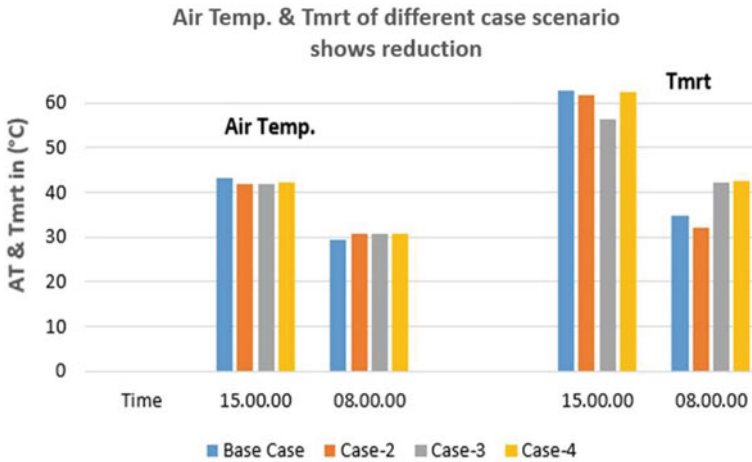
#### Hot Summer Day (09-05-2021)

The result for the hot summer day (09-05-2021) where raw data is extract in thematic map tool LEONARDO is for a particular hour at 15:00 which reports the highest temperature of the particular day in a year.

#### Result for Air Temperature and Tmrt

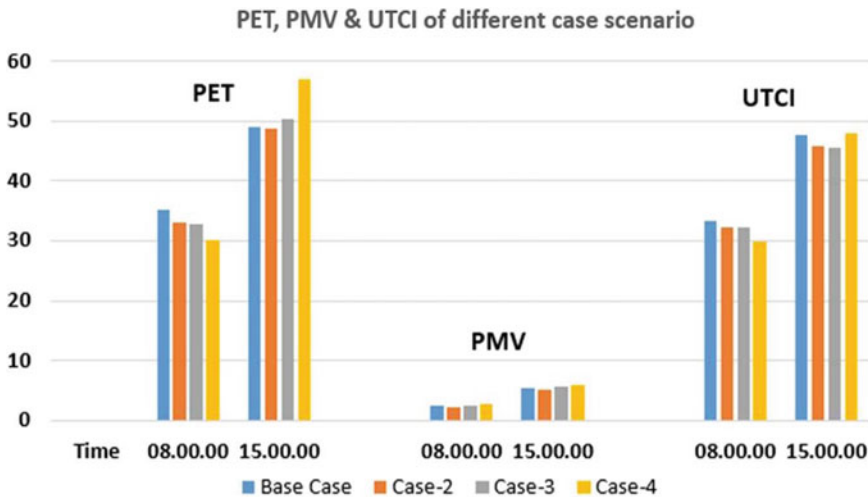
See Fig. 7.

The overall variation from case-1 to case-4 of Ta reduction at 15:00 is around 1.520–1.120 °C, the overall variation from case-1 to case-4 of Tmrt reduction at 15:00 is around 6.236–1.02 °C; as you can see on below graph, the overall variation from case-1 to case-4 of PET reduction at 08:00 AM (Min) is around 2.607 °C to 4.904 °C, the overall variation from case-1 to case-2 of PET reduction at 15:00 (Max)

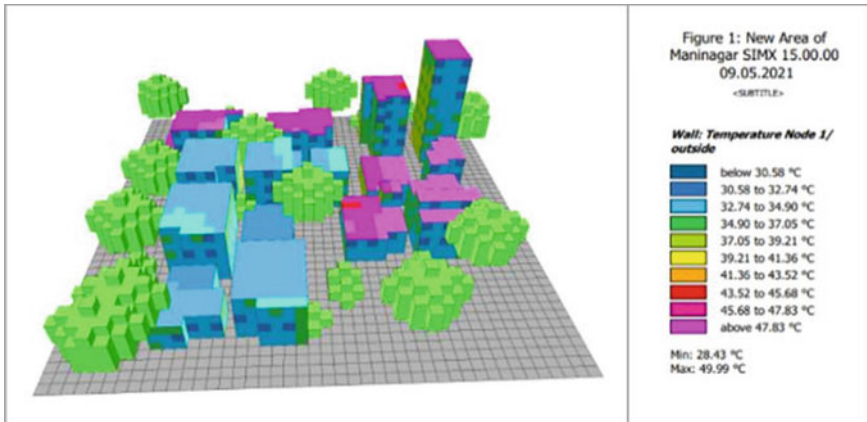


**Fig. 7** Graph shows the air temperature and Tmrt patterns for all the cases at particular time 15:00 & 08:00

is around 0.363 °C, the overall variation from case-1 to case-4 of PMV reduction at 08:00 AM (Min) is around 0.1868 °C, the overall variation from case-1 to case-2 of PMV reduction at 15:00 (Max) is around 0.2635 °C, the overall variation from case-1 to case-4 of UTCI reduction at 08:00 AM (Min) is around 0.922–3.444 °C, and the overall variation from case-1 to case-2 of UTCI reduction at 15:00 (Max) is around 1.698–2.188 °C (Fig. 8).



**Fig. 8** Graph show the PET, PMV and UTCI thermal indices patterns for all the cases at particular time 15:00 & 08:00



**Fig. 9** Image shows the wall: temp node 1/outside at 15:00 of study area in 3d view

### Result of roof and Façade greening

See Fig. 9.

The building which has roof and façade greenings has a wall greening material: green + mixed substrate & roof greening materials: only green is higher in temperature (hotter) as compared to the building which has wall greening material: green + mixed substrate and roof greening material: green + sandy loam substrate. It has a difference around 1.5 °C means green + sandy loam substrate is cooler than only green roof and has a variation around 1–3 °C. It provides more cooling effect on roof. (Wall: Air Temp. in front of façade).

### Cold Winter Day (17-12-2021)

The result for the cold winter day (17-12-2021) where raw data is extract in thematic map tool LEONARDO is for a particular hour at 07:00 which reports the lowest temperature of the particular day in a year.

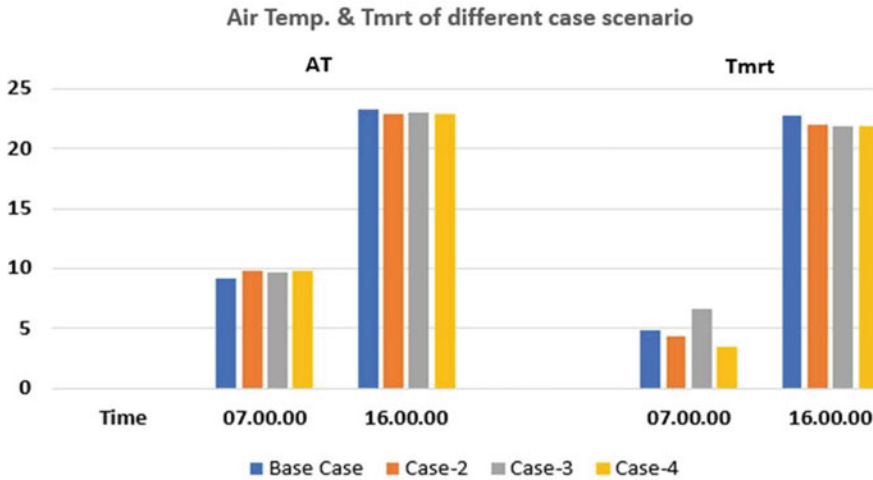
### Result for Air Temperature and Tmrt

See Fig. 10.

The overall variation (temperature increases) from case-1 to case-4 of Ta at 07:00 on 17-12-2021 in winter is around 0.6657–0.6822 °C, and the overall variation (temperature increases and decreases) from case-1 to case-4 of Tmrt at 07:00 on 17-12-2021 in winter is around 1.7017 °C (increase) to 0.6021 °C (decrease).

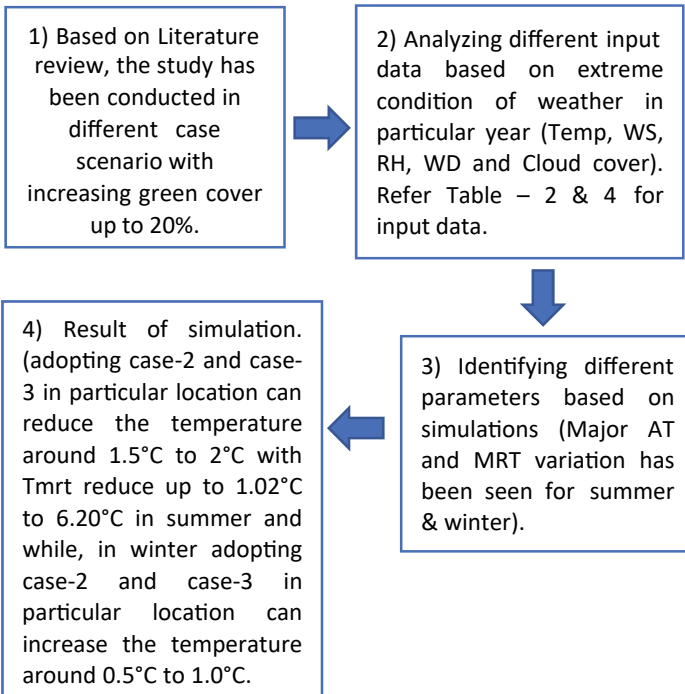
## 3.1 Strategies Planned During the Study

As per literature review, the study has been conducted hypothetically in Envi\_met (SPACES) model with have been planned from simulated results by taking two



**Fig. 10** Graph show the air temperature and patterns for all the cases at particular time 16:00 & 07:00

extreme condition in summer & winter. Below, methodology chart shows the different stages of analysis.



The simulated results (for a typical summer day 09 May 2021 at 15:00) show that the suggested strategies have an effect on OTC.

1. The building which has roof and façade greenings has a wall greening material: green + mixed substrate & roof greening materials: only green is higher in temperature (hotter) as compared to the building which has wall greening material: green + mixed substrate and roof greening material: green + sandy loam substrate. It is due to sandy loam substrate which is made up of soil along with varying amount of silt and clay.
2. As a design consideration, adopting or implementing case-4 (Façade and roof greening) in a hot humid climate can decrease the temperature of building at typical hottest day in a summer, and it has a more cooling effect than normal construction material used in buildings.
3. Increasing vegetation around 20% means: as a solution, planting a oak tree (which has a same significance of neem tree) on all four side of location or planting trees on the roadside (Road Arboriculture) means adopting case-2 in particular location can reduce the temperature around 1.5 °C and can provide more shade during the daytime as well it will help to reduce long and short wave radiation (mean radiant temperature) up to 1.02 °C and also thermal indices such as PET reduce around 0.37 °C, PMV 0.25 °C and UTCI up to 2.20 °C.
4. The 4 m hedges which was planted on road divider (central verge) can act as wind shielding to improve outdoor thermal comfort and reduce the wind speed as well. It can also be used to protect the soil from erosion and acts as a barrier to prevent accident and absorb sound to prevent from noise pollution.
5. Wind shielding/sheltering can be utilized to increase outdoor thermal comfort in a location where people like to congregate, such as café, courtyard and garden.
6. The key aim to increase the vegetation (green cover) to certain extent in (%) is to reduce the wind speed and air temperature as well.
7. As a solution, increasing vegetation around 20% means in case-3 that is random arrangement of the tree near the building area can be adopted or implemented to improve outdoor thermal comfort of a residential area.
8. As a design consideration, case-3 not only provides shade from radiation but also provides cooling effect to the near building area. It reduced the temperature around 1.5 °C and also helps to reduced short and long wave radiation (mean radiant temperature) up to 6.20 °C and also thermal indices such as PMV 0.240 °C and UTCI up to 2.19 °C.
9. A heaven tree (known as *Ailanthus excelsa*) planted near the building area can alone provide more shade to the occupant and reduce the air temperature in front of façade and has better effect on outdoor thermal comfort. It has one major benefit that is the most effective tree for absorbing suspended particulate matter.

The simulated results (for a typical coldest day 17 December 2021 at 07:00 AM) show that the suggested strategies have an effect on OTC.

10. As a design consideration, planting an oak tree (which has a same significance of neem tree) on all four side of location or planting trees on the roadside (Road Arboriculture) with deciduous tree means adopting case-2 can increase the temperature up to 0.5 °C to 1.0 °C and can allow solar radiation as well; here, MRT has been decreased around 0.6 °C, and also thermal indices such as PET increase approx. 0.04 °C, PMV approx. 0.36 °C and UTCI approx. 1.21 °C.
11. As a design consideration, adopting case-3 random arrangement of tree near the building area. It has a coniferous tree like pine, palm and conic, and large trunk improves heat comfort than broadleaves tree. The case-3 has an effective in increasing the temp up to 1.0 °C, and MRT has been increased up to 1.80 °C.

## 4 Conclusion

This research uses the ENVI-met model for microclimate numerical simulation to evaluate how different case scenarios affect the study area with environmental parameters consisting of air temperature,  $T_{mrt}$  and thermal indices along with PMV, PET and UTCI. Various heat mitigation strategies were planned during the study based on simulation results that were visualized as thematic map in LEONARDO for 24 h for the extreme condition that is on hottest day as well coldest day. The model shows the accuracy with simulated and measured environmental parameters for the validation. The validated model was used to investigate four case scenarios. (1) Base case scenario, (2) Number of trees at equal interval on all four side of corners, (3) Random arrangement of tree near the building area and (4) Façade and roof greening on building with some water bodies with base case scenario of tree arrangement.

This various heat mitigation strategies can be adopted in Ahmedabad City for improving outdoor thermal comfort, with Ahmedabad being one of the most developing cities of India, it is not economical nor it can be simple to implement high-tech urban design in a pre-existing area in a densely populated area, and hence, such issues can be addressed with adequate urban planning and other cost-effective measures. At the city level of Ahmedabad, the study provides a better understanding of heat mitigation strategies on human thermal comfort and the findings of this research provide the stakeholders with finer suggestion for improving outdoor thermal comfort environment of residential area and to developed sustainable cities, and also, it has direct impact on the health and wellbeing of occupants of outdoor spaces.

**Acknowledgements** First of all, I take this opportunity to express my intense feeling of gratitude towards my Guide Dr. Anurag Kandya, Associate Professor, Department of Civil Engineering, at Pandit Deendayal Energy University, Gandhinagar, India, for his guidance, abundant knowledge to specify my research identity and for the encouragement to gain my objectives precisely and constant inspiration at every stage of the work.

I, also, would give my appreciation to Mr. Aditya Vaghela working as Project Associate in ISRO Lab in PDEU for his help during the throughout project work and Thanks to my Guide Dr. Anurag Kandya, for support to provide me license of ENVI-met and Prof. M. Bruse (Inst. of Geography – University of Mainz) for the use of ENVI-met simulation model. Moreover, I would like to give special thanks to my friend Hiteshree Mithaiwala and my parents (Girish Bhavsar &



Mayuri Bhavsar) for their continuous support and motivation to pursue my research work in well method.

## References

- Abdollahzadeh et al (2021) Outdoor thermal comfort: Analyzing the impact of urban configurations on the thermal performance of street canyons in the humid subtropical climate of Sydney. *Front Arch Res* 10(2):394–409. <https://doi.org/10.1016/j.foar.2020.11.006>
- Atwa et al (2020) Evaluation of plantation design methodology to improve the human thermal comfort in hot-arid climatic responsive open spaces. *Sustain Cities Soc* 59. <https://doi.org/10.1016/j.scs.2020.102198>
- Barakat et al (2017) Urban design in favor of human thermal comfort for hot arid climate using advanced simulation methods. *Alexandria Eng J* 56(4):533–534. <https://doi.org/10.1016/j.aej.2017.04.008>
- J. Brozovsky et al (2021) Evaluation of sustainable strategies and design solutions at high-latitude urban settlements to enhance outdoor thermal comfort. *Energy Build* 244. <https://doi.org/10.1016/j.enbuild.2021.111037>
- Bruse M (1998) ENVI\_met. Retrieved from <https://www.envi-met.com/>
- Coisson et al (2016) Sustainable redevelopment of public spaces in city centres:: a bioclimatic approach. In: *World multidisciplinary civil engineering-architecture-urban planning symposium 2016, WMCAUS 2016*, vol 161, pp 1852–1857. <https://doi.org/10.1016/j.proeng.2016.08.704>
- Gajjar H (2019) Assessment of role of water body on thermal comfort in Ahmedabad, India. *IOP Conf Ser Earth Environ Sci* 281. <https://doi.org/10.1088/1755-1315/281/1/012023>
- Hunt J (2002) *London's environment*. Imperial College Press, London
- Karakounos I et al (2018) The influence of bioclimatic urban redevelopment on outdoor thermal comfort. *Energy Build* 158:1266–1274. <https://doi.org/10.1016/j.enbuild.2017.11.035>
- Koppen et al (n.d.) Köppen climate classification. Retrieved from [https://en.wikipedia.org/wiki/K%C3%B6ppen\\_climate\\_classification](https://en.wikipedia.org/wiki/K%C3%B6ppen_climate_classification)
- Kumar P et al (2020) Study on importance, procedure, and scope of outdoor thermal comfort. *Sustain Cities Soc* 61:1–47. <https://doi.org/10.1016/j.scs.2020.102297>
- Nora et al (2015) Urban heat island in Padua, Italy: Simulation analysis and migration strategies. *Urban Clim* 14:187–196. <https://doi.org/10.1016/j.uclim.2015.04.004>
- Othman et al (2020) The role of urban morphology on outdoor thermal comfort: the case of Al-Sharq City—Az Zarqa. *Urban Clim* 34. <https://doi.org/10.1016/j.uclim.2020.10.0706>
- Rajan et al (2020) Impact of building regulations on the perceived outdoor thermal comfort in the mixed-use neighbourhood of Chennai. *Front Arch Res* 10(1):148–163. <https://doi.org/10.1016/j.foar.2020.09.002>
- Salata et al (2017). Relating microclimate, human thermal comfort and health during heat waves: an analysis of heat island mitigation strategies through a case study in an urban outdoor environment. *Sustain Cities Soc* 34:76–96. <https://doi.org/10.1016/j.scs.2017.01.006>
- Salman et al (2021) The effect of Urban Heat Island mitigation strategies on outdoor human thermal comfort in the city of Baghdad. *Front Arch Res* 10(4):838–856. <https://doi.org/10.1016/j.foar.2021.07.002>
- Talgeni et al (2014) Outdoor thermal comfort within five different urban forms in the Netherlands. *Build Environ* 83:1–14. <https://doi.org/10.1016/j.buildenv.2014.03.014>

# Application of a Global Uncertainty and Sensitivity Analysis for Identifying Influential Sustainable Building Design and Operation Parameters



Ankit Rajput, Jishan H. Rajpal, Janak Chaudhary, Naimish Bhatt, and Shobhit Chaturvedi

**Abstract** The careful identification and treatment of sensitive building design and operation parameters can aid sustainable building modelling and optimization efforts. Using Design Builder software, this paper applies Latin hypercube sampling (LHS) and standard regression coefficient (SRC) for uncertainty and sensitivity analysis (UA/SA) to ascertain influential building design features influencing annual energy demands and thermal comfort levels. A commercial office building in Gandhinagar, India (Koppen-Geiger: Bsh climate), is chosen for analysis. The building's simulation model shows 90.01% agreement with the utility bills. Specifically, the influence of four unique wall constructions, five roof insulations, four window-to-wall ratios (WWR), five window types, four overhang depths, five air conditioner's (AC) coefficients of performance (COP) and five cooling set points (CSP) are assessed on building annual energy demand (AED) and annual thermal discomfort hours (ATDH) as per ASHRAE 55 2004. LHS permutes these eight parameters to produce 300 unique building design and operation possibilities, simulated sequentially to generate the model outputs. Notably, the lowest and highest AED and ATDH vary by a factor of four (5423–22923 kWh) and three (742–2242 h), respectively. The standard regression coefficient global SA identifies AC COP and CSP as the two critical influential parameters swaying AED, followed by WWR, Wall Construction and Roof Insulation. ATDH chiefly depends on AC CSP, followed by WWR, wall

---

A. Rajput · J. H. Rajpal · J. Chaudhary · N. Bhatt · S. Chaturvedi (✉)  
Pandit Deendayal Energy University, Gandhinagar, India  
e-mail: [shobhit.chaturvedi@sot.pdpu.ac.in](mailto:shobhit.chaturvedi@sot.pdpu.ac.in); [shobhitchaturvedi101@gmail.com](mailto:shobhitchaturvedi101@gmail.com)

A. Rajput  
e-mail: [ankitrajputa7@gmail.com](mailto:ankitrajputa7@gmail.com)

J. H. Rajpal  
e-mail: [jishanrajpal12@gmail.com](mailto:jishanrajpal12@gmail.com)

J. Chaudhary  
e-mail: [janakchaudhary728@gmail.com](mailto:janakchaudhary728@gmail.com)

N. Bhatt  
e-mail: [naimish.bhatt@sot.pdpu.ac.in](mailto:naimish.bhatt@sot.pdpu.ac.in)

construction and roof insulation. Thus, substantial AED and ATDH cutbacks can be achieved by selecting optimal AC COPs and CSP, WWR, wall construction and roof insulation. Other less influential parameters like building orientation and overhangs do not produce comparable benefits and do not require further optimization.

**Keywords** Building simulation · Design builder · Latin hypercube sampling · Standard regression coefficient

## 1 Introduction

The building sector is one of the most energy-intensive and most prominent greenhouse gas emitters, accounting for nearly 30% of global energy demands and CO<sub>2</sub> emissions (IEA 2017; Mariano-Hernández et al. 2021). So, building energy efficiency enhancement has become one of the key focus areas for researchers and policymakers worldwide (Chegari et al. 2021; Ikeda and Nagai 2021). Several building energy codes like leadership in energy and environmental design (LEED), building research establishment environmental assessment method (BREEAM) and Eco-Niwas Samhita (India) are being adopted to reduce building energy footprint and improve indoor thermal comfort (Evins 2013). However, sustainable building design is not a straightforward process and involves assessing the performance of a vast array of design and operational parameters (Kheiri 2018). The conventional design approach relies heavily on architect and engineer experience to make crucial decisions. This approach, although value-adding, often results in sub-optimal energy and cost performance. Further, manually analysing each design possibility becomes a strenuous, inaccurate and impractical exercise.

In recent times, building simulation programs (BSPs) have become the preferred option for selecting optimum building layout, envelope, air conditioning (AC), appliances, lighting, and energy systems as per prevailing weather and operational conditions (Mariano-Hernández et al. 2021). BSPs like EnergyPlus, Trnsys, IDE-ICE and ESP-r satisfy stringent performance requirements in low-energy residential and commercial buildings (Kheiri 2018; Shi et al. 2016). BSPs can appraise the influence of several design interventions linked to the envelope (roof, wall and window) and system (air conditioning and renewable energy) on final energy demands and indoor thermal comfort levels. But, not all strategies have a comparable effect on the building's energy footprint and thermal comfort. Simulating each building design intervention can magnify the time and energy spent during the predesign stage. Notably, depending on the building type, location, and operation patterns, a few design strategies can dominate others for attaining the desired outcomes.

The early identification and treatment of sensitive building design and operation parameters can aid sustainable building modelling and optimization efforts. Designers and modellers can prioritize their time and efforts towards the precise data collection and optimization of these sensitive parameters. As India gears to

significantly expand its present-day building stock in the coming decades, UA/SA-aided building design optimization efforts can help attain significant energy savings and better indoor comfort by adopting suitable design interventions (Fiorini and Aiello 2019; Mansouri et al. 2021). Thus, this paper applies an uncertainty and global sensitivity analysis to determine critical parameters influencing the energy and comfort performance of a commercial building in Gandhinagar (Koppen-Geiger: Bsh climate), India. Building's energy performance is represented by its annual energy demand, and indoor thermal discomfort is shown by annual thermal discomfort hours (ATDH) as per ASHRAE 55 2004 (Olesen and Brager 2004). Discomfort hours represent the duration when the zone humidity ratio and operative temperature are not in the ASHRAE 55-2004 summer or winter clothes region. For summer, the 0.5 Clo (0.08 m<sup>2</sup>K/W) level is used; for winter, the 1.0 Clo (0.08 m<sup>2</sup>K/W) level is used. This paper's findings shall help recognize influential building design and operation parameters and focus efforts on their assessment and optimization.

## 2 Uncertainty and Sensitivity Analysis

Uncertainty (UA) and sensitivity analysis (SA) offer an efficient mathematical framework to assess the relative influence of different input on various building performance criteria. UA considers different building design and operation possibilities to calculate the variation in building performance output. Latin hypercube sampling (LHS) is an efficient sampling method that divides the entire input space into  $N$  equal intervals to select samples with equal probability, thereby ensuring unbiased stratification and fast convergence (Pang et al. 2020). Post UA, SA identifies the main input parameters controlling the maximum proportion of output variance (Pianosi and Wagener 2015). Referring to SA results, designers can emphasize building design and optimization of these fewer but most important parameters (Heiselberg et al. 2009).

SA techniques are classified as local (LSA) and global (GSA) methods (Tian et al. 2018). Referred to as one-at-a-time (OAT) methods, LSA computes sensitivity indices (SI) by fluctuating one input at a time, keeping all other inputs fixed (Zeferina et al. 2019). LSA methods assume a linear relationship between inputs and output and ignore input correlations. Therefore, LSA is unsuitable for assessing large building energy models involving nonlinearity and interaction effects (Sun 2015). Unlike LSA, GSA techniques compute SI after simultaneous perturbation of all input parameters. Standardized regression coefficient (SRC) is a popular regression-based GSA technique due to its easy application and straightforward interpretation (Hopfe and Hensen 2011). The model response is estimated using a linear mathematical function of inputs. Silva and Ghisi employed SRC to assess the effects of occupant behaviour and physical parameters uncertainties on low-income housing energy demand in Brazil (Silva and Ghisi 2014). Recently Guo et al. developed an integrated SA-building optimization routine. SRC identified the influential parameters (wall-window ratio, internal thermal mass and air change rates) impacting the

office building's night ventilation (Guo et al. 2019). SRC also help focus optimization efforts solely on the influential design and operation parameters. Vukadinovic et al. adopted the NSGA II algorithm and a global SA for the structural and architectural optimization of a passive building with a sunspace in Serbia (Vukadinović et al. 2021). X. Chen et al. used the hybrid generalized pattern search particle swarm optimization (HGPPSO) to assess the impact of archetypes and confounding factors on high-rise solar building photovoltaic design systems (Chen et al. 2019). HGPPSO is fused with SRC before optimization stage for factor prioritizing and fixing.

### 3 Research Methodology

A four-step research methodology has been developed for this study.

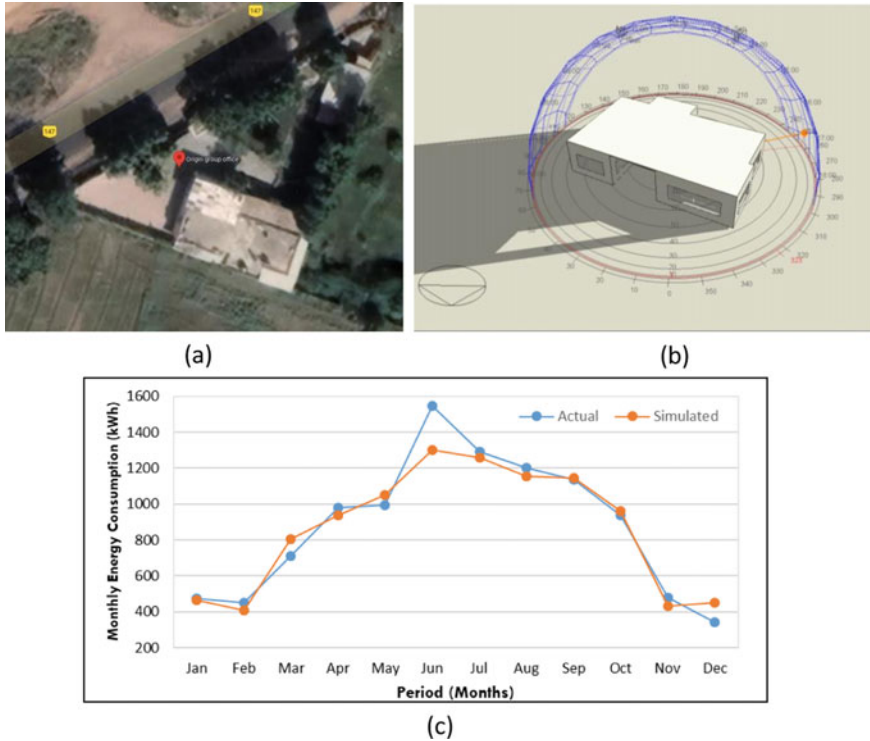
#### 3.1 Step 1: Building Energy Model Development

An office building (refer to Fig. 1) situated in Gandhinagar, India (23.18° N, 72.59° E), is selected for this study. Gandhinagar lies in a hot and dry region per the Indian National Building Code. Its location corresponds to the Bsh climate (Mid Latitude Steppe and Desert) as per the Köppen classification. The summer days are very hot, with a mean max temperature of 41.3 °C, and nights have a mean minimum temperature of 23.6 °C. Comparatively, winters exhibit mean and minimum temperatures of 30 °C and 15.4 °C. Further, the average annual rainfall is 782 mm, primarily from June to September.

The building is modelled using the EnergyPlus commercial front-end software, i.e. DesignBuilder. The chosen building comprises four naturally ventilated and five mixed-mode operated zones. The mixed-mode zones allow users to switch between



Fig. 1 Four-step research methodology to perform building uncertainty and sensitivity analysis



**Fig. 2** a Actual building location. b Rendered building model. c Monthly comparison between building’s actual and simulated energy demands

windows, roof-mounted fans and ACs to achieve thermal comfort, whereas naturally ventilated do not contain AC installations. A building energy usage survey is conducted before the modelling stage to collect necessary details regarding occupancy, appliances and AC installation and usage patterns. The model geometry, construction details, occupancy, appliances and AC installation and operation are fixed to resemble actual building energy use. The modelling precision is verified by comparing the actual and predicted monthly building energy utility bills. Building simulation performed using 2021 actual hourly weather records exhibits 90.01% (refer to Fig. 2c) match to actual utility bills.

### 3.2 Step 2: Develop Input Criteria

UA/SA are performed to ascertain dominant design and operation parameters swaying building energy demand and thermal comfort. Annual energy demand

(AED) and annual thermal discomfort hours (ATDH) are the two building performance criteria. UA and SA examine the influence of different wall construction materials, window-to-wall ratios (WWR), window construction, overhang depths, orientations, insulations, AC COP and cooling set points on ACED and ATDH. The different options for the eight-building design and operation parameters are listed in Table 1. As thermal transmittance strongly affects building elements' heat transfer, it is chosen as the primary criteria for selecting different walls (0.48–2.09) W/m<sup>2</sup>K, window (1.1–5.78) W/m<sup>2</sup>K and roof insulation (0.93–4.48) W/m<sup>2</sup>K, materials, as shown by the stepwise (low, medium and high) U value variations in Tables 2 and 3. In total, 160,000 building design and operation possibilities are considered.

**Table 1** Different building design options considered for uncertainty and sensitivity analysis

S. No.	Building design variable	Possibilities	Description
X1	Wall construction materials	4	AC block, fly ash brick, hand moulded Brunt Clay brick, calcium silicate Block
X2	Window-to-wall ratio	4	(10, 20, 30, 40)%
X3	Window type	5	Single clear glazing 6 mm, single clear 6 mm float glass, double clear 6 mm/6 mm air, low-E double glazing air filled 4–12–4 mm, clear triple glazing air filled 4–12–4–4 mm
X4	Window overhang depth	4	(0.3, 0.6, 0.9, 1.2) m
X5	AC coefficient of performance	5	(1, 2, 3, 4, 5)
X6	Building orientation	4	(0, 90, 180, 270)
X7	AC Cooling set point	5	(20, 22, 24, 26, 28)
X8	Roof insulation	5	No insulation, XPS insulation, glass wool insulation, EPS insulation, rock wool and gypsum board
Total combinations		(160,000)	

**Table 2** Construction details and thermophysical properties for the four wall constructions

Wall construction materials	Thickness (mm)	Density (kg/m <sup>3</sup> )	Specific heat (J/kgK)	Conductivity (W/m/K)	U-value (W/m <sup>2</sup> K)
Aerated concrete block	300	600	870	0.162	0.488
Fly ash brick	200	1700	1000	0.477	1.621
Hand moulded burnt clay brick	200	1600	880	0.624	1.766
Calcium silicate block	200	2071	970	0.712	2.086

**Table 3** Thermophysical properties for the different window types and roof insulation materials

Roof insulation material	U-value (W/m <sup>2</sup> K)	Window type	U-value (W/m <sup>2</sup> K)
XPS insulation	0.926	Single clear glazing 6 mm	5.78
Rock wool	0.967	Single clear 6 mm float glass	3.80
Glass wool insulation	1.028	Double clear 6 mm/6 mm air	3.09
Gypsum board	2.435	Low-E double glazing air filled 4–12–4 mm	1.60
RCC roof (no insulation)	4.48	Clear triple glazing air filled 4–12–4–4 mm	1.10

### 3.3 Step 3: Uncertainty Analysis

Uncertainty analysis is performed using Latin hypercube sampling to generate 300 unique simulation conditions, sequentially simulated using the DesignBuilder software. LHS divides sample space into distinct hypercubes such that each subspace is sampled with equal probability. This systematic selection ensures fast convergence and avoidance of similar samples. The results from 300 parametric simulations are collected to develop AED and ATDH histograms. These two outputs’ minimum, maximum and mean values are calculated to characterize their variation.

### 3.4 Step 4: Sensitivity Analysis

The sensitivity analysis is performed using the standard regression coefficient (SRC) method to attribute output variability to mutating input parameters. Using UA results, SRC generates a regression relationship between the model output (AED; ATDH) and the different model inputs, as shown in Eq. 1. Notably, regression coefficients ( $\beta_i, \dots, \beta_k$ ) from ordinary linear regression models are in different units (WWR, AC COP, CSEP, etc.); their direct comparison is not logical. A small regression coefficient may be much more important than a larger one. This issue resembles the classic problem of trying to compare apples to oranges. SRC coefficients eliminate this problem by expressing input coefficients in a single statistically equivalent unit for comparison, as shown in Eq. 2.

$$Y_i = c_o + \sum_i \beta_i x_{ii} + e_i \tag{1}$$

$$\text{SRC}(Y, x_j) = \beta_j S(x) / S(y) \tag{2}$$



where  $c_o$  represents the model intercept, and  $c_j$  and  $e_i$  represent the regression coefficients and error term associated with this model. Further, the SRC( $Y, x_j$ ) for an input parameter  $x_j$  is defined as the product of the regression coefficient  $\beta_j$  with the ratio of input's standard deviation  $S(x)$  to output's standard deviation  $S(y)$ . SRC estimates parameter significance such that a high SRC value indicates a more substantial parameter influence. Further, the SRC sign (+ve; -ve) indicates the nature of the influence; a positive SRC indicates a positive correlation between model input and output and vice versa.

## 4 Results

### 4.1 Uncertainty Analysis

Depending on the selected combination of input parameters, there is a considerable variation between the highest and lowest model output values. As shown in Fig. 3, the maximum, minimum and average building AED is 21743.67 kWh, 5422.53 kWh and 8964.57 kWh, respectively. The max/min and max/mean AED ratios equal 4 and 2.42, respectively. Further, AED exhibits skewness towards the right side, implying that most simulation combinations result in smaller than mean AED values. Thus, selecting building design and operation parameters consistent with the right skewed portion of the AED distribution is crucial for maximum AED reductions.

Further, as shown in Fig. 4, the maximum, mean and minimum ATDH estimates equal 2236.71 h, 741.87 h and 1396.22 h, respectively. Further, the max/min and

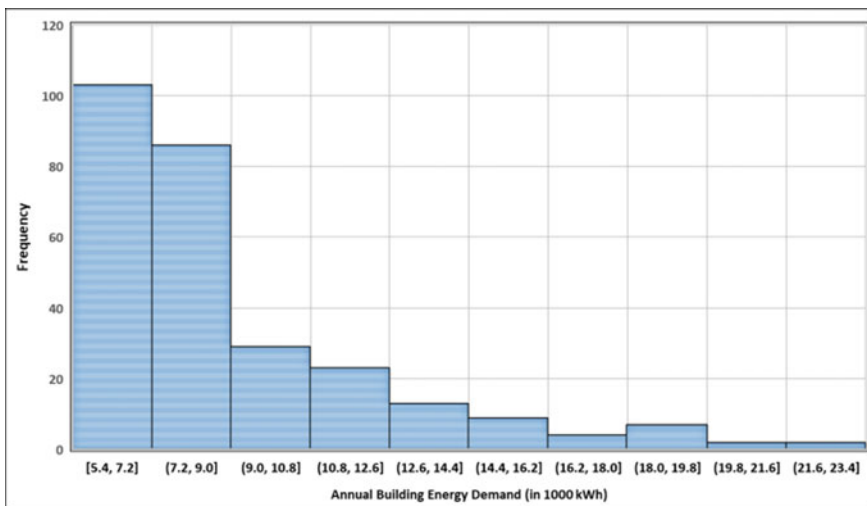


Fig. 3 Annual building energy demand distribution due to varying input conditions

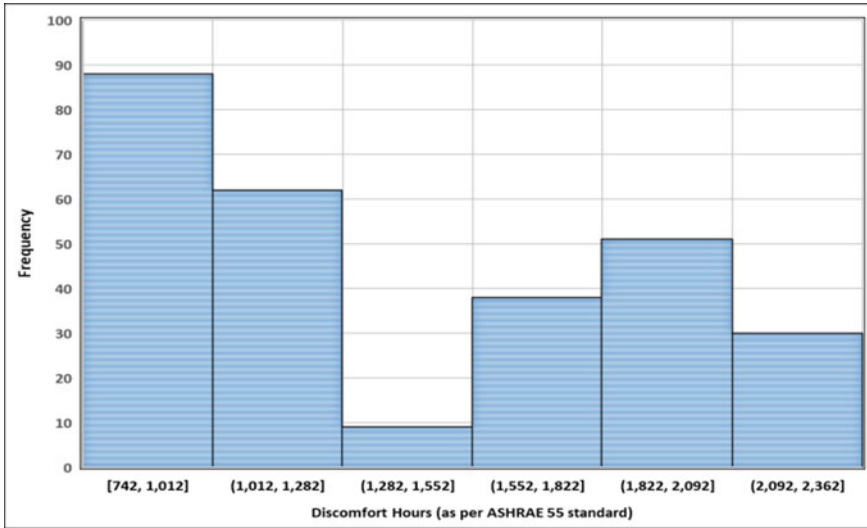


Fig. 4 Building discomfort hours distribution due to varying input conditions

max/mean ATDH ratios equal 3 and 1.6, respectively. Suitable building design and operation parameters limit building thermal discomfort levels. Unlike AED, ATDH exhibits uniform distribution characteristics, and comparable frequencies are visible across the full range from 742 to 2362 h except for between 1282 and 1552 h.

### 4.2 Sensitivity Analysis

Sensitivity analysis helps identify the influential design and operational parameters responsible for the maximum percentage of AED and ATDH variations (Table 4).

Building’s annual energy demand is mainly influenced by AC COP ( $S_i = -0.60$ ) and AC CSP ( $S_i = -0.51$ ) followed by WWR ( $S_i = 0.24$ ), wall construction ( $S_i = 0.18$ ), roof insulation and glazing type ( $S_i = -0.10$ ). Operational parameter influence dominates physical design in controlling AED, and smart operational strategies can help achieve maximum AED cutbacks. Air-conditioners with a high coefficient of performance produce the maximum AED cutbacks, as indicated by the high negative  $S_i$  values. The additional cost of buying high COP AC can be recovered by higher savings in the monthly energy bills. Similarly, higher comfort set points can limit building AED. Higher comfort CSPs are easier to maintain in centrally operated ACs inside commercial buildings than in residences. Better integration of natural ventilation and passive cooling opportunities reduces dependency on mechanical air cooling systems. Further, appropriate wall, roof and glazing systems must be chosen in line with building operation and ambient climatic conditions. In comparison, the

**Table 4** Sensitivity indices for the eight-building design and operation parameters and their importance rankings

Parameter	AED		ATDH	
	SRC	Rank	SRC	Rank
AC COP	-0.60	1	0.04	6
AC CSP (°C)	-0.51	2	0.94	1
Window-to-wall ratio	0.24	3	0.18	2
Wall construction	0.18	4	0.14	3
Roof insulation	0.12	5	0.11	4
Glazing type	-0.10	6	-0.09	5
Building orientation (°)	-0.06	7	0.02	7
Local shading	0.04	8	0.04	6

influence of building orientation ( $S_i = -0.06$ ) and local shading ( $S_i = 0.04$ ) is much less significant in energy-intensive commercial buildings.

Building's annual thermal discomfort hours are chiefly impacted by AC CSP ( $S_i = -0.51$ ). Increasing AC CSP negatively impacts building occupants' thermal comfort levels. Unlike AED, AC COP does not impact ATDH. Similar to AED, physical parameters have a much smaller sway on ATDH. However, appropriate WWR ( $S_i = 0.24$ ), wall construction ( $S_i = 0.14$ ), roof insulation ( $S_i = 0.11$ ) and glazing ( $S_i = -0.09$ ) selection slow down envelope heat transfer rates into the building, thereby maintaining indoor thermal comfort levels. In comparison, the effects of building orientation ( $S_i = 0.02$ ), AC COP ( $S_i = 0.04$ ) and local shading ( $S_i = 0.04$ ) are insignificant for ATDH estimations.

## 5 Conclusion

This paper applied uncertainty and sensitivity to ascertain the dominant design and operation parameters that influence annual building energy demand (AED) and thermal discomfort (ATDH) for a commercial office building in the hot and dry (Koppen-Geiger: Bsh) climate of Gandhinagar, India. Several options for walls, windows, window sizes, overhangs, roof insulation and AC coefficient of performance and cooling set point temperatures are scrutinized. AED and ATDH varied up to three and four times, depending on the selected building design and operational parameters. Markedly, AC CSP strongly impacts AED and ATDH, whereas AC COP exclusively impacts AED. Thus, higher COP AC installations can help achieve high AED cutbacks. High AC CSP reduces building AED but increases ATDH. Thus, a multi-objective approach is necessary to achieve a suitable tradeoff between these two performance criteria.

Further, window size and wall construction are the two main design parameters, followed by roof insulation and glazing type. Smaller window sizes are suitable

for reducing incoming solar radiation, but larger windows enhance natural ventilation and indoor illumination. Similarly, higher thermal resistance walls and roof insulations can reduce the heat-transmission rate into the building, thereby reducing mechanical cooling requirements and enhancing indoor thermal comfort. A multi-objective approach is necessary to balance different energy, thermal comfort and economic criteria. The less influential building orientation and window overhang depth can be dropped from the multi-objective optimization stage to reduce the computational burden. A follow-up study shall adopt these findings to identify the optimal building design and operation parameters consistent with the lowest AED and ATDH. Further, this study's approach can be adapted to other building typologies across different climates to ascertain dominant design and operation parameters impacting various building performance criteria.

## References

- Chegarı B et al (2021) Multi-objective optimization of building energy performance and indoor thermal comfort by combining artificial neural networks and metaheuristic algorithms. *Energy Build* 239:110839. <https://doi.org/10.1016/j.enbuild.2021.110839>
- Chen X, Yang H, Peng J (2019) Energy optimization of high-rise commercial buildings integrated with photovoltaic facades in urban context. *Energy* 172:1–17. <https://doi.org/10.1016/j.energy.2019.01.112>
- Evens R (2013) A review of computational optimisation methods applied to sustainable building design. *Renew Sustain Energy Rev* 22:230–245. <https://doi.org/10.1016/j.rser.2013.02.004>
- Fiorini L, Aiello M (2019) Energy management for user's thermal and power needs: a survey. *Energy Rep*, 1048–1076. <https://doi.org/10.1016/j.egy.2019.08.003>
- Guo R, Yue H, Liu M, Heiselberg P (2019) Influence of design parameters on the night ventilation performance in office buildings based on sensitivity analysis. *Sustain Cities Soc* 50(March):101661. <https://doi.org/10.1016/j.scs.2019.101661>
- Heiselberg P et al (2009) Application of sensitivity analysis in design of sustainable buildings. *Renew Energy* 9:2030–2036. <https://doi.org/10.1016/j.renene.2009.02.016>
- Hopfe CJ, Hensen JLM (2011) Uncertainty analysis in building performance simulation for design support. *Energy Build* 43(10):2798–2805. <https://doi.org/10.1016/j.enbuild.2011.06.034>
- IEA (2017) Global status report 2017
- Ikeda S, Nagai T (2021) A novel optimization method combining metaheuristics and machine learning for daily optimal operations in building energy and storage systems. *Appl Energy* 289(March):116716. <https://doi.org/10.1016/j.apenergy.2021.116716>
- Kheiri F (2018) A review on optimization methods applied in energy-efficient building geometry and envelope design. *Renew Sustain Energy Rev* 92(April):897–920. <https://doi.org/10.1016/j.rser.2018.04.080>
- Mansouri SA et al (2021) Energy management in microgrids including smart homes: a multi-objective approach. *Sustain Cities Soc* 69(March)
- Mariano-Hernández D et al (2021) A review of strategies for building energy management system: model predictive control, demand side management, optimization, and fault detect & diagnosis. *J Build Eng* 33(March 2020)
- Olesen BW, Brager GS (2004) A better way to predict thermal comfort. *ASHRAE J* (August), 20–26. <https://escholarship.org/uc/item/2m34683k%0A>; [http://repositories.cdlib.org/cedr/cbe/ieq/OlesenBrager2004\\_comfort/](http://repositories.cdlib.org/cedr/cbe/ieq/OlesenBrager2004_comfort/)

- Pang Z, O'Neill Z, Li Y, Niu F (2020) The role of sensitivity analysis in the building performance analysis: a critical review. *Energy Build* 209:109659. <https://doi.org/10.1016/j.enbuild.2019.109659>
- Pianosi F, Wagener T (2015) A simple and efficient method for global sensitivity analysis based on cumulative distribution functions. *Environ Model Softw* 67:1–11. <https://doi.org/10.1016/j.envsoft.2015.01.004>
- Shi X et al (2016) A review on building energy efficient design optimization from the perspective of architects. *Renew Sustain Energy Rev* 65:872–884. <https://doi.org/10.1016/j.rser.2016.07.050>
- Silva AS, Ghisi E (2014) Uncertainty analysis of user behaviour and physical parameters in residential building performance simulation. *Energy Build* 76:381–391. <https://doi.org/10.1016/j.enbuild.2014.03.001>
- Sun Y (2015) Sensitivity analysis of macro-parameters in the system design of net zero energy building. *Energy Build* 86:464–477. <https://doi.org/10.1016/j.enbuild.2014.10.031>
- Tian W et al (2018) A review of uncertainty analysis in building energy assessment. *Renew Sustain Energy Rev* 93(January 2017):285–301. <https://doi.org/10.1016/j.rser.2018.05.029>
- Vukadinović A et al (2021) Multi-objective optimization of energy performance for a detached residential building with a sunspace using the NSGA-II genetic algorithm. *Sol Energy* 224(March):1426–1444
- Zeferina V, Birch C, Edwards R, Wood R (2019) Sensitivity analysis of peak and annual space cooling load at simplified office dynamic building model. *E3S Web Conf* 111(May)

# Problems and Prospects for Conservation of Traditional Bazaars in Walled City of Jaipur



Shipra S. K. Goswami, Ashwani Kumar, and Satish Pipralia

**Abstract** India's steady economic growth since independence has positioned it as a leading emerging economy. This growth is crucial for overall development, with cities' commercial base serving as a major pillar. India's unique tradition of blending heritage with commerce contributes to both economic and cultural values. Notable examples of such commercial centres include the Walled City of Jaipur, Walled City of Ahmedabad, Hyderabad, and Delhi. These centres not only drive economic growth but also embody a rich blend of history, tradition, art, and culture. Therefore, safeguarding the resilience of these traditional commercial centres becomes imperative. The Walled City faces issues from changing needs, friction between tradition and development. Historic cities shape modern cities' functionality and economy, with 60% commercial activity in Jaipur's Walled City. Considering socio-economic prospects and development pressures, conserving the bazaars is vital. This study explores issues in Jaipur's traditional commercial centres and proposes sustainable empowerment. A holistic conservation strategy can address Walled City's problems and sustainably preserve its bazaars. The study's prospects act as directive principles, supporting the conservation objectives.

**Keywords** Conservation architecture · Walled City architecture · Urban planning

---

S. S. K. Goswami (✉) · A. Kumar · S. Pipralia  
Malaviya National Institute of Technology Jaipur, Jaipur, India  
e-mail: [2021RAR9006@mnit.ac.in](mailto:2021RAR9006@mnit.ac.in)

A. Kumar  
e-mail: [akumar.arch@mnit.ac.in](mailto:akumar.arch@mnit.ac.in)

S. Pipralia  
e-mail: [spipralia.arch@mnit.ac.in](mailto:spipralia.arch@mnit.ac.in)

## 1 Introduction

Commerce was an important aspect of civilisations all over the globe since historic times. The urban nature of settlements itself is an epitome of people deviating from agriculture and moving towards manufacturing, services, trade, and commerce. As was observed in the cities of Indus Valley Civilisation, people were involved in many different non-agricultural activities that formed the basis of urbanisation in these ancient cities. The Harappan people were involved in many primitive forms of industrial activities like tool manufacturing, precious and semi-precious ornaments, gold and silver jewellery, pottery, ship- building industry, etc. The extensive use of bronze tools led to agricultural surplus, thus making trade of grains possible. Along with agricultural trade, the Harappans also traded in lead from southern India, lapis-lazuli from Afghanistan, Copper from Khetri mines of Rajasthan, and other products like turquoise, jade, amethyst, agate, etc. This primitive form of trade and industry made them commercially active and their cities as important nodes of economic activity. As time progressed, newer economic activities started to arrive, and a financial system started to emerge and through this many different social classes and guilds sprung up in the society. These social classes were formed dominantly on the basis of their professions, and thus, the society started to take a stratified form based on the prosperity of each profession. The urban nature of society was thus driven by the clustering of people with similar profession and aggregation of these professions to form the central market places of the evolving cities. These markets became the economic nerve of the cities. With advancing time, the transition from ancient to medieval period saw the increment of non-agricultural activities, and thus, the commercially active concepts of bazaars emerged in India and with that city became a centre of attraction in terms of growth, opportunities, education, and health.

With the advent of modernity, the world saw a rapid change in technology, and economy became the central idea of growth and development. In the era of globalisation, nations are not just defined on the basis of their political boundaries but more on their economic prowess. This economic growth was majorly banked on the growth of cities, and hence, the economic and social character of urban areas has become highly significant. The central market places as discussed above were becoming the drivers of urban growth and thus came to be known as the central business districts (CBD). 'A CBD is dense area within a city which is characterised by high economic activity and is provisioned with adequate infrastructure and utilities to sustain this activity' (PHD Chamber of Commerce and Industry 2015). They help the economic empowerment of cities and impart a unique character to the region.

India being no exception to the globalised world order has its own share of economic prowess. Though the global average population of urban areas has moved above the halfway mark, India has a modest 31% population residing in the urban areas and a contribution of around 60–65% to the national GDP and is estimated that by 2030 it will reach 70–75%. With the rapidly urbanising cities, it is important to keep pace with such huge influx of people and sustain them with sufficient opportunities and utilities. The commercial centres of cities or CBDs hence act as a

pivot of economic and social development that can accommodate the aspirations and provide opportunities for the rising needs of the cities. With such significance, the commercial centres of cities need to be conserved to meet the demands of sustainable development.

## 2 Methodology

The study finds its base in the Walled City of Jaipur, wherein the commercial presence outweighs the economic contribution of the entire metropolitan city of Jaipur. Considering the importance of the commercial streets in the Walled City, the study is based on a broad exploration of the region through a critical visual survey.

The survey was furthered supplemented by informal interviews of the local shop owners. The responses have furthered strengthened the core of this study in terms of evaluating the risks, both economically and socially, to individuals and the community at large.

The output of the survey and interviews were used to determine the significance and characterisation of the study area. Based on these aspects, the pertinent issues were inferred as the problems occurring within the region. On the other hand, prospects in terms of plausible strategies to mitigate identified issues were derived from existing literature and similar cases.

## 3 Significance of Traditional Commercial Centres

The case of Indian city cores is quite unique in terms of their characteristics and evolution. The momentum carried on from ancient period, markets were established in the hearts of cities, and thus, they became the nerve of all economic and social activities of the medieval cities. Later on, with the coming of European powers and colonisation, most of the growth started to accumulate outside the walled cities, and with further technological exchanges and colonial demands of the British Raj, the traditional markets and the artisans were steadily losing their significance from the cities. The period of stagnancy though was side-lined after independence when these markets once again became the hub of economic activity despite the cities sprawling to newer boundaries.

These historic traditional centres have provided economic vibrancy while they also have also subjected to political as well as physical transformations to meet the contemporary needs of modern development. These central commercial centres host traditional economic activities like art, jewellery, handicrafts, textiles and wholesale business (Dhingra et al. 2016). The traditional economy of these commercial core areas is parallelly existing with the modern economical avenues of business corporations, industries and the service sector (Kumari 2020). Though the modern economy has induced a capitalist market-led growth in the society and are capital-intensive



sectors, the traditional commercial centres still continue to be predominantly labour-oriented. Hence, in a country like India, where human resource is more readily available than capital, it becomes indispensable that commercial centres be preserved keeping in mind the social prominence these regions have in Indian economy.

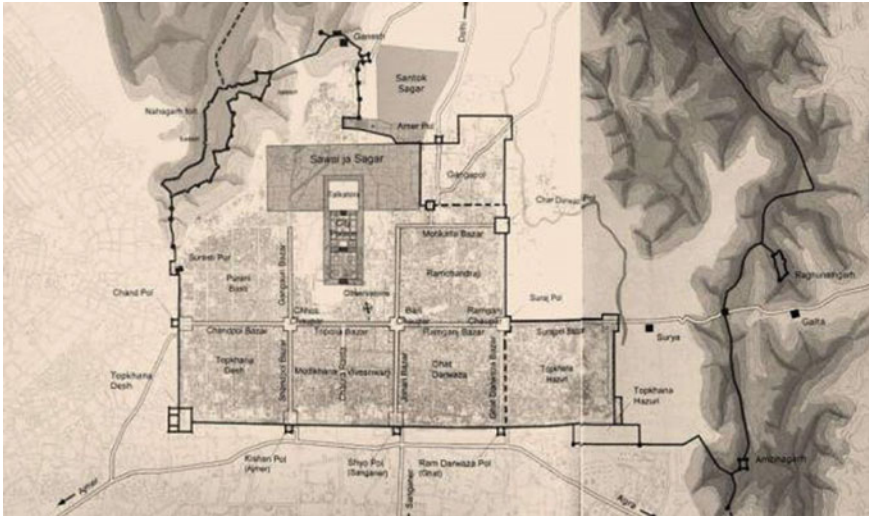
#### 4 Characterisation of Jaipur Walled City

Jaipur is a historic city and serves as the capital to the state of Rajasthan, India. The city of Jaipur is uniquely characterised by its Walled City region. The Walled City of Jaipur (Fig. 1), founded in 1727 by Sawai Jai Singh II, was built in a grid iron pattern and as per the traditional Prastara plan mentioned in the Vedic town planning principles, namely Vastu Shastra (Pusalkar 2022). Main streets donning uniform facades, chaupars, markets and shops, temples built along the main streets are the trademark features of the region. It was designed to be a commercial capital, and the city has maintained its local commercial, artisanal, and cooperative traditions to this day (UNESCO World Heritage 2022). The city was intended to be a trade capital in the region which has driven the market-oriented avenue planning; this feature has still retained in the Walled City through the characteristic bazaars of the city. The architectural marvels like Jantar Mantar, Hawa Mahal, City Palace, Govind Dev Temple, and the Nine Gates add to the heritage value of the Walled City. The meticulous integration of ancient Hindu and medieval Mughal architecture and Western ideas are distinctly visible in the layout of the city. The Walled City of Jaipur thus has served as a lighthouse to guide the development of similar towns in the Shekhawati region of Rajasthan.

The city also hosts the historic *Chattis Karkhanas* roughly translating as ‘36 industries’ which include the traditional industries like gemstones, miniature paintings, moorti-kala, fabric printing, lac jewellery, and few others dedicated on each street. A striking hierarchy of street pattern exists in the Walled City, wherein the traditional commercial shops have been established on the major streets (Funo et al. 2002). With the coming of British colonisation, the artisans and craftsmen found new admirers through the establishment of Rajasthan School of Arts and Albert Hall Museum. In the present time, these traditional activities have helped conserve the historic image of the commercial bazaars, and the flocking tourists have kept alive the interest in heritage of the Walled City of Jaipur.

The Walled City of Jaipur is under constant development pressures with increasing commercialization. Besides this, environmental hazards, poor solid waste management, lack of infrastructure, insufficient parking, unauthorised constructions, new interventions, encroachments, drainage and traffic problems, dilapidated historic structures, and misuse of historic structures are some of the issues that have become a threat for the city fabric.

Considering the socio-economic prospects of the Walled City of Jaipur and the contemporary development pressures, the nerve of socio-economic growth viz., the



**Fig. 1** Walled City of Jaipur (Borie et al. 2020)

bazaars need to be conserved in the overall context of the Walled City region. Considering the social stratification of these bazaars and variety of professions, the holistic understanding of the context becomes highly imperative through which measures can be taken and interventions can be made to target conservation efforts in the Walled City of Jaipur.

### 5 Problems Associated with the Commercial Areas in the Walled City, Jaipur

According to the Jaipur Master Plan 2025, around 60% of the commercial activity of the entire city is concentrated in the Walled City (Jaipur Development Authority, Master Development Plan 2025). At the outset, the Walled City had only four bazaars, namely *Johari Bazaar*, *Kishan Pol Bazaar*, *Gangauri Bazaar*, and *Sireh Deorhi Bazaar*. The unique feature of these bazaar was the presence of a specific craft or product in each rectangular block, and these blocks had shops lined along the streets. Hence, each street eventually came to be known by the name of the professions or community trading on that street, for example, Maniharo ka Raasta (lac bangle shops), Thateron ka Rasta (iron utensil shops), Nataniyo ka Raasta, Patwariyon ka Raasta, Ghee walo ka Raasta, Churukon ka Raasta, Partanion ka Raasta, Sango ka Raasta, Soothleewalon ka Raasta, Telipadon ka Rasta, and many others.

Table 1 depicts the list of traditional bazaars in the Walled City Region and the width of the main street abutting it. Through this Table 1, we can understand the

**Table 1** Important bazaars in Walled City of Jaipur (*Source* Author, Google Earth Pro)

S. No.	Name of bazaar	Abutting road width (m)
<i>North-south</i>		
1	Kishan Pol Bazar	30.40
2	Gangauri Bazar	30.31
3	Chaura Rasta	30.43
4	Johari Bazar	28.08
5	Sireh Deorhi Bazar	34.91
6	Ghat Darwaja Bazar	25.05
<i>East-west</i>		
7	Chand Pol Bazar	32.42
8	Tripolia Bazar	33.45
9	Ramganj Bazar	30.07
10	Suraj Pol Bazar	24

prominence given to the bazaars within the overall context of the Walled City of Jaipur and hence can help in exploring the issues within the region.

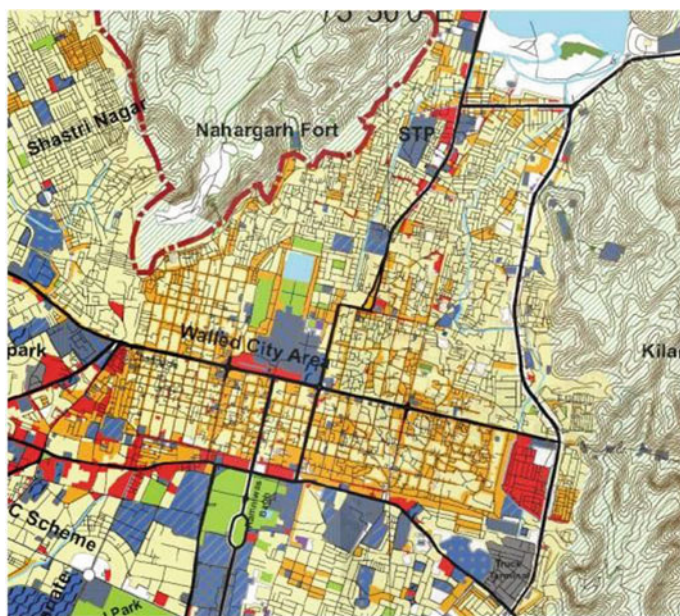
As can be conclusively seen that the main streets abutting the important bazaars in the Walled City region have adequate widths to assimilate the contemporary traffic conditions in ideal conditions, such was the long-sightedness of the planners of the region in the eighteenth century. Despite of such good planning, the city is not free from the encumbrances of contemporary developments and these issues are explored further.

In historic urban areas, the need to assimilate conservation efforts and revitalisation along with socio-economic development while preserving environmental quality is definitely challenging (Doratli et al. 2004). Following are the prominent issues arising in the Walled City region of Jaipur which need to be identified and studied on the detailed scale and approached holistically.

### ***5.1 Changing Functionality of the Walled City***

The Walled City of Jaipur was planned to be more of urban settlement with 62% of area allotted to residential usage while around 2.7% was for commercial aspects and close to 15% towards mixed use (Fig. 2 and Table 2) (SLAC, Town Planning Department, Special Area Heritage Development Plan 2041. Jaipur Nagar Nigam Heritage, Government Report). Despite of such small land share available, the Walled City has transitioned itself as the commercial hub of the entire Jaipur city. This points towards the centralisation of economic activity within the Walled City region and thus acting as a magnet to many other issues. This skewed commercialisation could possibly mean that the traditional economic activities in the Walled City might be getting

side-lined for the modern economic activities and hence becomes a serious issue in conservation of heritage art and livelihoods of traditional artisans and craftsmen.



**Fig. 2** Generalised existing land use in Walled City, Jaipur (SLAC, Town Planning Department, Special Area Heritage Development Plan 2041, Jaipur Nagar Nigam Heritage, Government Report)

**Table 2** Land use structure in Walled City, Jaipur (SLAC, Town Planning Department, Special Area Heritage Development Plan 2041, Jaipur Nagar Nigam Heritage, Government Report)

S. No.	Existing land use	Area (ha)	Percentage (%)
1	Residential	418.03	62
2	Commercial	17.92	2.7
3	Mixed	99.76	14.8
4	Industrial	0.58	0.1
5	Public/semi-public	37.71	5.6
6	Recreational	12.77	1.9
7	Circulation	66.22	9.8
8	Others	21.02	3.1
	Total	674	100

## **5.2 *Over-Densification of the Walled City Region***

The Walled City region is subjected to the highest density (930 pph) in entire Jaipur city. This trend is visible in almost all historic towns in India and across the globe too. Higher density might not be the absolute problem but the pressures exerted by high density on the commercial and social aspects within the region are matters to be considered. The densified core areas along with newer formal market invasion will definitely push for more space within the Walled City region and this might happen at the cost of traditional commerce thus affecting the heritage value.

## **5.3 *Traffic and Transportation***

The highest burden and pressure on the Walled City region of Jaipur is due the traffic and congestion. With the status of the commercial business district, the Walled City attracts a large number of people within its limit. The existing secondary and tertiary street network definitely does not support the prevalent traffic load, and hence, associated externalities are forced into the region. The main roads are wide enough to accommodate the flowing traffic, but during the peak hours the carrying capacity dwindles significantly due to increased pedestrian movement, informal encroachment, and on-road parking (Fig. 3). The commercial bazaars are primarily responsible for attracting traffic menace in the region. Along with the formal shops, the Walled City streets also host the informal traders with hand-driven carts. During the peak hours, these carts can be seen lined up along the main streets, and thus, the traffic carrying capacity of the wide main streets also shrink down.

## **5.4 *Obsolescence***

In the simplest terms, obsolescence means the lack of tangency between the available service and the contemporary requirements. By far, the Walled City of Jaipur is facing obsolescence in a qualified manner reflecting the need for in-depth understanding of the matter. Obsolescence can be derived in various forms like structural, functional, locational, legal and administrative, and image obsolescence. In case of physical or structural obsolescence, the traditional buildings might have faced deterioration (Fig. 4) due to various factors like time, weather, and poor maintenance. Hence, it becomes interesting that how over a period of more than 250 years of the city's establishment, the traditional bazaars are still standing tall. Though the situation of the structures seems to be sound today, the structural obsolescence issue cannot be ruled out completely.

Functional obsolescence depicts the mismatch between the design criteria of traditional bazaars and shops with respect to the modern economic activities (Fig. 5). The



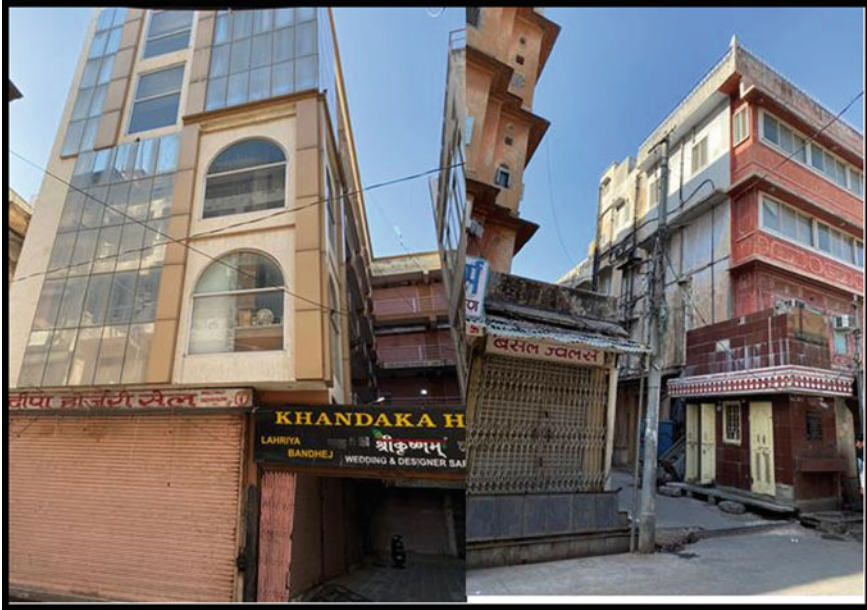


Fig. 3 Traffic situation on Walled City streets (Source Google Images)



Fig. 4 Physical deterioration leading to obsolescence (Source Author)

commercial areas of the Walled City have helped in preserving the traditional art and craft and thus the heritage but can this functionality alone can sustain the economic feasibility of the region. As the Walled City is also acting the central business district to the entire Jaipur city, thorough studies need to be attempted to evaluate any functional gaps within the traditional commerce and contemporary economic needs might be creating conflict for space within the market areas. On the other hand, locational



**Fig. 5** Replacement of the old heritage structure with new commercial complexes leading to Functional obsolescence (Source Author)

obsolescence can be derived from understanding the accessibility of the commercial areas in the larger context. In present time, if the commercial areas are equally accessible in terms of transport as well as logistics needs to be understood. This might otherwise pave way to ousting of traditional professions and thus loss of heritage.

Image obsolescence is the biggest threat the Walled City of Jaipur might face in the near future. The encumbrances like air pollution, poor drainage facilities, unhygienic conditions, noise pollution, encroachments, stagnant traffic, and congestion might give a bad character to the traditional bazaars of Walled City, and it will prove detrimental in the terms of tourism and attractiveness of the heritage sites.

### **5.5 Vulnerability to Hazards**

One of the biggest threat looming over the globe today is the increasing vulnerability towards hazards, and the risk is further compounded by the unsustainable practices prevalent in cities. Though hazard risk is uniformly high across all types of cities, the burden on historic city cores is extremely high due to heritage and the high quantum of livelihoods within such regions. The Walled City of Jaipur is facing urban hazards like urban floods and urban fires which bring the city to a standstill and significantly affects the daily lives of the people living therein. Urban fires have started to become

a frequent phenomenon and hence need to be given special attention as the risk of damage to property, life, and heritage is significantly high in such dense areas. For example, fire was reported on Khuteto ka Rasta in Kishanpole in a wooden warehouse and took almost four hours to bring under control (The Times of India 2018). Urban floods too are becoming common in the Walled City region due to poor drainage and often brings the commercial activities to a halt as water gushes in the shops and market areas. These hazards are hence serious issues grappling the traditional bazaars and need comprehensive attention.

### ***5.6 Community and Social Dynamics***

The traditional bazaars often host an economy that is driven more by social and religious character rather than solely relying on financial character. The invasion of newer formalised markets might affect the traditional commercial society and initiate a collapse of communities in the Walled City region. Along with the physical transformation, the risk to rapid transitions in cultural and social aspects thus will increase. With the changing functionality and pressure induced by densification couples with modern economic avenues, the old social order might get deprived of an appropriate platform to earn their livelihood. This could lead to successive deprivations to these communities and affect the further generations in a compounded manner. The traditional shop owners in the bazaars might fall victim to such deprivations leading to social marginalisation with respect to education, health care, dietary needs, and infrastructural facilities on individual, community, and class level (Naidu 1990).

## **6 Prospects to Conservation of Traditional Bazaars in Walled City of Jaipur**

The process undertaken to sustain the legacy of historic buildings by avoiding their damage and wearing is referred to as conservation. Conservation approaches can often be a subset of urban renewal mechanism working along with redevelopment and rehabilitation strategies. Conservation efforts in historic cities significantly help in extending the traditional built up with certain degree of freedom to make changes without affecting the heritage character of the region. It thus takes a holistic approach to socio-economic changes in the urban setting and preserving assets and historic fabric within the sustainable limits of environment and infrastructural capacities. Thus, it concerns the integration between maintenance and protection by controlling the dynamic changes associated with the processes of urban and social development (Mehanna and Mehanna 2019).



The traditional bazaars in the Walled City of Jaipur cannot be looked just to be economic activities and professions but rather as heritage assets. Though in the entirety of the Walled City region, the pressing issues like infrastructure development and improving quality of life are considered as priority matters, the conservation of traditional bazaars will help complement the efforts towards maintaining and preserving the urban heritage. Even the Sustainable Development Goal 11.4 targets the conservation of heritage and asks to strengthen efforts to protect and safeguard the cultural heritage (United Nations 2015). Hence, it becomes necessary to merge commercial aspects into culture and heritage and look at conservation strategies that will help resolve all issues in a comprehensive manner.

The prospective conservation could be done on both city level as well as community level. The Walled City itself has the status of a thriving city for more than 290 years now, also the economic activities are based on the community profession, and hence, conservation policies need to be devised on both levels. While the city level focuses more on tourism-related development, upgrading quality of life through infrastructure and job creation, the community level shall focus on imparting resilience against hazards, preserving the art and culture to thrive through the bazaar through community well-being and hence community participation. The subordinate activities necessary to guide both the city and community-level conservation would be the strategies like creating a 'sense of place' in the bazaars, bazaar identity and pride, and preservation of the profession.

## ***6.1 Community Conservation***

The biggest resource that can help in maintaining the heritage of the traditional bazaars of Walled City is the traditional professionals themselves. The heritage value of the region is not solely based on the historic buildings and landmarks, and they are equally reliant on the conservation of the art and culture. This art and culture are thriving only because of the market platform provided by the bazaars. Hence to conserve the bazaars, the people running the bazaar and their profession need to be conserved first.

Community participation-based research strategies can be devised in such situations which will help the stakeholders identify their needs and demands. These needs will then be mapped according to the priority of efforts needed to conserve the bazaars. In this way, the economic as well as social upliftment can be done without any loss in heritage value. The process of conservation under the community-based model equips the socio-economic resilience of the urban system and hence allows robust conservation efforts (Saez Ujaque et al. 2021).

## ***6.2 Conservation of Façade on Internal Commercial Streets***

The built structure and the façade adjoining the streets are the defining elements of the urban landscape and its value. The most remarkable feature of the main streets in the Walled City region is the uniform façade of the bazaars. This has helped in achieving the 'sense of place' and a specific identity for the region. The commercial streets are the most vital visual element of a historic city. The biggest drawback though is the absence of such uniformity within the inner streets of Walled City, Jaipur. This is one of the primary reasons that despite having a distinctive identity the internal streets of the bazaar do not have any 'sense of place' and an image that will help them to assimilate into the larger context of the Walled City. In order to protect and propagate the identity of the place, its built form needs to be protected through the implementation of legally binding principles and guidelines (Mohit and Kammeier 1996). Hence, the conservation of existing façade on major streets and development of uniform façade on inner commercial streets can be developed through regulations and induce a stronger sense of identity to the region, thus improving the prospects of the region.

## ***6.3 Markets and Traditional Commercial Streets***

The most prominent feature for conservation is the heritage markets in the Walled City of Jaipur. These bazaars are the hotspots of economic activities on daily basis and also are responsible for attracting heavy traffic both domestic and logistic within the region. It is rationally impossible to separate the traditional bazaars from the commercial streets as they are an amalgamation and not distinctive features in any historic city. Such features imparting the traditionality to the urban become the most noteworthy points and hence need to be revitalised through conservation efforts (Lee 1996). This linear format of commerce and economy hence can be seen in one light and approached with a similar strategy that will be symbiotic to each other. The integration can be classified and strategised in terms of temporal scale, functional scale, and by urban form (Feisal and Ibrahim 2009).

## ***6.4 Controlling Vehicular Movement Through One-Way Loop System***

Though the main streets are wide enough to accommodate the existing traffic load in ideal conditions, the encroachments, parking, and other encumbrances reduce their efficiencies. The secondary and tertiary streets are very narrow and hence cannot sustain even basic carrying capacity. Such congestions on the commercial streets are further aggravated by pedestrian movement and conflicts. These problems can be

overcome by redirecting the traffic movement. As the layout of the Walled City is based on the Prastara plan, the gird-iron pattern can be efficiently used to create loops of one-way street, thus doubling their traffic handling efficiency. With the provision of circulatory one-way street loops, enough road width will open up to accommodate even the informal trades and can solve parking issues to a significant level. Thus, there will be no need to widen the street network and put the heritage and bazaars at stake.

The efforts in Isfahan Central Business District in the country of Iran presents a viable solution towards reducing traffic congestions. The Isfahan CBD is also populated with historic buildings and commercial markets and hence has suitability with the Walled City of Jaipur. The reconfiguration of existing congested streets into one-way loop networks has shown promising and significant results in terms of reducing traffic congestion (Karimi et al. 2022).

### ***6.5 Logistic Management Plan***

The commercial bazaars, traditional as well as modern economic activities both need logistical support. As the bazaars also trade products like luxury furniture, carpets, fabric, metal, and many other, a constant supply chain needs to be maintained. This creates a conflict between pedestrians, domestic traffic and logistic traffic as the supply trucks and vans often take large amount of time for loading and unloading the materials. To solve this deadlock, it is necessary to evolve a Logistic Management Plan which can efficiently take care of the issues in the context. The solutions can vary based on the specific needs of specific bazaars and their trademark products hence a detailed Management Plan for logistics will help. Dedicated logistic streets can be assigned for logistic traffic to tread, or it could be made mandatory for the logistic traffic to load and unload in specific non-peak hours. This will help reduce the burden on the commercial streets and more space can be made available to the bazaars to work. The usage of trans-shipment networking platforms in densely crowded urban areas is a proven solution towards the efficient management of logistics (Merchan et al. 2016).

### ***6.6 Tourism Development***

The heart and soul of the traditional bazaars in the Walled City region are the tourist, local, national as well as international. The need to preserve the heritage and the traditional commercial bazaars solely finds its base in developing the tourism industry base in a country like India. With the development in tourism, various opportunities can be created for the local population, and the quality of life can also be enhanced. Tourism prospects thus can act as a catalyst for the conservation efforts in the Walled

City of Jaipur. A comprehensive tourism-oriented heritage conservation and management plan should be prepared that can address the issue with dedicated approach and assimilate the strategies.

The efforts of Jaipur Nagar Nigam Heritage have helped the preparation of the Special Area Heritage Development Plan targeting the horizon year of 2041. Decentralised conservation efforts in terms of reconstruction while retaining similar identity of the structure along with rehabilitation has proved to foster economical functionality to the otherwise dilapidated lesser important historic structures (Yulu 2021). The functional conversion thus can help achieve a dual goal of attracting commerce and economy while conserving the character and identity of the heritage.

## 7 Conclusion

The Walled City of Jaipur is one of the most significant nodes of Indian tourism industry. For a country like India that aims to foster growth and development on large scale has to focus on conserving its heritage and history through its cities. As these cities will attract people from all over the world, the conservation efforts will help India build a positive brand value and strengthen its position.

The study reveals the problems that the commercial streets face in terms of losing its identity due to contemporary demands from rapid urbanisation. The identification of problems in any system is always the most crucial stage towards conservation efforts, and hence, it has been attempted through this study. The most prevalent issues have been highlighted through the survey and have been presented as potential points where interventions are necessary. Based on various similar cases around the world, possible prospects have been suggested.

The traditional commercial bazaars of Walled City of Jaipur are hotspots of commercial activity in the entire Jaipur city which also happens to be the biggest city of Rajasthan. Hence, the importance of these bazaars and the need to conserve them is called for attention through this study. The problems of the Walled City if holistically approached can be addressed through an efficient conservation strategy, and the prospects put forth will act like the directive principles which will help the strategy to sustain the objectives of conservation of the traditional bazaars of Walled City, Jaipur.

## References

- Borie A, Catalàa F, Papillault R (2020) Jaipur: a planned city of Rajasthan. Altrim Publishers
- Dhingra M, Singh MK, Chattopadhyay S (2016) Rapid assessment tool for traditional Indian neighbourhoods: a case study of Alwar Walled City in Rajasthan. *Sustain Cities Soc* 26:364–382. <https://doi.org/10.1016/j.scs.2016.06.015>

- Doratli N, Hoskara SO, Fasli M (2004) An analytical methodology for revitalization strategies in historic urban quarters: a case study of the Walled City of Nicosia, North Cyprus. *Cities* 21(4):329–348. <https://doi.org/10.1016/j.cities.2004.04.009>
- Feisal Z, Ibrahim R (2009) The reality of traditional markets: an analytical study of the role of traditional markets in the contemporary city. Presented at the ARCHCAIRO conference
- Funo S, Yamamoto N, Pant M (2002) Space formation of Jaipur City, Rajasthan, India: an analysis on city maps (1925–28) made by survey of India. *J Asian Archit Build Eng* 1(1):261–269. <https://doi.org/10.3130/jaabe.1.261>
- Jaipur Development Authority, Master Development Plan 2025
- Karimi H, Ghadirifaraz B, Shetab Boushehri SN, Hosseininasab S-M, Rafiei N (2022) Reducing traffic congestion and increasing sustainability in special urban areas through one-way traffic reconfiguration. *Transportation* 49(1):37–60. <https://doi.org/10.1007/s11116-020-10162-4>
- Kumari S (2020) Historic cities in India—an overview, p 8
- Lee SL (1996) Urban conservation policy and the preservation of historical and cultural heritage: the case of Singapore. *Cities* 13(6):399–409. [https://doi.org/10.1016/0264-2751\(96\)00027-3](https://doi.org/10.1016/0264-2751(96)00027-3)
- Mehanna WAE-H, Mehanna WAE-H (2019) Urban renewal for traditional commercial streets at the historical centers of cities. *Alex Eng J* 58(4):1127–1143. <https://doi.org/10.1016/j.aej.2019.09.015>
- Merchan D, Blanco EE, Winkenbach M (2016) Transshipment networks for last-mile delivery in congested urban areas, p 11
- Mohit RS, Kammeier HD (1996) The Fort: opportunities for an effective urban conservation strategy in Bombay. *Cities* 13(6):387–398. [https://doi.org/10.1016/0264-2751\(96\)00026-1](https://doi.org/10.1016/0264-2751(96)00026-1)
- Naidu R (1990) *Old cities, new predicaments: a study of Hyderabad*. Sage, New Delhi, Newbury Park
- PHD Chamber of Commerce and Industry (2015) *Transforming central business districts: taking the smart route*. PWC India. [Online]. Available: <https://www.pwc.in/assets/pdfs/publications/2015/transforming-central-business-districts.pdf>
- Pusalkar S (2022) Understanding the Vastu shastra: city planning in Walled City of Jaipur. *Academia Lett* 9:61–72. <https://doi.org/10.53136/97912599480766>
- Saez Ujaque D, Roca E, de Balanzó Joue R, Fuertes P, Garcia-Almirall P (2021) Resilience and urban regeneration policies. Lessons from community-led initiatives. The case study of CanFugarolas in Mataró (Barcelona). *Sustainability* 13(22), Art. no. 22. <https://doi.org/10.3390/su132212855>
- SLAC, Town Planning Department, Special Area Heritage Development Plan 2041. Jaipur Nagar Nigam Heritage, Government Report
- Transforming our world: the 2030 agenda for sustainable development. United Nations, A/RES/70/1, 2015. [Online]. Available: <https://sustainabledevelopment.un.org>
- UNESCO World Heritage (2022) Jaipur City, Rajasthan. UNESCO World Heritage Centre. <https://whc.unesco.org/en/list/1605/>. Accessed 23 June 2022
- Wooden warehouse in Walled City gutted. *The Times of India*, Jaipur, 20 April 2018. [Online]. Available: [https://timesofindia.indiatimes.com/city/jaipur/wooden-warehouse-in-walled-city-gutted/articleshow/63837524.cms?utm\\_source=amp\\_slider&utm\\_medium=referral&utm\\_campaign=TOI&from=mdr](https://timesofindia.indiatimes.com/city/jaipur/wooden-warehouse-in-walled-city-gutted/articleshow/63837524.cms?utm_source=amp_slider&utm_medium=referral&utm_campaign=TOI&from=mdr)
- Yulu A (2021) The role of tourism in urban conservation: the case of Manila, The Philippines. *J Geogr*. <https://doi.org/10.26650/JGEOG2020-0011>

# A Framework of Internet of Things–Cloud–Building Information Modeling Based Life Cycle Management of Precast Components in Prefabricated Buildings



Arpit Solanki and Debasis Sarkar

**Abstract** Prefabricated buildings are adopted in the construction industry because they are more cost-effective, environmentally friendly, and faster to construct and provide higher quality and safety. The most essential and recognizable aspect of prefabricated buildings is precast components. Precast component management is still inefficient, and precast manufacturing efficiency is inadequate. The precast component lifecycle must be managed because the designers, manufacturing producers, and on-site installers are all from separate regions. Some of the most recent technologies include the Internet of Things (IoT) for real-time visibility and traceability, Cloud Computing for data management, and Building Information Modeling (BIM) for digital presentations and quality management, significantly reducing precast component lifecycle management difficulties in prefabricated buildings. BIM seems to be a model based information-sharing approach that allows multiple key stakeholders to collaborate on 3D BIM models. Cloud services enable project stakeholders to collaborate through the Internet and make decisions quickly from any location. RFID is an IoT technology that allows project stakeholders to monitor and track precast components in real time. Integrating BIM with RFID and Cloud technology enables the project stakeholders to access real-time information on precast components and prefabrication building lifecycle management. Therefore, this research study highlighted challenges in the life cycle management of precast components in prefabricated buildings and proposed a framework based on Internet of Things–Cloud–Building Information Modeling. The data flow model and information management systems are also described. Throughout the lifecycle of the precast component and the prefabricated building, this framework would improve real-time information communication among both the precast manufacturer and the construction project site so there will be no travel or duration gaps. Prefabricated component

---

A. Solanki (✉) · D. Sarkar

Department of Civil Engineering, School of Technology, Pandit Deendayal Energy University, Gandhinagar, India

e-mail: [arpit.sphd20@sot.pdpu.ac.in](mailto:arpit.sphd20@sot.pdpu.ac.in)

D. Sarkar

e-mail: [debasis.sarkar@sot.pdpu.ac.in](mailto:debasis.sarkar@sot.pdpu.ac.in)

and building lifecycle information may be tracked, and cost, quality, schedule, and safety management will be monitored.

**Keywords** Building Information Modeling (BIM) · Cloud Computing · Internet of Things (IoT) · Life Cycle Management · Prefabricated Buildings · Radio Frequency Identification Devices (RFID)

## 1 Introduction

Prefabricated buildings have gained popularity in the construction industry in various regions of the globe in the past few decades. A prefabrication building is defined as a structure manufactured and constructed using prefabricated components brought to the assembly on the construction site to finish the structure. Prefabricated buildings are employed for faster construction, higher quality, and better value for money in the construction industry. Precast components are the most important and recognizable aspect of prefabricated buildings. Compared to traditional constructions, the most recognizable and crucial part is producing building precast components in a manufacturing plant and delivering them to the installation site. Precast component manufacturing, delivery, and installation issues are caused due to a lack of standards and knowledge, poor collaboration and coordination, poor logistics planning, poor visibility, and a lack of traceability, which results in dimension variation, clash detections, poor handling, and reworking. The precast components are different parts of a single structure that were linked and fit together for the purpose of building the structure, commonly known as joineries. The joints of the precast components were appropriately sealed to prevent air and water entering in the structure. It was challenging to joinery on the installation site due to variations in the precast components' dimensions and quality. Due to a lack of investment, standardization, knowledge, and skilled workers in the manufacturing plant, the production of precast components suffers. Because the production plant is far from the installation site, the precast components were damaged or mishandled, and the installation was delayed. The connection of precast components is inappropriate due to poor design. The connection of precast components needs to be supervised and completed correctly on the installation site; otherwise, the structure may collapse. Therefore, special attention needs to be given to precast component management. The project manager, engineers, designers, contractors, and workers in precast buildings effectively manage all operations, emphasizing precast component management. Design, manufacturing, distribution, storing, assembly, and inspection of precast components seem time-consuming and costly (Valero et al. 2015). Lifecycle management is essential because of the large quantity and variety of precast components, such as beams, columns, walls, staircases, slabs, stationary, and pallets.

Lifecycle management of precast components is evaluating a product's environmental performance throughout the length of its entire or partial life span (Dong et al. 2013). Precast component lifecycle management is used to manage prefabricated

buildings' lifecycle (Han and Ye 2018). However, challenges in precast buildings remain to address information sharing, collaboration and coordination, poor data management, less accuracy, poor tracking, poor visibility, and poor traceability (Han and Ye 2018). The challenges in the management of the precast components are

1. Different parties, such as the designer, manufacturer, suppliers, on-site assemblers, and operation and maintenance parties, cannot share information and collaborate (Han and Ye 2018).
2. The information on precast concrete components (dimensions, materials, reinforcements, and so on) does not come immediately from the detailed design phase. Instead, it is manually gathered and recorded on paper, resulting in lesser accurate and trustworthy information (Han and Ye 2018).
3. Problems with current conventional methods to recognize, monitor, and track highly specialized prefabricated components lead to late delivery, double-handling and misplaced components, and improper installations, which cause time overruns and increased labor expenses (Ergen et al. 2007).
4. Furthermore, obtaining real-time data on the prefabricated component throughout its life cycle is challenging, leading to poor traceability and visibility (Han and Ye 2018). With the implementation of the Internet of Things, Cloud technologies, and Building Information Modeling, the owners, engineers, project managers, contractors, and supervisors are willing to connect their information management system with relevant applications in building modernization. Building Information Modeling (BIM) seems to be a highly interactive, model based strategy for the lifecycle management process that includes all project participants (Sun et al. 2014). Project team members work together in real time, and they can update in 3D models, review design alternatives, integrate structural, architectural, mechanical, electrical, and plumbing models, and avoid conflicts. Architects, producers, distributors, on-site installers, and operation and maintenance groups employ BIM models to make effective prefabricated building management decisions.

The Internet of Things is described as the connection of physical objects to the Internet in order to monitor them in real time. The Internet of Things (IoT) system architects have perception, network, and application layers. Data was collected in physical object perception layers via sensors and RFID. This data is transferred on the network layer through Wi-Fi, Ethernet, GSM, GPRS, and WSN, and it is managed and used by users via applications and software on the application layer (Jia et al. 2012). The Internet of Things (IoT) refers to the use of Radio Frequency Identification (RFID) tags attached to physical objects to identify, track, and monitor them using a Radio Frequency Identification (RFID) reader globally (Jia et al. 2012). Therefore, Radio Frequency Identification (RFID) has become more widely used in the precast industry to manage manufacturing, logistics, supply chains, facility and safety management, and continuous monitoring. The precast components are inspected in many stages, such as the manufacturing chain, material receiving, molds testing, sample strength feedback, logistics and shipping monitoring, all of which are monitored using RFID technology (Yin et al. 2009). The Internet of Things



(IoT), Cloud, and Building Information Modeling are the most recent technologies that may be used in the construction industry for real-time monitoring, collaboration, coordination, and visualization. Currently, precast components are manually tracked and monitored in prefabricated buildings, and decision-making on construction sites is a time-consuming and challenging process, especially with so many precast components. All these challenges will be resolved by integrating the Internet of Things (IoT), the Cloud, and Building Information Modeling. In comparison with manually tracking and monitoring, integrating the Internet of Things (IoT), the Cloud, and Building Information Modeling will automatically track and monitor precast components from the planning stage through the operation and maintenance phase. The precast component information is maintained on paper throughout its lifecycle in prefabricated buildings, increasing the possibility of mistakes and loss, but this will be decreased by adopting these technologies. In the Internet of Things (IoT), RFID may monitor and track products and construction site workers. RFID technology may be used to assure the effectiveness and precision of real-time on-site maintaining health and safety. RFID tags might retain information about each precast component's current state, enabling real-time monitoring and management of maintenance procedures (Valero et al. 2015).

The information collected from the Internet of Things and Building Information Modeling is not fully integrated and shared among stakeholders since architects, producers, distributors, and on-site installers are frequently from worldwide (Zhong et al. 2017). This problem has been solved by cloud technology. A cloud is something that exists in a remote area. The combination of all cloud computing models, such as software as a service (SaaS), platform as a service (PaaS), and infrastructure as a service (IaaS), are used because they enable Internet based collaboration to accelerate decision-making from any location. Therefore, the goal of this research is to propose a framework of Internet of Things (IoT)–Cloud–Building Information Modeling based life cycle management of precast components in prefabricated buildings. The actual information exchange of prefabricated building's precast components throughout the entire span could be improved, and the duration and location gaps among both the precast production plant and the installation site could be reduced, success can be attributed with the help of the Internet of Things (IoT), Cloud, and Building Information Modeling technological innovations.

## **2 Life Cycle Management of Prefabricated Buildings Through the Internet of Things (IoT)–Cloud–Building Information Modeling**

The lifecycle management of prefabricated buildings' precast components refers to handling the precast components through the typical stages of their life. The life cycle of prefabricated structures includes planning, designing precast components, manufacturing of precast components, modular fabrication, assembly on the construction

site, and building operation and maintenance. Precast component production is the more distinctive and difficult portion of the process. Throughout the construction life cycle, prefabricated building information is continuously produced and gathered. Thus, the significant problems in prefabricated buildings are smoothly and effectively utilizing information like construction documents, files, drawings, design, and records throughout the building life cycle and managing and maintaining the information systematically (Man et al. 2013).

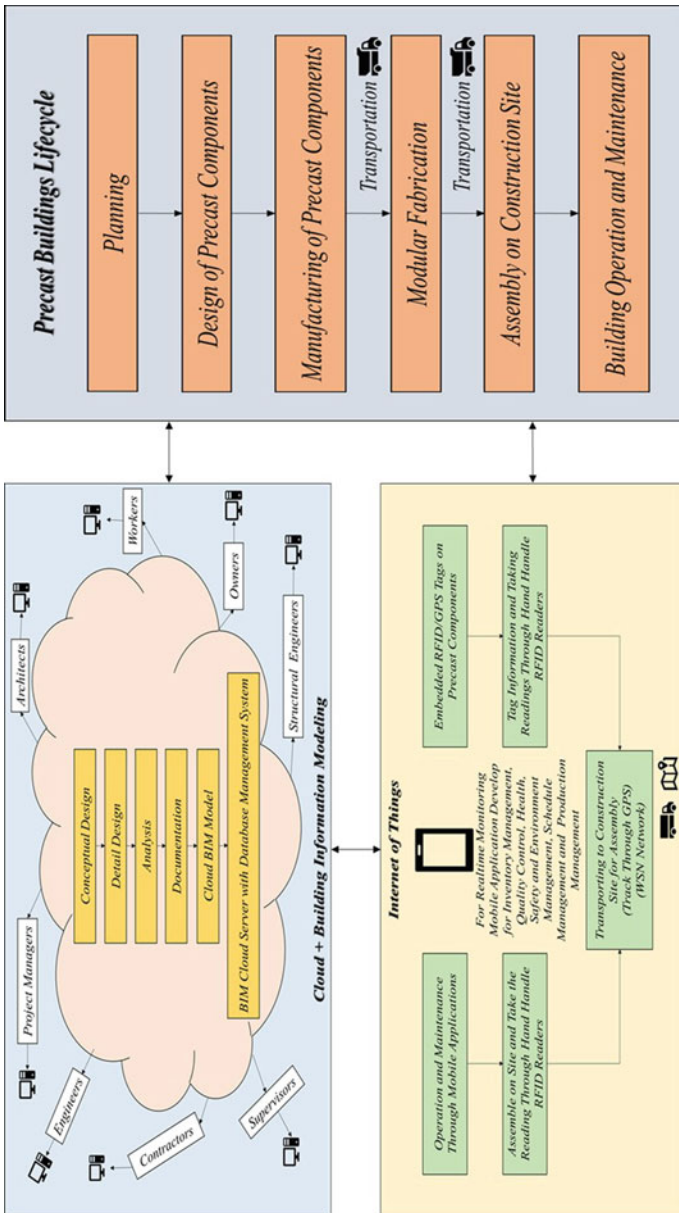
Prefabricated building lifecycle management is required to satisfy the demands and desires of owners, engineers, project managers, contractors, supervisors, and others. The Internet of Things–Cloud–Building Information Modeling technologies may be used to identify and adjust the properties of precast components' properties and monitor them without requiring active participation. Radio Frequency Identification Devices (RFID) is a wireless technology that employs tags and readers to track prefabricated components. They automatically recognize and track tags placed on precast components using electromagnetic fields. RFID integration with the BIM–Cloud platform enables real-time monitoring. The real-time decisions are actively taken by owners, engineers, project managers, contractors, supervisors, and others from RFID with the BIM–Cloud platform. Figure 1 shows the Internet of Things (IoT) framework–Cloud–Building Information Modeling based on the life cycle management of prefabricated buildings.

### 3 Internet of Things (IoT)–Cloud–Building Information Modeling Based Information Management Systems

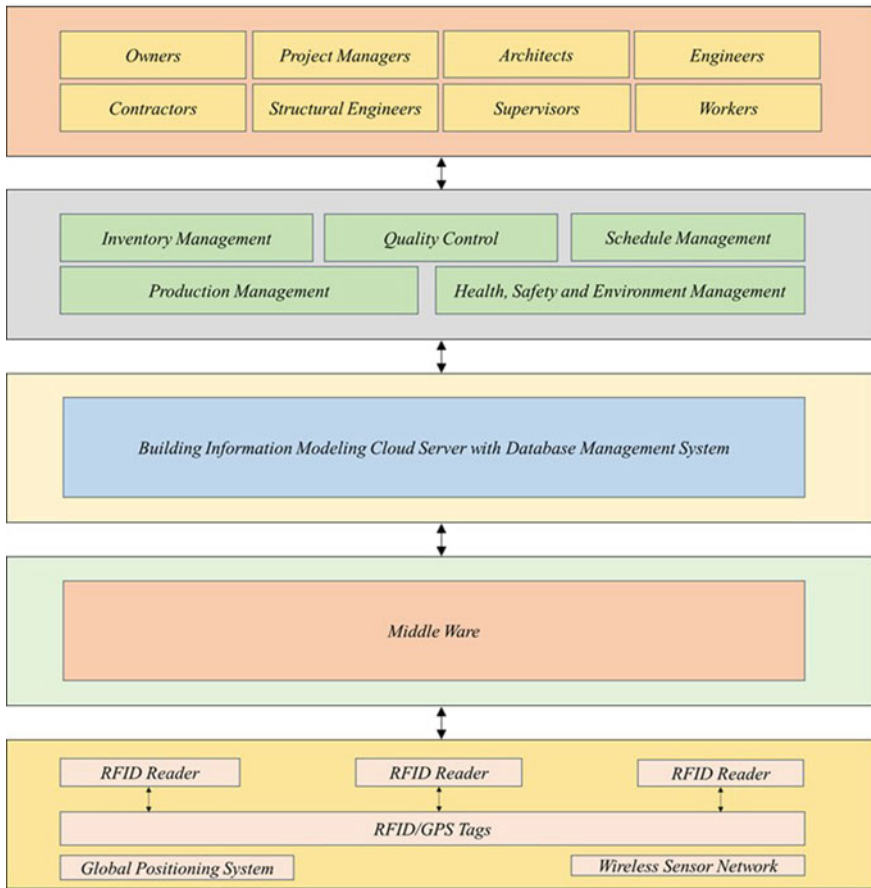
**The Conceptual Framework:** It is built on a wireless production system that provides real-time data transparency and track-and-trace, comparable to the manufacturing industry's lean production method. Building Information Modeling–Cloud allows all stakeholders to see and communicate on a single platform. From RFID, the precast components may trace and track through Global Positioning System (GPS). As a result, developing a system that combines Building Information Modeling, Cloud, and the Internet of Things is critical.

The conceptual framework is presented in Fig. 2. As shown in Fig. 2, the Internet of Things (IoT)–Cloud–Building Information Modeling found information management systems are made up of three subsystems: radio frequency identification devices subsystem, Building Information Modeling–Cloud subsystem, and business application subsystem.

Readers, tags, and middleware make up the RFID subsystem. RFID tags are classified into three categories (1) Active, (2) Passive, and (3) Semi-passive. There are five types of RFID readers (1) Fixed, (2) Handheld, (3) Low range serial, (4) Bluetooth, and (5) USB (Sarkar et al. 2022). The middleware is a software subsystem that stands between hardware and applications. The Global Positioning System (GPS)



**Fig. 1** Framework of Internet of Things (IoT)–Cloud–Building Information Modeling based life cycle management of prefabricated buildings



**Fig. 2** Internet of Things (IoT)–Cloud–Building Information Modeling Based Information Management Systems

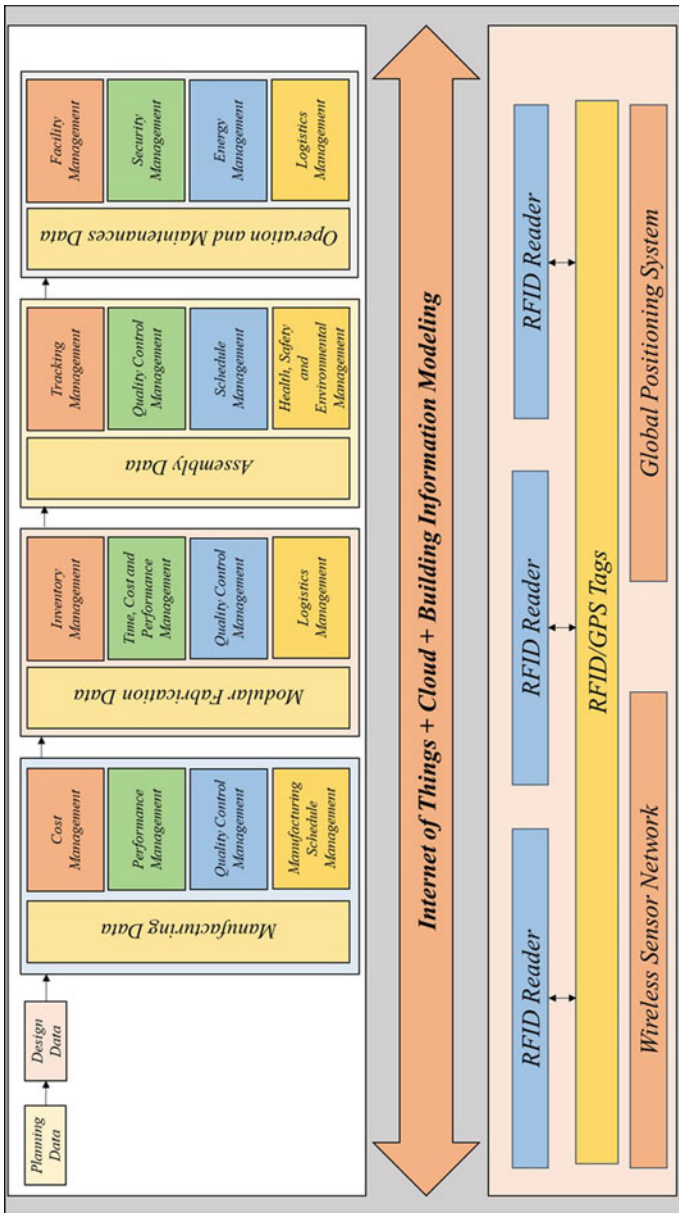
uses the signal from satellites to find the exact location of an object. A Wireless Sensor Network (WSN) is a collection of sensors that connect over wireless networks to monitor and record conditions in various locations. Because of the integrated global positioning system, radio frequency identification devices, and wireless sensor networks technologies, a large amount of real-time information about prefabricated buildings is gathered continuously. The RFID tags are implanted on precast components like beams, columns, walls, staircases, slabs, stationary, pallets, and other devices. The hand-held RFID readers and both active and passive RFID tags are used for real-time information collection in manufacturing, inventory, logistics, assembly, storage, and operation and maintenance. The RFID subsystem gathered real-time data such as description (unique id and dimensions), location (GPS coordinates), and condition (date, time, and environmental condition), then sent it to the

BIM–Cloud subsystem through middleware and updated it regularly. Relevant applications for management, such as quality control (unique id and dimensions), time, cost, and performance (unique id, GPS coordinates, dimensions, date, and time), manufacturing schedule (unique id, GPS coordinates, dimensions, date, time, and environmental condition), inventory (unique id, GPS coordinates, date, and time), tracking (unique id, GPS coordinates, date, and time), schedule (unique id, GPS coordinates, date, and time), facility (unique id, dimensions, and environmental condition), security (unique id, GPS coordinates, and environmental condition), energy (unique id and environmental condition), logistics (unique id, dimensions, GPS coordinates, date, time, and environmental condition), health, safety and environmental (unique id, GPS coordinates, date, time, and environmental condition), and others, are developed depending on the data gathered and the requirements of different people involved. As a result, this real-time information can control and monitor for management of decision-making and the effectiveness of operational activities.

**The Data Flow Model:** The flow of data in the Internet of Things (IoT)–Cloud–Building Information Modeling Based Information Management Systems is described in Fig. 3. The precast components of prefabricated buildings must be identified in the planning phase. A unique identification number should be assigned to the specified precast components during the design phase. The information mainly included in the detailed design phase is information of material, information of embedded parts, information of the projects, information of drawings, information of mold, and others.

When the design work is completed, comprehensive design information will be sent to the manufacturing monitoring systems. Rather than manually based on manufacturing execution system and Building Information Modeling, the details of the precast components for their manufacturing in the precast factory come instantly and automatically from the complete design model. RFID/GPS tags placed in precast components in the precast factory have a unique identification number and provide detailed design and production information, giving the RFID subsystem a beginning. All through the manufacturing process, engineers and technicians use handheld RFID readers to verify if the product satisfies the quality criteria. The real-time quality assessment outline is delivered to the Building Information Modeling–Cloud server database management system concurrently. The Database Management System (DBMS) in the BIM–Cloud server is database software that saves, retrieves, defines, and maintains information in the cloud through the BIM server. RFID subsystems and GPS tags are used in logistics and inventory management to accurately and effectively recognize, monitor, and locate prefabricated components in real time.

Throughout the operation and maintenance phase, the Building Information Modeling–Cloud server is updated in real time with information on labors, materials, equipment, vehicles, and facilities. From development through production and installation to operation and maintenance, the data in the tag is produced and gathered on a regular basis. Relevant applications for management, such as quality control, time, cost and performance, performance, manufacturing schedule, inventory, tracking, schedule, facility, security, energy, logistics, health, safety and environmental, and



**Fig. 3** Internet of Things (IoT)–Cloud–Building Information Modeling Data Flow Model

others, are built to improve the management level. As a result, information sharing and collaboration throughout the life cycle is achievable by integrating the Internet of Things (IoT), Cloud, and Building Information Modeling.

## 4 Conclusion

The framework for lifecycle management of precast components in prefabricated buildings using Internet of Things (IoT)–Cloud–Building Information Modeling proposed in this research paper. This proposed framework includes a radio frequency identification devices subsystem, a building information modeling subsystem, cloud subsystems, and a business application subsystem, and it enables real-time data visualization and traceability across several applications. This real-time data may be used to control and monitor decision-making and the effectiveness of operational activities.

This framework gives a novel viewpoint on prefabricated building and precast component lifecycle management in order to improve management decision-making efficiency and effectiveness. According to research, the adoption of Internet of Things (IoT) technology, such as radio frequency identification devices, enables the recognition and adjustment of characteristics, as well as the continuous monitoring of precast components as goods, resulting in essential precast component information management. The precast component's real-time data sharing and the prefabricated building's lifecycle would be improved by including radio frequency identification devices in the Building Information Modeling–Cloud platform. The Internet of Things (IoT)–Cloud–Building Information Modeling framework reduces the cost, time, and manual paperwork by 50% while managing the lifecycle of precast components in prefabricated buildings. This framework fulfils all stakeholders' and participants' needs and objectives, which is advantageous to sharing and cooperating with prefabricated building lifecycle information.

## References

- Dong Y, Wong C, Ng S, Wong J (2013) Life cycle assessment of precast concrete units. *Int J Civil Environ Eng* 7(3):230–235
- Ergen E, Akinci B, Sacks R (2007) Automation of effective tracking and locating precast components at a storage yard. *Autom Constr* 16(3):354–367
- Han C, Ye H (2018) A novel IoT-Cloud-BIM based intelligent information management system in building industrialization. In: International conference on construction and real estate management (ICCREM), Charleston, South Carolina, USA, 9–10 Aug 2018
- Jia X, Feng Q, Fan T, Lei Q (2012) RFID technology and its applications in Internet of Things (IoT). In: 2nd international conference on consumer electronics, communications and networks (CECNet), Yichang, China, 21–23 April 2012
- Man QP, Wang YW, Heng LI, Yuan C, Martin S (2013) Lifecycle information flow management system. *Int J Digit Content Tech Its Appl* 7(8):857–864

- Sarkar D, Patel H, Dave B (2022) Development of integrated cloud-based Internet of Things (IoT) platform for asset management of elevated metro rail projects. *Int J Constr Manag* 22(10):1993–2002
- Sun CS, Jiang F, Man QP (2014) A summary on BIM application in construction industry. *J Eng Manag* 28(3):28–31
- Valero E, Adan A, Cerrada C (2015) Evolution of RFID applications in construction: a literature review. *Sensors* 15(7):15988–16008
- Yin SYL, Tserng HP, Wang JC, Tsai SC (2009) Developing a precast production management system using RFID technology. *Autom Constr* 18(5):677–691
- Zhong RY, Peng Y, Xue F, Fang J, Zou W, Luo H, Ng ST, Lu W, Shen GQP, Huang GQ (2017) Prefabricated construction enabled by the Internet-of-Things. *Autom Constr* 76:59–70